Methods in Molecular Biology 1631

Springer Protocols

Ramanjulu Sunkar *Editor*

Plant Stress Tolerance

Methods and Protocols

Second Edition

Humana Press

METHODS IN MOLECULAR BIOLOGY

Series Editor
John M. Walker
School of Life and Medical Sciences
University of Hertfordshire
Hatfield, Hertfordshire, AL10 9AB, UK

For further volumes:
http://www.springer.com/series/7651

Plant Stress Tolerance

Methods and Protocols

Second Edition

Edited by

Ramanjulu Sunkar

Department of Biochemistry and Molecular Biology, Oklahoma State University, Stillwater, OK, USA

Humana Press

Editor
Ramanjulu Sunkar
Department of Biochemistry and Molecular Biology
Oklahoma State University
Stillwater, OK, USA

ISSN 1064-3745 ISSN 1940-6029 (electronic)
Methods in Molecular Biology
ISBN 978-1-4939-7134-3 ISBN 978-1-4939-7136-7 (eBook)
DOI 10.1007/978-1-4939-7136-7

Library of Congress Control Number: 2017942931

Printed on acid-free paper

This Humana Press imprint is published by Springer Nature
The registered company is Springer Science+Business Media LLC
The registered company address is: 233 Spring Street, New York, NY 10013, U.S.A.

Preface

The first edition of *Plant Stress Tolerance: Methods and Protocols* under the series of Methods in Molecular Biology was published in 2010. We were very gratified with its popularity. In the first edition all pertinent protocols could not be accommodated and also the fact that Plant Biology has witnessed a fast pace of molecular research over the last few years is the motivation to bring the second edition.

Given the more frequent episodes of drought, increasing heat or cold as well as saline--affected areas throughout the world, probing plant responses to abiotic stresses has become one of the top priority research areas now. This second edition begins with review chapters: Besides an updated review on oxidative stress responses newly emerging areas such as epigenetics, long noncoding RNAs, and microbiome in adaptation to abiotic stresses were included. The protocols included are genetic screens, quantifying in vivo molecular interactions, identifying DNA methylation and histone modifications, identifying stress-responsive genes that are differentially translated, proteomics, phosphoproteomics, posttranslational redox modifications, metabolomics, and lipidomics. Additionally, the protocols on determining sulfate, sulfite, thiosulfate, sulfolipids, and enzymes associated with sulfite toxicity as well as glutathione were included. The remaining methodology chapters cover a wide range of topics such as distinguishing superoxide dismutases, determining polyamines, quantifying ABA levels, silencing stress-responsive microRNAs, and identifying microbes that promote drought tolerance. I hope that this volume meets the demands of both new and established researchers who are interested in this area of plant biology research.

I thank the contributors who are instrumental in bringing this volume. I also thank Prof. John Walker, who gave me the opportunity to edit the second edition. Finally I also thank Prof. John Gustafson, Head, Department of Biochemistry and Molecular Biology, Oklahoma State University, for his encouragement to take up this task.

Stillwater, OK, USA ***Ramanjulu Sunkar***

Contents

Contributors

Ibtisam Al Harrasi • *Department of Biology, College of Science, Sultan Qaboos University, Muscat, Oman*

Rashid Al-Yahyai • *Department of Crop Science, College of Agriculture and Marine Sciences, Sultan Qaboos University, Muscat, Oman*

Carla António • *Plant Metabolomics Laboratory, Instituto de Tecnologia Química e Biológica António Xavier, Universidade Nova de Lisboa (ITQB-UNL), Oeiras, Portugal*

Jay Prakash Awasthi • *Department of Life Science and Bioinformatics, Plant Molecular Biotechnology Laboratory, Assam University, Silchar, Assam, India*

Pragya Barua • *National Institute of Plant Genome Research, Jawaharlal Nehru University Campus, New Delhi, India*

Aizat Bekturova • *French Associates Institute for Agriculture and Biotechnology of Drylands, Blaustein Institutes for Desert Research, Sede Boqer Campus, Ben-Gurion University, Beer Sheva, Israel*

Galina Brychkova • *Plant and AgriBiosciences Research Centre (PABC), School of Natural Sciences, National University of Ireland Galway, Galway, Ireland*

Niranjan Chakraborty • *National Institute of Plant Genome Research, Jawaharlal Nehru University Campus, New Delhi, India*

Subhra Chakraborty • *National Institute of Plant Genome Research, Jawaharlal Nehru University Campus, New Delhi, India*

Geeng Loo Chong • *Institute of Plant and Microbial Biology, Academia Sinica, Taipei, Taiwan; Molecular and Biological Agricultural Sciences Program, Taiwan International Graduate Program, Academia Sinica, Taipei, Taiwan; Graduate Institute of Biotechnology, National Chung-Hsing University, Taichung, Taiwan*

Kelly D. Craven • *Plant Biology Division, The Samuel Roberts Noble Foundation, Ardmore, OK, USA*

Shivakumar Devaiah • *Department of Biological Sciences, East Tennessee State University, Johnson City, TN, USA*

Karl-Josef Dietz • *Department of Biochemistry and Physiology of Plants, Faculty of Biology, Bielefeld University, Bielefeld, Germany*

Maria H. Florêncio • *Centro de Química e Bioquímica, Faculdade de Ciências, Universidade de Lisboa, Lisboa, Portugal; Departamento de Química e Bioquímica, Faculdade de Ciências, Universidade de Lisboa, Lisboa, Portugal*

Dipak Gayen • *National Institute of Plant Genome Research, Jawaharlal Nehru University Campus, New Delhi, India*

Xiaoqing Gong • *State Key Laboratory of Crop Stress Biology for Arid Areas, College of Horticulture, Northwest A&F University, Yangling, China*

Vandana K. Hivrale • *Department of Biochemistry, Dr. Babasaheb Ambedkar Marathwada University, Aurangabad, MS, India*

Guru Jagadeeswaran • *Department of Biochemistry and Molecular Biology, Oklahoma State University, Stillwater, OK, USA*

Ashwini R. Jamdhade • *Department of Biochemistry, Dr. Babasaheb Ambedkar Marathwada University, Aurangabad, MS, India*
Tiago F. Jorge • *Plant Metabolomics Laboratory, Instituto de Tecnologia Química e Biológica António Xavier, Universidade Nova de Lisboa (ITQB-UNL), Oeiras, Portugal*
Inna Khozin • *French Associates Institute for Agriculture and Biotechnology of Drylands, Blaustein Institutes for Desert Research, Sede Boqer Campus, Ben-Gurion University, Beer Sheva, Israel*
Aruna Kilaru • *Department of Biological Sciences, East Tennessee State University, Johnson City, TN, USA*
Derya Kirasi • *Dynamic Cell Imaging, Faculty of Biology, Bielefeld University, Bielefeld, Germany*
Assylay Kurmanbayeva • *French Associates Institute for Agriculture and Biotechnology of Drylands, Blaustein Institutes for Desert Research, Sede Boqer Campus, Ben-Gurion University, Beer Sheva, Israel*
Venkatachalam Lakshmanan • *Plant Biology Division, The Samuel Roberts Noble Foundation, Ardmore, OK, USA*
Nilesh Vikram Lande • *National Institute of Plant Genome Research, Jawaharlal Nehru University Campus, New Delhi, India*
Byeong-ha Lee • *Department of Life Science, Sogang University, Seoul, South Korea*
Yong-Fang Li • *College of Life Sciences, Henan Normal University, Xinxiang, Henan, China*
Guosheng Li • *Department of Biochemistry and Molecular Biology, Oklahoma State University, Stillwater, OK, USA*
Michael Liebthal • *Department of Biochemistry and Physiology of Plants, Faculty of Biology, University of Bielefeld, Bielefeld, Germany*
Ji-Hong Liu • *Key Laboratory of Horticultural Plant Biology, College of Horticulture and Forestry Sciences, Huazhong Agricultural University, Wuhan, China*
Ramamurthy Mahalingam • *Cereal Crops Research Unit, USDA-ARS, Madison, WI, USA*
Andrew Mort • *Department of Biochemistry and Molecular Biology, Oklahoma State University, Stillwater, OK, USA*
Sanjib Kumar Panda • *Plant Molecular Biotechnology Laboratory, Department of Life Science and Bioinformatics, Assam University, Silchar, Assam, India*
Christof Rampitsch • *Morden Research and Development Centre, Agriculture and Agrifood Canada, Morden, MB, Canada*
Prasun Ray • *Plant Biology Division, The Samuel Roberts Noble Foundation, Ardmore, OK, USA*
Moshe Sagi • *French Associates Institute for Agriculture and Biotechnology of Drylands, Blaustein Institutes for Desert Research, Sede Boqer Campus, Ben-Gurion University, Beer Sheva, Israel*
Smita Sahoo • *Plant Molecular Biotechnology Laboratory, Department of Life Science and Bioinformatics, Assam University, Silchar, Assam, India*
Thorsten Seidel • *Dynamic Cell Imaging, Faculty of Biology, Bielefeld University, Bielefeld, Germany*
Suhas Shinde • *Department of Biological Sciences, East Tennessee State University, Johnson City, TN, USA*
Yuepeng Song • *National Engineering Laboratory for Tree Breeding, College of Biological Sciences and Technology, Beijing Forestry University, Beijing, People's Republic of China; Key Laboratory of Genetics and Breeding in Forest Trees and Ornamental Plants, College*

of Biological Sciences and Technology, Beijing Forestry University, Beijing, People's Republic of China

Dominic Standing • *French Associates Institute for Agriculture and Biotechnology of Drylands, Blaustein Institutes for Desert Research, Sede Boqer Campus, Ben-Gurion University, Beer Sheva, Israel*

Chinta Sudhakar • *Department of Botany, Sri Krishnadevaraya University, Anantapuram, India*

Ramanjulu Sunkar • *Department of Biochemistry and Molecular Biology, Oklahoma State University, Stillwater, OK, USA*

Guiliang Tang • *College of Agronomy, Henan Agricultural University, Zhengzhou, China; Department of Biological Sciences, Michigan Technological University, Houghton, MI, USA*

Wilena Telman • *Department of Biochemistry and Physiology of Plants, Faculty of Biology, Bielefeld University, Bielefeld, Germany*

Sachin Teotia • *College of Agronomy, Henan Agricultural University, Zhengzhou, China; School of Biotechnology, Gautam Buddha University, Greater Noida, India; Department of Biological Sciences, Michigan Technological University, Houghton, MI, USA*

Patrick Treffon • *Department of Biochemistry and Physiology of Plants, Faculty of Biology, Bielefeld University, Bielefeld, Germany*

Gounipalli Veeranagamallaiah • *Department of Botany, Sri Krishnadevaraya University, Anantapuram, India*

Paul E. Verslues • *Institute of Plant and Microbial Biology, Academia Sinica, Taipei, Taiwan; Biotechnology Center, National Chung-Hsing University, Taichung, Taiwan*

Min May Wong • *Institute of Plant and Microbial Biology, Academia Sinica, Taipei, Taiwan; Molecular and Biological Agricultural Sciences Program, Taiwan International Graduate Program, Taipei, Taiwan; Graduate Institute of Biotechnology, National Chung-Hsing University, Taichung, Taiwan*

Mahmoud W. Yaish • *Department of Biology, College of Science, Sultan Qaboos University, Muscat, Oman*

Dmitry Yarmolinsky • *French Associates Institute for Agriculture and Biotechnology of Drylands, Blaustein Institutes for Desert Research, Sede Boqer Campus, Ben-Gurion University, Beer Sheva, Israel*

Si-in Yu • *Department of Life Science, Sogang University, Seoul, South Korea*

Deqiang Zhang • *National Engineering Laboratory for Tree Breeding, College of Biological Sciences and Technology, Beijing Forestry University, Beijing, People's Republic of China; Key Laboratory of Genetics and Breeding in Forest Trees and Ornamental Plants, College of Biological Sciences and Technology, Beijing Forestry University, Beijing, People's Republic of China*

Part I

Review Chapters

Chapter 1

Epigenetics and RNA Processing: Connections to Drought, Salt, and ABA?

Min May Wong, Geeng Loo Chong, and Paul E. Verslues

Abstract

There have been great research advances in epigenetics, RNA splicing, and mRNA processing over recent years. In parallel, there have been many advances in abiotic stress and Abscisic Acid (ABA) signaling. Here we overview studies that have examined stress-induced changes in the epigenome and RNA processing as well as cases where disrupting these processes changes the plant response to abiotic stress. We also highlight some examples where specific connections of stress or ABA signaling to epigenetics or RNA processing have been found. By implication, this also points out cases where such mechanistic connections are likely to exist but are yet to be characterized. In the absence of such specific connections to stress signaling, it should be kept in mind that stress sensitivity phenotypes of some epigenetic or RNA processing mutants maybe the result of indirect, pleiotropic effects and thus may perhaps not indicate a direct function in stress acclimation.

Key words Drought, Salinity, ABA signaling, Chromatin remodeling, Histone modification, DNA methylation, Alternative splicing, mRNA decapping, mRNA stability, Protein phosphatase 2Cs

1 Introduction

Plant tolerance of environmental stress is necessary for survival and is a key factor in agricultural productivity. Abiotic stresses such as drought and salinity have profound effects on plant growth and development and are among the major factors which lead to serious yield losses to agriculture worldwide [1, 2]. Plants respond to water limitation due to drought and salinity through a series of mechanisms which contribute to avoidance and tolerance of low water potential and reduced water uptake [2, 3]. Plants sense water limitation via unknown mechanisms which lead to changes in hormone levels and activation of stress signaling pathways [1, 4]. In particular, the phytohormone abscisic acid (ABA) accumulates during drought and salinity stress and is a central regulator of many downstream stress responses [5–7]. The core pathway of ABA signaling includes the Clade A protein phosphatase 2Cs (PP2Cs)

Ramanjulu Sunkar (ed.), *Plant Stress Tolerance: Methods and Protocols*, Methods in Molecular Biology, vol. 1631,
DOI 10.1007/978-1-4939-7136-7_1,

which interact with and are regulated by the Pyrabactin Resistance1/Pyrabactin Resistance1-Like/Regulatory Component of ABA Receptor (PYL/RCAR) family of ABA receptors [5, 6]. Inhibition of Clade A PP2C activity by PYL/RCAR binding allows autophosphorylation and activation of the Sucrose non-Fermenting Related-Related Kinase 2 (SnRK2) family of protein kinases and may also affect other signaling mechanisms, particularly other protein phosphorylation events or binding of Clade A PP2Cs to other protein complexes (Fig. 1). It has been stated [5] that a major remaining challenge is to connect the PYL/RCAR-PP2C-SnRK2 ABA signaling pathway to the great range of gene expression and protein activity changes that have been observed during drought stress. A similar statement can be made about ABA independent stress sensing and signaling mechanisms which act in parallel with ABA or alter ABA sensitivity. ABA-independent stress signaling mechanisms are diverse and as whole less well characterized than the core PYL/RCAR-PP2C-SnRK2 ABA signaling pathway [8, 9]. For example, several Dehydration Response Element/C-repeat binding factors (DREB/CBFs) are transcription factors that mediate abiotic stress responsive gene expression changes and are generally thought to act in an ABA-independent manner [10, 11]. It is also apparent from physiological studies that drought stressed plants have a very different response to ABA than unstressed plants [3, 12]; however, the molecular basis for such different ABA response in stressed versus unstressed plants remains obscure. Possibly, such differences in ABA sensitivity of stressed versus non-stressed plants are related to epigenetic mechanisms and stress memory [13–15]. There is also evidence that epigenetic mechanisms respond to reactive oxygen status of the plant and regulate metabolism [16] and these mechanisms are also relevant to abiotic stress responses.

Many studies have examined the effects of drought and salinity on gene expression and identified transcription factors controlling stress responsive gene expression (for example the DREBs mentioned above). Certainly more remain to be characterized. In addition, it has now become clear that drought, salinity, and other abiotic stresses cause remodeling of the epigenome and also alter splicing and stability of specific mRNAs. This has been shown both by studies of individual stress responsive loci as well as genome wide analyses [17–19]. Various histone marks (discussed below) as well as DNA methylation have been shown to be altered by abiotic stress [20–24]. Posttranscriptionally, there are indications that RNA-capping, alternative splicing, and RNA stability are strongly influenced by abiotic stress [25, 26] (as well as micro-RNA mediated regulation and selective translation of mRNAs, both of which lie outside the scope of this review). In this review, we provide a brief overview of key epigenetic and posttranscriptional RNA processing mechanisms and the evidence indicating that these

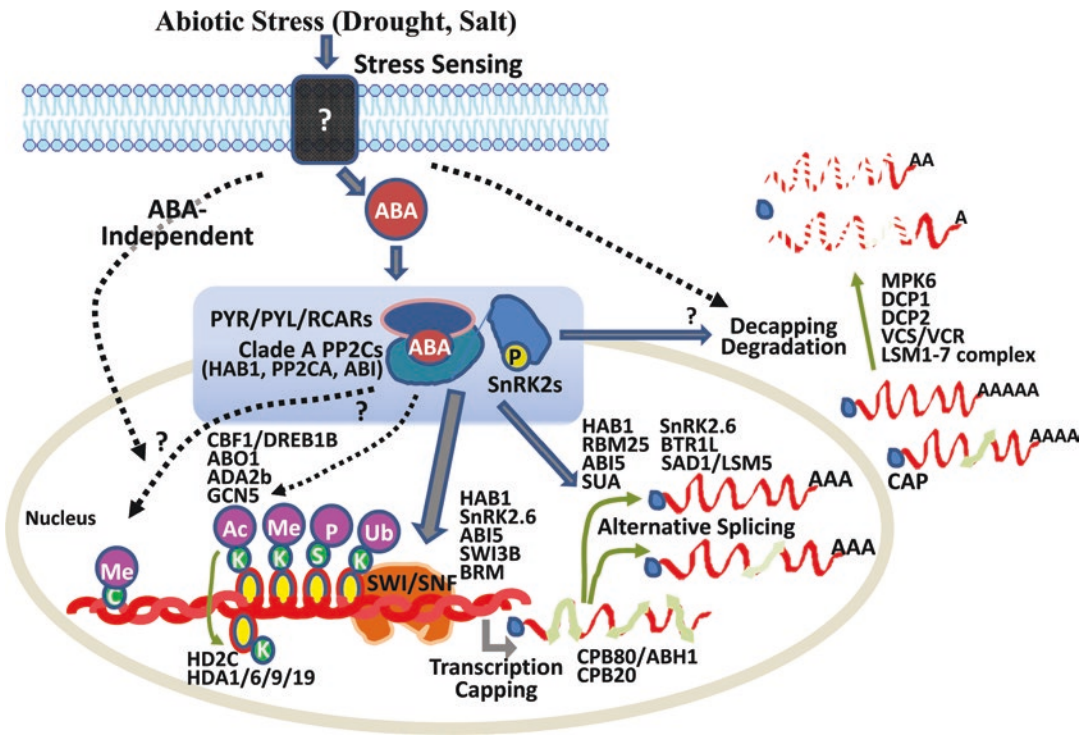

Fig. 1 Some major stress signaling, epigenetic, and RNA processing steps and their putative connections. Abiotic stresses such as drought and salinity are sensed by unknown mechanisms, perhaps including membrane-based sensor proteins. This upstream signaling elicits ABA accumulation which in turn is sensed through PYL/RCAR-Clade A PP2C-SnRK2 kinase protein complexes which constitute the core ABA signaling pathway. PYL/RCAR-PP2C-SnRK2 signaling can occur in both nucleus and cytoplasm. In some cases, such as chromatin remodeling by SWI/SNF complexes and some alternative splicing events, connections to the core ABA signaling pathway have been established. Other epigenetic and RNA processing, such as DNA methylation, are known to be affected by stress but the signaling controlling this has yet to be characterized. Stress sensing also elicits ABA-independent signaling which may affect epigenetic modifications and RNA processing but is less characterized. Key proteins described in the text are listed next to the processes they are involved in

processes influence responses to ABA, drought or salinity (Fig. 1). As one focus of our work is drought-related signaling, we also discuss the state of knowledge (or lack of knowledge) of mechanisms by which drought sensing and signaling or the core ABA signaling pathway can connect with and modulate epigenetic or RNA processing mechanisms. Interested readers are also referred to excellent recent reviews of Crisp et al. [13] who explore some of the same issues that we do here but with more emphasis on the role of epigenetics and RNA metabolism in stress memory and recovery from stress and of Shen et al. [16] who focus on the connections of redox state, metabolism and epigenetics.

2 Stress Epigenetics

2.1 Chromatin Remodeling Factors

Clade A PP2Cs play a key role in ABA signaling. Much of this occurs via regulation of SnRK2 kinase activity; however, identification of other proteins directly regulated by the Clade A PP2Cs has received relatively less attention. A notable exception to this is the interaction of Clade A PP2Cs with chromatin remodeling factors. Several Clade A PP2Cs including HAB1 (Hypersensitive to ABA1), ABI1 (ABA Insensitive 1), ABI2, and PP2CA, were found to interact with SWI3B, a subunit of SWI/SNF chromatin-remodeling complexes [27]. *Arabidopsis* SWI/SNF (Switch/Sucrose nonfermenting) chromatin remodeling subunits are encoded by multiple genes and form complexes consisting of the DNA-dependent ATPases SPLAYED (SYD) and BRAHMA (BRM) [28, 29], along with other subunits such as BUSHY (BSH), SWI3A, SWI3B, SWI3C, SWI3D, SWP73A, and SWP73B [30–32]. Chromatin Immunoprecipitation (ChIP) assays revealed that association of HAB1 with the promoter of RD29B and RAB18 (ABA regulated genes) is disrupted by ABA treatment, presumably because HAB1 is bound to PYL/RCARs in the presence of ABA. This suggests a direct involvement of HAB1 in the regulation of ABA-induced transcription [27], in addition to an indirect role via regulation of SnRK2 activity. This study has provided some of the most direct evidence to date for a link between ABA signaling and epigenetic regulation in plants. The function of Clade A PP2Cs in chromatin remodeling complexes as well as interaction of Clade A PP2Cs with other epigenetic or transcriptional regulatory factors are questions of continuing interest.

Chromatin remodeling complexes consist of several subunits and, given the interaction of Clade A PP2Cs with SWI/SNF chromatin remodeling complexes, it could be hypothesized that other subunits of such complexes may also influence abiotic stress responses. Consistent with this idea, Han et al. [33] demonstrated that mutation of another SWI2/SNF2 chromatin remodeling component, BRM, caused ABA hypersensitivity during postgermination growth arrest. They used ChIP assays to demonstrate that BRM binds to the *ABI5* (*ABA Insensitive5*) locus. ABI5 is a transcription factor that affects ABA sensitivity of seed germination. The same group further found direct interaction of BRM with HAB1 and SnRK2 kinases [34]. They also demonstrated that BRM is a direct substrate of SnRK2.6 and these phosphorylation sites are dephosphorylated by PP2CA (another Clade A PP2C). PP2CA dephosphorylation of BRM was blocked by addition of PYL/RCARs (in presence of ABA), consistent with formation of PYL-ABA-PP2C complexes which inhibit phosphatase activity. Furthermore, expression of phosphomimic BRM caused ABA hypersensitivity and increased expression of ABI5. This demonstrated that the BRM phosphorylation site targeted by SnRK2 and

PP2CA was functionally relevant to ABA response [34]. This research demonstrated that SnRK2/PP2C-regulated BRM phosphorylation/dephosphorylation is crucial for BRM-mediated control of ABA response.

Both the SWI3B and BRM studies provided some of the most direct evidence to date for a link between ABA signaling and epigenetic regulation in plants. Whether or not the Clade A PP2Cs interact with other epigenetic or transcriptional regulatory factors is a question of continuing interest. So far such evidence for direct regulatory links to ABA and stress signaling is lacking for other key epigenetic components including histone acetyltransferases (HAT)/histone deacetylase (HDAC) complexes and DNA methylation; however, more indirect evidence indicates that both histone modification and DNA methylation have substantial effects on stress and ABA sensitivity (see below). It is also worth noting that other chromatin remodeling components also are also associated with ABA-related phenotypes. For example, mutation of *PICKLE* (*PKL*), which encodes a SNF2-related helicase/ATPase domain protein, caused ABA hypersensitivity and increased expression of ABI3 and ABI5. ABA-treated *pkl* mutant showed low levels of H3K9me and H3K27me at ABI3 and ABI5 promoter sites [35]. However, it is not known whether ABA or stress signaling directly affects PKL function or whether the *pkl* mutant phenotypes are the result of more indirect effects. This type of question is also relevant to the other epigenetic mechanisms discussed below.

2.2 Histone Modifications During Drought and Salinity Stress

Modification of histone tails by acetylation, methylation, phosphorylation, and ubiquitination plays an essential role in epigenetic regulation of stress-responsive gene expression [17, 36, 37]. Histone acetylation is one of most important and best studied histone marks involved in gene regulation. Histone acetylation is mediated by antagonist activity of HATs and HDACs and occurs at the Ɛ-amino group of conserved lysine residue(s) of the histone N-terminal tail. Acetylation at these sites decreases the interaction between histones and negative charged DNA thus leading to a more accessible "looser" chromatin conformation [38–40].

In Arabidopsis, there are 12 putative HATs belonging to four different families. One of these HATs, GCN5 (General Control Non-depressible 5) which belongs to the GCN5 N-acetyltransferase (GNAT) subfamily is well characterized and acts as the catalytic subunit of several multiprotein HAT complexes [41, 42]. ADA (alteration/deficiency in activation) and SAGA (Spt-Ada-Gcn5-acetyltransferase) are two additional major components of GCN5-containing complexes. *Arabidopsis* ADA2b mutants display hypersensitivity to salt and abscisic acid [43, 44]. ADA2a and ADA2b were reported to interact with GCN5 and these three proteins also interacted with CBF1/DREB1B [45]. This suggested that CBF1 might stimulate transcription

through recruitment of ADA/SAGA-like HAT complexes to the promoters of its target genes [46]. Kaldis et al. [44] reported that a double mutant of *sgf29a-1* (*SAGA associated Factor 29*) and *ada2b-1* displayed similar phenotype with *ada2b-1* (i.e., hypersensitive to salt and similar reduced expression of several abiotic stress responsive genes), indicating that they may be involved in the same mechanism regulating stress responsive gene expression. Consistent with its interaction with CBF1, ADA2b positively regulated salt-induced gene expression of COR6.6, RAB18, and RD29b by maintaining locus-specific acetylation of Histone H4 and H3 [44]. This study supports the hypothesis that some DNA-binding transcription factors involved in abiotic stress response are capable of recruiting HAT complexes to their target promoters. Presumably, this regulation of histone acetylation involves CBF1-dependent recruitment of an ADA2b-containing HAT complex to target promoters; however, additional experiments such as ChIP assays are needed to see if HAT-complex components are indeed associated with stress responsive promoters, whether this promoter association is affected by stress or ABA and whether it is dependent on the presence of CBF1. As ChIP-sequencing techniques become more common and accessible, this would also be a promising approach to define the set of genes regulated by CBF1 recruitment of HAT complexes and determine whether control of histone acetylation is the predominant mechanism by which CBF1 regulates stress-responsive gene expression. CBF1 is one of the best studied abiotic stress-associated transcription factors; similar questions could be asked about other transcription factors that have been shown to regulate gene expression in response to abiotic stress. Conversely, one could also ask whether ADA2b and other HAT complex components interact with and are recruited by additional transcription factors involved in abiotic stress-responsive gene expression.

Other putative components of HAT complexes have also been proposed to be involved in ABA and stress responses. In Arabidopsis, mutants of ABO1/ELO2 (*ABA-Overly sensitive 1/Elongata 2*) are ABA hypersensitive in seed germination and seedling growth, have increased ABA-induced stomatal closure and altered drought resistance [47]. ABO1/ELO2 is an ortholog of yeast ELP1 which is one subunit of the yeast Elongator complex (a HAT complex) that functions in acetylation of Histone3 and Histone4 [48]. This study is consistent with the above mentioned results in that it suggests an important role for HAT complexes in abiotic stress. However, there is some uncertainty whether ABO/ELO2 affects stress responses via changes in histone acetylation or via other RNA processing mechanisms [48].

The activity of HAT complexes is counteracted by HDACs and there is also evidence that HDAC activity alters plant responses

to salt and drought stress. Expression of Arabidopsis HD2-type HDAC, AtHD2C, can be repressed by ABA. Overexpression of AtHD2C causes ABA insensitivity and alters salt and drought stress responses [49]. The other RPD3/HDA1 type HDACs, HDA6 and HDA19, also seem to be involved in gene regulation during ABA and salt stress in *Arabidopsis* [50, 51]. *hda6* and *hda19* mutant plants are more sensitive to ABA and salt stress compared with wild-type. In addition, salt- or ABA-responsive gene expression was decreased in *hda6* and *hda19* plants. A later study demonstrated that AtHD2C interacted physically with HDA6 and HDA19 and bound to histone H3, thus affecting histone H3 acetylation and methylation [52]. *hd2c-1*, *hda6*, and *hd2c-1hda6* mutants had increased H3K9K14 acetylation and H3K4 dimethylation in the promoter regions of ABI1 and ABI2 but not in the promoter of AtERF4 (Ethylene response factor) [19, 52]. Thus, the HD2C-HDA6-HDA19 protein complex may regulate gene expression involved in stress responses.

In contrast, HDA9 has phenotypic differences compared to HDA6 and HDA19. Mutants of HDA9 show increased root growth under salt and polyethylene glycol (PEG) treated seedlings compared to wild type [53], and, unlike HDA6 and HDA19, were hypersensitive to inhibition of seed germination by salt or ABA treatment. Mutation of HDA9 led to upregulation of water stress responsive genes. This is opposite to the downregulation of stress responsive genes in HDA6/HDA19 mutants. In the *hda9* mutant, H3K9 acetylation levels were much increased in the promoters of the 14 upregulated stress-responsive genes and decreased in downregulated genes [53]. The RPD3/HDA1 type HDACs in Arabidopsis most likely have distinct function and affect plant stress responses by regulating a different set of stress-responsive genes compared to other HDACs [50–53].

The overall pattern that emerges from these studies is that increased histone acetylation favors greater induction of stress responsive genes; however, in some cases there seems to be little or no change observed in the histone acetylation even when there is gene induction [examples are AtERF4, AtCYP1–1, and AtHSP90.2 [52, 53]]. While the overall evidence for the involvement of histone acetylation/deacetylation in abiotic stress response is strong, there are a number of questions unanswered, particularly questions about targeting to specific promoters. HATs and HDACs are targeted to specific genome regions in part by assembly into protein complexes containing DNA-binding proteins or transcription factors. The composition of these protein complexes and how stress signals influence their assembly and targeting to specific stress responsive promoters is not understood. Also, gene expression of several *HDAC*s is induced by abiotic stress but whether or not this induction is directly regulated by core ABA signaling or other stress signaling mechanism is unclear.

2.3 DNA Methylation

Cytosine methylation is a eukaryotic gene-silencing mechanism that affects gene expression by modulating DNA–protein interactions [54, 55]. DNA methylation status in plant is regulated by various physiological, developmental, and stress stimuli [21, 23, 24]. DNA methylation and histone modification are interrelated processes and the effect of various histone modifications (usually histone methylation or histone acetylation) can affect the establishment and maintenance of DNA methylation and eventually modulate gene expression [54, 56]. In plants, DNA methylation occurs at the three different cytosine sequence contexts: symmetric CG and CHG (where H is C, A, or T), and asymmetric CHH [58]. Distinct pathways are responsible for maintenance of methylation in each of these three sequence contexts [55] while de novo DNA cytosine methylation requires 24-nt small interfering RNAs (siRNA) that direct DRM2 (domains rearranged methyltransferase 2) to methylate all three sequence contexts via the RNA-directed DNA methylation (RdDM) pathway [58, 59]. The mechanisms controlling DNA methylation are complex and subject of substantial ongoing research. Here we focus on how DNA methylation affects gene expression under drought and salinity and the poorly understood ways in which stress signaling may modulate DNA methylation.

Studies from various plant species have shown that osmotic and salt stress could induce hypo/hypermethylation in different genome backgrounds. An early study of tobacco BY-2 cell suspension cultures, found that two nontranscribed heterochromatic loci were hypermethylated under osmotic and salt stress, which was reversible when the cells were reinoculated onto non stress media [60]. Water deficit also led to specific CG context hypermethylation in pea root tip [61]. Drought-induced hypermethylation and hypomethylation was also found in lowland rice cultivars and drought-tolerant rice cultivars [62]. In maize, salinity-induced methylation downregulated zmPP2C expression, while salinity-induced demethylation upregulated zmGST expression [63]. Several more recent studies have focused on genome scale profiling of stress-induced changes in DNA methylation. In *Arabidopsis*, genome-wide DNA methylation differences in response to low water potential stress (simulated drought imposed using polyethylene glycol-infused agar plates) have been identified [20]. In this study, the methylome was widely affected by changes in water potential, with the most dramatic DNA hypermethylation observed near transcription start sites (±500 bp) of protein-coding genes related to stress responses. However, in several cases, little correlation was identified between gene expression patterns and DNA methylation levels [18, 20]. Other studies have profiled DNA methylation changes in response to salt stress [22] or drought stress in barley [23]. In all of these studies, the authors proposed that altered DNA methylation patterns might be involved in stress

acclimation. In parallel, several other studies have advanced the idea that epigenetic mechanisms, particularly DNA methylation, are involved in transgenerational memory of various types of stress [13]. There can also be considerable differences in methylation patterns between different ecotypes/varieties with contrasting physiological characteristics [64, 65] and between different tissue and cell types [23, 66]. It seems likely that these methylation differences can contribute to phenotypic differences in stress resistance, although the relationship of methylation differences to stress phenotypes remains to be further characterized.

These genome wide studies have been complemented by more detailed investigations of methylation patterns of individual genes and there is a growing list of loci where stress-responsive methylation has been studied. For example, in soybean, salinity stress was shown to affect the methylation status of four transcription factors, i.e., *MYB*, *b-ZIP* and two *AP2/DREB f*amily members [67]. ChIP analysis indicated that at three of these four loci DNA methylation was correlated with an increased level of histone H3K4 trimethylation and H3K9 acetylation, and/or a reduced level of H3K9 demethylation in various parts of the promoter or coding regions [67]. A correlation of DNA hypermethylation at promoters and gene bodies with enrichment of H3K9me2 and depletion of H3K9ac and decreased gene expression has also been observed during abiotic stress [68]. In other studies it was shown that loss of CpG methylation in a *Methytransferase1* (*met1*) mutant resulted in the loss of H3K9 methylation [69, 70].

While the increased knowledge of DNA methylation patterns has been a major accomplishment in plant biology over recent years, an obvious next step is to ask which specific methylation sites or methylated regions are the key determinants of adaptation and stress memory, and then, how the differential methylation of these sites is regulated by stress signaling. Another key question is whether the sites of stress responsive DNA methylation changes correspond to key regulatory genes whose expression may in turn coordinate downstream stress responses. Also, while it is relatively well known that DNA methylation plays a crucial role in plant development, for example seed, embryo, and gametophyte development [17, 56], there is less information on the physiological consequences of DNA methylation for plant growth under stress. This is particularly true for drought stress. A limiting factor here is that mutants of the core enzymes directly mediating DNA methylation and demethylation have pleiotropic morphological defects [56] which complicates stress physiology analyses. Also, cross talk between DNA methylation and histone modification is still not much investigated under abiotic stress. Another key observation, which is perhaps not surprising given the technical challenges and newness of this field, is that the genome scale methylation analysis have not yet incorporated the

use of stress signaling mutants to test which stress sensing and signaling pathways may regulate methylation changes. It is also interesting to note that direct regulatory interactions between stress signaling proteins and components of the methylation machinery have yet to be observed at the protein level.

3 Alternative Splicing

By selectively joining different exons and generating different transcripts from a single gene, alternative splicing pathways provide a key mechanism for generating proteome diversity and functional complexity, as well as regulating gene expression. In contrast to transcriptional control, alternative splicing changes the structure of transcripts and can influence almost all aspects of protein function, such as binding properties, enzymatic activity, intracellular localization, posttranslational modification, or protein stability [71–73]. Four main types of alternative splicing are known: exon skipping, alternative 5′- and 3′-splice sites, and intron retention. Alternative splicing events do not randomly affect mRNA of all genes; rather they seem to occur preferentially to mRNAs of certain classes of genes commonly involved in signal transduction, or encoding enzymes, receptors and transcription factors [74, 75]. Several genome scale studies have profiled mRNA splicing patterns concluded that alternative splicing substantially alters protein function and localization during drought [72, 73, 76] or during heat and light responses in Physcomitrella patens [77, 78].

One of the best studied examples of stress-related alternative splicing to date involves the RNA-binding motif (RBM)-containing protein, RBM25 and its effect on splicing of the Clade A PP2C HAB1 which functions in ABA signaling [79, 80]. It was reported that *HAB1* has two transcripts, *HAB1.1* which encodes the full length active phosphatase and *HAB1.2* in which the third intron is retained. Retention of the third intron of HAB1 introduces a premature stop codon and leads to production of truncated HAB1 protein lacking the C-terminal 105 amino acids. This results in truncation of the catalytic domain and loss of phosphatase activity. The ratio of *HAB1.2/HAB1.1* transcripts was relatively low in wild type plants under normal growth conditions but increased after ABA treatment. In contrast, *HAB1.2/HAB1.1* ratio was increased dramatically in *rbm25* mutant under control conditions or after ABA treatment. The full length HAB1 acts as a repressor of ABA signaling by dephosphorylating SnRK2 kinases. The catalytically inactive HAB1 encoded by *HAB1.2* can still interact with SnRK2.6 but lacks the ability to repress SnRK2.6 activity [79]. Thus, HAB1.2 functions as a positive regulator of ABA signaling (in other words a dominant negative, negative regulator). By regulating the *HAB1.1–HAB1.2* ratio, RBM25 can affect ABA sensitivity.

Zhan et al. [80] showed that *RBM25* expression was upregulated by ABA treatment but the phosphorylation of RBM25 is downregulated by ABA. Reduced phosphorylation of RBM25 might be important for its activity as splicing factor or its protein stability under ABA treatment. However, the protein kinase(s) and phosphatase(s) responsible for controlling RBM25 phosphorylation status remain to be determined [79, 80]. Another connection of alternative splicing to ABA signaling was shown for ABI3 and control of its splicing by the splicing factor SUA, another RBM-domain protein [81].

These examples highlight the key roles of splicing factors and how their regulation can have broad implications for ABA and abiotic stress responses. Phosphoproteomic studies of wild type and *snrk2* mutants under control, ABA or dehydration stress treatments found many changes in splicing factor phosphopeptide abundance and identified several splicing factors as putative targets of SnRK2 phosphorylation [82, 83]. The RNA splicing factor Binding to Tomato mosaic virus RNA 1 Long (BTR1L) was confirmed to be a SnRK2.6 substrate by in vitro phosphorylation assay [83]. In our laboratory, quantitative phosphoproteomic analysis also found low water potential-induced changes in phosphopeptide abundance for splicing factors (G.B. Bhaskara, T.T. Nguyen, and P.E. Verslues, unpublished data). In most cases, the consequences of these protein phosphorylation changes in terms of specific alternative splicing events remain unknown. Also unknown is which protein phosphatases, and which kinases other than SnRK2s, may be direct regulators of splicing factor phosphorylation and function under abiotic stress. Interestingly, the genes encoding splicing factors themselves undergo extensive alternative splicing. For example, the relative levels of the splice variant encoding full-length SR30 protein, which has also been shown to affect splicing of its own pre-mRNA, have been recently reported to increase markedly under heat, light, and salt stress [72]. Whether or not alternative splicing of SR30 is related to splicing factor phosphorylation, or other stress signaling mechanisms, is an interesting question for future investigation.

In addition to the RBM proteins mentioned above, other types of RNA binding proteins (RBPs) have been associated with abiotic stress phenotypes [84–92]. In one example, the Arabidopsis *Supersensitive to ABA and Drought1* (*SAD1*) encodes Like-Sm 5 (LSm5) protein, a component of the U6 small nuclear ribonucleoprotein (snRNP) core [93]. Reduced levels of U6 snRNA and accumulation of unspliced pre-mRNAs have been observed in the *sad1/lsm5* mutant, suggesting that it has a role in pre-mRNA splicing by contributing to U6 stability [94, 95]. Whether or not the drought and ABA phenotypes of *sad1* represent a direct role of LSm5 in regulating stress-related transcripts or a pleiotropic effect of general RNA splicing disfunction is unclear. In another example,

Ambrosone et al. [86] found that an Arginine-Glycine-Glycine box protein encoded by *AtRGGA* was a stress-induced RNA binding protein localized in the cytoplasm and cytoplasmic perinuclear region. Mutation or overexpression of *AtRGGA* affected several abiotic stress phenotypes as well as ABA sensitivity and led to altered gene expression pattern during salt stress. As AtRGGA is localized in the cytoplasm, it is not involved in nuclear RNA processing. Rather, the authors hypothesized that AtRGGA could affect mRNA stability or translation efficiency [86]. Most of the RNA-binding proteins in the studies mentioned here were analyzed for stress phenotypes based on their stress-induced gene expression. Thus, in most cases there is a similar lack of mechanistic information of how their RNA binding activity leads to stress-related phenotypes.

4 RNA CAP Binding Proteins, Decapping, and mRNA Stability

The Cap binding complex binds to the 5′ RNA cap which is added cotranscriptionally to transcripts generated by RNA polymerase II. The Cap binding complex is important for splicing and RNA stability and there is evidence that components of the Cap binding complex can affect ABA sensitivity and abiotic stress responses. *ABA Hypersensitive 1* (*ABH1*) was identified in a forward genetic screen and encodes CAP-Binding protein 80 (CPB80) [96]. Subsequent studies found that ABH1/CPB80 mutants affected several aspects of ABA response, including ABA responses in guard cells [97] and mutants of CPB80 as well as CPB20 (the other component of the dimeric CAP-binding complex) were reported to be hypersensitive to salt stress [98]. Interestingly, *cpb80* and *cpb20* mutants exhibited alternative splicing of several stress-related genes including the gene encoding Δ^1-pyrroline-5-carboxylate synthetase 1 (P5CS1), a key enzyme in stress-induced proline accumulation [98].

After capping, polyadenylation and exit of mature mRNAs from the nucleus, there are still several steps of RNA metabolism which can impact abiotic stress responses. A key role of RNA metabolism in stress responses, and particularly in the ability of recover from stress and “reset” to a maximal growth state, has been proposed and reviewed by Crisp et al. [13]. The stability of cytosolic mRNAs is one of the key determinants of transcriptome composition and protein expression. Thus, rapid versus slow removal of stress-induced mRNAs has obvious implications for how long and how extensively plants maintain a stress response poise even after the stress is alleviated. In particular, removal of the 5′ mRNA cap is an important step in posttranscriptional regulation, as it represents movement away from active translation and functions as the rate-limiting prerequisite for exoribonuclease

degradation [99]. A recent study demonstrated that mutants of the LSM1–7 complex, which functions in mRNA decapping, were hypersensitive to several abiotic stress treatments including low water potential salt and cold [100]. The LSM1–7 complex targeted stress-responsive transcripts for degradation. Among these was the transcript encoding *9*-cis-*epoxycarotenoid dioxygenase 3* (*NCED3*), an enzyme required for stress-induced ABA accumulation [7]. Under certain conditions, LSM1–7 complex mutants had altered ABA accumulation [100], thus showing a direct effect of LSM1–7 mediated decapping on core stress response and signaling. How specific transcripts are selected for decapping and degradation under stress is not understood, although Park et al. [101] found that both 5′ and 3′ sequences were important for control of transcript degradation during stress. A connection of mRNA decapping to stress response was also shown by Xu and Chua [102] who found that dehydration stress activation of MPK6 led to phosphorylation of the decapping enzyme DECAPPING 1 (DCP1). Analysis of DCP1 phosphomimetic mutants suggests that phosphorylation enhances 5′ mRNA decapping. Impairing this process caused stress hypersensitivity and misregulation of dehydration-responsive transcripts [102].

Other studies have found that several proteins involved in cytosolic mRNA regulation through the 5′–3′ exonuclease degradation pathway experienced large changes in phosphorylation following a 5-min hyperosmotic challenge [103]. These proteins included members of the 5′ decapping complex: VARICOSE (VCS), VCS-Related protein (VCR), and the decapping enzyme DCP2. VCS was phosphorylated at multiple Ser residues, with some sites increasing and some decreasing their levels of phosphorylation in response to mannitol, reflecting a complex mechanism of phosphoregulation [103]. VCS functions in decapping and miRNA-mediated translational repression [104]. The stress phenotypes of other mutants related to RNA stability and decapping as well as how stress sensing and signaling control the selection of specific transcripts for decapping and degradation during stress remains unknown.

5 Conclusion

There is ample evidence that epigenetic mechanisms as well as alternative splicing and mRNA decapping and stability can all impact abiotic stress-related phenotypes. In some ways this is a case of too much of good thing. As more data accumulates and shows that mutation or overexpression of many epigenetic or RNA processing proteins alters abiotic stress phenotypes, it raises the possibility that some of the observed phenotypes are pleiotropic effects of a dysfunctional transcriptome and do not necessarily indicate

whether the mutated gene is directly involved in stress resistance. This concern is especially relevant where a mutant or transgenic line has a loss of fitness leading to inhibited growth or altered development even in the absence of stress treatment. Likewise differences in ABA sensitivity can also be the result of such indirect effects. The severity, timing, and type of stress phenotype assayed (survival versus growth) can all have a big impact the type of genes found to have stress phenotypes [3, 105, 106]. Conducting carefully controlled stress experiments and showing a positive stress phenotype of increased growth or tolerance to nonlethal stress treatment is important but does not totally alleviate the concern about indirect effects.

How then to identify the epigenetic and RNA metabolism factors that are directly and actively involved in abiotic stress resistance? In addition to careful and detailed phenotypic analyses, the best way is to mechanistically show how specific epigenetic and RNA splicing or metabolism proteins interact with and modify, or are modified by, stress-related signaling proteins or functionally important stress genes (for example *NCED3* and *P5CS1* mentioned above). In this regard, the association of Clade A PP2Cs with SWI3B on the promoters of stress responsive genes [27] as well as the effect of LSM1–7 on NCED3 decapping and degradation [100] and effect of CPB80/CPB20 on *P5CS1* splicing [98] are all good examples. In these cases chromatin remodeling and mRNA metabolism can be directly related to important and well characterized stress proteins. Likewise, the control of HAB1 splicing by RDM25 [79, 80] shows direct regulation of an important ABA signaling gene. In the case of RDM25 and HAB1, adding more context around the current results will be of interest in the future. For example, what other splicing events are regulated by RDM25 and do these also affect stress-related genes? How is the activity, particularly the phosphorylation, of RDM25 regulated and is this connected to stress signaling?

While these are good examples, overall there is limited information on how environmental signals are communicated to the epigenetic, splicing, or RNA metabolism machinery. Does this involve the core ABA signaling pathway or are other stress signaling mechanisms involved? Some of the most important results so far have come from studies of posttranslational protein modifications, particularly phosphorylation, and protein interactions. These techniques, along with genetic screens focused on specific phenotypes or gene regulation mechanisms, should reveal answers to some of these key questions. Ultimately, determining the epigenetic, alternative splicing, and RNA metabolism mechanisms most directly connected to stress sensing and signaling is important because these mechanisms will be most promising in efforts to improve plant productivity under abiotic stress while maintaining maximal growth and yield potential when environmental

conditions are favorable. This is the shared goal of many plant stress researchers no matter which level of organization, molecular, cellular, or physiological, we may focus on.

Acknowledgments

Research in the Verslues laboratory is supported by Academia Sinica and the Taiwan Ministry of Science and Technology. M.M.W. and G.L.C. have also received support from the Taiwan International Graduate Program.

References

1. Feng W, Lindner H, Robbins NE, Dinneny JR (2016) Growing out of stress: the role of cell- and organ-scale growth control in plant water-stress responses. Plant Cell 28:1769–1782
2. Skirycz A, Inze D (2010) More from less: plant growth under limited water. Curr Opin Biotechnol 21:197–203
3. Verslues PE, Agarwal M, Katiyar-Agarwal S, Zhu J, Zhu JK (2006) Methods and concepts in quantifying resistance to drought, salt and freezing, abiotic stresses that affect plant water status. Plant J 45:523–539
4. Haswell ES, Verslues PE (2015) The ongoing search for the molecular basis of plant osmosensing. J Gen Physiol 145:389–394
5. Cutler SR, Rodriguez PL, Finkelstein RR, Abrams SR (2010) Abscisic acid: emergence of a core signaling network. Ann Rev Plant Biol 61:651–679
6. Raghavendra AS, Gonugunta VK, Christmann A, Grill E (2010) ABA perception and signalling. Trends Plant Sci 15:395–401
7. Verslues PE (2016) ABA and cytokinins: challenge and opportunity for plant stress research. Plant Mol Biol 91:629–640
8. Nakashima K, Yamaguchi-Shinozaki K, Shinozaki K (2014) The transcriptional regulatory network in the drought response and its crosstalk in abiotic stress responses including drought, cold, and heat. In: Jain M, Garg R, Varshney RK (eds) Abiotic stress: molecular genetics and genomics. Frontiers E-Books, Lausanne, pp 25–31
9. Yoshida T, Mogami J, Yamaguchi-Shinozaki K (2014) ABA-dependent and ABA-independent signaling in response to osmotic stress in plants. Curr Opin Plant Biol 21:133–139
10. Stockinger EJ, Gilmour SJ, Thomashow MF (1997) *Arabidopsis thaliana* CBF1 encodes an AP2 domain-containing transcriptional activator that binds to the C-repeat/DRE, a cis-acting DNA regulatory element that stimulates transcription in response to low temperature and water deficit. Proc Natl Acad Sci U S A 94:1035–1040
11. Shinozaki K, Yamaguchi-Shinozaki K (2000) Molecular responses to dehydration and low temperature: differences and cross-talk between two stress signaling pathways. Curr Opin Plant Biol 3:217–223
12. Sharp RE, LeNoble ME (2002) ABA, ethylene and the control of shoot and root growth under water stress. J Exp Bot 53:33–37
13. Crisp PA, Ganguly D, Eichten SR, Borevitz JO, Pogson BJ (2016) Reconsidering plant memory: Intersections between stress recovery, RNA turnover, and epigenetics. Sci Adv 2:e1501340
14. Virlouvet L, Ding Y, Fujii H, Avramova Z, Fromm M (2014) ABA signaling is necessary but not sufficient for RD29B transcriptional memory during successive dehydration stresses in *Arabidopsis thaliana*. Plant J 79: 150–161
15. Ding Y, Fromm M, Avramova Z (2012) Multiple exposures to drought 'train' transcriptional responses in Arabidopsis. Nat Commun 3:740
16. Shen Y, Issakidis-Bourguet E, Zhou D-X (2016) Perspectives on the interactions between metabolism, redox, and epigenetics in plants. J Exp Bot 67:5291–5300
17. Van Oosten MJ, Bressan RA, Zhu J-K, Bohnert HJ, Chinnusamy V (2014) The role of the epigenome in gene expression control and the epimark changes in response to the environment. Crit Rev Plant Sci 33:64–87
18. Kinoshita T, Seki M (2014) Epigenetic memory for stress response and adaptation in plants. Plant Cell Physiol 55:1859–1863

19. Liu X, Luo M, Yang S, Wu K (2015) Role of epigenetic modifications in plant responses to environmental stresses. In: Pontes O, Jin H (eds) Nuclear functions in plant transcription, signaling and development. New York, NY, Springer New York, pp 81–92
20. Colaneri AC, Jones AM (2013) Genome-wide quantitative identification of DNA differentially methylated sites in Arabidopsis seedlings growing at different water potential. PLoS One 8:e59878
21. Zong W, Zhong X, You J, Xiong L (2013) Genome-wide profiling of histone H3K4-trimethylation and gene expression in rice under drought stress. Plant Mol Biol 81:175–188
22. Wibowo A, Becker C, Marconi G, Durr J, Price J, Hagmann J, Papareddy R, Putra H, Kageyama J, Becker J et al (2016) Hyperosmotic stress memory in Arabidopsis is mediated by distinct epigenetically labile sites in the genome and is restricted in the male germline by DNA glycosylase activity. *eLife* 5:e13546
23. Chwialkowska K, Nowakowska U, Mroziewicz A, Szarejko I, Kwasniewski M (2016) Water-deficiency conditions differently modulate the methylome of roots and leaves in barley (*Hordeum vulgare* L.) J Exp Bot 67:1109–1121
24. Sani E, Herzyk P, Perrella G, Colot V, Amtmann A (2013) Hyperosmotic priming of Arabidopsis seedlings establishes a long-term somatic memory accompanied by specific changes of the epigenome. Genome Biol 14:R59
25. Filichkin S, Priest HD, Megraw M, Mockler TC (2015) Alternative splicing in plants: directing traffic at the crossroads of adaptation and environmental stress. Curr Opin Plant Biol 24:125–135
26. Kuhn JM, Schroeder JI (2003) Impacts of altered RNA metabolism on abscisic acid signaling. Curr Opin Plant Biol 6:463–469
27. Saez A, Rodrigues A, Santiago J, Rubio S, Rodriguez PL (2008) HAB1–SWI3B interaction reveals a link between abscisic acid signaling and putative SWI/SNF chromatin-remodeling complexes in Arabidopsis. Plant Cell 20:2972–2988
28. Hurtado L, Farrona S, Reyes JC (2006) The putative SWI/SNF complex subunit BRAHMA activates flower homeotic genes in *Arabidopsis thaliana*. Plant Mol Biol 62:291–304
29. Wagner D, Meyerowitz EM (2002) SPLAYED, a novel SWI/SNF ATPase homolog, controls reproductive development in Arabidopsis. Curr Biol 12:85–94
30. Brzeski J, Podstolski W, Olczak K, Jerzmanowski A (1999) Identification and analysis of the *Arabidopsis thaliana* BSH gene, a member of the SNF5 gene family. Nucleic Acids Res 27:2393–2399
31. Sarnowska E, Gratkowska DM, Sacharowski SP, Cwiek P, Tohge T, Fernie AR, Siedlecki JA, Koncz C, Sarnowski TJ (2016) The role of SWI/SNF chromatin remodeling complexes in hormone crosstalk. Trends Plant Sci 21:594–608
32. Sarnowski TJ, Ríos G, Jásik J, Świeżewski S, Kaczanowski S, Li Y, Kwiatkowska A, Pawlikowska K, Koźbiał M, Koźbiał P (2005) SWI3 subunits of putative SWI/SNF chromatin-remodeling complexes play distinct roles during Arabidopsis development. Plant Cell 17:2454–2472
33. Han S-K, Sang Y, Rodrigues A, Wu M-F, Rodriguez PL, Wagner D (2012) The SWI2/SNF2 chromatin remodeling ATPase BRAHMA represses abscisic acid responses in the absence of the stress stimulus in Arabidopsis. Plant Cell 24:4892–4906
34. Peirats-Llobet M, Han SK, Gonzalez-Guzman M, Jeong CW, Rodriguez L, Belda-Palazon B, Wagner D, Rodriguez PL (2016) A direct link between abscisic acid sensing and the chromatin-remodeling ATPase BRAHMA via core ABA signaling pathway components. Mol Plant 9:136–147
35. Perruc E, Kinoshita N, Lopez-Molina L (2007) The role of chromatin-remodeling factor PKL in balancing osmotic stress responses during Arabidopsis seed germination. Plant J 52:927–936
36. Yuan L, Liu X, Luo M, Yang S, Wu K (2013) Involvement of histone modifications in plant abiotic stress responses. J Integr Plant Biol 55:892–901
37. Kim JM, Sasaki T, Ueda M, Sako K, Seki M (2015) Chromatin changes in response to drought, salinity, heat, and cold stresses in plants. Front Plant Sci 6:114
38. Han SK, Wagner D (2014) Role of chromatin in water stress responses in plants. J Exp Bot 65:2785–2799
39. Probst AV, Mittelsten Scheid O (2015) Stress-induced structural changes in plant chromatin. Curr Opin Plant Biol 27:8–16
40. Shahbazian MD, Grunstein M (2007) Functions of site-specific histone acetylation and deacetylation. Annu Rev Biochem 76:75–100
41. Lee KK, Workman JL (2007) Histone acetyltransferase complexes: one size doesn't fit all. Nat Rev Mol Cell Biol 8:284–295

42. Baker S, Grant P (2007) The SAGA continues: expanding the cellular role of a transcriptional co-activator complex. Oncogene 26:5329–5340
43. Hark AT, Vlachonasios KE, Pavangadkar KA, Rao S, Gordon H, Adamakis ID, Kaldis A, Thomashow MF, Triezenberg SJ (2009) Two Arabidopsis orthologs of the transcriptional coactivator ADA2 have distinct biological functions. Biochim Biophys Acta 1789:117–124
44. Kaldis A, Tsementzi D, Tanriverdi O, Vlachonasios KE (2011) *Arabidopsis thaliana* transcriptional co-activators ADA2b and SGF29a are implicated in salt stress responses. Planta 233:749–762
45. Mao YP, Pavangadkar KA, Thomashow MF, Triezenberg SJ (2006) Physical and functional interactions of Arabidopsis ADA2 transcriptional coactivator proteins with the acetyltransferase GCN5 and with the cold-induced transcription factor CBF1. Biochim Biophys Acta 1759:69–79
46. Stockinger EJ, Mao Y, Regier MK, Triezenberg SJ, Thomashow MF (2001) Transcriptional adaptor and histone acetyltransferase proteins in Arabidopsis and their interactions with CBF1, a transcriptional activator involved in cold-regulated gene expression. Nucleic Acid Res 29:1524–1533
47. Chen Z, Zhang H, Jablonowski D, Zhou X, Ren X, Hong X, Schaffrath R, Zhu JK, Gong Z (2006) Mutations in ABO1/ELO2, a subunit of holo-Elongator, increase abscisic acid sensitivity and drought tolerance in *Arabidopsis thaliana*. Mol Cell Biol 26:6902–6912
48. Versees W, De Groeve S, Van Lijsebettens M (2010) Elongator, a conserved multitasking complex? Mol Microbiol 76:1065–1069
49. Sridha S, Wu K (2006) Identification of AtHD2C as a novel regulator of abscisic acid responses in Arabidopsis. Plant J 46:124–133
50. Chen LT, Luo M, Wang YY, Wu K (2010) Involvement of Arabidopsis histone deacetylase HDA6 in ABA and salt stress response. J Exp Bot 61:3345–3353
51. Chen LT, Wu K (2010) Role of histone deacetylases HDA6 and HDA19 in ABA and abiotic stress response. Plant Signal Behav 5:1318–1320
52. Luo M, Wang YY, Liu X, Yang S, Lu Q, Cui Y, Wu K (2012) HD2C interacts with HDA6 and is involved in ABA and salt stress response in Arabidopsis. J Exp Bot 63:3297–3306
53. Zheng Y, Ding Y, Sun X, Xie S, Wang D, Liu X, Su L, Wei W, Pan L, Zhou D-X (2016) Histone deacetylase HDA9 negatively regulates salt and drought stress responsiveness in Arabidopsis. J Exp Bot 67:1703–1713
54. He X-J, Chen T, Zhu J-K (2011) Regulation and function of DNA methylation in plants and animals. Cell Res 21:442–465
55. Stroud H, Greenberg MV, Feng S, Bernatavichute YV, Jacobsen SE (2013) Comprehensive analysis of silencing mutants reveals complex regulation of the Arabidopsis methylome. Cell 152:352–364
56. Law JA, Jacobsen SE (2010) Establishing, maintaining and modifying DNA methylation patterns in plants and animals. Nat Rev Genet 11:204–220
57. Henderson IR, Jacobsen SE (2007) Epigenetic inheritance in plants. Nature 447:418–424
58. Matzke MA, Mosher RA (2014) RNA-directed DNA methylation: an epigenetic pathway of increasing complexity. Nat Rev Genet 15:394–408
59. Zhang H, Zhu J-K (2012) Seeing the forest for the trees: a wide perspective on RNA-directed DNA methylation. Genes Dev 26:1769–1773
60. Kovarik A, Koukalova B, Bezde M, Opatrn Z (1997) Hypermethylation of tobacco heterochromatic loci in response to osmotic stress. Theor Appl Genet 95:301–306
61. Labra M, Ghiani A, Citterio S, Sgorbati S, Sala F, Vannini C, Ruffini-Castiglione M, Bracale M (2002) Analysis of cytosine methylation pattern in response to water deficit in pea root tips. Plant Biol 4:694–699
62. Suji K, Joel AJ (2010) An epigenetic change in rice cultivars under water stress conditions. Electron J Plant Breed 1:1142–1143
63. Tan MP (2010) Analysis of DNA methylation of maize in response to osmotic and salt stress based on methylation-sensitive amplified polymorphism. Plant Physiol Biochem 48:21–26
64. Garg R, Chevala VN, Shankar R, Jain M (2015) Divergent DNA methylation patterns associated with gene expression in rice cultivars with contrasting drought and salinity stress response. Sci Rep 5:14992
65. Kawakatsu T, Huang SSC, Jupe F, Sasaki E, Schmitz RJ, Urich MA, Castanon R, Nery JR, Barragan C, He YP et al (2016) Epigenomic diversity in a global collection of *Arabidopsis thaliana* accessions. Cell 166:492–505
66. Kawakatsu T, Stuart T, Valdes M, Breakfield N, Schmitz RJ, Nery JR, Urich MA, Han XW, Lister R, Benfey PN et al (2016) Unique cell-type-specific patterns of DNA methylation in the root meristem. Nat Plant 2:16058

67. Song Y, Ji D, Li S, Wang P, Li Q, Xiang F (2012) The dynamic changes of DNA methylation and histone modifications of salt responsive transcription factor genes in soybean. PLoS One 7:e41274
68. Bilichak A, Ilnystkyy Y, Hollunder J, Kovalchuk I (2012) The progeny of *Arabidopsis thaliana* plants exposed to salt exhibit changes in DNA methylation, histone modifications and gene expression. PLoS One 7:e30515
69. Soppe WJ, Jasencakova Z, Houben A, Kakutani T, Meister A, Huang MS, Jacobsen SE, Schubert I, Fransz PF (2002) DNA methylation controls histone H3 lysine 9 methylation and heterochromatin assembly in Arabidopsis. EMBO J 21:6549–6559
70. Tariq M, Saze H, Probst AV, Lichota J, Habu Y, Paszkowski J (2003) Erasure of CpG methylation in Arabidopsis alters patterns of histone H3 methylation in heterochromatin. Proc Natl Acad Sci U S A 100:8823–8827
71. Duque P (2011) A role for SR proteins in plant stress responses. Plant Signal Behav 6:49–54
72. Filichkin SA, Priest HD, Givan SA, Shen R, Bryant DW, Fox SE, Wong WK, Mockler TC (2010) Genome-wide mapping of alternative splicing in *Arabidopsis thaliana*. Genome Res 20:45–58
73. Thatcher SR, Danilevskaya ON, Meng X, Beatty M, Zastrow-Hayes G, Harris C, Van Allen B, Habben J, Li B (2016) Genome-wide analysis of alternative splicing during development and drought stress in maize. Plant Physiol 170:586–599
74. Mazzucotelli E, Mastrangelo AM, Crosatti C, Guerra D, Stanca AM, Cattivelli L (2008) Abiotic stress response in plants: when post-transcriptional and post-translational regulations control transcription. Plant Sci 174:420–431
75. Raczynska KD, Stepien A, Kierzkowski D, Kalak M, Bajczyk M, McNicol J, Simpson CG, Szweykowska-Kulinska Z, Brown JWS, Jarmolowski A (2014) The SERRATE protein is involved in alternative splicing in *Arabidopsis thaliana*. Nucleic Acid Res 42:1224–1244
76. Remy E, Cabrito TR, Batista RA, Hussein MA, Teixeira MC, Athanasiadis A, Sa-Correia I, Duque P (2014) Intron retention in the 5'UTR of the novel ZIF2 transporter enhances translation to promote zinc tolerance in Arabidopsis. PLoS Genet 10:e1004375
77. Chang CY, Lin WD, Tu SL (2014) Genome-wide analysis of heat-sensitive alternative splicing in *Physcomitrella patens*. Plant Physiol 165:826–840
78. Wu HP, Su YS, Chen HC, Chen YR, Wu CC, Lin WD, Tu SL (2014) Genome-wide analysis of light-regulated alternative splicing mediated by photoreceptors in *Physcomitrella patens*. Genome Biol 15:R10
79. Wang Z, Ji H, Yuan B, Wang S, Su C, Yao B, Zhao H, Li X (2015) ABA signalling is fine-tuned by antagonistic HAB1 variants. Nat Commun 6:8138
80. Zhan X, Qian B, Cao F, Wu W, Yang L, Guan Q, Gu X, Wang P, Okusolubo TA, Dunn SL et al (2015) An Arabidopsis PWI and RRM motif-containing protein is critical for pre-mRNA splicing and ABA responses. Nat Commun 6:8139
81. Sugliani M, Brambilla V, Clerkx EJ, Koornneef M, Soppe WJ (2010) The conserved splicing factor SUA controls alternative splicing of the developmental regulator ABI3 in Arabidopsis. Plant Cell 22:1936–1946
82. Umezawa T, Sugiyama N, Takahashi F, Anderson JC, Ishihama Y, Peck SC, Shinozaki K (2013) Genetics and phosphoproteomics reveal a protein phosphorylation network in the Abscisic Acid signaling pathway in *Arabidopsis thaliana*. Sci Signal 6:270
83. Wang PC, Xue L, Batelli G, Lee S, Hou YJ, Van Oosten MJ, Zhang HM, Tao WA, Zhu JK (2013) Quantitative phosphoproteomics identifies SnRK2 protein kinase substrates and reveals the effectors of abscisic acid action. Proc Natl Acad Sci U S A 110:11205–11210
84. Ortega-Amaro MA, Rodriguez-Hernandez AA, Rodriguez-Kessler M, Hernandez-Lucero E, Rosales-Mendoza S, Ibanez-Salazar A, Delgado-Sanchez P, Jimenez-Bremont JF (2015) Overexpression of AtGRDP2, a novel glycine-rich domain protein, accelerates plant growth and improves stress tolerance. Front Plant Sci 5:782
85. Rai AN, Tamirisa S, Rao KV, Kumar V, Suprasanna P (2016) Brassica RNA binding protein ERD4 is involved in conferring salt, drought tolerance and enhancing plant growth in Arabidopsis. Plant Mol Biol 90:375–387
86. Ambrosone A, Batelli G, Nurcato R, Aurilia V, Punzo P, Bangarusamy DK, Ruberti I, Sassi M, Leone A, Costa A et al (2015) The Arabidopsis RNA-binding protein AtRGGA regulates tolerance to salt and drought stress. Plant Physiol 168:292–306
87. Dhandapani G, Kanakachari M, Padmalatha KV, Phanindra MLV, Singh VK, Raghavendrarao S, Jayabalan N, Prabha AL,

Kumar PA (2015) A gene encoding cold-circadian rhythm-RNA binding-like protein (CCR-Like) from upland Cotton (*Gossypium hirsutum* L.) confers tolerance to abiotic stresses in transgenic tobacco. Plant Mol Biol Rep 33:22–42

88. Du J-L, Zhang S-W, Huang H-W, Cai T, Li L, Chen S, He X-J (2015) The splicing factor PRP31 is involved in transcriptional gene silencing and stress response in Arabidopsis. Mol Plant 8:1053–1068
89. Huh SU, Paek KH (2014) APUM5, encoding a Pumilio RNA binding protein, negatively regulates abiotic stress responsive gene expression. BMC Plant Biol 14:75
90. Cao S, Jiang L, Song S, Jing R, Xu G (2006) AtGRP7 is involved in the regulation of abscisic acid and stress responses in Arabidopsis. Cell Mol Biol Lett 11:526–535
91. Kim JY, Park SJ, Jang B, Jung CH, Ahn SJ, Goh CH, Cho K, Han O, Kang H (2007) Functional characterization of a glycine-rich RNA-binding protein 2 in *Arabidopsis thaliana* under abiotic stress conditions. Plant J 50:439–451
92. Kwak KJ, Kim YO, Kang H (2005) Characterization of transgenic Arabidopsis plants overexpressing GR-RBP4 under high salinity, dehydration, or cold stress. J Exp Bot 56:3007–3016
93. Xiong L, Gong Z, Rock CD, Subramanian S, Guo Y, Xu W, Galbraith D, Zhu JK (2001) Modulation of abscisic acid signal transduction and biosynthesis by an Sm-like protein in Arabidopsis. Dev Cell 1:771–781
94. Perea-Resa C, Hernandez-Verdeja T, Lopez-Cobollo R, del Mar Castellano M, Salinas J (2012) LSM proteins provide accurate splicing and decay of selected transcripts to ensure normal Arabidopsis development. Plant Cell 24:4930–4947
95. Golisz A, Sikorski PJ, Kruszka K, Kufel J (2013) *Arabidopsis thaliana* LSM proteins function in mRNA splicing and degradation. Nucleic Acid Res 41:6232–6249
96. Hugouvieux V, Kwak JM, Schroeder JI (2001) An mRNA cap binding protein, ABH1, modulates early abscisic acid signal transduction in Arabidopsis. Cell 106:477–487
97. Hugouvieux V, Murata Y, Young JJ, Kwak JM, Mackesy DZ, Schroeder JI (2002) Localization, ion channel regulation, and genetic interactions during abscisic acid signaling of the nuclear mRNA cap-binding protein, ABH1. Plant Physiol 130:1276–1287
98. Kong XX, Ma L, Yang LM, Chen Q, Xiang N, Yang YP, Hu XY (2014) Quantitative proteomics analysis reveals that the nuclear cap-binding complex proteins Arabidopsis CBP20 and CBP80 modulate the salt stress response. J Proteome Res 13:2495–2510
99. Jonas S, Izaurralde E (2013) The role of disordered protein regions in the assembly of decapping complexes and RNP granules. Genes Dev 27:2628–2641
100. Perea-Resa C, Carrasco-Lopez C, Catala R, Tureckova V, Novak O, Zhang WP, Sieburth L, Jimenez-Gomez JM, Salinas J (2016) The LSM1-7 complex differentially regulates Arabidopsis tolerance to abiotic stress conditions by promoting selective mRNA decapping. Plant Cell 28:505–520
101. Park SH, Chung PJ, Juntawong P, Bailey-Serres J, Kim YS, Jung H, Bang SW, Kim YK, Do Choi Y, Kim JK (2012) Posttranscriptional control of photosynthetic mRNA decay under stress conditions requires 3′ and 5′ untranslated regions and correlates with differential polysome association in rice. Plant Physiol 159:1111–1124
102. Xu J, Chua NH (2012) Dehydration stress activates Arabidopsis MPK6 to signal DCP1 phosphorylation. EMBO J 31:1975–1984
103. Stecker KE, Minkoff BB, Sussman MR (2014) Phosphoproteomic analyses reveal early signaling events in the osmotic stress response. Plant Physiol 165:1171–1187
104. Brodersen P, Sakvarelidze-Achard L, Bruun-Rasmussen M, Dunoyer P, Yamamoto YY, Sieburth L, Voinnet O (2008) Widespread translational inhibition by plant miRNAs and siRNAs. Science 320:1185–1190
105. Skirycz A, Vandenbroucke K, Clauw P, Maleux K, De Meyer B, Dhondt S, Pucci A, Gonzalez N, Hoeberichts F, Tognetti VB et al (2011) Survival and growth of Arabidopsis plants given limited water are not equal. Nat Biotechnol 29:212–214
106. Verslues PE (2016) Time to grow: factors that control plant growth during mild to moderate drought stress. Plant Cell Environ 40(2):177–179. doi:10.1111/pce.12827

Chapter 2

The Fundamental Role of Reactive Oxygen Species in Plant Stress Response

Michael Liebthal and Karl-Josef Dietz

Abstract

Chemical, physical, and biotic factors continuously vary in the natural environment. Such parameters are considered as stressors if the magnitude of their change exceeds the current acclimation norm of the plant. Activation of genetic programs allows for conditional expansion of the acclimation norm and depends on specific sensing mechanisms, intracellular communication, and regulation. The redox and reactive oxygen species (ROS) network plays a fundamental role in directing the acclimation response. These highly reactive compounds like H_2O_2 are generated and scavenged under normal conditions and participate in realizing a basal acclimation level. Spatial and temporal changes in ROS levels and redox state provide valuable information for regulating epigenetic processes, transcription factors (TF), translation, protein turnover, metabolic pathways, and cross-feed, e.g., into hormone-, NO-, or Ca^{2+}-dependent signaling pathways. At elevated ROS levels uncontrolled oxidation reactions compromise cell functions, impair fitness and yield, and in extreme cases may cause plant death.

Key words Reactive oxygen species, Abiotic stress, Redox signaling, Redox regulation

1 Introduction

Plants are sessile organisms that have to cope with changing environmental conditions on time scales of minutes to years. On the one hand, plants exploit natural resources such as light and CO_2 in photosynthesis, mine minerals and tap water in the soil, and beneficially interact with bacteria and fungi. On the other hand, nutrient and water deficiencies, salinity, extreme temperatures, pathogens, and herbivores negatively interfere with plant fitness and yield. Regulatory circuitries allow for sensing the changing environmental parameters and control acclimation responses. If the intensity of such negative parameters increases, two effects reduce the fitness of plants: (1) The costs of activating and maintaining the acclimation and defense mechanisms compete for resource investments thereby decreasing growth, and (2) cumulative damage disturbs metabolism. Ultimately such disturbances

Ramanjulu Sunkar (ed.), *Plant Stress Tolerance: Methods and Protocols*, Methods in Molecular Biology, vol. 1631,
DOI 10.1007/978-1-4939-7136-7_2,

may cause cessation of growth and death. This stress concept is quite prevalent and has been extensively investigated in the last few decades, particularly with respect to the stress-specific signaling pathways, the involvement of redox- and ROS-related cues and the mechanisms mediating sensitivity and tolerance [1].

Most laboratory studies explore the effect of single stressors, while in nature organisms often encounter stress combination, e.g., high light, drought, and high temperature; or flood and salinity [2]. Abiotic stress can hardly be avoided and, from a global point of view, it impacts on plants stronger than biotic factors [3]. It is by now generally accepted that redox and ROS signaling decisively participate in perceiving stressful conditions, in regulating the acclimation response and in inducing damage progression and cell death. The qualitative and quantitative determination of relevant parameters often poses a challenge to the experimentalist. In the following the reader is introduced to the general stress concept and exemplarily to methods which have been used to assess the redox and ROS state of plant tissues under stress.

1.1 Generation of Reactive Oxygen Species

ROS are produced in discrete compartments of the plant cell.

1.1.1 Superoxide Anion Generation

In chloroplasts energy conversion is linked to the light-driven photosynthetic electron transport (PET). In mitochondria, the respiratory electron transport (RET) essentially converts reducing power generated from substrate oxidation to ATP. Within the transport chains electron carriers catalyze redox reactions and proton transfer to establish the electrochemical proton gradient for ATP synthesis. Both PET and RET can adopt a highly reduced state if energy input (light or NADH) is high and availability of intermediate carriers (plastoquinone, ubiquinone, cytochrome c) or terminal acceptors limited (NADP, O_2). Under such conditions superoxide anion ($^{\bullet}O_2^-$) can be generated at photosystem I, mitochondrial complexes I and III and the quinones [4–6]. Furthermore, plasma membrane-localized NADPH oxidase (respiratory burst oxidase homologue: RBOH) releases $^{\bullet}O_2^-$ into the apoplast which in particular participates in local and systemic signaling, plant immunity and stress responses [7, 8]. It should be noted that $^{\bullet}O_2^-$ can react with nitric oxide to produce peroxinitrite ($ONOO^-$) a highly reactive nitrogen species that cause protein nitration.

1.1.2 Singlet Oxygen

Photosensitizers such as excited chlorophylls in PS II are able to convert oxygen into its energized singlet state ($^1O_2$) being a highly reactive ROS that may damage the photosynthetic machinery. $^1O_2$-overproducing mutants revealed signaling functions in combination with oxylipins like 12-oxo-phytodienoic acid (OPDA) for stress acclimation and cell death [9].

1.1.3 Hydrogen Peroxide

Superoxide dismutase converts $^{\bullet}O_2^-$ to H_2O_2, which is a less reactive since more stable and thus more abundant ROS. In peroxisomes H_2O_2 is produced as side product of oxidase reactions such as photorespiratory glycolate oxidase but also for example xanthine oxidase. At ambient CO_2 and O_2 concentrations, photorespiratory H_2O_2 is generated in stoichiometric amounts of 30–40% relative to CO_2 fixation rate. H_2O_2 is decomposed by several antioxidant systems, most prominently catalase in peroxisomes, type III peroxidases in the apoplast, and thiol peroxidases and ascorbate peroxidases in most other compartments including cytosol, chloroplast, and mitochondrion. In addition, H_2O_2 functions as an important cellular messenger in context of regular and stress signaling [10, 11].

1.1.4 Hydroxyl Radical

Some authors considered H_2O_2 as potentially being more toxic than based on its reaction constants with proteins and other cell constituents. Generally accepted is the ability of H_2O_2 to react with $^{\bullet}O_2^-$, nitric oxide, some transition metals but also antioxidants such as ascorbate to produce $^{\bullet}OH$ (Eqs. 1–4) [12, 13].

$$H_2O_2 + {}^{\cdot}O_2^- \rightarrow {}^{\cdot}OH + OH^- + O_2. \quad (1)$$

$$H_2O_2 + NO \rightarrow {}^{\cdot}OH + HNO_2. \quad (2)$$

$$H_2O_2 + Fe^{2+} \rightarrow {}^{\cdot}OH + Fe^{3+} + OH^-. \quad (3)$$

$$H_2O_2 + Cu^+ \ \text{complex} + H^+ \rightarrow {}^{\cdot}OH + Cu^{2+} \ \text{complex} + H_2O. \quad (4)$$

The Fenton reaction where H_2O_2 is reduced by redox active metal ions such as Fe^{2+} and Cu^+, thereby generating $^{\bullet}OH$, also occurs in metal-containing protein complexes [14]. $^{\bullet}OH$ immediately reacts with proteins, nucleic acids, and lipids. Due to the high reactivity of $^{\bullet}OH$ with multiple cell components efficient detoxification is not possible, instead it can be quenched in part by high concentrations of low molecular mass antioxidants such as proline, which often accumulate under stress [15]. $^{\bullet}O_2^-$, H_2O_2 and $^{\bullet}OH$ exhibit distinct reactivity toward certain amino acid residues in proteins, lipids, carotenoids, and nucleic acids. Lipid peroxidation can initiate radical chain reactions, which accelerate lipid oxidation. Protein oxidation may inhibit protein function due to fragmentation, modification of functional amino acid groups, or protein cross-linking [16].

1.2 Antagonists of ROS Accumulation

The balance between mechanisms to suppress ROS generation and efficient detoxification establishes low resting ROS concentrations in cells under normal growth conditions. Under such conditions, the thiol redox potential in the cytosol and stroma as measured by redox-sensitized green fluorescent protein (roGFP) coupled to glutaredoxins (Grx) is rather negative [17]. Inhibition of metabolism often leads to decelerated consumption of reducing power

and ATP. Consequently ADP is unavailable for mitochondrial and chloroplast ATP synthase and $NADP^+$ is short as electron acceptor of photosystem I. Electron carriers of PET and RET get overreduced and the rate of electron transfer to O_2 increases. Thus, increasing stress intensity usually coincides with ROS accumulation and causes deviations from cell redox homeostasis. ROS detoxification takes place either by direct enzymatic reaction or by reductants that need to be regenerated.

The tripeptide glutathione (y-Glu-Cys-Gly, GSH) is present at millimolar concentrations in plasmatic compartments of the plant cells and functions as thiol buffer, electron donor, substrate for conjugation and phytochelatin synthesis, and by S-glutathionylation as regulator of proteins [18]. Redox regulation of protein functions to a major extent depends on cysteine thiols, which can undergo multiple posttranslational modifications, namely disulfide formation, sulfenylation, sulfinylation, sulfonylation, S-nitrosylation, S-acylation, and S-glutathionylation. Such modifications have strong impact on protein function, but may also trigger redox-linked signaling [19]. Glutathione stabilizes the cellular thiol redox state. Oxidized glutathione GSSG is regenerated by glutathione reductase (GR) using NADPH as electron donor [20]. GSH serves as substrate in synthesis of phytochelatins, which participate in binding and transport of some heavy metal and metalloid ions, e.g., cadmium and arsenic [21, 22]. Hydrophobic antioxidants like tocopherols and carotenoids are localized in the thylakoid membrane and other membranes and quench $^1O_2$ to protect lipid from peroxidation and to suppress radical chain reactions [23, 24].

Ascorbate is another important component of the plant redox system. In the Foyer-Halliwell–Asada cycle, ascorbate serves as reductant of H_2O_2 by ascorbate peroxidase (APX) [25, 26]. H_2O_2 originates from spontaneous breakdown or superoxide dismutase (SOD)-catalyzed conversion of $^\bullet O_2^-$ [27]. The Foyer-Halliwell–Asada cycle functions in many subcellular compartments and has a particularly important role in chloroplasts. Electrons are extracted from water in photosystem II in the PET and are conditionally transferred to O_2 as alternative acceptor to produce $^\bullet O_2^-$. This reaction allows for maintenance of electron flow through PET if other terminal acceptors are in short [28]. In addition to the thylakoid-bound ascorbate peroxidase (tAPX) and the soluble stromal sAPX in the chloroplast, APXs are present in the cytosol, the mitochondria and peroxisomes [29]. APX generates H_2O and monodehydroascorbate (MDHA), which is regenerated via dehydroascorbate (DHA), GSH and finally NADPH [30].

In parallel to the ascorbate-dependent water–water cycle, the ascorbate-independent thiol-based system detoxifies peroxides in many compartments. There are two main groups of high affinity thiol peroxidases, peroxiredoxins (PRX), and glutathione peroxidases (GPX) [31]. GPXs have a substrate preference for

lipid peroxides and the PRX group is able to react with a large spectrum of peroxides [32]. PRXs are classified according to their respective number of cysteines, binding interface and dimerization preference into groups of type A–D [33]. PRXs are characterized by a typical thioredoxin-like fold consisting of seven beta-sheets and five alpha-helices [34]. They reduce H_2O_2 to H_2O, alkylhydroperoxide to the corresponding alcohol and peroxinitrite to nitrite. Importantly, PRXs adopt different conformational states and physiological functions in dependence on their redox state such as peroxidase, chaperon, proximity-based oxidase, binding partner, and redox sensor in signaling [33].

Detoxification of generated ROS counteracts ROS accumulation, but cannot prevent eventual damage since the ROS molecules will diffuse from the site of generation through the cell until they are detoxified. Thus, the more efficient mechanism to decrease oxidative stress level is the suppression of ROS generation. In RET electrons are finally transferred to O_2 by complex IV, the cytochrome c oxidase (COX). Uncoupling protein and alternative oxidases (AOX) enable dissipation of excess reducing power and counteract ROS production in RET [35, 36]. In chloroplasts, the plastid terminal oxidase (PTOX) is part of chlororespiration and dissipates excess reducing power by transfer to O_2 [37, 38]. Thus, PTOX activation counteracts overreduction of the plastoquinone pool which otherwise could elicit oxidative stress [39, 40]. It should be noted that PTOX can produce $^{\bullet}O_2^-$ as side product and thus might contribute to oxidative stress under certain conditions [41].

2 Regulation of Stress Acclimation

On the one hand, the discussed mechanisms of activating redox safety valves, strengthening ROS detoxification by antioxidant systems and maintenance of a strong redox buffer stabilize plants against redox- and ROS-incidences in a fluctuating environment. However, on the other hand, the homeostasis mechanisms must be leaky in order to enable redox-triggered acclimation responses. In addition to stress-specific signaling and responses, redox sensing and ROS-dependent regulation function as overarching principle in stress acclimation. The concept of redox regulatory networks in all cells consisting of redox input elements, redox transmitters, redox targets, redox sensors, and final electron acceptors has been advanced and provides a functional framework [42–44]. This network depends on ROS for reoxidation of redox-regulated targets. The balance between metabolic electron pressure into the network and drainage of electrons by final electron acceptors defines the state of the network. From this consideration it becomes clear that our understanding of the cellular

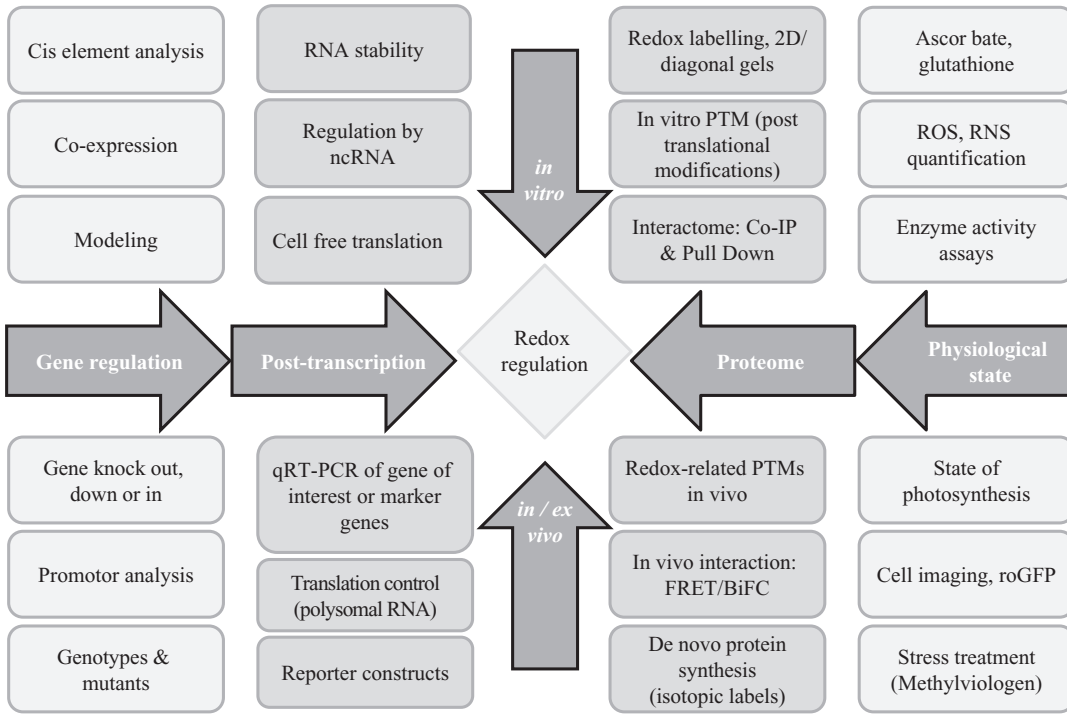

Fig. 1 Redox-focused overview of methods in redox and ROS research. The methods allow for various qualitative and quantitative assessments in the areas of transcriptome, proteome, and biochemical analyses

redox- and ROS-state must include sensitive analysis of the redox proteome and the involved regulatory mechanisms (*see* Fig. 1 for strategies).

Spatial and temporal specificity in ROS signatures comes from confined ROS generation, biological half-life time, substrate specificity and regulation of scavenging systems and compartmentation of sensors and targets [31, 45]. ROS and redox signaling pathways mutually interact with pathways controlled by Ca^{2+}-, reactive nitrogen species and phytohormones [46]. In the following paragraphs, three stressors, namely heat, high light, and salt, are exemplarily scrutinized to show the central role of ROS in plant stress responses.

2.1 ROS Response in Heat Stress

High temperatures have a huge impact on yield and productivity of plants [47, 48]. Rates of protein denaturation increase at higher temperatures. Therefore, mechanisms of protein stabilization by various types of chaperones and enhanced repair must counter protein inactivation and destabilization to maintain protein homeostasis and increase thermotolerance [49]. Responses to elevated temperatures include activation of ROS scavengers, heat shock transcription factors and proteins as well as increased osmolyte biosynthesis [50, 51]. Frank et al. [52] described significant correlations between ROS response and hormone signaling, sugar

accumulation and heat shock protein (HSP) translation. Transcript levels for stress markers like APX genes, RET and PET pathways, and heat shock factors are upregulated in maturing tomato microspores stressed for 2 h at 44 °C. The comparison between heat-tolerant and heat-sensitive cultivars indicates that oxidative stress functions as significant input signal for acquiring thermotolerance. This is especially reinforced by increased mRNA levels of ROS scavengers (tAPX, APX1, APX2, APX4-like, APX6-like, SIAPX3) in sensitive plants and basal levels of these markers before and after stress induction in tolerant plants. Tobacco bright-yellow 2 cells initiate the cell death program (PCD) after being subjected to a 55 °C heat-shock treatment. The PCD induction was associated with a twofold increased H_2O_2 accumulation and a tenfold increase of $^{\bullet}O_2^-$ relative to the control. V_{max} of cAPX activity decreases up to fivefold during ROS-induced cell death. Pretreatment with the antioxidant ascorbate or SOD prior to heat stress stabilizes cAPX activity and protein amount to a level of unstressed control. In addition the reduction state of ascorbate decreased from 80% to 50% after 24 h together with a decrease in protein amount and mRNA of cAPX by 80% and 90%, respectively. Impaired kinetic properties and lower APX quantity are correlated, so it was suggested that protein modifications and inhibitory effects associated with elevated temperatures feed into this redox-regulatory network resulting in low V_{max} [53]. ROS scavenging systems like the ascorbate-dependent and the thiol peroxidase-dependent water–water cycles maintain redox and ROS homeostasis also in stress situations like heat [31, 54, 55].

Protein stabilization, renaturation, and degradation are crucial processes in acclimation to elevated temperature. Heat shock protein (HSP) amounts increase 10- to 200-fold during heat stress. HSPs assist in protein folding and prevent aggregation [56, 57]. HSP translation in Mammalia and Drosophila was reported to be stimulated in response to stress-induced ROS accumulation. The translational stimulation involves protein kinase pathways. HSPs constitute a functionally highly conserved and similarly regulated mechanism in all organisms [58, 59]. Heat shock factors (HSF) are transcription factors, which control expression of HSPs and other stress response genes in the heat stress response. HSFs bind to the heat shock-motif nAGAAnnTTCTn which is contained not only in HSP promotors but also in many other stress-responsive genes with function in ROS signaling and detoxification, e.g., in cAPX1 [60–62]. The conserved mechanism in the heat stress response of humans and yeast involves H_2O_2-dependent phosphorylation [63, 64]. This mechanism was also identified in plants where mitogen-activated protein kinases (MAPK) transduce the heat stress signal in tomato [65] and in *A. thaliana* [66]. Two H_2O_2-sensitive MAPKs, namely MPK3 and MPK6 phosphorylate HSFA2 and HSFA4a and thereby connect the heat stress-induced signaling

with downstream activation of response genes [66]. A model for ROS-dependent oligomerization of AtHSFA8a and AtHSFA4a was suggested to trigger translocation to the nucleus and activation of target genes [67]. AtHSFA2 overexpressing Arabidopsis was subjected to short-term heat shock of 10 min. Upon heat shock HSFA2 could be detected in both the cytosol and nucleus. The *APX2* transcript accumulated 40-fold more in AtHSFA2 overexpressing plants than in wild type plants [68, 69]. Depending on the redox state of cysteine residues in HSFA8 in H_2O_2 treated protoplasts, a recent study indeed showed redox-dependent translocation to nucleus [70]. The Cys-Ser exchange in HSFA8 abolished the H_2O_2-induced translocation from the cytosol to the nucleus. This system should be tested in vivo.

Allakhverdiev et al. [71] reported that three processes in plant photosynthesis are especially vulnerable to elevated temperatures; (1) photosystem II (PSII) with its oxygen-evolving complex (OEC), (2) ATP-synthesis, and (3) carbon fixation in the Calvin-Benson cycle. Heat stress is associated with transient ROS accumulation. Accumulating H_2O_2 and $^1O_2$ inhibit PSII repair by interfering with translation of *psbA* mRNA in cyanobacteria and plants [72–74]. High temperatures and high lipid fluidity negatively affect electron transport in photosynthesis. Especially mobility of thylakoid-bound plastoquinone as electron transmitter is a rate-limiting factor in photosynthesis under heat stress [75]. Unstacking of grana at high temperature favors the mobility of formerly densely packed PSII complexes to stroma-exposed sites and as a consequence improves accessibility to repair mechanisms for D1 subunits [76, 77].

2.2 ROS Response in High Light (HL) Stress

Absorption of excessive excitation energy by photosynthesis triggers acclimation responses on very fast to long-term time scales [78]. Enhanced ROS generation and accumulation occurs as an early response within minutes after increasing the light intensity. Singlet oxygen originates from excited chlorophylls. β-Carotene is regarded as highly important quenching component in photosystem II. Its oxidized derivatives β-cyclocitral and dihydroactinidiolide appear to serve as retrograde signals from the chloroplast to the cytosol and nucleus [79, 80]. Transcript analyses on light-stressed *C. reinhardtii* indicate that these oxidized compounds activate signaling pathways that act on palindromic sequences in promoters called electrophile response elements for $^1O_2$-related stress responses [81]. Reprogramming of gene expression in response to photosynthetic light stress involves kinase activity which links ROS-sensing and downstream activation of target genes. Light stressed $^1O_2$-overproducing *flu* mutants overexpress *Oxidative Signal Inducible 1* (OXI1) which encodes an AGC kinase previously connected to cell death. Null mutants of *oxi1*

revealed less photo-induced oxidative damage and delayed cell death in high light [82]. Downstream activation of MAPKs through oxidative burst signaling was already reported as OXI1 function. Thus, there exists a tight coupling between ROS- and phosphorylation-dependent regulatory pathways and light stress-dependent gene expression [83].

The *flu* mutant is unable to suppress protochlorophyllide biosynthesis in darkness [84]. The accumulation of photosensitizers during darkness triggers $^1O_2$ release upon illumination and has allowed for studying the involved signaling pathways. Transcript profiling of *flu* plants showed upregulation of phytohormone-linked mRNAs previously reported for abscisic acid, ethylene, and jasmonate signaling, and also resembled patterns known from programmed cell death (PCD). The deduced mechanism assigns the decisive role to oxylipins, which control development of cell death or successful acclimation to $^1O_2$ stress [9].

A large scale microarray analysis in *flu* and the ROS-scavenging mutants *sod*, *cat2* and *apx1* exposed to various stresses including high light revealed overlapping and specific regulation of gene sets that illustrate the existence of complex redox signaling networks in plants. Cluster analysis of transcriptional responses pinpointed to nuclear-encoded signals characteristic for plastid $^1O_2$ production and provided evidence for patterns specific for the ROS type and subcellular localization. More than 500 annotated TFs in *A. thaliana* were differentially expressed showing the vast influence of changing ROS levels on plant cell transcription and redox regulation. Additionally these results identified unique transcriptional regulons based on specific bHLH, MYB, and NAM transcription factors found only in the high light stress sets [85]. A further transcript-targeted approach for ROS response focused on high light in catalase-deficient *A. thaliana* mutants with 65% or 20% residual catalase activity. This setup illustrated H_2O_2-dependent defense responses. Transcriptional control of NAC, MYB, WRKY, and AP2-related TFs and phosphorylation of MAPKs increased after 3 h HL compared to wild type. In addition, H_2O_2-dependent activation of photosynthetic proteins and ROS scavengers in plastids (e.g., peroxidases and PS I/II subunits) was delayed in catalase-deficient lines. The mutants were also interesting with regard to balanced resource investments into growth and defense. The energy-consuming translation machinery and protease activity were elevated in the catalase mutants indicative for increased protein turnover due to oxidation. Overall H_2O_2 is assumed to act together with master switches in the control of the light stress response [86, 87].

Chloroplast acclimation to high light is also linked to the redox state of the PQ pool [88–90]. The plastids have only a residual genome. Most genes for photosynthesis, respiration and also for

regulating redox imbalances like PQ redox state were transferred into nucleus genome. The communication between plastids and nucleus depends on retrograde signaling processes and includes information on ROS [91–95] in addition to metabolic, hormonal, and redox cues [78].

2.3 ROS Responses in Salt Stress

Salinity is a major threat for sustained crop production worldwide. Efficient salinity acclimation addresses osmolyte biosynthesis, ion homeostasis, transpiration control, and maintenance of ROS homeostasis [96, 97]. Stomatal closure decreases CO_2 availability and enhances processes leading to ROS accumulation such as photorespiration and Mehler reaction [98]. Guard cell contraction for gas control involves massive ion movement and often is mediated by ABA. The signaling also implicates MAPK and ROS synthesis [99, 100]. H_2O_2-treated *mpk9* and *mpk12* Arabidopsis were unable to close stomata like in WT controls [101]. The defect in H_2O_2 signaling was attributed to downstream elements such as nucleotide diphosphate kinase2 (AtNDK2), which is also needed for abiotic stress resistance and improved antioxidant capacity. AtNDK2 controls stress-dependent phosphorylation and signaling cascades by promoting AtMPK3/6 [102]. Rentel et al. [83] discovered additional components of signal transduction upstream of AtMPK3/6. As discussed above for light stress acclimation, OXI1 kinase activated AtMPK3/6 is suggested to act as a major player in oxidative burst mediated signaling. During ionic disturbances MPK6 acts as a regulatory hub in the control of Na^+/K^+ antiporters, supports membrane integrity and initiates RBOH-dependent signaling [103, 104]. MPK3 also promotes the expression of lipid transfer proteins and of the hybrid proline-rich protein (HyPRP) AZI1. These proteins improve seed germination and plant growth under salinity [105]. HyPRPs were reported to participate in cell wall cross-linking, thereby probably improving cell stability and membrane permeability against high salinity [106, 107].

Oxidative burst describes the sudden increase of ROS in the apoplastic space, which occurs as part of defense and signaling mechanisms. NADPH oxidases of the RBOH type transfer electrons from cytosolic NADPH to O_2 on the apoplastic site [108, 109]. Proline biosynthesis is enhanced by RBOH-dependent signaling and establishes safe osmotic relations in salt-stressed cultured tobacco cells [110, 111]. Salt stress activates expression of the RBOH isoforms C/D/F in Arabidopsis. This process depends on INT1 (increased tolerance to NaCl1) since it is significantly decreased in *int1* mutants [112]. Increased H_2O_2 concentrations in the apoplastic space and endomembrane vesicles also foster ABA-dependent stomatal response to salt stress [113]. ROS originating from AtRBOHC stabilizes *SOS1* mRNA under NaCl stress.

Indeed *SOS1* strongly responds to salt stress but not to methyl viologen-induced oxidative stress. RBOHC links Na^+ homeostasis, ROS, and Ca^{2+} signaling [114]. The RBOH protein structure is characterized by the presence of EF-hand motifs for Ca^{2+} binding and constitutes a phosphorylation target under the control of MAPKs, ROS, and Ca^{2+} [115].

3 Conclusion

Maintenance of redox homeostasis is essential for sustained growth in a changing environment. Deviations from redox equilibrium by increased ROS generation shift the system to increased defense at the expense of growth. ROS signatures are linked to other signaling cues such as Ca^{2+}, protein kinases and phosphatases, hormones, metabolites, and nitric oxide. The question as to how a limited number of ROS namely $^1O_2$, $^\bullet O_2^-$, H_2O_2, and $^\bullet OH$ can be involved in virtually all major stresses and how specificity of responses may be achieved is still unanswered. ROS signatures bear spatial and kinetic information depending on the type of abiotic stress [85]. Stress-dependent specificity of ROS signals might be encrypted in this type of poorly understood signature in time and space in combination with other signaling cues including activation of stress-specific sensors [45].

ROS action directly relates to redox homeostasis, cellular redox sensing, and the redox signaling network. Cysteine thiols play a unique role in this network. The thiol redox regulatory network consists of redox-switchable polypeptides and is composed of redox input elements, redox transmitters, redox targets, redox sensors, and ROS as final electron acceptors [42]. In addition to disulfide formation in and between polypeptides, Cys is subjected to S-glutathionylation, S-nitrosylation, sulfenylation, sulfinylation, sulfonylation, S-acetylation, and other modifications. Stress-induced disturbances are immediately recognized and responses elicited within seconds, e.g., upon high light exposure [116, 117]. Metabolic adjustment to new conditions is achieved by modulating the phosphoproteome, transcription factors, translation factors, and protein turnover. Often plants are not exposed to single stressors but face combinatorial stresses such as drought, heat, and high light. Understanding and dissecting the ROS pathways under such conditions pose a challenge to plant researchers. For this reason it is necessary to plan the projects along the proposed hypothesis, consider the available financial resources, and apply the most suitable methods. To this end, a selected overview of ROS-centered techniques is provided in Table 1.

Table 1
Exemplary overview of redox-targeted methods

Method	Advantage	Disadvandage	Scientific impact
ROS staining in tissues	Easy, visualization of ROS	Qualitative assessment of uncertain significance	*
Membrane integrity (lipid peroxidation, ion exchange)	Easy, ROS-related cell damage	Low sensitivity, late parameters of stress	*
Gel-based immune labeling by Western blotting	Easy assessment of PTMs	Requirement for specific antiserum, difficulty of blocking and labeling	**
Photosynthetic parameters	Eatablished devices and theory		***
Metabolites (GSH, ASC, ...) and ROS quantification	Access to cellular redox features	Enzyme-coupled or cycling assays, difficulty of quenching	***
Thiol quantification	Quantitative analysis for protein thiols and free thiols	Low specificity	**
Microarray/RNA-Seq	Genome-wide RNA analysis, high sensitivity	Often expensive outsourcing, need for bioinformatics, transcript level	****
Transcript analysis, qPCR	Quantitative analysis RNA regulation	Specific targets, primer designs and adjustment	****
[35S] methionine or isotope labelling	Protein translation in vivo, time resolution	Institutional requirements	****
Cell imaging, flourescent protein fusion	roGFP for redox balance, FRET and BiFC for interactions	Evaluation and controls require high experience, roGFP sensitivity range	****
Redox proteomics (2D redox gels, peptide identification)	Redox interaction on protein level, isolation and charecterization of targets	Need for sophisticated proteomics facilities	*****
Enzyme activity assays	Quantitative kinetic parameters	In vitro, complex redox assays	***
Isothermal titration calorimetry (ITC)	Kinetic parameters (K, n, H, G, S) interactions and dynamics	High purity and amounts of proteins	****
Mass spectrometry	Detection of PTMs	Intensive purification and database requirements; high expert level	*****
Chromatographic analysis of proteins	Visualization of dynamics, modifications isolation and purification of targets	Protein-dependent adjustments, protein instability	****

The summary provides additional remarks from the authors' perspective as to "Advantages" and "Disadvantages" as well as a rating in context of "Scientific Impact." Values are given between (*) for least and (*****) for highest scientific potential

References

1. Foyer CH, Noctor G (2011) Ascorbate and glutathione: the heart of the redox hub. Plant Physiol 155(1):2–18
2. Mittler R (2006) Abiotic stress, the field environment and stress combination. Trends Plant Sci 11(1):15–19
3. Gao JP, Chao DY, Lin HX (2007) Understanding abiotic stress tolerance mechanisms: recent studies on stress response in rice. J Integr Plant Biol 49(6):742–750
4. Biehler K, Fock H (1996) Evidence for the contribution of the Mehler-peroxidase reaction in dissipating excess electrons in drought-stressed wheat. Plant Physiol 112(1):265–272
5. Hideg É, Kálai T, Hideg K, Vass I (1998) Photoinhibition of photosynthesis in vivo results in singlet oxygen production detection via nitroxide-induced fluorescence quenching in broad bean leaves. Biochemistry 37(33):11405–11411
6. Navrot N, Rouhier N, Gelhaye E, Jacquot JP (2007) Reactive oxygen species generation and antioxidant systems in plant mitochondria. Physiol Plant 129(1):185–195
7. Liu Y, He C (2016) Regulation of plant reactive oxygen species (ROS) in stress responses: learning from AtRBOHD. Plant Cell Rep 35:995–1007
8. Rejeb KB, Benzarti M, Debez A, Bailly C, Savouré A, Abdelly C (2015a) NADPH oxidase-dependent H2O2 production is required for salt-induced antioxidant defense in *Arabidopsis thaliana*. J Plant Physiol 174:5–15
9. Laloi C, Havaux M (2015) Key players of singlet oxygen-induced cell death in plants. Front Plant Sci 6:39
10. Stone JR, Yang S (2006) Hydrogen peroxide: a signaling messenger. Antioxid Redox Signal 8(3–4):243–270
11. Mittler R, Berkowitz G (2001) Hydrogen peroxide, a messenger with too many roles? Redox Rep 6(2):69–72
12. Nappi AJ, Vass E (1998) Hydroxyl radical formation resulting from the interaction of nitric oxide and hydrogen peroxide. Biochim Biophys Acta 1380:55–63
13. Nappi AJ, Vass E (2000) Hydroxyl radical production by ascorbate and hydrogen peroxide. Neurotox Res 2:343–355
14. Scandalios JG (2005) Oxidative stress: molecular perception and transduction of signals triggering antioxidant gene defenses. Braz J Med Biol Res 38(7):995–1014
15. Signorelli S, Coitiño EL, Borsani O, Monza J (2014) Molecular mechanisms for the reaction between (˙)OH radicals and proline: insights on the role as reactive oxygen species scavenger in plant stress. J Phys Chem B118:37–47
16. Dat J, Vandenabeele S, Vranová E, Van Montagu M, Inzé D, Van Breusegem F (2000) Dual action of the active oxygen species during plant stress responses. Cell Mol Life Sci 57(5):779–795
17. Meyer AJ, Brach T, Marty L, Kreye S, Rouhier N, Jacquot JP, Hell R (2007) Redox-sensitive GFP in *Arabidopsis thaliana* is a quantitative biosensor for the redox potential of the cellular glutathione redox buffer. Plant J 52:973–986
18. Noctor G, Mhamdi A, Chaouch S, Han YI, Neukermans J, Marquez-Garcia B, Queval G, Foyer CH (2012) Glutathione in plants: an integrated overview. Plant Cell Environ 35(2):454–484
19. Zagorchev L, Seal CE, Kranner I, Odjakova M (2013) A central role for thiols in plant tolerance to abiotic stress. Int J Mol Sci 14(4):7405–7432
20. Rouhier N, Lemaire SD, Jacquot JP (2008) The role of glutathione in photosynthetic organisms: emerging functions for glutaredoxins and glutathionylation. Annu Rev Plant Biol 59:143–166
21. Jozefczak M, Keunen E, Schat H, Bliek M, Hernández LE, Carleer R, Remans T, Bohler S, Vangronsveld J, Cuypers A (2014) Differential response of Arabidopsis leaves and roots to cadmium: glutathione-related chelating capacity vs antioxidant capacity. Plant Physiol Biochem 83:1–9
22. Jozefczak M, Bohler S, Schat H, Horemans N, Guisez Y, Remans T, Vangronsveld J, Cuypers A (2015) Both the concentration and redox state of glutathione and ascorbate influence the sensitivity of Arabidopsis to cadmium. Ann Bot 116(4):601–612
23. Fryer MJ (1992) The antioxidant effects of thylakoid vitamin E (α-tocopherol). Plant Cell Environ 15(4):381–392
24. Havaux M, Eymery F, Porfirova S, Rey P, Dörmann P (2005) Vitamin E protects against photoinhibition and photooxidative stress in *Arabidopsis thaliana*. Plant Cell 17(12):3451–3469
25. Asada K (1999) The water-water cycle in chloroplasts: scavenging of active oxygens and dissipation of excess photons. Annu Rev Plant Biol 50(1):601–639
26. Foyer CH, Noctor G (2003) Redox sensing and signalling associated with reactive oxygen

in chloroplasts, peroxisomes and mitochondria. Physiol Plant 119(3):355–364

27. Tuna AL, Kaya C, Dikilitas M, Higgs D (2008) The combined effects of gibberellic acid and salinity on some antioxidant enzyme activities, plant growth parameters and nutritional status in maize plants. Environ Exp Bot 62(1):1–9
28. Asada K, Takahashi M (1987) Production and scavenging of active oxygen in photosynthesis. In: Kyle DJ, Osmond CB, Arntzen CJ (eds) Photoinhibition. Elsevier, Amsterdam, pp 227–287
29. Jimenez A, Hernandez JA, del Río LA, Sevilla F (1997) Evidence for the presence of the ascorbate-glutathione cycle in mitochondria and peroxisomes of pea leaves. Plant Physiol 114(1):275–284
30. Edwards EA, Enard C, Creissen GP, Mullineaux PM (1993) Synthesis and properties of glutathione reductase in stressed peas. Planta 192(1):137–143
31. Dietz KJ (2016) Thiol-based peroxidases and ascorbate peroxidases: why plants rely on multiple peroxidase systems in the photosynthesizing chloroplast? Mol Cells 39(1):20–25
32. Matamoros MA, Saiz A, Peñuelas M, Bustos-Sanmamed P, Mulet JM, Barja MV, Rouhier N, Moore M, James EK, Dietz KJ (2015) Function of glutathione peroxidases in legume root nodules. J Exp Bot 66:2979–2990
33. Dietz KJ (2011) Peroxiredoxins in plants and cyanobacteria. Antioxid Redox Signal 15(4):1129–1159
34. Noguera-Mazon V, Lemoine J, Walker O, Rouhier N, Salvador A, Jacquot JP, Lancelin JM, Krimm I (2006) Glutathionylation induces the dissociation of 1-Cys D-peroxiredoxin non-covalent homodimer. J Biol Chem 281(42):31736–31742
35. Dinakar C, Vishwakarma A, Raghavendra AS, Padmasree K (2016) Alternative oxidase pathway optimizes photosynthesis during osmotic and temperature stress by regulating cellular ROS, malate valve and antioxidative systems. Front Plant Sci 7:68
36. Millar AH, Whelan J, Soole KL, Day DA (2011) Organization and regulation of mitochondrial respiration in plants. Annu Rev Plant Biol 62:79–104
37. Carol P, Kuntz M (2001) A plastid terminal oxidase comes to light: implications for carotenoid biosynthesis and chlororespiration. Trends Plant Sci 6(1):31–36
38. Peltier G, Cournac L (2002) Chlororespiration. Annu Rev Plant Biol 53(1):523–555
39. Nawrocki WJ, Tourasse NJ, Taly A, Rappaport F, Wollman FA (2015) The plastid terminal oxidase: its elusive function points to multiple contributions to plastid physiology. Annu Rev Plant Biol 66:49–74
40. Trouillard M, Shahbazi M, Moyet L, Rappaport F, Joliot P, Kuntz M, Finazzi G (2012) Kinetic properties and physiological role of the plastoquinone terminal oxidase (PTOX) in a vascular plant. Biochim Biophys Acta 1817(12):2140–2148
41. Yu Q, Feilke K, Krieger-Liszkay A, Beyer P (2014) Functional and molecular characterization of plastid terminal oxidase from rice (*Oryza sativa*). Biochim Biophys Acta 1837: 1284–1292
42. Dietz KJ (2008) Redox signal integration: from stimulus to networks and genes. Physiol Plant 133(3):459–468
43. Ströher E, Dietz KJ (2008) The dynamic thiol–disulphide redox proteome of the *Arabidopsis thaliana* chloroplast as revealed by differential electrophoretic mobility. Physiol Plant 133(3):566–583
44. Winger AM, Taylor NL, Heazlewood JL, Day DA, Millar AH (2007) Identification of intra- and intermolecular disulphide bonding in the plant mitochondrial proteome by diagonal gel electrophoresis. Proteomics 7(22):4158–4170
45. Mittler R, Vanderauwera S, Suzuki N, Miller G, Tognetti VB, Vandepoele K, Gollery M, Shulaev V, Van Breusegem F (2011) ROS signaling: the new wave? Trends Plant Sci 16(6):300–309
46. Fujita M, Fujita Y, Noutoshi Y, Takahashi F, Narusaka Y, Yamaguchi-Shinozaki K, Shinozaki K (2006) Crosstalk between abiotic and biotic stress responses: a current view from the points of convergence in the stress signaling networks. Curr Opin Plant Biol 9(4):436–442
47. Boyer JS (1982) Plant productivity and environment. Science 218(4571):443–448
48. Boote KJ, Allen LH, Prasad PV, Baker JT, Gesch RW, Snyder AM, Pan D, Thomas JM (2005) Elevated temperature and CO2 impacts on pollination, reproductive growth, and yield of several globally important crops. J Agric Meteorol 60:469–474
49. Schroda M, Hemme D, Mühlhaus T (2015) The Chlamydomonas heat stress response. Plant J 82(3):466–480
50. Morimoto RI (1998) Regulation of the heat shock transcriptional response: cross talk between a family of heat shock factors, molecular chaperones, and negative regulators. Genes Dev 12(24):3788–3796

51. Kumar RR, Goswami S, Sharma SK, Singh K, Gadpayle KA, Singh SD, Pathak H, Rai RD (2013) Differential expression of heat shock protein and alteration in osmolyte accumulation under heat stress in wheat. J Plant Biochem Biotechnol 22(1):16–26
52. Frank G, Pressman E, Ophir R, Althan L, Shaked R, Freedman M, Shen S, Firon N (2009) Transcriptional profiling of maturing tomato (*Solanum lycopersicum* L.) microspores reveals the involvement of heat shock proteins, ROS scavengers, hormones, and sugars in the heat stress response. J Exp Bot 60(13):3891–3908
53. Vacca RA, de Pinto MC, Valenti D, Passarella S, Marra E, De Gara L (2004) Production of reactive oxygen species, alteration of cytosolic ascorbate peroxidase, and impairment of mitochondrial metabolism are early events in heat shock-induced programmed cell death in tobacco Bright-Yellow 2 cells. Plant Physiol 134(3):1100–1112
54. Asada K (2006) Production and scavenging of reactive oxygen species in chloroplasts and their functions. Plant Physiol 141(2):391–396
55. Dietz KJ, Jacob S, Oelze ML, Laxa M, Tognetti V, de Miranda SMN, Baier M, Finkemeier I (2006) The function of peroxiredoxins in plant organelle redox metabolism. J Exp Bot 57(8):1697–1709
56. Wahid A, Gelani S, Ashraf M, Foolad MR (2007) Heat tolerance in plants: an overview. Environ Exp Bot 61(3):199–223
57. Vierling E (1991) The roles of heat shock proteins in plants. Annu Rev Plant Biol 42(1):579–620
58. Arrigo AP (1998) Small stress proteins: chaperones that act as regulators of intracellular redox state and programmed cell death. Biol Chem 379(1):19–26
59. Nollen EA, Morimoto RI (2002) Chaperoning signaling pathways: molecular chaperones as stress-sensing 'heat shock' proteins. J Cell Sci 115(14):2809–2816
60. Rizhsky L, Davletova S, Liang H, Mittler R (2004) The zinc finger protein Zat12 is required for cytosolic ascorbate peroxidase 1 expression during oxidative stress in Arabidopsis. J Biol Chem 279(12): 11736–11743
61. Davletova S, Schlauch K, Coutu J, Mittler R (2005) The zinc-finger protein Zat12 plays a central role in reactive oxygen and abiotic stress signaling in Arabidopsis. Plant Physiol 139(2):847–856
62. Scharf KD, Berberich T, Ebersberger I, Nover L (2012) The plant heat stress transcription factor (Hsf) family: structure, function and evolution. Biochim Biophys Acta 1819(2): 104–119
63. Lee S, Carlson T, Christian N, Lea K, Kedzie J, Reilly JP, Bonner JJ (2000) The yeast heat shock transcription factor changes conformation in response to superoxide and temperature. Mol Biol Cell 11(5):1753–1764
64. Ahn SG, Thiele DJ (2003) Redox regulation of mammalian heat shock factor 1 is essential for Hsp gene activation and protection from stress. Genes Dev 17(4):516–528
65. Link V, Sinha AK, Vashista P, Hofmann MG, Proels RK, Ehness R, Roitsch T (2002) A heat-activated MAP kinase in tomato: a possible regulator of the heat stress response. FEBS Lett 531(2):179–183
66. Driedonks N, Xu J, Peters JL, Park S, Rieu I (2015) Multi-level interactions between heat shock factors, heat shock proteins, and the redox system regulate acclimation to heat. Front Plant Sci 6:999
67. Miller G, Mittler R (2006) Could heat shock transcription factors function as hydrogen peroxide sensors in plants? Ann Bot 98(2): 279–288
68. Ogawa D, Yamaguchi K, Nishiuchi T (2007) High-level overexpression of the Arabidopsis HsfA2 gene confers not only increased thermotolerance but also salt/osmotic stress tolerance and enhanced callus growth. J Exp Bot 58(12):3373–3383
69. Kotak S, Port M, Ganguli A, Bicker F, Von Koskull-Döring P (2004) Characterization of C-terminal domains of Arabidopsis heat stress transcription factors (Hsfs) and identification of a new signature combination of plant class A Hsfs with AHA and NES motifs essential for activator function and intracellular localization. Plant J 39:98–112
70. Giesguth M, Sahm A, Simon S, Dietz KJ (2015) Redox-dependent translocation of the heat shock transcription factor AtHSFA8 from the cytosol to the nucleus in *Arabidopsis thaliana*. FEBS Lett 589(6):718–725
71. Allakhverdiev SI, Kreslavski VD, Klimov VV, Los DA, Carpentier R, Mohanty P (2008) Heat stress: an overview of molecular responses in photosynthesis. Photosynth Res 98(1–3):541–550
72. Nishiyama Y, Yamamoto H, Allakhverdiev SI, Inaba M, Yokota A, Murata N (2001) Oxidative stress inhibits the repair of photodamage to the photosynthetic machinery. EMBO J 20(20):5587–5594
73. Nishiyama Y, Allakhverdiev SI, Murata N (2005) Inhibition of the repair of photosystem II by oxidative stress in cyanobacteria. Photosynth Res 84(1–3):1–7

74. Murata N, Takahashi S, Nishiyama Y, Allakhverdiev SI (2007) Photoinhibition of photosystem II under environmental stress. Biochim Biophys Acta 1767(6):414–421
75. Aminaka R, Taira Y, Kashino Y, Koike H, Satoh K (2006) Acclimation to the growth temperature and thermosensitivity of photosystem II in a mesophilic cyanobacterium, Synechocystis sp. PCC6803. Plant Cell Physiol 47(12):1612–1621
76. Khatoon M, Inagawa K, Pospíšil P, Yamashita A, Yoshioka M, Lundin B, Horie J, Morita N, Jajoo A, Yamamoto Y, Yamamoto Y (2009) Quality control of photosystem II: Thylakoid unstacking is necessary to avoid further damage to the D1 protein and to facilitate D1 degradation under light stress in spinach thylakoids. J Biol Chem 284:25343–25352
77. Nath K, Poudyal RS, Eom J-S, Park YS, Zulfugarov IS, Mishra SR, Tovuu A, Ryoo N, Yoon H-S, Nam HG, An G, Jeon J-S, Lee C-H (2013) Loss-of-function of OsSTN8 suppresses the photosystem II core protein phosphorylation and interferes with the photosystem II repair mechanism in rice (*Oryza sativa*). Plant J 76:675–686
78. Dietz KJ (2015) Efficient high light acclimation involves rapid processes at multiple mechanistic levels. J Exp Bot 66(9): 2401–2414
79. Triantaphylidès C, Havaux M (2009) Singlet oxygen in plants: production, detoxification and signaling. Trends Plant Sci 14(4):219–228
80. Havaux M (2014) Carotenoid oxidation products as stress signals in plants. Plant J 79(4):597–606
81. Fischer BB, Ledford HK, Wakao S, Huang SG, Casero D, Pellegrini M, Merchant SS, Koller A, Eggen RIL, Niyogi KK (2012) SINGLET OXYGEN RESISTANT 1 links reactive electrophile signaling to singlet oxygen acclimation in *Chlamydomonas reinhardtii*. Proc Natl Acad Sci 109(20):E1302–E1311
82. Shumbe L, Chevalier A, Legeret B, Taconnat L, Monnet F, Havaux M (2016) Singlet oxygen-induced cell death in Arabidopsis under high light stress is controlled by OXI1 kinase. Plant Physiol 170(3):1757–1771
83. Rentel MC, Lecourieux D, Ouaked F, Usher SL, Petersen L, Okamoto H, Knight H, Peck SC, Grierson CS, Hirt H, Knight MR (2004) OXI1 kinase is necessary for oxidative burst-mediated signalling in Arabidopsis. Nature 427(6977):858–861
84. Meskauskiene R, Nater M, Goslings D, Kessler F, op den Camp R, Apel K (2001) FLU: a negative regulator of chlorophyll biosynthesis in *Arabidopsis thaliana*. Proc Natl Acad Sci 98(22):12826–12831
85. Gadjev I, Vanderauwera S, Gechev TS, Laloi C, Minkov IN, Shulaev V, Apel K, Inzé D, Mittler R, Van Breusegem F (2006) Transcriptomic footprints disclose specificity of reactive oxygen species signaling in Arabidopsis. Plant Physiol 141(2):436–445
86. Vandenabeele S, Vanderauwera S, Vuylsteke M, Rombauts S, Langebartels C, Seidlitz HK, Zabeau M, Van Montagu M, Inzé D, Van Breusegem F (2004) Catalase deficiency drastically affects gene expression induced by high light in *Arabidopsis thaliana*. Plant J 39:45–58
87. Vanderauwera S, Zimmermann P, Rombauts S, Vandenabeele S, Langebartels C, Gruissem W, Inzé D, Van Breusegem F (2005) Genome-wide analysis of hydrogen peroxide-regulated gene expression in Arabidopsis reveals a high light-induced transcriptional cluster involved in anthocyanin biosynthesis. Plant Physiol 139(2):806–821
88. Karpinska B, Wingsle G, Karpinski S (2000) Antagonistic effects of hydrogen peroxide and glutathione on acclimation to excess excitation energy in Arabidopsis. IUBMB Life 50(1):21–26
89. Pfannschmidt T (2003) Chloroplast redox signals: how photosynthesis controls its own genes. Trends Plant Sci 8(1):33–41
90. Mühlenbock P, Szechyńska-Hebda M, Płaszczyca M, Baudo M, Mateo A, Mullineaux PM, Parker JE, Karpińska B, Karpiński S (2008) Chloroplast signaling and LESION SIMULATING DISEASE1 regulate crosstalk between light acclimation and immunity in Arabidopsis. Plant Cell 20(9):2339–2356
91. Escoubas JM, Lomas M, LaRoche J, Falkowski PG (1995) Light intensity regulation of cab gene transcription is signaled by the redox state of the plastoquinone pool. Proc Natl Acad Sci 92(22):10237–10241
92. Baier M, Dietz KJ (2005) Chloroplasts as source and target of cellular redox regulation: a discussion on chloroplast redox signals in the context of plant physiology. J Exp Bot 56(416):1449–1462
93. Nott A, Jung HS, Koussevitzky S, Chory J (2006) Plastid-to-nucleus retrograde signaling. Annu Rev Plant Biol 57:739–759
94. Pfannschmidt T, Bräutigam K, Wagner R, Dietzel L, Schröter Y, Steiner S, Nykytenko A (2009) Potential regulation of gene expression in photosynthetic cells by redox and energy state: approaches towards better understanding. Ann Bot 103(4):599–607
95. Oelze ML, Vogel MO, Alsharafa K, Kahmann U, Viehhauser A, Maurino VG, Dietz KJ (2012) Efficient acclimation of the chloroplast antioxidant defence of *Arabidopsis thaliana* leaves in response to a 10-or 100-fold

light increment and the possible involvement of retrograde signals. J Exp Bot 63(3): 1297–1313

96. Flowers TJ, Colmer TD (2008) Salinity tolerance in halophytes. New Phytol 179(4): 945–963
97. Hasegawa PM, Bressan RA, Zhu JK, Bohnert HJ (2000) Plant cellular and molecular responses to high salinity. Annu Rev Plant Biol 51(1):463–499
98. Gossett DR, Millhollon EP, Lucas M (1994) Antioxidant response to NaCl stress in salt-tolerant and salt-sensitive cultivars of cotton. Crop Sci 34(3):706–714
99. Kovtun Y, Chiu WL, Tena G, Sheen J (2000) Functional analysis of oxidative stress-activated mitogen-activated protein kinase cascade in plants. Proc Natl Acad Sci 97(6): 2940–2945
100. Wang P, Song CP (2008) Guard-cell signalling for hydrogen peroxide and abscisic acid. New Phytol 178(4):703–718
101. Jammes F, Song C, Shin D, Munemasa S, Takeda K, Gu D, Cho D, Lee S, Giordo R, Sritubtim S, Leonhardt N, Ellis BE, Murata Y, Leonhardt N (2009) MAP kinases MPK9 and MPK12 are preferentially expressed in guard cells and positively regulate ROS-mediated ABA signaling. Proc Natl Acad Sci 106(48):20520–20525
102. Moon H, Lee B, Choi G, Shin D, Prasad DT, Lee O, Kwak SS, Kim DH, Nam J, Bahk J, Hong JC, Lee SY, Cho MJ, Lim CO, Yun DJ (2003) NDP kinase 2 interacts with two oxidative stress-activated MAPKs to regulate cellular redox state and enhances multiple stress tolerance in transgenic plants. Proc Natl Acad Sci 100(1):358–363
103. Yu L, Nie J, Cao C, Jin Y, Yan M, Wang F, Liu J, Xiao Y, Liang Y, Zhang W (2010) Phosphatidic acid mediates salt stress response by regulation of MPK6 in *Arabidopsis thaliana*. New Phytol 188:762–773
104. Xing Y, Jia W, Zhang J (2008) AtMKK1 mediates ABA-induced CAT1 expression and H_2O_2 production via AtMPK6-coupled signaling in Arabidopsis. Plant J 54(3):440–451
105. Pitzschke A, Hirt H (2006) Mitogen-activated protein kinases and reactive oxygen species signaling in plants. Plant Physiol 141(2):351–356
106. Dvořáková L, Srba M, Opatrny Z, Fischer L (2011) Hybrid proline-rich proteins: novel players in plant cell elongation? Ann Bot 109(2):453–462
107. Qin LX, Zhang DJ, Huang GQ, Li L, Li J, Gong SY, Li XB, Xu WL (2013) Cotton GhHyPRP3 encoding a hybrid proline-rich protein is stress inducible and its overexpression in Arabidopsis enhances germination under cold temperature and high salinity stress conditions. Acta Physiol Plant 35(5): 1531–1542
108. Torres MA, Dangl JL (2005) Functions of the respiratory burst oxidase in biotic interactions, abiotic stress and development. Curr Opin Plant Biol 8(4):397–403
109. Sagi M, Fluhr R (2006) Production of reactive oxygen species by plant NADPH oxidases. Plant Physiol 141(2):336–340
110. Rejeb KB, Lefebvre-De Vos D, Le Disquet I, Leprince A-S, Bordenave M, Maldiney R, Jdey A, Abdelly C, Savouré A (2015b) Hydrogen peroxide produced by NADPH oxidases increases proline accumulation during salt or mannitol stress in *Arabidopsis thaliana*. New Phytol 208:1138–1148
111. Hoque MA, Banu MNA, Nakamura Y, Shimoishi Y, Murata Y (2008) Proline and glycinebetaine enhance antioxidant defense and methylglyoxal detoxification systems and reduce NaCl-induced damage in cultured tobacco cells. J Plant Physiol 165(8): 813–824
112. Sakamoto H, Matsuda O, Iba K (2008) ITN1, a novel gene encoding an ankyrin-repeat protein that affects the ABA-mediated production of reactive oxygen species and is involved in salt-stress tolerance in *Arabidopsis thaliana*. Plant J 56(3):411–422
113. Leshem Y, Seri L, Levine A (2007) Induction of phosphatidylinositol 3-kinase-mediated endocytosis by salt stress leads to intracellular production of reactive oxygen species and salt tolerance. Plant J 51(2):185–197
114. Chung JS, Zhu JK, Bressan RA, Hasegawa PM, Shi H (2008) Reactive oxygen species mediate Na+−induced SOS1 mRNA stability in Arabidopsis. Plant J 53(3):554–565
115. Kurusu T, Kuchitsu K, Tada Y (2015) Plant signaling networks involving Ca2+ and Rboh/Nox-mediated ROS production under salinity stress. Front Plant Sci 6:427
116. Vogel MO, Moore M, König K, Pecher P, Alsharafa K, Lee J, Dietz KJ (2014) Fast retrograde signaling in response to high light involves metabolite export, MITOGEN-ACTIVATED PROTEIN KINASE6, and AP2/ERF transcription factors in Arabidopsis. Plant Cell 26(3):1151–1165
117. Moore M, Vogel MO, Dietz KJ (2014) The acclimation response to high light is initiated within seconds as indicated by upregulation of AP2/ERF transcription factor network in *Arabidopsis thaliana*. Plant Signal Behav 9(10):976479

Chapter 3

The Role of Long Noncoding RNAs in Plant Stress Tolerance

Yuepeng Song and Deqiang Zhang

Abstract

Plants must adapt to multiple biotic and abiotic stresses; thus, sensing and responding to environmental signals is imperative for their survival. Moreover, understanding these responses is imperative for efforts to improve plant yield and consistency. Regulation of transcript levels is a key aspect of the plant response to environmental signals. Long noncoding RNAs (lncRNAs) have gained widespread attention in recent years with the advance of high-throughput sequencing technologies. As important biological regulators, lncRNAs have been implicated in a wide range of developmental processes and diseases in animals. However, knowledge of the role that lncRNAs play in plant stress tolerance remains limited. Here, we review recent studies on the identification, characteristics, classification, and biological functions of lncRNAs in response to various stresses, including bacterial pathogens, excess light, drought, salinity, hypoxia, extreme temperatures, and nitrogen/phosphate deficiency. We also discuss possible directions for future research.

Key words Abiotic stress, Long noncoding RNAs, Plant stress tolerance

1 Introduction

Plants can encounter, and thus must adapt to, multiple biotic and abiotic stresses including bacterial pathogens, excess light, drought, salinity, hypoxia, extreme temperatures, and heavy metals. Acute or chronic biotic and abiotic stresses can cause morphological, physiological, and biochemical changes that reduce photosynthesis, and thus limit plant growth and productivity [1, 2]. These stresses can cause devastating impacts on plant growth, yield, and the quality of plant-derived commodities. Thus, plants must have accurate mechanisms for sensing and responding to environmental signals [3]. Regulation of transcription, transcript levels, and translation, as the core of the plant genome-level response to environmental cues, alters gene expression and triggers protective mechanisms. Posttranscriptional regulation has pivotal functions in maintaining cellular homeostasis during stress and during recovery from stress [4].

Ramanjulu Sunkar (ed.), *Plant Stress Tolerance: Methods and Protocols*, Methods in Molecular Biology, vol. 1631,
DOI 10.1007/978-1-4939-7136-7_3,

Many protein-coding genes have been shown to have key functions in the well-studied stress-responsive signal transduction pathways [5], but the functions of noncoding RNAs (ncRNAs) have remained unclear. The discovery of microRNAs (miRNAs), which are short (21–24 nucleotides) noncoding RNAs (ncRNAs) that regulate the transcript levels of many genes, led to a paradigm shift in our understanding of gene regulation in plants. In addition to miRNAs, many types of ncRNAs have been found; these ncRNAs affect mRNA transcription, splicing, export, stability, and translation. Next-generation transcriptome sequencing in humans and yeast showed that ncRNAs accounted for approximately 90% of the transcripts in eukaryotes.

Based on their extraordinary differences in transcript lengths, biogenesis, and polarity, classification of ncRNAs remains difficult. Long noncoding RNAs (lncRNAs) are usually classified as ncRNAs of >200 nt. In the past decade, the focus on lncRNAs as regulators of gene expression has gradually increased. In eukaryotes, ncRNAs are mostly transcribed from intergenic regions, including antisense RNA transcripts, pseudogenes, and truncated transcripts [6]. Some lncRNAs overlap with or are interspersed between protein-coding transcripts [7]. Studies have shown that lncRNAs can upregulate and downregulate gene expression by modulating mRNA transcription, splicing, export, stability, and translation [7].

In plants, emerging research has identified the function of a few lncRNAs. *Enod40* was the first lncRNA discovered and was identified in *Medicago truncatula*; *Enod40* is induced at specific stages of plant development and functions in nodulation [8]. Work in *Arabidopsis thaliana* identified another lncRNA, *COOLAIR*, an antisense transcript of *FLOWERING LOCUS C* (*FLC*). *COOLAIR* represses the transcription of *FLC* in vernalization, a biological switch induced by cold temperatures, which induce flowering in the spring. This finding showed that lncRNAs play important regulatory functions in plant responses to environmental changes [9]. To date, approximately 49,000 putative lncRNAs have been identified in nine plant species including *A. thaliana*, *Zea mays*, *Triticum aestivum*, *Medicago sativa*, *Setaria italica*, *Populus trichocarpa*, *Brassica rapa*, and *Lycopersicon esculentum*. All of these putative lncRNAs play various roles in response to different biotic and abiotic stresses including infection by *Sclerotinia sclerotiorum*, tomato yellow leaf curl virus (TYLCV), stripe rust, and *Fusarium oxysporum*, as well as drought stress, heat stress, cold stress, osmotic stress, hypoxic stress, and nitrogen or phosphate deficiency.

Advances in high-throughput sequencing techniques will rapidly identify many more lncRNAs that function in the responses to different stresses. In this review, we first discuss the role of lncRNAs in plant stress tolerance, including stress-responsive lncRNA biogenesis, classification, and identification. Next, we describe the

transcriptional regulation of lncRNAs, the relationship between lncRNAs and epigenetics, and how lncRNAs affect small RNA pathways.

2 Biogenesis of Stress-Responsive lncRNAs

LncRNAs are transcribed from different regions of the genome and can be divided into four main categories according to their relationship to nearby protein-coding genes: (1) Sense lncRNAs are transcribed from the same strand as the protein-coding gene and usually overlap with one or more exons. (2) Antisense lncRNAs are transcribed from the opposite strand as the protein-coding gene. (3) Intronic lncRNAs and (4) intergenic lncRNAs (lincRNAs) are transcribed from introns or the regions between two genes on the same strand, respectively [10, 11].

In plants, intergenic transcription is performed by RNA Polymerase II (Pol II) [12]. Typically, lncRNAs transcribed by Pol II contain a 5′ cap and are polyadenylated at the 3′ end [13]. Two additional RNA polymerases, Pol IV and Pol V, have evolved from Pol II in plants through duplication and subfunctionalization of Pol II subunit genes. They specifically function to mediate RNA-directed DNA methylation and transcriptional silencing of retrotransposons and heterochromatic repeats [14–16]. Wierzbicki et al. [17] found that Pol V also produces lncRNAs, with some involvement of Pol II [12, 17]. Pol V-produced lncRNAs probably function in binding scaffolds for ARGONAUTE4 (AGO4_complexes with small interfering RNAs (siRNAs) [18]. Specific transcription factors, transcription elongation factors, and the mediator/histone modification complex are also necessary for transcription of lncRNAs [19]. Di et al. showed that lnc-173 and lnc-225 in *Arabidopsis* are potentially regulated by high light and PIF (PHYTOCHROME-INTERACTING FACTOR) transcription factors [20]. *COLD-ASSISTED INTRONIC NONCODING RNA* (*COLDAIR*), an intronic lncRNA, is required to establish stable, repressive chromatin at the *FLC* locus through its interaction with Polycomb Repressive Complex 2 (PRC2) and the P-TEFb transcription elongation factor [21, 22].

LncRNAs range in size from approximately 200 nt to over 100 kb and approximately 40–50% of lncRNA genes contain introns [13, 23, 24]. Thus, splicing is an important step in lncRNA biogenesis. The cap-binding proteins CPB20 and CBP80, with the associated protein SERRATE, regulate the biogenesis of approximately 20% of lncRNAs [13]. Primary transcripts of unspliced lncRNAs accumulate in *cpb20* and *cbp80* mutants [13, 25]. Many introns affect transcription, nuclear export of RNA, and suppression of the RNA silencing pathway [26–28]. Similar to mRNAs, the accurate splicing of introns is a key step in lncRNA biogenesis.

UP-frameshift (UPF) proteins are necessary factors for the nonsense-mediated decay (NMD) pathway to monitor the quality of lncRNAs [29]. The Arabidopsis upf mutants accumulated high levels of aberrant noncoding transcripts derived from protein-coding genes, intergenic regions, and natural antisense regions [30]. Although many studies have demonstrated that a deficiency of certain splicing factors affects the splicing of lncRNAs, the intron sequences of lncRNAs have not yet been characterized on a genome-wide scale and whether the intron sequences of lncRNAs and mRNA are different remains unclear.

RNA degradation also posttranscriptionally regulates lncRNAs. The exosome complex plays a central role in RNA metabolism and in *Arabidopsis*, a high abundance of lncRNAs negatively correlates with exosome activities [31]. Shorter poly (A) tails may explain why some lncRNAs are more sensitive to exosome-mediated degradation [32, 33]. The above studies suggest that the biogenesis of many polyadenylated lncRNAs is subject to mechanisms similar to those that regulate mRNA biogenesis.

Recent work in *Arabidopsis* and rice has also detected non-polyadenylated lncRNAs [34, 35]. Non-polyadenylated lncRNAs can be circular in structure, like circular RNAs (cRNAs), and are generated from back-spliced exons [36–38]. However, the mechanism by which non-polyadenylated lncRNAs form circular structures is still unclear.

3 The Functions of lncRNAs in Plants

LncRNAs function in *cis* and in *trans*. *Cis*-acting lncRNAs function near the site of synthesis and act directly on one or several contiguous genes on the same strand or chromosome. By contrast, *trans*-acting lncRNAs diffuse from the site of synthesis and can act directly on many genes at great distances, even on other chromosomes [39]. Their abundance may affect whether lncRNAs function in *cis* or *trans*: lncRNAs with low abundance likely act in *cis* and lncRNAs with higher abundance likely act in *trans* [40].

LncRNAs also can be processed into 21- to 24-nt small RNAs (smRNAs) (Fig. 1; Table 1). Some lncRNAs can form double-stranded RNA duplexes with natural antisense transcripts (NAT) to produce smRNAs and carry out their regulatory functions. In *Arabidopsis*, the transcripts of a Rab2-like small GTP-binding protein gene and a pentatricopeptide repeat protein-like gene produce an NAT pair from their complementary region processing of this NAT pair produces an endogenous siRNA [47]. Song et al. found two lncRNAs in *Populus simonii*, Psi-lncRNA00020674 and Psi-lnc00201294, which overlap with the genomic regions that produce the conserved miRNA166a and the *Populus*-specific miRNA27, suggesting that these lncRNAs may be the precursors of these miRNAs [48].

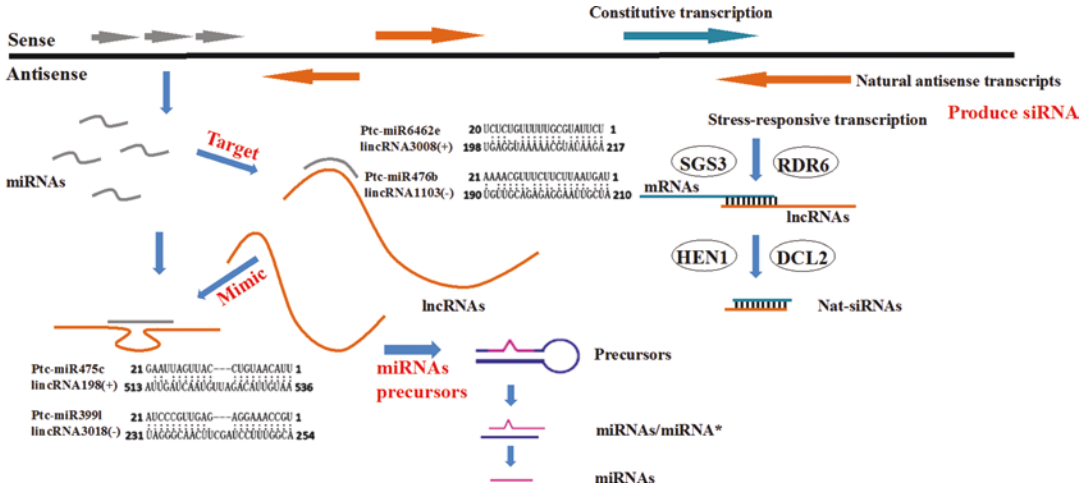

Fig. 1 Schematic diagram of stress-responsive lncRNAs involved in the small RNA pathway. Data of lncRNA mimics and targets of miRNA were cited from Shuai et al. [41]

LncRNAs can also function as miRNA target mimics; lncRNAs carrying an miRNA response element (MRE) can act as "sponges" for miRNAs, competing with the target mRNA for miRNA binding and thus blocking the action of the miRNA and relieving repression of its target gene [49]. In *Arabidopsis*, miRNA399 functions in regulating phosphate balance and is induced under phosphate deficiency [50]. *PHO2*, which encodes an E2 ubiquitin conjugase-related enzyme, is targeted by miR399. The lncRNA IPS1 (Induced by Phosphate Starvation 1) has a 23-nt motif that is partially complementary to miR399 and has a 3-nt central mismatch at the site where the miR399-mediated cleavage of *PHO2* mRNA occurs. Phosphate deficiency simultaneously induces IPS1 and *PHO2* [51]. IPS1, as a noncleavable target mimic and competitor to *PHO2*, can bind miR399 and weaken the miR399-mediated repression of *PHO2* [51] (Table 2).

LncRNAs can regulate transcription by affecting transcription factor binding to promoter regions [59]. In *Arabidopsis*, the lncRNA COOLAIR, which is produced by NAT from the *FLC* gene, can trigger the formation of a stable RNA–DNA triplex and an R-loop a single-stranded DNA [60, 61]. R-loop recruit inhibits factor of COOLAIR transcription, and *AtNDX*, resulting in repression of *FLC* (Table 2).

LncRNAs also function in protein–protein interactions [62], protein modification [63], assembly of protein complexes [64, 65], and subcellular protein localization [66, 67]. In *Medicago truncatula*, the enod40 RNA, together with RNA-Binding Protein 1 (MtRBP1), translocates from nuclear speckles to the cytosol in root cells during nodule development. In contrast, MtRBP1 is retained in the nucleus when enod40 is repressed [8, 68].

Table 1
Stress-responsive lncRNAs involved in the small RNA pathway

LncRNA	Type	Small RNA	Stress	Species	Expression pattern	Refs.
TalnRNA5	miRNA precursors	Ta-miR2004	Heat, Powdery mildew	*Triticum aestivum*	Induced	Xin et al. [42]
TahlnRNA27	miRNA precursors	Ta-miR2010	Heat stress	*Triticum aestivum*	Induced	Xin et al. [42]
TapmlnRNA8	miRNA precursors	Ta-miR2066	Powdery mildew	*Triticum aestivum*	Induced	Xin et al. [42]
TapmlnRNA19	miRNA precursors	Ta-miR2004	Powdery mildew	*Triticum aestivum*	Induced	Xin et al. [42]
TapmlnRNA2	Produce siRNA	siRNA	Powdery mildew	*Triticum aestivum*	Induced	Xin et al. [42]
TapmlnRNA7	Produce siRNA	siRNA	Powdery mildew	*Triticum aestivum*	Induced	Xin et al. [42]
TapmlnRNA9	Produce siRNA	siRNA	Powdery mildew	*Triticum aestivum*	Induced	Xin et al. [42]
TapmlnRNA11	Produce siRNA	siRNA	Powdery mildew	*Triticum aestivum*	Induced	Xin et al. [42]
TapmlnRNA15	Produce siRNA	siRNA	Powdery mildew	*Triticum aestivum*	Induced	Xin et al. [42]
TapmlnRNA16	Produce siRNA	siRNA	Powdery mildew	*Triticum aestivum*	Induced	Xin et al. [42]
TapmlnRNA23	Produce siRNA	siRNA	Powdery mildew	*Triticum aestivum*	Induced	Xin et al. [42]
TapmlnRNA24	Produce siRNA	siRNA	Powdery mildew	*Triticum aestivum*	Induced	Xin et al. [42]
TapmlnRNA26	Produce siRNA	siRNA	Powdery mildew	*Triticum aestivum*	Induced	Xin et al. [42]
TapmlnRNA28	Produce siRNA	siRNA	Powdery mildew	*Triticum aestivum*	Induced	Xin et al. [42]
TapmlnRNA29	Produce siRNA	siRNA	Powdery mildew	*Triticum aestivum*	Induced	Xin et al. [42]
TapmlnRNA31	Produce siRNA	siRNA	Powdery mildew	*Triticum aestivum*	Induced	Xin et al. [42]
TapmlnRNA32	Produce siRNA	siRNA	Powdery mildew	*Triticum aestivum*	Induced	Xin et al. [42]

TapmlnRNA34	Produce siRNA	siRNA	Powdery mildew	*Triticum aestivum*	Induced	Xin et al. [42]
TapmlnRNA38	Produce siRNA	siRNA	Powdery mildew	*Triticum aestivum*	Induced	Xin et al. [42]
TalnRNA21	Produce siRNA	siRNA	Heat stress	*Triticum aestivum*	Induced	Xin et al. [42]
TahlnRNA3	Produce siRNA	siRNA	Heat stress	*Triticum aestivum*	Induced	Xin et al. [42]
TahlnRNA14	Produce siRNA	siRNA	Heat stress	*Triticum aestivum*	Induced	Xin et al. [42]
TahlnRNA19	Produce siRNA	siRNA	Heat stress	*Triticum aestivum*	Induced	Xin et al. [42]
TahlnRNA36	Produce siRNA	siRNA	Heat stress	*Triticum aestivum*	Induced	Xin et al. [42]
TahlnRNA41	Produce siRNA	siRNA	Heat stress	*Triticum aestivum*	Induced	Xin et al. [42]
TahlnRNA42	Produce siRNA	siRNA	Heat stress	*Triticum aestivum*	Induced	Xin et al. [42]
TahlnRNA47	Produce siRNA	siRNA	Heat stress	*Triticum aestivum*	Induced	Xin et al. [42]
TahlnRNA52	Produce siRNA	siRNA	Heat stress	*Triticum aestivum*	Induced	Xin et al. [42]
IPS1	Target mimic	miR399	Phosphate deficiency	Arabidopsis	Induced	Bari et al. [43]
pti-MIR5472	miRNA precursors	miR5472	Phosphate deficiency	*Phaeodactylum tricornutum*	Induced	Cruz de Carvalho et al. [44]
pti-MIR5471	miRNA precursors	miR5471	Phosphate deficiency	*Phaeodactylum tricornutum*	Induced	Cruz de Carvalho et al. [44]
lincRNA1128	Target mimic	ptc-miR482a.1	Drought stress	*Populus trichocarpa*	Repressed	Shuai et al. [41]
lincRNA1393	Target mimic	ptc-miR6459b	Drought stress	*Populus trichocarpa*	Repressed	Shuai et al. [41]

(continued)

Table 1
(continued)

LncRNA	Type	Small RNA	Stress	Species	Expression pattern	Refs.
lincRNA3018	Target mimic	ptc-miR399i	Drought stress	*Populus trichocarpa*	Repressed	Shuai et al. [41]
lincRNA2752	Target mimic	ptc-miR169o	Drought stress	*Populus trichocarpa*	Induced	Shuai et al. [41]
lincRNA1795	Target mimic	ptc-miR476a	Drought stress	*Populus trichocarpa*	Repressed	Shuai et al. [41]
lincRNA20	Target mimic	ptc-miR476a	Drought stress	*Populus trichocarpa*	Induced	Shuai et al. [41]
lincRNA2623	Target mimic	ptc-miR156k	Drought stress	*Populus trichocarpa*	Repressed	Shuai et al. [41]
lincRNA2623	Target mimic	ptc-miR156c	Drought stress	*Populus trichocarpa*	Repressed	Shuai et al. [41]
lincRNA967	Target mimic	ptc-miR6462e	Drought stress	*Populus trichocarpa*	Not responsive	Shuai et al. [41]
lincRNA2762	Target mimic	ptc-miR156k	Drought stress	*Populus trichocarpa*	Repressed	Shuai et al. [41]
lincRNA1449	Target mimic	ptc-miR156k	Drought stress	*Populus trichocarpa*	Not responsive	Shuai et al. [41]
lincRNA179	Target mimic	ptc-miR156a	Drought stress	*Populus trichocarpa*	Not responsive	Shuai et al. [41]
TCONS_00012499	miRNA precursors	miR156	*S. sclerotiorum* infection	*Brassica napus*	Induced	Joshi et al. [45]
TCONS_00004577	miRNA precursors	miR156	*S. sclerotiorum* infection	*Brassica napus*	Induced	Joshi et al. [45]

TCONS_00004034	miRNA precursors	miR156	*S. sclerotiorum* infection	*Brassica napus*	Induced	Joshi et al. [45]
TCONS_00009614	miRNA precursors	miR156	*S. sclerotiorum* infection	*Brassica napus*	Induced	Joshi et al. [45]
TCONS_00015411	miRNA precursors	miR156	*S. sclerotiorum* infection	*Brassica napus*	Induced	Joshi et al. [45]
TCONS_00006568	miRNA precursors	miR169	*S. sclerotiorum* infection	*Brassica napus*	Induced	Joshi et al. [45]
TCONS_00018692	miRNA precursors	miR169	*S. sclerotiorum* infection	*Brassica napus*	Induced	Joshi et al. [45]
TCONS_000017152	miRNA precursors	miR169	*S. sclerotiorum* infection	*Brassica napus*	Induced	Joshi et al. [45]
TCONS_00008591	miRNA precursors	miR169	*S. sclerotiorum* infection	*Brassica napus*	Induced	Joshi et al. [45]
TCONS_000010926	miRNA precursors	miR169	*S. sclerotiorum* infection	*Brassica napus*	Induced	Joshi et al. [45]
TCONS_00027961	miRNA precursors	miR394	*S. sclerotiorum* infection	*Brassica napus*	Induced	Joshi et al. [45]
TCONS_00027962	miRNA precursors	miR394	*S. sclerotiorum* infection	*Brassica napus*	Induced	Joshi et al. [45]
TCONS_00011200	miRNA precursors	miR394	*S. sclerotiorum* infection	*Brassica napus*	Induced	Joshi et al. [45]
Slylnc0195	Target mimic	miR166	TYLCV infection	*Solanum lycopersicum*	Induced	Wang et al. [46]
Slylnc1077	Target mimic	miR399	TYLCV infection	*Solanum lycopersicum*	Repressed	Wang et al. [46]

Table 2
Function of lncRNA in response to biotic and abiotic stress in plants

LncRNA	Species	Stress	Regulation mechanism	Expression	Refs.
asHSFB2a	*Arabidopsis thaliana*	Heat stress	Antisense transcription	Induced	Wunderlich et al. [52]
COOLAIR	*Arabidopsis thaliana*	Cold stress	Promoter interference	Induced	Csorba et al. [53]; Marquardt et al. [54]
COLDAIR	*Arabidopsis thaliana*	Cold stress	Histone modification	Induced	Heo and Sung [21]
IPS1	*Arabidopsis thaliana*	Phosphate deficiency	Target mimicry	Induced	Franco-Zorrilla et al. [51]
Cis-NAT PHO1;2	*Oryza sativa*	Phosphate deficiency	Translation enhancer	Induced	Jabnoune et al. [55]
AtR8	*Arabidopsis thaliana*	Hypoxic stress	*trans*-acting factor	Repressed	Listerman et al. [56]; Wu et al. [57]
slylnc0195	*Solanum lycopersicum*	TYLCV infection	Targets of miRNAs	Induced	Wang et al. [46]
slylnc0049	*Solanum lycopersicum*	TYLCV infection	Unknown	Induced	Wang et al. [46]
TAR-66	*Arabidopsis thaliana*	*Fusarium oxysporum* infection	Unknown	Induced	Zhu et al. [58]
TAR-67	*Arabidopsis thaliana*	*Fusarium oxysporum* infection	Unknown	Induced	Zhu et al. [58]
TAR-191	*Arabidopsis thaliana*	*Fusarium oxysporum* infection	Unknown	Induced	Zhu et al. [58]
TAR-212	*Arabidopsis thaliana*	*Fusarium oxysporum* infection	Unknown	Induced	Zhu et al. [58]
TAR-224	*Arabidopsis thaliana*	*Fusarium oxysporum* infection	Unknown	Induced	Zhu et al. [58]

In *Arabidopsis*, at least 376 RBPs have been found that can potentially associate with lncRNAs to execute their functions and some of these RBPs have specific regulatory roles in plant development and stress responses [69].

LncRNAs also function in epigenetic regulation. Plants use all of the major epigenetic mechanisms present in eukaryotes, including DNA methylation, histone modification, and chromatin formation/remodeling [70]. DNA methylation is a strand-specific epigenetic mark and is commonly associated with gene silencing. Because lncRNAs have strand-specific distribution and expression patterns, lncRNAs are ideal regulators of DNA methylation. LncRNAs can form double-stranded RNA duplexes with NATs to produce siRNAs called NAT-siRNAs. Most NAT-siRNAs are produced in response to stress [71]. SiRNAs are key components of the RNA-directed DNA methylation pathway. Zhang et al. found that methylation interactions were characterized by an abundance of 24-nt small interfering RNAs in *Arabidopsis* [72]. In *Arabidopsis*, approximately 49% of lincRNAs overlap with transposable elements or repeats, producing the so-called repeat-containing lncRNAs [13, 73, 74]. These repeat-containing lncRNAs can also generate smRNAs.

Chromatin modifications, including histone methylation, acetylation, phosphorylation, ubiquitination, and SUMOylation, can regulate transcription in plants [75]. In the *Arabidopsis* genome, the *FLC* region has decreased levels of acetylation of lysine 9 and increased trimethylation of lysine 27 of histone 3 resulting in downregulation of *FLC* expression. In contrast, trimethylation of lysine 4 and lysine 36 of histone 3 increases *FLC* expression [76–80]. At cold temperatures, two lncRNAs, COLDAIR and COOLAIR, are transcribed from an intronic region and an antisense strand of the *FLC* gene, respectively, and directly interact with PRC2 to modify vernalization-mediated epigenetic repression on the *FLC* locus and repress *FLC* expression [21, 53, 54].

4 Role of lncRNAs in Plant Stress Tolerance

4.1 Temperature Stress

Work in wheat has identified 77 heat stress-responsive lncRNAs [42]. These lncRNAs have no homologs or significant matches in other plants, suggesting that wheat has evolved specific lncRNAs to regulate gene expression and cell activity. Among these heat stress-responsive lncRNAs, TalnRNA9 was differentially expressed in plant tissues including the leaves and flag leaf, suggesting that precise, tissue-specific regulatory mechanisms exist in wheat. Among these lncRNAs, TalnRNA5, TapmlnRNA8, TapmlnRNA19, and TahlnRNA27 were characterized as putative miRNA precursors. TapmlnRNA8 and TapmlnRNA19 were specific to powdery

mildew infection and TahlnRNA27 was specific to heat stress. TalnRNA5 and TapmlnRNA19 gave rise to the same miRNA, but they displayed distinctly different expression patterns, indicating that this miRNA could potentially be produced by different precursors under different stresses.

Heat stress transcription factors (HSFs) were originally identified as central regulators of heat stress responses. In *Arabidopsis*, *HSFB2a* is regulated by a natural, antisense lncRNA, *asHSFB2a*, which is involving in vegetative and gametophytic development [52]. Gene expression patterns and motif analysis showed one perfect heat shock element upstream of the transcription start sites of the heat-inducible genes *HSFB2a* (22 bp upstream) and *asHSFB2a* (71 bp upstream). AsHSFB2a is only expressed after heat stress and is dependent on the activity of HSFA1a/HSFA1b in leaves. By contrast, *HSFB2a* and *asHSFB2a* RNAs were also present in the absence of heat stress in the female gametophyte. Transgenic manipulations of *HSFB2a* and *asHSFB2a* showed that any deletion of these genes impaired the development of female gametophytes, suggesting that a dynamic balance of *HSFB2a* and *asHSFB2a* is necessary for the development of the female germline [52].

Vernalization is one of the best-studied plant responses to cold temperatures. In *Arabidopsis*, the *FLC* gene, a repressor of flowering time under cold temperature, regulated by the lncRNAs *COOLAIR* and *COLDAIR*, which are transcribed in the antisense orientation of the *FLC* gene and the intron of the *FLC* gene in the sense orientation, respectively [21, 42, 54]. In *FLC*, deacetylation of lysine 9 and trimethylation of lysine 27 of histone 3 have been found to be associated with *FLC* repression, whereas trimethylation lysine 4 and lysine 36 of histone 3 are positively correlated with *FLC* expression at cold temperatures [76, 79]. The RNA-binding proteins FCA and FPA, which contain a plant-specific RNA recognition motif, function in pre-mRNA processing, RNA polyadenylation, alternative splicing, RNA stability, RNA editing, mRNA export, RNA formation, and RNA degradation, and are negative regulators of *FLC* [80, 81]. FCA and FPA may be necessary for chromatin modifications of the *FLC* locus, implying that regulatory interactions may occur between RNA-binding and chromatin modification [79, 82–84].

Work in *Brassica rapa* identified 10,001 lncRNAs produced under cold and heat stress [85]. Among these lncRNAs, 9687 are novel lncRNAs and 50 are miRNA precursors. Of the lncRNAs, 468, 107, 14, 73, and 244 lncRNAs are show temperature-specific expression at −4, 0, 4, 25, and 44 °C, respectively. A total of 2236 lncRNAs were expressed in all the treatments. To investigate the relationship between temperature-responsive lncRNAs and protein-coding genes, co-expression networks were constructed and target genes were annotated. The results showed that most of the 67 targets of cold-responsive lncRNAs belonged to the cold response

proteins, such as CBF1, COR6.6, and LEA14, most of the 192 targets of heat-responsive lncRNAs belonged to heat response genes, such as *HSP*, *LTP*, and *CBF4*. Several of the targets, such as *KIN2*, were detected under cold and heat stress, implying that they might play important roles in the cross talk between cold and heat stress responses.

4.2 Phosphate and Nitrogen Stress

The essential elements phosphorus (P) and nitrogen (N) are often limiting nutrients for plant growth and development. The PHOSPHATE1 (PHO1) and PHO2 complex functions in phosphate loading into the xylem and is a key regulator of phosphate homeostasis in *Arabidopsis* [86]. *PHO2* encodes a ubiquitin-conjugating E2 enzyme and *PHO2* mRNA is targeted by miR399 [43]. Under phosphate deficiency, the lncRNA *IPS1* is induced and acts as a target mimic for miR399, implying that *IPS1* might be a positive regulator for phosphate homeostasis [51]. By contrast, *cis*-natural antisense RNAs transcribed from the *PHO1; 2* antisense strands have been identified as translational enhancers for the expression of its sense gene in rice [55].

In *Phaeodactylum tricornutum*, 1510 putative lincRNAs have been identified in response to P deficiency. Among these, 202 lncRNAs were specifically upregulated in response to P deficiency and downregulated when P was resupplied to the medium. Two lncRNAs, pti-MIR5472 and pti-MIR5471, have been identified as precursors of annotated miRNAs and were also significantly upregulated in response to P stress in *P. tricornutum* [44]. Among the most strongly upregulated lincRNAs in P stress, only two were significantly upregulated under N stress, revealing specific responses of the noncoding transcriptome to nutrient stress conditions.

In *Zea mays*, 7245 putative lncRNAs have been identified under N stress, including 6211 lncRNAs transcribed from intergenic regions and 1034 located within an intron of a protein-coding gene [87]. Among these lncRNAs, 637 (620 intergenic and 17 intronic) were differentially expressed under N stress. Co-expression network analysis showed that most of the lncRNAs (32 of 33) were enriched in a module, which comprises 32 N-responsive intergenic and intronic lncRNAs and 239 maize protein-coding genes. Gene ontology (GO) enrichment results indicated that oxidative phosphorylation, generation of precursor metabolites, oxidative reduction, and energy were been enriched in the biological process category. For molecular function, NADH dehydrogenase activity and oxidoreductase activity were significantly enriched among the identified GO categories.

4.3 High-Light Stress

Light is an important signal for plant development and response to environmental changes. In *Arabidopsis*, 37,238 sense–antisense transcript pairs have been found in response to high-light. Approximately 70% of *Arabidopsis* genes produce one or more antisense

transcripts [24]. Some transcripts may be involved in two or more pairs, e.g., AT1G05291 shares complementary sequences with two lncNATs, AT1TU005650 and AT1TU005660, at the 5′ and the 3′ end, respectively. Expression profiles of sense–antisense pairs showed spatial and developmental-specific light effects on 626 concordant and 766 discordant NAT pairs. Research showed that changes in the expression of 40–50% of light-responsive sense/antisense transcripts correlated with H3K9ac and/or H3K27ac, suggesting that a large number of the light-responsive NAT pairs are associated with histone modification peaks, and histone acetylation is dynamically correlated with the light-responsive expression changes of NATs. These results provide insight into possible antisense-mediated histone modification of sense transcripts in response to light, assuming a group of *Arabidopsis* antisense transcripts may direct histone modifications and regulate the expression of sense transcripts [24].

4.4 Hypoxic Stress

Twenty novel Pol III-dependent lncRNAs have been identified in *Arabidopsis* [57]. Among these, a root-specific AtR8 RNA that has a conserved promoter structure typically observed in U small nuclear RNA (snRNA) genes was selected as a candidate to study the function, precise location, stress response, and taxonomic conservation of these lncRNAs. AtR8 RNA showed no similarities to any protein-coding gene, either in sense or antisense and there are no target genes that specifically interact with it. Transcription of the AtR8 RNA and U6 snRNA genes is driven by the same type of promoter (Pol III). Unlike the constitutive expression of Pol III-dependent genes, AtR8 snRNA shows root specificity and increased accumulation under hypoxic conditions. Considering that Pol II accumulates upstream of the Pol III-dependent U6 snRNA gene in vivo and enhances transcription by Pol III in humans [56], AtR8 RNA might be regulated by *trans*-acting factors, one of which might be Pol II [57].

4.5 Drought Stress

Genome-wide systematic identification of drought stress-responsive lncRNAs in foxtail millet [88] identified 584 lncRNAs (494 lincRNAs and 90 NATs), ranging from 210 to 4168 nt. Of the lncRNAs, 35.45% harbored one or several introns and had twofold lower expression levels than the mean expression levels of the protein-coding genes. In total, 1489 of the lincRNAs and 126 of the NATs show conserved expression in foxtail millet and sorghum. Approximately 9% (51 lncRNAs) shared sequence conservation with their counterparts in sorghum, while 13 of the lncRNA pairs possessed synteny. Differential expression analysis showed that 19 lncRNAs (17 lincRNAs and 2 NATs) in foxtail millet responded to PEG-induced osmotic stress. Among these lncRNAs, only one of the drought-responsive lncRNAs had synteny with its sorghum counterpart. The expression of lincRNAs and neighboring

protein-coding genes showed no significant correlation. Two drought-responsive NATs were antisense overlapping transcripts of Si003758m and Si038715m. Si003758m is a homolog of the *Arabidopsis SAG21* gene, which has a role in oxidative stress tolerance and was induced by drought stress [89, 90]. Si003758m had two predicted antisense transcripts that contained overlapping regions at both ends of the sense partner. Si038715m encodes a hydroxyproline-rich glycoprotein family protein (HRGP), which is an important component of the plant cell wall and plays crucial roles in response to pathogens [91]. The antisense Si038715m transcript was a 3′ tail-to-tail transcript that ended within the second exon of Si038715m and overlapped with the last 74 nucleotides of the sense transcript. Under PEG-induced osmotic stress conditions, both the sense and antisense transcripts of Si003758m exhibited significantly increased expression, while the Si038715m transcript and its complementary lncRNA both exhibited significantly decreased expression, suggesting that the regulatory mechanisms of lncRNAs in response to drought stress may exist and are flexible. In *Medicago truncatula*, 7863 and 5561 lncRNAs were identified from osmotic stress-treated leaf and root samples, respectively. The transcript levels of 7863 lncRNAs in leaves and 5561 lncRNAs in roots changed in response to the osmotic stress. The expression of 1783 lncRNAs changed in both leaves and roots under osmotic stress [92].

Work in woody plants identified 2542 lincRNA candidates in *P. trichocarpa*, 504 of which were found to be drought responsive [41]. Fifty-one lincRNAs and 20 lincRNAs were identified as putative targets and target mimics of known *Populus* miRNAs. Among these, ptc-miR482a.1, ptc-miR476a, and ptcmiR156c were identified as targets or mimics of drought stress-responsive lncRNAs. LincRNA262 and lincRNA2623 is the target and target mimic of ptc-miR156c, respectively, while lincRNA1310 is a target of ptc-miR476a. LincRNA1851 has two target mimics, lincRNA20 and lincRNA1795. By contrast, Ptc-miR482a.1 was regulated by three lincRNAs (lincRNA1128, lincRNA1828, and lincRNA2623) through mimicry and regulates four lincRNAs (lincRNA1078, lincRNA1203, lincRNA2213, and lincRNA2252) and 27 disease-resistance transcripts through degradation, implying that it might be a key component of a subnetwork of the transcriptome.

4.6 Salt Stress

In *Medicago truncatula*, 7361 and 7874 lncRNAs were identified from salt stress-treated leaf and root samples, respectively [92]. GO terms were then examined for the genes that overlap with or are neighbors of the stress-responsive lncRNAs. This identified enrichment of GO terms in biological processes such as signal transduction, energy synthesis, molecule metabolism, detoxification, transcription, and translation. Expression analysis showed that 2148 lncRNAs changed in both leaves and roots under salt

stress. In leaves, more than half of the stress-responsive lncRNAs were common between osmotic stress (59.6%) and salt stress (63.7%). However, in roots, these values decreased to 47.0% and 33.2%, respectively. GO term enrichment analysis of co-expressed and neighboring genes (<100 kb) of lncRNAs showed that carbonate dehydratase activity, biotin carboxylase activity, structural constituents of ribosomes, zinc ion binding, and rRNA binding were enriched in the molecular functions category. For biological processes, carbon utilization and translation terms were enriched. In roots, GO term enrichments were greater than those in leaves, suggesting that roots are more sensitive to salt stress than leaves. Functional enrichment analysis showed that the stress-responsive lncRNAs may regulate genes involved in many biological processes in response to salt stress, including signal transduction, energy synthesis, molecule metabolism, detoxification, transcription, and translation. Interacting networks of co-expressed and neighboring genes (<100 kb) of lncRNAs showed that 13 protein-coding genes involved in oxidation/reduction reactions, transcription, energy synthesis, and signal transduction were regulated by the lncRNAs TCONS_00072494, TCONS_00074334, and TCONS_00075203. MYB and zinc finger families were regulated by TCONS_00119988. The lncRNA TCONS_00047650 was expressed from the regulatory region of the Medtr3g 069280 gene encoding phosphatidylinositol-specific phospholipase C, which hydrolyzes phosphatidylinositol 4,5-bisphosphate to the secondary messenger molecules inositol 1,4,5-trisphosphate and diacylglycerol [93], suggesting that TCONS_00047650 might affect signal transduction networks through regulation of the Medtr3g 069280 gene. The lncRNA TCONS_00116877, located approximately 3.9 kb upstream of Medtr7g094600 and encoding glutathione peroxidase, was upregulated in roots, implying that TCONS_00116877 may be involved in regulating plant tolerance to oxidative stress by modifying the expression of *POD*. Medtr1g081900, which codes for a vacuolar Na^+/H^+ antiporter mediating Na^+ influx into the vacuoles, was induced by salt stress in roots [94]. TCONS_00020253 has been found transcribed upstream of Medtr1g081900, suggesting that TCONS_00020253 might be a regulator of Medtr1g081900.

4.7 Biotic Stress

Sclerotinia sclerotiorum can cause *Sclerotinia* stem rot, which is a significant disease of canola (*Brassica napus*) worldwide. Considering that lncRNAs play important roles in the regulation of gene expression in plants, novel lncRNAs were identified that are responsive to *S. sclerotiorum* infection in *B. napus* at two time points after infection (24 and 48 hpi) [45]. In total, 3181 novel lncRNAs have been found including 2821 lincRNAs, 111 natural antisense transcripts, 76 with exonic overlap with the reference coding transcripts, and 173 novel lncRNA isoforms. Forty-one

lncRNAs were identified as the precursors for miRNAs, including miR156, miR169, and miR394, with significant roles in mediating plant responses to fungal pathogens. Among the identified lncRNAs, 2200 and 961 were assigned positions across nine and ten chromosomes of the CC (*B. oleracea*) and AA (*B. rapa*) genomes, respectively, suggesting that the CC genome contributed a larger number of lncRNAs to *B. napus*. In *B. oleracea*, 74.7% of lncRNAs were enriched in chromosome 6 and chromosome 7, including the majority of the stress-responsive *B. napus* lncRNAs. In the *B. rapa* genome, chromosome 3 had the highest number of lncRNA loci (138). Only 532 lncRNAs were conserved between the AA and CC genome, suggesting that the intergenic lncRNAs of *B. napus* may have evolved separately after speciation of *B. rapa* and *B. oleracea* or very recently after the speciation of *B. napus*. After *S. sclerotiorum* infection, 931 lncRNAs were differentially expressed. TCONS_00000966 is transcribed from the antisense strand of a plant defense gene with 90% overlapping regions and is induced at both infection stages, suggesting its involvement in the transcriptional regulation of defense responsive genes under *S. sclerotiorum* infection. Among the 2821 lincRNAs, 500 differentially expressed lncRNAs were annotated upstream and 512 differentially expressed lncRNAs were annotated at the 3′ UTR and downstream region of the coding transcripts. Nine pairs of sense/antisense transcripts that consist of the lincRNA and defense-responsive genes were significantly differentially expressed in response to *S. sclerotiorum* infection, suggesting that steric clashes of transcriptional machinery may lead to inactivation of the sense promoter [45].

The tomato yellow leaf curl virus (TYLCV) causes one of the most devastating diseases of tomato worldwide. A total of 1565 lncRNAs have been detected in control group and TYLCV-infected samples; these lncRNAs include 1074 lncRNAs expressed in both samples, 289 control group-specific lncRNAs, and 202 TYLCV-specific lncRNAs [46]. In total, 529 lncRNAs were differentially expressed between the control group and TYLCV-infected samples. Two lncRNAs that were significantly induced by TYLCV infection, slylnc0049 and slylnc0761, were selected for functional characterization. No disease symptoms of leaf curling and yellowing were observed after silencing slylnc0049 and slylnc0761, implying that candidate lncRNAs might have a function in the TYLCV regulatory network. A 5′ and 3′ rapid amplification of cDNA ends (RACE) experiment showed that slylnc0049 had a longer transcript than predicted from RNA-sequencing results. Slylnc0195 and slylnc1077 were predicted to be mimics for the conserved miRNAs miR166 and miR399, respectively. The expression of slylnc0195 has a negative correlation with miR166a. After slylnc0195 silencing, the class III HD-ZIP genes of the miR166a targets, which play important roles in plant development, showed

decreased transcript abundance, suggesting the existence of specific cross talk between slylnc0195 and the class III HD-ZIP genes through competitive binding of miR166a [46].

Fifteen lncNATs responsive to *F. oxysporum* infection were identified from *F. oxysporum*-inoculated plants at one and days post inoculation. Co-induced expression patterns of corresponding genes showed that stress-responsive *cis*-regulatory elements in the promoter regions of sense and antisense transcripts play important roles in response to *F. oxysporum* infection [58]. Of all 15 lncRNA sense–antisense pairs, none were predicted as the precursor of smRNAs, suggesting that smRNA-directed RNA silencing may not involved in the transcriptional regulation of *F. oxysporum*-responsive lncNATs. In total, 770 novel transcriptionally active regions (TARs) were found overlapping with or adjacent to (<200 bp) annotated genes, accounting for approximately 80% of TARs. Most of these TARs are transcribed in the same direction as their overlapping or adjacent genes. These observations suggested that these TARs might be independent lncRNAs associated with promoter or transcription terminator sequences or unannotated 5′ or 3′ UTR sequences of the overlapping or adjacent genes. Ten lincRNAs, which have potential antifungal functions, were investigated using knockout or knockdown plants infected with *F. oxysporum*. Faster and more severe disease symptom development was observed in five of the lines with depleted lincRNAs, indicating the importance of these lincRNAs in plant defense against *F. oxysporum* infection [58].

5 Conclusions and Future Perspectives

One focus of future research should be systematic identification of additional lncRNAs. The majority of plant lncRNAs are expressed at low levels, which may be caused by high enrichment of lncRNAs in a specific cell type or induction by a specific signal [13]. Thus, the identification of lncRNAs in specific cell types should be the focus of future studies. Isolation and collection of specific cell types combined with transcriptome analysis of single cells may provide new insights into lncRNA identification [95–97]. Meanwhile, transcriptome sequencing should be performed to a sufficient depth to enable the detection of as many lncRNAs as possible and the data sets should be submitted to the public databases for applications in other studies. Although many databases for lncRNAs have been established, including RNAcentral, lncRNAdb, TAIR, PLncDB, and PlantNATsDB [98–102], a specific database for stress-responsive lncRNAs is also needed.

Another aspect of lncRNA biology that merits additional study is the interaction of lncRNAs with transcription factors. LncRNAs play key roles in cellular functions and disease responses using

diverse mechanisms. In animals, lncRNAs can regulate the transcription machinery in many ways [103]. LncRNAs affect the DNA-binding activity of transcription factors through modifying transcription factor dimerization or trimerization [104], promoting transcription factor phosphorylation [62], or controlling transcription factor nuclear localization [105]. In addition, lncRNAs can also interact with mediator subunits and regulate mediator complex formation [105]. Another class of lncRNAs, enhancer RNAs (eRNAs), which are transcribed from the enhancer domains and/or transcription factor binding sites of genes, may regulate the transcription activities of neighboring genes through recruiting transcription activators/repressors and/or controlling chromatin topology [19, 106, 107]. Previous studies showed that stress-responsive *cis*-regulatory elements in promoter regions of sense and antisense transcripts play an important role in co-induced expression patterns. Considering the amount of lncRNAs transcribed from flanking regions of protein coding genes, their sequences may contain abundant *cis*-regulatory elements. These elements may play an important role in *cis*-regulatory function for expression of neighboring genes and the *trans*-regulatory function for expression of potential targets through recruiting transcription activators/repressors. Our recent study of heat stress-responsive lncRNAs indicated that the amount of motifs related to heat stress, including CCAATBOX1, HSE, HSELIKENTACIDICPR1, HSELIKENTGLN2, and OCSGMHSP26A enriched in the sequences of candidate lncRNAs, suggests that these motifs might be an important element for recruiting transcription factors and modifying transcription factor dimerization or trimerization (Fig. 2).

Novel and improved imaging technologies may shed light on how lncRNAs function in chromatin remodeling. TUP proteins can repress RNA Pol II processivity upstream of *fbp1* in humans [10]. The Atf1 activator binds to the UAS1 element, facilitating chromatin remodeling by RNA Pol II and the subsequent binding of Rst2 to a second UAS2 element under glucose deprivation. As further lncRNAs are transcribed, the chromatin structure around the *fbp1* initiation site is then accessible to the transcriptional machinery, allowing induction of gene expression to occur [10]. However, whether lncRNAs can facilitate chromatin remodeling in plants is still unclear. Genomic technologies that capture three-dimensional genome organization are rapidly advancing and have led to advances in the study of three-dimensional genome organization. High-throughput chromosome conformation capture (Hi-C) has been introduced as a method for identifying genome-wide higher-order chromatin interactions [108]. We believe that Hi-C can be coupled with the recent accumulation of noncoding transcriptome analyses to explore the mechanism of how lncRNAs affect chromatin remodeling in plants. The surface plasmon resonance (SPR) technique can measure biomolecular interactions in

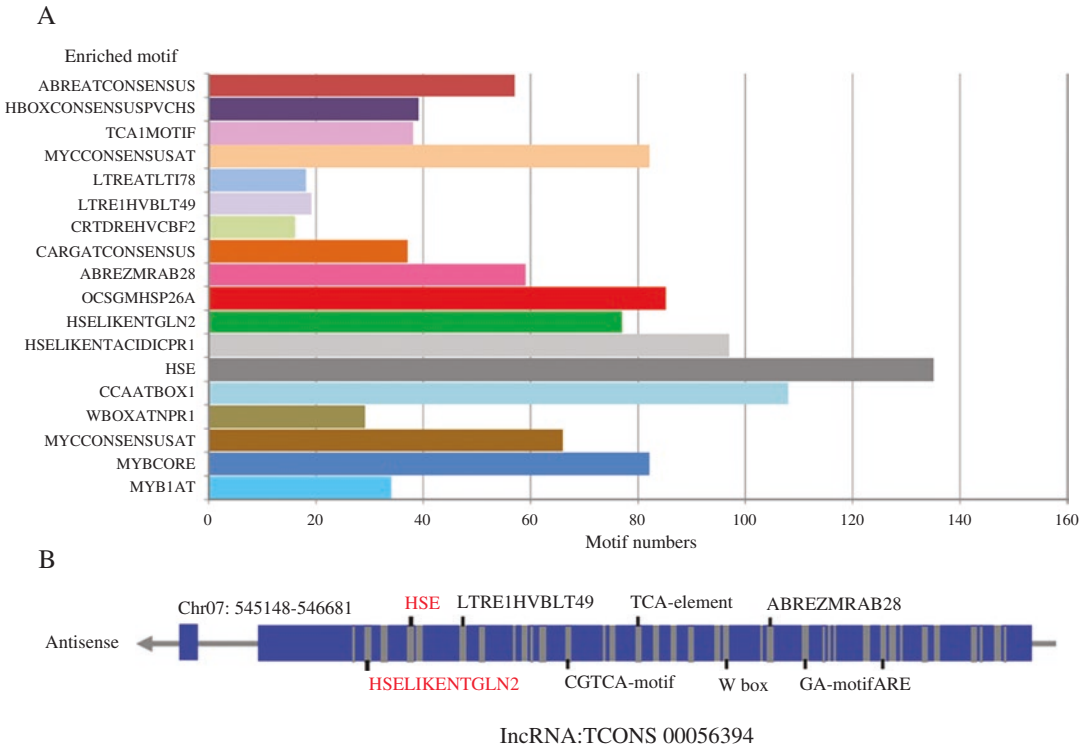

Fig. 2 Heat-responsive motifs enriched in the lncRNA body. (**a**) The number of motifs in heat-responsive lncRNAs. (**b**) The distribution of motifs in lncRNA TCONS_00056394

real-time with a high degree of sensitivity and without the need for labeling, providing a stable and high-throughput technique to validate interactions such as protein–protein, protein–nucleic acids, and nucleic acids–nucleic acids [109]. SPR is an ideal tool for validating of lncRNA–protein, lncRNA–mRNA, and lncRNA–miRNA interactions on a genome-wide level.

Another aspect of lncRNA function that remains mysterious is whether these "noncoding" RNAs can produce functional, small peptides. A string of in-frame sense codons beginning with a start codon and ending with a stop codon constitute a potentially translatable sequence that is defined as an open reading frame (ORF). ORFs are distinguished by their size; ORFs <100 codons are defined as small ORFs (sORFs). The smallest translated coding sORFs described so far is six codons long [110]. Not all sORFs are translated or are translatable [111]. Translatable sORFs have been found within the 5′ leader and 3′ trailer sequences within or overlapping with the previously known ORF of mRNAs and in various transcripts that have been previously thought to be noncoding RNAs (ncRNAs), including lncRNAs, intergenic, and antisense transcripts. Several short peptides encoded by sORFs (sPEPs) on intergenic regions and ncRNAs have been shown to be functional,

particularly in plants [111]. In legumes, *ENOD40* is expressed at an early stage in root nodule organogenesis, encoding two peptides of 12 and 24 amino acids. Both peptides specifically bind to the same 93-kDa protein, which was affinity-purified from soybean nodules [112]. The *Brk1* gene encodes a very small (approximately 8 kDa), novel peptide with no recognizable functional motifs or targeting sequences. However, database searches show this protein to be highly conserved throughout plants and animals. This conserved peptide promotes the polarized growth and division of maize leaf epidermal cells [113]. The *POLARIS* (*PLS*) gene is located within a short (500 nucleotides) auxin-inducible transcript and encodes a predicted polypeptide of 36 amino acid residues. Ectopic expression of the *PLS* ORF reduces root growth inhibition by exogenous cytokinins and increases leaf vascularization, demonstrating that PLS is required for auxin–cytokinin homeostasis to modulate root growth and leaf vascular patterning [114]. The *ROT4* ORF encodes a novel, small peptide that controls polarity-dependent cell proliferation during leaf morphogenesis [115]. Although stress-responsive lncRNAs continue to be identified in plants, the functions of the micropeptides encoded by lncRNAs in response to stress have not been reported.

RNA structure has crucial roles in processes ranging from ligand sensing to the regulation of translation, polyadenylation, and splicing [116–118] and although the RNA structures of smRNAs have been extensively examined, the role of structure in lncRNA function remains unclear. Comparisons of RNA secondary structure in vivo and in vitro reveal that RNAs might undergo conformational changes in response to stress [119]. Single nucleotide polymorphisms (SNPs) are thought to be the most widespread factor for RNA structural rearrangement. With the rapid identification of function-associated SNPs, there is a great demand to study SNPs in lncRNAs. The lncRNASNP database has been established in human and mouse and contains information on SNPs in lncRNAs and their potential functions [120]. In total, 495,729 and 777,095 SNPs in more than 30,000 lncRNA transcripts were identified in human and mouse, respectively, that had the potential to affect the miRNA–lncRNA interaction. In human and mouse lncRNAs, the average energy changes by SNPs are (1.30 ± 1.62) kcal/mol and (1.26 ± 1.27) kcal/mol [120]. SNPs in the miRNA target sites may destroy or create miRNA binding sites on lncRNAs, resulting in loss and/or gain of function of miRNA–lncRNA interactions. The presence of a large number of SNPs has the potential to disturb original miRNA target sites and/or create new potential miRNA target sites. In genome-wide association study (GWAS) results in humans, 197,827 lncRNA SNPs were found in the linkage disequilibrium regions. With advances in GWAS in plants, more genotype data will be available for the analysis of lncRNA SNPs. Our recent study on heat stress-responsive lncRNAs

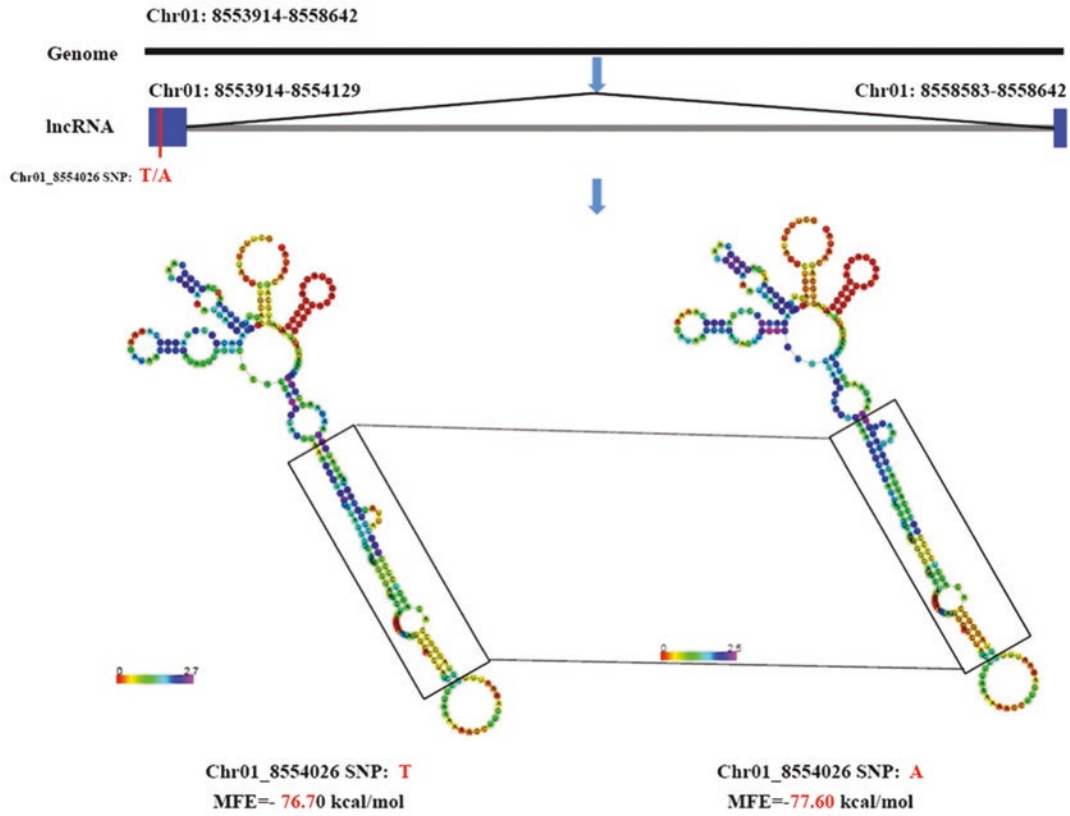

Fig. 3 SNPs of lncRNAs affect the RNA structure and minimal free energy (MFE)

indicated that a large amount of SNPs associated with temperature response are located in lncRNAs and significantly affect the RNA structure (Fig. 3). It will be interesting to further investigate the biological significance of this observation in the future.

LncRNAs can affect the RNA processing machinery through their complementary sequences, but the role of lncRNAs in splicing and other aspects of RNA processing remains an emerging, interesting story. In *Arabidopsis*, alternative splicing-competitor lncRNAs (ASCO-lncRNAs) can compete with nuclear speckle RNA-binding proteins (NSRs) with alternatively spliced mRNA targets altering the splicing pattern of mRNAs [121]. Classes of lncRNAs that lack both the 5′ cap structures and 3′ poly (A) tails have been found to be transcribed from introns [122–124]. These lncRNA ends correspond to positions of intronic small nucleolar (snoRNAs) and are named snoRNA-related lncRNAs (sno-lncRNAs). It has been demonstrated that sno-lncRNAs from the Prader–Willi syndrome critical regions and at least some of these are strongly associated with splicing factor Fox2, implying that these sno-lncRNAs may affect splicing patterns in cells [125].

Alternative splicing is a widespread mechanism that increases transcriptome complexity and proteome diversity and plays an important role in plant response to abiotic and biotic stress [126]. We believe that stress-responsive sno-lncRNAs are involved in the regulation of alternative splicing in plants and constitute an interesting topic for future lncRNA research that will provide a new insight for understanding the functions of lncRNAs.

References

1. Ashraf M, Harris PJC (2013) Photosynthesis under stressful environments: an overview. Photosynthetica 51:163–190
2. Wang WX, Vinocur B, Shoseyov O, Altman A (2001) Biotechnology of plant osmotic stress tolerance: physiological and molecular considerations. Acta Hort 560:285–292
3. Wani SH, Sah SK, Hussain MA, Kumar V, Balachandra SM (2016) Transgenic approaches for abiotic stress tolerance in crop plants. In: Al-Khayri JM, Jain SM, Johnson DV (eds) Advances in plant breeding strategies, vol 2. Agronomic, abiotic and biotic stress traits. Springer, Gewerbestrasse, pp 345–396
4. Sunkar R, Li YF, Jagadeeswaran G (2012) Functions of microRNAs in plant stress responses. Trends Plant Sci 17(4):196–203
5. Hirayama T, Shinozaki K (2010) Research on plant abiotic stress responses in the post-genome era: past, present and future. Plant J 61(6):1041–1052
6. Mercer TR, Dinger ME, Mattick JS (2009) Long non-coding RNAs: insights into functions. Nat Rev Genet 10:155–159
7. Brosnan CA, Voinnet O (2009) The long and the short of noncoding RNAs. Curr Opin Cell Biol 21:416–425
8. Campalans A, Kondorosi A, Crespi M (2004) *Enod40*, a short open reading frame-containing mRNA, induces cytoplasmic localization of a nuclear RNA binding protein in *Medicago truncatula*. Plant Cell 4(16):1047–1059
9. Swiezewski S, Liu FQ, Magusin A, Dean C (2009) Cold-induced silencing by long antisense transcripts of an Arabidopsis polycomb target. Nature 462(7274):799–802
10. Ponting CP, Oliver PL, Reik W (2009) Evolution and functions of long noncoding RNAs. Cell 136:629–641
11. Ma L, Bajic VB, Zhang Z (2013) On the classification of long non-coding RNAs. RNA Biol 10:925–933
12. Zheng B, Wang Z, Li S, Yu B, Liu JY, Chen X (2009) Intergenic transcription by RNA polymerase II coordinates Pol IV and Pol V in siRNA-directed transcriptional gene silencing in Arabidopsis. Genes Dev 23:2850–2860
13. Liu J, Jung C, Xu J, Wang H, Deng S, Bernad L, Arenas-Huertero C, Chua NH (2012) Genome-wide analysis uncovers regulation of long intergenic noncoding RNAs in Arabidopsis. Plant Cell 24:4333–4345
14. Herr AJ, Jensen MB, Dalmay T, Baulcombe DC (2005) RNA polymerase IV directs silencing of endogenous DNA. Science 308:118–120
15. Kanno T, Huettel B, Mette MF, Aufsatz W, Jaligot E, Daxinger L, Kreil DP, Matzke M, Matzke AJ (2005b) Atypical RNA polymerase subunits required for RNA-directed DNA methylation. Nat Genet 37:761–765
16. Pontier D, Yahubyan G, Vega D, Bulski A, Saez-Vasquez J, Hakimi MA, Lerbs-Mache S, Colot V, Lagrange T (2005) Reinforcement of silencing at transposons and highly repeated sequences requires the concerted action of two distinct RNA polymerases IV in Arabidopsis. Genes Dev 19:2030–2040
17. Wierzbicki AT, Ream TS, Haag JR, Pikaard CS (2009) RNA polymerase V transcription guides ARGONAUTE4 to chromatin. Nat Genet 41:630–634
18. Wierzbicki AT, Cocklin R, Mayampurath A, Lister R, Rowley MJ, Gregory BD, Ecker JR, Tang H, Pikaard CS (2012) Spatial and functional relationships among Pol V-associated loci, Pol IV-dependent siRNAs, and cytosine methylation in the Arabidopsis epigenome. Genes Dev 26(16):1825–1836
19. Liu X, Hao LL, Li DY, Zhu LH, Hu SN (2015) Long non-coding RNAs and their biological roles in plants. Genomics Proteomics Bioinformatics 13:137–147
20. Di C, Yuan J, Wu Y, Li J, Lin H, Hu L, Zhang T, Qi Y, Gerstein MB, Guo Y, Lu ZJ (2014) Characterization of stress-responsive lncRNAs in *Arabidopsis thaliana* by integrating expression, epigenetic and structural features. Plant J 80(5):848–861

21. Heo JB, Sung S (2011) Vernalization-mediated epigenetic silencing by a long intronic noncoding RNA. Science 331:76–79
22. Wang ZW, Wu Z, Raitskin O, Sun Q, Dean C (2014) Antisense mediated FLC transcriptional repression requires the P-TEFb transcription elongation factor. Proc Natl Acad Sci U S A 111:7468–7473
23. Ulitsky I, Bartel DP (2013) lincRNAs: genomics, evolution, and mechanisms. Cell 154:26–46
24. Wang H, Chung PJ, Liu J, Jang IC, Kean MJ, Xu J, Chua NH (2014) Genome-wide identification of long noncoding natural antisense transcripts and their responses to light in Arabidopsis. Genome Res 24:444–453
25. Laubinger S, Sachsenberg T, Zeller G, Busch W, Lohmann JU, Ratsch G, Weigel D (2008) Dual roles of the nuclear cap-binding complex and SERRATE in pre-mRNA splicing and microRNA processing in *Arabidopsis thaliana*. Proc Natl Acad Sci U S A 105:8795–8800
26. Rose AB (2002) Requirements for intron-mediated enhancement of gene expression in Arabidopsis. RNA 8:1444–1453
27. Christie M, Croft LJ, Carroll BJ (2011) Intron splicing suppresses RNA silencing in Arabidopsis. Plant J 68:159–167
28. Akua T, Shaul O (2013) The *Arabidopsis thaliana* MHX gene includes an intronic element that boosts translation when localized in a 5′ UTR intron. J Exp Bot 64:4255–4270
29. Kim SH, Koroleva OA, Lewandowska D, Pendle AF, Clark GP, Simpson CG, Shaw PJ, Brown JW (2009) Aberrant mRNA transcripts and the nonsense-mediated decay proteins UPF2 and UPF3 are enriched in the Arabidopsis nucleolus. Plant Cell 21:2045–2057
30. Kurihara Y, Matsui A, Hanada K, Kawashima M, Ishida J, Morosawa T, Tanaka M, Kaminuma E, Mochizuki Y, Matsushima A, Toyoda T, Shinozaki K, Seki M (2009) Genome-wide suppression of aberrant mRNA-like noncoding RNAs by NMD in Arabidopsis. Proc Natl Acad Sci U S A 106:2453–2458
31. Chekanova JA, Gregory BD, Reverdatto SV, Chen H, Kumar R, Hooker T, Yazaki J, Li P, Skiba N, Peng Q, Alonso J, Brukhin V, Grossniklaus U, Ecker JR, Belostotsky DA (2007) Genome-wide high-resolution mapping of exosome substrates reveals hidden features in the *Arabidopsis* transcriptome. Cell 131:1340–1353
32. Gy I, Gasciolli V, Lauressergues D, Morel JB, Gombert J, Proux F, Proux C, Vaucheret H, Mallory AC (2007) *Arabidopsis FIERY1*, *XRN2*, and *XRN3* are endogenous RNA silencing suppressors. Plant Cell 19:3451–3461
33. Kurihara Y, Schmitz RJ, Nery JR, Schultz MD, Okubo-Kurihara E, Morosawa T, Tanaka M, Toyoda T, Seki M, Ecker JR (2012) Surveillance of 3′ noncoding transcripts requires *FIERY1* and *XRN3* in *Arabidopsis*. G3 2:487–498
34. Liu TT, Zhu D, Chen W, Deng W, He H, He G, Bai B, Qi Y, Chen R, Deng XW (2013) A global identification and analysis of small nucleolar RNAs and possible intermediate-sized non-coding RNAs in *Oryza sativa*. Mol Plant 6:830–846
35. Wang Y, Wang X, Deng W, Fan X, Liu TT, He G, Chen R, Terzaghi W, Zhu D, Deng XW (2014) Genomic features and regulatory roles of intermediate-sized non-coding RNAs in *Arabidopsis*. Mol Plant 7:514–527
36. Memczak S, Jens M, Elefsinioti A, Torti F, Krueger J, Rybak A, Maier L, Mackowiak SD, Gregersen LH, Munschauer M, Loewer A, Ziebold U, Landthaler M, Kocks C, le Noble F, Rajewsky N (2013) Circular RNAs are a large class of animal RNAs with regulatory potency. Nature 495:333–338
37. Salzman J, Chen RE, Olsen MN, Wang PL, Brown PO (2013) Cell-type specific features of circular RNA expression. PLoS Genet 9:e1003777
38. Zhang XO, Wang HB, Zhang Y, Lu X, Chen LL, Yang L (2014a) Complementary sequence-mediated exon circularization. Cell 159:134–147
39. Lee JT (2012) Epigenetic regulation by long noncoding RNAs. Science 338:1435–1439
40. Yang L, Froberg JE, Lee JT (2014) Long noncoding RNAs: fresh perspectives into the RNA world. Trends Biochem Sci 39:35–43
41. Shuai P, Liang D, Tang S, Zhang Z, Ye CY, Su Y, Xia X, Yin W (2014) Genome-wide identification and functional prediction of novel and drought-responsive lincRNAs in *Populus trichocarpa*. J Exp Bot 65(17):4975–4983
42. Xin MM, Wang Y, Yao YY, Song N, Hu ZR, Qin DD, Xie CJ, Peng HR, Ni ZF, Sun QX (2011) Identification and characterization of wheat long non-protein coding RNAs responsive to powdery mildew infection and heat stress by using microarray analysis and SBS sequencing. BMC Plant Biol 11:61
43. Bari R, Datt Pant B, Stitt M, Scheible WR (2006) PHO2, micro-RNA399, and PHR1 define a phosphate-signaling pathway in plants. Plant Physiol 141:988–999
44. Cruz de Carvalho MH, Sun HX, Bowler C, Chua NH (2016) Noncoding and coding

transcriptome responses of a marine diatom to phosphate fluctuations. New Phytol 210(2):497–510

45. Joshi RK, Megha S, Basu U, Rahman MH, Kav NN (2016) Genome wide identification and functional prediction of long non-coding RNAs responsive to *Sclerotinia sclerotiorum* infection in *Brassica napus*. PLoS One 11(7):e0158784
46. Wang J, Yu W, Yang Y, Li X, Chen T, Liu T, Ma N, Yang X, Liu R, Zhang B (2015) Genome-wide analysis of tomato long non-coding RNAs and identification as endogenous target mimic for microRNA in response to TYLCV infection. Sci Rep 5:16946
47. Katiyar-Agarwal S, Morgan R, Dahlbeck D, Borsani O, Villegas A Jr, Zhu JK, Staskawicz BJ, Jin H (2006) A pathogen-inducible endogenous siRNA in plant immunity. Proc Natl Acad Sci U S A 103:18002–18007
48. Song YP, Ci D, Tian M, Zhang DQ (2016) Stable methylation of a non-coding RNA gene regulates gene expression in response to abiotic stress in *Populus simonii*. J Exp Bot 67(5):1477–1492
49. Liu J, Wang H, Chua NH (2015) Long non-coding RNA transcriptome of plants. Plant Biotechnol J 13:319–328
50. Aung K, Lin SI, Wu CC, Huang YT, Su CL, Chiou TJ (2006) pho2, a phosphate over accumulator, is caused by a nonsense mutation in a microRNA399 target gene. Plant Physiol 141:1000–1011
51. Franco-Zorrilla JM, Valli A, Todesco M, Mateos I, Puga MI, Rubio-Somoza I, Leyva A, Weigel D, Garcia JA, Paz-Ares J (2007) Target mimicry provides a new mechanism for regulation of microRNA activity. Nat Genet 39:1033–1037
52. Wunderlich M, Gross-Hardt R, Schöffl F (2014) Heat shock factor HSFB2a involved in gametophyte development of *Arabidopsis thaliana* and its expression is controlled by a heat-inducible long non-coding antisense RNA. Plant Mol Biol 85(6):541–550
53. Csorba T, Questa JI, Sun Q, Dean C (2014) Antisense COOLAIR mediates the coordinated switching of chromatin states at FLC during vernalization. Proc Natl Acad Sci U S A 111:16160–16165
54. Marquardt S, Raitskin O, Wu Z, Liu F, Sun Q, Dean C (2014) Functional consequences of splicing of the antisense transcript COOLAIR on FLC transcription. Mol Cell 54:156–165
55. Jabnoune M, Secco D, Lecampion C, Robaglia C, Shu QY, Poirier Y (2013) A rice *cis*-natural antisense RNA acts as a translational enhancer for its cognate mRNA and contributes to phosphate homeostasis and plant fitness. Plant Cell 25:4166–4182
56. Listerman I, Bledau AS, Grishina I, Neugebauer KM (2007) Extragenic accumulation of RNA polymerase II enhances transcription by RNA polymerase III. PLoS Genet 3:e212
57. Wu J, Okada T, Fukushima T, Tsudzuki T, Sugiura M, Yukawa Y (2012) A novel hypoxic stress-responsive long non-coding RNA transcribed by RNA polymerase III in Arabidopsis. RNA Biol 9(3):302–313
58. Zhu QH, Stephen S, Taylor J, Helliwell CA, Wang MB (2014) Long noncoding RNAs responsive to *Fusarium oxysporum* infection in *Arabidopsis thaliana*. New Phytol 201(2):574–584
59. Martianov I, Ramadass A, Serra Barros A, Chow N, Akoulitchev A (2007) Repression of the human dihydrofolate reductase gene by a noncoding interfering transcript. Nature 445:666–670
60. Sun Q, Csorba T, Skourti-Stathaki K, Proudfoot NJ, Dean C (2013) Rloop stabilization represses antisense transcription at the Arabidopsis FLC locus. Science 340:619–621
61. Wahba L, Koshland D (2013) The Rs of biology: R-loops and the regulation of regulators. Mol Cell 50:611–612
62. Wang P, Xue Y, Han Y, Lin L, Wu C, Xu S, Jiang Z, Xu J, Liu Q, Cao X (2014) The STAT3-binding long noncoding RNA lnc-DC controls human dendritic cell differentiation. Science 344:310–313
63. Yang F, Zhang H, Mei Y, Wu M (2014) Reciprocal regulation of HIF-1alpha and lincRNA-p21 modulates the Warburg effect. Mol Cell 53:88–100
64. Chen LL, Carmichael GG (2009) Altered nuclear retention of mRNAs containing inverted repeats in human embryonic stem cells: functional role of a nuclear noncoding RNA. Mol Cell 35:467–478
65. Yang L, Lin C, Liu W, Zhang J, Ohgi KA, Grinstein JD, Dorrestein PC, Rosenfeld MG (2011) ncRNA- and Pc2 methylation-dependent gene relocation between nuclear structures mediates gene activation programs. Cell 147:773–788
66. Audas TE, Jacob MD, Lee S (2012) Immobilization of proteins in the nucleolus by ribosomal intergenic spacer noncoding RNA. Mol Cell 45:147–157
67. Batista PJ, Chang HY (2013) Cytotopic localization by long noncoding RNAs. Curr Opin Cell Biol 25:195–199

68. Dey M, Complainville A, Charon C, Torrizo L, Kondorosi A, Crespi M, Datta S (2004) Phytohormonal responses in enod40-overexpressing plants of *Medicago truncatula* and rice. Physiol Plant 120:132–139
69. Lorkovic ZJ (2009) Role of plant RNA-binding proteins in development, stress response and genome organization. Trends Plant Sci 14:229–236
70. Matzke M, Kanno T, Huettel B, Jaligot E, Mette MF, Kreil DP, Daxinger L, Rovina P, Aufsatz W, Matzke AJM (2005) RNA-directed DNA methylation. In: Meyer P (ed) Plant epigenetics. Blackwell Publishing, Oxford, pp 69–96
71. Borsani O, Zhu J, Verslues PE, Sunkar R, Zhu JK (2005) Endogenous siRNAs derived from a pair of natural cis-antisense transcripts regulate salt tolerance in Arabidopsis. Cell 123(7):1279–1291
72. Zhang Q, Wang D, Lang Z, He L, Yang L, Zeng L, Li Y, Zhao C, Huang H, Zhang H, Zhang H, Zhu JK (2016) Methylation interactions in Arabidopsis hybrids require RNA-directed DNA methylation and are influenced by genetic variation. Proc Natl Acad Sci U S A 113(29):E4248–E4256
73. Dunoyer P, Brosnan CA, Schott G, Wang Y, Jay F, Alioua A, Himber C, Voinnet O (2010) An endogenous, systemic RNAi pathway in plants. EMBO J 29:1699–1712
74. Kapusta A, Kronenberg Z, Lynch VJ, Zhuo X, Ramsay L, Bourque G, Yandell M, Feschotte C (2013) Transposable elements are major contributors to the origin, diversification, and regulation of vertebrate long noncoding RNAs. PLoS Genet 9:e1003470
75. Jenuwein T, Allis CD (2001) Translating the histone code. Science 293:1074–1080
76. Crevillen P, Yang H, Cui X, Greeff C, Trick M, Qiu Q, Cao X, Dean C (2014) Epigenetic reprogramming that prevents transgenerational inheritance of the vernalized state. Nature 515(7528):587–590
77. He Y (2012) Chromatin regulation of flowering. Trends Plant Sci 17:556–562
78. He Y, Amasino RM (2005) Role of chromatin modification in flowering time control. Trends Plant Sci 10:30–35
79. Liu F, Quesada V, Crevillen P, Baurle I, Swiezewski S, Dean C (2007) The Arabidopsis RNA-binding protein FCA requires a lysine specific demethylase 1 homolog to downregulate FLC. Mol Cell 28:398–407
80. Simpson GG (2004) The autonomous pathway: epigenetic and posttranscriptional gene regulation in the control of Arabidopsis flowering time. Curr Opin Plant Biol 7:570–574
81. Maris C, Dominguez C, Allain FH (2005) The RNA recognition motif, a plastic RNA-binding platform to regulate post-transcriptional gene expression. FEBS J 272:2118–2131
82. Baurle I, Dean C (2008) Differential interactions of the autonomous pathway RRM proteins and chromatin regulators in the silencing of Arabidopsis targets. PLoS One 3:e2733
83. Baurle I, Smith L, Baulcombe DC, Dean C (2007) Widespread role for the flowering-time regulators FCA and FPA in RNA-mediated chromatin silencing. Science 318:109–112
84. Veley KM, Michaels SD (2008) Functional redundancy and new roles for genes of the autonomous floral-promotion pathway. Plant Physiol 147:682–695
85. Song XM, Liu GF, Huang ZN, Duan WK, Tan HW, Li Y, Hou XL (2016) Temperature expression patterns of genes and their coexpression with LncRNAs revealed by RNA-Seq in non-heading Chinese cabbage. BMC Genomics 17:297
86. Hamburger D, Rezzonico E, MacDonald-Comber Petetot J, Somerville C, Poirier Y (2002) Identification and characterization of the Arabidopsis PHO1 gene involved in phosphate loading to the xylem. Plant Cell 14:889–902
87. Lv Y, Liang Z, Ge M, Qi W, Zhang T, Lin F, Peng Z, Zhao H (2016) Genome-wide identification and functional prediction of nitrogen-responsive intergenic and intronic long non-coding RNAs in maize (*Zea mays* L.) BMC Genomics 17(1):350
88. Qi X, Xie S, Liu Y, Yi F, Yu J (2013) Genome-wide annotation of genes and noncoding RNAs of foxtail millet in response to simulated drought stress by deep sequencing. Plant Mol Biol 83(4–5):459–473
89. Seki M, Narusaka M, Abe H, Kasuga M, Yamaguchi-Shinozaki K, Carninci P, Hayashizaki Y, Shinozaki K (2001) Monitoring the expression pattern of 1300 Arabidopsis genes under drought and cold stresses by using a full-length cDNA microarray. Plant Cell 13(1):61–72
90. Salleh FM, Evans K, Goodall B, Machin H, Mowla SB, Mur LA, Runions J, Theodoulou FL, Foyer CH, Rogers HJ (2012) A novel function for a redox-related LEA protein (SAG21/AtLEA5) in root development and biotic stress responses. Plant Cell Environ 35(2):418–429

91. Deepak S, Shailasree S, Kini RK, Hause B, Shetty SH, Mithofer A (2007) Role of hydroxyproline-rich glycoproteins in resistance of pearl millet against downy mildew pathogen *Sclerospora graminicola*. Planta 226(2):323–333
92. Wang TZ, Liu M, Zhao MG, Chen R, Zhang WH (2015) Identification and characterization of long non-coding RNAs involved in osmotic and salt stress in *Medicago truncatula* using genome-wide high-throughput sequencing. BMC Plant Biol 15:131
93. Xiong LM, Schumaker KS, Zhu JK (2002) Cell signaling during cold, drought, and salt stress. Plant Cell 14:S165–S183
94. Yamaguchi T, Aharon GS, Sottosanto JB, Blumwald E (2005) Vacuolar Na^+/H^+ antiporter cation selectivity is regulated by calmodulin from within the vacuole in a $Ca2^+$- and pH-dependent manner. Proc Natl Acad Sci U S A 102(44):16107–16112
95. Belmonte MF, Kirkbride RC, Stone SL, Pelletier JM, Bui AQ, Yeung EC, Hashimoto M, Fei J, Harada CM, Munoz MD, Le BH, Drews GN, Brady SM, Goldberg RB, Harada JJ (2013) Comprehensive developmental profiles of gene activity in regions and subregions of the Arabidopsis seed. Proc Natl Acad Sci U S A 110:E435–E444
96. Iyer-Pascuzzi AS, Zurek PR, Benfey PN (2013) High-throughput, noninvasive imaging of root systems. Methods Mol Biol 959:177–187
97. Moussaieff A, Rogachev I, Brodsky L, Malitsky S, Toal TW, Belcher H, Yativ M, Brady SM, Benfey PN, Aharoni A (2013) High-resolution metabolic mapping of cell types in plant roots. Proc Natl Acad Sci U S A 110:E1232–E1241
98. Bateman A, Agrawal S, Birney E, Bruford EA, Bujnicki JM, Cochrane G, Cole JR, Dinger ME, Enright AJ, Gardner PP, Gautheret D, Griffiths-Jones S, Harrow J, Herrero J, Holmes IH, Huang HD, Kelly KA, Kersey P, Kozomara A, Lowe TM, Marz M, Moxon S, Pruitt KD, Samuelsson T, Stadler PF, Vilella AJ, Vogel JH, Williams KP, Wright MW, Zwieb C (2011) RNAcentral: a vision for an international database of RNA sequences. RNA 17:1941–1946
99. Chen D, Yuan C, Zhang J, Zhang Z, Bai L, Meng Y, Chen LL, Chen M (2012) PlantNATsDB: a comprehensive database of plant natural antisense transcripts. Nucleic Acids Res 40:D1187–D1193
100. Jin J, Liu J, Wang H, Wong L, Chua NH (2013) PLncDB: plant long non-coding RNA database. Bioinformatics 29:1068–1071
101. Lamesch P, Berardini TZ, Li D, Swarbreck D, Wilks C, Sasidharan R, Muller R, Dreher K, Alexander DL, Garcia-Hernandez M, Karthikeyan AS, Lee CH, Nelson WD, Ploetz L, Singh S, Wensel A, Huala E (2012) The Arabidopsis Information Resource (TAIR): improved gene annotation and new tools. Nucleic Acids Res 40:D1202–D1210
102. Quek XC, Thomson DW, Maag JL, Bartonicek N, Signal B, Clark MB, Gloss BS, Dinger ME (2014) lncRNAdb v2.0: expanding the reference database for functional long noncoding RNAs. Nucleic Acids Res 43:168–173
103. Goodrich JA, Kugel JF (2006) Non-coding-RNA regulators of RNA polymerase II transcription. Nat Rev Mol Cell Biol 7:612–616
104. Willingham AT, Orth AP, Batalov S, Peters EC, Wen BG, Aza-Blanc P, Hogenesch JB, Schultz PG (2005) A strategy for probing the functionof noncoding RNAs finds a repressor of NFAT. Science 309:1570–1573
105. Lai F, Orom UA, Cesaroni M, Beringer M, Taatjes DJ, Blobel GA, Shiekhattar R (2013) Activating RNAs associate with Mediator to enhance chromatin architecture and transcription. Nature 494:497–501
106. Ariel F, Jegu T, Latrasse D, Romero-Barrios N, Christ A, Benhamed M, Crespi M (2014) Noncoding transcription by alternative RNA polymerases dynamically regulates an auxin-driven chromatin loop. Mol Cell 55:383–396
107. Lam MT, Li W, Rosenfeld MG, Glass CK (2014) Enhancer RNAs and regulated transcriptional programs. Trends Biochem Sci 39:170–182
108. Dixon JR, Selvaraj S, Yue F, Kim A, Li Y, Shen Y, Hu M, Liu JS, Ren B (2012) Topological domains in mammalian genomes identified by analysis of chromatin interactions. Nature 485(7398):376–380
109. Zeng S, Baillargeat D, Ho HP, Yong KT (2014) Nanomaterials enhanced surface plasmon resonance for biological and chemical sensing applications. Chem Soc Rev 43(10):3426–3452
110. Law GL, Raney A, Heusner C, Morris DR (2001) Polyamine regulation of ribosome pausing at the upstream open reading frame of S adenosylmethionine decarboxylase. J Biol Chem 276:38036–38043
111. Andrews SJ, Rothnagel JA (2014) Emerging evidence for functional peptides encoded by short open reading frames. Nat Rev Genet 15:193–204
112. Röhrig H, Schmidt J, Miklashevichs E, Schell J, John M (2002) Soybean *ENDO40*

encodes two peptides that bind sucrose synthase. Proc Natl Acad Sci 99(4):1915–1920

113. Frank MJ, Smith LG (2002) A small, novel protein highly conserved in plants and animals promotes the polarized growth and division of maize leaf epidermal cells. Curr Biol 12:849–853
114. Casson SA, Chilley PM, Topping JF, Evans M, Souter MA, Lindsey K (2002) The POLARIS gene of Arabidopsis encodes a predicted peptide required for correct root growth and leaf vascular patterning. Plant Cell 14:1705–1721
115. Narita NN, Moore S, Horiguchi G, Kubo M, Demura T, Fukuda H, Goodrich J, Tsukaya H (2004) Overexpression of a novel small peptide ROTUNDIFOLIA4 decreases cell proliferation and alters leaf shape in *Arabidopsis thaliana*. Plant J 38:699–713
116. Buratti E, Muro AF, Giombi M, Gherbassi D, Iaconcig A, Baralle FE (2004) RNA folding affects the recruitment of SR proteins by mouse and human polypurinic enhancer elements in the fibronectin EDA exon. Mol Cell Biol 24:1387–1400
117. Cruz JA, Westhof E (2009) The dynamic landscapes of RNA architecture. Cell 136:604–609
118. Kozak M (2005) Regulation of translation via mRNA structure in prokaryotes and eukaryotes. Gene 361:13–37
119. Ding Y, Tang Y, Kwok CK, Zhang Y, Bevilacqua PC, Assmann SM (2013) *In vivo* genome-wide profiling of RNA secondary structure reveals novel regulatory features. Nature 505:696–700
120. Gong J, Liu W, Zhang JY, Miao XP, Guo AY (2015) lncRNASNP: a database of SNPs in lncRNAs and their potential functions in human and mouse. Nucleic Acids Res 43:D181–D186
121. Bardou F, Ariel F, Simpson CG, Romero-Barrios N, Laporte P, Balzergue S, Brown JW, Crespi M (2014) Long noncoding RNA modulates alternative splicing regulators in Arabidopsis. Dev Cell 30:166–176
122. Rearick D, Prakash A, McSweeny A, Shepard SS, Fedorova L, Fedorov A (2011) Critical association of ncRNA with introns. Nucleic Acids Res 39:2357–2366
123. Salzman J, Gawad C, Wang PL, Lacayo N, Brown PO (2012) Circular RNAs are the predominant transcript isoform from hundreds of human genes in diverse cell types. PLoS One 7:e30733
124. Yang L, Duff MO, Graveley BR, Carmichael GG, Chen LL (2011) Genome wide characterization of non-polyadenylated RNAs. Genome Biol 12:R16
125. Yin QF, Yang L, Zhang Y, Xiang JF, Wu YW, Carmichael GG, Chen LL (2012) Long noncoding RNAs with snoRNA ends. Mol Cell 48(2):219–230
126. Chang CY, Lin WD, Tu SL (2014) Genome-wide analysis of heat-sensitive alternative splicing in *Physcomitrella patens*. Plant Physiol 165(2):826–840

Chapter 4

Toward a Resilient, Functional Microbiome: Drought Tolerance-Alleviating Microbes for Sustainable Agriculture

Venkatachalam Lakshmanan, Prasun Ray, and Kelly D. Craven

Abstract

In recent years, the utilization of novel sequencing techniques opened a new field of research into plant microbiota and was used to explore a wide diversity of microorganisms both inside and outside of plant host tissues, i.e., the endosphere and rhizosphere, respectively. An early realization from such research was that species richness and diversity of the plant microbiome are both greater than believed even a few years ago, and soil is likely home to the most abundant and diverse microbial habitats known. In most ecosystems sampled thus far, overall microbial complexity is determined by the combined influences of plant genotype, soil structure and chemistry, and prevailing environmental conditions, as well as the native "bulk soil" microbial populations from which membership is drawn. Beneficial microorganisms, traditionally referring primarily to nitrogen-fixing bacteria, plant growth-promoting rhizobacteria, and mycorrhizal fungi, play a key role in major functions such as plant nutrition acquisition and plant resistance to biotic and abiotic stresses. Utilization of plant-associated microbes in food production is likely to be critical for twenty-first century agriculture, where arable cropland is limited and food, fiber, and feed productivity must be sustained or even improved with fewer chemical inputs and less irrigation.

Key words Mycorrhiza, Next-generation sequencing, Phytobiome, Plant-associated microbiomes, Sustainable agriculture

1 Introduction

Currently, agriculture consumes 75% of global water and that percentage could double in the next 50 years, if trends in population growth and current food production practices continue [1]. However, intensive agriculture with increased productivity to meet global food demands for an ever increasing human population creates serious environmental hazards, including drought and salinity [2]. These hazards are exacerbated by climate change, and represent major threats to plant survival and agricultural productivity [3]. Indeed, drought is commonly seen as the most important abiotic factor limiting plant growth and yield in many areas [3, 4]. Defined as a feature of climate that is characterized by a period of below-average rainfall sufficiently long and intense to result in

Ramanjulu Sunkar (ed.), *Plant Stress Tolerance: Methods and Protocols*, Methods in Molecular Biology, vol. 1631,
DOI 10.1007/978-1-4939-7136-7_4, © Springer Science+Business Media LLC 2017

water shortages and crop failures, drought is a major driver of very serious environmental and socioeconomic stresses in the afflicted area(s). In fact, drought is one of the most costly natural hazards in the USA each year. While commonly described as arising from a combination of lack of precipitation and high temperatures, in reality drought is a complex set of interacting, anthropogenic processes that ties changes in land cover, such as deforestation and overgrazing, to moisture recycling and can ultimately even lead to reductions in rainfall. The detrimental effects of drought on environment, economy, and society are manifold [5, 6] and will not be discussed further here. Instead, we will focus on potential biologically based solutions, where plant–microbe relationships are manipulated, and eventually engineered to improve plant productivity and resist severe weather events of various kinds in an agronomic setting. With the world's natural resources being depleted at an alarming rate, the race is on to find technologies that can ameliorate drought-related losses and also meet the requisites of economic, social, and environmental sustainability [7].

In general, there are four main categories of drought, namely (a) meteorological drought, (b) agricultural drought, (c) hydrological drought, and (d) socioeconomic drought. Agricultural drought refers to the deficit in water requirements of crops during different growing stages. Under such water deficit conditions, the plant's ability to produce sufficient above and below-ground biomass is highly reduced. The growth retardation aboveground creates a negative feedback, as photosynthesis-derived carbohydrates fuel root growth as well. Tolerance to this abiotic stress is a complex phenomenon, comprising a number of physiobiochemical processes at both cellular and whole organism levels, even potentially activated at different stages of plant development. Alterations in gene expression, the accumulation of metabolites such as the phytohormone abscisic acid (ABA) or other osmotically active compounds, and the synthesis of specific proteins that function to scavenge oxygen radicals, keep other proteins properly folded (chaperone proteins), etc. are common [8].

Research on promoting drought tolerance in plants largely involves molecular marker-assisted breeding and/or genetic engineering techniques. The basic strategy of using genetic engineering to impart drought tolerance is to introduce functional genes that are directly involved in mitigating the plant response to these events [9]. Another method approaches the problem from the perspective of understanding the behavior of the whole plant rather than individual genes or set of genes that regulate specific pathways. Here, the objective is to identify phenotypic traits that play key roles in drought tolerance and use this information for superior genotype selection by molecular breeding [10]. Still, ameliorating drought tolerance in plants by genetic engineering is expensive both in terms of time and resources required. Further, we have to

acknowledge the significant public perception and regulatory issues involved in this approach. While nontransgenic crop improvement through molecular breeding does not have to pass through regulatory channels, it still time-consuming and often difficult to achieve. Further, the likely polygenic nature of such complex traits as drought tolerance can be challenging not only to dissect but to effectively integrate and regulate in a target plant species. An alternative approach that, while certainly not novel, has gained momentum in recent years involves achieving drought resistance or tolerance through the incorporation of microbes that form symbiotic associations with plants.

In addition to intrinsic systems that serve to protect against biotic and abiotic stresses, plants can establish beneficial associations with a number of microorganisms present in the rhizosphere that can alleviate drought stress symptoms [11–13]. Collectively referred to as the plant microbiome, these microbes represent a second genome to the plant that has untapped potential for exerting positive effects on plant health and productivity [14]. This microbiome encompasses an extensive and functionally diverse gene pool, comprising viruses, prokaryotes, and eukaryotes, each associated with distinct plant tissues or organs as well as those residing in the soil immediately adjacent to the root surface, known as the rhizosphere [15]. The rhizosphere can be conceptualized as the soil area that is directly growing or responding to the release of root exudates through a process called "rhizodeposition." The use of molecular approaches based on high-throughput sequencing is dramatically improving our current knowledge of plant rhizosphere and the microbiota that reside there [16]. Although largely still a black box, the microbial diversity and their assemblage and the species richness in different plant and soil compartments has been established in the model plant *Arabidopsis* [17–20], as well as certain cultivated crop plants [21–23] and ecosystems [24, 25]. Indeed, a growing number of studies support the notion that various factors in addition to plant exudates, including the host genome, plant tissue type, and developmental stage, and different agronomic practices all play a role in determining the structure and complexity of soil and rhizosphere microbiomes [22, 26–28]. Despite these advances, harnessing the plant microbiome for the promotion of drought tolerance or other plant health and fitness objectives remains very limited [29, 30].

Historically, the manipulation of the plant microbiome has been largely limited to a few fungi or bacteria that have a significant impact on plant nutrient acquisition or on plant health by reducing the incidence of pests and diseases [31, 32], thereby increasing productivity [33–35]. The improvement of plant performance by alleviating abiotic or biotic stress has been documented more recently, and involves beneficial plant growth-promoting bacteria (PGP), endowed with

the capacity to produce 1-aminocyclopropane-1-carboxylate (ACC) deaminase or induce its production in the plant host directly (ACCd) [36]. ACC is a precursor to the plant stress hormone ethylene, and thus its cleavage can lower ethylene levels and reduce stress associated with drought or other environmentally challenging conditions in plants [37]. Fungi can also play a significant role in plant fitness and abiotic stress tolerance. Mycorrhizas are mutualistic associations between certain soil fungi and the roots of the vast majority of plant species, and have a multitude of beneficial effects on plant performance including growth promotion, increased nutrient uptake, enhanced seed production, and increased resistance against different biotic and abiotic stresses. Mycorrhizal fungi belonging to the family Serendipitaceae (Class Basidiomycota; Order Sebacinales) are one such group and our research has demonstrated that these symbiotic microbes have dramatic plant growth-promoting properties, even under drought conditions [38]. These positive effects have been documented in numerous agronomically important plant species, suggesting that serendipitoid fungi should be considered as a previously hidden, but amenable and effective microbial tool for enhancing plant productivity and stress tolerance [39].

In this book chapter we summarize mainly published studies on the plant microbiome, its functional importance, and its potential relationship to the establishment of a host phenome, specifically promoting plant tolerance against drought. We also present suggestions and recommendations for future research on the plant microbiome, with the aim of fostering innovative approaches for sustainable, low-input agriculture.

2 Plant-Associated Microbiomes

Every part of the plant is associated with various microorganisms including bacteria, fungi, oomycetes, nematodes, protozoa, algae, viruses, archaea, and arthropods. The microbial composition is more abundant and complex in the rhizosphere, the narrow zone surrounding plant roots, with 10^9 cells per gram in typical rhizospheric soil comprising up to 10^6 taxa. Despite these astounding numbers, only a very small fraction of the microbial community has been cultured on various artificial media or growth conditions [40]. It remains unclear what percent of the remaining microbiome is truly unculturable, and certainly many more await isolation on growth media that more closely approximate their dietary and metabolic needs. What is clear is that it has been culture-*independent* approaches based on DNA sequencing technologies that have had the largest impact on our understanding of microbiomes and their population dynamics in space and time. Such efforts primarily originated with the discovery of a conserved small subunit ribosomal RNA gene (rRNA) gene sequence and its application, via the

polymerase chain reaction or PCR, in the identification of microorganisms [41, 42]. The rRNA, consisting of the 16S rRNA gene for bacteria and the 18S rRNA gene for eukarya, contains highly conserved regions that can be used for PCR primer design and more variable regions that, once sequenced, can be used to group the microorganisms into operational taxonomic units (OTUs) that approximate species boundaries. Advances in molecular methods, most notably in high-throughput sequencing technologies referred to collectively as next-generation sequencing (NGS) have enabled researchers to describe soil bacterial and fungal communities with unprecedented depth and accuracy [16]. NGS platforms include the 454 Genome Sequencer (Roche Diagnostics), the HiSeq 2000 (Illumina), and the AB SOLiD System (Life Technologies) [16]. In general, each of these platforms involves DNA extraction from the microbial community or microbiome of interest, followed by PCR amplification and sequencing of rDNA, followed by data analysis and interpretation. However, as powerful as these new tools are, biases and uncertainties associated with nucleic-acid based methods and NGS must be considered [43]. Documented sources of error and bias include sampling and handling methods [44], DNA extraction efficiency [45], template properties (e.g., GC content and secondary structure) and PCR amplification [46, 47], and finally, sequencing itself, which has an intrinsic error rate [48]. To date, there have been rigorous improvements achieved for each of these techniques, including marker gene surveys, in which a portion of a conserved sequence such as the 16S rRNA gene is amplified, sequenced, and used to quantify the organisms or operational taxonomic units (OTUs) that make up a microbial community [49, 50]. Armed with these new technologies and improving statistical or methodological approaches for dealing with the biases that arise from each, researchers over the last 5 years have characterized root microbiomes associated with several agronomically important plants, including rice [21], maize [22], sugarcane [51], sweet potato [52], cultivated agave [53], banana [54], domesticated barley [23], as well as those found in the root systems of grasslands [55] and the model plant, *Arabidopsis thaliana* [18, 19, 23, 56].

The taxonomic composition and abundance of soil microbial communities depends upon various primary soil properties, such as pH, temperature, texture, moisture, and prevailing agronomic practices [57–60], but also on more complex, biotic interactions [27, 28, 61]. In general, microbial communities of aboveground and belowground plant tissues are distinct, differing in both their taxonomic diversity and structure, as well as their putative functionality [28, 62]. Root exudates generally vary substantially in quantity and composition between different plant species and genotypes and can depend on a variety of factors, such as nutrient levels, disease, stress, and even the microbial community itself [63]. Plant functional groups, such as legumes and grasses, differ

in litter quality and the amount of carbon and nitrogen released to the soil [64]. Many plant functional groups or guilds, i.e., species with similar morphological, phenological, and physiological traits, differ in litter quality and the amount of carbon and nitrogen released to the soil [65], thereby affecting microbial composition [64]. Similarly, the developmental stage or physiological age of the plant has an effect on the structure and function of the rhizospheric microbiome [26, 28, 66]. Last but definitely not least, the plant's immune system can impact rhizosphere microbiomes. Recent studies showed that the plant defense-related hormone salicylic acid (SA) plays a role in the assembly of the microbiome in the interior of *Arabidopsis* roots [20, 67]. Lebeis and colleagues analyzed the rhizospheric and endophytic root microbiomes of SA-biosynthesis and signaling mutants and found that plants with altered SA-signaling have root microbiomes that differ in the relative abundance of specific bacterial families, as compared with those of wild type. This was taken as strong evidence that SA or SA-mediated plant processes play an important role in modulating colonization of the roots by specific bacterial families, thereby acting as gatekeepers that preferentially give access to the root interior, or endosphere, to specific bacterial taxa in the microbial community [20]. In another study it was reported that jasmonic acid (JA) signaling mutants of *Arabidopsis*, *myc2* and *med2* released lower amounts of asparagine, ornithine, and tryptophan, and *med25* released less glutamic acid, resulting in changes in the abundance of rhizosphere microbial populations [67]. Further, root exudates released in response to changes in JA signaling have been shown to influence the relative abundances of bacteria and archaea in the rhizosphere [67]. Collectively, these findings highlight the critical role that plant immunity plays in the process of microbiome assembly in both the rhizosphere, and ultimately the endosphere.

3 Drought Tolerance-Alleviating Microbes

Perhaps one of the most impending and potentially catastrophic consequences of climate change is a warming and drying planet. As the microbiome influences a plant's overall health and responsiveness to environmental conditions such as drought and salinity, and some fungi can even extend their mycorrhizal filaments beyond plant roots to tap additional nutrients or water, microbial approaches to mitigate drought stress has received substantial attention [12, 68–70]. Plant growth-promoting rhizobacteria (PGPR) are known that colonize monocot and dicot crop species and help their host plants tolerate biotic and abiotic stresses through a variety of mechanisms [12]. Examples of plant drought tolerance induced by rhizobacteria documented in the scientific literature have been shown to occur via: (1) the production of

phytohormones like abscisic acid (ABA), gibberellic acid, and indole-3-acetic acid (IAA); (2) the production of ACC-deaminase to reduce levels of ethylene in the roots; (3) bacterial exopolysaccharides (summarized in Table 1).

Physiologically, the most active phytohormone in plant growth and development is IAA which influences such diverse programs as cell division, initiation of lateral and adventitious roots, elongation of stems and roots, and orientation of root and shoot growth in response to both light and gravity [90]. Some microbes, such as various *Azospirillum* spp. or *Bacillus thuringiensis*, are able to synthesize phytohormones like IAA themselves and can demonstrably enhance the formation of lateral roots and root hairs, thus helping plants to cope with water deficit [73]. Similarly, ABA and gibberellin-producing strains of *Azospirillum lipoferum* can impart water loss regulation in their maize plant hosts by controlling stomatal closure and stress signal transduction pathways [71]. Some PGPR produce ACC-deaminase, an enzyme that hydrolyzes 1-aminocyclopropane-1-carboxylate (ACC), the immediate precursor of ethylene (ET), into ammonia and alpha-ketobutyrate instead of converting it into ET [91, 92]. The overall ACC and ET levels in the rhizoplane are reduced, thus eliminating the higher ET concentrations, and reducing the stress levels in the host plant [91]. For example, treatment of tomato (*Solanum lycopersicum* L.) and pepper (*Capsicum annuum* L.) seedlings with *Achromobacter piechaudii* ARV8, a bacterium capable of producing ACC deaminase, resulted in reduced ET concentrations (by cleaving ACC), which most likely contributed to the observed drought tolerance [77]. Another group of PGPR strains secrete hydrophilic exopolysaccharides (EPS), which impart the architectural structure and often much of the functionality to biofilms. Such biofilms can improve plant performance under drought (water-restricted) conditions. For instance, EPS producing *Pseudomonas* spp. and *Acinetobacter* spp. promoted drought tolerance of pepper plant through the formation of a hydrophilic biofilm around the roots that imparted protection against desiccation [11]. In fact, some PGPR strains have been documented as producing EPS with water retention properties exceeding 70 g water per gram of polysaccharide [93]. .

Fungal symbionts conferring drought tolerance to plants can be grossly categorized into (a) endophytic fungi that live entirely within the plant, either systemically or specifically in certain tissues such as roots, stems, and/or leaves; and (b) mycorrhizal fungi that colonize only the plant roots but extend their thread-like mycelium out into the rhizosphere. Various fungal endophytes have been shown to confer drought tolerance in a wide variety of plants, including monocots and dicots. Often, such tolerance is achieved through enhanced or accelerated growth of roots or root hairs, by means of osmoregulation and stomatal regulation, by production of plant hormones and by regulating plant drought stress-related

Table 1
Drought tolerance promoting microbes, and its mechanisms (adopted and updated from [69, 70]

Microorganisms	Crop	Mechanisms	Reference
Bacterial—phytohormone modulators			
Azospirillum lipoferum	Maize	Gibberellins and increased ABA. Better control of stomata closure mediated by ABA and more developed root system	[71]
Azospirillum sp.	Wheat	IAA enhanced root growth, and increased uptake of water and nutrients	[72]
Bacillus thuringiensis	*Lavandula dentata*	IAA increased in higher K^- proline	[73]
Phyllobacterium brassicacearum STM196	*Arabidopsis*	Increased ABA content resulted in decreased transpiration	[74]
Bacillus subtilis	*Platycladus orientalis*	Increased ABA levels and the stomatal conductance	[75]
Rhizobium leguminosarum LR-30, *Mesorhizobium ciceri* CR-30 and CR-39, and *Rhizobium phaseoli* MR-2	Wheat	IAA improved the growth, biomass and drought tolerance index	[76]
Bacterial—ACC deaminase (ACCd) producers			
Achromobacter piechaudii ARV8	Tomato and pepper	Reduced ET production and increased fresh and dry weight	[77]
Pseudomonas fluorescens ACC-5	Pea	Induced longer roots and increased uptake of water	[78]
Burkholderia phytofirmans, *Enterobacter* spp.	Maize	Increased chlorophyll content	[79]
Bacillus thuringiensis AZP2	wheat	Reduction of volatile emissions and higher photosynthesis	[80]
Bacterial—exopolysaccharide producers			
Pantoea agglomerans	Wheat	EPS	[81]
Rhizobium spp., *Pseudomonas putida*	Sunflower	EPS	[82]
Bacillus spp.	Maize	EPS	[83]
Acinetobacter, *Pseudomonas*	Grapevine	EPS	[11]
Fungi			
Piriformospora indica	Chinese cabbage	Stimulating antioxidant enzymes, the expression of drought-related genes and the plastid-localized CAS protein	[84]

(continued)

Table 1
(continued)

Microorganisms	Crop	Mechanisms	Reference
Sebacina vermifera	Switchgrass	Increased root biomass	[38]
Glomus mosseae; G. etunicatum	Winter wheat	Improved water and nutrient uptake	[85]
Fungal endophyte	Wild barley	Increased root biomass	[86]
Neotyphodium spp.	Cool season grasses	Improved water uptake from the soil by an extensive root system	[87]
Fusarium culmorum	American dune grass; Rice; Wild tomatoes	Decrease in water consumption	[88]
Trichoderma hamatum	Cocoa	Stomatal conductance, net photosynthesis, green fluorescence emissions	[89]

We apologize to all colleagues whose work could not be cited because of space limitations

genes [84, 87, 94–96]. Perhaps as a consequence of enhanced or accelerated host development, such plant–microbe interactions often confer a more *global*, *adaptive* advantage to their hosts, and may even allow the expansion of the ecological and/or geographical range that can be successfully adapted to by the host plant(s). A classic example of this phenomenon is the ability of perennial rye grass to spread over large areas of the southeastern USA that would otherwise be too hot and dry [97, 98].

Many drought responsive genes have been identified in plants, some affecting primary characteristics such as stomatal response time [99, 100] and others implicated more indirectly in abiotic stress tolerance. For each pathway or physiological response that can impart drought tolerance, there is likely a microbe or a combination of microbes that can induce the response either directly or indirectly [101]. *Piriformospora indica*, belonging to the fungal order Serendipitaceae, has shown to alleviate drought stress by modulating several stress-related genes in plants [84, 102]. Similar regulation of drought responsive genes in the Cacao plant has been observed when colonized with another beneficial fungal endophyte *Trichoderma hamatum*, eventually resulting in delayed drought-induced changes in stomatal conductance, net photosynthesis, and green fluorescence emissions [89]. Arbuscular mycorrhizae (AM) are often cited to improve plant resistance to water deficit and drought stress through the alteration of plant physiology and the expression of plant genes [99]. AM fungi have reportedly improved both the osmotic adjustment in plants under drought stress as well as gene sets that play a critical role in ameliorating drought-related stress either by avoidance or by tolerance.

Avoidance can occur via maintenance of high internal water potential, and tolerance can be achieved by survival of low internal water potential [99, 103]. In particular, the role of abscisic acid (ABA) had been suggested as they primary driver of the AM-mediated stress response in lettuce [104]. In terms of altering plant physiology, mycorrhized plants showed improved root biomass, potassium content, and water content [99, 105–108].

4 Conclusions and Future Perspectives

There is ample research evidence to support the notion that a great many soil bacteria and fungi can improve drought tolerance in plants through one of many distinct mechanisms, often in combination with one another. Some responses are common among different plant families, and others can only be initiated by distinct microbial taxa (Table 1). In nature, plants interact simultaneously with an astounding array of potentially beneficial microbes, ultimately forming a number of symbiotic relationships with both cultivable and uncultivable microbes and interacting with the plant to function effectively as a holobiont, or *phytobiome*. This amalgamation of macro and micro, sharing space and functioning as a dynamic community, may be able to respond and evolve to environmental fluctuations more effectively than could either on their own. It is possible, and perhaps even likely, that anthropomorphic climate change may challenge the stability and effective functioning of these phytobiome-based ecosystems, and that rational design of their constituency may allow us to avoid or ameliorate the worst consequences of a drying, warming Earth. Ultimately, our ability to harness these relationships for agronomic gain rests upon identification of the rules governing the initiation, effectiveness and ultimately, the resilience of these mutualistic interactions.

The majority of the NGS-based studies provide the phylogenetic structure of the soil microbial community and thus give a snapshot of community structure and even mechanisms underlying their assembly (reviewed by [27, 109–111]. However, there is currently a transition already underway in research focus, from simple community profiling based upon rDNA sequencing to a combinatorial approach integrating this data with other -omics-based data, such as metaproteomics and metatranscriptomics. Both are in early stages of development, particularly in a more complex, field environment, and face many challenges due to sampling constraints and the overall paucity of representation in publicly available protein and metabolite databases [112]. Although headway can be made toward understanding the functional responses between the soil microbiome and their host plants in from controlled laboratory and greenhouse studies, assigning large-scale proteomics or metabolomics data from a complex, field environment in a temporally and spatially informative way is much more challenging. Reproducibility is replaced by

unpredictability, and double-digit improvements observed in the former often shrink to single number fluctuations in the latter, more complex environment. The incorporation of ecological and energy-flux modeling will perhaps improve this incongruence, but ample field data must be generated in a variety of ecological habitats and cropping systems to populate these models.

Finally, microbiologists of the sort that study phytobiomes need to be more involved in the plant breeding process. Traditionally, microbes have only been incorporated in any crop improvement program during the final stages of their development, and mostly as an afterthought. While we agree that screening a large population of microbes against a large number of plant genotypes for identifying the *perfect genotypic match* is practically impossible, we also cannot deny that optimizing the pairing of microbe and plant genotypes holds great potential for maximizing performance of the symbiosis. If we do not, then we are accepting the very real possibility that we have not reached optimal performance and/or stress tolerance. Recently, a few potential promising routes have been outlined to engineer rhizosphere microbiomes for optimizing the plant phenotype of interest [68]. To conclude, we believe engineering microbiomes for crop improvement and ameliorating biotic and abiotic stress can indeed be realized, where a production potential greater than the sum of the parts can be achieved and the resilient, productive and predictable power of the microbiome unleashed [113]. Combined with other advances in plant breeding, genetic modification, and precision fertilizer and water application, we can forge a new and potentially transformative paradigm in plant health, nutrition, and sustainable agriculture.

Acknowledgments

This work was supported by the US Department of Energy, Bioenergy Research Center, through the Office of Biological and Environmental Research in the DOE Office of Science and The Samuel Roberts Noble Foundation. We declare no conflict of interests inherent to this submission.

References

1. Molden D, Oweis TY, Pasquale S, Kijne JW, Hanjra MA et al (2007) Pathways for increasing agricultural water productivity. In: Water for food, water for life, a comprehensive assessment of water management in agriculture. Earthscan and International Water Management Institute, London, pp 279–310
2. Golldack D, Li C, Mohan H, Probst N (2014) Tolerance to drought and salt stress in plants: unraveling the signaling networks. Front Plant Sci 15:151–161
3. Trenberth KE, Fasullo JT, Branstator G, Phillips AS (2014) Seasonal aspects of the recent pause in surface warming. Nat Clim Chang 4:911–916

4. Rejeb IB, Pastor V, Mauch-Mani B (2014) Plant responses to simultaneous biotic and abiotic stress: molecular mechanisms. Plants 3:458–475
5. Pandey S, Bhandari H, Hardy B (2007) Economic costs of drought and rice farmers' coping mechanisms. A crosscountry comparative analysis. International Rice Research Institute/World Scientific Publishing, Los Baños, Philippines/Singapore, pp 1–9
6. Dijk AI, Beck HE, Crosbie RS, Jeu RA, Liu YY et al (2013) The millennium drought in southeast Australia (2001–2009): natural and human causes and implications for water resources, ecosystems, economy, and society. Water Resour Res 49:1040–1057
7. Ray P, Craven KD (2016) Sebacina vermifera: a unique root symbiont with vast agronomic potential. World J Microbiol Biotechnol 32:1–10
8. Reddy AR, Chaitanya KV, Vivekanandan M (2004) Drought-induced responses of photosynthesis and antioxidant metabolism in higher plants. J Plant Physiol 161:1189–1202
9. Umezawa T, Fujita M, Fujita Y, Yamaguchi-Shinozaki K, Shinozaki K (2006) Engineering drought tolerance in plants: discovering and tailoring genes to unlock the future. Curr Opin Biotechnol 17:113–122
10. Sinclair TR (2011) Challenges in breeding for yield increase for drought. Trends Plant Sci 16:289–293
11. Rolli E, Marasco R, Vigani G, Ettoumi B, Mapelli F et al (2015) Improved plant resistance to drought is promoted by the root-associated microbiome as a water stress-dependent trait. Environ Microbiol 17:316–331
12. Ngumbi E, Kloepper J (2016) Bacterial-mediated drought tolerance: Current and future prospects. Appl Soil Ecol 105:109–125
13. Zolla G, Badri DV, Bakker MG, Manter DK, Vivanco JM (2013) Soil microbiomes vary in their ability to confer drought tolerance to Arabidopsis. Appl Soil Ecol 68:1–9
14. Berendsen RL, Pieterse CM, Bakker PA (2012) The rhizosphere microbiome and plant health. Trends Plant Sci 17:478–486
15. Rout ME, Southworth D (2013) The root microbiome influences scales from molecules to ecosystems: the unseen majority 1. Am J Bot 100:1689–1691
16. Caporaso JG, Lauber CL, Walters WA, Berg-Lyons D, Huntley J et al (2012) Ultra-high-throughput microbial community analysis on the Illumina HiSeq and MiSeq platforms. ISME J 6:1621–1624
17. Bai Y, Müller DB, Srinivas G, Garrido-Oter R, Potthoff E et al (2015) Functional overlap of the Arabidopsis leaf and root microbiota. Nature 528:364–369
18. Bulgarelli D, Rott M, Schlaeppi K, van Themaat EVL, Ahmadinejad N et al (2012) Revealing structure and assembly cues for Arabidopsis root-inhabiting bacterial microbiota. Nature 488:91–95
19. Lundberg DS, Lebeis SL, Paredes SH, Yourstone S, Gehring J et al (2012) Defining the core *Arabidopsis thaliana* root microbiome. Nature 488:86–90
20. Lebeis SL, Paredes SH, Lundberg DS, Breakfield N, Gehring J et al (2015) Salicylic acid modulates colonization of the root microbiome by specific bacterial taxa. Science 349:860–864
21. Edwards J, Johnson C, Santos-Medellín C, Lurie E, Podishetty NK et al (2015) Structure, variation, and assembly of the root-associated microbiomes of rice. Proc Natl Acad Sci 112:E911–E920
22. Peiffer JA, Spor A, Koren O, Jin Z, Tringe SG et al (2013) Diversity and heritability of the maize rhizosphere microbiome under field conditions. Proc Natl Acad Sci 110:6548–6553
23. Bulgarelli D, Garrido-Oter R, Münch PC, Weiman A, Dröge J et al (2015) Structure and function of the bacterial root microbiota in wild and domesticated barley. Cell Host Microbe 17:392–403
24. Fierer N, Ladau J, Clemente JC, Leff JW, Owens SM et al (2013) Reconstructing the microbial diversity and function of pre-agricultural tallgrass prairie soils in the United States. Science 342:621–624
25. Tautges NE, Sullivan TS, Reardon CL, Burke IC (2016) Soil microbial diversity and activity linked to crop yield and quality in a dryland organic wheat production system. Appl Soil Ecol 108:258–268
26. Chaparro JM, Badri DV, Vivanco JM (2014) Rhizosphere microbiome assemblage is affected by plant development. ISME J 8:790–803
27. Lakshmanan V (2015) Root microbiome assemblage is modulated by plant host factors. Adv Bot Res 75:57–79
28. Wagner MR, Lundberg DS, Tijana G, Tringe SG, Dangl JL et al (2016) Host genotype and age shape the leaf and root microbiomes of a wild perennial plant. Nat Commun 7:12151. doi:10.1038/ncomms12151
29. Kiers ET, Duhamel M, Beesetty Y, Mensah JA, Franken O et al (2011) Reciprocal rewards

stabilize cooperation in the mycorrhizal symbiosis. Science 333:880–882

30. Werner GD, Strassmann JE, Ivens AB, Engelmoer DJ, Verbruggen E et al (2014) Evolution of microbial markets. Proc Natl Acad Sci 111:1237–1244
31. Van Loon LC, Rep M, Pieterse C (2006) Significance of inducible defense-related proteins in infected plants. Annu Rev Phytopathol 44:135–162
32. Bhattacharyya P, Jha D (2012) Plant growth-promoting rhizobacteria (PGPR): emergence in agriculture. World J Microbiol Biotechnol 28:1327–1350
33. Vessey JK (2003) Plant growth promoting rhizobacteria as biofertilizers. Plant Soil 255:571–586
34. Lugtenberg B, Kamilova F (2009) Plant-growth-promoting rhizobacteria. Annu Rev Microbiol 63:541–556
35. Kloepper J, Schroth M (1978) Plant growth-promoting rhizobacteria on radishes. Proceedings of the 4th international conference on pathogenic bacteria, Tours, pp 879–882
36. Glick BR, Cheng Z, Czarny J, Duan J (2007) Promotion of plant growth by ACC deaminase-producing soil bacteria. Eur J Plant Pathol 119:329–339
37. Glick BR (2004) Bacterial ACC deaminase and the alleviation of plant stress. Adv Appl Microbiol 56:291–312
38. Ghimire SR, Craven KD (2011) The ectomycorrhizal fungus *Sebacina vermifera*, enhances biomass production of switchgrass (*Panicum virgatum* L.) under drought conditions. Appl Environ Microbiol 77:7063–7067
39. Ray P, Ishiga T, Decker SR, Turner GB, Craven KD (2015) A novel delivery system for the root symbiotic fungus, *Sebacina vermifera*, and consequent biomass enhancement of low lignin COMT switchgrass lines. Bioenergy Res 8:922–933
40. Tringe SG, Von Mering C, Kobayashi A, Salamov AA, Chen K et al (2005) Comparative metagenomics of microbial communities. Science 308:554–557
41. Woese CR, Fox GE (1977) Phylogenetic structure of the prokaryotic domain: the primary kingdoms. Proc Natl Acad Sci 74:5088–5090
42. Mullis KB, Erlich HA, Arnheim N, Horn GT, Saiki RK, et al (1987) Process for amplifying, detecting, and/or-cloning nucleic acid sequences. US 4683195 A
43. Pinto AJ, Raskin L (2012) PCR biases distort bacterial and archaeal community structure in pyrosequencing datasets. PLoS One 7:e43093
44. Zhou J, Jiang Y-H, Deng Y, Shi Z, Zhou BY et al (2013) Random sampling process leads to overestimation of β-diversity of microbial communities. MBio 4:e00324–e00313
45. Feinstein LM, Sul WJ, Blackwood CB (2009) Assessment of bias associated with incomplete extraction of microbial DNA from soil. Appl Environ Microbiol 75:5428–5433
46. Aird D, Ross MG, Chen W-S, Danielsson M, Fennell T et al (2011) Analyzing and minimizing PCR amplification bias in Illumina sequencing libraries. Genome Biol 12:R18
47. Ahn J-H, Kim B-Y, Song J, Weon H-Y (2012) Effects of PCR cycle number and DNA polymerase type on the 16S rRNA gene pyrosequencing analysis of bacterial communities. J Microbiol 50:1071–1074
48. Kennedy K, Hall MW, Lynch MD, Moreno-Hagelsieb G, Neufeld JD (2014) Evaluating bias of Illumina-based bacterial 16S rRNA gene profiles. Appl Environ Microbiol 80:5717–5722
49. D'Amore R, Ijaz UZ, Schirmer M, Kenny JG, Gregory R et al (2016) A comprehensive benchmarking study of protocols and sequencing platforms for 16S rRNA community profiling. BMC Genomics 17:55–74
50. Gohl DM, Vangay P, Garbe J, MacLean A, Hauge A et al (2016) Systematic improvement of amplicon marker gene methods for increased accuracy in microbiome studies. Nat Biotechnol 34:942–949
51. Yeoh YK, Paungfoo-Lonhienne C, Dennis PG, Robinson N, Ragan MA et al (2015) The core root microbiome of sugarcanes cultivated under varying nitrogen fertilizer application. Environ Microbiol 18:1338–1351
52. Marques JM, da Silva TF, Vollu RE, Blank AF, Ding G-C et al (2014) Plant age and genotype affect the bacterial community composition in the tuber rhizosphere of field-grown sweet potato plants. FEMS Microbiol Ecol 88:424–435
53. Coleman-Derr D, Desgarennes D, Fonseca-Garcia C, Gross S, Clingenpeel S et al (2016) Plant compartment and biogeography affect microbiome composition in cultivated and native *Agave* species. New Phytol 209:798–811
54. Köberl M, Dita M, Martinuz A, Staver C, Berg G (2015) Agroforestry leads to shifts within the gammaproteobacterial microbiome of banana plants cultivated in Central America. Front Microbiol 6:91
55. Zhang K, Shi Y, Jing X, He J-S, Sun R et al (2016) Effects of short-term warming and altered precipitation on soil microbial

communities in alpine grassland of the Tibetan plateau. Front Microbiol 7:1032

56. Schlaeppi K, Dombrowski N, Oter RG, van Themaat EVL, Schulze-Lefert P (2014) Quantitative divergence of the bacterial root microbiota in *Arabidopsis thaliana* relatives. Proc Natl Acad Sci 111:585–592
57. Steenwerth K, Drenovsky R, Lambert J-J, Kluepfel D, Scow K et al (2008) Soil morphology, depth and grapevine root frequency influence microbial communities in a Pinot noir vineyard. Soil Biol Biochem 40:1330–1340
58. Habekost M, Eisenhauer N, Scheu S, Steinbeiss S, Weigelt A et al (2008) Seasonal changes in the soil microbial community in a grassland plant diversity gradient four years after establishment. Soil Biol Biochem 40:2588–2595
59. Le Roux X, Schmid B, Poly F, Barnard RL, Niklaus PA et al (2013) Soil environmental conditions and microbial build-up mediate the effect of plant diversity on soil nitrifying and denitrifying enzyme activities in temperate grasslands. PLoS One 8:e61069
60. Nuccio EE, Anderson-Furgeson J, Estera KY, Pett-Ridge J, Valpine P et al (2016) Climate and edaphic controllers influence rhizosphere community assembly for a wild annual grass. Ecology 97:1307–1318
61. Lakshmanan V, Selvaraj G, Bais HP (2014) Functional soil microbiome: belowground solutions to an aboveground problem. Plant Physiol 166:689–700
62. Kembel SW, O'Connor TK, Arnold HK, Hubbell SP, Wright SJ et al (2014) Relationships between phyllosphere bacterial communities and plant functional traits in a neotropical forest. Proc Natl Acad Sci 111:13715–13720
63. Lankau RA (2011) Resistance and recovery of soil microbial communities in the face of *Alliaria petiolata* invasions. New Phytol 189:536–548
64. Breulmann M, Schulz E, Weißhuhn K, Buscot F (2012) Impact of the plant community composition on labile soil organic carbon, soil microbial activity and community structure in semi-natural grassland ecosystems of different productivity. Plant Soil 352:253–265
65. Lange M, Habekost M, Eisenhauer N, Roscher C, Bessler H et al (2014) Biotic and abiotic properties mediating plant diversity effects on soil microbial communities in an experimental grassland. PLoS One 9:e96182
66. Bressan M, Roncato M-A, Bellvert F, Comte G, el Zahar HF et al (2009) Exogenous glucosinolate produced by *Arabidopsis thaliana* has an impact on microbes in the rhizosphere and plant roots. ISME J 3:1243–1257
67. Carvalhais LC, Dennis PG, Badri DV, Kidd BN, Vivanco JM et al (2015) Linking jasmonic acid signaling, root exudates, and rhizosphere microbiomes. Mol Plant-Microbe Interact 28:1049–1058
68. Qin Y, Druzhinina IS, Pan X, Yuan Z (2016) Microbially mediated plant salt tolerance and microbiome-based solutions for saline agriculture. Biotechnol Adv 34:1245–1259
69. Kaushal M, Wani SP (2016) Rhizobacterial-plant interactions: strategies ensuring plant growth promotion under drought and salinity stress. Agric Ecosyst Environ 231:68–78
70. Vurukonda SSKP, Vardharajula S, Shrivastava M, SkZ A (2016) Enhancement of drought stress tolerance in crops by plant growth promoting rhizobacteria. Microbiol Res 184:13–24
71. Cohen AC, Travaglia CN, Bottini R, Piccoli PN (2009) Participation of abscisic acid and gibberellins produced by endophytic Azospirillum in the alleviation of drought effects in maize. Botany 87:455–462
72. Arzanesh MH, Alikhani H, Khavazi K, Rahimian H, Miransari M (2011) Wheat (*Triticum aestivum* L.) growth enhancement by *Azospirillum* sp. under drought stress. World J Microbiol Biotechnol 27:197–205
73. Armada E, Roldán A, Azcon R (2014) Differential activity of autochthonous bacteria in controlling drought stress in native Lavandula and Salvia plants species under drought conditions in natural arid soil. Microb Ecol 67:410–420
74. Bresson J, Varoquaux F, Bontpart T, Touraine B, Vile D (2013) The PGPR strain Phyllobacterium brassicacearum STM196 induces a reproductive delay and physiological changes that result in improved drought tolerance in Arabidopsis. New Phytol 200:558–569
75. Liu F, Xing S, Ma H, Du Z, Ma B (2013) Cytokinin-producing, plant growth-promoting rhizobacteria that confer resistance to drought stress in *Platycladus orientalis* container seedlings. Appl Microbiol Biotechnol 97:9155–9164
76. Hussain MB, Zahir ZA, Asghar HN, Asghar M (2014) Can catalase and exopolysaccharides producing rhizobia ameliorate drought stress in wheat. Int J Agric Biol 16:3–13
77. Mayak S, Tirosh T, Glick BR (2004) Plant growth-promoting bacteria that confer resistance to water stress in tomatoes and peppers. Plant Sci 166:525–530

78. Zahir Z, Munir A, Asghar H, Shaharoona B, Arshad M (2008) Effectiveness of rhizobacteria containing ACC deaminase for growth promotion of peas (*Pisum sativum*) under drought conditions. J Microbiol Biotechnol 18:958–963
79. Naveed M, Mitter B, Reichenauer TG, Wieczorek K, Sessitsch A (2014) Increased drought stress resilience of maize through endophytic colonization by *Burkholderia phytofirmans* PsJN and Enterobacter sp. FD17. Environ Exp Bot 97:30–39
80. Timmusk S, El-Daim IAA, Copolovici L, Tanilas T, Kännaste A et al (2014) Drought-tolerance of wheat improved by rhizosphere bacteria from harsh environments: enhanced biomass production and reduced emissions of stress volatiles. PLoS One 9:e96086
81. Amellal N, Burtin G, Bartoli F, Heulin T (1998) Colonization of wheat rhizosphere by EPS producing Pantoea agglomerans and its effect on soil aggregation. Appl Environ Microbiol 64:3740–3747
82. Alami Y, Achouak W, Marol C, Heulin T (2000) Rhizosphere soil aggregation and plant growth promotion of sunflowers by an exopolysaccharide-producing Rhizobiumsp. Strain isolated from sunflower roots. Appl Environ Microbiol 66:3393–3398
83. Vardharajula S, Zulfikar Ali S, Grover M, Reddy G, Bandi V (2011) Drought-tolerant plant growth promoting *Bacillus* spp.: effect on growth, osmolytes, and antioxidant status of maize under drought stress. J Plant Interact 6:1–14
84. Sun C, Johnson JM, Cai D, Sherameti I, Oelmüller R et al (2010) Piriformospora indica confers drought tolerance in Chinese cabbage leaves by stimulating antioxidant enzymes, the expression of drought-related genes and the plastid-localized CAS protein. J Plant Physiol 167:1009–1017
85. Al-Karaki G, McMichael B, Zak J (2004) Field response of wheat to arbuscular mycorrhizal fungi and drought stress. Mycorrhiza 14:263–269
86. Murphy B, Martin Nieto L, Doohan F, Hodkinson T (2015) Fungal endophytes enhance agronomically important traits in severely drought-stressed barley. J Agron Crop Sci 201:419–427
87. Malinowski DP, Belesky DP (2000) Adaptations of endophyte-infected cool-season grasses to environmental stresses: mechanisms of drought and mineral stress tolerance. Crop Sci 40:923–940
88. Rodriguez RJ, Henson J, Van Volkenburgh E, Hoy M, Wright L et al (2008) Stress tolerance in plants via habitat-adapted symbiosis. ISME J 2:404–416
89. Bae H, Sicher RC, Kim MS, Kim S-H, Strem MD et al (2009) The beneficial endophyte Trichoderma hamatum isolate DIS 219b promotes growth and delays the onset of the drought response in *Theobroma cacao*. J Exp Bot 60:3279–3295
90. Glick BR (1995) The enhancement of plant growth by free-living bacteria. Can J Microbiol 41:109–117
91. Glick BR, Penrose DM, Li J (1998) A model for the lowering of plant ethylene concentrations by plant growth-promoting bacteria. J Theor Biol 190:63–68
92. Shaharoona B, Arshad M, Zahir Z (2006) Effect of plant growth promoting rhizobacteria containing ACC-deaminase on maize (*Zea mays* L.) growth under axenic conditions and on nodulation in mung bean (*Vigna radiata* L.) Lett Appl Microbiol 42:155–159
93. Vu B, Chen M, Crawford RJ, Ivanova EP (2009) Bacterial extracellular polysaccharides involved in biofilm formation. Molecules 14:2535–2554
94. Bacon C, Hill N (1996) Symptomless grass endophytes: products of coevolutionary symbioses and their role in the ecological adaptations of grasses. In: Redlin SC, Carris LM (eds) Endophytic fungi in grasses and woody plants. American Phytopathologycal Society Press, St Paul, MN, pp 155–178
95. Marulanda A, Barea J-M, Azcón R (2009) Stimulation of plant growth and drought tolerance by native microorganisms (AM fungi and bacteria) from dry environments: mechanisms related to bacterial effectiveness. J Plant Growth Regul 28:115–124
96. James EK, Gyaneshwar P, Mathan N, Barraquio WL, Reddy PM et al (2002) Infection and colonization of rice seedlings by the plant growth-promoting bacterium *Herbaspirillum seropedicae* Z67. Mol Plant-Microbe Interact 15:894–906
97. Singh LP, Gill SS, Tuteja N (2011) Unraveling the role of fungal symbionts in plant abiotic stress tolerance. Plant Signal Behav 6:175–191
98. Hahn H, McManus MT, Warnstorff K, Monahan BJ, Young CA et al (2008) Neotyphodium fungal endophytes confer physiological protection to perennial ryegrass (*Lolium perenne* L.) subjected to a water deficit. Environ Exp Bot 63:183–199
99. Augé RM (2000) Stomatal behavior of arbuscular mycorrhizal plants Arbuscular mycorrhizas: physiology and function. Springer, New York, NY, pp 201–237

100. Duan X, Neuman DS, Reiber JM, Green CD, Saxton AM et al (1996) Mycorrhizal influence on hydraulic and hormonal factors implicated in the control of stomatal conductance during drought. J Exp Bot 47:1541–1550
101. Shinozaki K, Yamaguchi-Shinozaki K, Seki M (2003) Regulatory network of gene expression in the drought and cold stress responses. Curr Opin Plant Biol 6:410–417
102. Sherameti I, Venus Y, Drzewiecki C, Tripathi S, Dan VM et al (2008) PYK10, a β-glucosidase located in the endoplasmatic reticulum, is crucial for the beneficial interaction between *Arabidopsis thaliana* and the endophytic fungus *Piriformospora indica*. Plant J 54:428–439
103. Levitt J (1980) Responses of plants to environmental stresses Volume II Water, radiation, salt, and other stresses. Academic, Cambridge, MA
104. Aroca R, Vernieri P, Ruiz-Lozano JM (2008) Mycorrhizal and non-mycorrhizal *Lactuca sativa* plants exhibit contrasting responses to exogenous ABA during drought stress and recovery. J Exp Bot 59:2029–2041
105. Subramanian KS, Charest C (1995) Influence of arbuscular mycorrhizae on the metabolism of maize under drought stress. Mycorrhiza 5:273–278
106. Azcón R, Tobar RM (1998) Activity of nitrate reductase and glutamine synthetase in shoot and root of mycorrhizal *Allium cepa*: effect of drought stress. Plant Sci 133:1–8
107. Tarafdar J (1996) The role of vesicular arbuscular mycorrhizal fungi on crop, tree and grasses grown in an arid environment. J Arid Environ 34:197–203
108. Augé RM (2001) Water relations, drought and vesicular-arbuscular mycorrhizal symbiosis. Mycorrhiza 11:3–42
109. Huang X-F, Chaparro JM, Reardon KF, Zhang R, Shen Q et al (2014) Rhizosphere interactions: root exudates, microbes, and microbial communities. Botany 92:267–275
110. Turner TR, James EK, Poole PS (2013) The plant microbiome. Genome Biol 14:209–219
111. Berg G, Grube M, Schloter M, Smalla K (2015) Unraveling the plant microbiome: looking back and future perspectives. Front Microbiol 5:148
112. Knief C (2014) Analysis of plant microbe interactions in the era of next generation sequencing technologies. Front Plant Sci 5:216
113. Turner TR, Ramakrishnan K, Walshaw J, Heavens D, Alston M et al (2013) Comparative metatranscriptomics reveals kingdom level changes in the rhizosphere microbiome of plants. ISME J 7:2248–2258

Part II

Methodology Chapters

Chapter 5

Mining and Quantifying In Vivo Molecular Interactions in Abiotic Stress Acclimation

Thorsten Seidel and Derya Kirasi

Abstract

Stress acclimation is initialized by sensing the stressor, transducing the signal, and inducing the response. In particular, the signal transduction is driven by protein–protein interactions and the response might involve de novo complex formation, shifts in subcellular localization and, thus, transportation that is mediated by other proteins. The investigation of protein–protein interactions and their regulation upon abiotic stress is crucial for a deeper understanding of the underlying mechanisms. FRET measurements by sensitized emission allow for the analysis of protein–protein interactions in real time and have a high potential to provide new insights into the regulation of protein–protein interaction with respect to subcellular localization and time. Within this section protocols are provided which allow for FRET analysis on the single cell level, the image acquisition procedure is described in detail and ImageJ plugins are suggested for the data evaluation.

Key words Förster resonance energy transfer (FRET), Fluorescent proteins, Protein–protein interactions, Sensitized emission, ImageJ

1 Introduction

The importance of Förster resonance energy transfer (FRET) in life sciences benefits from the engineering of fluorescent proteins. This facilitated the analysis of protein–protein interactions (PPI) in vivo [1]. In the recent years FRET pairs of cyan and yellow fluorescent proteins have been applied frequently and effort was spent to the improvement of these spectral variants, resulting in enhanced cyan fluorescent protein (ECFP), Cerulean3, SCFP3 and 4, mTurquoise2 as donors and enhanced yellow fluorescent protein (EYFP), SYFP, Citrine, or Venus as acceptor (summarized in Subheading 2). A comparatively easy way to measure FRET in living plant cells is 3-filter FRET that takes advantage of the sensitized acceptor emission in the presence of a donor. The technical requirements are fulfilled in most laboratories and comprise fluorescent microscopes with three appropriate filter sets or confocal laser

Ramanjulu Sunkar (ed.), *Plant Stress Tolerance: Methods and Protocols*, Methods in Molecular Biology, vol. 1631,
DOI 10.1007/978-1-4939-7136-7_5,

scanning microscope with two detectors and appropriate laser lines. This methodology was applied to map proteins within enlarged protein complexes, to confirm protein–protein interactions in living cells and to observe conformational alterations [3–6].

Stress- and effector-dependent FRET measurements were performed to analyze the impact of changing redox conditions on the conformation of the plastidic 2-cystein peroxiredoxin in *Arabidopsis thaliana* and dimerization of the transcription factor NAC089 [6–9]. Another dataset dealt with the question if the structural integrity of the vacuolar proton pump V-ATPase is linked to the glucose availability [5]. These examples for successful applications of FRET demonstrate its potential for the analysis of dynamic alterations of protein–protein interactions in response to stress or effector application. In the following a procedure is described for single cell analysis, but the measurement can be easily transferred to transgenic plants and the analysis of tissues expressing fluorescent protein-tagged interaction partners. Typical pitfalls and characteristic limitations will be addressed and strategies will be provided to reduce the bias of inadequate donor–acceptor ratios. The data evaluation by ImageJ is explained and plugins are compared.

2 Materials

2.1 Plasmid Isolation (Large Scale)

1. 3 M sodium acetate, pH 5.2.
2. 1 M Tris–HCl, pH 8 (stock solution, use concentrated HCl for pH).
3. 0.5 M EDTA, pH 8 (stock solution, EDTA dissolves at pH 8).
4. 10 mM Tris–HCl, pH 8.
5. 10 M ammonium acetate pH 7.5.
6. 5 M lithium chloride.
7. 100% isopropanol.
8. 100% ethanol.
9. 70% (v/v) ethanol.
10. Tris-buffered phenol (DNA is soluble in aqueous phenol, *see* **Note 1**).
11. Chloroform.
12. Solution 1: 50 mM glucose, 25 mM Tris–HCl pH 8, 10 mM EDTA (autoclave).
13. Solution 2: 0.2 N NaOH, 1.0% SDS (do *not* autoclave!).
14. Lysozyme solution: 10 mg/mL lysozyme in 10 mM Tris–HCl, pH 8.
15. PEG solution: 20% (w/v) PEG 8000 in water (heat to dissolve), 2.5 M NaCl (*see* **Note 2**).

16. TE buffer: 10 mM Tris–HCl pH 8, 1 mM EDTA.
17. LB Media: 1.0% tryptone, 0.5% yeast extract, 1.0% sodium chloride, pH 7 (autoclave).
18. SOC Media: 2.0% tryptone, 0.5% yeast extract, 10 mM sodium chloride, 2.5 mM potassium chloride, 10 mM magnesium chloride, 10 mM magnesium sulfate, 20 mM glucose, pH 7 (filter-sterilize).
19. Transformation buffer I: 30 mM potassium acetate, 50 mM manganese chloride, 100 mM rubidium chloride, 10 mM calcium chloride, 15% glycerol, pH 5.8 (filter-sterilize).
20. Transformation buffer II: 10 mM MOPS pH 7, 75 mM calcium chloride, 10 mM rubidium chloride, 15% glycerol (filter-sterilize).

2.2 Protoplast Isolation and Transfection

1. 100 mM MES, pH 5.7 (stock, autoclave).
2. 1 M mannitol (heat to dissolve).
3. 1 M calcium chloride.
4. Enzyme solution: 1.5% cellulose R10, 0.4% macerozyme R10, 0.1% BSA, 0.4 M mannitol, 20 mM potassium chloride, 20 mM (200 mL of stock per liter) MES pH 5.7, 10 mM calcium chloride (autoclave *without* enzymes and BSA, add enzymes and BSA prior to use) (*see* **Note 3**).
5. W5 solution: 154 mM sodium chloride, 125 mM calcium chloride, 5 mM potassium chloride, 5 mM glucose, 2 mM (20 mL of stock per liter) MES pH 5.7 (autoclave) (*see* **Note 4**).
6. MMG solution: 0.4 M mannitol, 15 mM magnesium chloride, 4 mM (40 mL of stock per liter) MES pH 5.7 (autoclave).
7. PEG solution: 40% PEG4000, 0.2 M (2 mL of stock per 10 mL) mannitol, 100 mM (1 mL of stock per 10 mL) calcium chloride (PEG4000 contributes vastly to the volume, only 65% (v/v) (3.5 mL for 10 mL, if stocks are used) of water are required, heat moderately to dissolve PEG 4000 and mannitol).
8. Plasmids for the expression in protoplasts, for instance: 35S–ECFP-NosT, 35S–EYFP-NosT [3], 35S–ECFP-C, 35S–EYFP-C [4], 35S–mCherry-NosT, 35S–mCherry-C [8], 35S–mTurquoise2-NosT [2].
9. Nylon mesh, 100–500 μm pore diameter, funnel, and 10-mL centrifugation-tubes. All materials should be detergent-free.

2.3 Microscopy

1. Technical requirements for fluorescence microscopy: Besides an appropriate light source for epi-illumination filter sets with bandpass characteristics are required that allow for specific excitation and detection of the donor (donor-filter set) and the acceptor (acceptor-filter set), respectively, and detection of

the acceptor upon excitation of the donor (FRET-filter set). The microscope stand should provide a camera-port equipped with a camera for digital image acquisition (*see* **Note 5**). Here, a monochromatic camera is recommended due to higher sensitivity. Anyway, color imaging is not of advantage due to the properties of the bandpass filters. Objectives with at least 40-fold magnification are suitable for protoplast imaging. Water-dipping objectives are recommended for upright stands, while long distance water immersion objectives are the best choice for inverted stands. To check the viability of cells, a long-pass filter set with an excitation at around 480 nm and an emission filter in the range of 500–700 nm can be used.

2. Additional technical requirements for confocal laser scanning microscopy: Appropriate laser lines for the excitation of donor and acceptor, two detectors that allow for spectrally separated detection of donor and acceptor. Dichroic mirrors or acousto-optical beam splitters (AOBS) that allow for sequential application of both laser lines in a line-by-line scanning mode. Most confocal laser scanning microscopes allow for line-wise sequential excitation with 458 nm/514 nm or 488 nm/543(561) nm.

2.4 Calibration of FRET Measurements (Protein Expression)

1. Lysis buffer: 10 mM imidazole, 300 mM sodium chloride, 50 mM NaH_2PO_4, pH 8.
2. Washing buffer: 20 mM imidazole, 300 mM sodium chloride, 50 mM NaH_2PO_4, pH 8.
3. Elution buffer: 250 mM imidazole, 300 mM sodium chloride, 50 mM sodium dihydrogen phosphate, pH 8.
4. 1 M K-Phosphate buffer pH 7 (stock): adjust pH to 7 by mixing 1 M potassium dihydrogen phosphate and 1 M dipotassium hydrogen phosphate.
5. LB Media: 1.0% tryptone, 0.5% yeast extract, 1.0% sodium chloride, pH 7 (autoclave).
6. SOC Media: 2.0% tryptone, 0.5% yeast extract, 10 mM sodium chloride, 2.5 mM potassium chloride, 10 mM magnesium chloride, 10 mM magnesium sulfate, 20 mM glucose, pH 7 (filter-sterilize).
7. Plasmids for single fluorophores: His-ECFP, His-EYFP, His-EGFP, His-mTurquoise2, His-mCherry, His-mVenus [2, 10].
8. Plasmids for donor–acceptor fusions: His-ECFP-EYFP (E_c = 0.46), His-mTurquoise2-mVenus (E_c = 0.62), His-EYFP-mCherry (E_c = 0.45) [2, 8]. Donor–acceptor fusions C5V, C17V, C32V of the Vogel-Lab are recommended for Cerulean and Venus as FRET pair [11]. The FRET efficiencies E_c were 0.43 ± 0.024, 0.38 ± 0.03, and 0.31 ± 0.02 for C5V, C17V, and C32V, respectively [11].

9. Technical requirements for absorption spectra: UV–Vis spectrophotometer, UV cuvettes.
10. Technical requirements for excitation and emission spectra (fluorescence): fluorescence spectrometer, quartz cuvettes for fluorescence.

2.5 Evaluation of FRET Measurements

The computer used for data evaluation should be up to date with sufficient RAM (≥ 8 GB). For ImageJ/FIJI, any operating system can be used. The following plugins are available for analyzing sensitized emission:

Fret and Colocalization Analyzer: http://rsb.info.nih.gov/ij/plugins/fret-analyzer/fret-analyzer.htm

RiFRET: http://www.biophys.dote.hu/rifret/

*Pix*FRET:http://www.unil.ch/cig/home/menuinst/research/research-groups/prof-desvergne.html#tabs-ad1640159a2e492d8b8dd070d9b95ae6

All Plugins can be downloaded and the .jar-file copied to the „plugin"-folder within the ImageJ-folder (typically C:/programs/imagej/plugins). After a restart of ImageJ, the plugin can be started.

3 Methods

3.1 Plasmid Isolation (Maxi-Preparation)

Maxipreparation of plasmid DNA is performed to gain high amounts of highly concentrated suspensions. The following protocol is suitable to gain up to 1 mg of high copy plasmid DNA out of 400 mL overnight culture.

1. Transform appropriate *Escherichia coli* strains (e.g., DH5α) with the plasmids of interest.
2. Thaw the chemically competent cells on ice.
3. Add 2 μL of plasmid to the cells (one vial of competent cells per plasmid).
4. Incubate the cells for 30 min on ice.
5. Perform a heat shock at 42 °C for 30–60 s.
6. Incubate the cells on ice for 2 min.
7. Add 250 μL of SOC media to the cells.
8. Incubate the cells at 37 °C for 30–60 min while horizontally shaking at 140 rpm.
9. Transfer the sample to a 50 mL-Erlenmeyer flask with 10 mL LB and appropriate concentration of desired antibiotics (e.g., 50–100 μg of ampicillin).
10. Incubate overnight at 37 °C while shaking at 140 rpm.

11. Transfer the preculture to a 1000 mL-Erlenmeyer flask with 400 mL LB and appropriate concentration of desired antibiotics (e.g., 50–100 µg/mL of ampicillin).
12. Incubate overnight at 37 °C while shaking at 140 rpm.
13. Harvest the cells by centrifugation at 4500 × *g* and 4 °C for 20 min.
14. Resuspend the cells in 9 mL Solution 1 (*see* **Note 6**).
15. Add 1 mL of Lysozyme solution and 20 mL of Solution 2.
16. Incubate for 10 min at room temperature.
17. Add 10 mL of 3 M sodium acetate pH 5.2.
18. Incubate for 10 min at 4 °C.
19. Centrifuge at 4000 × *g* and 4 °C for 15 min.
20. Filtrate the supernatant through two layers of miracloth.
21. Fill the tube to the 50 mL-mark with isopropanol (*see* **Note 7**).
22. Incubate at room temperature for 10 min.
23. Centrifuge at 4000 × *g* and room temperature for 20 min.
24. Resuspend the pellet with 6 mL TE (*see* **Notes 8** and **9**).
25. Add 6 mL 5 M lithium chloride.
26. Centrifuge at 4000 × *g* and 4 °C for 20 min.
27. Add 12 mL isopropanol to the supernatant.
28. Centrifuge at 4000 × *g* and room temperature for 20 min.
29. Discard the supernatant and wash the pellet with 70% ethanol.
30. Resuspend the pellet with 1.2 mL of TE (*see* **Note 8**), add 2.4 µL of RNase solution.
31. Transfer the samples to 2 mL safe lock reaction tubes.
32. Incubate at 37 °C for at least 1 h.
33. Add 800 µL of PEG solution (*see* **Note 1**).
34. Incubate at 4 °C for 10 min.
35. Centrifuge at 16,000 × *g* and 4 °C for 5 min.
36. Resuspend the pellet with 800 µL of TE (*see* **Note 2**).
37. Add 800 µL of phenol–chloroform and vortex for 15 s (*see* **Note 10**).
38. Centrifuge at 16,000 × *g* and 4 °C for 5 min.
39. Transfer the upper aqueous phase to a new 2 mL safe lock tube.
40. Add 800 µL of chloroform.
41. Centrifuge at 16,000 × *g* and 4 °C for 5 min.
42. Split the upper aqueous phase into two 1.5-mL tubes.
43. Add 100 µL of 10 M ammonium acetate pH 7.5 and 1 mL 100% ethanol to each tube.

44. Incubate at room temperature for 10 min.
45. Centrifuge at 16,000 × *g* and 4 °C for 5 min.
46. Discard the supernatant and wash the pellet with 70% ethanol.
47. Dry the pellet completely to remove the ethanol.
48. Resuspend the pellet with 50–200 µL 10 mM Tris–HCl pH 8 (*see* **Note 11**).
49. Quantify the DNA by measuring the OD_{260nm} of an1:100 dilution, adjust the concentration to 5 µg/µL.

3.2 Protoplast Isolation and Transfection

The protoplast isolation is established for mesophyll cells of *Arabidopsis thaliana*, but the protocol can be adjusted to any other plant species and tissue. Separation of mesophyll cells, guard cells, and epidermal cells can be achieved by density centrifugation [12]. Two alternate protocols are given. One is suggested for inverse stands and the other for upright stands.

1. Twenty microliters of enzyme solution is sufficient for 4 g of leaves, pour the enzyme solution into a 90-mm petri dish (*see* **Note 12**).
2. Cut the leaves perpendicular to the midvein into strips of approximately 1–2 mm, transfer the slices immediately to the enzyme solution to prevent drying. Alternatively, epidermis could be stripped or removed by sandpaper instead of cutting.
3. Vacuum-infiltrate the leaves, e.g., for 3 min, reventilate carefully (*see* **Note 13**).
4. Transfer the dish to a platform shaker and incubate for at least 2 h with slight shaking at for example 40–50 rpm for a Heidolph Unimax 1010 shaker (*see* **Note 14**).
5. Release the protoplasts by accelerated shaking speed for 1 min, e.g., 90 rpm for a Heidolph Unimax 1010.
6. Filtrate the cells through a nylon mesh to separate the cells from the leaf strips.
7. Sediment the cells by centrifugation at 100 × *g* and 4 °C for 3 min.
8. Carefully remove the supernatant and resuspend the cells with 5 mL of W5 solution (use plastic Pasteur pipettes for media removal), keep the protoplasts on ice for 30 min (protoplast preparation ends here, the isolated cells in W5 can be subjected to other analyses. The following steps are required for transfection).
9. Sediment the cells by centrifugation at 100 × *g* and 4 °C for 1 min (*see* **Note 15**).
10. Resuspend the cells in 3 mL MMG solution and keep the protoplasts on ice for 30 min.

11. Mix the plasmids according to the pairs of proteins that have to be analyzed, consider replicates.
12. For inverted microscopes: Place 20 µL protoplasts in the center of a well, e.g., that of an 8-well slide for each transfection (*see* **Note 16**).
13. Add 5 µL of the plasmid mix to the cells by gently pipetting and distribute the plasmid mix all over the cell resuspension (*see* **Note 17**).
14. Add 25 µL PEG solution immediately after addition of the plasmid, again by gently pipetting (*see* **Note 18**).
15. Dilute the PEG by stepwise addition of W5: begin with adding 50 µL W5 solution followed by 8 min of incubation. Repeat the dilution step with 100 µL and two times 200 µL W5 solution, each step followed by 8–15 min of incubation at room temperature (*see* **Notes 19** and **20**).
16. Transfer the 8-well slide to an incubator adjusted to 25 °C and incubate the cells in the dark overnight. The incubation time can be adjusted with respect to the maturation time of the analyzed proteins and the fluorescent proteins.

3.2.1 Alternative Procedure for Upright Microscope Stands Following Step 11

12. Place 200 µL protoplasts in the center of a 60-mm petri dish. Prepare a dish for each transfection.
13. Add 20 µL of the plasmid mix to the cells by gently pipetting and distribute the plasmid mix all over the cell resuspension.
14. Add 220 µL PEG solution immediately after addition of the plasmid, again by gently pipetting (*see* **Note 18**).
15. Dilute the PEG by stepwise addition of W5: begin with adding 0.5 mL W5 solution followed by 8 min of incubation. Repeat the dilution step with 1 mL, 2 mL, and 4 mL W5 solution, each step followed by 8–15 min of incubation at room temperature (*see* **Notes 19** and **20**).
16. Transfer the dishes to an incubator adjusted to 25 °C and incubate the cells in the dark overnight. The incubation time can be adjusted with respect to the maturation time of the analyzed proteins and the fluorescent proteins.

3.3 Microscopy

The suggested procedure for FRET measurements applies confocal laser scanning microscopes.

1. Check the transfection efficiency and fitness of protoplasts by bright-field and fluorescence microscopy. The cells should be perfectly round-shaped. In case of mesophyll cells, the chlorophyll-fluorescence should be clearly visible as dark-red fluorescence emission upon blue light excitation, if a long pass-filter is used.

2. Allow the light source to gain a stable output. For confocal laser scanning microscopy with an argon ion laser, start the laser at least 1 h before you intend to use it. Before, the laser intensity will show fluctuations (*see* Fig. 1). The actual time point depends on the setup and needs to be determined first. To this end, perform a time series with <1 fps for 3 h directly after starting the laser. Detect the emission of the laser by the trans-detector and finally plot the emission against the time to visualize fluctuations over time (Fig. 1). Determine the time the laser requires for a smooth and stable performance.
3. Define the settings for FRET measurements, e.g., for measurements applying cyan and yellow fluorescence proteins the cyan donor and the yellow acceptor can be excited by the 458 nm and the 514 nm line, respectively. Appropriate detection ranges for donor and acceptor are 470–510 and 530–600 nm, respectively (*see* **Notes 21–23**). This results in three channels, one for the donor, one for the FRET, one for the acceptor. The corresponding emission intensities are named I_D, I_F, and I_A, respectively (Fig. 2). Adjust the offset to a grainy background. Full suppression of background noise has to be avoided. Generally, a 12-bit scanning should be performed at moderate speed and moderate laser intensity without line averaging. Apply the transdetector to estimate the laser intensity (*see* **Note 24**).

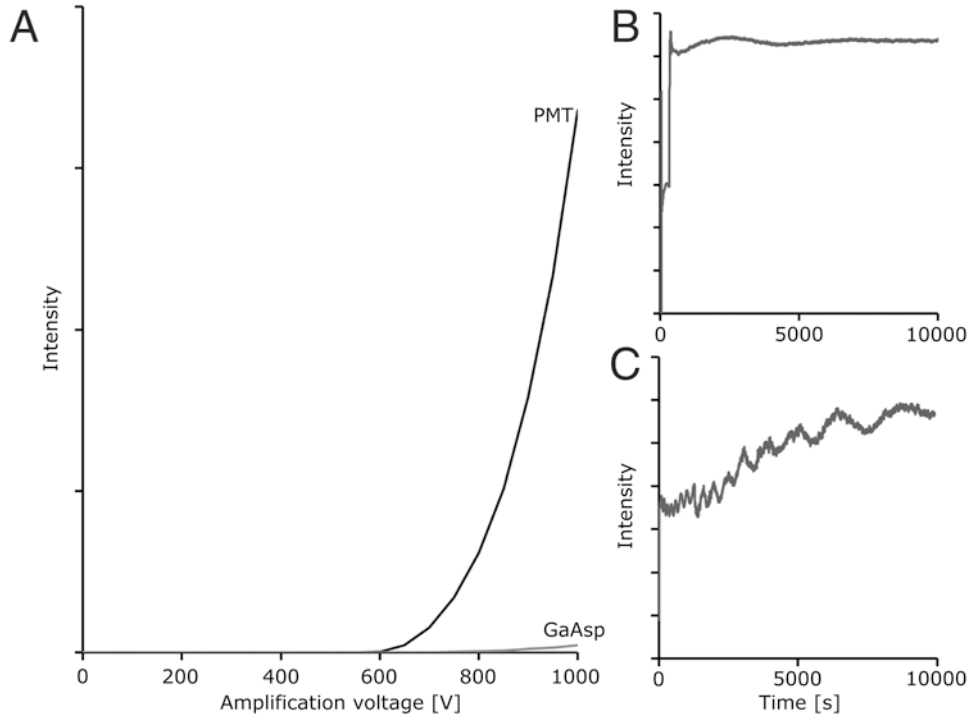

Fig. 1 LSM performance. (**a**) Photomultipliers and GaAsp detectors differ in their background noise. (**b**, **c**) 488-nm output of two argon ion lasers monitored for more than 2 h

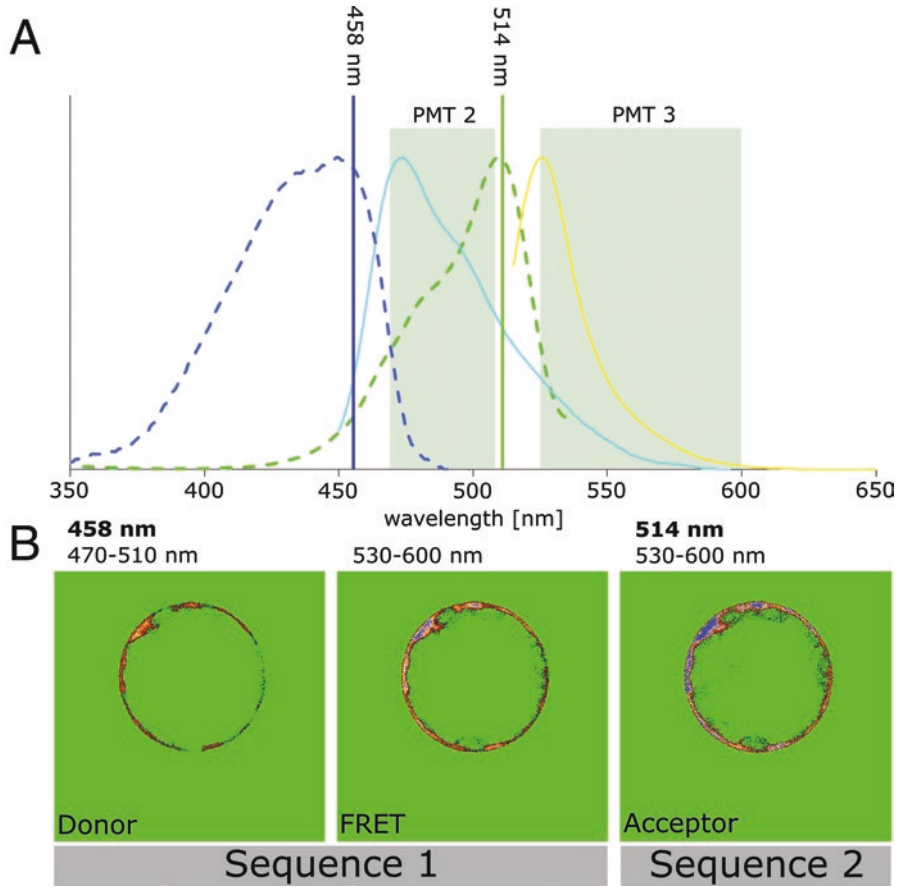

Fig. 2 Detection of donor and acceptor by three-filter FRET or sensitized emission, depicted for cyan and yellow fluorescent proteins as FRET pair. (**a**) absorption spectra (*dashed lines*) and emission spectra (*solid lines*) are given for ECFP and EYFP. Two detectors (PMT1 and PMT2) and excitation at 458 nm is required to obtain the donor and the FRET image. One detector (PMT2) and excitation at 514 nm is applied to obtain the acceptor image. (**b**) The images are obtained by sequential scanning, recording donor (CFP) and FRET simultaneously, and the acceptor (YFP) in a second scanning sequence. Keeping PMT settings identical for both sequences allows for sequential scanning in the line by line mode

4. Start the measurement with your sample of interest (*see* **Note 25**). Carefully adjust the gain voltage so that the full dynamic range of the detector is used. Dynamic range means the range between background noise and highest emission detected in your sample. For dynamic measurements determine the conditions of highest signal intensity in the FRET channel and donor channel first. Then use these conditions to determine the gain and thus, the dynamic range of your measurement. Each set of settings requires a full set of control measurements. Once you change a setting, another set of controls is required. Controls comprise the determinations of DSBT, ASBT and the calibration measurements. Acquire Images of ≥20 cells for statistical data evaluation.

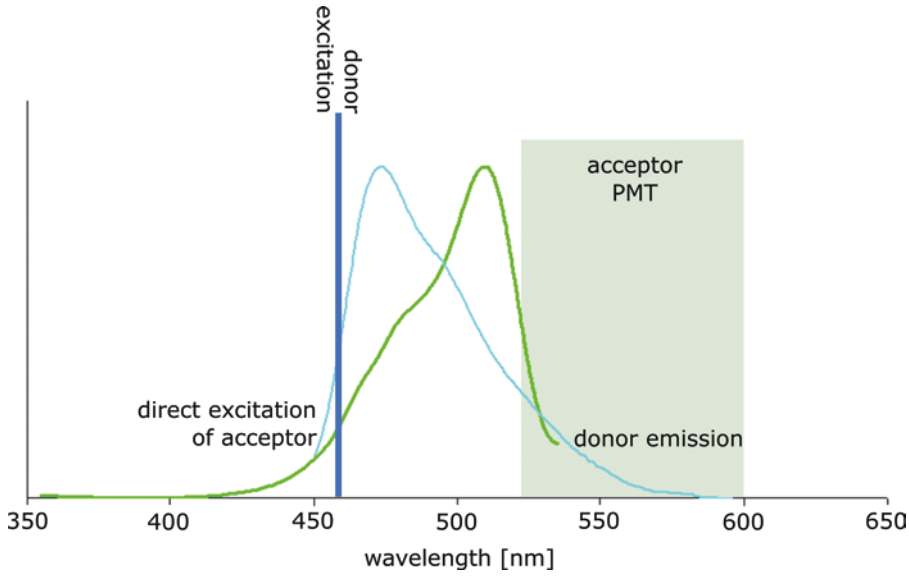

Fig. 3 Origins of DSBT and ASBT. Donor spectral bleed through (DBST) and acceptor spectral bleed through (ASBT) originate by the broad emission spectra of the donor and the direct excitation of the acceptor, respectively. The correction factors β and α are the ratios of the intensities in the FRET channel and in the donor/acceptor reference channels for cells expressing donor only and acceptor only, respectively

5. Fluorescent proteins show broad emission spectra (Fig. 3). Thus, the donor emission can be detected in the same wavelength range as the acceptor emission (donor spectral bleed through, DSBT). Analyze cells expressing donor only.
6. The acceptor might be excited at the wavelength that is used for donor/FRET excitation, too (Fig. 3). This direct acceptor excitation results in acceptor emission in the absence of FRET (acceptor spectral bleed through, ASBT). Analyze cells expressing acceptor only.
7. Record images for a FRET construct of known FRET efficiency E_c. This can be achieved by expressing a donor–acceptor fusion protein in the cells and applying the identical settings as used for the FRET measurements. These images are required for calibration and calculation of the coefficient ξ which expresses the linear relationship between sensitized emission I_{SE} and donor quenching I_{DQ}. Optionally, the system can be calibrated by an acceptor-based approach. In this case, γ represents the ratio of donor's and acceptor's absorption coefficients ε at the donor's excitation wavelength while significant ASBT is mandatory.
8. Keep the settings constant for all measurements, if the variance of emission intensities allows for.

3.4 Data Evaluation, Readout of FRET Data

The raw data obtained by confocal laser scanning microscopy are quantitative images. Next, the pixel intensities have to be read out so that SBTs as well as ξ or γ can be determined and finally the FRET efficiency can be calculated (*see* **Notes 26** and **27**). To get the FRET efficiency from areas, go to "Histo(gram)," define a region of interest within the area to get the mean intensities of all three images in this region. Denominate the donor intensity I_D, the FRET intensity I_F, and the acceptor intensity I_A. For structures of low spatial dimensions, a line profile across the structure is recommended. The intensities of the structure are read out by the maxima of the resulting three line profiles. Ensure that the maxima are co-localized and export the data as txt file. This way, the data can easily be imported to any spreadsheet.

1. Donor spectral bleed through (DSBT): Determine the extent β of DSBT by analyzing cells expressing donor only. Then β is given as ratio of the emission in the FRET channel I_F and the emission in the donor channel I_D:

$$\beta = \frac{I_F}{I_D}$$

2. Acceptor spectral bleed through (ASBT): Determine the extent α of ASBT by analyzing cells expressing acceptor only. Then α is given as ratio of the emission in the FRET channel I_F and the emission in the acceptor channel I_A:

$$\alpha = \frac{I_F}{I_A}$$

3. Calibrate the measurements by obtaining I_D, I_F, and I_A for an intramolecular FRET construct of known FRET efficiency E_c [13]. The coefficient ξ is calculated based on this dataset ($I_{DQ} = \xi I_{SE}$). ξ enables the quantification of FRET efficiency E on the basis of donor quenching (*see* **Note 29**):

$$E = 1 - \frac{I_D}{I_D + I_{DQ}} = 1 - \frac{I_D}{I_D + \xi I_{SE}} = 1 - \frac{I_D}{I_D + \xi(I_F - \alpha I_A - \beta I_{D)}}$$

Optionally, acceptor-based calculation of γ is enabled by obtaining I_D, I_F, I_A for a reference construct of known E_c, too (*see* **Note 28**):

$$E = 1 - \frac{\varepsilon_A}{\varepsilon_D}\left(\frac{I_F - \beta I_D}{\alpha I_A}\right) = 1 - \gamma\left(\frac{I_F - \beta I_D}{\alpha I_A}\right)$$

so that γ can be calculated as follows:

$$\gamma = \frac{E_c}{\frac{I_F - \beta I_D}{\alpha I_A} - 1}$$

4. Combine the data in a spreadsheet.

3.5 Data Evaluation, Visualization of FRET Results

Displaying of FRET efficiencies in images obtained by confocal laser scanning microscopy is enabled for instance by the ImageJ plugins "FRET and Colocalization Analyzer," "PixFRET," and "RiFRET". Thereby the FRET efficiency is given in dependency on the subcellular localization and usually shown for a representative cell (*see* **Note 30**).

3.5.1 Installation

ImageJ and its plugins work with iOS, Windows, and Unix.

1. Download the zip file.
2. Place the ".jar" file in the "Plugins" folder in ImageJ.
3. Start ImageJ again to display the new plugin in the "Plugins" menu.

3.5.2 FRET and Colocalization Analyzer

The ImageJ plugin "FRET and Colocalization Analyzer" [14] analyzes FRET images obtained by confocal microscopy (*see* **Note 31**). The plugin uses the "sensitized FRET emission" evaluation. The donor is excited and the sensitized emission of the acceptor fluorophore is recorded in the FRET channel. To estimate the spectral bleed through (SBT) of the fluorophores, corrections factors are calculated and defined as constants to subtract the SBT from the raw data of the FRET channel. The calculation is based on Youvan et al. [15]. The result is a FRET image, which displays the acceptor emission intensities caused by FRET in a pixel-wise manner. The plugin also provides the ability to verify the calculated SBT-values and to eliminate false-positive FRET signals. The elimination of false-positive FRET signals relies on the co-localization of the donor and acceptor fluorophores by correlating co-localization and FRET. The plugin edits images with up to 8-bit [14]. The compression of 16- to 8-bit images results in a loss of information accompanied by the risk of modification of the FRET data.

1. Open the "bleed through" window for DSBT and ASBT evaluation.
2. Define number of controls for samples expressing only the donor: Indicate the number n of fields of control images that will be used to evaluate the mean of the donor bleed through (max: 10).
3. Open the required donor channel images and FRET channel images of cells expressing the donor fluorophore only.

4. Go to "File," press "Refresh files list," names of the images appear in the rolling image menu.
5. Optional: press "Show controls" to perform a regression analysis and plot a regression graph, that assigns either donor or acceptor intensities to FRET intensities at given pixel coordinates in the images.
6. "Get": to perform the calculation of the DSBT parameters of the images (**step 2**).
7. Repeat **steps 1–5** for another set of images.
8. Acceptor spectral bleed-through evaluation: repeat **steps 3–6** with acceptor channel images and FRET channel images of cells expressing the Acceptor fluorophore only. Then "Get" results in the calculation of ASBT parameters.
9. Select the window "FRET calculation": Open a set of images of donor, acceptor, and FRET channel. These images are obtained from cells co-expressing donor and acceptor.
10. "Refresh files list."
11. Optional: choose "FRET min and max," in addition to the FRET index image, minimum and maximum FRET-index images are generated. These consider either the maximal SBT contribution (minimum) or the minimum SBT contribution (maximum) according to the range of values obtained for DSBT and ASBT before.
12. Optional: choose "Colocalization and FRET," displays a co-localization correlation diagram for donor and acceptor intensities. FRET efficiencies are displayed color-encoded. Within this graph pixels can be selected for the "co-localized FRET-index" image by box-drawing. This option enables a background correction of FRET.
13. Press "FRET-index": all FRET images including the optional images will be generated.

3.5.3 PixFRET

The "PixFRET" plugin [16] generates normalized FRET images by pixel-wise calculation of intensities in the three channels "donor," "acceptor," and "FRET." The calculation refers to Xia and Liu [17] and was designed to adjust for varying donor to acceptor ratio (*see* **Note 25**):

$$\mathrm{NFRET} = \frac{I_\mathrm{F} - \alpha I_\mathrm{A} - \beta I_\mathrm{D}}{\sqrt{I_\mathrm{D} I_\mathrm{A}}}$$

In addition, SBT values can be entered for the donor and acceptor, these values can also be determined from the images of the three channels. First, the background values of the channels and then the average SBT are calculated. This plugin allows further

for adjusting SBT as either a linear (linNFRET) or exponential (expNFRET) function of donor abundance/intensity. By clicking the "Compute FRET" button a normalized 8-bit FRET image is generated [16].

1. The PixFRET plug-in requires three different sets of images:
2. For FRET analysis, a set of three images taken with the FRET, donor, and acceptor settings.
3. For DSBT determination, a set of two images of cells expressing the donor only and taken with the FRET and donor settings.
4. For ASBT determination, a set of two images of cells expressing the acceptor only and taken with the FRET and Acceptor settings.
5. FRET Calculation: Click on "Donor Model" to enter or acquire DSBT parameters.
6. If SBT parameters have been determined offline, clicking "Accept" in the background dialog box allows to directly select the appropriate model for donor SBT estimation in the dialog box beneath (e.g., "constant") and to enter the values manually. Click on the "Accept" button and then skip points 7–10.
7. Open the image set for DSBT determination.
8. Select a region-of-interest (ROI) to determine the background outside cells and click on the "Get" button. The average background intensity values in the ROI are displayed in the two boxes below. It can be reset by clicking the "Reset" button. Values can also be entered manually.
9. Select a ROI in which the SBT will be determined and click the "Get" button.
10. Click the "Accept" button to use the SBT values obtained.
11. Perform similar operations for the acceptor. Go to the FRET menu and open the set of images for FRET calculation.
12. Select a ROI in the background and click "Get" in the background box to obtain the background values, these can be entered manually, too.
13. Enter the value for the Gaussian blur and mark the "show blurred images" box to visualize the image.
14. Enter the "threshold correction factor." FRET and NFRET are calculated only, if pixel values are above a given threshold that is set to average background values as default.
15. Select the normalization method for processing the final FRET image. With normalization, the FRET values will be divided for each pixel by (a) the value of the donor intensity, (b) the acceptor intensity, (c) the product of donor and acceptor intensities, or (d) the square root of the product of donor and

acceptor intensities for the given pixel (NFRET). The latter is recommended.

16. Generation of FRET images: After clicking the "Compute FRET" button, the software calculates for each pixel the normalized FRET (NFRET) value and displays two images.
17. Save the images.

3.5.4 RiFRET

The RiFRET plugin calculates intensity-based ratiometric FRET efficiencies pixel by pixel. Two calibration methods are provided so that the experimentator has the choice to determine the FRET efficiency of the reference constructs by antibody labeling or by acceptor bleaching. If images of the donor, acceptor and FRET channel are available, a FRET image can be calculated. The calculation can also be performed for z-stacks or time series. At the beginning, the background of the respective images is subtracted. Optionally, the influence of cellular autofluorescence can be determined by background-corrected images of unlabeled cells. At the end a FRET image is generated [18].

The SBT correction factors S_1–S_4 can be either manually entered or calculated based on images of donor (S_1, S_3) only or acceptor (S_2, S_4) only. S_1 and S_2 correspond to the previously introduced factors β and α, respectively. S_3 and S_4 represent the SBT of the donor into the acceptor channel and the SBT of the acceptor into the donor channel: $S_3 = I_A/I_D$ and $S_4 = I_D/I_A$. Often, the values of S_3 and S_4 are practically 0 due to the spectral properties of the dyes.

Roszik and coworkers introduced a novel factor that they denominated α. The factor α is the ratio of the fluorescence intensities of a given number of excited acceptor molecules (measured in the FRET channel) and fluorescence intensities of the same number of excited donor molecules in the donor channel [18].

Calculation of FRET efficiency E is performed pixel-by-pixel and bases on A and α:

$$A = \frac{1}{\propto} \frac{S_1 S_2 \left[I_F \left(1 - S_3 S_4\right) - I_D \left(S_1 - S_2 S_3\right) - I_A \left(S_2 - S_1 S_4\right) \right]}{\left(S_1 - S_2 S_3\right)\left(I_D S_2 - I_F S_4\right)}$$

In case that $S_3 = 0$ and $S_4 = 0$, the equation is:

$$A = \frac{1}{\propto} \frac{S_1 S_2 \left(I_F - I_D S_1 - I_A S_2\right)}{S_1 S_2 I_D}$$

In living cells, α can be determined by donor–acceptor fusions with a fluorophore expression ratio of consumably 1. For simplicity the calculations are given for $S_3 = 0$ and $S_4 = 0$. Further, the ratio of dyes bound to antibodies L_D/L_A is not applicable here and set to 1. Otherwise, the complete calculations can be found in Roszik et al. [18]. The calculation is performed by iterative approximation starting with $E = 0$ to get an initial value for α, then this α is used

to calculate E again, which in turn is used to calculate α in the second iteration. Three to five iterations are sufficient to get optimized values for E and α [18].

$$\propto = \frac{I_A S_2 (1-E)}{I_D} \frac{\varepsilon_D}{\varepsilon_A} = \frac{I_A S_2 (1-E)}{I_D} \frac{I_F - S_1 I_D - S_2 I_A}{S_2 I_A E_c}$$

The ratio of the absorption coefficients ε can be calculated with a dataset obtained with cells expressing the donor–acceptor fusions of known FRET efficiency E_c, too.

$$\frac{\varepsilon_D}{\varepsilon_A} = \frac{I_F - S_1 I_D - S_2 I_A}{S_2 I_A E_c}$$

Finally, E is given by

$$E = \frac{A}{1+A}$$

1. Calculate or set S_1, S_2, S_3, and S_4 correction factors.
2. For S_1 and S_2 use cells expressing donor only.
3. For S_2 and S_4 use cells expressing acceptor only.
4. Calculate or set α.
5. Open and set the donor, FRET, and acceptor images (*see* **Note 32**).
6. Subtract average of a background Region of Interest (ROI) within the donor, transfer, and acceptor images.
7. Optional: Blur the donor, transfer, and acceptor images. This will result in a Gaussian blurring of the images.
8. Set threshold for donor, transfer, and acceptor channel images to define upper and lower limits, if desired.
9. Create the FRET image.
10. Select ROIs and start measurements to obtain the FRET efficiency.

4 Notes

1. Tris-buffered phenol was used to avoid unwanted dissolving of DNA in the organic phase. DNA is soluble in aqueous phenol.
2. Take care of proper labeling of the PEG solution to avoid its usage in protoplast transfection.
3. Enzyme solution can be reused at least for one more time; filter-sterilize the solution and store it at −20 °C after first use.
4. The composition of media might be adapted to specific experimental requirements such as omitting sodium chloride for the investigation of salinity effects. Attention should then be paid

to osmotic effects. Any treatment or pest potentially affects the transfection efficiency. 6-carboxyfluoresceindiacetate staining can be applied to display vitality of cells.

5. If a conventional fluorescent microscope is used, the pixel intensities depend on the exposure time of the camera. In this case an automated shutter that controls the epi-illumination and a motorized filter-wheel are recommended to avoid unwanted exposure and, thus, bleaching effects. The exposure times should be identical for the measurements and the controls.
6. Usually, 9 mL of solution is sufficient to resuspend the pellet of a 400-mL culture.
7. Isopropanol precipitation subsequent to alkaline lysis should be performed with at least 30% of isopropanol.
8. To facilitate resuspending of the pellet, remove as much of isopropanol, ethanol, or PEG solution-containing supernatant as possible before resuspending the plasmid DNA.
9. Adjust resuspension volumes according to the gained pellet. If resuspension is incomplete, increase the volume stepwise until the pellet is resuspended.
10. Due to the toxicity of phenol the phenol extraction was performed with 2-mL safe-lock tubes and a refrigerated centrifuge. All steps were performed within a fume hood with closed sash. Phenol and chloroform were mixed before usage and centrifuged for 1 min to separate the organic solvents from water. At the end, clean the centrifuge carefully to prevent phenol-mediated corrosion.
11. Start the final elution with 50 µL 10 mM Tris–HCl pH 8 and increase the volume in steps of 50 µL until the pellet is resuspended. Due to the viscosity of highly concentrated plasmid DNA, prepare 1:100 dilutions for NanoDrop measurements. This also prevents extremely high absorption values far from linearity.
12. Age and health of plants is crucial for successful transfection. For instance, young leaves are inappropriate for CaMV35S-driven protein expression. Before starting the experiments, compare healthy plants of different developmental stages under your preferred growth conditions to identify the most promising stage. Keep in mind that this likely affects the comparison of stress responses at different developmental stages.
13. Some petri dishes do not tolerate stacking during vacuum infiltration and collapse.
14. Theoretically, digestion of leaves can be extended up to overnight treatments, though altered fitness and conditional state of the cells might occur then.
15. Protoplasts sediment in W5 by time, so that centrifugation can be avoided if desired.

16. Cut the pipet tips before usage to avoid shearing of cells.
17. The ratio of donor and acceptor plasmids does not necessarily match the resulting protein ratio. Differences in molecular weight, processing, and transport likely result in differences in protein abundance.
18. High amount of plasmid DNA results more in PEG-mediated precipitation of DNA rather than in an improved transfection.
19. The incubation time subsequent transfection depends on your protein of interest. Among others, the time required for expression depends on the molecular weight, complexity of folding and subcellular localization. Estimating the time point of appearance is helpful for considering shuttling and transport dynamics between compartments and identifying overexpression artefacts by flooding cellular compartments with the protein of interest. Transfection efficiency increases with the temperature while survival rate decreases. With incubation at 25 ° C sufficient transfection efficiency can be obtained by proper cell survival [19]. Raising the temperature to 30 °C reduces cell survival but increases the transfection efficiency.
20. Protoplasts should settle in the media. Media that allow protoplasts to float are inappropriate.
21. The wavelengths that are used for the excitation of donor and acceptor differ in their absorption by the pigments of the cell. In autotrophic plant cells the excitation light of yellow fluorescent proteins is less affected by cellular absorption while the excitation of cyan fluorescent proteins is significantly affected by cellular absorption. This effect results in a bias of FRET measurements by an apparent donor quenching. Thus, areas should be considered that are close to the objective. Alternatively, data evaluation has to be performed in areas that are characterized by short distances of the excitation light within the cell. In protoplasts, the basal areas facing the objective and the equatorial regions fulfill this requirement.
22. According to the previous note, the choice of the microscopic setup is of importance. Protoplast are characterized by an altered morphology, the chloroplasts lack anchoring and follow the gravity. They are concentrated at the bottom of the protoplasts. Using an upright stand equipped with a water immersion objective designed for electro physiology are of advantage to analyze the upper basal area of the cell without an impact by the plastidic absorption. In contrast, inverse stands show higher impacts by the plastidic absorption at the basal area. Both setups show the same applicability for the peripheral equatorial regions.
23. A central prerequisite for protein interactions is the co-localization of the proteins subjected to analysis. The interaction

can be limited by spatial and temporal dynamics, so that time-dependent observation of the localization might be required as preparatory work.

24. Setting the image resolution to 8-bit seems to be sufficient since FRET efficiencies range from 0 to 1 and 256 intensities are available, resulting in a precision of apparently 0.01. That's below the error of the experiment. The situation changes once DSBT and ASBT are considered. Then the FRET-derived intensity-range decreases and does no longer provide appropriate precision. For instance, assuming $\beta = 0.6$ and $\alpha = 0.2$ and saturated donor, FRET and acceptor images, the intensity-range for FRET-derived emission will be around 0–50. Thus, 12-bit scanning is recommended, 16-bit scanning is not of additional advantage.
25. FRET quantification by sensitized emission is sensitive to changes in the donor–acceptor ratio. In particular, an excess of the donor decreases the average FRET efficiency of the ensemble. Swapping the fluorophores and changing the donor–acceptor ratio provide information on different expression levels of donor and acceptor.
26. FRET depends on the orientation of donor and acceptor. If the donor dipole and acceptor dipole are placed perpendicularly, FRET will not occur. Therefore, lack of energy transfer does not necessarily correspond to the lack of interaction. One way out is the additional application of circular permutated fluorescent proteins, e.g., cpVenus as acceptor for cyan fluorescent proteins.
27. FRET further depends on the availability of acceptors in the unexcited ground state S_0. Long fluorescent lifetimes of the acceptor decrease the probability of FRET, if the acceptor lifetime exceeds the donor lifetime.
28. Most acceptor-based calculations depend on an ASBT-value $\alpha > 0$, since the denominator is multiplied by α in most equations. For donors with large Stokes shifts an acceptor-based calculation might be inappropriate.
29. Besides the standard deviation and the standard error, calculating the FRET efficiency with the maximal and the minimal SBT provides further information on the reliability and precision of the obtained FRET efficiency.
30. Among others, the main criteria for "representative image" are that the FRET efficiencies shown in the FRET image match the mean FRET efficiencies of all analyzed cells and the appearance of the cell and the subcellular distribution of the analyzed proteins are similar in all cells.
31. To use the plugin *FRET and Colocalization Analyzer*, the recorded microscope images must be 8 bit. Therefore, the images have to be compressed to 8 bit before running the analysis.

32. With *RiFRET*, images that have been defined as "acceptor," "donor," or "Fret" can be erroneously used again for a different channel, without occurrence of an error message. Therefore, all images that have been already defined and used for a calculation should be closed.

References

1. Gadella T, van der Krogt G, Bisseling T (1999) GFP-based FRET microscopy in living plant cells. Trends Plant Sci 4:287–291
2. Müller SM, Galliardt H, Schneider J, Barisas B, Seidel T (2013) Quantification of Förster resonance energy transfer by monitoring sensitized emission in living plant cells. Front Plant Sci 4:413
3. Seidel T, Golldack D, Dietz KJ (2005) Mapping of C-termini of V-ATPase subunits by in vivo-FRET measurements. FEBS Lett 579: 4374–4382
4. Seidel T, Schnitzer D, Golldack D, Dietz KJ (2008) Organelle-specific isoenzymes of plant V-ATPase as revealed by in vivo-FRET analysis. BMC Cell Biol 9:28
5. Schnitzer D, Seidel T, Sander T, Golldack D, Dietz KJ (2011) The cellular energization state affects peripheral stalk stability of plant vacuolar H+-ATPase and impairs vacuolar acidification. Plant Cell Physiol 52:946–956
6. Muthuramalingam M, Seidel T, Laxa M, de Miranda SM, Gärtner F, Wu JR, Ströher E, Kandlbinder A, Dietz KJ (2009) Multiple redox and non-redox interactions define 2-Cys peroxiredoxin as a regulatory hub in the chloroplast. Mol Plant 2:1273–1288
7. Klein P, Seidel T, Stöcker B, Dietz KJ (2012) The membrane-tethered transcription factor ANAC089 serves as redox-dependent regulator of stromal ascorbate peroxidase gene expression. Front Plant Sci 3:247
8. Seidel T, Seefeld B, Sauer M, Dietz KJ (2010) In vivo analysis of the 2-Cys peroxiredoxin by two-step FRET. J Biotechnol 149:272–279
9. Wolf H, Barisas BG, Dietz KJ, Seidel T (2013) Photo-convertible Kaede enables the detection of protein homo-aggregation and conformational alterations in plant cells. Mol Plant 6:1453–1462
10. Seefeldt B, Kasper R, Seidel T, Tinnefeld P, Dietz KJ, Heilemann M, Sauer M (2008) Fluorescent proteins for single-molecule fluorescence applications. J Biophotonics 1:74–82
11. Koushik SV, Chen H, Thaler C, Puhl HL, Vogel SS (2006) Cerulean, Venus, and VenusY67C FRET reference standards. Biophys J 91:L99–L101
12. Pandey S, Wang XQ, Coursol SA, Assmann SM (2001) Preparation and applications of *Arabidopsis thaliana* guard cell protoplasts. New Phytol 153:517–526
13. Beemiller P, Hoppe A, Swanson J (2006) A phosphatidylinositol-3-kinase-dependent signal transition regulates ARF1 and ARF6 during Fcγ receptor-mediated phagocytosis. PLoS Biol 4:e162
14. Hachet-Haas M, Converset N, Marchal O, Matthes H, Gioria S, Galzi J, Lecat S (2006) FRET co-localization analyzer—a method to validate measurements of sensitized emission FRET acquired by confocal microscopy and available as an ImageJ plug-in. Microsc Res Technnol 69:941–956
15. Youvan D, Silva C, Bylina E, Coleman W, Dilworth M, Yang M (1997) Calibration of fluorescence resonance energy transfer in microscopy using genetically engineered GFP-derivatives on nickel chelating beads. Biotechnology 3:1–18
16. Feige J, Sage D, Wahli W, Desvergne B, Gelman L (2005) PixFRET, an ImageJ plugin for FRET calculation that can accommodate variations in spectral bleed-throughs. Microsc Res Technol 68:51–58
17. Xia Z, Liu Y (2001) Reliable and global measurement of fluorescence resonance energy transfer using fluorescence microscopes. Biophys J 81:2395–3402
18. Roszik J, Lisboa D, Szollosi J, Vereb G (2009) Evaluation of intensity-based ratiometric FRET in image cytometry approaches and a software solution. Int Soc Adv Cytom A 74A:761–767
19. Seidel T, Kluge C, Hanitzsch M, Ross J, Sauer M, Dietz KJ, Golldack D (2004) Colocalization and FRET-analysis of subunits c and a of the vacuolar H^+-ATPase in living plant cells. J Biotechnol 112:165–175

Chapter 6

Generation of a Stress-Inducible Luminescent Arabidopsis and Its Use in Genetic Screening for Stress-Responsive Gene Deregulation Mutants

Si-in Yu and Byeong-ha Lee

Abstract

In order to understand plant stress tolerance and its application, it is important to identify the signaling components involved in the stress-regulated gene expression. One initial step for this is generation of a stress-inducible luminescent Arabidopsis and its use in genetic mutant screening. Here, we describe how to generate a transgenic Arabidopsis line harboring a single copy of the *STABILIZED1* (*STA1*) promoter-driven luciferase transgene (*STA1p-LUC*) as an example. *STA1* is a pre-mRNA splicing factor Prp6p homolog and is induced by cold and heat stresses. In addition, generation of the STA1p-LUC mutant pool and a luminescence imaging-based screening for *STA1p-LUC* deregulated mutants are described.

Key words Arabidopsis, Cold stress, Heat stress, Thermal stress, STA1, STABLIZED1, Luminescence imaging, Genetic screening, EMS mutagenesis

1 Introduction

Because plants are immobile, their ability of adaption to environmental changes is essential to survive. Among these adaptations, gene expression changes under abiotic stresses are key mechanisms for stress tolerance. Thus, it is important to understand how these stress-responsive genes are regulated.

Once environmental stimuli are recognized by plant cells, these signals are transduced to the nuclei through many signaling components such as second messengers, protein kinases, protein phosphatases, and transcription factors. Within nuclei, transcription factors either activate or repress the stress-regulated genes by binding to the promoters of the target genes. Despite this rather straightforward scheme of stress signaling, many signaling components still await their identification.

Ramanjulu Sunkar (ed.), *Plant Stress Tolerance: Methods and Protocols*, Methods in Molecular Biology, vol. 1631,
DOI 10.1007/978-1-4939-7136-7_6,

One approach to identify signaling components is isolation of genetic mutants defective in stress-responsive gene expression and identification of the responsible genes for the mutations. To this end, generation of plants harboring a stress-inducible gene promoter-driven reporter is the method of choice to initiate the genetic screening. There are several reporter systems for gene regulation studies or genetic screenings [1–3]. In our study, we selected the firefly luciferase as a reporter gene because of several advantages. Coupled with the luminescence imaging system, the luciferase system makes it possible to monitor the gene expression *in planta*. In addition, due to the short half-life time (3 h) of luciferase, it is possible to apply a second stress on one sample after a first stress as long as there is an enough intermission to allow luciferase to decay; hence, the multiple luminescence imagings for each stress mutant screening are possible. These advantages enable a high-throughput mutant screening.

The Arabidopsis *STABILIZED1* (*STA1*) gene encodes a putative pre-mRNA splicing factor that is similar to the human U5 snRNP-associated 102-kDa protein (PRPF6) and the pre-mRNA splicing factors, PRP1p and Prp6p of fission and budding yeast, respectively [4]. *STA1* was shown to be involved in RNA stability, pre-mRNA splicing, microRNA processing, and RNA-directed DNA methylation [5–7]. Interestingly, the *STA1* gene expression is induced by cold or heat stress. Indeed, *sta1-1*, a *STA1* defective mutant, is hypersensitive to cold or heat stress [4, 5]. Thus, with the *STA1* gene as an example, we describe how to generate Arabidopsis harboring a *STA1* promoter-driven luciferase gene (*STA1p-LUC*) and how to use this line in genetic screening for mutants with altered expression of *STA1p-LUC*.

2 Materials

2.1 Preparation and Conditions for Seedling Growth

1. MS (Murashige and Skoog)–agar medium: 1× MS basal salt mixture with 2% sucrose and 0.3% Gelrite (or Phytagel). Dissolve 4.43 g of MS basal salt mixture and 20 g of sucrose in 800 mL of deionized water, and adjust pH to 5.8 with 0.5 N KOH. Add 3 g of Gelrite and deionized water to bring the final volume to 1 L. Autoclave at 121 °C and 15 psi for 15 min. Pour the MS agar medium into 150 mm sterile petri plates and allow for solidification. To make the selection plates (MS agar), add 1 mL of 25 mg/mL hygromycin B in 1 L MS agar medium just before pouring plates.
2. Seed sterilization solution: Bleach with 0.01% Tween 20.
3. Soil and fertilizer: Soil mixes such as Sunshine® Mix 5 or equivalent. Slow fertilizer-releasing pellets such as Osmocote® or nutrient solution may be added to soil.

4. Plant growth chamber: 22 °C, 70% relative humidity, and continuous or cycle-controllable light conditions with illumination of approximately 100 μmol/m² s.
5. Cold room or refrigerator and heat chamber.

2.2 Luminescence Imaging Components

1. 100 mM luciferin stock: Dissolve 318.4 mg luciferin (Promega, USA) in a final volume of 10 mL sterile distilled water. Store the stock in aliquots of 100 μL at −80 °C (*see* **Note 1**).
2. 1 mM luciferin working solution: Dilute a 100 μL of 100 mM luciferin stock to 1 mM working concentration by adding 9,900 μL of deionized water with 0.01% Triton X-100. Keep in dark at 4 °C before use.
3. Luciferin sprayer: Fine misting sprayer with a 30-mL spray bottle. A nasal sprayer can be used.
4. Luciferase Imaging System (Fig. 1): Camera controller (Model # 7513–0002, Roper Scientific, USA), Charge coupled device camera (CCD camera; Lumazone 1300B, Roper Scientific, USA) with a liquid nitrogen cooling system, imaging lens

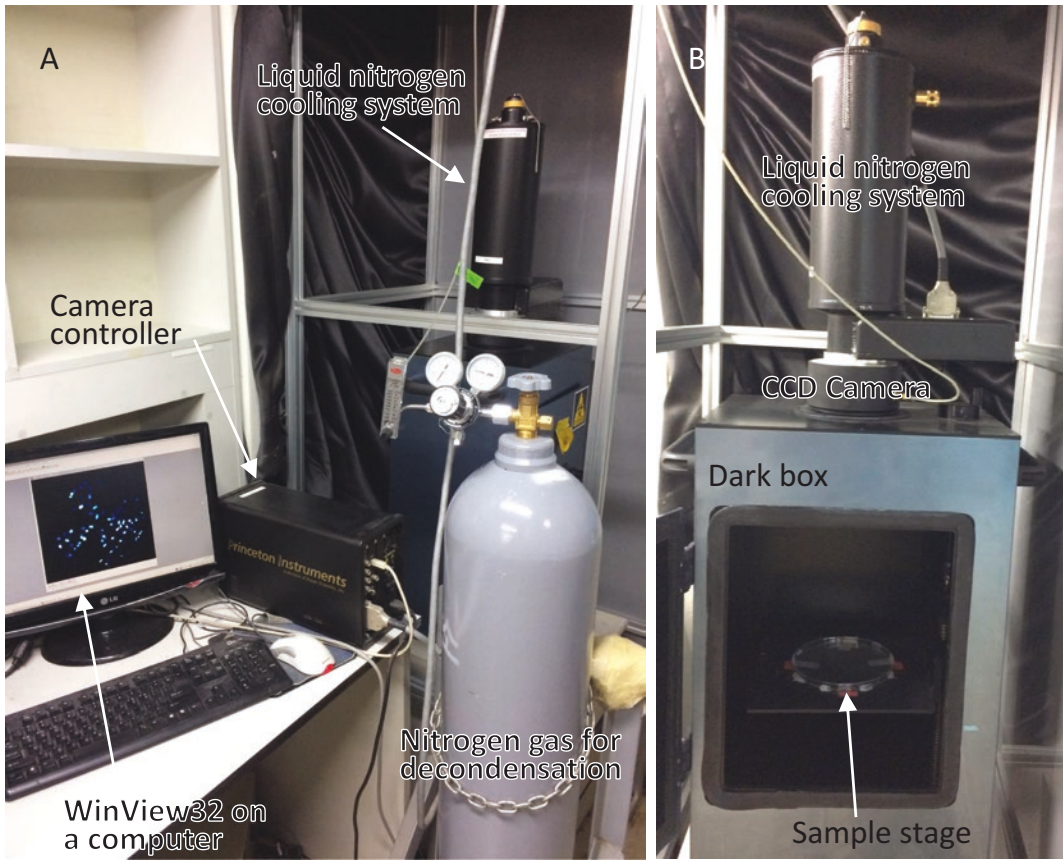

Fig. 1 Luminescence imaging system

(F-mount NIKKOR f/1.2 lens, 50 mm, Nikon, Japan), Dark box (650 × 380 × 300 mm) with a sample stage, Nitrogen gas supplier for CCD camera decondensaton, Computer, and WinView32 software (version 2.5.20.2, Roper Scientific, USA).

3 Methods

3.1 Construction of the STA1p-LUC Arabidopsis

1. Construct the *STA1p-LUC* containing vector: Insert the STA1 promoter sequence in front of the promoterless *LUC* coding sequence preferably in a binary vector. In our case, the GUS coding sequence in pCAMBIA1381Z is replaced with the *LUC* coding sequence, producing a binary vector named pCAMBIA1381Z-LUC. The 1475 bp of DNA sequence upstream from the STA1 translation initiation codon is inserted in front of the *LUC* conding sequence of pCAMBIA1381Z-LUC to make the *STA1p-LUC* construct.
2. Transform *Arabidopsis* Columbia plants with the *STA1p-LUC* vector into via *Agrobacterium* mediated *Arabidopsis* transformation. The trichome-lacking Arabidopsis Columbia *gl1* mutant can be used to avoid the possible interference of luminescence with trichomes.
3. Plate the T1 seeds from the floral-dipped plants on MS agar plates with hygromycin (25 μg/mL) for transformant selection. Transfer the selected seedlings into soil and allow the self-pollination of T1 or cross T1 to the background line (Columbia *gl1*) for F1 seeds. Harvest the T2 seeds from each self-pollinated T1 transformant. Also harvest the F2 seeds from the F1 seedlings derived from crosses between Columbia *gl1* and T1. T2 or F2 seeds should be individually harvested and analysis of F2 seeds can be carried out after T2 analysis (*see* below).
4. For a single transgene locus analysis, plate the T2 seeds of each individual line on hygromycin plates and select the lines that show a 3:1 segregation ratio of hygromycin resistance to sensitivity. Evaluate co-segregation of hygromycin resistance with temperature-induced *STA1p-LUC* luminescence by luminescence imaging of seedlings grown on hygromycin plate after temperature stress treatments. All hygromycin resistant seedlings should show high luminescence. Co-segregation can also be confirmed through cold- or heat-induced luminescence imaging and genotyping of the hygromycin resistance gene in the seedlings with high luminescence. Similarly, a single transgene locus and co-segregation can be tested with F2 seeds derived from Columbia *gl1* x T1 through the same approach described above (Fig. 2, Table 1).
5. Identify a homozygote of *STA1p-LUC* among the T3 seeds derived from the confirmed *STA1p-LUC* single copy line by

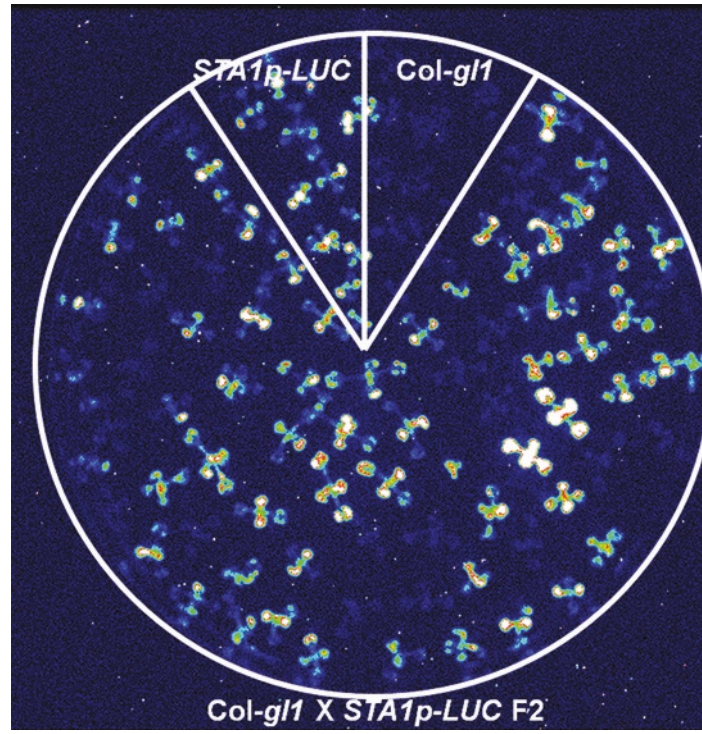

Fig. 2 Confirmation of a single transgene locus. Luminescence imaging after cold stress treatment (0 °C for 2 days). 13-day seedlings were used. Columbia *gl1* (Col-*gl1*) is a negative control

Table 1
Genetic analysis of transgenic *STA1p-LUC* plants (cross: [a]Col-*gl1* x *STA1p-LUC*, [a]*STA1p-LUC* x Col-*gl1*)

	Luminescence			Hygromycin		
Samples	**High**	**Low**	**Ratio**	**Resistant**	**Sensitive**	**Ratio**
Col-*gl1* x *STA1p-LUC* F2	68	24	2.8: 1	76	25	3.0: 1
STA1p-LUC x Col-*gl1* F2	81	32	2.5: 1	92	33	2.8: 1

[a]Female × male

examining the hygromycin resistance and temperature-induced high luminescence. For this, harvest the T3 seeds separately from individual T2 lines, single-locus insertion and co-segregation of which have been confirmed. Plate the T3 seeds on hygromycin-containing MS agar plates and luminescence-image the T3 seedlings after temperature stress treatments.

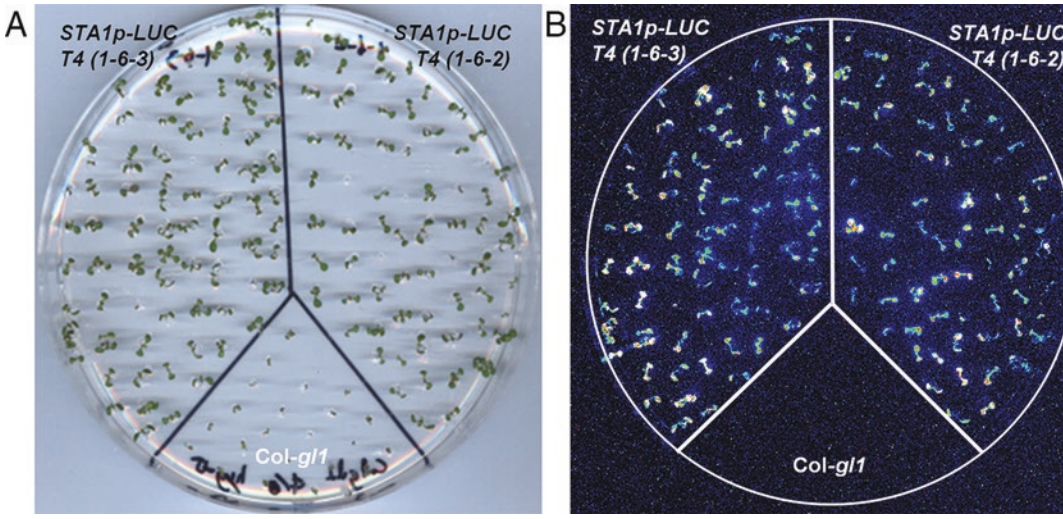

Fig. 3 Luminescence analysis of *STA1p-LUC* T4 lines on hygromycin plates. (**a**) Image of a hygromycin plate containing 11-day-old T4 seedlings, used for luminescence image (**b**); (**b**) Luminescence image of (**a**) after cold stress treatment (0 °C for 2 days. Col-*gl1* was a negative control. Here T4 generation was used instead for normal T3. Figure as originally published in *Yu S-i, Han J-H, Chhoeun C and Lee B-h (2016). Front. Plant Sci. 7:618. doi: 10.3389/fpls.2016.00618*

The homozygotes of *STA1p-LUC* transgenic plants will show 100% hygromycin resistance and 100% high luminescence (Fig. 3).

6. Evaluate a single copy of the transgene by using real-time PCR amplification of the transgene in comparison with the control (genomic DNA of wild type without transgene). Please note that a single locus insertion can still be a repeated transgene insertion (multiple copies) in the locus and this repeated sequence can be epigenetically regulated, possibly resulting in discrepancy of the reporter gene expression and the endogenous gene expression. In our case, we designed the primers for the *STA1* promoter sequence used for the STA1p-LUC construct and an internal control (UBQ10 gene; UBQ10_F, 5′-AACGGGAAAGACGATTAC-3′, UBQ10_R, 5′-ACAAGA TGAAGGGTGGAC-3′). Prepare the same amount of wild type genomic DNA (Columbia *gl1*) and the *STA1p-LUC* transgenic plants genomic DNA. The genomic DNA concentration can be estimated using spectrophotometer. A range of 0.5–50 ng of genomic DNA can be tested (*see* **Note 2**). Carry out real time PCR with these genomic DNA and *STA1* promoter primers. The relative expression value of *STA1* promoter in *STA1p-LUC* should be 2 if the transgenic plant has a single copy of the transgene (Fig. 4).
7. Compare kinetics of luminescence intensities of the homozygote lines of *STA1p-LUC* with those of the endogenous *STA1*

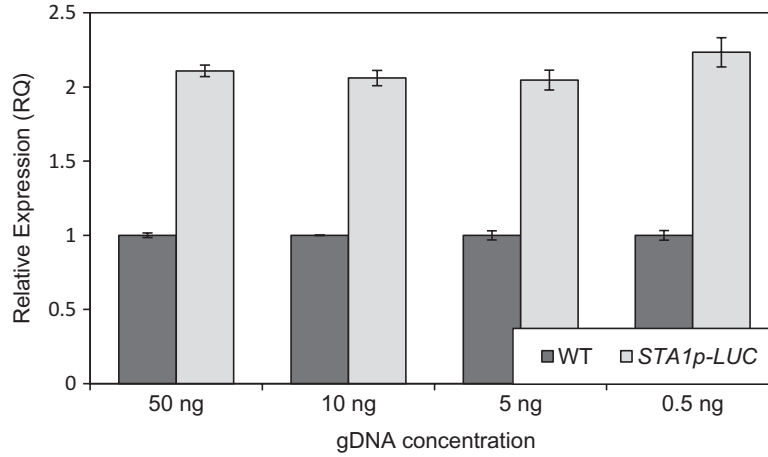

Fig. 4 Transgene copy number measurement by real-time PCR. The copy number of *STA1p-LUC* transgene measured by real-time PCR. Wild type (WT) plants without a transgene were used as a reference

transcript levels to validate the reliability of *STA1p-LUC* expression in monitoring the endogenous STA1 expression. Grow WT and *STA1p-LUC* half and half on an MS agar plate. Prepare the same number of plates as the treatment time-points. Measure luminescence intensities and RNA levels of WT and *STA1p-LUC* at different time points under temperature stresses.

8. Backcross the confirmed *STA1p-LUC* line to the wild type to dilute and remove potential mutations that might occur during Agrobacterium-mediated transformation. Cross F2 plants (from **step 4**) to Arabidopsis Columbia *gl1* plant. Usually 5–6 generation after the original backcross will be enough.
9. It is also recommended to locate the transgene locus. Sometimes gene interruption by the transgene insertion might result in unexpected gene regulation. To this end, perform TAIL-PCR with genomic DNA from the confirmed *STA1p-LUC* line. Carry out the three rounds of TAIL-PCR as described previously [8] with modified primers. Modified primers used in *STA1p-LUC*'s case are three T-DNA specific primers: LB1, 5′-TCCGAGGGCAAAGAAATAGA-3′; LB2, 5′-TTCCTATAGGGTTTCGCTCA-3′; LB3, 5′-TTCTAATT CCTAAAACCAAAATCCA-3′. After the transgene position is located, confirm the location by PCR with T-DNA specific primers (LB1, LB2, and LB3) and flanking plant genomic DNA-specific primers. In our case, At3g23165-F (5′-CCGGA GGGAATGGAAAATAA-3′) and K14B15–24.42 K–R (5′-GG GTCAAACTTGTTTTTCTCG-3′) are used. The *STA1p-LUC* is found not to interrupt any endogenous gene structure as it is inserted in the intergenic region.

10. T-DNA insertion can sometimes cause altered regulation of neighboring gene expression mainly due to the hyperactivity of 35S promoters in the transgene [9–12]. Once the transgene locus has been identified, evaluate the expression levels of neighboring genes by RT-PCR or RNA blotting analysis. *STA1p-LUC* is inserted between At3g23165 and At3g23167, both of which encode a member of a family of small, secreted cysteine-rich proteins similar in sequence to a pollen coat protein. RT-PCR analysis with the gene specific primers confirmed no altered expression of these neighboring genes [4].

3.2 Mutant Generation

1. Weigh 2.5 g (~100,000 seeds) of the *STA1p-LUC* homozygote seeds.
2. Imbibe the seeds in the plastic container with wet tissue for overnight at cold room.
3. Place the seeds in a 50-mL conical tube with 45 mL of water and add ethyl methanesulfonate (EMS) to the seeds-containing tube to a final concentration of 0.2–0.4% and gently shake for 15 h at room temperature (*see* **Note 3**).
4. Remove the EMS solution from the tube and wash the seeds with 45 mL of water ten times. After ten times of wash, move the seeds to a 1 L flask and wash the seeds with 200 mL of water five times. The resultant seeds are now at M1 generation. For complete washing, each time shake the seed container for 30 min. All EMS-contaminated solutions should be decanted into 2 N NaOH in a volume ratio of 7:1 (EMS: NaOH solutions) and leave it overnight (> 6 h).
5. Sow the seeds with a density of approximately 100 seeds per 540 × 270 mm flat. A squeeze bottle can be used for even distribution of the seeds when planting.
6. Grow the M1 plants in a growth room at 22 °C. Make sure of no cross-contamination. As the *STA1p-LUC* is generated from Arabidopsis Columbia *gl1* mutant, the trichome-lacking phenotype can be a good indicator to evaluate the cross-contamination. To check the efficiency of EMS treatment, open a silique of at least 50 M1 plants and count the albino seeds. In a successful mutagenesis, 0.5–3% of M1 plants segregate chlorophyll deficient plants in their M2 progeny
7. Harvest the seeds from M1 individuals or in a 10–20 plant pool. Individual harvest is useful to isolate the lethal mutants.

3.3 Seedling Preparation on MS Agar Plates

1. Perform seed surface sterilization: Seeds should be less than 200–500 counts in 1.5-mL microtube. If more than 500 seeds, use 15-mL conical tubes. Add 1 mL of bleach with 0.01% Tween 20 and vortex. Five minutes later, remove bleach and immediately add sterile distilled water. After vortexing, change water. Repeat this washing step at least five times.

2. Sow the seeds on MS agar plates. The plates can be divided into several sections for multiple line plating. Seal the plate with Parafilm and keep the plates at 4 °C at least for 2 days for synchronized germination. For freshly harvested seeds, an extended cold treatment (aka stratification) is necessary.
3. After stratification up to 7 days, grow the seedlings under normal conditions for about 10 days until just two true leaves appear.

3.4 Stress Treatments

1. Cold stress: Prepare 10–13-day-old seedlings grown in MS agar plates. Place the plates at 0 °C for desired durations.
2. Heat stress: Prepare 10–13-day-old seedlings grown in MS agar plates. Place at 37 °C for desired durations. If multiple stresses can be applied, the same seedlings used for cold stress imaging can be heat-stressed after at least 1 day incubation for luciferase decay (*see* below).

3.5 Luminescence Imaging

1. Prior to imaging, add liquid nitrogen to cool the camera down to −110 °C. Turn on the WinView32 program and check the camera temperature. This cooling process takes more than 1 h.
2. Adjust the camera focusing. The camera is fixed to the top of the dark imaging chamber. Control the distance between sample and camera using movable sample stage. Check the sample plate orientation. Use these parameters for adjusting the camera focusing: ADC Rate = 1 MHz, Exposure time = 10 ms.
3. Change the parameters to take the sample luminescence: ADC Rate = 100 KHz, Exposure time = 10 min.
4. After stress treatment, spray 1 mM luciferin working solution evenly on the seedlings. 2–3 shots of sprays of luciferin will be enough for a 150-mm plate. Immediately, place the plates in a dark imaging chamber for 5 min to remove autofluorescence from chlorophyll.
5. After the 5-min incubation, take the luminescence image. In our case, 10-min exposure is used to detect luminescence signals from seedlings. All the preparation for imaging after temperature stress should be carried out in the exactly same temporal steps. It is because luminescence is based on the enzyme activity. Therefore, a different incubation time particularly after cold stress will result in differently warmed-up luciferase activity.

3.6 Mutant Screening

1. Take the luminescence image of M2 seedlings on MS agar plates after stress treatments. Align the plate to the luminescence image and mark positions of putative mutants with altered luminescence intensity; higher or lower than wild type (*STA1p-LUC* plant). Try cold stress imaging first and incubate the plates under normal conditions at least for 24 h to allow decay of luciferase. After that, proceed to heat treatment and luminescence imaging.

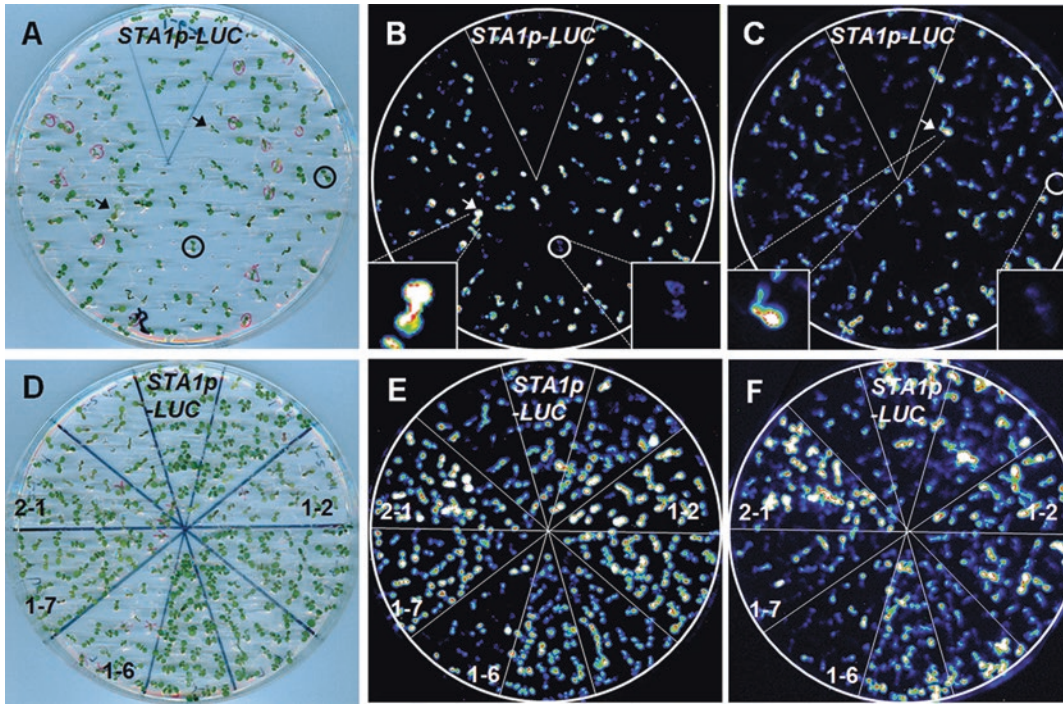

Fig. 5 *STA1p-LUC* deregulated mutant screening**.** (**a**) Plate containing 11-day-old M2 seedlings for B and C; (**b**) Luminescence image taken after cold stress treatment (0 °C for 36 h); (**c**) Luminescence image taken after heat treatment (37 °C for 15 h). In comparison with *STA1p-LUC*, putative mutants with higher luminescence were marked with *white arrow* and ones with lower luminescence were marked with *circles*; (**d**) Plate containing 11-day-old putative mutant seedlings (M3 generation) for confirmation (**e** and **f**); (**e**) and (**f**) Luminescence images taken after cold stress (**e**) and heat stress (**f**). The confirmed mutants without segregation were labeled with mutant numbers. Some showed altered luminescence by both stress, while others showed only by one stress

2. Transfer the marked putative M2 mutant individuals to soil. Recovering period of 2–3 days after stress treatments is recommended before soil transfer.
3. Harvest M3 seeds form each putative M2 mutant individual.
4. Confirm the putative mutant phenotype (altered *STA1p-LUC* expression) by imaging luminescence of M3 seedlings from each M2 mutant (Fig. 5). Once confirmed, the endogenous *STA1* expression in confirmed mutants can be examined. A further characterization and mutant gene cloning should be carried out.

4 Notes

1. Luciferin should be stored in dark because of its sensitivity to photo-oxidation.
2. Analysis with the serial dilutions of genomic DNA is recommended to improve accuracy and reproducibility (Fig. 4).

3. When working with EMS, always wear lab coat, goggles, and gloves and work in fume hood because EMS is a very strong mutagen.

Acknowledgment

The work was supported by Next-Generation BioGreen21 Program (PJ011006), Rural Development Administration, Republic of Korea and the National Research Foundation of Korea (NRF) grant (2014R1A1A2058769) funded by the Ministry of Education, Republic of Korea.

References

1. Haseloff J, Siemering KR, Prasher DC, Hodge S (1997) Removal of a cryptic intron and subcellular localization of green fluorescent protein are required to mark transgenic Arabidopsis plants brightly. Proc Natl Acad Sci U S A 94:2122–2127
2. Jefferson RA, Kavanagh TA, Bevan MW (1987) GUS fusions: beta-glucuronidase as a sensitive and versatile gene fusion marker in higher plants. EMBO J 6:3901–3907
3. Ow DW, Wet DE, Helinski DR, Howell SH, Wood KV, Deluca M et al (1986) Transient and stable expression of the firefly luciferase gene in plant cells and transgenic plants. Science 234:856–859
4. Yu SI, Han JH, Chhoeun C, Lee BH (2016) Genetic screening for Arabidopsis mutants defective in STA1 regulation under thermal stress implicates the existence of regulators of its specific expression, and the genetic interactions in the stress signaling pathways. Front Plant Sci 7:618
5. Lee BH, Kapoor A, Zhu J, Zhu JK (2006) STABILIZED1, a stress-upregulated nuclear protein, is required for pre-mRNA splicing, mRNA turnover, and stress tolerance in Arabidopsis. Plant Cell 18:1736–1749
6. Ben Chaabane S, Liu R, Chinnusamy V, Kwon Y, Park JH, Kim SY, Zhu JK, Yang SW, Lee BH (2013) STA1, an Arabidopsis pre-mRNA processing factor 6 homolog, is a new player involved in miRNA biogenesis. Nucleic Acids Res 41:1984–1997
7. Dou K, Huang CF, Ma ZY, Zhang CJ, Zhou JX, Haung HW, Cai T, Tang K, Zhu JK, He XJ (2013) The PRP6-like splicing factor STA1 is involved in RNA-directed DNA methylation by facilitating the production of Pol V-dependent scaffold RNAs. Nucleic Acids Res 41:8489–8502
8. Liu YG, Mitsukawa N, Oosumi T, Whittier RF (1995) Efficient isolation and mapping of *Arabidopsis thaliana* T-DNA insert junctions by thermal asymmetric interlaced PCR. Plant J 8:457–463
9. Yoo SY, Bomblies K, Yoo SK, Yang JW, Choi MS, Lee JS, Weigel D, Ahn JH (2005) The 35S promoter used in a selectable marker gene of a plant transformation vector affects the expression of the transgene. Planta 221: 523–530
10. Singer SD, Cox KD, Liu Z (2010) Both the constitutive cauliflower mosaic virus 35S and tissue-specific AGAMOUS enhancers activate transcription autonomously in *Arabidopsis thaliana*. Plant Mol Biol 74:293–305
11. Singer SD, Liu Z, Cox KD (2012) Minimizing the unpredictability of transgene expression in plants: the role of genetic insulators. Plant Cell Rep 31:13–25
12. Zheng X, Deng W, Luo K, Duan H, Chen Y, McAvoy R, Song S, Pei Y, Li Y (2007) The cauliflower mosaic virus (CaMV) 35S promoter sequence alters the level and patterns of activity of adjacent tissue- and organ-specific gene promoters. Plant Cell Rep 26:1195–1203

Chapter 7

Detection of Differential DNA Methylation Under Stress Conditions Using Bisulfite Sequence Analysis

Ibtisam Al Harrasi, Rashid Al-Yahyai, and Mahmoud W. Yaish

Abstract

DNA methylation is the most important epigenetic change affecting gene expression in plants grown under normal as well as under stress conditions. Therefore, researchers study differential DNA methylation under distinct environmental conditions and their relationship with transcriptome abundance. Up to date, more than 25 methods and techniques are available to detect DNA methylation based on different principles. Bisulfite sequencing method is considered as a gold standard since it is able to distinguish 5-methylcytosine from cytosine using the bisulfite treatment. Therefore, it is useful for qualitative and semiquantitative measurement of DNA methylation. However, the reliability of data obtaining from this technique is mainly depending on the efficiency of bisulfite conversion and number of sequencing clones representing the target-converted sequence. Therefore, it is labor intensive and time-consuming. Revolution of next generation DNA sequencing (NGS) has allowed researches to combine conventional bisulfite sequencing methods with high-throughput Illumina sequencing in a technique called whole genome bisulfite sequencing (WGBS). This technique allows a single nucleotide resolution of 5-methylcytosine on a genome scale. WGBS technique workflow involves DNA fragmentation, processing through end blunting, terminal A(s) addition at 3′ end and adaptor ligation, bisulfite treatment, PCR amplification, sequencing libraries and assembling, and finally alignment with the reference genome and data analysis. Despite the fact that WGBS is more reliable than the conventional clone-based bisulfite sequencing, it is costly, requires large amount of DNA and its output data is not easily handled.

Key words DNA methylation, Cytosine, Methylcytosine, Bisulfite, WGBS, Illumina

1 Introduction

Epigenetics is the study of heritable changes in gene expression caused by mechanisms without change in the original DNA sequences [1]. Epigenetic changes can be classified into three main distinct mechanisms, which are DNA methylation, histone modifications, and RNA-mediated gene silencing [2]. Among these mechanisms, DNA methylation is the most extensively studied in both plants and mammals [3, 4]. In DNA methylation, a methyl group (CH_3) is added to the cytosine base at carbon 5 position through a covalent attachment [5]. Unlike mammalian genome,

Ramanjulu Sunkar (ed.), *Plant Stress Tolerance: Methods and Protocols*, Methods in Molecular Biology, vol. 1631,
DOI 10.1007/978-1-4939-7136-7_7,

which is limited to CG dinucleotide sequence context, plant DNA methylation occurs in three sequence contexts (CG, CHG, CHH, where H = A, C, or T) [3]. Cytosine methylation (mC) of mammalian cell DNA can be oxidized by 10–11 translocation methylcytosine dioxygenase 1 (TET1) family and converted to 5-hydroxymethylcytosine [5]. However, this enzyme has not been reported in plants [6].

There is a growing evidence for DNA methylation effects on regulating gene expression in response to abiotic stress [4, 7–14]. Nevertheless, studies have shown significant differences in DNA methylation response patterns among different species [8–11]. It has been reported that exposure to various abiotic stresses led to increase in global DNA methylation in *Arabidopsis thaliana* genome probably to enhance tolerance to stress [8]. Similarly, exposure of *Populus trichocarpa* to drought increased cytosine methylation [10]. Another study on *Mesembryanthemum crystallinum* methylome found that the methylation level of CHG context of the nuclear genome increased twice under salt stress and that was coupled with satellite DNA hypermethylation [9]. Such an increase was also observed in the DNA extracted from the root tissues of *Medicago* species [7].

In contrast, it has been noticed a genome wide demethylation in root tissues of maize under cold stress. Overall, the existing evidence indicates that DNA methylation is responsible for plant phenotypic variation in response to stress [15]. Generally, stress induced changes in epigenome can be inherited over successive generations (transgeneration memory of stress) and can also persist over a long period of time in plants [16].

Over the years, many techniques have been developed to analyze DNA methylation. These techniques are basically underlying one of three principles: methylation-sensitive restriction, bisulfite conversion, and affinity purification [18]. Techniques based on the first principle are methylation-sensitive polymerase chain reaction (MS-PCR), methylation-sensitive amplification polymorphism (MSAP), differential methylation hybridization (DMH), microarray-based integrated analysis of methylation by isoschizomers (MIAMI), and cytosine extension assay. However, the bisulfite conversion-based techniques are quantitative analysis of methylated alleles (QAMA), enzymatic regional methylation assay (ERMA), methylation-sensitive-single strand conformation analysis (MS-SSCA), fluorescence melting curve analysis (FMCA), methylation-sensitive-single nucleotide primer extension (MS-SNuPE), and whole genome bisulfite sequencing (WGBS). The two principles can be applied in one technique such as combined bisulfite restriction analysis (COBRA). Finally, the affinity purification principle is involved in high-performance liquid chromatography (HPLC), thin-layer chromatography (TLC), matrix-assisted laser desorption/ionization (MALDI)

mass spectrometry, fluorescent capillary electrophoresis (FCE), immunoprecipitation, and Southern blotting [17].

This chapter discusses the conventional method of bisulfite sequencing and high-throughput technique of whole genome bisulfite sequencing (WGBS).

Bisulfite sequencing is considered as a fundamental method in DNA methylation analysis [17]. This technique has gained a significant improvement when accompanied with the recent DNA sequencing technologies [18]. This technology provides efficient qualitative and semiquantitative measurement of DNA methylation [17]. Hence, it can be used for detecting differential DNA methylation levels of specific targeted genes under control and stress conditions.

Under the harsh condition of bisulfite treatment, including high salt concentration, high temperature and low pH, the unmethylated cysteine bases will be deaminated into uracil(s). Latter after PCR amplification, these converted uracil bases will be read as thymine(s). However, bisulfite treatment does not affect the methylated cytosine residues, which remain intact and read as cytosine(s) [18]. The methylated cytosine(s) are identified by sequencing the PCR products from the targeted regions. Ideally each methylation site should be confirmed by sequencing of at least ten different clones of each category (control and treatment samples). However, next generation sequencing will provide a more quantitative method to determine the methylation level at a particular site since it is very common that the certain cytosine will be covered 20–40 times during the sequencing procedure. Regardless of the sequencing method, the most critical point for accurate determination of methylation level is the complete conversion of unmethylated cytosine(s) under the bisulfite treatment. Therefore, in parallel with the target gene, it is important to use a negative control. If the sequencing procedure involves a cloning procedure step, this control can be a plasmid DNA isolated from a DNA methylation mutant strain of bacteria [6].

For the bisulfite sequencing procedure, which is based on the cloning protocol, data of bisulfite sequencing analysis can be simply interpreted by aligning the sequenced insert of the target gene with the original unconverted DNA sequence. Essentially, all unmethylated cytosine(s) in the original sequence are converted and sequenced as thymine(s). In contrast, the presence of a C-peak indicates the presence of a methylated cytosine in the original sequence (*see* Fig. 1). Then the percentage of methylation can be calculated by dividing the number of sequenced clones confirming the presence of methylated cytosine or cytosine in one position over the total number of sequenced clones of the same targeted region. For example, if only four sequences showing cytosine(s) and the rest six sequences showing thymine(s) at a particular site then, the parentage of DNA methylation at that position is 40%.

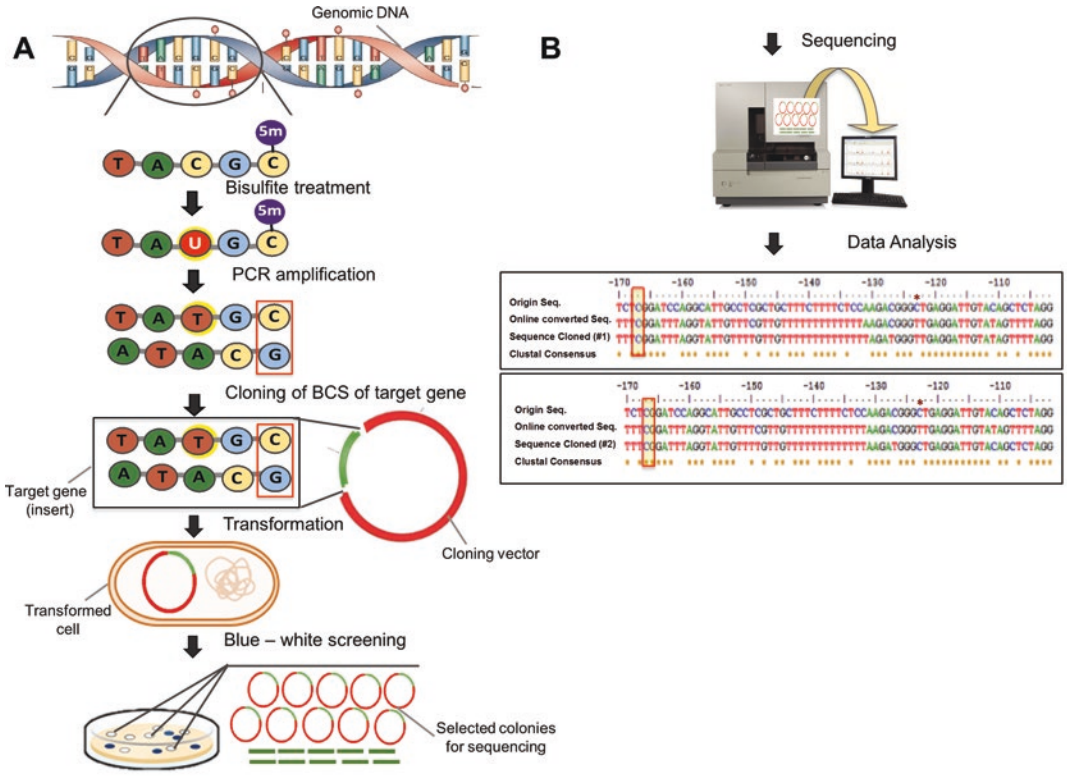

Fig. 1 Schematic representation of the bisulfite sequencing technique. (**a**) Genomic DNA is first treated with sodium bisulfite, and then, the bisulfite-converted sequence (BCS) of the gene of interest is amplified with methylation-specific PCR (MSP) primers. The amplified fragment is cloned into a cloning vector and then transformed into competent *E. coli* cells. (**b**) DNA methylation detection and semiquantitative measurement. In order to detect the methylation status of the target gene, the resultant sequence of the insert is aligned to the converted sequence and the original sequence using BioEdit software

Whole genome bisulfite sequencing (WGBS) is a genome-wide sequencing technology combining bisulfite chemistry with high-throughput next generation sequencing of the genomic DNA [19]. In general, the successive flow of this procedure is starting with DNA fragmentation by sonication or enzymatic digestion, followed by generating blunt ends, terminal A(s) addition at 3′ end, adaptor ligation, bisulfite treatment of the DNA libraries, and PCR amplification; subsequently, sequencing the libraries using Illumina platform and, finally, identification of bisulfite sequence reads (*see* Fig. 2). This technique is considered to be the most comprehensive among different DNA methylation analyzing techniques [18]. By using bioinformatics tools, such as Integrative Genomic Viewer (IGV) [20] and MethGo [21], this technique allows screening of the differentially methylated regions under both control and stress conditions. It allows quantifying and mapping the distribution of methylated cytosine (s) of three sequence

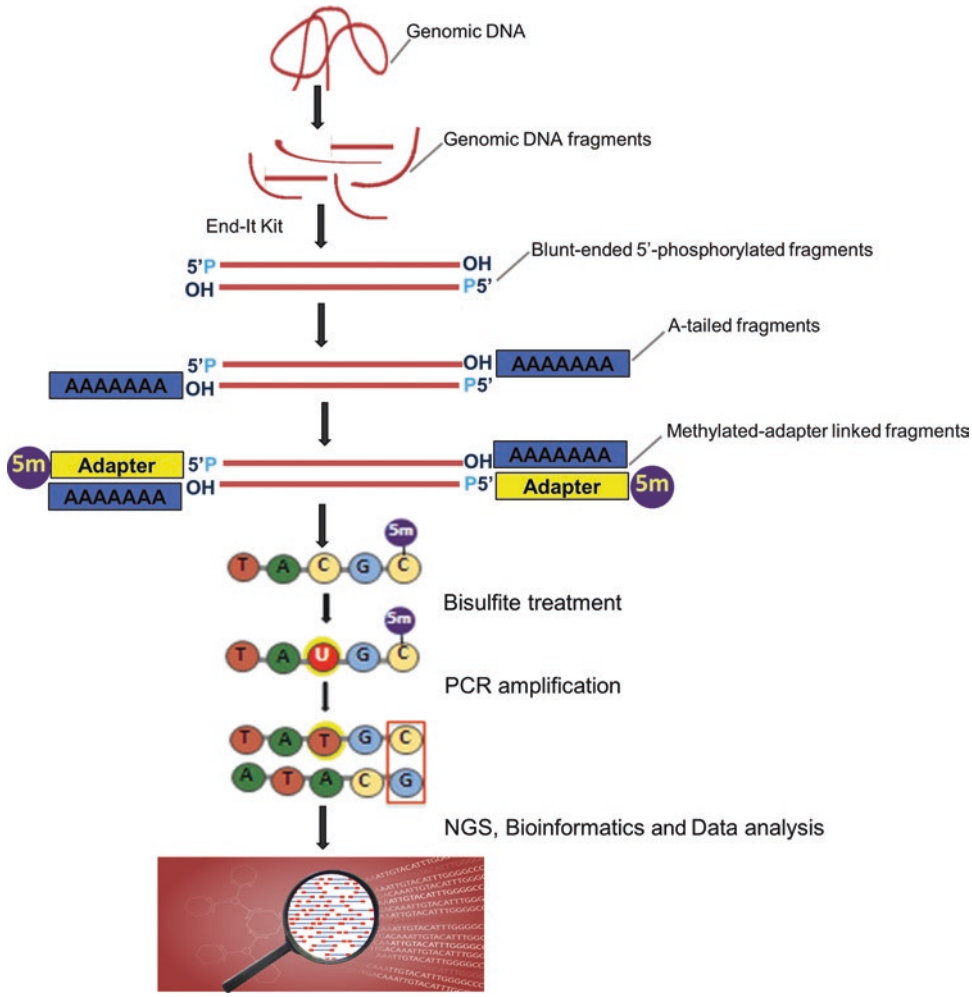

Fig. 2 Schematic representation of the whole genome bisulfite sequencing (WGBS) technique. Generally, genomic DNA is fragmented either by sonication or through enzymatic digestion. Subsequently, the fragments are processed via library constructing steps including end-blunting, terminal A(s) addition at 3′ end, and methylated adaptor ligation. After that, the resultant libraries are undergone a bisulfite treatment and PCR amplification. The bisulfite libraries are sequenced using Illumina platform and finally the bisulfite sequence reads are passed through bioinformatics tools for data analysis

contexts among different gene features (promoter, exon, and introns). Despite these advantages, few limitations are associated with this technique which include large amount of DNA, higher cost, and difficult handling of NGS data [18, 22]. Recently, the reduced representation bisulfite sequencing (RRBS) has been developed to alleviate limitations found in WGBS [23].

There are some considerations need to be addressed when WGBS technique is chosen for stress induced-methylation detection. Firstly, the presence of a suitable negative control of methylation-free genomic DNA (control vs. treatment genomic DNA). Secondly, the use of an internal control such as the chloroplastic genome is

essential to estimate the cytosine conversion efficiency [24, 25]. In addition, the nuclear gene IND (INDEHISCENT) and the mitochondrial genes, NAD (NICOTINAMIDE ADENINE DINUCLEOTIDE) and ATP1 (ATPase SUBUNIT 1) can be used as universal endogenous controls for the bisulfite conversion [26]. Thirdly, a balance between the number of replicates and the sequencing coverage per replicate (5×–15× depth range) is extremely important [27]. Combining the reads of the biological replicates, the total methylome should give at least 30× sequencing coverage [28]. In this case, two biological replicates with 15× coverage each should be sufficient according to The NIH Roadmap Epigenomics Project [27]. However, in case of one biological replicate 30× coverage can be obtained from 15× per strand due to strand specificity of this technique. The performance of this technique is mainly affected by the alignment efficiency of bisulfite-converted sequencing reads to the reference genome [29]. Therefore, a high reference genome sequence quality is important [27, 28].

2 Materials

2.1 Bisulfite Sequencing Method

1. *Arabidopsis thaliana* plants.
2. DNA extraction kit.
3. Freshly prepared NaOH (3 M).

2.1.1 DNA Extraction and Denaturation

2.1.2 Sulfonation and Deamination

1. Sodium metabisulfite (7.6 g $Na_2O_5S_2$).
2. Sodium hydroxide (10 M NaOH).
3. Quinol (100 mM) (0.55 g of C_6H_4 $(OH)_{2)}$.
4. Mineral oil.
5. Water bath.
6. pH meter.

2.1.3 Desalting and Alkali Desulfonation

1. Desalting columns.
2. Sodium hydroxide (3 M NaOH).
3. Yeast tRNA (10 mg/mL).
4. Ammonium acetate (5 M NH_4OAc (pH 7.0)).
5. Ice-cold 100% ethanol.
6. Tris–EDTA (TE) buffer (10 mM Tris–HCl, pH 7.5. 1 mM EDTA).

2.1.4 Bisulfite PCR Amplification

1. MethPrimer program.

CpG Islands Prediction and Primer Design

PCR Reaction and Cycling Conditions

1. High-Fidelity PCR Master Mix (2×).
2. Specific primers (10 pmol/μL).
3. Dimethyl sulfoxide (DMSO).
4. Nuclease-free water.
5. 50× Tris–acetate–EDTA (TAE buffer).
6. 2% agarose gel (2 g agarose. 100 mL 1× TAE buffer).
7. Electrophoresis apparatus.

PCR Purification

1. 1% agarose gel (1 g agarose. 100 mL 1× TAE buffer).
2. UV source.
3. Gel and PCR purification kit.
4. NanoDrop spectrometer

2.1.5 Cloning and Transformation

1. 2× Rapid Ligation Buffer.
2. pGEM®-T Easy Vector (50 ng).
3. T4 DNA ligase (3 Weiss units/μL).
4. Commercially available cloning strains of *Escherichia coli* (*E. cloi*) competent cells (e.g., 10-beta, 5-alpha, Stable, Turbo Competent/Electrocompetent *E. coli*).
5. *E. cloi* JM110 competent cells (*dam* and *dcm*)
6. Electroporation system.
7. Electroporation cuvette (0.2 cm).
8. Super Optimal Broth (SOB) with Catabolite Repression with added glucose (SOC).
9. Luria–Bertani (LB) agar.
10. Ampicillin (100 μg/mL).
11. Isopropyl β-D-1-thiogalactopyranoside (IPTG) (0.5 M).
12. X-gal (80 μg/mL).
13. Luria–Bertani (LB) broth.

2.1.6 Plasmid Purification

1. Mini Plasmid Prep Kit.
2. 1.5% agarose gel (1.5 g agarose. 100 mL 1× TAE buffer).
3. NanoDrop spectrophotometer.

2.1.7 Sequencing and Data Analysis

1. T7 Promoter Primer.
2. SP6 Promoter Primer.
3. Sequencer (ABI Applied Biosystems or Beckman Coulter).
4. BioEdit software.

2.2 Whole Genome Bisulfite Sequencing (WGBS) Technique

2.2.1 Genomic DNA Fragmentations

1. NanoDrop spectrophotometer.
2. dsDNA Shearase™ Plus enzyme.
3. 5× dsDNA Shearase™ Plus Reaction Buffer.
4. dsDNA Shearase™ Plus.
5. Nuclease-free water.
6. DNA Cleaning kit.

2.2.2 MethylC-Seq Library Construction

1. End-It DNA end repair kit.
2. DNA cleaning kit.

End Repair

Adenosine Tailing

1. Klenow (5 U/μL).
2. DNA cleaning kit.

Methylated Adapter Ligation

1. 10× DNA ligase buffer with ATP.
2. T4 DNA ligase (400 U/μ).
3. Nuclease-free water.
4. DNA cleaning kit.

2.2.3 Bisulfite Conversion

1. Nuclease-free water.
2. Bisulfite conversion kit.

2.2.4 Amplification of Bisulfite-Converted Genomic DNA

1. 25× PCR primer mix.
2. 2× KAPA HiFi uracil+ ReadyMix.
3. PCR product cleaning kit.

2.2.5 Sequencing, Alignment, and Data Analysis

1. Agilent 2200 TapeStation.
2. Illumina Hiseq instrument.
3. Alignment and assembly software (e.g., Bowtie).

3 Methods

3.1 Bisulfite Sequencing Method

3.1.1 DNA Extraction and Denaturation

1. Use appropriate genomic DNA extraction method to obtain a high concentration (1–2 μg) (*see* **Note 1**).
2. In a total volume of 20 μL, denature genomic DNA samples by adding 2 μL of freshly prepared NaOH (3 M), and incubate them at 37 °C for 15 min and then at 90 °C for 2 min.
3. Directly put the denatured samples on ice for 5 min to maintain the DNA single-stranded.
4. Centrifuge at 10,000 × *g* for few seconds at 4 °C.

3.1.2 Sulfonation and Deamination

1. Prepare fresh solutions of bisulfite reaction mix, which contains saturated sodium metabisulfite, pH 5.0 (*see* **Note 2**) and 10 mM Quinol (*see* **Note 3**).
2. Prepare the bisulfite reaction mix for each sample up to a total volume of 240 μL by adding 208 μL of saturated sodium metabisulfite and 12 μL of 10 mM Quinol, to 20 μL of denatured DNA sample.
3. Mix all reagents gently and centrifuge briefly to ensure all of the reaction components are at the bottom of the tube and then overlay each sample with 200 μL of mineral oil.
4. Incubate the samples at 55 °C for 4–16 h depending on the quality and quantity of the DNA samples (*see* **Notes 4** and **5**).
5. After elapsed incubation time, briefly spin the tubes and recover the bisulfite treated DNA samples from the mineral oil either by carefully pipetting of DNA samples from the bottom of the tube or snap-freezing tubes and removing unfrozen top layer of mineral oil.

3.1.3 Desalting and Alkali Desulfonation

1. After complete removal of mineral oil, pass the treated DNA sample through a desalting column to remove any bisulfite ions (*see* **Note 6)** and collect the pure DNA sample which is eluted in 50 μL of nuclease-free water.
2. Desulfonate the eluted DNA by adding 5 μL of 3 M (NaOH) and then incubate at 37 °C for 15 min.
3. After incubation, centrifuge briefly and add 1 μL of (10 mg/mL) tRNA.
4. Add 33 μL of 5 M NH_4OAc (pH 7.0) to neutralize the solution.
5. Precipitate the DNA by adding 2× volume of ice-cold 100% ethanol and mix well and then incubate the samples at −20 °C for at least 1 h (*see* **Note 7**).
6. Centrifuge at 16,000 × *g* for 15–20 min at 4 °C.
7. Remove the supernatant and air-dry the DNA sample.
8. Resuspend the DNA pellet in 50 μL of nuclease-free water or TE buffer and make sure that the pellet is completely dissolved.
9. The DNA can be used directly in polymerase chain reaction (RNA) or stored at −20 °C for long-term storage (*see* **Note 8**).

3.1.4 Bisulfite PCR Amplification

1. Specify your target genomic region which includes CpG islands.

CpG Islands Prediction and Primer Design

2. Use MethPrimer program [30] to predict the number of CpG islands and locate them among the target genomic region and use this information to design bisulfite conversion-based methylation primers (*see* **Note 9**).

PCR Reaction and Cycling Conditions

1. Prepare PCR reaction in a final volume of 25 μL containing of 12.5 μL of the high-fidelity PCR master mix (2×), 2.5 μL from each primer (10 pmol/μL), 1.5 μL bisulfite-converted genomic DNA (original concentrations), 0.75 μL dimethyl sulfoxide (DMSO), and 5.25 μL nuclease-free water.
2. Perform PCR using normal thermal cycler as follows: One cycle of initial denaturation step of 4 min at 95 °C, followed by 36 cycles of 95 °C for 30 s, (predicted Tm) °C for 30 s (not exceeding 450 bp) and 72 °C for 40 s and then a final extension at 72 °C for 7 min.
3. Visualize PCR products in 2% agarose gel in 1× Tris–acetate–EDTA buffer at 100 V for 40 min. For successful PCR amplification, single, intense, and specific band should be obtained (*see* **Notes 10** and **11**).

PCR Purification

1. After gel-based verification of the PCR product of the target sequence, repeat the PCR reaction in a total volume of 50 μL or more.
2. Use commercially available kits to purify the target sequence directly from the PCR product (in case of precise amplified band) or extracted from the gel (in case of nonspecific amplifications) following the manufacturers' protocol (*see* **Note 12**).

3.1.5 Cloning and Transformation

1. Prepare ligation reaction mixture of 2.5 μL of 2× Rapid Ligation Buffer, the required amounts of the purified PCR product (depending on (insert–vector) molar ratio optimization), and 0.5 μL from both pGEM®-T Easy Vector (50 ng) and T4 DNA ligase (3 Weiss units/μL), up to a final volume of 5 μL.
2. Incubate the mixture overnight at room temperature.
3. Add 1 μL of the ligation mixture to 50 μL of the commercially available cloning strains of *E. coli* and mix it well.
4. Transfer the cells to pre-cold cuvette and incubate on ice for a while.
5. Make sure to wipe off ice or water from the cuvette before use the electroporation system.
6. Set up the electroporation system according to its catalog instructions and then introduce the cloning vector into the competent cells.
7. Immediately, add 200 μL of SOC (Super Optimal Broth with Catabolite Repression, SOB with added glucose) to the cells and incubated for 1 h at 37 °C before plating.
8. Meanwhile, prepare growth plates by adding Ampicillin to a final concentration of 100 μg/mL, 0.5 M of IPTG (Isopropyl β-D-1-thiogalactopyranoside), 80 μg/mL X-gal.

9. Plate the cells in prepared LB agar and incubate overnight at 37 °C.
10. Next day choose ten white colonies as well as a single blue colony, as a negative control, and inoculate each in LB broth with ampicillin (*see* **Note 13**).
11. Incubate the selected colonies overnight at 37 °C with a shaking at 250 rpm.
12. In a parallel experiment, use a negative control for sodium bisulfite reaction as mentioned above.
13. Amplify the target sequence using regularly designed PCR primers, clone it in pGEM®-T Easy Vector and transform into JM110 strain of *E. coli* (*see* **Note 14**).
14. Perform the coming steps for both sequences (target and control).

3.1.6 Plasmid Purification

1. Purify plasmids of each colony culture using a mini plasmid prep kit following the manufacturer's protocol.
2. Check the purity and the quantity of the plasmids on a 1.5% agarose gel in 1× Tris-acetate EDTA buffer at 100 V for 40 min.
3. Check again the quality and the quantity of plasmid DNA using a NanoDrop spectrophotometer (ND-1000).

3.1.7 Sequencing and Data Analysis

1. Use T7 and\or SP6 Promoter Primer to sequence the inserts by Sanger Sequencing method (at least ten sequence clones are required for each gene).
2. Use BioEdit software to align the sequences with original sequence (unconverted sequence) and the converted sequence by the MethPrimer program (*see* Fig. 1b).
3. Referring to the original sequence, identify the methylated sites (unconverted cytosines) and check the same site over 10 sequenced clones.
4. Calculate the methylation percentage at that specific site.
5. Repeat the same last two steps for all predicted sites of methylation.

3.2 Whole Genome Bisulfite Sequencing (WGBS) Technique

3.2.1 Genomic DNA Fragmentations

1. Extract genomic DNA with a proper extraction method and make sure to obtain enough amounts (~ 1 μg) of a good quality. (*see* **Note 15**)
2. For DNA fragmentation, digest ~500 ng of genomic DNA with 2 units of dsDNA Shearase™ Plus enzyme. (*see* **Note 16**)
3. Prepare digestion reaction mixture by including 4 μL of 5× dsDNA Shearase™ Plus Reaction Buffer, 5 μL 100 ng/μL DNA, 9 μL nuclease-free water, and 2 μL dsDNA Shearase™ Plus in an eppendorf tube. (*see* **Note 17**)

4. Mix all components gently by flicking the tube, then centrifuge briefly at room temperature to collect the components at the tube bottom.
5. Incubate the mixture at 42 °C for 20 min then directly incubate it at 65 °C for 5 min to stop the reaction.
6. Purify the DNA using commercially available kits following the manufacturers' protocol.

3.2.2 MethylC-Seq Library Construction

1. Use End-It DNA end repair kit to blunt the sticky ends of the DNA fragments.

End Repair

2. Prepare for each reaction using the following mixture: (1–34) μL DNA (based on the concentration, up to 5 μg), 5 μL 10× End-Repair Buffer, 5 μL dNTP Mix, 5 μL ATP, 1 μL End-Repair Enzyme, and x μL nuclease-free water up to a reaction volume of 50 μL.
3. Mix the reaction gently, centrifuge briefly at room temperature and then incubate at room temperature for 45 min.
4. Purify repaired fragments from end-repair reaction components using commercially available kits for DNA cleaning following the manufacturers' protocol

Adenosine Tailing

1. Add 8 μL of A-tailing reaction mixture (5 μL 10× dA-tailing buffer and 3 μL klenow (3′–5′ exo–; 5 U/μL)) to the sample up to a total volume of 50 μL.
2. Mix the mixture gently, centrifuge briefly at room temperature, then incubate it at 37 °C for 45 min.
3. Purify the A-tailed fragments using commercially available kits for DNA cleaning following the manufacturers' protocol.

Methylated Adapter Ligation

1. Prepare for each sample the following reaction mixture; 2 μL methylated adapter (25 μM) (**Note 18**), 2.5 μL 10× DNA ligase buffer with ATP, 1.25 μL T4 DNA ligase (400 U/μ), and 3 μL nuclease-free water (*see* **Note 19**).
2. Mix the mixture gently, centrifuge briefly at room temperature, then incubate the mixture at 16 °C overnight.
3. Before purification, bring the volume of ligation mixture to 50 μL with nuclease-free water.
4. Purify adapter-linked fragments using commercially available kits for DNA cleaning following the manufacturers' protocol.

3.2.3 Bisulfite Conversion

1. Adjust the volume of adapter-linked gDNA sample to 20 μL (≤ 450 ng). If it is less bring the volume to 20 μL with nuclease-free water.

2. Perform the bisulfite conversion using commercially available kits following the manufacturers' instructions (*see* **Note 20**).

3.2.4 Amplification of Bisulfite-Converted Genomic DNA

1. Transfer bisulfite treated samples to 0.2-mL PCR tubes and add 27 μL of the reaction mixture (2 μL 25× PCR primer mix and 2× KAPA HiFi Uracil+ ReadyMix).
2. Run the samples under the following PCR program: one cycle of initial denaturation step of 2 min at 95 °C, followed by another two cycles of denaturation of 30 s at 98 °C, then [3–6] cycles of 98 °C for 15 s denaturation, 60 °C for 30 s annealing, and 72 °C for 1 min extension, and then a final extension at 72 °C for 10 min. (*see* **Note 21**).
3. Purify bisulfite-converted libraries using a commercially available kit following the manufacturer's protocol.

3.2.5 Sequencing, Alignment, and Data Analysis

1. Measure the concentration of genomic DNA libraries using Agilent 2200 TapeStation.
2. Sequence the libraries using Illumina Hiseq instrument.
3. Identify the sequence reads of MethylC-seq libraries using standard Illumina base-calling software.
4. Analyze the reads using alignment software like Bismark (http://www.bioinformatics.babraham.ac.uk/projects/bismark/).
5. Construct Index files by a bismark-genome-preparation command using the entire *Arabidopsis thaliana* as a reference genome.
6. Use *Arabidopsis thaliana* chloroplast genome to calculate the bisulfite conversion rate.
7. Estimate the methylation level of each cytosine as follows: the number of reads covering a cytosine divided by the total number of reads covering a cytosine or thymine.
8. Perform Fisher's exact test, combined with a robust False Discovery Rate (FDR) correction, for each cytosine with a minimum coverage of five aligned sequence reads ($P < 0.05$).
9. Use IGV (https://www.broadinstitute.org/igv/UserGuide) to analyze and visualize the data as the following:
   (a) Detect methylation percentage at each particular site under both control and stress conditions.
   (b) Identify DNA methylation regions (DMRs) in three sequence contexts: mCG, mCHG, and mCHH.
   (c) Quantifying and mapping the distribution of methylated cytosines of three sequence contexts among different gene features (promoter, exon, and introns).

4 Notes

1. High concentration of DNA is needed because large portion of DNA will be degraded during the harsh condition of bisulfite conversion (high temperature and low pH) and\or lost during purification.
2. Saturated sodium metabisulfite can be prepared by dissolving 7.6 g $Na_2O_5S_2$ in 15 mL water. Adjust the pH with 464 μL of fresh 10 M NaOH for complete dissolving of sodium metabisulfite. Optimal pH 5.0 is required for complete cytosine to uracil conversion.
3. Quinol (100 mM) can be prepared by dissolving 0.55 g of $C_6H_4(OH)_2$ in 15 mL of water. Then this can be diluted to obtain 10 mM Quinol.
4. DNA with poor quality, low molecular weight, and/or low concentration (100 ng) can be converted in 4 h, but for DNA with high quality, high molecular weight, and/or high concentration (500 ng to 2 μg), the conversion always takes 6–16 h.
5. The bisulfite conversion process should take place in the dark to avoid oxidation. Therefore, in case you are using an open system like a water bath for 55 °C incubation it is recommended to wrap the tubes with aluminum foil.
6. Desalting columns are available from different suppliers. Therefore, the procedure can be different based on the manufacturer's protocol.
7. For better DNA precipitation, incubate the DNA samples at −20 °C overnight.
8. For downstream applications, it is always recommended to prepare fresh bisulfite-modified DNA for best results. Converted DNA is not stable so, avoid repeated freeze and thaw cycles during storage.
9. Depending on your research purpose MethPrimer can design Methylation-Specific PCR (MSP), Bisulfite-Sequencing PCR (BSP), or Bisulfite-Restriction PCR primers. The principle of such software is to replace all cytosine (s) in the original sequence with thymine (s), mimicking the bisulfite treatment. The following criteria should be considered during bisulfite primers selection:
   (a) Avoid CpG dinucleotides in primer sequence because their methylation status is still unknown.
   (b) Primer sequence should contain at least 25% thymine (s) converted from cytosine (s) to ensure conversion specificity.
   (c) Avoid hairpin structures and primer dimers.

(d) To ensure their specificity, the length of bisulfite primers should be in the range of 25–30 bp.

(e) Amplicon size should not exceed 450 bp due to potential degradation of bisulfite-treated DNA.

10. In case of insufficient PCR product, a nested PCR is recommended to obtain more intensive bands.
11. The obtained PCR product will be cloned in a proper cloning system (e.g., pGEM-T Easy vector) to confirm the methylation pattern of the target sequence in many isolated colonies (at least ten colonies).
12. During band excising, minimize extra gel weight as much as possible.
13. Perform colony PCR for quick screening of inserts directly from the selected colonies of *Escherichia coli* using specific primers of your target sequence.
14. JM110 Competent cells are used as a negative control because they are deficient for two methylases (Dam and Dcm) present in most strains of *E. coli*. Dam methylase recognizes the GATC sequence and add a methyl group at the adenine residue at the N-6 position, while Dcm methylase recognizes CCAGG and CCTGG sequences and methylates the C-5 position of the internal cytosine.
15. The optical density (OD) at 260/280 readings should be greater than 1.7. High quality genomic DNA is highly demanded for constructing MethylC-seq libraries. This is help avoiding imbalanced cytosine (s) coverage in the genome, which might be reflected in biased sequencing results.
16. Instead of enzymatic digestion some protocols are using sonication for fragmenting the genomic DNA into ~200 bp fragments.
17. dsDNA Shearase™ Plus should be the last component added to the reaction mix and its ratio to genomic DNA must be 1 unit of enzyme per 250 ng of DNA.
18. Methylated adapter is designed to contain 5′-methyl-cytosine instead of cytosine bases.
19. When preparing the ligation reaction, put the samples tubes on ice and the reaction components as ordered. In case of multiple samples, making a master mix is not recommended, so prepare a separate reaction for each sample.
20. The elution volume depends on the number of PCR reactions planned to perform. For each PCR run, an elution of at least 23 μL is required. Multiple PCR is recommended to increase the sequencing depth.
21. To amplify adapter-linked genomic DNA fragments for sequencing, four cycle of PCR are enough to ensure low PCR duplicates.

References

1. Goldberg AD, Allis CD, Bernstein E (2007) Epigenetics: A landscape takes shape. Cell 128:635–638
2. Jablonka E, Raz G (2009) Transgenerational epigenetic inheritance: prevalence, mechanisms, and implications for the study of heredity and evolution. Q Rev Biol 84:131–176
3. Cokus SJ, Feng S, Zhang X, Chen Z, Merriman B, Haudenschild CD, Pradhan S, Nelson SF, Pellegrini M, Jacobsen SE (2008) Shotgun bisulphite sequencing of the Arabidopsis genome reveals DNA methylation patterning. Nature 452:215–219
4. Yaish MWF, Peng M, Rothstein SJ (2009) AtMBD9 modulates Arabidopsis development through the dual epigenetic pathways of DNA methylation and histone acetylation. Plant J 59:123–135
5. Saze H, Tsugane K, Kanno T, Nishimura T (2012) DNA methylation in plants: Relationship to small RNAs and histone modifications, and functions in transposon inactivation. Plant Cell Physiol 53:766–784
6. Erdmann RM, Souza AL, Clish CB, Gehring M (2014) 5-Hydroxymethylcytosine is not present in appreciable quantities in Arabidopsis DNA. G3 (Bethesda) 5:1–8
7. Al-Lawati A, Al-Bahry S, Victor R, Al-Lawati AH, Yaish MW (2016) Salt stress alters DNA methylation levels in alfalfa (Medicago spp). Genet Mol Res 15:15018299
8. Boyko A, Blevins T, Yao Y, Golubov A, Bilichak A, Ilnytskyy Y, Hollander J, Meins F, Kovalchuk I (2010) Transgenerational adaptation of Arabidopsis to stress requires DNA methylation and the function of dicer-like proteins. PLoS One 5:e9514
9. Dyachenko OV, Zakharchenko NS, Shevchuk TV, Bohnert HJ, Cushman JC, Buryanov YI (2006) Effect of hypermethylation of CCWGG sequences in DNA of *Mesembryanthemum crystallinum* plants on their adaptation to salt stress. Biochemistry (Mosc) 71:461–465
10. Liang D, Zhang Z, Wu H, Huang C, Shuai P, Ye C-Y, Tang S, Wang Y, Yang L, Wang J, Yin W, Xia X (2014) Single-base-resolution methylomes of *Populus trichocarpa* reveal the association between DNA methylation and drought stress. BMC Genet 15:S9
11. Steward N (2002) Periodic DNA Methylation in maize nucleosomes and demethylation by environmental stress. J Biol Chem 277: 37741–37746
12. Yaish MW ((2013)) DNA methylation-associated epigenetic changes in stress tolerance of plants. In: Rout GR, Das AB (eds) Molecular stress physiology of plants. Springer, Dordrecht, pp 427–440
13. Yaish MW, Colasanti J, Rothstein SJ (2011) The role of epigenetic processes in controlling flowering time in plants exposed to stress. J Exp Bot 62:3727–3735
14. Yaish MW, Peng M, Rothstein SJ (2013) Global DNA methylation analysis using Methyl-Sensitive Amplification Polymorphism (MSAP). Methods Mol Biol 1062:285–298
15. Sahu PP, Pandey G, Sharma N, Puranik S, Muthamilarasan M, Prasad M (2013) Epigenetic mechanisms of plant stress responses and adaptation. Plant Cell Rep 32:1151–1159
16. Molinier J, Ries G, Zipfel C, Hohn B (2006) Transgeneration memory of stress in plants. Nature 442:1046–1049
17. Li Y, Tollefsbol TO (2011) DNA Methylation detection: bisulfite genomic sequencing analysis. Methods Mol Biol 791:11–21
18. Kurdyukov S, Bullock M (2016) DNA methylation analysis: choosing the right method. Biol 5:3
19. Hardcastle TJ (2013) High-throughput sequencing of cytosine methylation in plant DNA. Plant Methods 9:16
20. Robinson JT, Thorvaldsdóttir H, Winckler W, Guttman M, Lander ES, Getz G, Mesirov JP (2011) Integrative genomics viewer. Nat Biotechnol 29:24–26
21. Liao W-W, Yen M-R, Ju E, Hsu F-M, Lam L, Chen P-Y (2015) MethGo: a comprehensive tool for analyzing whole-genome bisulfite sequencing data. BMC Genomics 16:S11
22. Urich MA, Nery JR, Lister R, Schmitz RJ, Ecker JR (2015) MethylC-seq library preparation for base-resolution whole-genome bisulfite sequencing. Nat Protoc 10:475–483
23. Lee Y, Jin S, Duan S, Lim Y, Ng DPY, Lin X, Yeo GSH, Ding C (2014) Improved reduced representation bisulfite sequencing for epigenomic profiling of clinical samples. Biol Proced Online 16:1
24. Ahlert D, Stegemann S, Kahlau S, Ruf S, Bock R (2009) Insensitivity of chloroplast gene expression to DNA methylation. Mol Genet Genomics 282:17–24
25. Fojtová M, Kovařík, A., and Matyášekek, R. (2001) Cytosine methylation of plastid genome in higher plants. Fact or artefact? Plant Sci 160:585–593
26. Wang J, Wang C, Long Y, Hopkins C, Kurup S, Liu K, King GJ, Meng J (2011) Universal endogenous gene controls for bisulphite con-

version in analysis of plant DNA methylation. Plant Methods 7:39

27. Ziller MJ, Hansen KD, Meissner A, Aryee MJ (2015) Coverage recommendations for methylation analysis by whole-genome bisulfite sequencing. Nat Methods 12:230–232
28. Stevens M, Cheng JB, Li D, Xie M, Hong C, Maire CL, Ligon KL, Hirst M, Marra MA, Costello JF, Wang T (2013) Estimating absolute methylation levels at single-CpG resolution from methylation enrichment and restriction enzyme sequencing methods. Genome Res 23:1541–1553
29. Krueger F, Kreck B, Franke A, Andrews SR (2012) DNA methylome analysis using short bisulfite sequencing data. Nat Methods 9:145–151
30. Li L-C, Dahiya R (2002) MethPrimer: designing primers for methylation PCRs. Bioinformatics 18:1427–1431

Chapter 8

ChIP-Seq Analysis for Identifying Genome-Wide Histone Modifications Associated with Stress-Responsive Genes in Plants

Guosheng Li, Guru Jagadeeswaran, Andrew Mort, and Ramanjulu Sunkar

Abstract

Histone modifications represent the crux of epigenetic gene regulation essential for most biological processes including abiotic stress responses in plants. Thus, identification of histone modifications at the genome-scale can provide clues for how some genes are 'turned-on' while some others are "turned-off" in response to stress. This chapter details a step-by-step protocol for identifying genome-wide histone modifications associated with stress-responsive gene regulation using chromatin immunoprecipitation (ChIP) followed by sequencing of the DNA (ChIP-seq).

Key words Abiotic stresses, Chromatin immunoprecipitation (ChIP), Epigenome, Gene regulation, Histone modifications

1 Introduction

The basic unit of chromatin is the nucleosome, in which 146 bp of DNA wraps around an octameric histone core. This histone core contains two copies each of the four histones H2A, H2B, H3, and H4. The histone proteins contain an NH_2-terminal "tail" that protrudes from the nucleosome core and is accessible for protein–protein and protein–DNA interactions [1]. The tail region also contains the lysine and arginine amino acid residues that are frequently modified as part of reversible posttranslational modifications. The histone octamer aids in compacting DNA into a chromosome. Modifications such as methylation of lysines (monomethylation, dimethylation, trimethylation), methylation of arginine (monomethylation and assymetric or symmetric dimethylation), acetylation of lysine, phosphorylation of serine and threonine, ubiquitination of lysine, sumoylation of lysine, and poly-ADP ribosylation of glutamate residues of histones determine the chromatin state of a gene [2]. Although both H3 and H4 are targets for most

Ramanjulu Sunkar (ed.), *Plant Stress Tolerance: Methods and Protocols*, Methods in Molecular Biology, vol. 1631,
DOI 10.1007/978-1-4939-7136-7_8,

posttranslational modifications, H3 is the most frequently modified histone. Typically, H3 lysine acetylation is a mark for transcriptional activation [3], whereas, depending on which lysine (K4, K9, K27, K36, and K79) of H3 is methylated, can serve as a mark for either activation or silencing [3]. For instance, H3K4, H3K36, and K79 methylations represent marks for transcriptional activation, while H3K9 and H3K27 are marks for gene silencing [3, 4]. Overall, these epigenetic modifications particularly methylation/acetylation at specific positions mainly on H3 and H4 dictate where and when a gene should be expressed or silenced [5].

Plant adaptation to stress involves numerous changes such as altered metabolites, increased antioxidant system, altered hormone biosynthesis and signaling, repression of energy-consuming processes, and readjustment of growth and development, which require the induction/activation or suppression of numerous genes. The altered metabolic profiles as well as other numerous responses at the genome level could be due to a combination of the following states; (a) the induction of new genes, (b) strengthened transcription of genes that are expressed without stress, (c) downregulation of genes that are expressed without stress, and (d) complete silencing of genes. While binding of a transcription factor to the *Cis*-elements in the promoter region confers one aspect of gene regulation, access to the *Cis*-elements in the DNA itself is regulated by the chromatin structure at a specific locus. Only active/open chromatin allows for binding of transcriptional regulators. On the other hand, closed/inactive chromatin does not allow for transcription and thus the corresponding gene is silenced. The active/inactive state of chromatin is controlled by covalent modifications to histones, a structural component of chromatin.

Plant stress responses are being studied in many plant species through "-omic" approaches to unravel molecular, biochemical, physiological, and morphological mechanisms important for stress tolerance [6–8]. Recently, epigenetic regulation has emerged as the upstream layer of gene regulation in plants and animals. DNA methylation and histone modifications, commonly known as "epigenetic modifications," regulate gene expression by altering the chromatin state. Genome-wide analyses of histone modifications have provided novel insights into correlations between histone modifications and gene expression under stress in plants [9–13]. For the purpose of identifying genome-wide histone modifications important for gene regulation, histone methylation and acetylation are most frequently analyzed given that their contributions to gene regulation are well established in plants. For instance, trimethylation of histone H3 Lys27 (H3K27me3) is generally regarded as a negative marker of transcription, whereas trimethylation of histone H3 Lys4 (H3K4me3) and acetylation of histone H3 Lys9 (H3K9ac) are often used as a positive marker of gene transcription.

In rice, H3K4me2 (dimethylation of histone H3 Lys4) and H3K4me3 marks on two submergence/hypoxia-inducible genes, alcohol dehydrogenase 1 (*ADH1*) and pyruvate decarboxylase 1 (*PDC1*), during the process from submergence to re-aeration were analyzed [14]. The K4 residues of H3 on the coding region of both *ADH1* and *PDC1* changed from a dimethylated to a trimethylated state, which was accompanied by transcriptional activation [14]. In Arabidopsis, the histone modifications on four dehydration stress-responsive genes, *RD29A*, *RD29B*, *RD20*, and an *AP2* transcription factor (At2g20880) during drought stress have been reported, and at all these loci, there was an enrichment of H3K4me3 and H3K9ac in response to dehydration stress [10]. In rice, H3K27me3 modification gradually decreases at the loci of two cold-responsive genes, *COR15A* and *AtGolS3*, during exposure to cold temperatures [11]. The decrease in H3K27me3 could lead to the upregulation or activation of gene expression on these genes, which play an important role during cold tolerance. In soybean, H3K4me3 and H3K9ac levels were elevated, leading to the activation of bZIP, AP2/EREB, NAC, and MYB transcription factors [15]. Thus, altered histone modifications have been observed under stress, which in turn affects the gene expression,thus potentially contributing for adaptation to stress [13, 16].

Chromatin immunoprecipitation (ChIP) has become the method of choice for identifying genome-wide histone modifications implicated in gene regulation. At the end, ChIP DNA can be analyzed by adopting hybridization to a microarray (ChIP-chip) or by high-throughput sequencing (ChIP-seq) [17, 18]. In recent years, ChIP-seq has gained popularity over ChIP-chip, an array-based technique limited to probes spotted in an array. Furthermore, ChIP-seq needs only a reference genome for analyzing the sequences and is more sensitive than ChIP-chip analysis. With the cost of sequencing coming down considerably, combined with ease of access and improvements in high-throughput sequencing, the ChIP-seq is increasingly adopted under varied biological experiments. Although several platforms exist for sequencing of ChIP DNA, Illumina Genome Analyzer is widely followed by researchers worldwide. In this chapter, we outline a detailed protocol based on this platform. In ChIP-seq, histones are covalently cross-linked to their genomic DNA to generate chromatin complexes followed by breaking the chromatin into smaller fragments. Antibodies specific to modified histones (e.g., monomethylation, dimethylation, or trimethylation of specific lysines) of interest are then employed for immunoprecipitation of the cross-linked chromatin fragments. After reversing the cross-links, ChIP DNA can be purified and used for constructing a library. In the end, ChIP generates a library of DNA enriched with modified histone-bound sites in vivo [19].

2 Materials

2.1 Cross-Linking Tissue Samples

1. Formaldehyde.
2. 2 M glycine stock.
3. Glass beakers.
4. Vacuum setup.

2.2 Chromatin Purification from Plant Tissue

1. Extraction Buffer 1:
   0.4 M Sucrose.
   10 mM Tris–HCl pH 8.0.
   10 mM $MgCl_2$.
   (Add 5 mM β-mercaptoethanol, 1× protease inhibitor, and 1 mM PMSF; *see* **Note 1**).
2. Extraction Buffer 2:
   0.25 M sucrose.
   10 mM Tris–HCl pH 8.0.
   10 mM $MgCl_2$.
   1% Triton X-100.
   (Add 5 mM β-mercaptoethanol, 1× protease inhibitor, and 1 mM PMSF; *see* **Note 1**).
3. Extraction Buffer 3:
   1.7 M sucrose.
   10 mM Tris–HCl pH 8.0.
   2 mM $MgCl_2$.
   0.15% Triton X-100.
   (Add 5 mM β-mercaptoethanol, 1× protease inhibitor, and 1 mM PMSF; *see* **Note 1**)
4. Centrifuge.
5. Miracloth.
6. Tubes (1.5 mL and 50 mL).
7. SDS lysis buffer.

2.3 Chromatin Immunoprecipitation (ChIP)

1. Sonicator.
2. Vortex mixer.
3. Incubator or water bath.
4. Protein A agarose/salmon sperm DNA.
5. Chromatin immunoprecipitation (ChIP) assay kit.
6. ChIP grade antibodies (specific for histone modification, e.g., H3K4me3 or H3K27me3).

7. Elution buffer (1% SDS, 0.1 M $NaHCO_3$, freshly made).
8. Proteinase K.
9. Phenol–chloroform (1:1).
10. Phase-lock gel tube.
11. Glycogen.
12. Sodium acetate.
13. Ethanol 70%.

2.4 ChIP-Seq Sample Preparation

1. End-It DNA end repair kit.
2. 100 mM dNTP stock.
3. Klenow enzyme.
4. T4 DNA ligase with 10× buffer.
5. Adaptors and PCR primers compatible with Illumina sequencing.
6. MinElute PCR Purification Kit.
7. QIAquick PCR Purification Kit.
8. QIAgen Gel extraction kit.
9. Low adhesion tubes.

3 Methods

3.1 Chromatin Cross-Linking

1. Wrap the plant tissue to be cross-linked in aluminum foil and keep it immersed in a beaker containing 1% formaldehyde.
2. Cross-link the proteins to DNA in the chromatin by applying vacuum for about 10–15 min and release vacuum slowly (*see* **Note 2**).
3. Stop cross-linking by keeping the sample in a beaker with formaldehyde containing 0.125 M glycine (final concentration) and apply vacuum for 5 min and release vacuum slowly.
4. Rinse the sample three times in sterile water to remove any traces of formaldehyde remaining in the sample (*see* **Note 3**).
5. Continue with chromatin preparation (*see* **Note 4**).

3.2 Chromatin Preparation

1. Grind about 2 g of cross-linked tissue to a fine powder in a precooled pestle and mortar with liquid nitrogen.
2. Using a cold spatula, transfer the tissue powder to a 50-mL tube and add 20 mL of prechilled Extraction Buffer 1 (*see* **Note 5**).
3. Vortex the solution until it becomes homogenous, and then place on ice for 15 min.

4. Filter the homogenate through two layers of Miracloth into a fresh 50 mL centrifuge tube placed on ice.
5. Centrifuge the filtered solution at 12,000 × *g* at 4 °C for 10 min.
6. Gently remove the supernatant and resuspend the pellet thoroughly in 5 mL of prechilled Extraction Buffer 2, and centrifuge as in **step 3**.
7. Remove the supernatant and resuspend the pellet thoroughly in 1.2 mL of prechilled Extraction Buffer 3 (*see* **Note 6**).
8. Add 300 μL of prechilled Extraction Buffer 3 in to an Eppendorf tube, carefully layer 300 μL of resuspensions (from **step 7**; equally aliquoted in four tubes) over the Extraction Buffer 3, and centrifuge at 16,000 × *g* at 4 °C for 1 h.
9. Remove the supernatant with pipette carefully.
10. Resuspend the chromatin pellet in 300 μL of SDS lysis buffer (Millipore Chromatin Immunoprecipitation Assay Kit) by pipetting the solution up and down or by vortexing gently and proceed for sonication to shear the chromatin (*see* **Note 7**).

3.3 Chromatin Immunoprecipitation (ChIP)

1. Sonicate the resuspended chromatin solution in a probe sonicator; Save 10 μL of the solution prior to sonication for comparison with sonicated sample later (*see* **Notes 8** and **9**).
2. Centrifuge the sonicated chromatin at 12,000 × *g* at 4 °C for 10 min to pellet the debris. Remove the supernatant and resuspend the pellet in SDS lysis buffer and save about 10 μL from each sample to serve as the "input DNA."
3. Measure the volume of the chromatin sample and add ChIP dilution buffer (chromatin immunoprecipitation kit) to bring the final volume to 3 mL.
4. Divide the chromatin solution for each sample equally in three tubes of 1 mL each (two tubes for immunoprecipitation reactions, one for no-antibody control).
5. To each tube, add 40 μL of protein A-agarose beads and preclear the solution by incubating at 4 °C for 1 h with gentle rotation.
6. Centrifuge the chromatin solutions with beads at 12,000 × *g* at 4 °C for 1 min and transfer the supernatant to fresh tubes (*see* **Note 10**).
7. Add 5 μL of the chosen antibody (*see* **Note 11**) to two of the three tubes; the third tube without antibody is the "no-antibody control." Incubate all three tubes at 4 °C overnight with gentle rotation.

8. Add 50 μL of protein A-agarose beads to each tube and collect the immune complexes by incubation at 4 °C for 2 h with gentle rotation.
9. Recover the beads by centrifugation at no more than 3800 × *g* at 4 °C for 1 min to avoid damaging the beads and remove the supernatant.
10. Wash the beads at 4 °C with gentle rotation, using the appropriate buffer from the ChIP Assay Kit sequentially: Quick wash in low-salt wash buffer followed by a second wash for 5 min; Quick wash in high-salt wash buffer followed by a second wash for 5 min; Quick wash in TE wash buffer followed by a second wash for 5 min. After each wash, recover the beads by centrifugation at 3800 × *g* at 4 °C for 1 min. After the last wash, carefully remove as much TE buffer as possible from the beads.
11. Add 200 μL of freshly prepared elution buffer to elute the immune complexes from the beads.
12. Vortex briefly to mix and incubate the tubes at 65 °C for 15 min with gentle rotation (*see* **Note 12**).
13. Centrifuge the beads at 3800 × *g* at 15–25 °C for 2 min and carefully transfer each supernatant fraction to a fresh tube. Repeat this step with 200 μL of elution buffer and combine the two eluates for each sample.
14. Reverse the cross-linking by adding 16 μL of 5 M NaCl to each sample followed by incubation at 65 °C overnight; Also incubate the "input DNA" (from **step 2** of Subheading 3.3).
15. To each sample of eluate and to the "input DNA" control, add the following:

0.5 M EDTA	8 μL
1 M Tris–HCl pH 8.0	16 μL
10 mg/mL proteinase K	2 μL
Incubate at 45 °C for 1 h	

16. Extract the DNA with phenol–chloroform (1:1), using a phase-lock gel tube.
17. Recover the DNA by precipitation with ethanol in the presence of 0.3 M sodium acetate (pH 5.2) and 2 μL glycogen carrier (10 mg/mL) overnight at −20 °C.
18. Wash the DNA pellets with 70% ethanol and resuspend the pellet in 20 μL of nuclease-free water.

3.4 ChIP-Seq Sample Preparation

1. Perform end repair by mixing the following components in a low-adhesion tube, and incubate at room temperature (18–20 °C) for 45 min (*See* **Note 13**).

ChIP DNA	28 μL
10× End-repair buffer	5 μL
2.5 mM dNTP mix	5 μL
10 mM ATP	5 μL
Water to bring reaction volume to 49 μL	X μL
End-repair enzyme mix	1 μL
Total reaction volume	50 μL

2. Purify DNA from **step 1** on a QIAquick column from the QIAquick PCR purification kit and protocol. Elute in 34 μL of elution buffer.
3. For A-tailing, combine and mix the following components in a PCR tube and incubate for 30 min at 37 °C (e.g., in PCR machine).

DNA from **step 2**	34 μL
Klenow buffer (NEB buffer 2)	5 μL
1 mM dATP	10 μL
Klenow fragment (3′-5′ exonuclease minus)	1 μL
Total reaction volume	50 μL

4. Purify DNA from **step 3** on a QIAquick MinElute column using the MinElute PCR purification kit and elute in 17 μL of elution buffer.
5. For adaptor ligation, combine and mix the following components in a Lo-bind tube and incubate for 20–22 h at 16 °C (e.g., in PCR machine).

DNA from **step 4**	16.5 μL
10× DNA ligase buffer	2 μL
Illumina adaptor oligo mix (1:10–1:50)	1 μL
T4 DNA ligase	0.5 μL
Total reaction volume	20 μL

6. Purify the DNA using the QIAquick PCR Purification Kit and elute in 30 μL elution buffer.

7. To amplify and carry out PCR, set up the master mix by combining the following components in a PCR tube. Reagents per reaction is given below

5× Phusion buffer	10 µL
2.5 mM dNTP	4 µL
Phusion enzyme	0.8 µL
dH_2O	3.2 µL
Total reaction volume	18 µL

8. In a PCR tube combine:

DNA (from **step 6**)	30 µL
Master mix (from **step 7**)	18 µL
PCR primer 1.1 (Illumina)	1 µL
PCR primer 2.1 (Illumina)	1 µL
Total reaction volume	50 µL

9. Amplify the DNA using the following PCR protocol:

   30 s at 98 °C.

   10 s at 98 °C.

   30 s at 65 °C.

   30 s at 72 °C.

   18–20 cycles total.

   5 min at 72 °C.

   Hold at 4 °C.

10. Purify on one QIAquick MinElute column using the MinElute PCR purification kit and protocol. Elute in 20 µL EB.
11. Test for enrichment using qPCR.
12. Gel purification: Run PCR product on a 2% agarose gel poured with 1/10,000 (vol/vol) GelRed.
13. Excise a large band in the range 250–500 bp with a clean scalpel. Be sure to take photos of the gel both before and after the slice is excised. Estimate and record the median product size.
14. Purify the DNA from the agarose slice using a Qiagen Gel extraction kit. Elute in 30 µL of elution buffer.
15. Quality control: Test for enrichment using qPCR.
16. Measure the DNA concentration and size by picogreen assay (Invitrogen Q-bit) or Agilent BioAnalyzer DNA 1000 chip.

4 Notes

1. Protease inhibitor and freshly prepared PMSF must be added just prior to using the buffer.
2. The amount of plant tissue and the duration of cross-linking are highly variable and needs to be determined empirically.
3. Remove as much as water as possible to remove all formaldehyde by gently blotting with paper towels.
4. Cross-linked plant sample can now be stored by flash-freezing in liquid nitrogen and keeping at −80 °C.
5. All buffers should be kept cold at all times and tissue samples should not be allowed to thaw at any stage.
6. This step may take time, but complete resuspension is needed for thorough homogenization.
7. The chromatin pellet at this stage can be stored at −80 °C until used.
8. Sonication procedure (the number of sonication cycles and duration of each cycle) needs to be optimized depending on the plant species and tissue sample. This can be done by checking the DNA purified from the sonicated chromatin by running a 2% agarose gel after incubating at 65 °C overnight. A DNA smear of desired size (100–400 bp) should be seen.
9. The sonicated solution at this point can be stored at −80 °C.
10. Care must be taken not to transfer any of the agarose beads while transferring.
11. The amount of antibody needs to be determined empirically.
12. Incubation can be done in a rotating hybridization oven at 65 °C; if a water bath is used manually mix by rotating the tubes every 3 min.
13. Because of the low amount of DNA, low-adhesion microfuge tubes need to be used to reduce nonspecific binding of DNA to tubes and avoid further loss of DNA).

Acknowledgments

The work in RS laboratory was supported by the Oklahoma Center for Advancement of Science and Technology and Oklahoma Agricultural Experiment Station. AM acknowledges the Stevens endowed Chair professorship in Agricultural Biotechnology of DASNR, OSU.

References

1. Temel A, Janack B, Humbeck K (2015) Epigenetic regulation in plants. Chichester, John Wiley & Sons, Ltd. doi:10.1002/9780470015902.a0021848
2. Lauria M, Rossi V (2011) Epigenetic control of gene regulation in plants. Biochim Biophys Acta 1809:369–378
3. Kouzarides T (2007) Chromatin modifications and their function. Cell 128:693–705
4. Yuna L, Liu X, Luo M, Yang S, Wu K (2013) Involvement of histone dmofications in plant abiotic stress responses. J Int Plant Biol 55:892–901
5. Grunstein M (1997) Histone acetylation in chromatin structure and transcription. Nature 389:349–352
6. Zhu J-K (2002) Salt and drought stress signal transduction in plants. Annu Rev Plant Biol 53:247–273
7. Bartels D, Sunkar R (2005) Drought and salt tolerance in plants. Crit Rev Plant Sci 24:23–58
8. Juenger T (2013) Natural variation and genetic constraints on drought tolerance. Curr Opin Plant Biol 16:274–281
9. Zhang X, Clarenz O, Cokus S, Bernatavichute YV, Pellegrini M, Goodrich J, Jacobsen SE (2007) Whole-genome analysis of histone H3 lysine 27 trimethylation in Arabidopsis. PLoS Biol 5:e129
10. Kim JM, To TK, Ishida J, Morosawa T, Kawashima M, Matsui A, Toyoda T, Kimura H, Shinozaki K, Seki M (2008) Alterations of lysine modifications on the histone H3 N-tail under drought stress conditions in *Arabidopsis thaliana*. Plant Cell Physiol 49:1580–1588
11. Kwon CS, Lee D, Choi G, Chung W (2009) Histone occupancy-dependent and -independent removal of H3K27 trimethylation at cold-responsive genes in Arabidopsis. Plant J 60:112–121
12. van Dijk K, Ding Y, Malkaram S, Riethoven JJ, Liu R, Yang J, Laczko P, Chen H, Xia Y, Ladunga I, Avramova Z, Fromm M (2010) Dynamic changes in genome-wide histone H3 lysine 4 methylation patterns in response to dehydration stress in *Arabidopsis thaliana*. BMC Plant Biol 10:238
13. Han SK, Wagner D (2014) Role of chromatin in water stress responses in plants. J Exp Bot 65:2785–2799
14. Tsuji H, Saika H, Tsutsumi N, Hirai A, Nakazono M (2006) Dynamic and reversible changes in histone H3-Lys4 methylation and H3 acetylation occurring at submergence-inducible genes in rice. Plant Cell Physiol 47:995–1003
15. Song Y, Ji D, Li S, Wang P, Li Q, Xiang F (2012) The dynamic changes of DNA methylation and histone modifications of salt responsive transcription factor genes in soybean. PLoS One 7:e41274
16. Chinnusamy V, Zhu JK (2009) Epigenetic regulation of stress responses in plants. Curr Opin Plant Biol 12:133–139
17. Iyer VR, Horak CE, Scafe CS, Botstein D, Snyder M, Brown PO (2001) Genomic binding sites of the yeast cell-cycle transcription factors SBF and MBF. Nature 409:533–538
18. Barski A, Cuddapah S, Cui K, Roh TY, Schones DE, Wang Z, Wei G, Chepelev I, Zhao K (2007) High-resolution profiling of histone methylations in the human genome. Cell 129:823–837
19. Ren B, Robert F, Wyrick JJ, Aparicio O, Jennings EG, Simon I, Zeitlinger J, Schreiber J, Hannett N, Kanin E et al (2000) Genome-wide location and function of DNA binding proteins. Science 290:2306–2309

Chapter 9

Isolation of Polysomal RNA for Analyzing Stress-Responsive Genes Regulated at the Translational Level in Plants

Yong-Fang Li, Ramamurthy Mahalingam, and Ramanjulu Sunkar

Abstract

Alteration of gene expression is an essential mechanism, which allows plants to respond and adapt to adverse environmental conditions. Transcriptome and proteome analyses in plants exposed to abiotic stresses revealed that protein levels are not correlated with the changes in corresponding mRNAs, indicating regulation at translational level is another major regulator for gene expression. Analysis of translatome, which refers to all mRNAs associated with ribosomes, thus has the potential to bridge the gap between transcriptome and proteome. Polysomal RNA profiling and recently developed ribosome profiling (Ribo-seq) are two main methods for translatome analysis at global level. Here, we describe the classical procedure for polysomal RNA isolation by sucrose gradient ultracentrifugation followed by highthroughput RNA-seq to identify genes regulated at translational level. Polysomal RNA can be further used for a variety of downstream applications including Northern blot analysis, qRT-PCR, RNase protection assay, and microarray-based gene expression profiling.

Key words Polysome, Ribosome, Stress, Sucrose density gradient, Translatome, Translational regulation, Ultracentrifugation

1 Introduction

Gene expression profiling is a central tool for identifying the various pathways associated with plant responses to various stresses. Measurement of steady-state mRNA abundances, rather than the rates of protein synthesis, is the main method currently used to study global gene expression changes in response to stresses, because simple and reliable tools are available for RNA isolation [1]. Microarray and the advent of high-throughput sequencing techniques have revolutionized our understanding of the content of transcriptome and transcriptional regulatory networks associated with various stresses. However, more and more evidence shows that mRNA levels do not necessarily correlate with the levels

Ramanjulu Sunkar (ed.), *Plant Stress Tolerance: Methods and Protocols*, Methods in Molecular Biology, vol. 1631,
DOI 10.1007/978-1-4939-7136-7_9,

of proteins, indicating that control of protein synthesis is another key regulator of gene expression [1–6].

Protein synthesis is an energetically expensive anabolic process and is sensitive to the environmental changes [7, 8]. Messenger RNA translation is an intricate process that takes place on ribosomes and it can be divided into three stages: initiation, elongation, and termination [9]. In plants, it has been shown that initiation is the main rate-limiting stage in protein synthesis. In this stage, translation initiation factors recruit an mRNA to a 40S ribosomal subunit to form initiation complex, which will scan the mRNA from 5′ to 3′ till the initiation codon, then, a 60S subunit joins the complex to form 80S ribosome and initiate protein synthesis. During elongation stage, other ribosomes can initiate translation on the same mRNA to form polysomes. Recent studies have shown regulation of elongation also plays important roles through cis-regulatory elements on the transcripts, codon bias, or mRNA structure [2, 10, 11]. Mass spectrometry is the popular method to measure protein expression levels at global level; however, sequencing technologies usually provide deeper measurement than mass spectrometry measurements [3]. Thus, a reliable measurement of the translation of mRNA is the degree of its association with ribosomes. Measurements of the translatome, which refers to all mRNAs associated with ribosomes, can effectively monitor the translational status under various physiological conditions.

Polysome profiling is the traditional standard method to study translatome, which separates mRNAs based on the bound ribosome number using a sucrose gradient ultracentrifugation (Fig. 1). Combined with microarrays or high-throughput RNA sequencing technique, polysome profiling can identify the actively translated mRNAs at global level [8, 12–14]. Recently, a new high-throughput sequencing approach named ribosome profiling (Ribo-seq) has been developed for global analysis of translation at near nucleotide resolution. Ribo-seq detects the RNaseI digestion footprint of an mRNA on a ribosome, and also helps to identify the number of ribosomes on each mRNA [7, 15–18]. Although ribosome profiling has been proven to be powerful in defining ribosome positions on the entire transcriptome, polysome profiling is still a valuable and flexible method.

Polysomes can be divided into small polysome complex (two to four ribosomes per mRNA) and large polysome complex (more than four ribosomes per mRNA), which represent moderately translated mRNAs and actively translated mRNAs, respectively [5, 9]. Gene expression can even be checked with the RNA collected from each gradient fraction. Polysome profiling is ideal for analyzing translatome or specific mRNA changes in response to stresses. The distribution of specific mRNAs in the gradients can be monitored by reverse-transcription quantitative polymerase chain reaction, Northern blot, or RNase protection assay [14]. These downstream

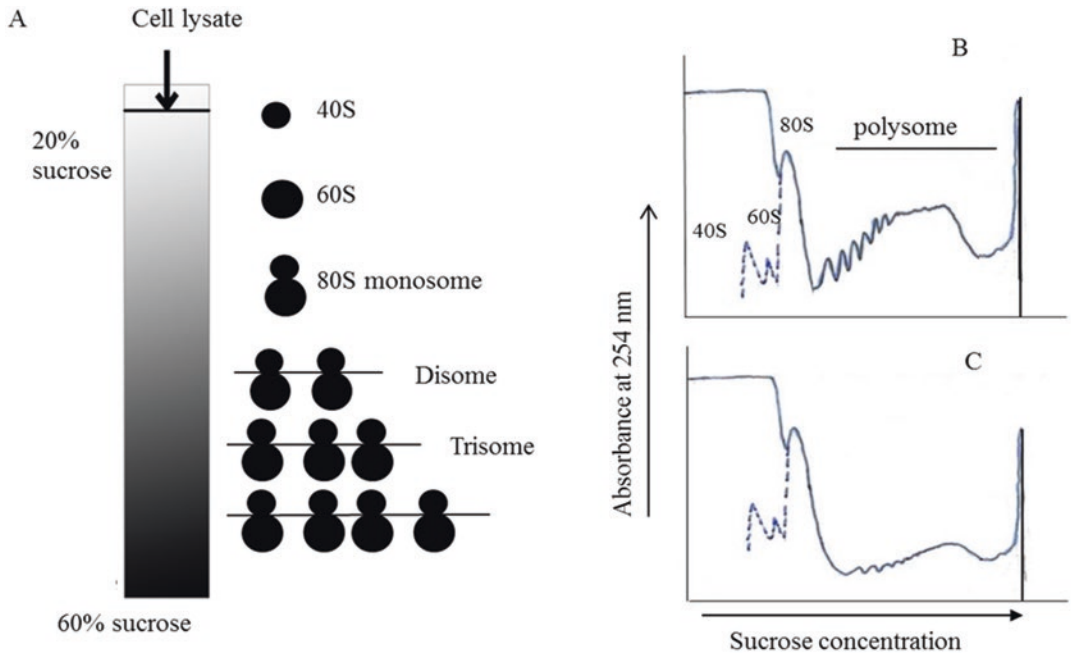

Fig. 1 Sucrose gradient ultracentrifugation and fractionation. (**a**) distribution of ribosome subunits, monosome and polysome in sucrose gradient. (**b, c**) polysome profile of rice seedlings under control and salinity stress, respectively. The decrease in polysome part is a clear indication of reduced protein synthesis in responsive to salinity stress. Since plant cell lysate contains high amounts of chlorophyll, high absorbance is observed in light sucrose density part, peaks of ribosome subunits usually cannot be seen. However, 80S monosome peak is clear and visible. Dashed line indicates the approximate position of 40S and 60S ribosome subunit

procedures are not possible using ribosome profiling. Here, we describe polysome RNA-seq (psRNA-seq) in conjunction with total RNA-seq to study stress responsive genes in plant (Fig. 2). Comparison of the transcriptome/translatome profile under control and stress condition will reveal the stress responsive genes at transcriptional/translational level. Comparison of the transcriptome and translatome profile under same condition will aid in identifying the noncorrelative genes and thus reveal their regulatory mechanism. Integrative analysis of these profiles will help us understand the gene networks operative in response to stresses. RNA-seq is quite well documented and is only described briefly here. Polysomal isolation is the challenging step for successful analysis of the translatome. Here we describe the procedure we adopted from the published protocols [5, 6, 19]. Using this procedure, we have successfully isolated polysomal RNA from Arabidopsis, Medicago, rice, and barley.

2 Materials

All solutions, pipette tips, and tubes should be RNase free. All solutions are prepared with nano-pure water unless indicated.

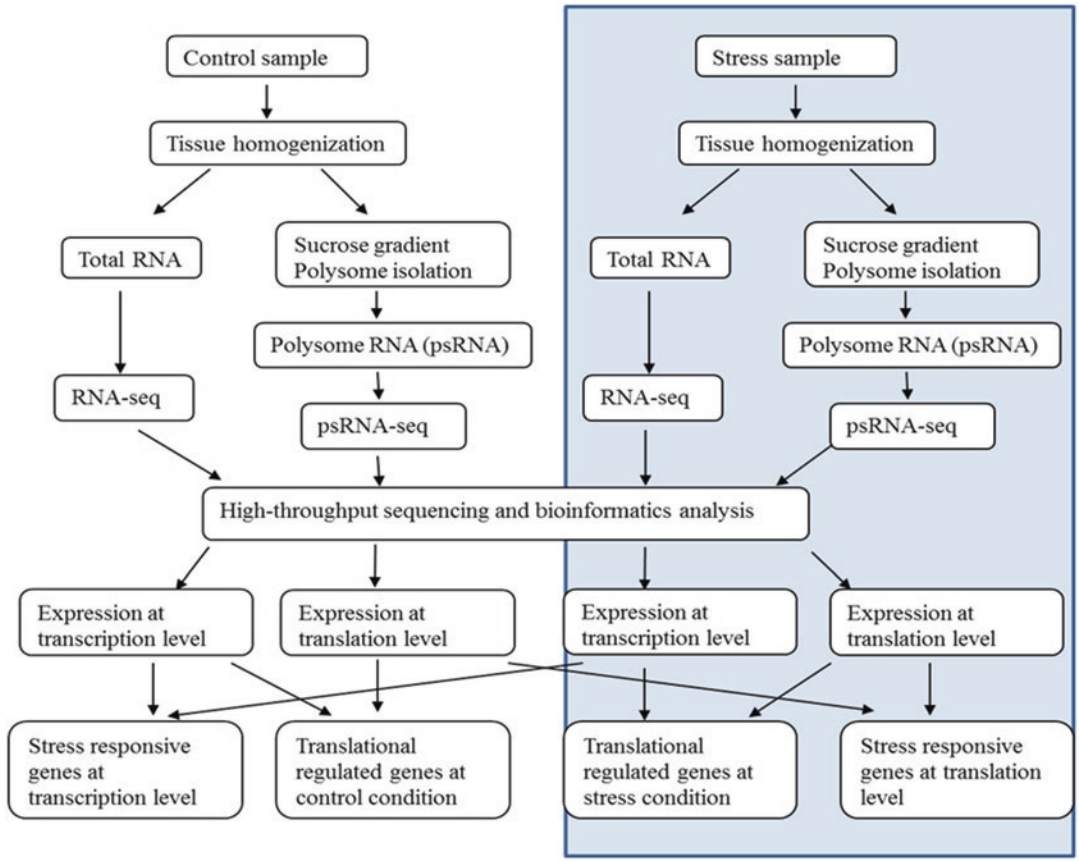

Fig. 2 Workflow for analyzing stress responsive genes using total RNA and polysomal RNA

2.1 Polysome Isolation

1. 2 M sucrose (*see* **Note 1**).
2. 10× sucrose salts: 0.4 M Tris–HCl pH 8.4, 0.2 M KCl, 0.1 M $MgCl_2$.
3. 2 M Tris–HCl, pH 9.0.
4. 2 M KCl.
5. 0.25 M EGTA (ethylene glycol-bis(2-aminoethylether)-N,N,N′,N′-tetraacetic acid), pH 8.3 (*see* **Note 2**).
6. 1 M $MgCl_2$.
7. 20% (v/v) polyoxyethylene 10 tridecyl ether (PTE) (*see* **Note 3**).
8. 10% sodium deoxycholate (DOC) (*see* **Note 4**).
9. 20% detergent mix (*see* **Note 5**): 20% (w/v) polyoxyethylene(23)lauryl ether (Brij-35), 20% (v/v) Triton X-100, 20% (v/v) octylphenyl-polyethylene glycol (Igepal CA630), 20% (v/v) polyoxyethylene sorbitan monolaurate 20 (Tween 20).

The above solutions should be autoclaved and can be kept at room temperature. The following stocks should not be autoclaved and are stored at −20 °C in aliquots.

10. 0.5 M dithiothreitol (DTT).
11. 50 mg/mL cycloheximide, dissolved in ethanol.
12. 50 mg/mL chloramphenicol, dissolved in ethanol.
13. 0.5 M phenylmethylsulfonyl fluoride (PMSF), dissolved in isopropanol (*see* **Note 4**).
14. Heparin (*see* **Note 6**).
15. RNase inhibitor (*see* **Note 6**).
16. Plant material: Plant tissues under control and stress condition must be harvested and immediately frozen in liquid nitrogen. If the tissues are not used immediately, it is better to grind tissues to fine powder using sufficient liquid nitrogen and keep pulverized tissue samples at −80 °C until use.

2.2 Other Kits and Chemicals

1. TRIzol reagent.
2. Chloroform.
3. Isopropanol.
4. Ethanol.
5. Nuclease-free water.
6. Glycogen.
7. Illumina TruSeq® Stranded mRNA-Seq kit.
8. Fluorinet™ FC-40.

2.3 Equipment and Tubes

1. Benchtop centrifuge.
2. Ultracentrifuge and swinging bucket rotor: We have used Beckman Optima LE-80 K ultracentrifuge (Beckman-Coulter) and Beckman swinging bucket rotor SW55.T1.
3. Open-top polyclear ultracentrifuge tubes (Seton Scientific Co.; Los Gatos, CA) of 13 × 51 mm size. Tubes are immersed in 0.1% DEPC water overnight and dried prior to use.
4. Density gradient fractionator Retriever 500 (Teledyne-ISCO Lincoln, NE).
5. BioAnalyzer 2100 (Agilent).
6. NanoDrop 1000.

3 Methods

3.1 Sucrose Gradient Preparation

Open-top 5-mL polyclear ultracentrifuge tubes are used for preparing sucrose gradients and polysome isolation. Sucrose gradients can be prepared by using commercial gradient marker per manufacturer's guidance. Here we introduce the freeze-thawing method, which is easy to perform and suitable for preparation of multiple sucrose gradients in advance. The frozen gradients can be stored for several months at −80 °C.

Table 1
Preparation of sucrose gradients

Sucrose content (%)	2 M sucrose (mL)	10× sucrose salt (mL)	DEPC H_2O (mL)	Chloramphenicol and cycloheximide (μL)	Volume per gradient (mL)
60 (Bottom)	22	2.5	0.5	2.5	0.75
45	33	5	12	5	1.5
30	22	5	23	5	1.5
20 (top)	7.25	2.5	15.25	2.5	0.75

1. Prepare 20%, 30%, 45%, and 60% sucrose solution according to Table 1, which is enough for 30 gradient tubes.
2. Place the Seton ultracentrifuge tubes in a rack, which can withstand −80 °C.
3. Starting with the 60% sucrose layer, pipette 0.75 mL into the ultracentrifuge tubes avoiding any air bubbles, and freeze tubes for 1 h at −80 °C.
4. Add 1.5 mL 45% sucrose layer above the frozen 60% sucrose layer, freeze again, and then 1.5 mL of 30% and 0.75 mL of 20% sucrose layer successively.
5. Keep sucrose gradients at −80 °C till ready to use.

3.2 Tissue Homogenization and Ultracentrifugation

Preparation on the working day:

(a) Take out sucrose gradient tubes (20–60% sucrose) from −80 °C, place them into rotor buckets and warm at 37 °C for 1 h, then cool at 4 °C for at least 1 h before usage (*see* **Note 7**).

(b) Prepare polysome extraction buffer according to Table 2. PEB should be mixed freshly and kept on ice. 20% detergents should be warmed at 42 °C till all ingredients are dissolved prior to use.

The following steps should be carried out on ice or at 4 °C unless stated.

1. Grind plant tissues to fine powder using liquid nitrogen.
2. Place 750 μL of packed tissue powder into chilled 2.0 mL tubes, then immediately add 1.25 mL polysome extraction buffer to the tubes and mix the extract by stirring with spatula.
3. Place tubes on ice for 10 min with occasional inversion for thorough mixing (do not vortex).
4. Centrifuge the extract for 2 min at 16,000 × *g* at 4 °C using a benchtop centrifuge.

Table 2
Preparation of polysome extraction buffer (PEB)

Items	Stock concentration	Volume for 10 mL	Final concentration
Tris (pH 9.0)	2 M	1 mL	0.2 M
KCl	2 M	1 mL	0.2 M
EGTA (pH 8.3)	0.25 M	1 mL	0.025 M
$MgCl_2$	1 M	0.35 mL	0.035 M
H_2O		to 7.9 mL	
Detergent mix	20%	0.5 mL	1%
DOC	10%	1 mL	1%
PTE	20%	0.5 mL	1%
Cycloheximide	50 mg/mL	10 µL	50 µg/mL
Chloramphenicol	50 mg/mL	10 µL	50 µg/mL
DTT	0.5 M	0.1 mL	5 mM
PMSF	0.5 M	20 µL	1 mM
Heparin			1 mg/mL

5. Transfer the supernatant into a QIA shredder (QIAGEN), and centrifuge the column for 1 min at 16,000 × *g* at 4 °C. The column can be reused. Combine the flow through (cell lysate).
6. Carefully load 700 µL of cell lysate on the top of sucrose gradient. Aliquot 300 µL cell lysate into a separate tube for later total RNA isolation.
7. Balance gradient tubes with buckets within 0.01 g using either excess cell lysate or polysome extraction buffer.
8. Ultracentrifuge the tubes for 140 min at 152,000 × *g* at 4 °C using Beckman Optima LE-80 K ultracentrifuge (*see* **Note 8**).

3.3 Polysome Fractionation

1. Turn on the density gradient fractionator during ultracentrifugation, at least 30 min before polysome analysis.
2. Assemble the peristaltic pump and gradient holder according to the manufacturer's instructions. Adjust the absorbance detector to 1.0 sensitivity.
3. Prerun a sucrose gradient with 700 µL polysome extraction buffer loaded on top of the gradients to establish the baseline absorbance profile. Meanwhile, determine the dead volume of the detector–collector system and the corresponding time delay between particular peak detection and its elution from the ISCO instrument.

4. After centrifugation, carefully remove the buckets from the rotor, place the buckets on ice. Place the 1st gradient tube in the UV detector holder, puncture the tube from bottom, and pump forward Fluorinet™ FC-40 into the tube at 1 mL/min flow rate (*see* **Note 9**). Record the A254 nm absorbance with paper chart recorder at 60 cm/h chart speed (and use an external data acquisition module equipped with an appropriate software if available). Collect fractions at 16 drops per tube for 14 tubes (*see* **Note 10**), and place tubes on ice immediately to avoid RNA degradation.
5. After the whole tube sucrose gradient is fractionated retrieve Fluorinet™ FC-40 by reversing pump flow direction. Then continue fractionation with the second gradient tube, as described in **step 4**.
6. Combine polysome fractions. Usually, two pools are combined. The first is the non-polysome pool (fraction tubes No. 1–7), which contains ribosomal subunits and monosomes, representing the nontranslated transcripts. The second is the polysomes (fraction tube No. 8–13), containing the actively translated mRNAs. For accurate collection of corresponding fractions, we recommend taking the dead volume and the corresponding time delay into account. The dead volume and time delay vary with flow rate and the detector–collector connection tube length, which can be determined during the prerun with the sucrose gradient. If you prefer to do analysis on individual fractions, do not combine the tubes.

3.4 Polysomal RNA and Total RNA Isolation

We use TRIzol reagent to isolate polysomal RNA and total RNA. Combined ploysome fractions are used for polysomal RNA isolation. Total RNA is isolated from the aliquot cell lysate (Subheading 3.2).

1. Quantify the volume of polysomal fractions/cell lysate, add 1.5× volume of TRIzol reagent (Invitrogen), shake the tubes vigorously for 15 s, and incubate at room temperature for 10 min.
2. Add 0.3 volume chloroform to the tubes, shake vigorously for 15 s, and incubate at room temperature for 2–3 min.
3. Spin at 16,000 × *g* for 15 min at 4 °C.
4. Transfer the aqueous phase (clear portion) to a new tube, add 1 μL glycogen and 1× aqueous phase volume of isopropanol, vortex well and keep in −80 °C for 30 min.
5. Spin at 16,000 × *g* for 30 min at 4 °C and carefully discard the supernatant (*see* **Note 11).**
6. Wash pellet with 1 mL of 75% ethanol, spin at 13,000 × *g* for 2 min at 4 °C, and discard ethanol.

7. Quick-spin and remove residual ethanol with a pipette, and air-dry pellet at room temperature for 2 min.
8. Add appropriate quantity of RNase free water to dissolve RNA pellet to get approximately final concentration of 1.0 μg/μL.
9. Check RNA quality with Bioanalyzer 2100 (Agilent) and RNA concentration with Nanodrop 1000 (Thermo Scientific).
10. Store RNA samples at −80 °C until use.

3.5 RNA-Seq Library Preparation

RNA isolated from polysome is used for polysome mRNA-seq library (ps-RNA-seq) preparation, which represents the whole translatome; RNA isolated from cell lysate is used for generating total mRNA-seq library, which represents the whole transcriptome. Illumina TrueSeq™ stranded mRNA sample preparation kit is used for RNA-seq libraries preparation. Briefly, Poly(A) RNA is isolated from 4 μg of polysome/cell lysate RNA using PCR plates with a magnetic stand. Poly(A) RNA is fragmented into small pieces using Fragment, Prime and Finish mix at 94 °C for 8 min. mRNA fragments are copied into cDNA using random-primers and reverse transcriptase followed by second strand cDNA synthesis. Double stranded cDNA fragments go through an end repair process and 3′ end adenylation. Pair-end adaptors with different index are ligated. It is advisable to choose the manufacturer recommended combination of indexes to allow multiplex sequencing later. Ligated DNA is selectively enriched by 15 cycles of PCR. Following PCR product purification and quality analysis using BioAnalyzer (Agilent), libraries are pooled for Illumina Hi-SEQ sequencing.

4 Notes

1. Use high-purity sucrose to ensure RNase-free sucrose gradient.
2. EGTA will not dissolve till pH is adjusted to 8.3 with 10 M NaOH.
3. Mix well before aliquoting the solution.
4. Wear protective mask while weighing sodium deoxycholate and PMSF.
5. Warm solution at 42 °C before use; pipette detergent mix using 1-mL tips with cut end.
6. Heparin can be omitted; RNase inhibitor may be added to polysome extraction buffer to prevent RNA degradation.
7. Sucrose gradient can be thawed at 4 °C overnight to form continuous sucrose gradient; Thawed gradients should be handled carefully.

8. To reduce centrifugation time, speed can be increased to 237,000 × *g* for 90 min. Centrifugation at 116,000 × *g* for 160 min also generates good polysome profile.
9. Pump Fluorinet™ FC-40 slowly till a little FC-40 flows out from the orifice on the needle before inserting the gradient tube onto UV detector holder. This helps to avoid air bubbles that can disrupt the sucrose gradient.
10. Fractions can be collected based on number of drops per tube or based on volume.
11. Be careful to not disturb the RNA pellet.

Acknowledgment

This work was partly supported by Starting-up grant of Henan Normal University (5101049470095) and Program for Innovative Research Team in Science and Technology in University of Henan Province (17IRTSTHN017) to YFL. The work in RS laboratory was supported by the Oklahoma Agricultural Experiment Station.

References

1. King HA, Gerber AP (2016) Translatome profiling: methods for genome-scale analysis of mRNA translation. Brief Funct Genomics 15:22–31
2. Zupanic A, Meplan C, Grellscheid SN, Mathers JC, Kirkwood TB et al (2014) Detecting translational regulation by change point analysis of ribosome profiling data sets. RNA 20:1507–1518
3. Kuersten S, Radek A, Vogel C, Penalva LO (2013) Translation regulation gets its 'omics' moment. Wiley Interdiscip Rev RNA 4:617–630
4. Matsuura H, Ishibashi Y, Shinmyo A, Kanaya S, Kato K (2010) Genome-wide analyses of early translational responses to elevated temperature and high salinity in *Arabidopsis thaliana*. Plant Cell Physiol 51:448–462
5. Branco-Price C, Kawaguchi R, Ferreira RB, Bailey-Serres J (2005) Genome-wide analysis of transcript abundance and translation in Arabidopsis seedlings subjected to oxygen deprivation. Ann Bot 96:647–660
6. Reynoso MA, Blanco FA, Bailey-Serres J, Crespi M, Zanetti ME (2013) Selective recruitment of mRNAs and miRNAs to polyribosomes in response to rhizobia infection in *Medicago truncatula*. Plant J 73:289–301
7. Michel AM, Baranov PV (2013) Ribosome profiling: a Hi-Def monitor for protein synthesis at the genome-wide scale. Wiley Interdiscip Rev RNA 4:473–490
8. Juntawong P, Girke T, Bazin J, Bailey-Serres J (2014) Translational dynamics revealed by genome-wide profiling of ribosome footprints in Arabidopsis. Proc Natl Acad Sci U S A 111:203–212
9. Beilharz TH, Preiss T (2004) Translational profiling: the genome-wide measure of the nascent proteome. Brief Funct Genomic Proteomic 3:103–111
10. Arava Y, Boas FE, Brown PO, Herschlag D (2005) Dissecting eukaryotic translation and its control by ribosome density mapping. Nucleic Acids Res 33:2421–2432
11. Leprivier G, Remke M, Rotblat B, Dubuc A, Mateo AR et al (2013) The eEF2 kinase confers resistance to nutrient deprivation by blocking translation elongation. Cell 153:1064–1079
12. Puckette M, Iyer NJ, Tang Y, Dai XB, Zhao P et al (2012) Differential mRNA translation in *Medicago truncatula* accessions with contrasting responses to ozone-induced oxidative stress. Mol Plant 5:187–204
13. Larsson O, Sonenberg N, Nadon R (2010) Identification of differential translation in genome wide studies. Proc Natl Acad Sci U S A 107:21487–21492

14. Arava Y (2003) Isolation of polysomal RNA for microarray analysis. Methods Mol Biol 224:79–87
15. Ingolia NT, Brar GA, Rouskin S, McGeachy AM, Weissman JS (2012) The ribosome profiling strategy for monitoring translation in vivo by deep sequencing of ribosome-protected mRNA fragments. Nat Protoc 7:1534–1550
16. Baudin-Baillieu A, Hatin I, Legendre R, Namy O (2016) Translation analysis at the genome scale by ribosome profiling. Methods Mol Biol 1361:105–124
17. Ingolia NT, Ghaemmaghami S, Newman JR, Weissman JS (2009) Genome-wide analysis in vivo of translation with nucleotide resolution using ribosome profiling. Science 324: 218–223
18. Jackson R, Standart N (2015) The awesome power of ribosome profiling. RNA 21:652–654
19. Mustroph A, Juntawong P, Bailey-Serres J (2009) Isolation of plant polysomal mRNA by differential centrifugation and ribosome immunopurification methods. Methods Mol Biol 553:109–126

Chapter 10

Global Proteomic Profiling and Identification of Stress-Responsive Proteins Using Two-Dimensional Gel Electrophoresis

Pragya Barua, Dipak Gayen, Nilesh Vikram Lande, Subhra Chakraborty, and Niranjan Chakraborty

Abstract

Global proteome profiling is a direct representation of the protein set in an organism, organ, tissues, or an organelle. One of the main objectives of proteomic analysis is the comparison and relative quantitation of proteins under a defined set of conditions. Two-dimensional gel electrophoresis (2-DE) has gained prominence over the last 4 decades for successfully aiding differential proteomics, providing visual confirmation of changes in protein abundance, which otherwise cannot be predicted from genome analysis. Each protein spot on 2-DE gel can be analyzed by its abundance, location, or even its presence or absence. This versatile gel-based method combines and utilizes the finest principle for separation of protein complexes by virtue of their charge and mass, visual mapping coupled with successful mass spectrometric identification of individual proteins.

Key words Global proteome, Two-dimensional gel electrophoresis, Mass spectrometry, Stress-responsive proteins

1 Introduction

In this chapter, we demonstrate the technique of two-dimensional gel electrophoresis (2-DE), practiced for separation of complex mixture of proteins from various biological samples. This method is used to investigate which proteins are conditionally expressed and how strongly are they affected under two or more different conditions. It is a multistep process which commences with protein extraction and solubilization, followed by their separation, and culminates with the identification of individual components, as shown in Fig. 1. Here, we briefly describe the process of protein isolation, emphasize on the method for their separation in each dimension and focus on the detection and identification of stress-responsive proteins. The method applied for protein isolation

Ramanjulu Sunkar (ed.), *Plant Stress Tolerance: Methods and Protocols*, Methods in Molecular Biology, vol. 1631,
DOI 10.1007/978-1-4939-7136-7_10,

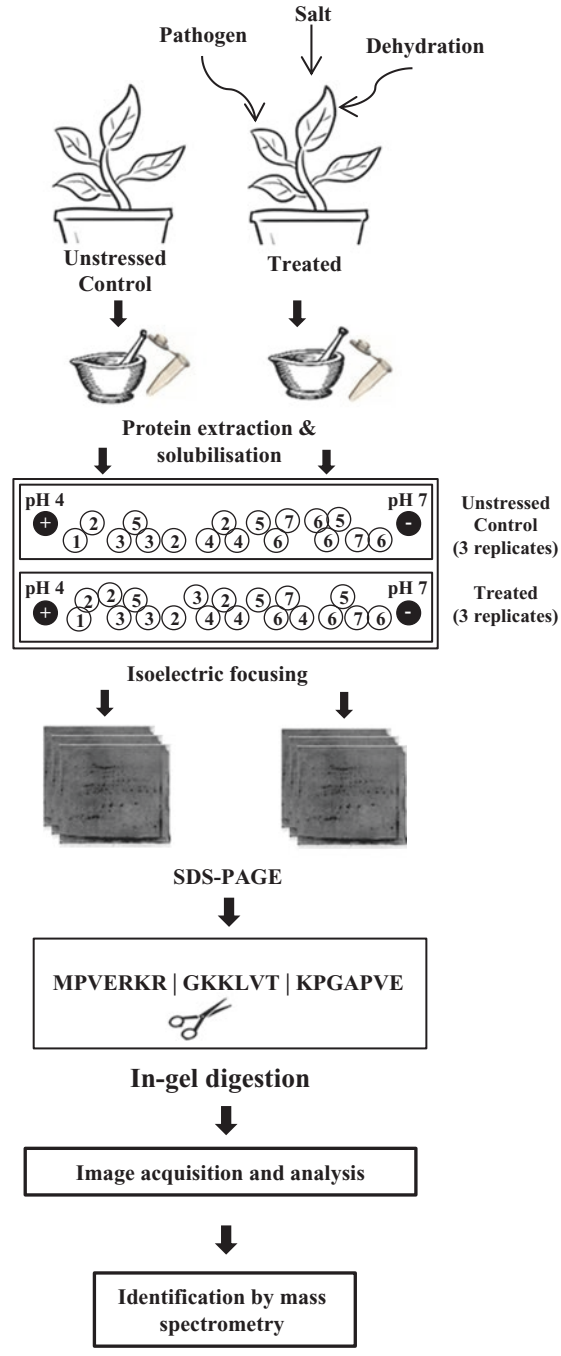

Fig. 1 Workflow depicting the steps involved in the study for identification of stress-responsive proteins by 2D gel electrophoresis. The sample from unstressed control and treated are processed simultaneously

essentially depends upon the source tissue and the type of analysis required to be done. For global proteomic analysis, overall changes in the expression pattern of total cellular protein is studied in response to different stress [1]. In case of fraction-specific study, for example, subcellular compartments or extracellular space, additional steps of isolation of particular fraction of interest and protein extraction needs to be carried out [2–4]. Once the proteins are extracted, they are dissolved in a solubilization cocktail containing strong detergents and chaotropes. While SDS (detergent) solubilizes the proteins, high concentrations of urea and thiourea (chaotropes) aid in denaturation. This cocktail, popularly referred to as 2D rehydration buffer, is capable of solubilizing vast majority of proteins and is compatible with the downstream electrophoretic separation.

In the first dimension, the proteins are resolved according to their isoelectric point (pI), followed by molecular weight (MW) in the second dimension. In 1975, O'Farrell for the first time gave a detailed successful report of the application of 2-DE for separation of proteins [5]. During the early years, one of the greatest challenges faced was to obtain run-to-run reproducibility when pH gradient used to be generated in tube gels by mixture of ampholytes [6]. In the 1980s, introduction of immobilized pH gradient (IPG) strips and protein identification with Edman sequencing gave the technique its much awaited impetus [7]. The quantum leap in speed, sensitivity, and in-depth protein characterization occurred with the advent and evolution of mass spectrometry. Since then the method has gained special importance as a primary tool for differential proteomics analysis with the ability to resolve over thousands of proteins in a single gel [8]. In combination with in silico image evaluation for qualitative and quantitative analyses, this technique has not only created a revolutionary contribution in the field of proteomics science but also allowed interlaboratory comparison of datasets.

Contrary to what the name suggests, 2-DE is a multistep process wherein each step is crucial and must be carefully executed in order to achieve overall success of the experiment. Although in present scenario, it is no longer the only experimental workflow for modern differential proteomics analysis [9], it is still a robust, reliable technique for detection of proteins and measurement of relative abundance. The process however offers difficulty in separation of hydrophobic membrane proteins and those having extreme acidic and basic pI [10, 11]. The low abundant proteins tend to get masked by the high abundant proteins and also by the dynamic range of the stain used [12, 13]. However, with the rapid increase in genomic and protein sequence databases on the public domain, and availability of high resolution mass spectrometry, the power of this technique has increased manifold [14, 15]. In addition to this, direct access to the spot-pattern database enables comparison of electrophoretic results which provides impetus toward coordinated

proteome research worldwide. In this chapter, the principal methods of separation and identification of stress-responsive proteins by 2D electrophoresis have been discussed.

2 Materials

2.1 Equipment

1. Isoelectric focusing system. We use Ettan IPGphor 3 (GE Healthcare) and PROTEAN® i12™ (Bio-Rad).
2. IEF strip holder or IEF tray.
3. SDS-PAGE electrophoresis system.
4. Gel caster.
5. Set of glass plates.
6. Forceps.
7. Electrophoresis power supply.

2.2 Buffers and Solutions

2.2.1 Protein Isolation

1. *Homogenization buffer*: 50 mM HEPES–KOH (pH 7.5), sucrose (40%), β-mercaptoethanol (1%), 1 mM EDTA (pH 7.5), 60 mM sodium fluoride, protease inhibitor cocktails 1 and 2 (Sigma-Aldrich). Add protease inhibitors just prior to use. The buffer can be stored at 4 °C up to 1 week.
2. *Extraction solution*: Tris-saturated phenol.
3. *Precipitation solution*: 0.1 mM ammonium acetate in methanol.
4. *Washing solution*: 80% acetone.

2.2.2 2-DE

1. First dimension.
   - *2D rehydration buffer (RB)*: 8 M urea, 2 M thiourea, 2% CHAPS, 0.5% (v/v) carrier ampholytes, traces of bromophenol blue. Add 2.8 mg/mL of DTT prior to use.
   - Mineral oil.
2. Second dimension
   (a) *Equilibration buffer*: 5.4 g urea, 0.3 g SDS, 3.8 mL 1.5 M Tris–HCl, pH 8.8, 3 mL glycerol in a 50-mL centrifuge tube. Adjust the total volume to 15 mL with MQ-water. Dissolve with shaking, but do not use any heat.
   (b) *Equilibration buffer A*: 120 mg DTT in 7.5 mL equilibration buffer.
   (c) *Equilibration buffer B:* 150 mg iodoacetamide in 7.5 mL equilibration buffer.
   (d) *Stock solutions*
      - Acrylamide stock: 30% acrylamide–bis solution (29:1).
      - SDS stock: 10% SDS in MQ-water.
      - Tris stock: 1.5 M Tris–HCl, pH 8.8.

- APS stock: 10% ammonium persulfate (prepare fresh by dissolving 0.1 g APS in 1 mL MQ-water.
- 10× Tris–glycine running buffer: 30 g Tris, 144 g glycine, 10 g SDS. Make up the volume to 1 L with Milli-Q water.
- Agarose sealing solution: 0.5 g agarose, 10 mL of 10× Tris–glycine running buffer, 30 mL glycerol. Adjust the total volume to 100 mL with water. Add 1 mL of 1% BPB. This reagent can be stored at room temperature and used repeatedly over several months.

(e) *Gel solution* (for 1 L of 12.5% gel): 250 mL Tris stock, 416 mL acrylamide stock, 318 mL MQ-water, 5 mL SDS stock, 10 mL APS stock, 1 mL TEMED. Add TEMED and APS just before use.

(f) Running buffer (1×): 100 mL of 10× Tris–glycine buffer, 900 mL MQ-water.

2.2.3 In-Gel Trypsin Digestion

(a) *Destaining solution*: 100 mM sodium thiosulfate, 30 mM potassium ferricyanide (for silver staining), 50 mM ammonium bicarbonate in 50% acetonitrile (ACN).

(b) Gel washing solution: 50% acetonitrile, 50 mM ammonium bicarbonate.

(c) *Reducing* buffer: 10 mM DTT in 50 mM ammonium bicarbonate.

(d) *Alkylation buffer*: 50 mM iodoacetamide in 50 mM ammonium bicarbonate.

(e) *Digestion buffer*: Resuspend lyophilized trypsin (20 μg/vial) in 20 μL of the 50 mM acetic acid solution provided with trypsin, yielding a 1 μg/μL stock solution. Dilute that stock to 1 μg/50 μL with 50 mM ammonium bicarbonate (50-fold dilution, 20 ng/μL). Aliquot and store at −70 °C. Avoid repeated freeze–thaw of trypsin stock solutions more than once.

(f) Extraction solution: 50% ACN–1% trifluoroacetic acid (TFA) for MALDI-TOF/TOF and in 50% ACN–1% HCOOH for LC-MS/MS.

3 Methods

3.1 Extraction and Solubilization of Proteins from Unstressed Control and Treated Samples

Depending upon the source of protein, different extraction methods can be applied to yield maximum quantity of protein. One might be interested in the study of total or fractionated cellular proteins such as nuclear, mitochondrial, cytoplasmic, or membrane. The aim of the experiment dictates the extraction procedure for retrieving proteins. The general technique and procedure for isolation of protein from various source of interest

includes TCA–acetone precipitation [16], phenol extraction [17], chloroform–methanol extraction [18], among others. Different extraction procedure suits different types of source tissue in terms of yield as well as well as clarity of the resolution of separated protein spots. The method of protein extraction and solubilization should be exactly similar for both unstressed control and treated samples. Any alteration in the protocol might induce unintended variation, which may not truly represent a stress response. Ideally all the proteins must be solubilized, without any modification added to them.

3.1.1 Extraction of Total Cellular Protein

The procedure for extraction of total protein is comparatively simple, gives good yield of protein and less time-consuming. Here we outline the procedure for total protein extraction from aerial parts of developing chickpea (*Cicer arietinum*) seedlings.

1. Chill a mortar with liquid nitrogen and then grind the experimental tissues in it using liquid nitrogen to fine powder.
2. Transfer 2 g of the grounded tissue into prechilled 50-mL centrifuge tube containing 10 mL homogenization buffer.
3. Vortex and mix the homogenate and filter through cheesecloth in order to remove cell debris.
4. Add 15 mL of Tris-saturated phenol to the filtrate and place the tube on a rocker platform for 30 min at 4 °C followed by centrifugation at 5000 × *g* for 15 min.
5. Collect the upper phase and precipitate with 0.1 mM ammonium acetate in methanol for overnight at −20 °C.
6. Precipitate the protein by centrifugation at 10,000 × *g* for 15 min at 4 °C.
7. Wash the protein with 80% acetone and solubilize in 2D rehydration buffer (*see* **Note 1**).

3.1.2 Extraction of Organellar Proteins

Study of organellar proteome is important for understanding the regulation of proteins found in particular fraction. The organellar proteomics study mainly includes isolation and purification of organelle of interest, followed by extraction and solubilization of proteins from the isolated fraction. Additionally, one needs to perform purity assessment of the isolated organelle using antibody and/or specific biochemical assays and quantitative tests for other contaminants. Isolation of proteins from different fraction has been extensively described before [19–21]. As mentioned above, the rehydration buffer containing chaotropic agents such as urea, thiourea and detergents such as CHAPS, serves as a strong solubilizing cocktail, which dissolves most of the proteins.

3.2 Quantification of Protein

Protein extracted from the unstressed control and treated samples must be individually quantified in replicates using standard Bradford assay or BCA assay. Accuracy in quantification is crucial

as one need to use equal amount of protein from each sample so as to be able to assign any protein as truly differential or stress-responsive (*see* **Note 2**).

3.3 Isoelectric Focusing (IEF)

In this step, referred to as first dimension separation or IEF, the proteins are separated or focused by differences in their isoelectric point (pI). The pI of a protein is the pH at which the net charge carried by a protein becomes zero. Proteins show a considerable variation in pI, usually in the range of pH 3–12, with majority distributed within pH 4–7. In addition to its amino and carboxyl termini, a protein is capable of carrying both positive and negative charge in its amino acid side chains. When the pH < pI, a protein has net positive charge and at pH > pI becomes negatively charged. Thus, proteins with acidic pI migrate toward the cathode and those with basic pI toward the anode. In a pH gradient, under the influence of electric field a protein migrates to a position where it has no net charge. If a protein diffuses away from its pI, it again gains charge and moves back. This method allows the proteins to be separated even by a small difference in charge. Successful IEF requires stable, linear, and reproducible pH gradient over extensive focusing runs. Use of immobilized pH gradient (IPG) strips ensures higher resolution, reproducibility, and protein loads [22].

3.3.1 Rehydration of IPG Strips

Separate IPG strip of same length is required for each of the control and treated samples and all of them must be processed in parallel (*see* **Note 3**) (Table 1). Rehydration for reswelling of frozen gel strips can be carried out with or without the sample added to the rehydration buffer (Table 1).

1. Level the rehydration tray and ensure that the tray is dry and clean (*see* **Note 4**).
2. Mix the protein sample with appropriate volume of rehydration and IPG buffer, and pipette the mixture to the reswelling slot.
3. Remove the protective cover from the IPG strip carefully and position the IPG strip with the gel side down.
4. Hold one end of the strip with the help of blunt end tweezers not touching the gel and gently lay the strip on the sample from one end. Be vigilant not to trap bubbles below the strip.
5. Overlay the IPG strip with cover fluid (mineral oil) in order to prevent evaporation and urea crystallization.
6. Slide the lid of the rehydration tray and allow the IPG strip to rehydrate overnight (10–12 h).

3.3.2 Sample Loading

There are three different methods for loading of IPG strips:

(a) *Rehydration*: It can be active or passive depending upon whether current is applied. Appropriate volume of quantified protein sample when added to the rehydration buffer in previous

Table 1
Suitable protein amount and volume of rehydration solution required per IPG strip

Immobiline strip (pH 4–7 linear) length (cm)	Silver/fluorescent stain (detection limit 0.5–2 ng)	Colloidal CBB stain (detection limit 5–10 ng)	Total volume/ strip (μL)
7	2–8 μg	10–20 μg	135
11	10–20 μg	15–40 μg	200
13	15–30 μg	30–80 μg	250
18	30–60 μg	60–180 μg	340
24	50–100 μg	90–200 μg	450

Subheading 3.3.1, the process is referred to as passive rehydration. In case of active rehydration, current is applied while the proteins are being taken up by the gel. Instead of rehydration tray, the strips are placed in manifold inside the electrophoresis unit in correct orientation with the electrodes set at both ends and the rehydration is completed in a comparatively shorter time span (4–5 h).

(b) *Cup loading*: It can be anodic or cathodic depending upon loading of very basic or acidic proteins, respectively. It is suitable for proteins with pIs at extreme pH ranges.

1. Follow **steps 1–3** of Subheading 3.3.1. Place the rehydrated IPG strips with gel side up in adjacent groves of the ceramic manifold with anodic end facing back of the instrument.
2. Choose the sample cups of appropriate size suitable with the length of IPG strip and carefully place them over strips typically at anodic end causing a perfect seal.
3. Dampen two electrode wicks per strip with 150 μL MQ-water each, and place in the groves with one end of the wick overlapping with the ends of the gel in the strip.
4. Put the electrode assemblies in place where wicks overlap the gel.
5. Cover the strips with cover fluid to prevent evaporation.
6. Pipette samples into the cups. Overlay the sample with mineral oil in the cups. Close the lid and begin isoelectric focusing.

(c) *Paper bridge loading*: It provides better resolution for very basic or acidic subproteomes. It also offers higher sample load and the sample can be conserved by reusing the paper bridge on other pH range gels. For example, up to 5 mg protein can be loaded on 18 cm long narrow pH range strip.

1. Follow **step 1–3** according to cup loading protocol.
2. Paper bridges can be prepared with filter paper. Depending on the sample load, the length and breadth of the bridge can be adjusted accordingly.
3. Load the sample in the paper bridge and place the bridge at the anodic end of the rehydrated strip with an overlap of 0.5 cm on top of the strip.
4. Electrodes are placed at the far end of the paper bridge at the anode end and also at the cathode end of the strip.
5. Samples are loaded from the bridge to the strip by applying 200 V overnight.
6. One can remove the bridges after loading the samples and reset the electrodes to the ends of the IPG strip. (*see* **Note 5**)

3.3.3 Focusing Conditions and Electrophoresis

Focusing condition varies according to sample complexity, sample composition, IPG strip length, and pH range. Electrical conductivity of the gel changes with time, during the IEF run. The current is relatively high at the beginning due to large number of charge carriers present. As proteins and ampholytes move toward their pIs, the current gradually decreases due to the decrease in the charge on individual proteins and carrier ampholytes.

1. Remove the IPG strip from its slot with the help of forceps and rinse with Milli-Q water to remove excess rehydration solution, which may hinder electrophoresis causing urea crystallization.
2. Place the IPG strip with gel side up over filter paper to soak the excess moisture.
3. Transfer the strips with gel side up immediately to adjacent slots of the ceramic tray with the positive end toward the back of the instrument.
4. Follow **step 3–6** of the cup-loading protocol and place the movable electrode assembly properly at the cathodic and anodic end of the strip.
5. For ramping conditions, it is suitable to begin with the recommended guidelines provided with the IEF unit to be used and then optimize according to desired outcomes.
6. Following IEF, the strips can be stored at −80 °C immersed in mineral oil for maximum 2 months (*see* **Note 6**).

3.4 Second-Dimension Electrophoresis

In second-dimension electrophoresis, the isoelectrically focused proteins are further resolved according to their molecular weights by traditional SDS-PAGE.

3.4.1 Casting Gel for Second-Dimension

Simultaneously prepare separate gels for each of the IEF strip used, just prior to the completion of focusing. Multiple gels can be cast at the same time using multicasting chamber. One can also use

commercially available precast or hand cast gels as well as gradient or isocratic gels. Generally single percentage gels (12.5%) are better for resolution in particular mass range (15–80 kDa) and is most commonly used. Array of vertical electrophoresis units are commercially available and one can choose according to the size of the gel to be cast.

1. Prepare the gel caster. Each item (gel caster, glass plates, separator sheets, blank cassette inserts) must be clean and dirt free, as any residual dust could result in artifacts on the gel images.
2. Assemble the gel cassettes inside the caster and make it leakproof.
3. Select the gel percentage according to range of separation required. Add APS and TEMED to the gel solution immediately before casting. Stacking gels are not required for vertical 2D gels.
4. Overlay each gel with water-saturated butanol to minimize exposure to oxygen.
5. Allow the gels to be polymerized for a minimum of 4 h. If not used immediately, gels can be stored at 4 °C for up to 2 weeks after overlaying with gel storage solution and covering with Parafilm or Saran Wrap.

3.4.2 Equilibration of Strips

The equilibration step saturates the strips with SDS, which is a prerequisite for separation by SDS-PAGE.

1. With the help of forceps, place the IPG strips inside the equilibration tubes, with support film toward tube wall.
2. Add appropriate amount of equilibration Buffer A (containing reducing agent) to the tube (15 mL/strip).
3. Cap the tubes and place them on a rocker and equilibrate for 15 min. The strips must be dipped in the solution all the time.
4. Pour off the buffer carefully, and add equilibration Buffer B (containing alkylating agent). Again seal the tubes and keep on the rocker for additional 15 min.

3.4.3 Loading of Equilibrated Strips onto SDS Gels

1. Gently hold the equilibrated strip at one end with the help of forceps and gently wash it with Milli-Q water. Soak the excess solution with a tissue paper.
2. Position the strips with acidic end to the left and gently push them between the glass plates, holding the gel with the plastic back facing one of the glass plates. The top surface of the slab must be in uniform contact with the entire lower edge of the IPG strip (*see* **Note 7**).
3. Apply protein MW marker by soaking 15–20 μL of the solution on to a small piece of filter paper and then by using forceps

apply it on the top surface of the gel next to one end of the strip. The markers should contain 200–1000 ng of each component for CBB staining and ~10–50 ng of each component for silver staining.

4. Seal the IPG strip in place with agarose sealing solution having BPB which acts as a tracking dye during the run (*see* **Note 8**). The sealing solution prevents the IPG strip from getting displaced or floating in the electrophoresis buffer.

3.4.4 Running the Gels

1. Insert the gel cassettes in the cassette carriers and place the gels inside the electrophoresis unit. Fill the empty slots, if any, with blanks.
2. Prepare anode and cathode running buffer and fill both lower and upper buffer chambers.
3. Attach and close the lid properly and connect the power leads to the power supply in the correct order.
4. Run the gels at constant voltage which can be increased or decreased within a range. Generally gels are run at 100 V which ensures proper resolution. It takes almost 10–12 h for completion of a run.
5. Stop electrophoresis when the dye front is approximately 1 mm from the bottom of the gel. This ensures gel-to-gel reproducibility in terms of coordinates of each protein spot.
6. After electrophoresis, carefully remove gels from their gel cassettes and prepare them for staining.

3.5 Staining of 2D Gels

In order to visualize the proteins resolved by 2-DE, the gels are stained by any of the well-established staining methods. The most popular staining technique used is silver staining, owing to its high sensitivity over other staining methods. One can either use commercially available staining kits or can manually stain the gels. For different staining techniques and their detection limits refer to Table 1. High sensitivity, wide linear dynamic range, and compatibility with mass spectrometry are the three main features to be looked into for staining the gels. To analyze the stress-responsive proteome, it is crucial to stain the unstressed control as well as treated gels in a uniform manner, and desirably simultaneously for a uniform time.

3.6 Image Acquisition

In complex proteome studies with gel patterns containing several thousand protein spots, it is practically impossible to detect the appearance of a few novel spots or the disappearing of spots. Therefore, image collection hardware and image assessment software are indispensable to detect these alterations as well as to acquire maximum information from the gel patterns. Therefore, post-staining protein patterns are digitized in order to be analyzed.

Table 2
Commercially available gel imagers and gel analysis software

Type of imager	Light source options	Applicable for	Image analysis software
Densitometer Example: GS800, Typhoon FLA 7000	Epi-illumination and transillumination of white light	Colorimetric stains (Silver, CBB)	PDQuest, ProteomWeaver (Bio-Rad), SigmaScan (Sigma), ImageMaster (GE Healthcare)
CCD- camera based Example: ChemiDoc™ MP	UV and white light transillumination and epi-illumination white, red, green, and blue	Colorimetric and fluorescent stains, DIGE	
CCD-camera based Example: Gel-Doc	UV and white light transillumination	Colorimetric and UV stain, DIGE	
Laser-based Example; PharosFX™, Typhoon FLA 7000/9500	External laser	Fluorescent staining and multiplexing	

A number of imaging systems are available which are compatible with downstream analysis. Selection of the imaging device primarily depends upon the staining technique used. Several imaging systems are commercially available with multiple detection modes, which can be used with a variety of applications (Table 2). Densitometer (for visible light absorbing stains such as CBB or silver stain) or laser based imaging system (SYPRO Ruby) are most commonly used. It is crucial to image the unstressed control as well as treated gels with the same set of parameters in order to facilitate downstream analysis (*see* **Note 9**).

3.7 Quantitative Analysis of 2D Gel Images

A number of commercial software packages compatible with different gel imagers are available to complete digital 2-DE gel analysis. ImageMaster, PDQuest, ProteomWeaver, Delta 2D are few well-known software programs used for analysis of 2D gels. The aim of software-assisted 2-DE gel analysis is detection of protein spots, match them between replicate gels within an experiment, and then identify any differences in protein expression between sets of samples. The representative images are shown in Fig. 2. It is beyond the scope of the chapter to outline each step of the analysis. Briefly, one has to define data that can be exported as spreadsheets and one can identify the list of upregulated or downregulated proteins. Successful quantification of protein expression levels is largely dependent on the algorithms for spot matching, normalization, and background subtraction provided by analysis software. Here, we briefly outline the computational analysis using PDQuest verion 7.2.0.

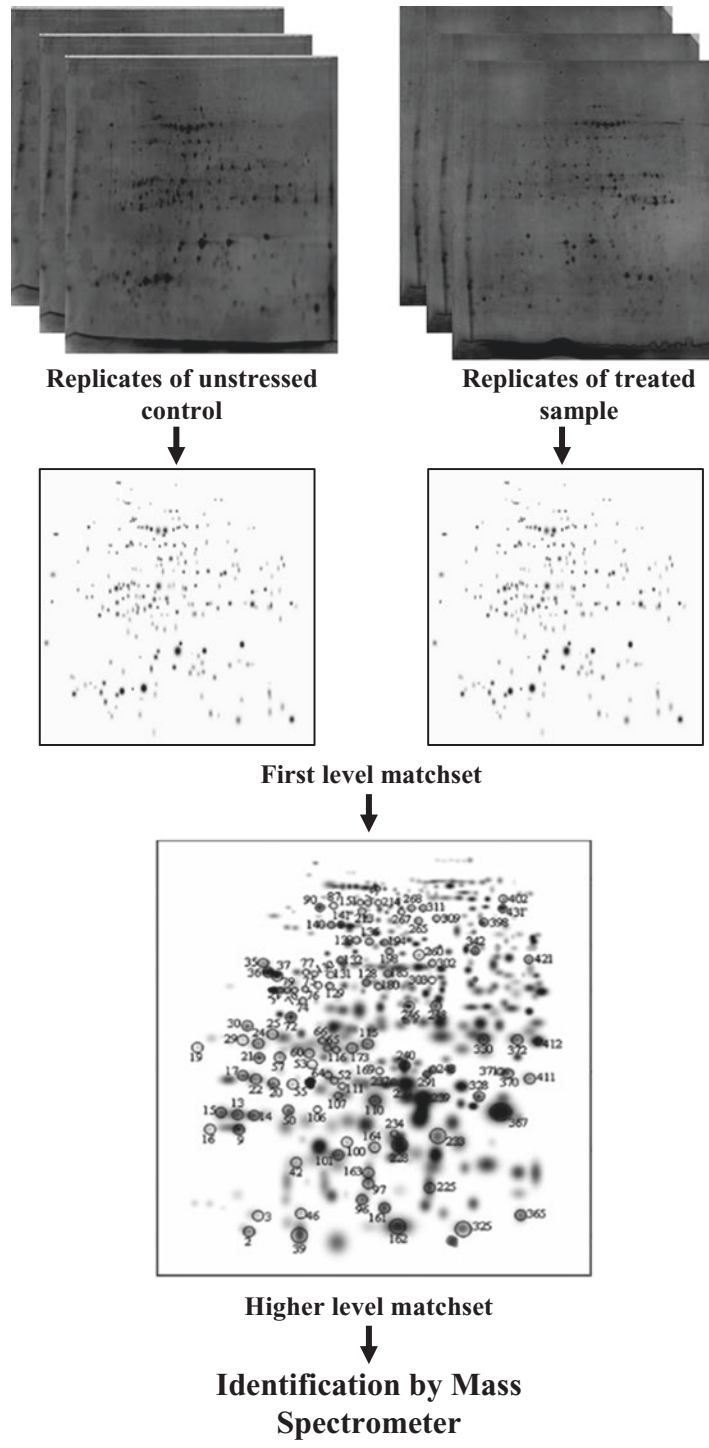

Fig. 2 Electrophoretic separation of proteins followed by in silico analysis of the acquired 2D gel images by available software. The first level match set represents the complete set of proteins present in at least two of the three replicates for a particular sample. The higher level match set, generated by comparison between the first level match sets, indicates the common as well as differentially expressed proteins across all time points

1. At least three replicates of stained 2-DE gels are computationally combined to generate the standard gels, referred to as first level match set.
2. Each spot included on the standard gel should meet several criteria:
   (a) It must be present in, at least, two of the three replicates and must be qualitatively consistent in size and shape.
   (b) Spots with quality score less than 30 must be defined as "low quality" spots and are therefore eliminated from further analysis.
   (c) The remaining high quality spot quantities are used to calculate the mean value for a given spot, and this value is used as the spot quantity on the standard gel.
   (d) The spot densities from the first level match set are normalized against the total density in the gel image.
   (e) The replicate gels used for making the first level match set must have a correlation coefficient value of at least 0.8.
3. After obtaining the first level match sets, a second level match set which allows a comparison of the standard gels from each of the control and treated time point is obtained.
4. A second normalization is done with a set of three unaltered spots identified from across the time points.
5. From this match set, the filtered spot quantities from the standard gels are assembled into a data matrix of high quality spots from all the time points for further analysis.
6. Decide on the change in fold value in terms of intensity in order to assign a protein spot to be differential. A protein can thus be termed as upregulated or downregulated.
7. Finally, statistical analysis (t-test, ANOVA, 2-way-ANOVA) is considered for unbiased identification of differentially expressed protein for comparative study.

3.8 In-Gel Digestion of Excised Protein Spots

1. Excise the candidate differential protein spots from silver or CBB stained gels manually or using spot picker (*see* **Note 10**).
2. Wash the excised spots twice with deionized water.
3. Destain twice for 15 min each with respective destaining solution for the particular stain used.
4. Next, wash the gel pieces twice with washing solution for 10 min each.
5. Shrink gel pieces by soaking in 100% acetonitrile.
6. Remove acetonitrile, and air-dry the gel pieces for 20–30 min.
7. Add appropriate amount of digestion solution and incubate at 30 °C overnight. 1:20 ratio for trypsin–protein is widely used. Collect the digestion solution having the digested peptides.

8. For reextraction, soak the gel pieces in extraction solution with gentle agitation for 30–60 min. Pool the extracts, vacuum-dry and suspend in 50% (v/v) ACN and 0.1% (v/v) TFA for MALDI-TOF/TOF, and 50% (v/v) ACN and 0.1% (v/v) HCOOH for LC-MS/MS analysis.

3.9 Identification by Mass Spectrometry

One can use both MALDI-MS or ESI-MS for protein identification. Also there are several search engines available for examining the spectra, the most widely used being Mascot and Sequest. For protein identification using Mascot search engine (www.matrixscience.com), the mass spectra are searched against the following parameters: maximum allowed missed cleavage 1, fixed amino acid modification as carbamidomethylation and variable amino acid modification oxidation (M), taxonomy set to viridiplantae (for plants), and database used NCBInr or Swissprot. For stringency in searching in case of MALDI/TOF/TOF, the peptide fragment and precursor mass tolerance are set at 100 ppm, 0.3 Da, whereas 100 ppm and 0.4 Da for ESI-LC-MS. We consider only those protein spots as positive identification whose MOWSE score is above the significant threshold level as determined by MASCOT (Fig. 3).

4 Notes

1. Air dry the pellet for sufficient amount of time so that no trace of acetone remains. Presence of acetone hinders solubilization of protein in aqueous solution. Do not overdry the pellet.
2. It is important to load equal amount of proteins from both unstressed control and treated sample and therefore accuracy in quantification is necessary.
3. To avoid differences due to handling and minimize technical error, control and treated samples should be processed in parallel.
4. Uneven levelling or tilted tray may result in uneven distribution of sample across the strip and incomplete rehydration.
5. Care should be taken that the IEF gel does not get damaged.
6. It is better to proceed immediately for second dimension separation. Improper storage may cause damage to the IEF strip.
7. Ensure that no air bubbles are trapped between the IPG strip and the slab gel surface or between the gel backing and the glass plate. The agarose sealing solution prevents the strip from dislocating or floating in the electrophoresis buffer.
8. Tracking dye allows the progress of the gel to be monitored.
9. Different software programs are compatible for processing gel images obtained from different imagers.
10. Gloves must be worn throughout the process to avoid keratin contamination.

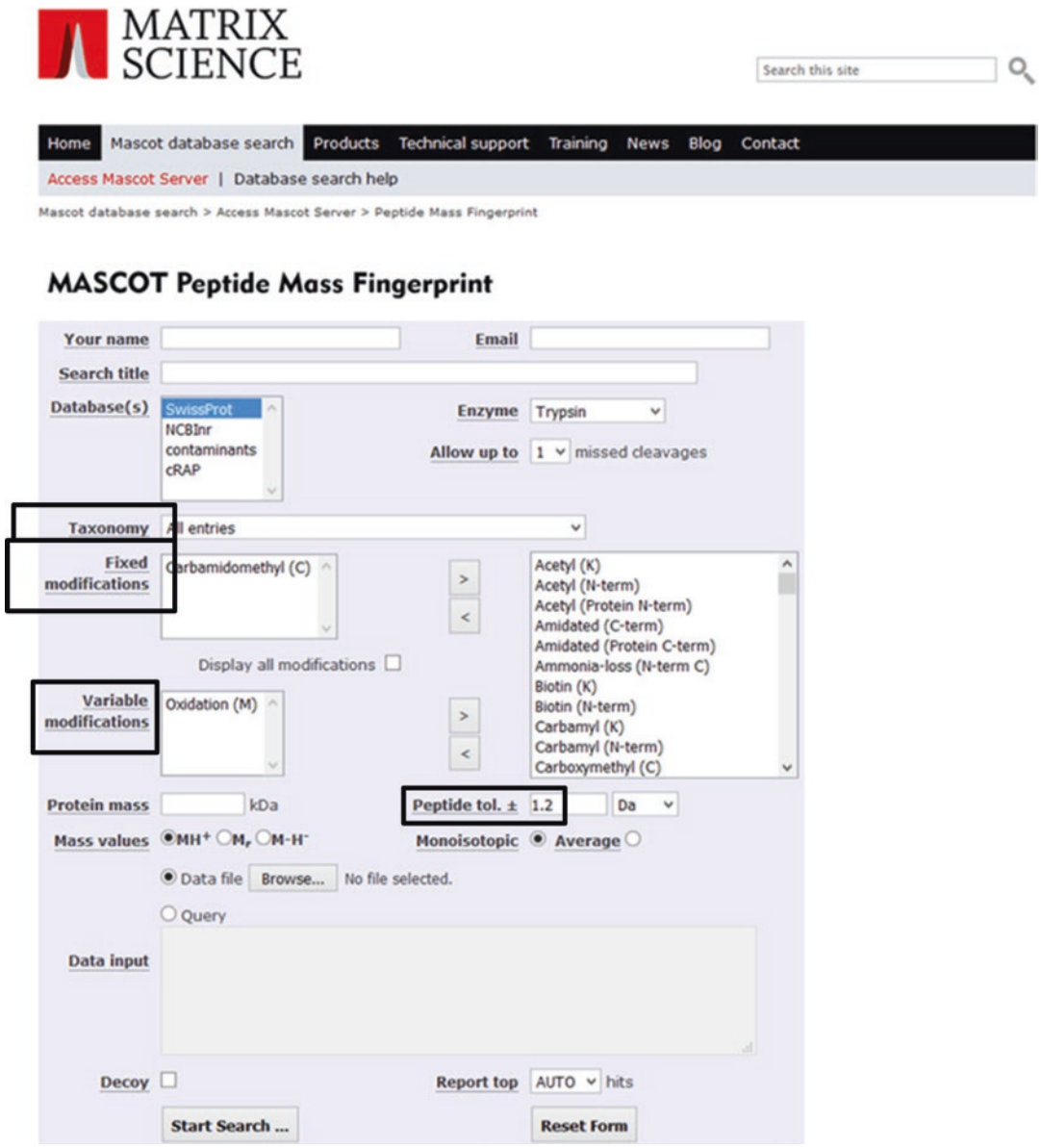

Fig. 3 Screenshot image of MASCOT webpage highlighting the parameters required to be set, in order to search database for obtaining successful identifications by peptide mass fingerprinting

Acknowledgment

This work was supported by grants from the Department of Biotechnology (DBT) (BT/AGR/CG-Phase II/01/2014), India and the Council of Scientific and Industrial Research (CSIR) (38-1385/14/EMR-II), India. The authors thank Mr. Jasbeer Singh for illustrations and graphical representations in the manuscript.

References

1. Agapito-Tenfen SZ, Guerra MP, Wikmark OG, Nodari RO (2013) Comparative proteomic analysis of genetically modified maize grown under different agroecosystems conditions in Brazil. Proteome Sci 11(1)
2. Nouri MZ, Komatsu S (2010) Comparative analysis of soybean plasma membrane proteins under osmotic stress using gel-based and LC MS/MS-based proteomics approaches. Proteomics 10:1930–1945
3. Kruft V, Eubel H, Jänsch L, Werhahn W, Braun HP (2001) Proteomic approach to identify novel mitochondrial proteins in Arabidopsis. Plant Physiol 127:1694–1710
4. Printz B, Morais RDS, Wienkoop S, Sergeant K, Lutts S, Hausman JF, Renaut J (2015) An improved protocol to study the plant cell wall proteome. Front Plant Sci 6:237
5. O'Farrell PH (1975) High resolution two-dimensional electrophoresis of proteins. J Biol Chem 250:4007–4021
6. Barnouin K (2004) Two-dimensional gel electrophoresis for analysis of protein complexes. In: Fu H (ed) Protein-protein interactions: methods and applications 261. Humana Press Inc., New Jersey
7. Rabilloud T, Chevallet M, Luche S, Lelong C (2010) Two-dimensional gel electrophoresis in proteomics: past, present and future. J Proteome 73:2064–2077
8. Khoudoli GA, Porter IM, Blow JJ, Swedlow JR (2004) Optimisation of the two-dimensional gel electrophoresis protocol using the Taguchi approach. Proteome Sci 2:1
9. Liu GT, Ma L, Duan W, Wang BC, Li JH, Xu HG et al (2014) Differential proteomic analysis of grapevine leaves by iTRAQ reveals responses to heat stress and subsequent recovery. BMC Plant Biol 14:110
10. Rabilloud T, Vaezzadeh AR, Potier N, Lelong C, Leize-Wagner E, Chevallet M (2009) Power and limitations of electrophoretic separations in proteomics strategies. Mass Spectrom Rev 28:816–843
11. Bunai K, Yamane K (2005) Effectiveness and limitation of two-dimensional gel electrophoresis in bacterial membrane protein proteomics and perspectives. J Chromatogr B 815: 227–236
12. Chevalier F (2010) Standard dyes for total protein staining in gel-based proteomic analysis. Materials 3:4784–4792
13. Gauci VJ, Wright EP, Coorssen JR (2011) Quantitative proteomics: assessing the spectrum of in-gel protein detection methods. J Chem Biol 4:3–29
14. Van den Bergh G, Arckens L (2005) Recent advances in 2D electrophoresis: an array of possibilities. Expert Rev Proteomics 2:243–252
15. Lilley KS, Razzaq A, Dupree P (2002) Two-dimensional gel electrophoresis: recent advances in sample preparation, detection and quantitation. Curr Opin Chem Biol 6:46–50
16. Santa C, Anjo SI, Manadas B (2016) Protein precipitation of diluted samples in SDS-containing buffer with acetone leads to higher protein recovery and reproducibility in comparison with TCA/acetone approach. Proteomics 6:1847–1851
17. Subba P, Barua P, Kumar R, Datta A, Soni KK, Chakraborty S, Chakraborty N (2013) Phosphoproteomic dynamics of chickpea (Cicer arietinum L.) reveals shared and distinct components of dehydration response. J Proteome Res 12:5025–5047
18. Barua P, Subba P, Lande NV, Mangalaparthi KK, Prasad TK, Chakraborty S, Chakraborty N (2016) Gel-based and gel-free search for plasma membrane proteins in chickpea (Cicer arietinum L.) augments the comprehensive data sets of membrane protein repertoire. J Proteome 143:199–208
19. Zychlinski AV, Gruissem W (2009) Preparation and analysis of plant and plastid proteomes by 2DE. In: Sheehan D, Tyther R (eds) Two-dimensional electrophoresis Protocols. Humana Press, New Jersey, pp 205–220
20. Santoni V (2007) Plant plasma membrane protein extraction and solubilization for proteomic analysis. In: Thiellement H, Zivy M, Damerval C, Méchin V (eds) Plant proteomics: methods and Protocols. Humana Press, New Jersey, pp 93–109
21. Zabel C, Klose J (2009) Protein extraction for 2DE. In: Sheehan D, Tyther R (eds) Two-dimensional electrophoresis protocols. Humana Press, New Jersey, pp 171–196
22. Stastna M, Slais K (2005) Two-dimensional gel isoelectric focusing. Electrophoresis 26:3586–3591

Chapter 11

Phosphoproteomics Analysis for Probing Plant Stress Tolerance

Christof Rampitsch

Abstract

Protein phosphorylation is a key signaling mechanism during the plant biotic and abiotic stress response. Signaling cascades communicate between the cell surface, where the stress is perceived, and the nucleus, where a response can be enacted. Many of these signals involve the specific, transient phosphorylation of proteins by kinases, a signal which is usually amplified through cascades. The advent of high-throughput phosphoproteomics, pioneered mainly in yeast and mammalian cells, has made it possible to discover novel phosphorylation events rapidly and efficiently in a data-dependent manner and this has greatly enlarged our understanding of the plant's response to stress. This chapter describes a simple gel-free protocol for high-throughput phosphoproteomics, which is amenable to most labs engaged in plant stress research.

Key words IMAC, Phosphoproteomics, Signaling, TiO_2

1 Introduction

Protein phosphorylation is one of the most common posttranslational modifications found in any biological system. Given its importance in transmitting intracellular signals, often from the cell surface to the nucleus and its ability to control protein function, it is not surprising then that it is also one of the most studied, most frequently published and reviewed. Phosphoproteomics is the attempt to discover, catalog—and more recently quantitate—these posttranslational modifications (PTM) in a high-throughput manner as a preliminary step to understanding their function in cells. For recent reviews on phosphoproteomics the reader is referred to the following reviews on general phosphoproteomics [1]; quantitative phosphoproteomics [2]; plant phosphoproteomics [3]; and crop phosphoproteomics [4].

In spite of the high level of interest and intense research activity, progress has been limited by some key factors, which include the following. *Protein phosphorylation often has a low stoichiometry.* The signaling proteins are usually not abundant because the signal is

Ramanjulu Sunkar (ed.), *Plant Stress Tolerance: Methods and Protocols*, Methods in Molecular Biology, vol. 1631,
DOI 10.1007/978-1-4939-7136-7_11,

subtle and amplified as it proceeds through the pathway. This makes detecting signaling intermediates challenging: without some form of enrichment, it is difficult or impossible to detect low abundance proteins reliably as preparations will be heavily contaminated with abundant proteins whose detection will be favored. *Protein phosphorylation is dynamic*. A protein of interest may only be phosphorylated for a very short period of time, just long enough to do its job and in addition the onset of signaling may be very rapid, often occurring within seconds of stimulus (e.g., ref. [5]). Timing of the treatment and treatment administration to ensure a synchronous response are therefore important factors to consider during planning and when executing an experiment. *The phosphodiester bond is relatively labile*. This is a problem mainly during sample preparation, where phosphatases must be inactivated or chemically inhibited. During analysis, the labile nature of the O-phosphodiester bond is something of an advantage as it almost always produces a neutral loss product ion that is diagnostic of phosphorylation [6]. This signature neutral loss product is most common with phosphoserine and threonine, but not with phosphotyrosine. Figure 1 shows a typical product ion (MS2) spectrum from a peptide phosphorylated on serine and shows this prominent neutral loss ion. *Tryptic peptides will not reveal all phosphorylation sites*. Trypsin cuts peptides reliably after a K or R residue, yielding peptides that are predominantly doubly charged during electrospray ionization, and typically with an m/z ratio of 300:1500. If peptides are too short and it is impossible determine their sequence and phosphorylation site using trypsin, alternate enzymes (and even alternate fragmentation modes) can be considered [7]. In special cases where the sequence is known, synthetic peptides have been used to confirm phosphorylation [8]. Peptides with very high charged states or which are very long may also be challenging to analyze. However, these tend to be the exception and many phosphoproteins will yield to the analysis described herein.

This chapter is written with plant biotic stress researchers in mind. It is aimed at readers who do not necessarily have good access to state-of-the-art instrumentation and software—although some level of access to these is inevitably required. Phosphoproteomics is not for the faint of heart, but it is possible for anyone to achieve some level of success because the most difficult aspect of this research is getting a high quality biological sample to begin with. It is critical to emphasize again the speed of the phosphorylation response and the low quantity of many important phosphoproteins.

This chapter describes a bottom-up approach to phosphoproteomics where tryptic peptides are first produced and then fractionated by ion exchange HPLC and subsequently enriched either by TiO_2 [9] or Fe-III IMAC [10] chromatography or both [11]— as presented here—prior to analysis by LC-MS and identification by database matching. Although other strategies have been reported, this approach forms the backbone of many high-throughput phosphoproteomics experiments, and it can easily be adapted to suit

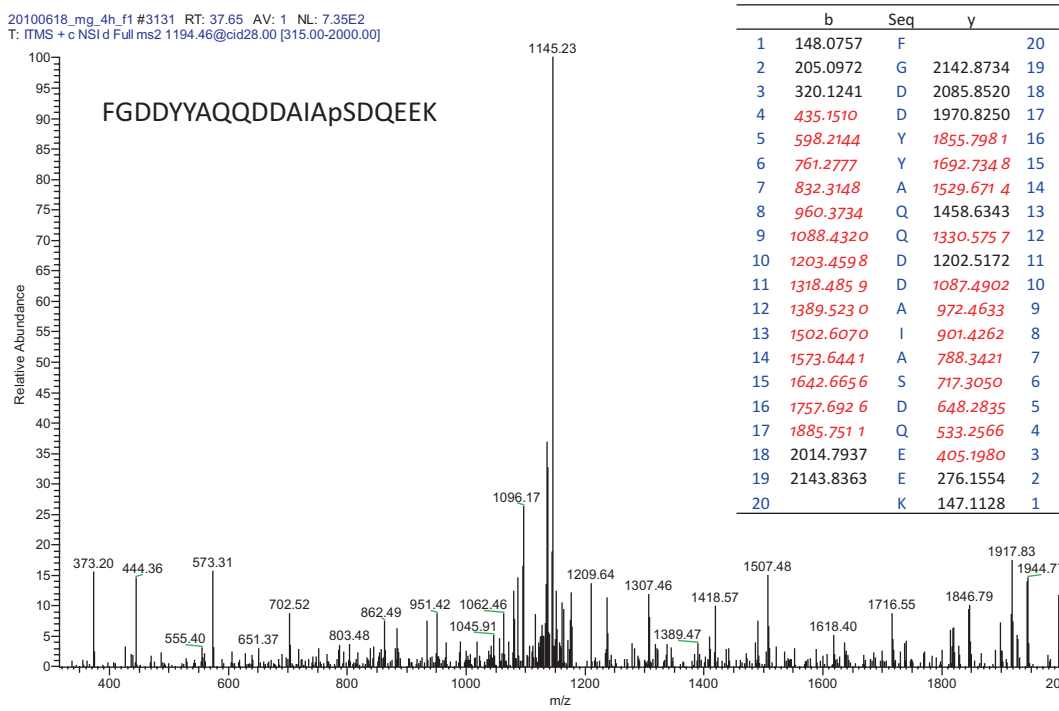

	b	Seq	y	
1	148.0757	F		20
2	205.0972	G	2142.8734	19
3	320.1241	D	2085.8520	18
4	*435.1510*	D	1970.8250	17
5	*598.2144*	Y	*1855.798 1*	16
6	*761.2777*	Y	*1692.734 8*	15
7	*832.3148*	A	*1529.671 4*	14
8	*960.3734*	Q	1458.6343	13
9	*1088.4320*	Q	*1330.575 7*	12
10	*1203.459 8*	D	1202.5172	11
11	*1318.485 9*	D	*1087.4902*	10
12	*1389.523 0*	A	*972.4633*	9
13	*1502.6070*	I	*901.4262*	8
14	*1573.644 1*	A	*788.3421*	7
15	*1642.665 6*	S	*717.3050*	6
16	*1757.692 6*	D	*648.2835*	5
17	*1885.751 1*	Q	*533.2566*	4
18	2014.7937	E	*405.1980*	3
19	2143.8363	E	276.1554	2
20		K	147.1128	1

Fig. 1 A typical MS2 spectrum of a phosphopeptide with O-phosphorylation on serine showing a conspicuous neutral loss ion. The precursor ion was doubly charged with m/z = 1194.46. Neutral loss of H_3PO_4 during collision-induced dissociation yields a prominent ion with m/z = 1145.23. The mass difference of 49.23 is multiplied by 2 to yield 98.46, corresponding to the mass of H_3PO_4. The mass spectrum displayed a near-complete series of sequence specific b-type peptide fragment ion signals (inset table: *italic font* represents ions that were detected) identifying a tryptic peptide of a conserved hypothetical protein (FGSG_05502) from *Fusarium graminearum*, a serious pathogen of wheat and other cereals. The y-ion series (inset table: *italic font*) further confirms the match to FGDDYYAQQDDAIApSDQEEK, which was returned from a Mascot search. The Mascot ions score was 100 (Ions score is $-10\log P$, where P is the probability that the observed match is a random event. Individual ions scores >21 indicate identity or extensive homology ($p < 0.05$)). The Mascot Delta score was 88, indicating that the next best match, a peptide with the sequence MDDGNLGENIQEETEVIEDR scored only 12. Since there are no ST residues close to the phosphorylated residue, the assignment is likely correct. The spectrum was acquired in a hybrid linear ion-trap/Orbitrap mass spectrometer

many labs. The technique is easy to execute even with a minimum of equipment, and the MS analysis can be performed under contract at a core facility. This method can also be expanded to produce quantitative data, although this is more challenging (e.g., ref. [12]).

2 Materials

2.1 Instrumentation

Aside from common laboratory equipment, the procedures outlined here require a high-pressure liquid chromatography (HPLC) system (*see* **Note 1**) and a mass spectrometer.

2.1.1 HPLC

This system should be equipped with a UV detector, a fraction collector and should be capable of 0.5–1 mL/min of flow.

2.1.2 LC-MS

The mass spectrometer should be part of a nanoflow LC-MS system. It is very important to use a high-resolution mass spectrometer with a time-of-flight or Orbitrap detector. Lower-resolution instruments (e.g., ion traps) lack the necessary mass accuracy for confident identification. Access to an instrument capable of electron transfer dissociation is an advantage, but not essential [7]. Since the analysis program to be used is quite generic, it is possible to use the services of a core facility for the MS analysis (*see* **Note 2**).

2.2 Chemicals

For all procedures, the highest grade of chemicals available should be used; the water used should have a resistance of at least 18 MΩ and all solutions should be freshly prepared.

2.2.1 Protein Purification and Digestion with Trypsin

For general contamination precautions, *see* **Note 3**.

1. 10% (w/v) trichloroacetic acid (TCA).
2. Acetone.
3. 100 mM dithiothreitol (DTT) stock in water, kept frozen in small aliquots.
4. Compressed nitrogen gas.
5. Bradford assay kit with BSA or IgG standard (available from Bio-Rad Laboratories Hercules CA).
6. 100 mM ammonium bicarbonate buffer.
7. Iodoacetamide.
8. Modified trypsin for proteomics (Promega; this kit comes with its own buffer optimized for protein digestion).
9. Benchtop Centrifuge (e.g., Eppendorf 5415R: Brinkmann Instruments, Mississauga, Canada).
10. Dialysis cups with a 5–10 kDa cutoff and centrifugal spin filters also with a 5–10 kDa cutoff.
11. Incubator, heating blocks, or water bath capable of maintaining 56 °C and 37 °C.

2.2.2 Desalting

1. HPLC system with a UV detector and fraction collector, or C_8 SPE cartridges. In our lab we use an analytical HPLC pump (Ultimate 3000: Dionex, Germany) equipped with an autosampler, a UV detector (220 nm), and a fraction collector.
2. Short C_8 HPLC column. In our lab we use a 5-cm reversed phase (MOS1-Hypersil: ThermoFisher), for desalting.
3. Mobile Phase A: 2% (v/v) acetonitrile (ACN) 0.1% (v/v) trifluoroacetic acid (TFA).

4. Mobile Phase B: 50% (v/v) acetonitrile (ACN) 0.1% (v/v) formic acid (FA).
5. 100 mM KCl solution to measure void volume if desired.
6. SpeedVac concentrator.

2.2.3 Strong Cation Exchange Chromatography

1. HPLC system with a UV detector and fraction collector, or centrifugal spin devices and ion exchange slurry.
2. Strong cation exchange HPLC column. In our lab we have a 15 cm SCX column (BioBasic: ThermoFisher, USA) for ion exchange.
3. Mobile Phase A: 7 mM KH_2PO_4, pH 2.65, 30% ACN (v/v). Adjust the pH prior to adding ACN.
4. Mobile Phase B: A + 350 mM KCl
5. Mobile Phase C: 50 mM K_2HPO_4, 500 mM NaCl, pH 7.5.

2.2.4 Enrichment 1: Fe-III IMAC

1. Precharged IMAC resin (PHOS-Select Iron Affinity Gel: Sigma-Aldrich, St. Louis MO). Other suppliers produce IMAC beads and enrichment kits which may be more convenient.
2. Gel loader tips (e.g., for loading sequencing gels).
3. 40% (v/v) ACN, 25 mM formic acid.
4. 50 mM KH_2PO_4, pH 10.
5. 0.1% (v/v) TFA.
6. ZipTips (EMD Millipore, Merck KGaA, Darmstadt, Germany).

2.2.5 Enrichment 2: TiO_2

1. TopTips TiO_2 (Canadian Life Science, Peterborough ON). Other suppliers produce TiO_2 beads and enrichment kits, which may be more convenient.
2. 70% (v/v) ACN, 1 M glycolic acid, 5% (v/v) TFA.
3. 70% (v/v) ACN, 5% (v/v) TFA.
4. NH_4OH, pH 11.3.

2.2.6 LC-MS Analysis

1. Nano-scale HPLC system capable of forming a gradient with two mobile phases and producing a flow of 250 nL per min.
2. Capillary column, 15 cm in length, 75 μm internal diameter, packed with C_{18} beads of 3–5 μm diameter.
3. High-resolution mass spectrometer capable of MS2 with a nano-spray ionization source.
4. Mobile phases A: 0.1% (v/v) formic acid in 2% (v/v) aqueous acetonitrile.
5. Mobile Phase B: 0.1% (v/v) formic acid in acetonitrile.

3 Methods

Sample preparation is one of the key steps to a successful phosphoproteome enrichment. Since there are many different protocols for protein extraction from many diverse plant tissues, this section is written assuming that this step has already been achieved; however, some suggestions are presented here. The first consideration is to choose the experimental plant system and the stress stimulus. Changes in phosphorylation can be very rapid: Schulze and colleagues [5] were able to detect phosphorylation of the flagellin receptor FLS2 and the receptor-like kinase BAK1 within just 15 s of stimulation with the known stress signal flg22. It is therefore important to consider the experimental design to ensure a synchronous response to the stimulus. For this reason many researchers use suspension cell cultures (typically from *Arabidopsis thaliana*) as their biological material because of the challenges of executing such a precisely timed experiment with whole plants. However, suspension cells are not suitable for many stresses and it is often necessary to stimulate whole plants to achieve a biologically relevant result. The reader is referred to a recent review summarizing experiments in stress-related crop phosphoproteomics [4].

The next step is to isolate proteins from the plants in such a way that the posttranslational phosphorylation remains intact. A good starting point for protein extraction is the acetone TCA precipitation published by Darmeval [13], because this method rapidly inactivates phosphatases during the extraction step. A step-by-step protocol for producing an acetone powder from leaf tissue is described by Rampitsch and Bykova [14]. This procedure is applicable here although any procedures that are adapted for phosphoproteomics must include consideration for inhibiting or deactivating phosphatases. At least 5–20 mg of protein should be extracted (Bradford assay, BSA equivalents).

Once a protein extract has been obtained and prior to trypsin digestion the proteins must first be dissolved, then reduced with DTT and alkylated to prevent re-formation of disulfide bonds. This step is essential to produce linear tryptic peptides suitable for MS analysis. The steps to achieve this are described below.

3.1 Reduction and Alkylation

1. Depending on the tissue used, dissolving the acetone powder can be challenging. It is first necessary to ensure that no traces of acetone remain in the powder. Acetone can be removed with a gentle stream of N_2 gas, taking care not to blow away any of the powder.
2. Once the powder is dry, add a small volume (e.g., 0.5 mL) of buffer that is compatible with trypsin. Please refer to the manufacturer's instructions for optimal buffers and compatible chaotropes (urea) and salts.

3. It is usually possible (and necessary) to add urea to 1 M, and to sonicate the sample to aid dissolution. Sonication should be performed in a water bath set to 20 °C to prevent carbamylation of proteins [15].
4. Once as much protein has dissolved as possible, centrifuge the samples to rid them of insoluble debris at 10,000 × *g* for 10 min.
5. Bring samples to 10 mM DTT.
6. Incubate for 45 min at 56 °C.
7. Cool to room temperature and add 55 mM iodocaetamide.
8. Incubate in the dark at room temperature for 30 min.
9. It is important not to exceed this time as over alkylation may result [16].
10. Dialyze the protein against several changes of 100 mM NH_4HCO_3 taking care that the proteins do not come out of solution. If they do they should be redissolved as far as possible be adding back chaotrope or salts (again, they must be compatible with trypsin) which may have been removed by dialysis.
11. It may be necessary to reduce the final volume, which can be done using a centrifugal spin device with a cutoff of 5–10 kDa.

3.2 Digestion with Trypsin

1. Prepare 10 mL of digestion buffer: 100 mM NH_4HCO_3, 10% (v/v) acetonitrile, and 2.5 mM $CaCl_2$ (add $CaCl_2$ from a 0.5 M stock solution last to avoid precipitation) (*see* **Note 4**).
2. Dissolve 1 trypsin vial with 200 µL of 50 mM acetic acid standard resuspension buffer (supplied by the manufacturer) to prepare a stock solution with 0.1 µg trypsin per µL, and keep it on ice until starting the reaction.
3. Add trypsin stock solution to the samples to yield a final concentration of 12 ng per µL in the digestion buffer.
4. Close the lids of the tubes well to prevent evaporation and incubate at 37 °C overnight.

3.3 Desalting and Strong Cation Exchange Chromatography

As mentioned in **Note 2**, this procedure can be performed without HPLC using ion exchange slurry and centrifugal devices. First the peptides (after trypsin digestion) must be desalted. This can be achieved using a disposable SPE cartridge, or by HPLC as described below.

1. Connect the MOS1 Hypersil column to the HPLC unit and equilibrate it with 2% (v/v) ACN in 0.1% (v/v) trifluoroacetic acid (TFA) at 1 mL per min until the baseline (220 nm) is stable.
2. Determine the void volume of the column by injecting 100 µL of 100 mM KCl.
3. Once the baseline is stable, inject the peptide sample.

4. Unbound material will elute with the void volume.
5. Elute the peptides from the column with 50% (v/v) ACN, 0.1% (v/v) FA.
6. Collect all fractions eluting under the 220 nm peak.
7. Pool these and dry them using a SpeedVac concentrator.
8. Reequilibrate the column before the next use.

Once desalted, the peptides are ready to be separated into fractions by SCX. The following separation is based on the one described by Villén and Gygi [17].

9. The HPLC is programmed to run a salt gradient of KCl from 0 to 300 mM over 30 min, after an initial 5 min of isocratic flow. The gradient is run in 7 mM KH_2PO_4, pH 2.65 and 30% (v/v) ACN. To clean the column a 5-min slug of 0.5 M NaCl is applied in 7 mM KH_2PO_4, pH 2.65. Please refer to Subheading 2.2.3 for the exact composition of the three mobile phases. The column is then reequilibrated for 10 min for the next sample injection.
10. Attach the bioBasic column to the HPLC and equilibrate it in mobile phase A (7 mM KH_2PO_4, pH 2.65, 30% (v/v) ACN).
11. It is advisable to run a blank first by injecting a sample containing no peptides. This ensures all equipment is functioning.
12. The samples (i.e., desalted peptides) are dissolved in 0.2–0.5 mL mobile phase A.
13. The samples are then injected using the autosampler. The program is executed as described in **step 8**.
14. Monitor the eluant and collect twenty 1 mL fractions as soon as the first peak elutes. Although it is possible to collect more than 20 fractions, the vast majority of the peptides will be contained in the first few fractions (*see* **Note 5**).
15. Desalt the fraction as described in **steps 1–7**, or use a disposable SPE cartridge as described by Villén and Gygi [17]. The automation afforded by HPLC is an advantage when dealing with multiple samples.
16. Lyophilize the desalted peptides using a SpeedVac in preparation for enrichment.

3.4 Enrichment 1: Fe-III IMAC

1. Dissolve the peptides for enrichment in 200 µL 40% (v/v) ACN, 25 mM formic acid for 10 min.
2. In the meantime prime 50 µL of IMAC slurry by washing three times in 200 µL 40% (v/v) ACN, 25 mM formic acid.
3. Incubate sample with beads for 1 h with shaking (to maintain beads in suspension).

4. Transfer the slurry into a constricted gel-loader tip (the tip is constricted at the end using pliers; this will hold the beads within the tips).
5. Save the breakthrough fraction.
6. Wash with 50 μL of 40% (v/v) ACN, 25 mM formic acid.
7. Retain the unbound fractions for TiO_2 enrichment.
8. Repeat the wash and pool the all of the breakthrough fractions (Subheading 3.5).
9. Elute phosphopeptides by adding 200 μL 50 mM KH_2PO_4, pH 10.
10. Repeat the elution, allowing 5 min of contact with the beads per elution.
11. Add 200 μL formic acid to acidify the sample before drying in a SpeedVac.
12. Resuspend the dried fractions in water with 0.1% TFA and desalt using ZipTips in preparation for MS analysis.

3.5 Enrichment 2: TiO_2

1. Prepare the pooled unbound fractions from Subheading 3.3, **step 8** for enrichment as follows.
2. Desalt the peptides using a ZipTip and dry using a SpeedVac.
3. Load peptides in 70% (v/v) ACN, 1 M glycolic acid, 5% (v/v) TFA.
4. Wash in the same solution, but with no glycolic acid.
5. Elute with NH_4OH, pH 11.3.
6. Desalt this fraction with a ZipTip in preparation for MS analysis.

3.6 Mass Spectrometry

This section is written for an analysis performed on a Q-Exactive mass spectrometer and an Easy nLC HPLC unit (ThermoFisher Scientific, San Jose CA). This is a commonly used instrument combination in many core labs, but the method, simply a data-dependent acquisition of MS2 spectra of peptides eluting with an acetonitrile gradient, is very commonly seen in proteomics and can easily be applied to other instruments too.

1. Samples are dissolved in mobile phase A and loaded using an autosampler into a flow path of 2% (v/v) ACN in 0.1% (v/v) FA.
2. Once sample loading is complete the HPLC delivers a gradient of 2% (v/v) ACN to 40% (v/v) ACN (both in 0.1% (v/v) FA) over 60 min at 250 nL per min. The run time can be extended or decreased depending on sample complexity; however, excessive lengthening will lead to broadening of chromatographic peaks and should be avoided.

3. The gradient is terminated by bringing the content of ACN to 90% (v/v) for 2 min. The Easy nLC system automatically equilibrates the column to mobile phase A prior to sample loading, so a column equilibration step should not be programmed into the method. However, other HPLC systems may not do this and it is important to load all samples onto a column equilibrated with mobile phase A. Phosphopeptides tend to be hydrophilic and some will elute directly in 2% (v/v) ACN without appreciable retention by the column.
4. The mass spectrometer should be programmed to acquire 12 MS2 scans per survey scan. In the Q-Exactive both spectra are acquired in the Orbitrap mass analyzer. The settings should be chosen with care, but in principle they are no different to settings generally used for data-dependent proteomics analyses. Kalli et al. [18] have provided a detailed discussion of settings for Orbitrap mass analyzers and the reader is referred to this article (*see* **Note 6**). After acquisition the raw data file must be converted to a form readable by the search engine to be used. Again, there are several options depending on the search engine to be used. In our lab we use Mascot Distiller (MatrixScience, London UK) to produce MGF files, which can be searched by Mascot.

3.7 Data Analysis

Although not strictly a part of the laboratory procedure, it is well to make a few observations on this important topic. After mass spectrometry, spectra will need to be matched against a suitable database, using either a commercial or free online software. Examples of these are Mascot [19], Sequest [20], and X!Tandem [21]. Perhaps the most important consideration is that the plant under study should have a fully sequenced genome with the sequence available and annotated at least to some degree. Working with unsequenced plants greatly increases the chances of misidentifying phosphopeptides and phosphorylation sites; even under optimal circumstances with good spectra and reliable sequences this task can be challenging. A few other considerations are set out below.

1. Search parameters for Mascot (or any of the other search programs) must include variable modifications for phospho ST and Y. The fixed modification carbamidomethyl (CAM) must be specified for cysteine, since reduction and alkylation with IAA (iodoacetamide) was performed (Subheading 3.1). In addition, the variable modifications of M (oxidation) and NQ (deamidation) can also be used as these are frequently observed in our lab.
2. The Q-Exactive instrument permits a very high mass accuracy setting of 5 ppm for the precursor ion (or even lower, especially if lock masses were used during the acquisition) and 0.1 Da for the product ions, since both are measured in the Orbitrap.

3. To estimate the level of false positive returns a decoy database should be used. The false discovery threshold is typically set to 1% or lower.
4. It is useful to include a contaminants database. This should contain entries for keratin, trypsin and BSA [22]. These proteins are not present in plants and their spectra can lead to weak matches with plant proteins.
5. Finally, after the search, one should be careful when assigning phosphorylation sites to particular S, T, or Y residues in a high-throughput manner. In many cases there will be ambiguity, especially if there are neighboring S, T, or Y residues. Figure 1 shows an example of a correctly assigned phosphorylation site and the legend explains how it was interpreted. Unfortunately, it is not practical to check each spectrum manually in a high-throughput experiment, which can automatically assign thousands of phosphorylation sites. For this reason it is necessary to use phosphorylation site assignment software to lend confidence to the assignments. Examples of these are Ascore [23] and Scaffold PTM (proteomesoftware.com). If the search is performed with Mascot, the Delta Score is a useful aid [24].

4 Notes

1. It is possible to perform the ion exchange step without HPLC. Ion exchange resin (approximately 0.5 mL) can be held in a centrifugal spin device and loaded with peptides in low salt. Peptides can then be eluted in batches with increasing salt slugs as described by Rampitsch et al. [25]. SCX HPLC with a salt gradient will yield superior results however.
2. A typical run would be 60 min in length with peptides separated on an acetonitrile gradient on a reversed phase (C_{18}) column. A top10 method selects the ten most abundant peaks from the survey scan for MS2 analysis in each duty cycle. It is not necessary to perform a "neutral loss" scan (MS3) as this has been shown not to be advantageous in increasing identification [26].
3. Fresh 50–100 mL stocks of water, ammonium bicarbonate buffer, formic acid and acetonitrile should be used to prepare each new series of samples. Environmental dust accumulates rapidly in solutions and contaminates samples with keratin and polymeric detergents. Gloves without talcum powder should be worn. The solutions for extraction should be freshly made in tubes suitable and stable for acetonitrile and formic acid (siliconized Eppendorf tubes).
4. The manufacturer provides detailed instructions on trypsin digestion. Sequencing Grade Modified Trypsin (Promega),

100 µg total amount with 5 vials per 20 µg lyophilized powder, store at −20 °C (for maximum 12 months). Specific activity ≥5 U/µg protein. Dissolve one vial in 200 µL of 50 mM acetic acid (resuspension buffer included) to prepare 0.1 µg/µL stock solution. Excess trypsin stock solution can be aliquoted (20 µL), frozen and stored at −20 °C for 1–2 months. Thaw the aliquot only once just before preparing the digestion buffer.

5. After MS analysis the user can decide how many fractions to collect for future analyses. A good option is to pool higher fractions into a single fraction to lessen the amount of processing and MS analysis required.
6. In our lab, using a Q-Exative instrument, we typically use inject times of 40 ms and 100 ms for MS and MS2 respectively, and an AGC target of 5×10^5 and 1×10^5 ions for MS and MS2 respectively. The chromatographic peak width is determined empirically, but is typically set to 20–40 s, normalized collision energy set to 30, dynamic exclusion is enabled and set to 10–20 s, charged states of +1 and "unassigned" are rejected, and the underfill ratio is set to 1% [18].

Acknowledgments

Funding for proteomics research to CR originates from Agriculture and Agrifood Canada. I thank Slavica Djuric-Ciganovic for critical comments on the manuscript.

References

1. Engholm-Keller K, Larsen M (2013) Technologies and challenges in large-scale phosphoproteomics. Proteomics 13:910–931
2. Nilsson CL (2011) Advances in quantitative phosphoproteomics. Anal Chem 84:735–746
3. Silva-Sanchez C, Li H, Chen S (2015) Recent advances and challenges in plant phosphoproteomics. Proteomics 15:1127–1141
4. Rampitsch C, Bykova NV (2012) The beginnings of crop phosphoproteomics: exploring early warning systems of stress. Front Plant Sci 3:144
5. Schulze B, Mentzel T, Jehle AK, Mueller K, Beeler S, Boller T, Felix G, Chinchilla D (2010) Rapid heteromerization and phosphorylation of ligand-activated plant transmembrane receptors and their associated kinase BAK1. J Biol Chem 285:9444–9451
6. Mann M, Ong S-E, Grønborg M, Jensen ON, Pandey A (2002) Analysis of protein phosphorylation using mass spectrometry: deciphering the phosphoproteome. Trends Biotechnol 6:261–268
7. Molina H, Horn DM, Tang N, Mathivanan S, Pandey A (2007) Global proteomic profiling of phosphopeptides using electron transfer dissociation tandem mass spectrometry. Proc Natl Acad Sci U S A 104:2199–2204
8. Mughal W, Nguyen L, da Silva Rosa SC, Piotrowski S, Chapman D, Du M, Alli NS, Grigull J, Halayko AJ, Aliani M, Topham MK, Epand RM, Hatch GM, Kereliuk S, McDermott JC, Rampitsch C, Dolinsky VW, Gordon JW (2015) A conserved MADS-box phosphorylation motif regulates differentiation and mitochondrial function in skeletal, cardiac, and smooth muscle cells. Cell Death Dis 6:e1944
9. Mazanek M, Mituloviæ G, Herzog F, Stingl C, Hutchins JR, Peters JM, Mechtler K (2007) Titanium dioxide as a chemo-affinity solid

phase in offline phosphopeptide chromatography prior to HPLC-MS/MS analysis. Nat Protoc 2:1059–1069

10. Ficarro SB, Salomon AR, Brill LM, Mason DE, Stettler-Gill M, Brock A, Peters EC (2005) Automated immobilized metal affinity chromatography/nano-liquid chromatography/electrospray ionization mass spectrometry platform for profiling protein phosphorylation sites. Rapid Commun Mass Spectrom 19:57–71
11. Thingholm TE, Jensen ON, Robinson PJ, Larsen MR (2007) SIMAC (sequential elution from IMAC), a phosphoproteomics strategy for the rapid separation of monophosphorylated from multiply phosphorylated peptides. Mol Cell Proteomics 7:661–671
12. Zhang H, Zhou H, Berke L, Heck AJR, Mohammed S, Scheres B, Menke FLH (2013) Quantitative phosphoproteomics after Auxin-stimulated lateral root induction identifies an SNX1 protein phosphorylation site required for growth. Mol Cell Proteomics 12: 1158–1169
13. Damerval C (1986) Technical improvements in two-dimensional electrophoresis increases the level of genetic variation detected in wheat seedling proteins. Electrophoresis 7:52–54
14. Rampitsch C, Bykova NV (2009) Methods for functional proteomic analyses. In: Somers D et al (eds) Methods in molecular biology, vol 513. Humana press, Totowa NJ, pp 93–110
15. Kollipara L, Zahedi RP (2013) Protein carbamylation: in vivo modification or in vitro artefact? Proteomics 13:941–944
16. Boja ES, Fales HM (2001) Overalkylation of a protein digest with iodoacetamide. Anal Chem 73:3576–3582
17. Villén J, Gygi S (2008) The SCX/IMAC enrichment approach for global phosphorylation analysis by mass spectrometry. Nat Protoc 3:1630–1638
18. Kalli A, Smith GT, Sweredoski MJ, Hess S (2013) Evaluation and optimization of mass spectrometric settings during data-dependent acquisition mode: focus on LTQ-Orbitrap mass analyzers. J Proteome Res 12:3071–3086
19. Perkins D, Pappin D, Creasy D, Cottrell J (1999) Probability-based protein identification by searching sequence databases using mass spectrometry data. Electrophoresis 20:3551–3567
20. Eng JK, McCormak AL, Yates JR (1994) An approach to correlate tandem mass spectral data of peptides with amino acid sequences in a protein database. J Am Soc Mass Spectrom 5:976–989
21. Craig R, Cortens JP, Beavis RC (2004) Open source system for analyzing, validating and storing protein identification data. J Proteome Res 3:1234–1242
22. Keller BO, Sui J, Young AB, Whittal RM (2008) Interferences and contaminants encountered in modern mass spectrometry. Anal Chim Acta 627:71–81
23. Beausoleil SA, Villén J, Gerber SA, Rush J, Gygi SP (2006) A probability-based approach for high-throughput protein phosphorylation analysis and site localization. Nat Biotechnol 24:1285–1292
24. Savitski MM, Lemeer S, Boesche M, Lang M, Mathieson T, Bantscheff M, Kuster B (2011) Confident phosphorylation site localization using the Mascot delta score. Mol Cell Proteomics 10:M110.003830
25. Rampitsch C, Subramaniam R, Djuric-Ciganovic S, Bykova NV (2010) The phosphoproteome of *Fusarium graminearum* at the onset of nitrogen starvation. Proteomics 10:124–140
26. Villén J, Beausoleil SA, Gygi SP (2008) Evaluation of the utility of neutral-loss-dependent MS3 strategies in large-scale phosphorylation analysis. Proteomics 8:4444–4452

Chapter 12

Probing Posttranslational Redox Modifications

Patrick Treffon, Michael Liebthal, Wilena Telman, and Karl-Josef Dietz

Abstract

Reactive molecular species (RMS) can damage DNA, lipids, and proteins but as signaling molecules they also affect the regulatory state of the cell. RMS consist of reactive oxygen (ROS), nitrogen (RNS), and carbonyl species (RCS). Besides their potentially destructive nature, RMS are able to modify proteins at the posttranslational level, resulting in regulation of structure, activity, interaction as well as localization. This chapter addresses methods to analyze and quantify posttranslational redox modifications in vitro and ex vivo, such as sulfenic acid generation of cysteine residues and oxidative carbonylation of proteins. In addition, by use of isothermal titration calorimetry, redox-dependent interaction studies of proteins will be described.

Key words Posttranslational redox modifications, Sulfenylation, Carbonylation, Hydrogen peroxide, Peroxiredoxin, Isothermal titration calorimetry, Dimedone, DNPH

1 Introduction

Posttranslational modifications (PTMs) of proteins are involved in a multitude of metabolic processes [1, 2]. These biochemical mechanisms, in which amino acid residues are chemically modified, allow the dynamic alteration of protein function in response to metabolic requirements [3]. Covalent modifications, such as phosphorylation or acetylation, can be classified according to the affected amino acid side chain, the family of the enzymes involved in this modification, as well as the extent of reversibility. Redox-dependent posttranslational modifications of proteins receive increasing attention as important redox regulatory mechanism in biology [4]. Here, reactive molecular species (RMS), derived from oxygen (ROS), nitrogen (RNS) or the reaction with carbon (RNS), are responsible for the modification of certain protein site chains. RMS are by-products of physiological metabolism and increase after exposure to various kind of stresses. As a consequence, redox-dependent PTM and in particular the oxidation of sulfur-containing amino acids takes place (*see* Fig. 1a). The reactive thiolate anion of

Ramanjulu Sunkar (ed.), *Plant Stress Tolerance: Methods and Protocols*, Methods in Molecular Biology, vol. 1631,
DOI 10.1007/978-1-4939-7136-7_12,

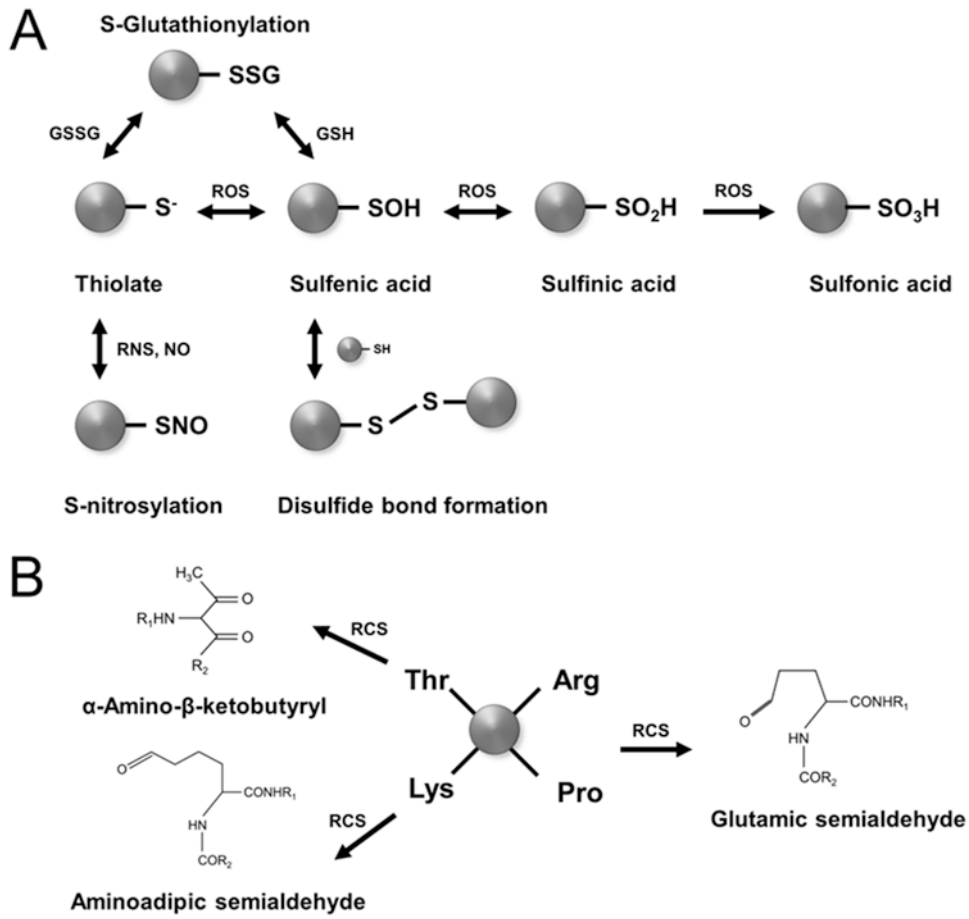

Fig. 1 Example of important posttranslational protein modifications by oxidation. (**a**) ROS and RNS related changes on protein cysteine residues. (**b**) Oxidative carbonylation on threonine, lysine, arginine, and proline amino acids. See text for details. Abbreviations: *GSH* reduced glutathione, *GSSG* oxidized glutathione, *NO* nitric oxide

cysteine residues can directly be oxidized to sulfenic acid (-SOH). Further reaction with ROS result in sulfinic acid ($-SO_2H$) and sulfonic acid ($-SO_3H$) formation. Oxidation up to sulfinic acid derivatives are reversible by thiol-dependent reduction, whereas hyperoxidation to sulfonylated protein species are considered to be irreversible [5]. Despite this, cysteines can also interact with the tripeptide glutathione (glutathionylation) or with other thiol containing proteins (S-S), forming mixed disulfide and intermolecular disulfide bonds, respectively. In addition, in the presence of RNS like NO, thiolate anions can be S-nitrosylated. The irreversible oxidative carbonylation of particular amino acid residues (arginine, lysine, threonine, or proline, *see* Fig. 1b) also commonly occurs as oxidative protein modification. Introducing carbonyl groups, aldehyde and ketones, in reaction with reactive carbonyl species

leads to alteration in protein activity, proteolytic breakdown or aggregate formation [6]. In this chapter, methods are presented to access redox-dependent posttranslational modifications and their impact on protein function using various techniques. We focus on the identification of sulfenylated protein species using the chemoselective probe dimedone with subsequent mass spectrometric analysis, approach the extent of carbonylation of proteins spectrophotometrically and by Western blotting and, finally, will introduce isothermal titration calorimetry to study redox-dependent protein–protein interactions.

2 Materials

All solutions are prepared with high-quality ultrapure water and all chemicals are of reagent grade and used without further purification.

2.1 Identification of Sulfenic Acid Derivatives in Proteins Using Dimedone

2.1.1 Chemical Reduction of Proteins

1. Sample buffer: 0.1 M Tris–HCl, pH 8.0.
2. Heterologously expressed and purified protein in sample buffer.
3. Dithiothreitol (DTT) stock solution: 1 M in 0.1 M Tris–HCl, pH 8.0 (*see* **Note1a**).
4. Incubator at 25 °C.
5. PD-10 desalting columns (GE Healthcare, Munich, Germany).
6. Coomassie Brilliant Blue Dye-G250 solution, e.g., Roti-Quant (Roth, Karlsruhe, Germany).
7. 5,5′-dithiobis-(2-nitrobenzoic acid) DTNB: 6 mM prepared fresh in sample buffer (*see* **Note 1b**).
8. 96-well microtiter plates.

2.1.2 Labeling of Oxidized Proteins with Dimedone

1. Hydrogen peroxide: 100 mM stock is prepared directly in sample buffer just prior to use. Working solutions are prepared by further dilutions in sample buffer.
2. Dimedone: 100 mM stock in DMSO-sample buffer (1:1).
3. 80% acetone (v/v).

2.1.3 Mass Spectrometric Analysis (ESI-MS)

1. 30% EtOH (v/v).
2. 100% formic acid.
3. ESI-MS mass spectrometer: e.g., Esquire 3000 Plus Quadrupole Ion Trap Mass Spectrometer (Bruker Daltonics, Bremen, Germany).
4. Software that uses the MS data to obtain the molecular weights of the proteins via deconvolution, e.g., DataAnalysis Version 3.2 or higher (Bruker Daltonics, Bremen, Germany).

2.2 Spectrophotometric Quantification of Protein Carbonyl Groups by DNPH-Assay

1. Triton X-100 (Merck Millipore, Darmstadt, Germany). Prepare a 10% (v/v) Triton X-100 aliquot just prior to use by stirring gently to avoid foam formation.
2. Ten percent (w/v) streptomycin sulfate in ultrapure water. Store stock solutions at −20 °C.

2.2.1 Nucleic Acid Removal by Precipitation

2.2.2 Derivatization of Carbonyl Groups and Protein Precipitation

1. Derivatization blank solution: 2 M HCl.
2. Derivatization solution: 10 mM 2,4-dinitrophenylhydrazine (DNPH; Sigma-Aldrich, Munich, Germany) in 2 M HCl. The water content of DNPH (33% in minimum) should be taken into account (*see* **Note 2a**).
3. Ice-cold 100% (w/v) trichloroacetic acid (TCA) solution. Store at 4 °C in dark bottle (*see* **Note 2b**).
4. Washing solution: Ice-cold ethanol–ethylacetate (1:1, v/v) to remove any free DNPH molecules. Store tightly sealed at −20 °C.
5. 6 M guanidine hydrochloride in 20 mM potassium phosphate buffer (pH 2.3) to solubilize protein precipitates. Adjust the pH dropwise with 85% H_3PO_4.
6. Centrifuge at 4 °C.

2.2.3 Spectrophotometric Quantification

1. Precision cuvettes made of Quartz SUPRASIL® with a light path of 10 mm (Type No. 105.250-QS; Hellma, Müllheim, Germany).
2. Washing solution to clean the quartz cuvettes for each measurement: 6 M guanidine hydrochloride in 20 mM potassium phosphate buffer (pH 2.3). Prepare 100 mL and adjust the pH dropwise with 85% H_3PO_4.
3. UV–Vis spectrophotometer (e.g., Varian Cary 300 Bio UV-Vis Series II spectrophotometer).

2.3 OxyBlot

2.3.1 DNPH Derivatization of Protein Mixture

1. Components required for the derivatization reaction are contained in the OxyBlot Protein Oxidation Detection Kit (Merck Millipore, Darmstadt, Germany). Store at 4 °C:
   (a) 1× 2,4-dinitrophenylhydrazine (DNPH) solution.
   (b) 1× derivatization control solution.
   (c) Neutralization solution.
2. 12% (w/v) SDS solution in water. Store at room temperature.
3. Reducing agent: 2-mercaptoethanol (AppliChem, Darmstadt, Germany). Store at room temperature (*see* **Note 2c**).

2.3.2 SDS–Polyacrylamide Gel Electrophoresis

1. Stacking gel buffer: 0.5 M Tris–HCl, pH 6.8.
2. Separating gel buffer: 1.5 M Tris–HCl, pH 8.8.
3. Thirty percent (w/v) acrylamide–bisacrylamide solution (ratio 37.5:1) (Roth, Karlsruhe, Germany). Store in dark bottle (*see* **Note 2d**).
4. N,N,N′,N′-tetramethylethylenediamine (TEMED) (Sigma-Aldrich, Seelze, Germany). Store at 4 °C.
5. Ten percent (w/v) ammonium persulfate (APS) solution. Store at 4 °C and prepare fresh weekly.
6. Isopropanol (100%) to overlay the separating gel to ensure a flat surface and to exclude oxygen during polymerization.
7. Running gel buffer (10×): 125 mM Tris, 960 mM glycine, 0.5% (w/v) SDS. Store at room temperature. For 1× running buffer, add 100 mL of 10× running buffer to 900 mL ultrapure H_2O.
8. SDS electrophoresis system: chamber, comb, set of glass plates, spacer, rubber gum, clamps, power supply, cables. A Hamilton syringe to apply the samples and additional 10-mL syringe fitted with a 20-gauge needle to wash the wells after removing the comb.
9. Loading Buffer (5×): 225 mM Tris–HCl, pH 6.8, 5% (w/v) SDS, 50% glycerol, 0.05% bromophenol blue (without reducing agent). For 1× loading buffer dilute 200 μL 5× loading buffer in 800 μL deionized H_20. Store at room temperature.
10. Mixture of standard proteins with attached 2,4-dinitrophenylhydrazone (DNP) residues (Merck Millipore, Darmstadt, Germany). Prepare 5 μL aliquots and store at −20 °C to avoid subsequent freeze–thaw cycles.
11. PageRuler™ Prestained Protein Ladder and PageRuler™ Unstained Protein Ladder (ThermoFisher, Oberhausen, Germany).

2.3.3 Western Blot and Immunodetection of Carbonyl Groups

1. Electroblot transfer buffers. Store at 4 °C:
   (a) 10× anode buffer: 300 mM Tris–NaOH (pH 10.4), 20% (v/v) methanol.
   (b) 1× anode buffer: add 100 mL of 10× anode buffer to 900 mL ultrapure H_2O.
   (c) Cathode buffer: 25 mM Tris–HCl (pH 9.4), 40 mM caproic acid, 20% (v/v) methanol.
2. Blotting system and required materials: transfer apparatus, nitrocellulose membrane (0.45 μm pore size), blotting absorbent filter paper, power supply.

3. 10× Phosphate buffered saline (PBS): 188 mM sodium dihydrogen phosphate monohydrate (NaH_2PO_4*H_2O), 810 mM sodium hydrogen phosphate (Na_2HPO_4), 1.454 M sodium chloride (*see* **Note 2e**). Adjust the pH to 7.2–7.5 using NaOH or HCl. To prepare 1× PBS add 100 mL of 10× PBS to 900 mL ultrapure H_2O.
4. Blocking buffer: 1% (w/v) bovine serum albumin (BSA) in 1× PBS. Adjust the pH to 7.2–7.5 as mentioned in **step 3** and store at 4 °C.
5. 1× Phosphate buffered saline Tween 20 (PBST): add 0.5 mL of Tween 20 to 100 mL 10× PBS and 899.5 mL ultrapure H_2O to a final concentration of 0.05%.
6. Components required for the immunodetection are obtained from the OxyBlot Protein Oxidation Detection Kit (Merck Millipore, Darmstadt, Germany). Store at 4 °C:
   (a) 1° Antibody: rabbit anti-DNP antibody stock solution. Dilute 1° antibody stock solution 1:150 with blocking buffer (*see* **Note 2f**).
   (b) 2° Antibody: goat anti-rabbit IgG (HRP-conjugated) stock solution. Dilute 2° antibody stock solution to 1:300 with blocking buffer (*see* **Note 2f**).
7. Chemiluminescent reagent solution has to be prepared just prior to use. Mix 1 mL of solution A with 0.3 µL 30% hydrogen peroxide and 100 µL of solution B (use 0.05 mL/cm^2 of membrane):
   (a) Solution A: dissolve 50 mg Luminol (Sigma-Aldrich, Munich, Germany) in 200 mL Tris–HCl (0.1 M, pH 8.6). Store at 4 °C in dark bottle.
   (b) Solution B: dissolve 11 mg p-coumaric acid (Sigma-Aldrich, Munich, Germany) in 10 mL dimethyl sulfoxide (DMSO). Store at room temperature in dark bottle.
   (c) Thirty percent hydrogen peroxide. Store at 4 °C.
8. Concentrated developer solution (Kodak T-Max, Chalon-sur-Saône, France). Prepare a 1:4 dilution in H_2O. Dilution is stable for weeks at room temperature in dark bottle.
9. Concentrated fixer solution (Kodak GBX, Bagnolet, France). Prepare a 1:4 dilution in H_2O. Dilution is stable for weeks at room temperature in dark bottle.
10. Kodak Scientific Imaging film.

2.3.4 Coomassie Brilliant Blue G-250 Staining

1. Staining solution: 40% (v/v) ethanol, 10% (v/v) acetic acid, 0.1% (w/v) Coomassie Brilliant Blue G-250. May be used several times.
2. Destaining solution: 40% (v/v) ethanol, 10% (v/v) acetic acid.

2.4 Redox-Dependent Interaction Studies of Proteins by ITC

1. ITC instrument (MicroCal Inc. Northampton, MA, USA) and connected PC for software.
2. Degassing device and stirrer, preferable in a single unit.
3. Handling materials: 5-mL test tubes with plain bottom for optimal stirring, magnet stirrers, 1-mL glass tube for syringe loading (MircoCal Inc. Northampton, MA, USA), a Hamilton syringe for cell loading and cleaning, and a filling syringe with loading tube for syringe loading and cleaning.
4. Dialysis sacks and clips (Visking Cellulose, 14 kDa cutoff, Roth, Karlsruhe, Germany, *see* **Note 3a**).
5. Syringe and filter units (0.45 μm pore size, Macheray-Nagel, Düren, Germany).
6. Dithiothreitol (DTT, 1 M), freshly prepared in water (*see* **Note 3b**).
7. Hydrogen peroxide (H_2O_2) stock solution: 100 mM.
8. Buffer: 35 mM HEPES (pH 8.0).
9. MilliQ water (Merck Chemicals GmbH, Darmstadt, Germany) for buffer preparation and cleaning (*see* **Note 3c**).
10. Protein solution at a concentration of around 50 μM, e.g., heterologously expressed in *E. coli* and purified to 95% or higher purity (*see* **Note 3d**).
11. Origin software (OriginLab Corporation, Northampton, MA, USA) with ITC plugin for data evaluation.

3 Methods

3.1 Identification of Sulfenic Acid Derivatives in Proteins Using Dimedone

Proteins are susceptible to reversible oxidation–reduction (redox) reactions in order to control RMS production and maintain redox homeostasis [7]. Cysteine thiol groups are most prone towards oxidation and undergo various redox-dependent modifications (*see* Fig. 1). Such PTMs affect cell functions like enzyme activity, control of gene expression and signaling pathway therefore rely on reversible posttranslational modifications of cysteine residues [8]. As a consequence, protein thiols are important factors in maintaining biological equilibrium and their redox state can vary in response to oxidative stress [4]. The method described here enables the detection of protein sulfenic acids (-SOH) using the chemoselective probe dimedone [9]. In combination with mass spectrometric techniques, which provide highly accurate molecular weight information on intact molecules, protein–dimedone adducts can be identified due to a mass shift of 140 Da (*see* Fig. 2). This method offers a potentially powerful approach to monitor changes in thiol oxidation state of proteins in vitro.

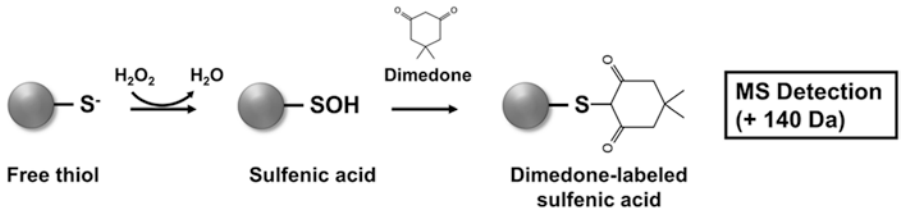

Fig. 2 Mechanism of dimedone labeling. Oxidation of protein thiols with H_2O_2 results in sulfenic acid formation. Subsequent reaction of dimedone with sulfenylated proteins allows the detection by mass spectrometric analysis due to the mass shift of 140 Da

3.1.1 Reduction of Proteins

1. Adjust protein to a concentration of 20–50 μM in sample buffer.
2. Complete reduction: Incubate 20–50 μM (198 μL) protein with 2 μL of 1 M DTT (10 mM) at room temperature for 30 min.

3.1.2 Removal of Excess DTT

Remove excess DTT after the reaction by size exclusion chromatography (PD-10 columns) with gravity flow.

1. Column equilibration: Fill up the column with sample buffer and allow the buffer to enter the packed bed completely. Repeat this step four times, so that in total 30 mL sample buffer is used for equilibration. Discard the flow-through.
2. Sample application: Add the sample slowly on top of the column. After the sample has entered the packed bed completely, add sample buffer.
3. Elution: Elute with 6 mL sample buffer and collect the eluate in 0.5 mL fractions.
4. Analysis of protein-enriched fractions: Prepare 160 μL H_2O with 40 μL of Roti-Quant per fraction and aliquot it into a microtiter plate. Add 10 μL of fractions, mix well by pipetting and incubate it at room temperature for 5 min. Protein-enriched samples appear blue. To test whether these fractions contain DTT, mix 80 μL H_2O with 20 μL DTNB and 20 μL of the fractions. A yellow color indicates the presence of DTT, which occurs usually at fractions 10–11.

3.1.3 Reaction of Reduced Thiol Proteins with Hydrogen Peroxide and Dimedone

1. Combine the protein-enriched, desalted samples and adjust the concentration to 50 μM reduced protein in sample buffer and add 1 μM–50 μM H_2O_2 (final concentration). Incubate for 30 min at room temperature. For controls skip the addition of hydrogen peroxide and dimedone and proceed further with **step 2**.
2. Stop the reaction by adding 800 μL of ice-cold (−20 °C) acetone to the samples, mix by vortexing and incubate on ice for 1 h.

3. Centrifuge at 20,000 × *g* and 4 °C for 15 min to obtain the precipitated proteins.
4. Wash the pellet in 1 mL of cold 80% acetone (*see* **Note 1c**).
5. Repeat **steps 3** and **4**.
6. Collect final protein precipitate by centrifugation at 20,000 × *g* at 4 °C for 15 min.
7. Carefully remove the acetone solution completely without disturbing the pellet and dry samples under dry air to eliminate any acetone residue (*see* **Note 1d**).
8. Resuspend final pellet in 50 µL ultrapure water (*see* **Note 1e**).

3.1.4 Mass Spectrometric Analysis (ESI-MS)

The mass of intact modified and unmodified proteins is determined by ESI-MS.

1. Instrumental parameters for Esquire 3000 Plus Quadrupole Ion Trap Mass Spectrometer, which gave the best ion abundances for identification of dimedone-labeled (formerly sulfenylated) protein species, are explained in the following. Check the parameters with your instrument. Capillary voltage = 2.000 V. Nebulizer gas pressure = 15 psi. Drying gas flow = 4.0 L/min. Drying gas temperature = 200 °C. The mass-to-charge (*m/z*) values depend on the molecular weight of the analyzed protein (*see* **Note 1f**).
2. Sample preparation: Mix 10–25 µL of the protein solution with 489–474 µL 30% ethanol and 1 µL formic acid and vortex (*see* **Note 1g**).
3. Inject the sample with a flow rate of 180 µL/h. Check the parameter with your instrument.
4. Start the acquisition and process the resulting mass spectra with any deconvolution software, e.g., DataAnalysis (Bruker Daltonics, Bremen, Germany) according to the manufacturer's instructions (Figs. 3, 4 and Table 1).

To identify oxidized proteins in vivo, this method can be refined with optimized dimedone-derived probes (e.g., DYn-2) that can be detected using azide-based tags by standard click technique and subsequent LC-mass spectrometric analysis.

3.2 Spectrophotometric DNPH-Assay and OxyBlot to Access Carbonylated Proteins

Oxidative carbonylation of specific amino acid residues leads to an often irreversible and stable posttranslational modification (*see* Fig. 1b). It was reported to be involved in various regulatory pathways, e.g., as a consequence of protein dysfunction, in proteolytic degradation and during leaf senescence [10–12]. In order to quantify oxidative modifications of proteins by introduction of carbonyl groups during oxidative stress, these reactive groups are derivatized with 2,4-dinitrophenylhydrazine (DNPH). DNPH reacts specifically with carbonyl groups (ketones and aldehydes) to

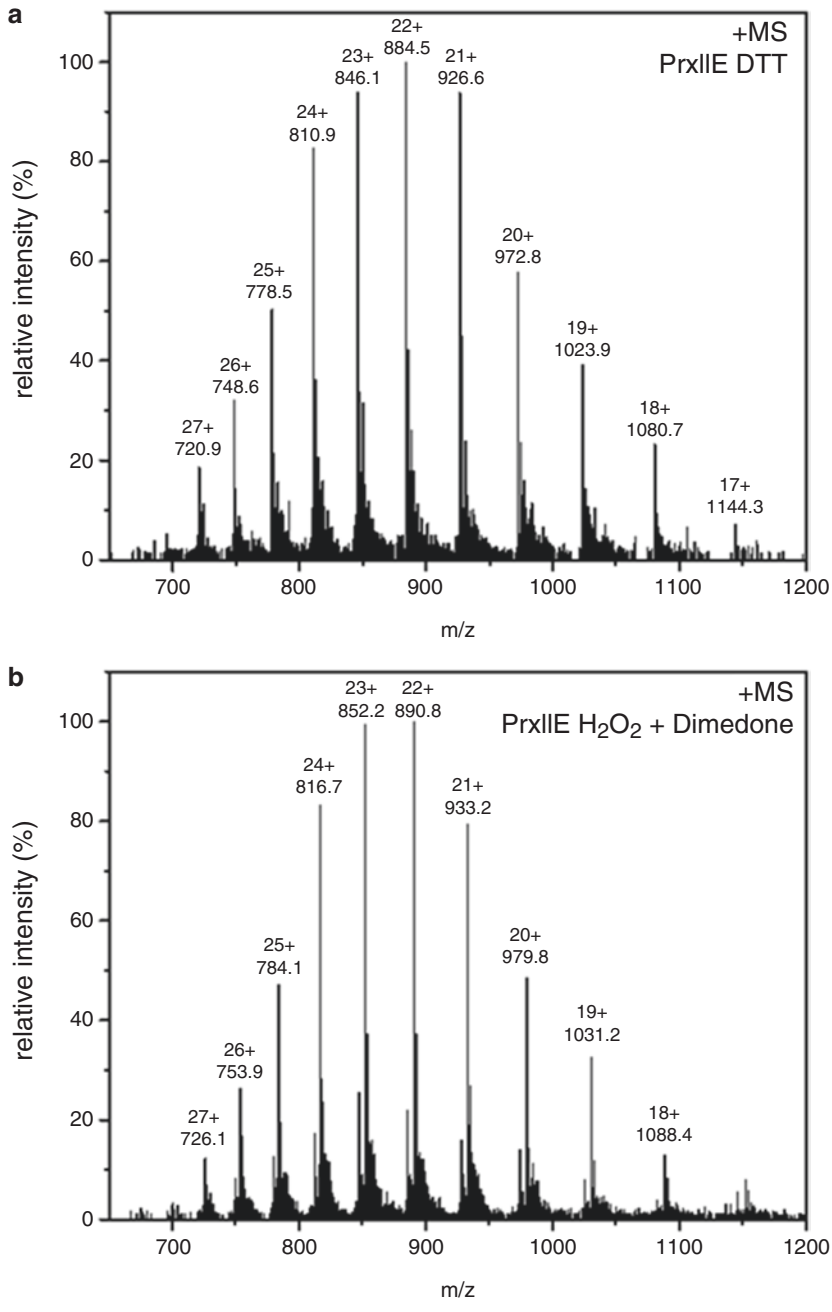

Fig. 3 ESI-MS spectra of reduced and dimedone-labeled PrxIIE. Mass spectra of the heterologously expressed *Arabidopsis thaliana* peroxiredoxin IIE (PrxIIE; At3g52960). (**a**) Relative ion intensities of the reduced form of the protein with their corresponding charge. The distribution of charge states occur after multiple protonation of the protein (in positive ion mode). The eleven charge states from +17 to +27 with a maximum at +22 are plotted. ESI-MS generates highly charged ion species, resulting in multiple peaks that differ by one charge. (**b**) Oxidation with 10 μM H_2O_2 and labeling of generated sulfenic acid derivative with 5 mM dimedone was achieved by incubation for 30 min at room temperature. The oxidized and labeled protein is presented in 10 charge states, from +18 to +27

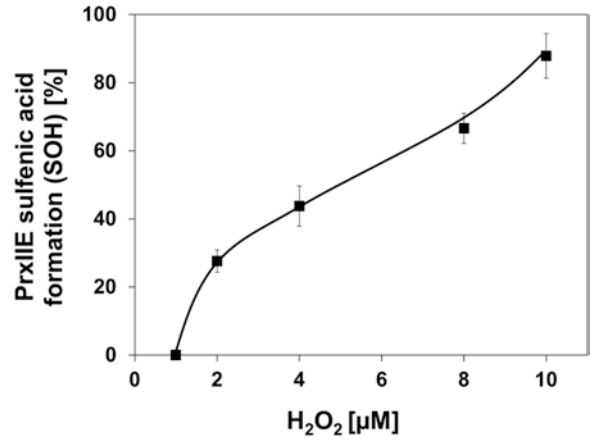

Fig. 4 Rate of PrxIIE oxidation with H_2O_2. The extent of sulfenic acid generation was estimated from the ratio of the peak intensities for the reduced (SH; 19.437 Da) and dimedone-labeled, oxidized (SOH; 19.577 Da) protein species in the deconvoluted ESI-MS spectra

produce a chemically stable 2,4-dinitrophenylhydrazone (DNP) which absorbs ultraviolet light [13]. These hydrazones can be detected spectrophotometrically at an absorbance of 370 nm, thus allowing the quantification of carbonylated proteins [14]. Since nucleic acids also contain carbonyl groups, a complete removal of nucleic acids is needed for reliable carbonyl group quantification [15]. As an alternative method to analyze protein carbonylation, 1D–SDS-PAGE followed by Western blot immunoassay with specific anti-DNPH antibody is presented. The derivatization reaction with DNPH may be performed directly before SDS-PAGE. This semiquantitative technique provides a more sensitive and specific detection of carbonylated proteins in context of applied redox-dependent stresses ex vivo.

3.2.1 Spectrophotometric Quantification of Protein Carbonyl Groups

Nucleic Acid Precipitation

1. For each measurement two replicates of each sample with at least 0.5 mg of protein are required. One of the samples will be derivatized with DNPH, the other will serve as blank. Use the same volume for every protein extract (e.g., 200 µL). When a volume other than 200 µL is used, adjust the volumes of other reagents accordingly.
2. Incubate the samples with 0.03% (v/v) Triton X-100 and 1% (w/v) streptomycin sulfate for 20 min on ice to remove the nucleic acids.

Derivatization of Carbonyl Groups and Protein Precipitation

1. Centrifuge at 20,000 × *g* at 4 °C and incubate the supernatants (200 µL) with 300 µL of 10 mM DNPH in 2 M HCl for 1 h at room temperature. The blanks are incubated in 2 M HCl instead of the derivatization solution.

Table 1
H_2O_2-dependent sulfenic acid formation of PrxIIE and cysteine variants using dimedone

	PrxIIE WT		PrxIIE C121S		PrxIIE C146S		PrxIIE C121S/C146S	
Treatment	**Mass [kDa] ± SD**	**Cys modification**	**Mass [kDa] ± SD**	**Cys modification**	**Mass [kDa] ± SD**	**Cys modification**	**Mass [kDa] ± SD**	**Cys modification**
DTT (control)	19,438.02 ± 0.42	None (SH)	19,422.10 ± 0.14	None (SH)	19,422.04 ± 0.59	None (SH)	19,405.56 ± 0.15	None
1 µM H_2O_2	19,438.08 ± 0.35	None (SH)	19,422.18 ± 0.22	None (SH)	19,421.84 ± 0.38	None (SH)	19,405.74 ± 0.20	None
2 µM H_2O_2	19,437.74 ± 0.13 19,576.50 ± 0.42	None (SH) **Oxidation (SOH)*** **	19,422.16 ± 0.26	None (SH)	19,422.44 ± 0.11 19,561.60 ± 0.45	None (SH) **Oxidation (SOH)*** **	19,405.78 ± 0.30	None
4 µM H_2O_2	19,437.90 ± 0.58 19,576.12 ± 0.52	None (SH) **Oxidation (SOH)*** **	19,422.08 ± 0.14	None (SH)	19,422.32 ± 0.17 19,561.10 ± 0.74	None (SH) **Oxidation (SOH)*** **	19,405.98 ± 0.28	None
8 µM H_2O_2	19,437.67 ± 0.41 19,576.40 ± 0.45	None (SH) **Oxidation (SOH)*** **	19,422.08 ± 0.32	None (SH)	19,422.74 ± 0.61 19,561.08 ± 0.51	None (SH) **Oxidation (SOH)*** **	19,405.82 ± 0.21	None
10 µM H_2O_2	19,437.88 ± 0.40 19,576.10 ± 0.61	None (SH) **Oxidation (SOH)*** **	19,422.34 ± 0.15	None (SH)	19,422.10 ± 0.56 19,561.04 ± 0.55	None (SH) **Oxidation (SOH)*** **	19,406.04 ± 0.13	None

Proteins were reduced with DTT, desalted and treated with H_2O_2 and dimedone for 30 min at RT and then analyzed by ESI-MS. Generation of dimedone-labeled Cys increases the mass of the protein by 140 Da. PrxIIE contains two cysteines at positions 121 and 146, respectively. To test for the cysteine residue at which oxidation occurs, Cys-Ser mutated PrxIIE variants were analyzed. The data reveal the peroxide concentration dependent sulfenylation of the peroxidatic Cys121. Significant difference to controls (T-test): *** $p < 0.001$.

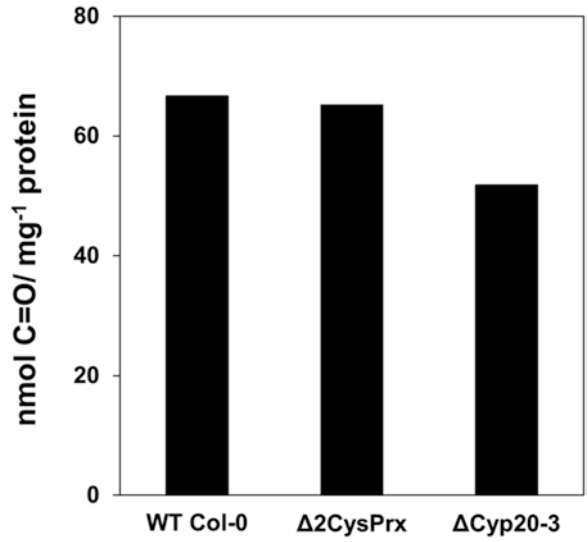

Fig. 5 Quantification of carbonylated proteins derivatized with DNPH. *Arabidopsis thaliana* WT (WT Col-0), 2-cysteine peroxiredoxin mutant (Δ2CysPrx) and cyclophilin 20–3 mutant (ΔCyp20-3) plants were grown for 5 weeks and then stressed for 1 h at 42 °C. Estimated values are in the range as previously reported [14]

2. Add ice-cold 100% (w/v) TCA to a final 10% (v/v) TCA concentration and vortex immediately to avoid aggregation of precipitated proteins. The precipitation is performed overnight at −20 °C.
3. Centrifuge at 20,000 × *g* at 4 °C for 10 min, decant the supernatant and wash the precipitates three times with ice-cold ethanol–ethylacetate 1:1 (v/v) solution. Tap the tubes on a clean paper towel to remove residual washing solution without disturbing the pellet.
4. Dissolve each protein precipitate (derivatized and blank samples) in 500 μL 6 M guanidine hydrochloride in 20 mM potassium phosphate buffer (pH 2.3). The samples are ready for spectrophotometric measurements at 280 nm and 370 nm (Fig. 5).

Spectrophotometric Quantification

1. Before and between the spectrophotometric measurements all Quartz cuvettes should be cleaned with washing solution (6 M guanidine hydrochloride, 20 mM potassium phosphate buffer, pH 2.3).
2. Measure the absorbance of each DNPH-treated sample and their respective blanks (without DNPH) at wavelengths of 280 nm and 370 nm.
3. For later calculation and quantification of protein carbonyl groups use a molar absorption coefficient for aliphatic hydrazones at 370 nm of 22,000 M^{-1} cm^{-1}. Estimation of

protein content in the samples is done by using an average molar absorption coefficient at 280 nm of 50,000 M^{-1} cm^{-1} (*see* **Note 2g**).

3.2.2 OxyBlot

DNPH-Derivatization of Protein Mixture

1. Fifteen to twenty micrograms of protein is needed for the derivatization with DNPH. Prepare two aliquots of each sample with a final concentration of 5 μg/μL. One aliquot will be treated with DNPH. The second aliquot will serve as a negative control by using the 1× derivatization-control solution instead of the 1× DNPH solution. In order to visualize all proteins, a third aliquot can be prepared for protein separation via SDS-PAGE and protein staining with Coomassie Brilliant Blue G-250.
2. Transfer 5 μL of protein samples (5 μg/μL) into new 1.5-mL eppendorf tubes. If other volumes than 5 μL are used, be sure to scale up the volume of subsequent reagents accordingly.
3. Denature each 5 μL aliquot by adding 5 μL of 12% (w/v) SDS solution to a final concentration of 6% (w/v) SDS.
4. Add 10 μL of 1× DNPH Solution to one of the aliquots and 10 μL of 1× Derivatization control solution to the negative control samples.
5. Incubate both tubes at room temperature for 15 min. Do not allow the reaction to proceed more than 30 min as unspecific reactions may occur.
6. Add 7.5 μL of neutralization solution to each sample.
7. Add 5% (v/v) of 2-mercaptoethanol in order to reduce the proteins (*see* **Note 2c**).

SDS–Polyacrylamide Gel Electrophoresis

1. These instructions assume the use of an SDS-PAGE system with gels of 18 cm (width) × 10 cm (height) × 1 mm (thickness). The volumes can be easily adapted to other formats.
2. Clean all components of the gel electrophoresis system (e.g., the glass plates, spacers and combs) with 70% ethanol and a lint-free tissue (e.g., Kimwipes).
3. Assemble the system according to the manufacturer's recommendations.
4. Prepare 20 mL of 12% separating gel by mixing 6.9 mL water, 4.9 mL separating gel buffer, 8 mL acrylamide solution (*see* **Note 2d**), 20 μL TEMED, and 133 μL APS solution for each gel. The polymerization process will start as soon as APS and TEMED have been added.
5. Pour the gel between the plates carefully, overlay with 1 mL of 100% isopropanol, and wait until the gel is polymerized (takes approximately 20 min).

6. Pour off the isopropanol and rinse twice with distilled water. Remove the water completely using a lint-free tissue.
7. Prepare 10 mL of 6% stacking gel by mixing 5.3 mL water, 2.5 mL stacking gel buffer, 2 mL acrylamide solution, 10 μL TEMED, and 100 μL APS solution for each gel.
8. Pour the stacking gel and carefully insert the comb, avoid the introduction of air bubbles.
9. Once the stacking gel is polymerized (takes approximately 20 min), assemble the gel electrophoresis system by attaching the gel to the chamber and fill the reservoir chambers with 1× running buffer. After removing the comb, wash the wells with 1× running buffer using a Hamilton syringe.
10. Do not heat the samples prior to loading into the gel. It is not necessary to add 5× gel loading buffer to the samples, since the glycerol (32%, w/v) in the neutralization solution makes the samples dense enough to sink to the bottom of the well.
11. If a third aliquot is prepared, add 5× gel loading buffer containing 100 mM DTT to final 1× gel loading buffer (e.g., 25 μL sample and 6,25 μL 5× gel loading buffer with reducing agent). Heat the samples at 95 °C for 5 min, cool on ice and centrifuge briefly to remove drops from the lid.
12. Add 5 μL of the mixture of standard proteins with attached DNP residues to 22.5 μL of 1× gel loading buffer. This molecular weight protein standard will serve as an internal positive control.
13. Apply 27.5 μL of sample per well using the Hamilton syringe.
14. Run the gel at constant current (60 mA) until the running front reaches the bottom.

Western Blot and Immunodetection of Carbonyl Groups

1. Cut 6 blotting absorbent filter papers and the nitrocellulose membrane (0.45 μm in pore size) fitting the size of the gel.
2. Incubate the gel and the nitrocellulose membrane for 5 min in cathode buffer and 1× anode buffer, respectively.
3. Prepare a semidry transfer sandwich of blotting absorbent filter papers, nitrocellulose membrane and gel (ensure there are no air bubbles). Soak therefore the filter papers in transfer buffers as followed:
   (a) Two filter papers in 10× anode buffer.
   (b) One filter paper in 1× anode buffer.
   (c) Three filter papers in cathode buffer.
4. Transfer the proteins from the gel onto the nitrocellulose membrane via blotting for 30 min using 2 mA/cm^2 of membrane.

5. Remove the membrane and block nonspecific binding sites with blocking solution (1× PBS containing 1% (w/v) BSA) at room temperature for 1 h with gentle shaking.
6. Dilute the 1° anti-DNP antibody stock 1:150 in blocking solution (*see* **Note 2f**). Incubate the membrane in the 1° antibody solution for 1 h with gentle shaking at room temperature or at 4 °C overnight. Use 0.15 mL/cm^2 of membrane.
7. Wash the membrane with 1× PBST for 15 min, then twice for 5 min.
8. Dilute the 2° anti-rabbit IgG antibody (HRP-conjugated) stock 1:300 in blocking solution (*see* **Note 2f**). Incubate the membrane in the 2° antibody solution for 1 h with gentle shaking at room temperature. Use 0.15 mL/cm^2 of membrane.
9. Wash the membrane as in **step 7**.
10. Prepare the chemiluminescent substrate. Use 0.025 mL/cm^2 of membrane.
11. Drain the membrane on filter towels to remove 1× PBST as far as possible and place the membrane air bubble-free an on saran wrap.
12. Pipette the chemiluminescent substrate completely evenly on the membrane. Cover the membrane immediately with another layer of saran wrap (air bubble-free) and incubate for 2 min in dark. Carefully squeeze out the complete liquid with a lint-free tissue.
13. All further steps are performed in the dark room. Cut Kodak Scientific Imaging films in size of the membrane.
14. Carefully place the film without blurring on the membrane and mark the corners (for later prestained protein ladder tracing). Select an exposure time with clear signal and low background (e.g., 30 s–15 min).
15. Develop the film in the developer solution (1:4 dilution of developer concentrate). Select at this point also a develop time with clear signal and low background.
16. Rinse the film in water and incubate in fixing solution for at least 3 min.
17. Let the film dry and trace the prestained protein ladder. Semiquantitative and comparable analysis can be performed using an image-processing application (e.g., ImageJ) (Fig. 6).

Coomassie Brilliant Blue G-250 Staining

1. Carefully remove the complete stacking gel after SDS–polyacrylamide gel electrophoresis and put the gel into a clean box with 50 mL staining solution. Ensure the whole gel is covered.
2. Incubate the gel in the staining solution overnight with gentle shaking (*see* **Note 2h**).

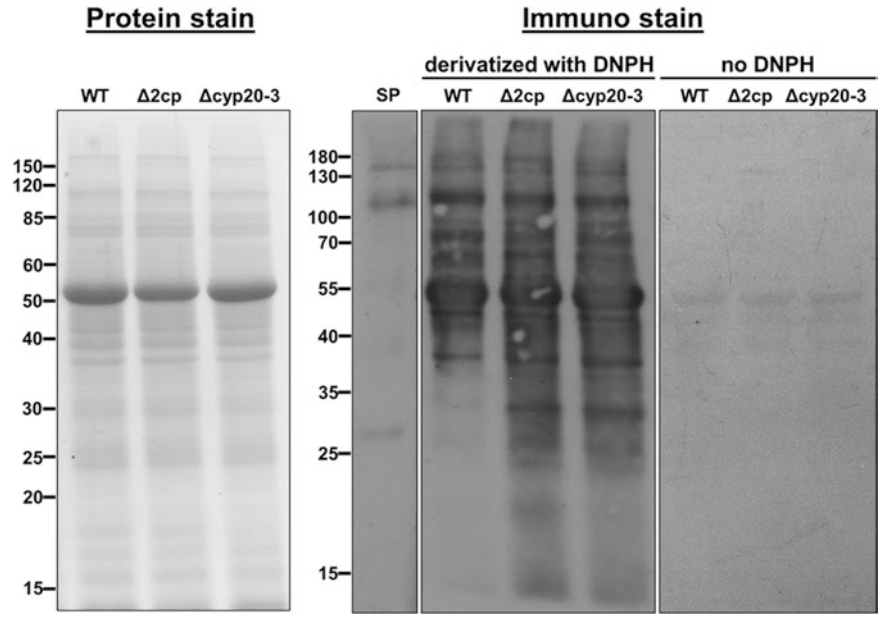

Fig. 6 Visualization of protein carbonyl groups in heat-stressed *Arabidopsis thaliana* WT Col-0 (WT), 2-cysteine peroxiredoxin mutant (Δ2cp) and cyclophilin 20–3 mutant (Δcyp20–3) by OxyBlot. Plants were grown for 5 weeks and followed by heat stress at 42 °C for 1 h. Protein extracts of leaves (25 μg) were treated with or without 2,4-dinitrophenylhydrazine (DNPH) and separated by SDS-PAGE. Untreated samples were visualized by Coomassie Brilliant Blue staining (*left*). Protein carbonyl groups were detected using an anti-DNP antibody (1:75 dilution). Standard proteins with attached DNP-residues (SP; 5 μL) were used as positive control. Molecular weight markers are indicated in the panel on the left. DNPH treated Δ2cp and Δcyp20–3 samples show higher signal intensity in the range of 15–55 kDa compared to the WT. This result indicates that more proteins are carbonylated in mutants after heat stress application. Negative controls (*right* immuno stain) show a slight crossreactivity of the anti-DNP antibody with proteins in the range of 55 kDa

3. Discard the staining solution and rinse the gel with water.
4. Destain the gel with destaining solution until clear bands with no background are visible (*see* **Note 2h**). Periodically change the solution to ensure a faster destaining process.

3.3 Redox-Dependent Interaction Studies of Proteins by ITC

Isothermal titration microcalorimetry is a versatile tool to obtain quantitative biochemical and biophysical information. Its strength is based on the laws of thermodynamics which allow for characterizing the entropy (S) and Gibbs free energy (G) of a dynamic but well-defined system as given in the Gibbs–Helmholtz Eq. (1).

$$\Delta G = \Delta H - T\Delta S \tag{1}$$

(T = absolute temperature, H = enthalpy)

$$K_c = \frac{k^r}{k^f} = \frac{C^c}{P^p L^l} \tag{2}$$

(P = protein, L = ligand, C = protein–ligand complex)

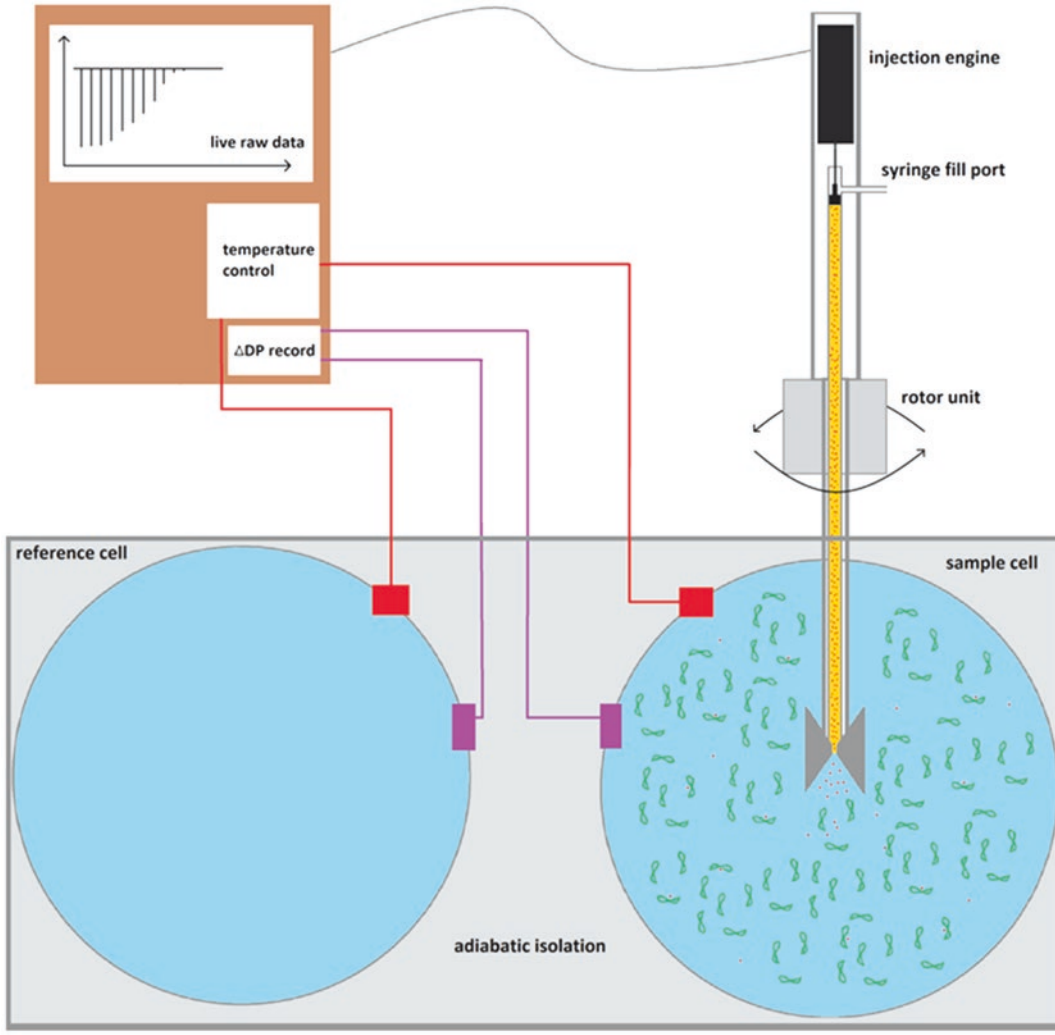

Fig. 7 Schematic illustration of ITC devices. The lower schematic depicts the setup with measuring and reference cell, the syringe for repeated injections and the exemplary readout

The Gibbs energy is connected to the reaction equilibrium (Eq. 2).

$$\Delta G = -RT \ln K_c \tag{3}$$

(R = gas constant)

An ITC measurement gives insight into binding affinities, mechanisms and stoichiometry, enthalpy changes and kinetics based on Eqs. (1) and (3). The device is able to sense ΔT = 0.001 between a reference cell and the sample cell while both are adiabatic isolated (*see* Fig. 7). Precisely defined injections of target proteins or ligands into the sample cell will potentially result in a binding (or not) and its energy signature. Collecting input

information and experimental data, software is able to calculate ΔG, ΔS and therefore ΔH for a specific interaction set as well as binding affinities in a range of $K_A = 10^2$–10^{10} M^{-1} (For more details check [16–18]).

3.3.1 Protein Preparation

1. Protein concentrations need to be optimized; here 50–70 μM are chosen.
2. Redox-state is adjusted by incubation for 2 h with DTT or H_2O_2 at a final concentration of 10 mM DTT/H_2O_2 in protein solution (*see* **Note 3e**).
3. Treated protein solutions are dialyzed against 35 mM HEPES, pH 8.0 overnight at 4 °C. Adjust final DTT concentration in dialysis buffer to stabilize the reducing conditions (*see* **Notes 3a** and **3f**). If possible, proteins used in interaction measurements should be dialyzed in the same buffer flask for identical background. Stirring at 250 revolutions per minute improves buffer substitution.
4. Filtration of protein solutions and buffers removes particles or aggregates.
5. Determination of protein concentration to compensate for dialysis dilution.
6. Aliquots are prepared with a minimum of fivefold higher concentrated of injected protein than receiving solution in the cuvette (*see* **Note 3g** and **3h**). Dialyses buffer from **step 3** is used for dilution. For optimal loading, 600-μL aliquots are loaded in the syringe and 2-mL volumes in the sample cell. Both solutions are frozen in liquid nitrogen to retain redox conditions and only thawed out prior to use (*see* **Note 3i**).

3.3.2 Titration

1. No preheat phase is needed for ITC devices. Connection to PC and recognition by analysis software is assumed. Room temperature and ventilation should be observed to be constant.
2. Cleaning of syringe and cells is done with MilliQ water 3–5 times and additionally twice with buffer, except reference cell for replicates. Syringe cleaning demands raising plugger tip above the actual fill port by clicking on “Open Fill Port” in the software menu.
3. Aliquots are thawed or directly used after dialysis and quantification. Degassing is done for 5–10 min with smooth stirring at 400 rpm (*see* **Note 3j**).
4. Sample loading is done identical to cleaning. Cells are loaded up to a metal ring surrounding the loading hole with buffer or protein solution (around 1.4 mL). Avoid trapping of gas in the syringe during loading. 1 mL glass tubes fit into the pipette

stirrer tip and are used for injectant loading (around 400 μL). Press "Close Fill Port" when done. Exact sample volumes in syringe are ensured by pressing "Purge Refill" in the software menu (*see* **Note 3k**).

5. Running parameters are entered into software interface. Experimental Parameters: "Total Number of Injections": 40; "Cell Temperature": 25 °C; "Reference Power": 10 μcal/s; "Initial Delay": 60 s; "Syringe/Cell concentrations": 0.05/0.01 mM; "Stirring Speed": 580 rpm.
6. Label experiment with necessary details in "Data File Name".
7. Injection Parameters: "Volume": 10 μL; "Duration": 10 s; "Spacing": 60 s; "Filter Period": 2 s. Set "All Same" in "Edit Mode" and keep rest to default (*see* **Note 3l**).
8. If loading and parameter setup is complete, the syringe can be inserted into sample cell. Clean the pipette tip on the outside before starting the titration. Press "RUN" to start (*see* **Note 3m**).

3.3.3 Data Evaluation

1. Use Origin software and VP-ITC plug-in with .itc files. Minimize inner window and start "ITC Data Analysis" in submenu "Format" followed by "Menu". Press "Read Data..." to find and open raw data of an .itc-experiment.
2. Automated function fitting and calculations will be done by pressing "One set of sites" for most interactions (*see* **Note 3n**).
3. Regression curves are corrected with further fitting iterations by clicking on "100 Iter." or "1 Iter." until "Chi-Sqr" is stable. "Fitting Function Parameters" dialog box is used to set N, K, and H and improve fitting (*see* **Note 3o**).
4. An output window containing important information (n, K_d, and H) appears in the raw data sheet. For publication figures copy data label, execute "Final Figure" in "ITC" submenu and paste in suitable location (*see* Figs. 8 and 9). Changing axis scale can facilitate reading of figures.

4 Notes

1. Identification of sulfenic acid derivatives in proteins using dimedone.
   (a) Preparing aliquots of DTT and/or storage at −20 °C for single use is recommended, because DTT is highly prone to oxidation by air.
   (b) DTNB is soluble at neutral pH values. At higher concentrations neutralization with NaOH is required. Too much NaOH causes a sudden deepening of the yellow color so

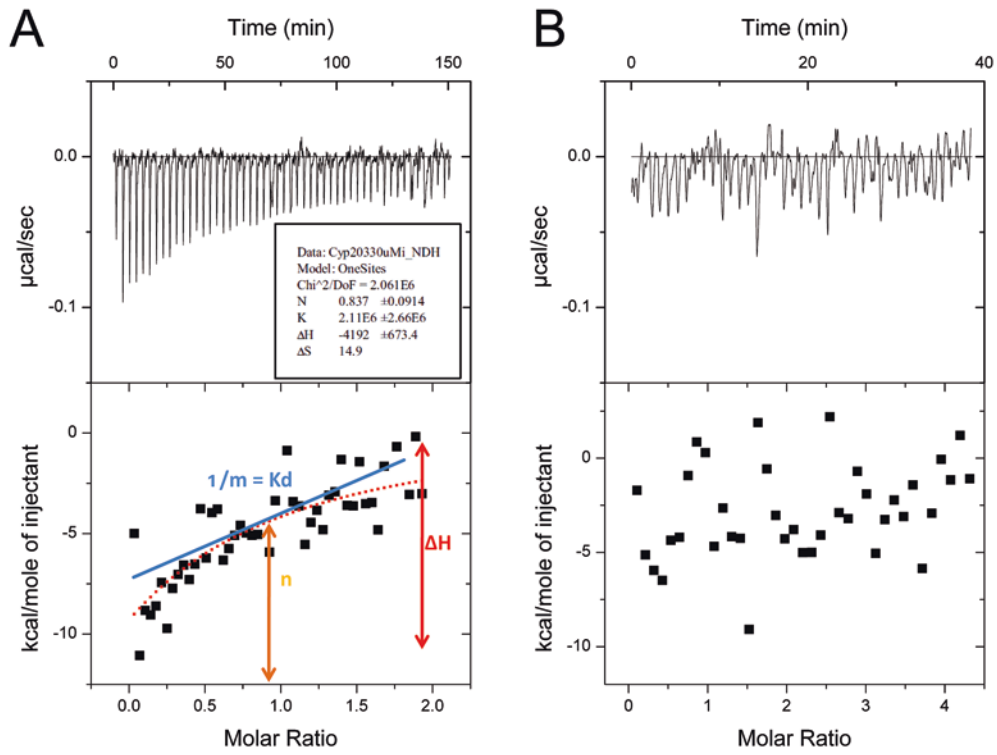

Fig. 8 Finalized figure for cyclophilin 20–3/2-cysteine peroxiredoxin interaction under reducing (**A**) and oxidizing conditions (**B**). Raw titration data are displayed in upper part while integrated enthalpy values and fitting curve in lower part. Cyclophilin 20–3 (60 µM) was titrated into 2-cysteine peroxiredoxin (10 µM). Weak interactions of the reduced forms indicate low affinity. Valuable data extraction is indicated in (**A**) for *n*, K_d and ΔH

that a positive reaction is masked; too little NaOH and the reagent might not be alkaline enough to react quickly with thiol groups.

(c) Be sure to thoroughly resuspend the pellet by pipetting or vortexing.

(d) Allow the acetone to evaporate from the open tube at room temperature. Do not overdry pellet, otherwise it may not dissolve properly. Instead of air drying, the pellet can be dried by inverting the tube and placing it on a Kimwipes for 15 min at 37 °C.

(e) Samples can be shock-frozen in liquid N_2 and stored at −80 °C prior to mass spectrometric analysis.

(f) For the ~19 kDa peroxiredoxin II E (At3g52960) a range between 650 and 1200 *m/z* achieved good results.

(g) Ionization depends on the protein. Instead of the buffer mentioned above a (80%) acetonitrile, (0.1%) trifluoroacetic acid solution can be used.

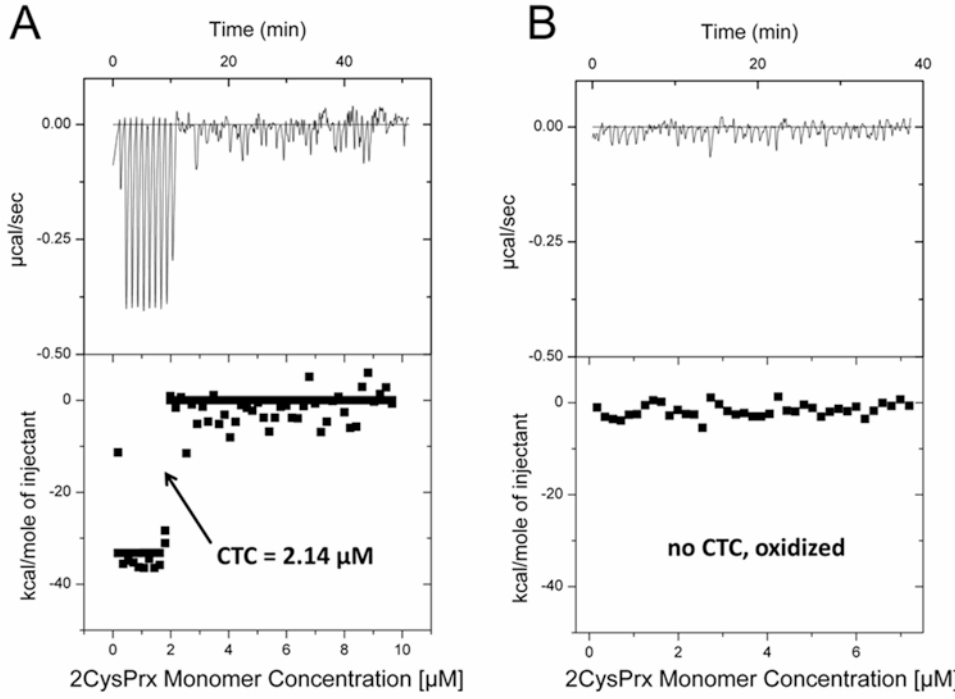

Fig. 9 Exemplary measurements for a redox-dependent conformation analysis. 2-cysteine peroxiredoxin exists in five distinct conformations. A shift from reduced dimer to decamer form is induced at increasing dimer concentrations. Similar to the critical micelle concentration of detergents, a critical transition concentration of 2.14 µM was determined for 2-cysteine peroxiredoxin at pH 8 [19, 20]

2. Spectrophotometric DNPH-assay and OxyBlot to access carbonylated proteins.
   (a) To dissolve the correct amount of DNPH in 2 M HCl it is recommended to crystallize the moist solid [21]. For this, heat 2 M HCl to 50 °C. Dissolve DNPH as much as possible in hot HCl and let the solution cool to room temperature. Collect the crystals by filtration through a filter paper and dissolve them in fresh 2 M HCl to a final concentration of 10 mM DNPH. Stock solutions are stable for months.
   (b) TCA is a strong acid and causes severe burns. Handle with care and wear appropriate personal protective equipment.
   (c) Other reducing agents than 2-mercaptoethanol may be used (e.g., DTT at a final concentration of 1–100 mM). No adverse effect on the reaction with DNPH and following steps has been reported.
   (d) Acrylamide is a toxin and may cause mutagenic effects. Handle with care and use personal protective equipment.

(e) Since Na_2HPO_4 has a poor solubility in water, it is necessary to dissolve Na_2HPO_4 first. When solubilized, add the other components of 10× PBS and dissolve them in water.

(f) According to the manufacturer's manual of the OxyBlot Protein Oxidation Detection Kit (Merck Millipore, Darmstadt, Germany), the indicated antibody dilutions should be adequate to detect femtomoles of carbonyl groups. However, in case of low signal the antibody dilutions may be decreased.

(g) You may use the molar absorption coefficient for proteins at 280 nm of 50,000 M^{-1} cm^{-1} if the molar absorption coefficient of the protein is not known. For more details, *see* [13]. However, it is recommended to use another assay to determine the protein concentration more precisely.

(h) Staining and destaining will be accelerated if the gel in the staining or destaining solution is heated in the microwave (600 W) for approximately 30 s (!) without boiling.

3. Redox-Dependent interaction studies of proteins by ITC.

(a) Dialysis and filtration are crucial steps for ITC measurement. Due to its high sensitivity, protein aggregates and particles and even small differences in buffer composition may disturb the equilibration of the system and might cover the real energy signature. Consider protein and ligand properties prior to dialysis. Choose the right dialysis tubing (MWCO) and pore size (filtration).

(b) DTT (1 M) in water is oxidized by air and by repeated freeze/thaw cycles. Therefore it is recommended to prepare freshly or to use aliquots stored at −20 °C in tightly sealed containers.

(c) The ITC reaction cells are coated with a high conductive and corrosion-resistant material. Even though ions or organic solvents may pollute the poorly accessible heat chambers. Using pure water for cleaning and preparation minimizes false-positive signals and eases reproducibility.

(d) Due to high sensitivity of ITC analysis only work with pure samples can result in valid data. Proteins should be checked on SDS-PAGE by appropriate staining methods like silver staining. If heterologous expression was used to generate proteins a purification-tag might influence interaction. Cleavage is highly recommended and must again be confirmed. Various methods for further protein purification can be applied to increase target concentration like ion-exchange, size-exclusion, or affinity chromatography.

(e) Oxidation and reduction processes are protein-specific. Adjusting time and especially reductant concentration might be necessary.

(f) Reduced proteins must be stable during dialysis, so a small amount is helpful. Concerning buffers it is obligatory to use same buffer for reduced/oxidized interaction partners and dilute only with filtered dialysis buffer. Even small dilution effects can interfere with ITC analysis. Choice of buffer may vary depending on pH optimum for proteins and should be checked for protonation signals lowering the signal to noise ratio.

(g) Suitable concentrations should be considered beforehand. Optimal graphs can be obtained if targeting for a *c*-value of 20–100:

$$c = K_a c_{cell} n$$

(K_a = binding constant, c_{cell} = cell sample concentration, n = stoichiometry)

(h) Use concentrations equivalent to 10–50 times dissociation constant (K_d) of the sample cell molecule if binding constant is unknown. It is further recommended to use high concentration of proteins for low affinities and low concentrations of proteins for high affinities in case of protein–ligand binding. Consider collecting and reisolating the molecules of interest from the sample cell if preparation is difficult.

(i) This step is helpful if oxidation of reduced samples occurs in air.

(j) Gas bubbles have a negative influence on the titration, decrease the signal to noise ratio and may cause readout artifacts during the measurement. Air bubbles should be removed carefully.

(k) A software controlled refill is necessary in order to control titration and syringe volume limits.

(l) Settings can be adjusted to improve reaction performances. Besides concentration dependencies for optimal curve output and fitting, also the injection and volume can be modified to reach 1:1 stoichiometry after 10–15 injections. Injection spacing and duration should be set to allow ITC heating or cooling to reach the base line again in time. Reference power depends on exothermic (30 µcal/s) and endothermic (2 µcal/s) activities in the interacting sample. In detail, reference power is adjusted to keep the differential power (DP) positive during runs.

(m) Titration process is automated from here on. Single titrations start after DP and temperature adjustment for cells. The time for every run depends on time-related settings (duration, spacing, injections) and temperature equilibration.

(n) "One set of sites" can be used in many interaction evaluations when all binding sites feature same K and H values. For different interaction sites "Two set of sites" can be used while adjusting $H1/2$ and $K1/2$ to a fitting curve.

(o) Obtained curve can be read out for n, K_a, and ΔH (*see* Fig. 8a). More models like Sequential Binding Sites, Competitive Binding, Dissociation and Enzyme Assays are available.

References

1. Mieyal JJ, Chock PB (2012) Posttranslational modification of cysteine in redox signaling and oxidative stress: focus on s-glutathionylation. Antioxid Redox Signal 16:471–475
2. Walsh CT, Garneau-Tsodikova S, Gatto GJ (2005) Protein posttranslational modifications: the chemistry of proteome diversifications. Angew Chem Int Ed Engl 44:7342–7372
3. Seo J-W, Lee K-J (2004) Post-translational modifications and their biological functions: proteomic analysis and aystematic approaches. J Biochem Mol Biol 37:35–44
4. Mock H-P, Dietz K-J (2016) Redox proteomics for the assessment of redox-related posttranslational regulation in plants. Biochim Biophys Acta 1864:967–973
5. Woo HA, Kang SW, Kim HK, Yang K-S, Chae HZ, Rhee SG (2003) Reversible oxidation of the active site cysteine of peroxiredoxins to cysteine sulfinic acid. Immunoblot detection with antibodies specific for the hyperoxidized cysteine-containing sequence. J Biol Chem 278:47361–47364
6. Suzuki YJ, Carini M, Butterfield DA (2010) Protein carbonylation. Antioxid Redox Signal 12:323–325
7. Lennicke C, Rahn J, Lichtenfels R, Wessjohann LA, Seliger B (2015) Hydrogen peroxide - production, fate and role in redox signaling of tumor cells. Cell Commun Signal 13:39
8. Bartosz G (2009) Reactive oxygen species: destroyers or messengers? Biochem Pharmacol 77:1303–1315
9. Gupta V, Carroll KS (2014) Sulfenic acid chemistry, detection and cellular lifetime. Biochim Biophys Acta 1840:847–875
10. Dalle-Donne I, Rossi R, Giustarini D, Milzani A, Colombo R (2003) Protein carbonyl groups as biomarkers of oxidative stress. Clin Chim Acta 329:23–38
11. Dalle-Donne I, Scaloni A, Butterfield DA (eds) (2006) Redox proteomics: from protein modifications to cellular dysfunction and diseases, Wiley-interscience series in mass spectrometry. Wiley-Interscience, Hoboken, N.J
12. Havé M, Leitao L, Bagard M, Castell J-F, Repellin A, Adams W (2015) Protein carbonylation during natural leaf senescence in winter wheat, as probed by fluorescein-5-thiosemicarbazide. Plant Biol (Stuttg) 17:973–979
13. Levine RL, Williams JA, Stadtman ER, Shacter E (1994) Carbonyl assays for determination of oxidatively modified proteins. Methods Enzymol 233:346–357
14. Romero-Puertas MC, Palma JM, Gomez M, Del Rio LA, Sandalio LM (2002) Cadmium causes the oxidative modification of proteins in pea plants. Plant Cell Environ 25:677–686
15. Levine RL, Garland D, Oliver CN, Amici A, Climent I, Lenz AG et al (1990) Determination of carbonyl content in oxidatively modified proteins. Methods Enzymol 186:464–478
16. Todd MJ, Gomez J (2001) Enzyme kinetics determined using calorimetry: a general assay for enzyme activity? Anal Biochem 296:179–187
17. Chaires JB (2008) Calorimetry and thermodynamics in drug design. Annu Rev Biophys 37:135–151
18. Freyer MW, Lewis EA (2008) Isothermal titration calorimetry: experimental design, data dnalysis, and probing macromolecule/ligand binding and kinetic interactions. In: Biophysical tools for biologists, volume one: in vitro techniques, vol 84. Elsevier, Amsterdam; Boston, pp 79–113
19. Barranco-Medina S, Kakorin S, Lázaro JJ, Dietz K-J (2008) Thermodynamics of the dimer–decamer transition of reduced human and plant 2-Cys peroxiredoxin. Biochemistry 47:7196–7204
20. Liebthal M, Strüve M, Li X, Hertle Y, Maynard D, Hellweg T et al (2016) Redox-dependent conformational dynamics of decameric 2-cysteine Peroxiredoxin and its interaction with Cyclophilin 20-3. Plant Cell Physiol 57:1415–1425
21. Matsui K, Sugimoto K, Kakumyan P, Khorobrykh SA, Mano J (2010) Volatile oxylipins and related compounds formed under stress in plants. In: Armstrong D (ed) Lipidomics. Humana Press, Totowa, NJ, pp 17–28

Chapter 13

Zymographic Method for Distinguishing Different Classes of Superoxide Dismutases in Plants

Ashwini R. Jamdhade, Ramanjulu Sunkar, and Vandana K. Hivrale

Abstract

In plants, especially in chloroplasts, superoxide radical is generated when an electron is transferred to dimolecular O_2 due to decreased activity of Photosystem I. The superoxide (O_2^-) radical accumulation is more rampant in plants exposed to abiotic stresses due to oxidation of photosystem components. Excessive superoxide radical accumulation will lead to oxidative damage to the cellular macromolecules. The ubiquitous superoxide dismutases (SODs) represent critical enzymatic antioxidant system present in cells, which can catalyze the disproportion of superoxide (O_2^-) radical rapidly into hydrogen peroxide (H_2O_2) and molecular oxygen. Depending on the metal cofactor present, the plant SODs are classified into Cu/ZnSOD, MnSOD, and FeSOD. The activity of SODs can be quantified zymographically. Additionally, using this method, different classes of SODs can be distinguished by using H_2O_2, KCN, and NaN_3.

Key words Classes of SODs, SOD activity, Electrophoresis, NBT, Riboflavin, Characterization of SOD

1 Introduction

In almost all aerobic organisms, superoxide dismutases (SOD) (EC1.15.1.1) play defensive roles against the toxic reactive oxygen species (ROS) accumulation and represent the most important antioxidant system in plant cells. These enzymes eliminate toxic oxygen (superoxide radical) produced as a result of decreased PSI activity or xanthine oxidase, NADPH oxidase, and alternate oxidase activities [1] or even as byproduct of cellular respiration [2, 3]. The activity of different classes of superoxide dismutases relies upon a specific redox active metal ion. Depending on the metal cofactor present, the plant SODs are classified into Cu/ZnSOD, MnSOD, and FeSOD [4].

The reaction of SOD is as follows:

$$2H^+ + 2\ O_2^- \rightarrow H_2O_2 + O_2$$

Ramanjulu Sunkar (ed.), *Plant Stress Tolerance: Methods and Protocols*, Methods in Molecular Biology, vol. 1631,
DOI 10.1007/978-1-4939-7136-7_13,

The produced hydrogen peroxide is then detoxified by catalase or peroxidase [5]. In plants, chloroplasts and mitochondria are major sites of superoxide radical production [6]. Different classes of SOD enzymes and their isoforms can be detected by using electrophoresis method on 10% polyacrylamide gel and visualized by using NBT and riboflavin. NBT competes with enzyme for free radical. Free radicals are generated by riboflavin in presence of TEMED and oxygen, by the action of enzyme white colored activity bands are visualized against dark blue background in presence of light condition.

Different classes of SOD enzymes can be distinguished by using different inhibitors. NaN_3 inhibits FeSOD activity, whereas H_2O_2 inhibits both Cu/ZnSOD and FeSOD activities. MnSOD activity is not inhibited by either treatment. Thus, the SOD enzymes can be characterized by electrophoresis method in which the enzyme is preincubated with H_2O_2, KCN and sodium azide (NaN_3) for 20 min at 37 °C. This reaction mixture is then separated on a 10% polyacrylamide gel. After electrophoresis, the gel is processed for the photochemical reaction using NBT and riboflavin. The principle involved in detecting SOD activity is based on NBT reduction. Initially the gel is soaked in NBT solution and then in riboflavin solution. Afterward, exposing the gel to light causes the riboflavin to generate a superoxide radical flux in the presence of oxygen and TEMED. NBT and SOD in the gel competes for superoxide radical at the same time. At the locations where enzyme exists, the gel remains transparent in contrast to those areas without SOD where the gel becomes purple-blue due to NBT reduction.

2 Materials

Prepare all solutions using distilled water and analytical grade reagents. Prepare and store all reagents at room temperature (unless indicated otherwise). Follow all waste disposal regulations when disposing of waste materials.

1. Crude SOD enzyme extract isolated from plant species.
2. Buffer (0.15 M Tris–HCl, pH 7.5) for extracting the crude enzyme.
3. Resolving gel buffer: 1.5 M Tris–HCl, pH 8.8. Dissolve 181.7 g Tris in approximately 900 mL distilled water. Adjust the pH using HCl. Make up the final volume to 1 L. Store at 4 °C.
4. Stacking gel buffer: 1 M Tris, pH 6.8 (Dissolve 30 g of Tris in 200 mL distilled water and adjust the pH to 6.8 using HCl. Makeup the final volume to 250 mL with distilled water and store at 4 °C.

5. 30% acrylamide–bisacrylamide gel solution: Dissolve 30 g acrylamide and 1.04 g bisacrylamide in 50 mL of water using a magnetic stirrer and make the volume to 100 mL (*see* **Note 1**). Keep the solution away from sunlight and store at 4 °C (*see* **Note 2**).
6. Ammonium persulfate: 10% solution in water (*see* **Note 3**).
7. *N*, *N*, *N*, *N* -tetramethyl-ethylenediamine (TEMED). Store at 4 °C (*see* **Note 4**).
8. Stacking gel stock solution: Take 17 mL of acrylamide–bisacrylamide solution and add 12 mL of Stacking gel buffer to it and mix them together. Dilute it to 100 mL with distilled water and store in the refrigerator.
9. 10× Electrode buffer: Dissolve 30 g of Tris, 144 g of glycine in 800 mL distilled water and adjust pH to 8.3 and make the final volume to 1000 mL. Dilute to 1:10 with distilled water before use.
10. Sample buffer: 2.5 mL glycerol, 1.6 mL stacking gel buffer, few crystals of bromophenol blue and make up the final volume to 5 mL using distilled water.
11. Solution A [nitrobluetetrazolium (NBT)]: 1.23 mM NBT (Dissolve 0.123 g of NBT in 100 mL of distilled water).
12. Solution B [riboflavin and tetramethylethylenediamine]: 1 mg of riboflavin (0.028 mM) + 324 μL TEMED (28 mM) add to 100 mL of 0.1 M Tris–HCl (pH –7.8) [0.1 M Tris–HCL preparation—Dissolve 1.21 g Tris in 75 mL distilled water and adjust the pH to 7.8 using concentrated HCl and make the final volume to 100 mL).
13. H_2O_2 (100 mM): Add 6 μL of hydrogen peroxide to 5 mL of distilled water.
14. KCN (100 mM): Dissolve 0.0325 g of potassium cyanide in 5 mL of distilled water.
15. NaN_3 (100 mM): Dissolve0.0325 g of sodium azide in 5 mL of distilled water.

3 Methods

3.1 Extraction of Crude SOD Enzymes from Plant Tissues [7]

1. Harvest plant tissue and immediately freeze in liquid nitrogen.
2. Grind the tissue into fine powder using liquid nitrogen.
3. Mix with 3 mL of extraction buffer (0.15 M Tris–HCl, pH 7.5).
4. Centrifuge the samples 14,000 × *g* for 10 min at 4 °C.
5. Repeat the centrifugation for thrice to clear the debris.
6. Transfer the supernatant and use it for the enzyme activity determination.

3.2 Assembling the Glass Plates

1. Assemble the glass plate on a clean surface. Lay the longer glass plate (the one with spacer) down first and place the shorter glass plate on top of it.
2. Embed them into the casting frame and clamp them properly to make sure that the bottom ends of the glass plates are properly aligned.
3. Then place it on the casting stand.

3.3 Casting the Gel

1. 10% resolving gel: Take 12.5 mL distilled water and add 7.5 mL resolving gel buffer and 10 mL 30% acrylamide–bisacrylamide solution to it (*see* **Note 5**).
2. Add 100 μL of 10% APS and 20 μL TEMED to solution (just before pouring) and mix thoroughly. Pour the solution and add a layer of butanol or distilled water on top of the gel so as to level the poured gel.
3. Allow the gel to polymerize for 45 min to 1 h. After polymerization drain the butanol.
4. Stacking gel can be prepared by taking 10 mL of Stacking gel stock solution, add 100 μL APS and 20 μL TEMED and mix well and pour between the plates.
5. Place a comb in the stacking gel and allow it to polymerize for 30 min (*see* **Note 6**).

3.4 Running the Gel

1. To assemble, take out the gels from the casting frame and clamp them in the gel apparatus (Make sure that the short plate always faces inside).
2. When the plates are secured, place them in the gel running tank.
3. Then lock them properly in the cassette.
4. Fill the inner chamber of the tank with buffer (Now it is easy to remove the comb, since it is lubricated).
5. Remove the comb carefully without breaking the wells (Now the gel is ready to load samples).
6. Mix the samples (test and standard) with sample buffer in 1:2 ratio and load into each well with the help of micropipettes and then subject it to electrophoresis at 20 mA through the stacking gel for 15 min and at the constant current of 30 mA through the separating gel (*see* **Notes 7** and **8**).
7. Attach the power supply by putting the lid. Set the voltage up to 180 V and run for 1 h. Do not allow the dye front to go out of the gel.
8. After electrophoresis, remove the plate from the unit (a modified photochemical method of Beauchamp and Fridovich [1971] is used to locate SOD activities on gels).

9. Take 25 mL of 1.23 mM NBT (solution A) in a small tray and cover it with the help of aluminum foil so as to maintain the darkness and soak the gel for 15–20 min.
10. Then briefly wash the gel to remove the excess of reagent and soak it in 30 mL of 100 mM potassium phosphate buffer (pH 7.0) containing 28 mM TEMED and 2.8×10^{-2} mM riboflavin (solution B); carefully cover the tray with aluminum foil for another 15–20 min.
11. Briefly wash the gel again and then place it on a light box with a light intensity of 30 $m\text{Em}^{-2}$ s^{-1} for 15 min to initiate the photochemical reaction.
12. Transparent bands of SOD enzyme on purple colored gel can be observed.
13. Scan the gel to detect the SOD enzymes.

3.5 Characterization of SOD Enzyme [8]

1. Preincubate 30 µL of enzyme extract with 20 µL of H_2O_2 (100 mM), KCN (100 mM) and NaN_3 (sodium azide) (100 mM) in separate eppendorf tubes along with control (containing only enzyme) for 25–30 min at 37 °C (*see* **Note 9**).
2. Mix the samples with sample buffer in 1:2 ratio and load each sample into a well with the help of micropipettes and then subject it to electrophoresis at 20 mA through the stacking gel for 15 min and at the constant current of 30 mA through the separating gel.
3. After the electrophoresis subject the gel to the photochemical reaction using NBT and riboflavin to detect the SOD enzyme isoforms and their inhibition by respective inhibitors.
4. Take 25 mL of 1.23 mM NBT (solution A) in a small tray and cover it with an aluminum foil to maintain darkness and soak the gel for 15–20 min.
5. Then briefly wash the gel to remove the excess reagent and soak it in 30 mL of 100 mM potassium phosphate buffer (pH 7.0) containing 28 mM TEMED and 2.8×10^{-2} mM riboflavin (solution B). Carefully cover the tray with aluminum foil for another 15–20 min.
6. Briefly wash the gel again, and then place it on a light box with a light intensity of 30 $m\text{Em}^{-2}/s$ for 15 min to initiate the photochemical reaction.
7. Transparent bands of SOD enzyme in purple colored gel can be observed.
8. Scan the gel to detect the bands of SOD enzyme inhibition with reference to that of control.
9. Inhibition of bands by KCN indicates the presence of Cu/ZnSOD enzyme.

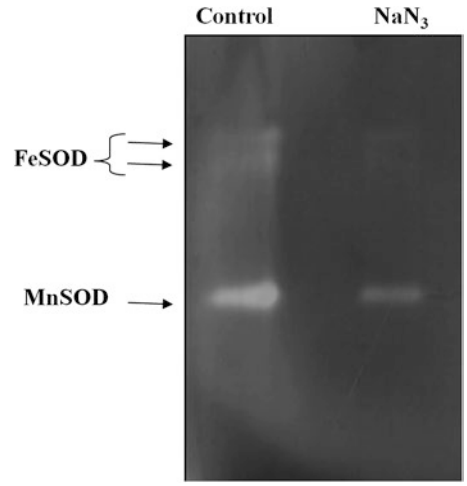

Fig. 1 Differentiation of FeSOD and MnSOD activities. NaN_3 inhibits FeSOD activity, but not MnSOD activity

10. Inhibition of bands by H_2O_2 indicates the presence of FeSOD and Cu/ZnSOD enzyme.
11. Inhibition of bands by NaN_3 (sodium azide) indicates the presence of FeSOD enzyme. An example is shown in Fig. 1.
12. If the bands are not inhibited by H_2O_2/KCN/NaN_3, then those bands correspond to the MnSOD in the sample.

4 Notes

1. Wear a mask when weighing acrylamide. Unpolymerized acrylamide is a neurotoxin and hence care must be taken to avoid skin contact.
2. The acrylamide solution can be stored at 4 °C for 1 month.
3. Prepare fresh APS each time.
4. Storing TEMED at 4 °C reduces its pungent smell.
5. The gel cassette is sealed at the base using 1% agarose. Overlaying the resolving gel of 10% followed by the layer of saturated butanol to prevent contact with atmospheric oxygen (which inhibits acrylamide polymerization) in addition to helping to level the resolving gel solution.
6. Before running the gel make sure that the gel, and samples are ready.
7. Centrifuging the samples prior to the run helps remove insoluble components, which could produce streaks in the protein lanes.

8. This allows you to visualize approximately where the sample is as it runs through the gel.
9. Potassium cyanide is highly toxic, so handle with extreme care and awareness.

Acknowledgment

ARJ gratefully acknowledges the BARTI, Pune for providing the junior research fellowship.

References

1. Asada K, Takahashi M (1987). Production and scavenging of active oxygen in chloroplasts. In DJ Kyle, CB Osmond, CJ Arntzen, (eds), Photoinhibition Elsevier, Amsterdam, pp 227–287
2. Vázquez-Juárez R, Vargas-Albores F, Ochoa JL (1993) A computer program to calculate superoxide dismutase activity in crude extracts. J Microbiol Methods 17:239–244
3. Khutan H, Haussmann HJ, Werringloe J (1986) A spectrophotometric assay for superoxide dismutase activities in crude tissue fractions. Biochem J 237:175–180
4. Culotta VC, Yang M, O'Halloran TV (2006) Activation of superoxide dismutases: putting the metal to the pedal. Biochim Biophys Acta 1763:747–758
5. Chen CN, Pan SM (1996) Assay of superoxide dismutase activity by combining electrophoresis and densitometry. Bot Bull Acad Sin 37: 107–111
6. Alscher RG, Erturk N, Heath LS (2002) Role of superoxide dismutases (SODs) in controlling oxidative stress in plants. J Exp Bot 53:1331–1341
7. Beauchamp C, Fridovich I (1971) Superoxide dismutase: improved assays and an assay applicable to acrylamide gels. Anal Biochem 44:276–287
8. Lomate PR, Sangole KP, Sunkar R, Hivrale VK (2015) Superoxide dismutase activities in the midgut of Helicoverpaarmigera larvae: identification and biochemical properties of a manganese superoxide dismutase. Insect Physiology 5:13–20

Chapter 14

Determination of Enzymes Associated with Sulfite Toxicity in Plants: Kinetic Assays for SO, APR, SiR, and In-Gel SiR Activity

Galina Brychkova, Assylay Kurmanbayeva, Aizat Bekturova, Inna Khozin, Dominic Standing, Dmitry Yarmolinsky, and Moshe Sagi

Abstract

The amino acid cysteine plays a major role in plant response to abiotic stress by being the donor of elemental sulfur for the sulfuration of the molybdenum cofactor, otherwise the last step of ABA biosynthesis, the oxidation of abscisic aldehyde, is inactivated. Additionally, cysteine serves as a precursor for the biosynthesis of glutathione, the reactive oxygen species scavenger essential for redox status homeostasis during stress. Cysteine is generated by the sulfate reductive pathway where sulfite oxidase (SO; EC 1.8.3.1) is an important enzyme in the homeostasis of sulfite levels (present either as a toxic intermediate in the pathway or as a toxic air pollutant that has penetrated the plant tissue via the stomata). SO is localized to the peroxisomes and detoxifies excess sulfite by catalyzing its oxidation to sulfate. Here we show a kinetic assay that relies on fuchsin colorimetric detection of sulfite, a substrate of SO activity. This SO assay is highly specific, technically simple, and readily performed in any laboratory.

5′-adenylylsulfate (APS) reductase (APR, E.C. 1.8.4.9) enzyme regulates a crucial step of sulfate assimilation in plants, algae and some human pathogens. The enzyme is upregulated in response to oxidative stress induced by abiotic stresses, such as salinity and hydrogen peroxide, to generate sulfite an intermediate for cysteine generation essential for the biosynthesis of glutathione, the hydrogen peroxide scavenger. Here we present two robust, sensitive, and simple colorimetric methods of APR activity based on sulfite determination by fuchsin.

Sulfite reductase (SiR) is one of the key enzymes in the primary sulfur assimilation pathway. It has been shown that SiR is an important plant enzyme for protection plant against sulfite toxicity and premature senescence. Here we describe two methods for SiR activity determination: a kinetic assay using desalted extract and an in-gel assay using crude extract.

Due to the energetically favorable equilibrium, sulfurtransferase (ST) activity measured as sulfite generation or consumption. Sulfite-generating ST activity is determined by colorimetric detection of SCN^- formation at 460 nm as the red $Fe(SCN)_3$ complex from cyanide and thiosulfate using acidic iron reagent. Sulfite-consuming (MST) activity is detected as sulfite disappearance in the presence of thiocyanate (SCN^-) or as SCN^- disappearance. To abrogate interfering SO activity, total ST activities is detected by inhibiting SO activity with tungstate.

Key words 5′-Adenylylsulfate (APS) Reductase, Coupled reaction, Fuchsin colorimetric detection method, In-gel assay, Kinetic assay, Sulfite, Sulfite oxidase, Sulfite reductase, Sulfur transferase

Ramanjulu Sunkar (ed.), *Plant Stress Tolerance: Methods and Protocols*, Methods in Molecular Biology, vol. 1631,
DOI 10.1007/978-1-4939-7136-7_14,

1 Introduction

Sulfur is necessary for proper growth and development of living organisms; however, it is the least abundant of the essential plant mineral macronutrients. There is about 30-fold more nitrogen, eightfold more potassium and twofold more phosphorus than sulfur in plant shoot dry matter [1]. Sulfur amino acids are nearly always directly involved in the catalytic, structural, or electrochemical functions of proteins, give rise to key enzymatic cofactors, and play an essential role in cellular redox homeostasis through glutathione (GSH) [2]. Thus, the sulfur-containing amino acids methionine and cysteine are essential for human and animal nutrition. Sufficient sulfur supply is therefore important for yield and quality of crops.

However, due to the substantial reduction in sulfur-rich fertilizers and in sulfur dioxide emissions [3], a greater portion of agricultural soils are becoming sulfur deficient. This results in reduced plant growth, increased susceptibility to abiotic and biotic stresses, and reduced content of sulfur-containing amino acids in the seed storage proteins and thus a lower baking quality of flour [3–5]. Because sulfur deficiency is a relatively new situation, increasing sulfur use efficiency is important. Sulfur is available to plants as an oxidized anion sulfate, which is taken up, reduced to sulfide, and incorporated into cysteine in a pathway of sulfate assimilation ([6], *see* Fig. 1).

Apart from sulfate, plants are capable of utilizing alternative sources of sulfur, i.e., atmospheric gases such as sulfur dioxide (SO_2) that is readily hydrated in water to form the sulfite ions, HSO_3^{1-} and SO_3^{2-} that are strong nucleophiles that can deleteriously affect plant health [7]. SO_2 enters plants via their stomata and below toxic levels plants are able to utilize SO_2. The amount of SO_2 taken up by the leaves can regulate sulfate transporters in roots [8]. Above a certain threshold, SO_2 toxicity leads to visible effects that include chlorosis (chlorophyll destruction), necrosis (plant tissue death), and long-term yield reduction [9–13].

1.1 Multiple Pathways for Sulfite/SO_2 Utilization

Sulfite occupies a central position in sulfur assimilation. After sulfite's formation by APS reductase (APR, EC 1.8.4.9., *see* Fig. 1) or entry via the stomata, it can follow four avenues. (1) One pathway is ferredoxin-dependent sulfite reduction catalyzed by sulfite reductase (SiR, EC 1.8.7.1), to yield the reduced sulfide (S^{2-}) in the primary sulfate assimilation. (2) Another pathway for sulfite utilization/detoxification is its incorporation into sulfolipids, the initial step being catalyzed by the SQD1 protein [14]. (3) Excess sulfite can be reoxidized back to sulfate by the molybdenum cofactor-containing enzyme, sulfite oxidase, localized to the peroxisomes [15] and encoded in *Arabidopsis* by a single gene [16].

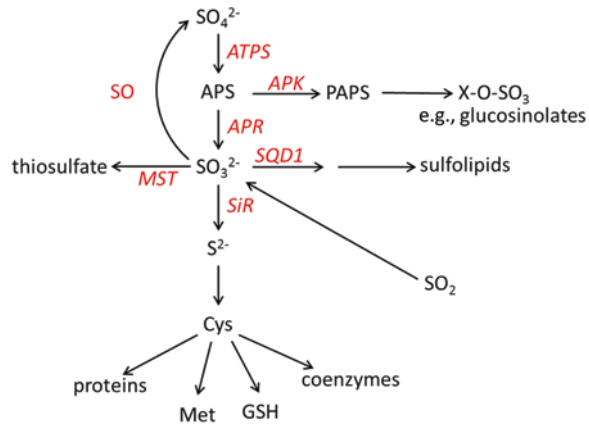

Fig. 1 Pathway of sulfate assimilation. Sulfate is activated to adenosine 5′-phosphosulfate (APS) by ATP sulfurylase (ATPS). APS is either reduced by APS reductase (APR) to sulfite or further phosphorylated by APS kinase (APK) to activated sulfate PAPS, which is used for synthesis of sulfated secondary metabolites such as glucosinolates. Sulfite can be further reduced by sulfite reductase (SiR) to sulfide and incorporated into cysteine, which in turn is the source of reduced sulfur for synthesis of methionine, glutathione, and various coenzymes. Sulfite is also formed from atmospheric SO_2 and can be used for synthesis of sulfolipids by SQD1 enzyme, metabolized to thiosulfate by MST1 protein, or oxidized in peroxisomes to sulfate by sulfate oxidase (SO). The "sulfite network" forming enzymes APR, SiR, SO, SQD1, and MST/ST are highlighted in *red*

(4) Alternatively, the nucleus-, chloroplast-, mitochondrion-, and cytosol-localized multigene family (20 gene members in Arabidopsis) of β-mercaptopyruvate sulfurtransferases (*MST* or *ST*) has been shown to catalyze the synthesis of the less toxic compound thiosulfate in the presence of β-mercaptopyruvate and sulfite [17, 18].

We present here a more detailed laboratory protocols for APR (two kinetic assays) and SiR methods (kinetic assay and in-gel assay) previously described by Brychkova et al. ([19] and [20] respectively).

2 Materials

2.1 Sulfite Oxidase Activity

2.1.1 Extraction Solution

1. Prepare 1 L of 1 M Tris–acetate buffer, pH 7.25 by dissolving 121.1 g of Trizma base in 800 mL of Milli-Q water and carefully adjusting the pH to 7.25 with glacial acetic acid). Make up to 1 L with Milli-Q water.
2. Prepare 5 mg mL^{-1} stock solutions of protease inhibitors: aprotinin, leupeptin, and pepstatin A by dissolving individually 5 mg of aprotinin and 5 mg of leupeptin in 1 mL Milli-Q water. To dissolve 5 mg pepstatin A use 1 mL ethanol (*see* **Note 1**).

3. Prepare 50 mL of 0.1 M Tris–acetate, pH 7.25 extraction solution (5 mL of 1 M Tris–acetate, pH 7.25 in 50 mL H_2O) with 10 μL of prepared pepstatin A and aprotinin.
4. Prepare G25 columns for protein extraction. To do so, remove the cap and bottom from the column, allow the storage liquid to pass through the column, and wash the Sephadex G-25 with 0.1 M Tris–acetate, pH 7.25 by passing 3 mL through the column 3 times. Avoid column drying.
5. Prepare 250 mM tungstic acid.

2.1.2 Materials for Protein Detection

1. Prepare Protein Assay reagent for protein detection by diluting 1 mL of Bio-Rad Protein Assay Dye Reagent Concentrate to 10 mL with Milli-Q water.
2. Prepare the 100 μg/mL BSA stock solution for standard curve by diluting 25 μL of Quick Start Bovine Serum Albumin Standard with 475 μL Milli-Q water.
3. Prepare the dilutions for the standard curve from 0 to 10 μg/mL BSA (Table 1).

2.1.3 Materials for the Sulfite Standard Curve

1. Prepare 100 mM sodium sulfite stock by dissolving 126 mg Na_2SO_3 in 10 mL DDW (*see* **Note 2**).
2. Prepare 1 mM Na_2SO_3 solution by diluting 0.1 mL of 100 mM sodium sulfite in 9.9 mL of 0.1 M Tris–acetate, pH 7.25.
3. Prepare the dilutions for the standard curve for sulfite from 0 to 500 μM (Table 2).

2.1.4 Sulfite Detection Reagents

1. Prepare **Reagent A** (acid-discolored fuchsin solution) by adding 4 mg of Basic Fuchsin to 8.25 mL ice-cold Milli-Q water, place on ice and then carefully add 1.25 mL of concentrated sulfuric acid. Keep solution on ice.

Table 1
Dilutions for the BSA standard curve

Final BSA, μg/mL	μL of 100 μg/mL BSA	μL, Milli-Q water
0	0	1000
1	10	990
2	20	980
4	40	960
6	60	940
8	80	920
10	100	900

Table 2
Dilutions for the sulfite standard curve

Final sulfite concentration, μM	μL of 1 mM sulfite	μL, 0.1 M Tris–acetate, pH 7.25
0	0	200
10	2	198
20	4	194
50	10	190
100	20	180
200	40	160
300	60	140
500	100	100

2. Prepare **Reagent B solution** by diluting 0.320 μL formaldehyde in 9.68 mL Milli-Q water.
3. The **Color reagent** should be prepared fresh prior to use. To make this, 1 mL of **Reagent A** should be added to 7 mL Milli-Q water followed by 1 mL **Reagent B**.

2.2 Adenosine 5′-Phosphosulfate (APS) Reductase (APR) Colorimetric Detection Assays

All the solutions should be prepared using Milli-Q grade water. All working solutions should be freshly prepared and stored on ice, unless indicated otherwise. Waste should be disposed of according to local waste disposal regulations.

2.2.1 Extraction Solution

1. Prepare 1 L of 1 M Tris–acetate buffer, pH 7.25 by dissolving 121.1 g of Trizma base in 800 mL of Milli-Q water and carefully adjusting the pH to 7.25 with glacial acetic acid. Make up to 1 L with Milli-Q water.
2. Prepare sulfate buffer (0.5 M Na_2SO_4 in 0.1 M Tris–acetate, pH 8.0) by adding 5 mL 1 M Tris–acetate buffer, pH 7.25 to 30 mL Milli-Q water and 3.6 g of anhydrous Na_2SO_4. Make up to 50 mL with Milli-Q water. Do not adjust the pH, as once we have added the sodium sulfate it reaches 8.0.
3. Prepare 5 mg/mL stock solutions of protease inhibitors: aprotinin, leupeptin, and pepstatin A by dissolving, individually, 5 mg of aprotinin and 5 mg of leupeptin in 1 mL Milli-Q water. To dissolve 5 mg pepstatin A, use 1 mL ethanol (*see* **Note 1**).
4. Prepare 10 mL extraction solution by adding 10 μL aprotinin, leupeptin, and pepstatin A solutions to sulfate buffer, pH 8.0.
5. Prepare 4.2 M ammonium sulfate solution by dissolving 7.2 g ammonium sulfate in 13 mL DDW)

6. Prepare 0.32 M tungstic acid by dissolving 80 mg Tungstic acid in 1 mL Milli-Q water.
7. Prepare G25 columns for protein extraction. To do so, remove the cap and bottom from the column, allow the storage liquid to pass through the column, and saturate Sephadex G-25 with sulfate buffer, pH 8.0 by passing 3 mL of sulfate buffer through the column three times. Avoid column drying.

2.2.2 Materials for Protein Detection (BSA standards, diluted Protein Assay reagents, etc. as Shown in Subheading 2.1.2)

Materials for the Detections of Sulfite oxidase (SO), Sulfite Reductase (SiR) and 5′-adenylylsulfate (APS) reductase activity (BSA standards, diluted Protein Assay reagents, etc. as Shown in Subheading 2.1.2).

2.2.3 Materials for the Sulfite Standard Curve

1. Prepare 100 mM sodium sulfite stock by dissolving126 mg Na_2SO_3 in 10 mL DDW (*see* **Note 1**).
2. Prepare 1 mM Na_2SO_3 solution by diluting 0.1 mL of 100 mM sodium sulfite in 9.9 mL of sulfate buffer, pH 8.0.
3. Prepare the dilutions for the standard curve from 0 to 500 μM (Table 3).

2.2.4 Materials for the Kinetic Assay

1. Prepare 50 mM GSH by dissolving 23.1 mg of reduced L-glutathione in 1.5 mL sulfate buffer, pH 8.0
2. Prepare 10 mM APS solution by dissolving 6.83 mg adenosine 5′-phosphosulfate sodium salt in 1.6 mL Milli-Q water. This should be used as a substrate for the one-step assay.
3. Prepare 50 mM MgATP by dissolving 26.7 mg adenosine 5′-triphosphate (ATP) disodium salt hydrate and 10.15 mg

Table 3
Dilutions for the sulfite standard curve

Final sulfite concentration, μM	μL of 1 mM sulfite	μL, sulfate buffer, pH 8.0
0	0	200
10	2	198
20	4	194
50	10	190
100	20	180
200	40	160
300	60	140
500	100	100

$MgCl_2$ in 1 mL Milli-Q water. This is used as a cofactor for the coupled reaction.

4. Prepare 1.2 U ATPS by dissolving 6 mg adenosine-5′-triphosphate sulfurylase in 2 mL sulfate buffer, pH 8.0. This reagent should be used in the coupled reaction to generate APS from sulfate.
5. Prepare 100 mM EDTA solution by dissolving 292 mg ethylenediaminetetraacetic acid in 10 mL sulfate solution, pH 8.0.

2.2.5 One-Step APR Activity Reaction Mix

1. Prepare the reaction mix by combining 50 µL sulfate buffer (pH 8.0), 1 µL 100 mM EDTA, 3 µL 10 mM APS, 9.6 µL 50 mM GSH, and 16.4 µL Milli-Q water per reaction point, including a Time 0.

2.2.6 Inactive Coupled APR Activity Reaction Mix

1. Prepare inactive 7.79 mL preincubation solution by combining 3 mL sulfate buffer, pH 8.0, 2.1 mL 50 mM MgATP, 960 µL 50 mM GSH, and 1.73 mL Milli-Q water. Keep on ice.

2.2.7 Sulfite Detection Reagents

1. Prepare **Reagent A (**acid-discolored fuchsin solution) by adding 4 mg of Basic Fuchsin to 8.25 mL ice-cold Milli-Q water, place on ice and then add 1.25 mL concentrated sulfuric acid. Keep solution on ice.
2. Prepare **Reagent B** solution by diluting 0.320 mL formaldehyde in 9.68 mL Milli-Q water.
3. The **Reagent** should be mixed fresh prior to use by adding 1 mL of **Reagent A** to 7 mL Milli-Q water followed by 1 mL **Reagent B**.

2.3 SiR Activity Determination

Prepare all solutions using ultrapure Milli-Q water and analytical grade reagents.

2.3.1 Materials for Protein Extraction for SiR Kinetic Activity

1. Prepare 1 M stock of KH_2PO_4 and K_2HPO_4: dissolve individually 68.045 g of KH_2PO_4 and 87.1 of K_2HPO_4 in 500 mL of Milli-Q water. After dissolving, filter solution solutions through 0.22-µm filters to avoid contamination of the buffers.
2. Prepare protease inhibitors (aprotinin, leupeptin, and pepstatin A) by dissolving, individually, 5 mg of aprotinin and leupeptin in 1 mL of Milli-Q water and 5 mg of pepstatin A in 1 mL of ethanol (*see* **Note 1**).
3. Sucrose.
4. 10% Triton X-100: dissolve 1 g of Triton X-100 in 10 mL of Milli-Q water.
5. G25 columns for protein extraction.

2.3.2 Materials for Protein Extraction for SiR In-Gel Activity

1. Prepare 1 M stock of Tris–HCl, pH 7.5 by dissolving 60.5 g of Trizma base in 300 mL of Milli-Q water. After dissolving, carefully adjust the pH to 7.5 with HCl.

2. 100 mM EDTA: dissolve 292 mg of EDTA in 10 mL of DDW.
3. Prepare protease inhibitors (aprotinin, leupeptin, and pepstatin A) by dissolving, individually, 5 mg of aprotinin and leupeptin in 1 mL of Milli-Q water and 5 mg of pepstatin A in 1 mL of ethanol (*see* **Note 1**).
4. Sucrose.
5. 10% Triton X-100: dissolve 1 g of Triton X-100 in 10 mL of Milli-Q water.

2.3.3 Materials for Protein Detection (BSA standards, diluted Protein Assay reagents, etc. as Shown in Subheading 2.1.2)

1. To prepare 25 mM phosphate buffer, pH 7.5, dilute 1.88 mL of 1 M KH_2PO_4 and 8.12 mL of 1 M K_2HPO_4 in 100 mL of Milli-Q water. Check the pH (The preparation of potassium phosphate buffer with specific pH is described at http://nature.berkeley.edu).
2. 6 mM O-acetyl-L-serine: dissolve 22 mg of OAS in 200 μL of 100 mM HEPES-NaOH, pH 7.5.

2.3.4 Materials for the Kinetic Assay

3. 6 mM sodium dithionite stock solution: dissolve 209 mg sodium dithionite and126 mg $NaHCO_3$ in 10 mL of Milli-Q water.
4. NADPH—β-nicotinamide adenine dinucleotide 2′-phosphate reduced tetrasodium salt hydrate.
5. 0.7 mM methyl viologen: dissolve 18 mg MVH in 5 mL of 25 mM phosphate buffer, pH 7.5.
6. 10% trichloroacetic acid (TCA): dissolve 10 g of TCA in 100 mL of DDW. Store at room temperature.
7. Ninhydrin solution: (work in a fume hood) to 250 mg of ninhydrin add 6 mL of glacial acetic acid and 4 mL of 32% HCl. Loosely cover with aluminum foil and mix for 30 min at RT to dissolve the ninhydrin. Prepare fresh for use.
8. 10 mM L-cysteine: dissolve 1.21 mg of L-cysteine in 1 mL of Milli-Q water.

2.3.5 Materials for Native PAGE

1. 4× separating buffer, pH 8.48: dissolve 11.47 g of Tris in 50 mL DDW. Carefully add 28.92 mL concentrated HCl and make up to 100 mL with DDW.
2. Monomer solution for separating gel (40%:5%): dissolve 38 g of acrylamide and 2 g of bis-acrylamide in 100 mL of DDW.
3. 4× stacking buffer, pH 6.9: dissolve 1.92 g of Tris in 25.6 mL of H_3PO_4, add DDW until 100 mL.
4. Monomer solution for stacking gel (6.25%:20%): dissolve 5 g of acrylamide and 1.25 g of bis-acrylamide in 100 mL of DDW.
5. 10% (w/v) ammonium persulfate: dissolve 1 g of ammonium persulfate in 10 mL of DDW.

6. TEMED—N,N,N′,N′-tetramethylethylenediamine.
7. Lower tank buffer (63 mM Tris, 50 mM HCl, pH 7.47): dissolve 22.7 g of Trizma base in 150 mL of HCl and make up to 3 L with DDW. Check the pH.
8. Upper tank buffer (37.6 mM Tris and 40 mM glycine, pH 8.89): dissolve 4.56 g of Trizma base and 3 g of glycine in 1 L of DDW. Check the pH.
9. Sample buffer: dissolve 5 g of sucrose and 100 mg bromophenol blue in 10 mL of DDW.

2.3.6 Materials for In-Gel Assay

1. 1 M Tris–HCl, pH 7.5: dissolve 1.21 g of Tris in 10 mL of DDW.
2. 2-mercaptoethanol.
3. 6 mM sodium dithionite stock solution: dissolve 209 mg sodium dithionite and126 mg $NaHCO_3$ in 10 mL of Milli-Q water.
4. 0.7 mM methyl viologen: dissolve 18 mg in 5 mL of 25 mM phosphate buffer, pH 7.5.
5. NADPH—β-nicotinamide adenine dinucleotide 2′-phosphate reduced tetrasodium salt hydrate.
6. 40 mM lead acetate: dissolve 15 mg of lead(II) acetate trihydrate in 1 mL of DDW.

2.4 Sulfurtransferase Activity

2.4.1 Extraction Solution

1. Prepare 1 L of 1 M Tris–acetate buffer, pH 7.25 by dissolving 121.1 g of Trizma base in 800 mL of Milli-Q water and carefully adjust pH with glacial acetic acid. Make up to 1 L with Milli-Q water.
2. Prepare 5 mg/mL stock solutions of protease inhibitors: aprotinin, leupeptin, and pepstatin A by dissolving, individually, 5 mg of aprotinin and 5 mg of leupeptin in 1 mL Milli-Q water. To dissolve 5 mg pepstatin A use 1 mL ethanol (*see* **Note 1**).
3. Prepare 50 mL of 0.1 M Tris–acetate, pH 7.25 extraction solution (5 mL of 1 M Tris–acetate, pH 7.25 in 50 mL DDW) with 10 μL of prepared pepstatin A and aprotinin.
4. Prepare G25 columns for protein extraction. To do so, remove the cap and bottom from the column, allow the storage liquid to pass through the column, and wash the Sephadex G-25 with 0.1 M Tris–acetate, pH 7.25 by passing 3 mL through the column three times. Avoid column drying.
5. Prepare 250 mM tungstic acid.

2.4.2 Materials for Protein Detection (BSA standards, diluted Protein Assay reagents, etc. as Shown in Subheading 2.1.2)

Materials for the detection of Sulfurtransferase Activity (BSA standards, diluted Protein Assay reagents, etc. as Shown in Subheading 2.1.2)

2.4.3 Materials for the Sulfite Standard Curve (Prepare the dilutions for the Sulfite standard curve as Shown in Subheading 2.1.3)

Materials for the Sulfite Standard Curve (Prepare the dilutions for the Sulfite standard curve as Shown in Subheading 2.1.3)

2.4.4 Materials for the Thiocyanate Standard Curve

1. Prepare 10 mM sodium thiocyanate stock by dissolving 8.17 mg NaSCN in 10 mL DDW.
2. Prepare 1 mM NaSCN solution by diluting 1 mL of 10 mM sodium thiocyanate in 9.0 mL of 0.1 M Tris–acetate, pH 7.25.
3. Prepare the dilutions for the standard curve from 0 to 200 μM (Table 4).

2.4.5 Materials for the Sulfite Detection Kinetic Assay of Sulfurtransferase Activity

1. Prepare 1 M Tris–HCl buffer, pH 9.5.
2. Prepare 100 mM sodium sulfite stock by dissolving 126 mg Na_2SO_3 in 10 mL DDW (*see* **Note 2**).
3. Prepare 10 mM sodium thiocyanate stock by dissolving 8.17 mg NaSCN in 10 mL DDW.

2.4.6 Preparation of the Reaction mix for the Sulfite Detection Kinetic Assay of Sulfurtransferase Activity

1. Prepare the reaction mix by combining 1 mL 1 M Tris–HCl, pH 9.5, 50 μL of 100 mM Na_2SO_3, 50 μL of 10 mM NaSCN, 3.9 μL β-mercaptoethanol and dilute till 10 mL with Milli-Q water.
2. Final concentration for Reaction mix:

   M Tris–HCl buffer, pH 9.5.

Table 4
Dilutions for the thiocyanate standard curve

Concentration μM	Working NASCN solution μL (final volume 1000 μL)	Dilution water μL (final volume 1000 μL)
0	0	1000
20	20	980
50	50	950
100	100	900
200	200	800

0.5 mM Na_2SO_3.

5 mM β-mercaptoethanol.

50 μM NaSCN.

2.4.7 Materials for Thiosulfate Rhodanese Sulfurtransferase Activity

1. Prepare 1 M Tris–HCl buffer, pH 9.0.
2. Prepare 100 mM sodium thiosulfate stock by dissolving 158 mg $Na_2S_2O_3$ in 10 mL DDW.
3. Prepare 100 mM potassium cyanide stock by dissolving 62 mg KCN in 10 mL DDW.
4. KCN in 7.5 mL 0.1 M Tris–HCl, pH 9.0.

2.4.8 Preparation of the Reaction Mix for Thiosulfate Rhodanese Sulfurtransferase Activity

1. Prepare the reaction mix by combining 1 mL 1 M Tris–HCl, pH 9.0, 500 μL of 100 mM $Na_2S_2O_3$, 500ul of 100 mM KCN, 3.9 μL β-mercaptoethanol and dilute till 10 mL with Milli-Q water.
2. Final concentration for Reaction mix.

   M Tris–HCl buffer, pH 9.0.

   5 mM $Na_2S_2O_3$.

   5 mM β-mercaptoethanol.

   10 mM KCN.

2.4.9 Thiocyanate Detection Reagents

1. Prepare **Acidic Iron Reagent** (AIR) by adding 1 g $FeCl_3$ and 4 mL HNO_3 to 20 mL of DDW.

2.4.10 Sulfite Detection Reagents

1. Prepare **Reagent A** (acid-discolored fuchsin solution) by adding 4 mg of Basic Fuchsin, to 8.25 mL ice-cold Milli-Q water, place on ice and then add 1.25 mL of concentrated sulfuric acid. Keep solution on ice prior to use.
2. Prepare **Reagent B** solution by diluting 0.320 mL formaldehyde in 9.68 mL Milli-Q water.
3. The **Color reagent** is prepared by adding 1 mL of Reagent A to 7 mL Milli-Q water followed by 1 mL reagent B. Prepare fresh prior to use.

3 Methods

3.1 Sulfite Oxidase Activity

3.1.1 Protein Extraction Quantification and Preparation for Kinetic Assay

1. Collect 150 mg of plant samples (use leaves from the same position), finely chop them with a sharp razor blade, flash-freeze in liquid nitrogen and store at −80 °C prior to extraction.
2. For the extraction take the samples stored at −80 °C and crush them in ice-cold mortar and pestle with 5 mg white quartz sand. Add 1 mL extraction solution and crush until homogenous.

3. Transfer samples to 2.0 mL SafeSeal microcentrifuge tubes (Sarstedt) and centrifuge at 18,400 × *g* for 10 min at 4 °C.
4. Transfer 0.9 mL of supernatant to a new 2-mL tube.
5. Add 0.1 mL of 4.2 M ammonium sulfate solution (7.2 g ammonium sulfate in 13 mL DDW) to the supernatant.
6. Centrifuge at 17,600 × *g* for 10 min at 4 °C to precipitate the very small proteins. This step also helps to clear the sample.
7. Transfer the supernatant to new 2-mL tubes containing 460 mg ammonium sulfate. Centrifuge at 17,600 × *g* for 10 min at 4 °C to precipitate all the proteins.
8. Discard the supernatant and dissolve the pellet in 0.5 mL extraction buffer.
9. Add 500 μL of protein to the G-25 column, equilibrated with 0.1 M Tris–acetate, pH 7.25. Allow to completely absorb into the column before eluting the protein with 1 mL of 0.1 M Tris–acetate, pH 7.25 into a new tube.
10. To measure the protein concentration dilute 10 μL of protein in 240 μL of Milli-Q water. Add 20 μL of diluted protein to 200 μL of diluted PA reagent. Proteins should be measured at 595 nm. Standard curve should be measured similarly.
11. Prepare 400 μL protein equalized to 50 μg/μL protein, taking into account that 20 μL of protein will be used per assay.
12. Prepare another 400 μL protein equalized to 50 μg/μL protein and add 3.2 μL tungstic acid and incubate for 30 min at 4 °C to inactivate the molybdoenzyme sulfite oxidase enzyme.

3.1.2 Kinetic Assay for SO Activity

The reaction can be performed in PCR strips. A schematic of the assay is shown in Fig. 2.

Time 20:

1. Take 80 μL of protein/protein with tungstate and add 20 μL of 0.5 mM SO_3. Incubate the reaction at 30 °C for 20 min.
2. Take 80 μL of standard curve add 20 μL of 0.1 M Tris–acetate, pH 7.25. Incubate the reaction at 30 °C for 20 min
3. Add 180 μL Color reagent to the wells of a flat 96-well microplate.
4. After 20 min, using a multichannel pipette, simultaneously transfer 20 μL of the protein/protein with tungstate/standard curve into 180 μL Color reagent.

Time 0:

1. Take 80 μL of protein/protein with tungstate and add 20 μL of 0.5 mM SO_3 mix and simultaneously transfer into 180 μL color reagent.

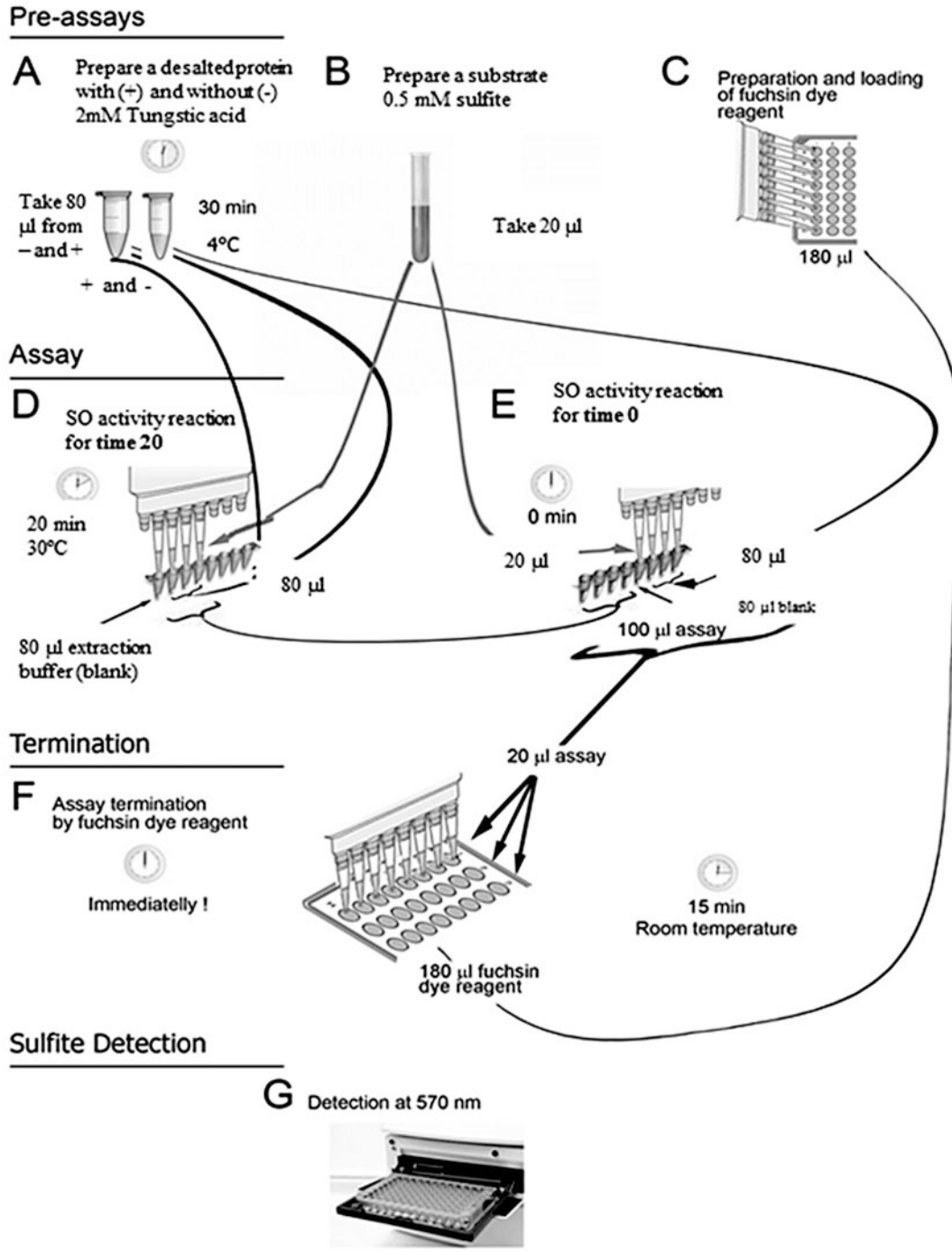

Fig. 2 Schematic illustrating of the main steps of SO activity kinetic assay employing 0.5 mM sulfite as the substrate. Proteins are extracted in 0.1 M Tris-acetate buffer, pH 7.25, and after desalting, half of the proteins should undergo preincubated with 2 mM tungstate for 30 min at 4 °C prior to the assay (**A**). Using a multichannel pipette, the assay is initiated by adding 20 µl substrate [0.5 mM sulfite (**B**)] to 80 µl desalted protein (**A**). The addition of substrate to 80 µl protein treated with tungstic acid serves as the blank control. To terminate the reaction 180 µl Colour Reagent is loaded into the 96-well plate (**C**) followed by the addition of 20 µl time 20 min [T20 (**D**)] and time 0 min (T0) of SO reactions (**E**). 80 µl extraction buffer added to 20 µl substrate (**B**) serves as blank. After 15 min incubation at room temperature [RT (**F**)], the optical density (OD) of developed colour is measured at 570 nm (**G**)

Sulfite Detection

Note: Time 20 and Time 0 should be transferred into 180 µL Color reagent at the same time.

1. Incubate the plate for 15 min at room temperature and read the absorbance of the developed purple color at 570 nm. Determine the absorbance differences of the sample:

$$\Delta = (T_0 - T_{20})_{\text{without tungstate}} - (T_0 - T_{20})_{\text{with tungstate}}$$

2. Calculate the Δ of SO activity per min based on the protein concentration per assay. The calculation should be performed with reference to the corresponding standard curve.

3.2 Adenosine 5′-Phosphosulfate (APS) Reductase (APR) Colorimetric Detection Assays

3.2.1 Protein Extraction, Quantification and Preparation for Kinetic Assay

1. Collect 100 mg of plant samples (use leaves from the same position), finely chop them with a sharp razor blade, flash-freeze in liquid nitrogen and store at −80 °C prior to extraction.
2. For extraction take the samples stored at −80 °C and crush them in an ice-cold mortar and pestle with 5 mg white quartz sand. Add 1 mL extraction solution and crush until homogenous.
3. Transfer samples to 2.0 mL SafeSeal microcentrifuge tubes (Sarstedt) and centrifuge at 18,400 × *g* for 10 min at 4 °C.
4. Transfer 0.9 mL of the supernatant to new 2-mL tubes.
5. Add 0.1 mL of 4.2 M ammonium sulfate solution (dissolve 7.2 g ammonium sulfate in 13 mL DDW) to the supernatant.
6. Centrifuge at 17,600 × *g* for 10 min at 4 °C to precipitate the very small proteins. This step is also helps to clear the sample.
7. Transfer the supernatant to new 2-mL tubes containing 460 mg ammonium sulfate. Centrifuge at 17,600 × *g* for 10 min at 4 °C to precipitate all the proteins.
8. Discard the supernatant and dissolve the pellet in 0.5 mL extraction buffer.
9. Add 500 µL protein to the G-25 column, equilibrated with sulfate buffer, pH 8.0. Elute the protein fraction with 1 mL sulfate buffer, pH 8.0 into a new tube.
10. To measure the protein concentration, dilute 10 µL protein in 240 µL Milli-Q water. Add 20 µL diluted protein to 200 µL diluted Protein Assay reagent (1 mL of Bio-Rad Protein Assay Dye Reagent Concentrate to 10 mL with Milli-Q water). Protein concentration should be measured at 595 nm. Standard curve should be measured similarly.
11. Prepare 320 µL equalized protein with concentrations ranging from 7.15 to 21.45 µg/protein assay for *Arabidopsis* and

3.57–14.30 μg/protein assay for tomato, taking into account that 20 μL of protein will be used per assay.

12. Add 1 μL tungstate to 320 μL equalized protein and incubate for 30 min at 4 °C to inactivate the molybdoenzyme sulfite oxidase.

3.2.2 One-Step APR Activity

1. Add 80 μL one-step APR activity reaction mix to 20 μL protein/standard curve/blanks (this can be performed in PCR strips). Incubate the reaction at 30 °C for 10 min.
2. Add 180 μL Color reagent to wells of a flat 96-well microplate.
3. Add 80 μL one-step APR activity reaction mix to 20 μL protein/blanks (Time 0 min).
4. Using a multichannel pipette simultaneously transfer 20 μL of the protein/standard curve/blanks (Time 10 and Time 0) into 180 μL Color reagent.
5. Incubate the plate for 15 min at room temperature.
6. Read the developed purple color at 570 nm (Fig. 2).
7. Calculate the APR activity per min based on the protein concentration per assay. The calculation should be performed with reference to the corresponding standard curve.

3.2.3 Coupled APR Activity

1. Add 80 μL one-step APR activity reaction mix to 20 μL protein/standard curve/blanks (this can be performed in PCR strips). Incubate the reaction at 30 °C for 10 min.
2. Add 180 μL Color reagent to wells of a flat 96-well microplate.
3. Add 80 μL one-step APR activity reaction mix to 20 μL protein/blanks (Time 0 min).
4. Using a multichannel pipette simultaneously transfer 20 μL of the protein/standard curve/blanks (Time 10 and Time 0) into 180 μL Color reagent.
5. Incubate the plate for 15 min at room temperature.
6. Read the developed purple color at 570 nm (Fig. 3).
7. Calculate the APR activity per min based on the protein concentration per assay. The calculation should be performed with reference to the corresponding standard curve.

3.3 SiR Activity Determination

3.3.1 Sample Preparation for SiR Kinetic Activity

1. Prepare extraction solution by dissolving 1 g of sucrose, 25 μL of 10% Triton X-100, and 10 μL of each protease inhibitor in 10 mL of 25 mM phosphate buffer, pH 7.5.
2. Crush 150 mg plant tissue into powder using mortar and pestle with liquid nitrogen and add 600 μL of extraction solution.

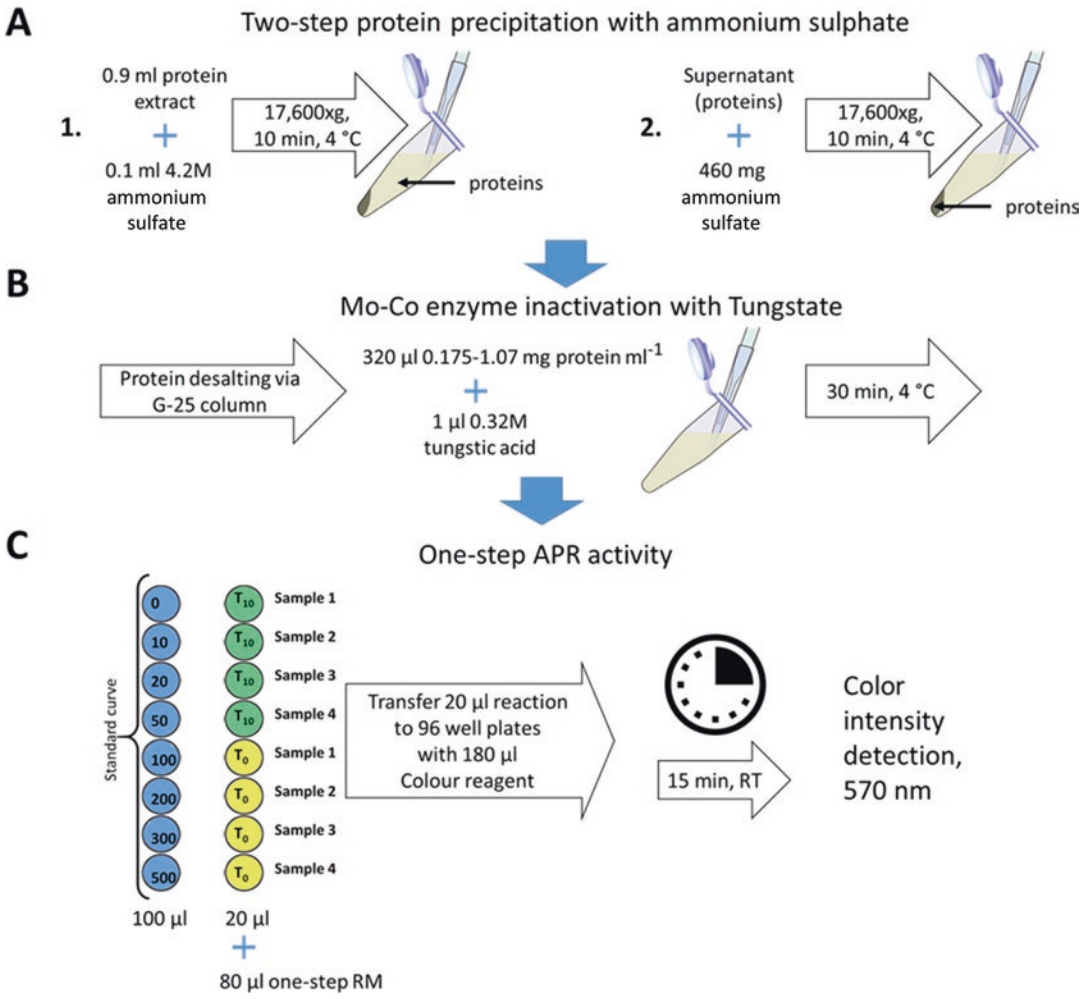

Fig. 3 Schematic illustrating the main steps of APR activity kinetic assay employing APS as a substrate. Proteins are extracted in 0.1 M Tris–acetate buffer, pH 8.0, with 0.5 M sulfate and, after desalting (**a**), preincubated with 1 mM tungstate for 30 min at 4 °C prior to the assay (**b**). Using a multichannel pipette, the assay is initiated by adding 80 µL reaction assay (50 µL sulfate buffer, pH 8.0; 1 µL of 100 mM EDTA; 3 µL 10 mM APS; 9.6 µL 50 mM GSH; and 16.4 µL Milli-Q) to 20 µL desalted protein. The addition of reaction mix to 20 µL extraction solution serves as blank control. To detect APR activity 180 µL Color reagent is loaded into the 96-well plate followed by the addition of 20 µL T10 and T0 APR reactions. After a 15-min incubation at RT, the intensity of developed color is measured at 570 nm

3. Transfer sample into 1.5-mL microcentrifuge tube and centrifuge for 15 min at 18,400 × *g*.
4. Collect the supernatant and heat the sample at 55 °C for 90 s. This helps to release SiR proteins from the chloroplast matrix.
5. Centrifuge for 5 min at 18,400 × *g* and collect the supernatant.

6. Equilibrate Sephadex G-25 columns by saturation with 25 mM phosphate buffer, pH 7.5 three times. Avoid column drying.
7. Pass 500 µL of the sample through Sephadex G-25 columns. After proteins have entered into the columns, place them into 10 mL tubes and add to the top 1 mL 25 mM P-buffer, pH 7.5. The flow-through contains the proteins.
8. Measure the protein concentration: first, dilute 10 µL of protein in 240 µL of Milli-Q water, then add 20 µL of diluted protein to 200 µL of diluted protein assay reagent (dilute 1 mL of Bio-Rad Protein Assay Dye Reagent Concentrate in 9 mL of Milli-Q water). Similarly prepare standards and measure spectrophotometrically in 595 nm.
9. Equalize proteins to 0.1 OD in 1 mL volume.

3.3.2 SiR Activity

1. Prepare reaction solution containing 188 µL of 1 M KH_2PO_4 and 812 µL of 1 M K_2HPO_4, 1 mL of dithionite solution, 1 mL of MVH solution, 1.1 mg of NADPH (*see* **Note 3**), 200 µL of OAS stock and make up with Milli-Q water to 10 mL.
2. Prepare standards in 25 mM P-buffer, pH 7.5, using 0.2 mM L-Cysteine from 0 to 50 µM. To prepare 0.2 mM L-Cysteine dilute 200 µL of 10 mM L-Cysteine in 10 mL of Milli-Q water (Table 5).
3. Initiate the reaction with by adding 50 µL of SiR reaction mix to the 50 µL Proteins (or cysteine standards).
4. Incubate for 30 min for at 37 °C, afterward add 25 µL 10% TCA to terminate the reaction.
5. Use TCA inhibited proteins as a blank.
6. In the fume hood add 100 µL of acetic acid and 100 µL of ninhydrin solution to all the samples and standards. Make sure to add the acetic acid first.
7. Mix well, centrifuge at 18,400 × *g*, 4 °C for 3 min, then transfer supernatant to the new tubes.
8. Heat for 10 min at 100 °C and then cool fast in ice-water bath.
9. Transfer 150 µL of sample to a 96-well microplate, add 50 µL of 95% ethanol and mix (color is stable for 20 min).
10. Measure at 560 nm. Calculate the enzyme activity as the delta between T_{30} and blank.

3.3.3 Sample Preparation for SiR In-Gel Activity

1. Prepare extraction solution: 856 mg of sucrose, 25 µL of 10% Triton X-100, 150 µL of 100 mM EDTA, 500 µL of 1 M Tris–HCl, pH 7.5, and 10 µL of each protease (leupeptin, aprotinin, pepstatin A) inhibitor. Make up to 10 mL with DDW.

Table 5
Dilutions for cysteine standard curve

Concentration, μM	0.2 mM L-cysteine, μL	25 mM P-buffer, pH 7.5, μL
0	0	1000
5	25	985
10	50	950
20	100	900
30	150	850
40	200	800
50	250	750

2. Crush 30 mg plant tissue into powder using mortar and pestle with liquid nitrogen and add 600 μL of extraction solution.
3. Transfer sample into 1.5-mL microcentrifuge tube and centrifuge 15 min at 18,400 × *g*.
4. Collect supernatant and measure the protein concentration at 595 nm with Protein Assay (described in Subheading 3.1, **step 8**).
5. Heat samples at 55 °C for 90 s. This helps to release SiR proteins from the chloroplast matrix.
6. Centrifuge for 15 min at 18,400 × *g* and collect supernatant.
7. Equalize proteins to 5 μg/60 μL. Add loading dye in a ratio 1:10.

3.3.4 Gel Running Protocol

1. To prepare a 7.5% separating gel (quantities are for one gel) put 4.22 mL of water, 1.88 mL of separating buffer and 1.41 mL of monomer solution for separating gel. Then add 75 μL of 10% ammonium persulfate, 7.5 μL of TEMED and mix gently (*see* **Note 4**). Pipette the gel solution into the gap between the glass plates in a gel casting frame (do not fill to the top). Fill the remaining space (*see* **Note 5**) with water. Allow 20–30 min for the gel to set completely.
2. Prepare the stacking gel solution in a beaker (quantities are for one gel). Put 1.25 mL of water, 1.25 mL of stacking buffer and 2.5 mL of monomer solution for stacking gel and mix with 50 μL of 10% ammonium persulfate and 4 μL of TEMED. Pour out the water in the first step and pipette the stacking gel solution into the gap and carefully insert the comb. Allow 20-30 min for the gel to set completely.
3. To prepare the electrophoresis chamber fill the inner chamber with upper buffer and outer chamber with lower buffer.

4. Load 60 μL of samples into the wells and set 15 mA to run the electrophoresis.
5. Run native PAGE with ice refrigeration until the dye is 0.5–1 cm above the bottom of the gel.

3.3.5 Staining the In-Gel Activity

1. Prepare a reaction solution containing 1 mL of Tris–HCl, pH 7.5, 70 μL of β-mercaptoethanol (fume hood), 1 mL of dithionite solution, 1 mL of MVH solution, 1.1 mg of NADPH, and DDW up to 20 mL (*see* **Note 3**). After addition of the methyl viologen the solution should become dark purple.
2. Place the gel into a container and carefully pour the solution so that the gel is completely covered. Do not shake the container as the solution might oxidize.

Add 400 μL of 40 mM lead acetate and let it incubate for a few hours (*see* **Note 6**).

3.4 Sulfurtransferase Activity

3.4.1 Protein Extraction Quantification and Preparation for Kinetic Assay

1. Collect 150 mg of plant samples (use leaves from the same position on plants), finely chop them with sharp razor blade, flash-freeze in liquid nitrogen and store at −80 °C prior to extraction.
2. For the extraction take the samples stored at −80 °C and crush them using an ice-cold mortar and pestle with 5 mg white quartz sand. Add 1 mL extraction solution and crush until homogenous.
3. Transfer samples to 2.0 mL SafeSeal microcentrifuge tubes (Sarstedt) and centrifuge at 18,400 × *g* for 10 min at 4 °C.
4. Transfer 0.9 mL of supernatant to new 2-mL tubes.
5. Add 0.1 mL of 4.2 M ammonium sulfate (dissolve 7.2 g ammonium sulfate in 13 mL DDW) solution to the supernatant.
6. Centrifuge at 17,600 × *g* for 10 min at 4 °C to precipitate the very small proteins. This step also helps clean the sample.
7. Transfer the supernatant to new 2-mL tubes containing 460 mg ammonium sulfate. Centrifuge at 17,600 × *g* for 10 min at 4 °C to precipitate all the proteins.
8. Discard the supernatant and dissolve the pellet in 0.5 mL extraction buffer.
9. Add 500 μL of protein to the G-25 column, 0.1 M Tris–acetate, pH 7.25. Elute with 1 mL 0.1 M Tris–acetate, pH 7.25 into new tube.
10. To measure the protein concentration first it is necessary to dilute the 10 μL of protein in 240 μL of Milli-Q water. Then, 20 μL of diluted protein should be added to 200 μL of diluted PA reagent. Proteins should be measured at 595 nm. Standard curve should be measured similarly.

11. Prepare 1 mL protein equalized to 50 μg/μL protein, add 20 μL tungstic acid and incubate for 30 min at 4 °C to inactivate the molybdoenzyme sulfite oxidase.

3.4.2 Kinetic Assay for Sulfite-consuming activity of MST

The reaction can be performed in PCR strips.

Time 20:

1. Take 80 μL of protein/blank (*see* **Note 7**), add 20 μL of Reaction mix for the sulfite detection assay and incubate for 20 min at 37 °C.
2. Take 80 μL of standard curve samples, add 20 μL of Reaction mix (without NaSCN) for the sulfite detection assay and incubate for 20 min at 37 °C together with Time 20.
3. Add 180 μL Color reagent to the wells of a flat 96-well microplate.
4. After 20 min using a multichannel pipette simultaneously transfer 20 μL of the protein/standard curve/blanks into 180 μL Color reagent (*see* **Note 8**).

Time 0:

1. Take 80 μL of protein/blank add 20 μL of Reaction mix (without NaSCN) for the sulfite detection assay and, using a multichannel pipette, simultaneously transfer 20 μL into 180 μL Color reagent (*see* **Note 8**).
2. Incubate the plate for 15 min at room temperature.
3. Read the absorbance of the purple color at 570 nm.

Colorimetric detection of sulfite disapperance

1. Determine the absorbance differences ($T_0 - T_{20}$) for blank and samples.
2. Subtract the absorbance difference (Δ) of the blank from the absorbance Δ of the sample:

$$\Delta = (T_0 - T_{20})_{\text{sample}} - (T_0 - T_{20})_{\text{blank}}.$$

3. Calculate the ST activity per min based on the protein concentration per assay. The calculation should be performed with reference to the corresponding standard curve.

3.4.3 Kinetic Assay for Thiosulfate Rhodanese Sulfurtransferase Activity

The reaction can be performed in 1.5-mL tubes (Fig. 4).

Time 40:

1. Take 150 μL of Reaction mix for the thiocyanate detection kinetic assay and add 50 μL of protein/blank (*see* **Note 7**) then incubate for 40 min at 37 °C.
2. Take 150 μL of Reaction mix (without $Na_2S_2O_3$) and add 50 μL standard curve for the thiocyanate detection kinetic v then incubate for 40 min at 37 °C.

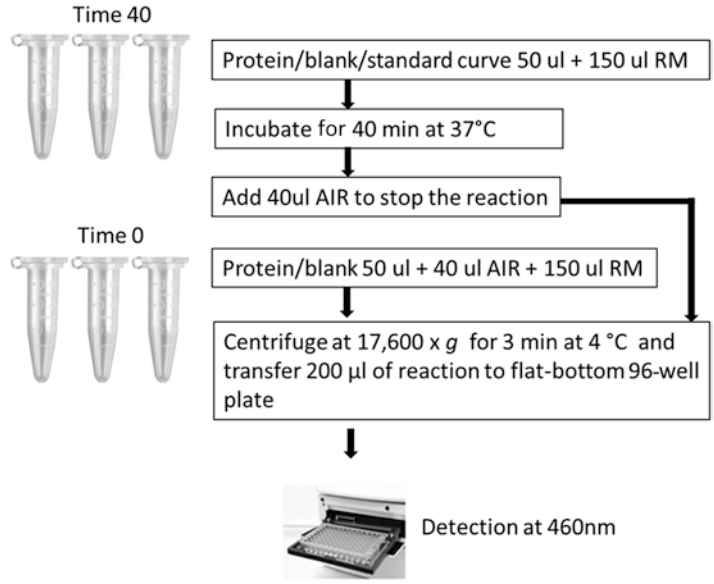

Fig. 4 Schematics of thiosulfate rhodanese sulfurtransferase activity

3. After 20 min stop the reaction by adding 40 µL of AIR. The color should be yellow-brownish.
4. Centrifuge at 17,600 × *g* for 3 min at 4 °C and transfer to the plate 200 µL.

Time 0:

1. Take 150 µL of Reaction mix (without $Na_2S_2O_3$) for the thiocyanate detection kinetic assay and add 40 µL of AIR, mix and 50 µL of protein/blank. The color should be yellow-brownish. Centrifuge at 17,600 × *g* for 3 min at 4 °C and transfer 200 µL of the supernatant to each well of a flat-bottom 96-well plate for detection.

Read the absorbance of the red $Fe(SCN)_3$ formed at 460 nm. The net sulfite-generating activity is estimated as the difference between sulfite consumption activity and sulfite generation activities of STs and expressed as nmol sulfite min^{-1}/mg protein.

4 Notes

1. Make 10-µL aliquots of the protease inhibitors and store them at −20 °C.
2. Na_2SO_3 is highly reactive and should be prepared fresh for each assay. Keep on ice.

3. If accurately weighing 1.1 mg is problematic, then prepare 0.5 mL of 10 mM NADPH by dissolving 4.2 mg NADPH in 0.5 mL Milli-Q water and adding 132 μL of this stock to the reaction solution.
4. Once you add APS and TEMED polymerization starts. When you are ready to pour the gel add the TEMED and ensure that the solution is well mixed. Pour the gel as soon as possible after mixing.
5. You need to leave enough space so that there is a gap of ~1 cm between the bottom of the comb teeth and the start of the running gel.
6. If, after a few hours bands have not appeared, or the solution becomes transparent, renew the reaction solution and leave the gel to incubate overnight.
7. Use blank-extraction solution instead of protein.
8. Time 20 and Time 0 reactions should be transferred into 180 μL Color reagent at the same time.

References

1. Marschner H (2005) Mineral nutrition of higher plants, 2nd edn. Academeic Press, London
2. Saito K (2000) Regulation of sulfate transport and synthesis of sulfur-containing amino acids. Curr Opin Plant Biol 3:188–195
3. Lewandowska M, Sirko A (2008) Recent advances in understanding plant response to sulfur-deficiency stress. Acta Biochim Pol 55(3):457–471
4. Rausch T, Wachter A (2005) Sulfur metabolism: a versatile platform for launching defence operations. Trends Plant Sci 10(10):503–509
5. Muttucumaru N, Halford NG, Elmore JS, Dodson AT, Parry M, Shewry PR, Mottram DS (2006) Formation of high levels of acrylamide during the processing of flour derived from sulfate-deprived wheat. J Agric Food Chem 54(23):8951–8955
6. Leustek T, Martin MN, Bick JA, Davies JP (2000) Pathways and regulation of sulfur metabolism revealed through molecular and genetic studies. Ann Rev Plant Phys Plant Mol Biol 51:141–165
7. Murray F (1997) Urban air pollution and health effects. In: Brune D, Chapman DV, Gwynne MD, Pacyna JM (eds) The global environment: science, technology and management. Scandinavian Science Publisher, Weinheim, Germany
8. Herschbach C, Rennenberg H (2001) Significance of phloem-translocated organic sulfur compounds for the regulation of sulfur nutrition. Prog Bot 62:177–192
9. Van der Kooij TAW, De Kok LJ, Haneklaus S, Schnug E Uptake and metabolism of sulfur dioxide by *Arabidopsis thaliana*. New Phytol 135:101–107
10. Noji M, Saito M, Nakamura M, Aono M, Saji H, Saito K (2001) Cysteine synthase overexpression in tobacco confers tolerance to sulfur-containing environmental pollutants. Plant Physiol 126:973–980
11. Legge AH, Krupa SV (2002) Effects of sulphur dioxide. In: Bell JNB, Treshow M (eds) Air pollution and plant life, 2nd edn. John Wiley, Chichester
12. Matityahu I, Kachan L, Ilan IB, Amir R (2006) Transgenic tobacco plants overexpressing the Met25 gene of *Saccharomyces cerevisiae* exhibit enhanced levels of cysteine and glutathione and increased tolerance to oxidative stress. Amino Acids 30:185–194
13. Brychkova G, Xia Z, Yang G, Yesbergenova Z, Zhang Z, Davydov O, Fluhr R, Sagi M (2007) Sulfite oxidase protects plants against sulfur dioxide toxicity. Plant J 50:696–709
14. Sanda S, Leustek T, Theisen MJ, Garavito RM, Benning C (2001) Recombinant Arabidopsis SQD1 converts UDP-glucose and sulfite to the

sulfolipid head group precursor UDP-sulfoquinovose in vitro. J Biol Chem 276: 3941–3946

15. Eilers T, Schwarz G, Brinkmann H, Witt C, Richter T, Nieder J, Koch B, Hille R, Hänsch R, Mendel RR (2001) Identification and biochemical characterization of *Arabidopsis thaliana* sulfite oxidase: a new player in plant sulfur metabolism. J Biol Chem 276:46989–46994
16. Kopriva S (2006) Regulation of sulfate assimilation in *Arabidopsis* and beyond. Ann Bot 97:479–495
17. Papenbrock J, Schmidt A (2000) Characterization of two sulfurtransferase isozymes from *Arabidopsis thaliana*. Eur J Biochem 267:5571–5579
18. Tsakraklides G, Martin M, Chalam R, Tarczynski MC, Schmidt A, Leustek T (2002) Sulfate reduction is increased in transgenic *Arabidopsis thaliana* expressing 5′-adenylylsulfate reductase from *Pseudomonas aeruginosa*. Plant J 32:879–889
19. Brychkova G, Yarmolinsky D, Sagi M (2012) Kinetic assays for determining in vitro APS reductase activity in plants without the use of radioactive substances. Plant Cell Physiol 53(9):1648–1658
20. Brychkova G, Yarmolinsky D, Ventura Y, Sagi M (2012) A novel in-gel assay and an improved kinetic assay for determining in vitro sulfite reductase activity in plants. Plant Cell Physiol 53(8):1507–1516

Chapter 15

Determination of Total Sulfur, Sulfate, Sulfite, Thiosulfate, and Sulfolipids in Plants

Assylay Kurmanbayeva, Galina Brychkova, Aizat Bekturova, Inna Khozin, Dominic Standing, Dmitry Yarmolinsky, and Moshe Sagi

Abstract

In response to oxidative stress the biosynthesis of the ROS scavenger, glutathione is induced. This requires the induction of the sulfate reduction pathway for an adequate supply of cysteine, the precursor for glutathione. Cysteine also acts as the sulfur donor for the sulfuration of the molybdenum cofactor, crucial for the last step of ABA biosynthesis. Sulfate and sulfite are, respectively, the precursor and intermediate for cysteine biosynthesis and there is evidence for stress-induced sulfate uptake and further downstream, enhanced sulfite generation by 5′-phosphosulfate (APS) reductase (APR, EC 1.8.99.2) activity. Sulfite reductase (SiR, E.C.1.8.7.1) protects the chloroplast against toxic levels of sulfite by reducing it to sulfide. In case of sulfite accumulation as a result of air pollution or stress-induced premature senescence, such as in extended darkness, sulfite can be oxidized to sulfate by sulfite oxidase. Additionally sulfite can be catalyzed to thiosulfate by sulfurtransferases or to UDP-sulfoquinovose by SQD1, being the first step toward sulfolipid biosynthesis.

Determination of total sulfur in plants can be accomplished using many techniques such as ICP-AES, high-frequency induction furnace, high performance ion chromatography, sulfur combustion analysis, and colorimetric titration. Here we describe a total sulfur detection method in plants by elemental analyzer (EA). The used EA method is simple, sensitive, and accurate, and can be applied for the determination of total S content in plants.

Sulfate anions in the soil are the main source of sulfur, required for normal growth and development, of plants. Plants take up sulfate ions from the soil, which are then reduced and incorporated into organic matter. Plant sulfate content can be determined by ion chromatography with carbonate eluents.

Sulfite is an intermediate in the reductive assimilation of sulfate to the essential amino acids cysteine and methionine, and is cytotoxic above a certain threshold if not rapidly metabolized and can wreak havoc at the cellular and whole plant levels. Plant sulfite content affects carbon and nitrogen homeostasis Therefore, methods capable of determining sulfite levels in plants are of major importance. Here we present two robust laboratory protocols which can be used for sulfite detection in plants.

Thiosulfate is an essential sulfur intermediate less toxic than sulfite which is accumulating in plants in response to sulfite accumulation. The complexity of thiosulfate detection is linked to its chemical properties. Here we present a rapid, sensitive, and accurate colorimetric method based on the enzymatic conversion of thiosulfate to thiocyanate.

The plant sulfolipid sulfoquinovosyldiacylglycerol (SQDG) accounts for a large fraction of organic sulfur in the biosphere. Aside from sulfur amino acids, SQDG represents a considerable sink for sulfate in plants and is the only sulfur-containing anionic glycerolipid that is found in the photosynthetic membranes of plastids. We present the separation of sulfolipids from other fatty acids in two simple ways: by one- and two-dimensional thin-layer chromatography.

Ramanjulu Sunkar (ed.), *Plant Stress Tolerance: Methods and Protocols*, Methods in Molecular Biology, vol. 1631,
DOI 10.1007/978-1-4939-7136-7_15,

Key words Total sulfur, Elemental analyzer, Sulfate, Ion chromatography, Sulfite detection, NADH coupled reaction, Fuchsin colorimetric detection, OAS-TL/SiR coupled reaction, Thiosulfate, Sulfite, Rhodanese, Sulfurtransferases, Colorimetric detection, SQDG, Fatty acids, Thin-layer chromatography, 1D, 2D

1 Introduction

As a plant macronutrient, sulfur is important for yield production and quality of crops. In nature, sulfur is mostly available in its fully oxidized anion sulfate form, which is taken up, reduced, and incorporated into cysteine via sulfite and sulfide generation in the sulfate assimilation pathway [1] (Fig. 1).

In addition to its presence in the amino acids cysteine and methionine, sulfur is an important component of oligopeptides such as glutathione, coenzymes, prosthetic groups, vitamins and secondary metabolites, and lipids [1, 2]. In the latter case, the chloroplast membrane containing sulfolipids [sulfoquinovosyldiacylglycerol (SQDG)] is one of the primary sulfur-containing components in higher plants [3]. Sulfite, a less oxidized form of sulfate, is an intermediate in the assimilation of sulfur and a potentially cytotoxic molecule [4] that if not rapidly metabolized can wreak havoc at the cellular [5, 6] and whole plant levels [7, 8]. Roots obtain sulfate from the soil and sulfite is generated from sulfate in the leaves by the chloroplast-localized 5′-adenylylsulfate (APS) reductases [APR, EC 1.8.4.9, (*AtAPR1*, *2*, and *3* in *Arabidopsis*)] [9]. Another source of sulfite is atmospheric, originating from microbial, volcanic, or anthropogenic activities and entering the plant via the stomata or through the root system. In mammal tissue, endogenous sources for sulfite are thought to be formed during the degradation of the S-containing amino acids [10–12]. Such scavenging has not been explored in plants.

1.1 Multiple Pathways for Sulfite/SO_2 Utilization

Since sulfite is cytotoxic at elevated concentrations [4], it can be expected that cellular levels of sulfite are tightly regulated in an interplay between its production and conversion. Known avenues for *in planta* sulfite assimilation and detoxification make up a potential network for the control of sulfite turnover (*see* Fig. 1). One pathway is ferredoxin-dependent sulfite reduction catalyzed by chloroplast-localized sulfite reductase (SiR, EC 1.8.7.1) to yield a reduced sulfide (S^{2-}) in primary sulfate assimilation [13]. Another pathway for sulfite utilization is its incorporation into sulfolipids, where sulfite is catalyzed by chloroplast-localized UDP-sulfoquinovose synthase (SQD1, EC 3.13.1.1) protein [6]. Sulfite can be reoxidized back to sulfate by the molybdenum cofactor-containing enzyme, sulfite oxidase, localized to the peroxisomes [14]. Alternatively, the nucleus-, chloroplast-, mitochondrion-, and cytosol-localized β-mercaptopyruvate sulfurtransferase

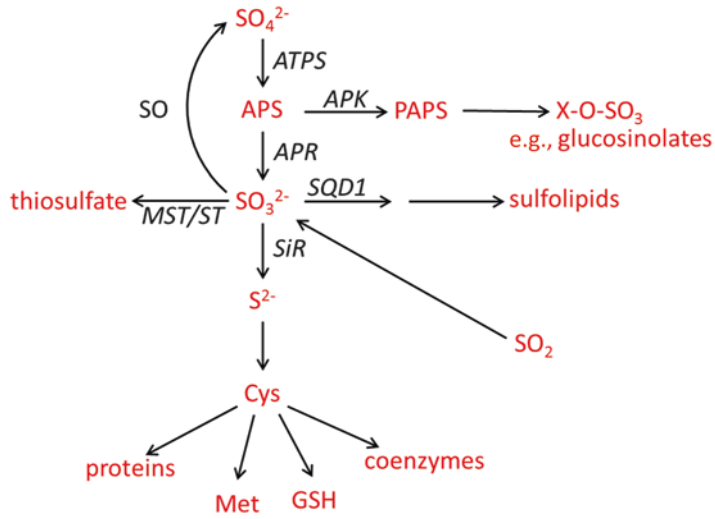

Fig. 1 Pathway of sulfate assimilation. Sulfate is activated to adenosine 5′-phosphosulfate (APS) by ATP sulfurylase (ATPS). APS is rather reduced by APS reductase (APR) to sulfite or further phosphorylated by APS kinase (APK) to activated sulfate PAPS, which is used for synthesis of sulfated secondary metabolites such as glucosinolates. Sulfite can be further reduced by sulfite reductase (SiR) to sulfide and incorporated into cysteine, which in turn is the source of reduced sulfur for the synthesis of methionine, glutathione, and various coenzymes. Sulfite is also formed from atmospheric SO_2 and can be used for synthesis of sulfolipids by SQD1 enzymes, metabolized to thiosulfate by sulfurtransferases such as MST1 protein, or oxidized in peroxisomes to sulfate by sulfite oxidase (SO). The "sulfite network" metabolites are highlighted in *red*

(ST) multigene family (20 gene members in Arabidopsis) has been shown to catalyze the synthesis of the less toxic compound thiosulfate in the presence of β-mercaptopyruvate and sulfite [15, 16].

2 Materials

2.1 Detection of Total Sulfur in Plants

1. Prepare plant materials and dry (*see* **Notes 1** and **2**).
2. Accurately record the mass of the samples before and after drying.
3. Grind dried materials as finely as possible in mortar and pestle to ensure sample homogeneity.
4. Prepare reference materials GSH or Cys as standards. Weigh three standards of slightly different masses (2.0, 2.5, 3.0 mg for example).

2.2 Sulfate Determination in Plants by Ion Chromatography

Prepare all solutions using ultrapure Milli-Q water and analytical grade reagents.

1. 200 mM Na_2CO_3/75 mM $NaHCO_3$: Dissolve 2.1 g of Na_2CO_3 and 0.63 g of $NaCO_3$ in 100 mL of Milli-Q. Store at +4 °C.

2. Formaldehyde.
3. Syringe-driven filter units (PVDF, 0.22 μm).
4. Sterile syringe.
5. IonPac polymeric column (AS 4ASC; Dionex).

2.3 Sulfite Detection in Plants

2.3.1 Protocol 1. Sulfite Detection with Basic Fuschin

Here we describe in detail the laboratory protocols briefly described in Brychkova et al. [17]. Sulfite detection with basic fuchsin has several advantages, such as rapidity, very low cost and the possibility to use the protein fraction for other analyses. This method is very convenient for *Arabidopsis* samples, but has some complications if one needs to detect sulfite levels in plants with strong coloration, as the plant color can interfere with fuchsin stain. It is also necessary to prepare the color reagent as described, since temperature can alter fuchsin color. Note that external sulfite addition to the reaction prevents internal sulfite from been oxidized.

All the solutions should be prepared using Milli-Q grade water. All working solutions should be freshly prepared and stored on ice, unless indicated otherwise.

Materials for Sample Deproteinization

1. Prepare 1 L of 1 M Tris–acetate buffer, pH 7.25 by dissolving 121.1 g of Trizma base in 800 mL of Milli-Q water. Adjust the pH with glacial acetic acid and make up to 1 L with Milli-Q water.
2. Prepare Sulfate buffer (0.5 M Na_2SO_4 in 0.1 M Tris–acetate, pH 8.0) by adding 5 mL 1 M Tris–acetate buffer, pH 7.25 to 30 mL H_2O and 3.6 g of anhydrous Na_2SO_4. Make up to 50 mL with Milli-Q water. Do not adjust the pH, as it will become 8.0 after adding the sodium sulfate.
3. Prepare G25 columns to separate proteins from metabolites. To do so, remove the cap and bottom from the column, allow the storage liquid to pass through the column, and saturate the Sephadex G-25 with sulfate buffer, pH 8.0 by passing 3 mL of sulfate buffer three times through the column. Avoid column drying.

Materials for Sulfite Standard Curve

1. Prepare 100 mM sodium sulfite stock by dissolving 126 mg Na_2SO_3 in 10 mL DDW.
2. Prepare 1 mM Na_2SO_3 solution by diluting 0.1 mL of 100 mM sodium sulfite in 9.9 mL of sulfate buffer, pH 8.0.
3. Prepare dilutions for the standard curve from 0 to 500 μM (Table 1)

Materials for Sulfite Detection Reagents

1. Prepare the 0.5 mM sulfite solution in water by diluting 50 μL of 100 mM Na_2SO_3 in 10 mL of Milli-Q water.
2. Prepare **Reagent A (**Acid-discolored fuchsin solution) by adding 4 mg of basic fuchsin to 8.25 mL ice-cold Milli-Q water,

Table 1
Dilutions for the standard curve

Final sulfite concentration, μM	μL of 1 mM sulfite	μL, sulfate buffer, pH 8.0
0	0	200
10	2	198
20	4	194
50	10	190
100	20	180
200	40	160
300	60	140
500	100	100

place on ice for 5 min, and then add 1.25 mL of concentrated sulfuric acid. Keep the solution on ice while adding sulfuric acid (exothermic reaction).

3. Prepare **Reagent B solution** by diluting 0.320 mL formaldehyde in 9.68 mL Milli-Q water.
4. The **Color reagent** should be mixed fresh prior to use. To do so, 1 mL of **Reagent A** should be added to 7 mL Milli-Q water followed by addition of 1 mL **Reagent B**.

2.3.2 Protocol 2. Sulfite Detection with Sulfite Oxidase Enzyme

The method provided below contains some modifications from Sulfite UV test kit (R-Biopharm AG, Darmstadt, Germany, Cat. No. 10725854035) protocol. The kit is essential for sulfite detection in plant samples.

All the solutions should be prepared using Milli-Q grade water. All working solutions should be freshly prepared and stored on ice, unless indicated otherwise. Waste should be disposed of according to local waste disposal regulations.

Materials for Sample Deproteinization

1. Prepare 1 L of 1 M Tris–HCl buffer, pH 8.0 by dissolve 121.1 g Trizma base in 800 mL Milli-Q water and carefully adjust pH to 8.0 with concentrated HCl. Make up to 1 L with Milli-Q water.
2. Prepare Sulfate buffer (0.5 M Na_2SO_4 in 0.1 M Tris–HCl, pH 8.0) by adding 5 mL 1 M Tris–HCl, pH 8.0 to 30 mL H_2O and 3.6 g anhydrous Na_2SO_4. Make up to 50 mL with Milli-Q water. Adjust to pH 8 with concentrated HCl if needed.
3. Prepare G25 columns to separate proteins from metabolites. To do so, remove the cap and bottom from the column, allow the storage liquid to pass through the column, and saturate

Sephadex G-25 with sulfate buffer, pH 8.0 by passing 3 mL of sulfate buffer through the column three times. Avoid column drying.

Materials for the Sulfite Standard Curve

1. Prepare 100 mM sodium sulfite stock by dissolving126 mg Na_2SO_3 in 10 mL DDW.
2. Prepare 1 mM Na_2SO_3 solution by diluting 0.1 mL of 100 mM sodium sulfite in 9.9 mL sulfate buffer, pH 8.0.
3. Prepare the dilutions for the standard curve from 0 to 200 μM (Table 2).

Materials for Sulfite Detection Reagents

The Sulfite UV test kit (R-Biopharm, Cat. No. 10725854035) was used according to instructions but with some modifications. The volumes are recalculated to have 210.7 μL in one reaction. Bottle 1 contains triethanolamine buffer, pH 8.0; Bottle 2 contains reduced nicotinamideadenine dinucleotide (NADH) tablets, approx. 0.4 mg each; Bottle 3 contains 0.3 mL suspension, consisting of enzyme NADH-peroxidase (NADH-POD), approx. 3 U; Bottle 4 contains 1.6 mL of chicken sulfite oxidase ($S0_2$-OD).

1. Prepare reaction mixture **1&2**. To do so, dissolve 1 NADH tablet from **Bottle 2** in 1 mL of triethanolamine buffer from **Bottle** 1. Keep the mixture on ice.
2. Immediately prior to starting the reaction, add 10 μL of NADH-POD solution from the **Bottle 3** (carefully mix prior to use) to the **1&2** premix. This will result in **1&2&3 reagent**.

2.4 Enzymatic Detection of Thiosulfate in Plant Tissues

All the solutions should be prepared using Milli-Q grade water. All working solutions should be freshly prepared and stored on ice, unless indicated otherwise. Waste should be disposed of according to local waste disposal regulations.

Table 2
Dilutions for the standard curve

Final sulfite concentration, μM	μL, 1 mM sulfite	μL, sulfate buffer, pH 8.0
0	0	1000
5	5	995
10	10	990
20	20	980
50	50	950
100	100	900
200	200	800

2.4.1 Materials for Extraction

1. Prepare 1 M Tris–HCl buffer, pH 9.0. To do so, dissolve 121.1 g of Trizma base in 800 mL of Milli-Q water. Adjust the pH to 9.0 by adding concentrated HCl (approximately 30 mL). Make up to 1 L with Milli-Q water.
2. Prepare 1 L 0.1 M Tris–HCl buffer, pH 9.0 by diluting 100 mL of 1 M Tris–HCl to 1 L with Milli-Q water.
3. Prepare 0.1 M HCl by adding 4.12 mL concentrated HCl to 400 mL Milli-Q water, and then make up to 500 mL with Milli-Q water.

2.4.2 Materials for Detection

1. Prepare a working solution of rhodanese enzyme from bovine liver (R1756, Sigma) by dissolving 1 mg of rhodanese (119 U) in 2 mL of 0.1 M Tris–HCl, pH 9.0.
2. Prepare 10 mL **solution F** by adding 1.36 mL 12 M HCl and 48.6 mg anhydrous $FeCl_3$ to 3 mL water and make up to 10 mL with water. Keep the solution in the dark by covering tube in the aluminum foil and on ice.
3. Prepare **solution D** by adding 8.2 mL 12 M HCl to 1.8 mL water and dissolving 41.8 mg N,N-dimethyl-p-phenylenediammonium dichloride in it.
4. Prepare 10 mM dithiothreitol solution by dissolving 23 mg DL-dithiothreitol in 15 mL 0.1 M Tris–HCl, pH 9.0.

2.4.3 Materials for the Standard Curve

1. Prepare a stock of 10 mM sodium thiosulfate by dissolving 15.8 mg sodium thiosulfate in 10 mL 0.1 M Tris–HCl, pH 9.0.
2. Prepare 100 μM thiosulfate solution by diluting 0.1 mL of 10 mM sodium thiosulfate in 9.9 mL 0.1 M Tris–HCl, pH 9.0.
3. Prepare the dilutions for the standard curve from 0 to 30 μM (Table 3).

2.5 Detection of Sulfolipids in Plants

Prepare and store all reagents at room temperature under the fume hood and use DD water, glass test tubes and vials. 0.01% butylated hydroxytoluene (BHT) should be added to all solvents.

2.5.1 Materials for Lipid Extraction

1. Use only glass tubes with Teflon lined screw caps and glass vials, glass Pasteur pipettes.
2. Isopropanol with 0.01% butylated hydroxytoluene (BHT) to limit oxidation. BHT 0.01% w/v.
3. Prepare 2:1:0.8 mL methanol–chloroform–water (v:v:v) solution
4. Prepare chloroform and water, separately.

2.5.2 Materials for Washing Solution

1. Washing solution: 65:25 mL chloroform–methanol, v/v.

Table 3
Dilutions for the thiosulfate standard curve

Final thiosulfate concentration, μM	μL of 100 μM thiosulfate	μL, 0.1 M Tris–HCl, pH 9.0
0	0	1000
2	20	980
5	50	950
7	70	930
10	100	900
15	150	850
20	200	800
30	300	700

2.5.3 Materials for 1D TLC and 2D TCL

1. For 1D TCL: Polar lipid separation solution 85:20:10:4 v/v chloroform–methanol–acetic acid–water.
2. For 2D TLC: System A: 65:25:4 v/v/v chloroform-methanol-water and System B: 65:35:5:0.5 v/v/v/v Chloroform-methanol-NH_4OH-Isopropylamine

2.5.4 Materials to Visualize the Fatty Acid Spots

1. 10% v/v sulfuric acid (concentrated) in methanol.
2. UV solution: 50 mg of 8-anilinonaphthalene-1-sulfonic acid (ANS) dissolve in 100 mL methanol.

3 Methods

3.1 Detection of Total Sulfur in Plants (for Flash 2000EA, Running Eager Xperience Software)

1. Using an analytical scale accurately weigh 2–3 mg of the powdered plant material and standards into tin capsules, record the mass, add 5–10 mg vanadium pentoxide, mix (*see* **Note 3**), and seal the tin capsule (*see* **Note 4**).
2. The sample order should be as follows: Bypass, Blank, Standard (×3), Sample (*see* **Note 5**).
3. Place capsules inside the autosampler making sure that the autosampler lid is correctly seated after all the capsules are in.
4. Using the software set up or use an existing method (*see* **Note 6**).
5. Enter sample type (blank, bypass, standard, sample), filename, and mass, where appropriate.
6. Make sure that the software recognizes the table by clicking anywhere outside the table and then click "OK."

7. When the EA reactor has reached its working temperature, a leak test has been performed, the samples loaded and the table correctly filled in with sample type, filename and mass (where appropriate) the run is ready to start.

3.2 Sulfate Determination in Plants by Ion Chromatography

3.2.1 Sample Preparation

1. Prepare extraction solution extraction solution by diluting 1 mL of 200 mM Na_2CO_3/75 mM $NaHCO_3$ solution in 100 mL of DDW. Add formaldehyde, 24 mM at final concentration.
2. With liquid nitrogen grind 20 mg plant tissue into a fine powder using a mortar and pestle. Add extraction solution extraction solution in ratio 1:100 (w/v).
3. Centrifuge at 18,400 × *g* for 15 min at 4 °C. Transfer supernatant to new tubes.
4. Centrifuge for a further 15 min at 18,400 × *g* collect supernatant, put on ice.
5. Incubate samples for 1 h at −20 °C.
6. Centrifuge for 15 min at 18,400 × *g*, collect supernatant.
7. Filter supernatant through 0.22 μm PVDF filters, to avoid the column inlet becoming clogged.
8. Samples can be transferred to separation columns for immediate detection or frozen at −80 °C until needed.

3.2.2 Ion Chromatography

1. Equilibrate the system with eluent before use. It takes at least 30 min.
2. Inject a standard containing 10 mg/L sulfate in methanol. The column is equilibrated when two consecutive injections of the standard produce identical retention times. Retention times of 3.57 and 3.90 min distinguish sulfite from sulfate, respectively (*see* **Note 7**).

3.3 Sulfite Detection in Plants

3.3.1 Protocol 1. Sulfite Detection with Basic Fuschin

Sulfite Extraction

1. Collect 100 mg of plant samples (use leaves from the same position on the plants), finely chop them with sharp razor blade, flash-freeze in liquid nitrogen and store at −80 °C prior to extraction.
2. For the extraction take the samples stored at −80 °C and place them in an ice-cold mortar with 5 mg white quartz sand. Crush the samples with an ice-cold pestle for 1 min, then add 600 μL sulfate buffer and crush until homogenous.
3. Transfer samples to 2.0 mL SafeSeal microcentrifuge tubes and centrifuge at 18,400 × *g* for 10 min at 4 °C.
4. Collect supernatant into new 2.0-mL tubes and then transfer 500 μL of the supernatant into the G25 the column equilibrated with sulfate buffer. Allow sample to completely absorb into the G25 matrix.

5. To separate the proteins from the metabolites add 1000 μL of sulfate buffer to the G25 columns. Allow the buffer to be completely absorbed into the G25 Sephadex. The 1 mL released from the column contains the proteins. They can be collected and used for other analyses, where sulfate presence will not affect the results. To collect metabolites, transfer the column into a new 15-mL tube, add 1.5 mL of sulfate buffer to the G25 column. According to the G25 column specification, the released 1.5 mL solution contains most of the metabolites. Use the solution immediately.

Sulfite Detection

1. Add 30 μL plant extract/standard/blank to the wells of a flat 96-well microplate, containing 5 μL 0.5 mM sulfite solution in water. Use 30 μL sulfate buffer, containing 5 μL 0.5 mM sulfite solution in water as a blank.
2. Using a multichannel pipette simultaneously add 215 μL freshly prepared Color reagent and mix it with the sample/standard/blank.
3. Incubate samples for 10 min at room temperature and measure sulfite concentration at spectrophotometrically at 570 nm.

When calculating sulfite levels take into account all dilutions (Fig. 2a). Note that extraction through the column results in a threefold dilution.

3.3.2 Protocol 2. Sulfite Detection with Sulfite Oxidase Enzyme

The method provided below contains some modifications from Sulfite UV test kit (R-Biopharm AG, Darmstadt, Germany) protocol. The kit is essential for sulfite detection in plant samples.

Method for Sulfite Detection with Chicken Sulfite Oxidase (SOC)

Sulfite Extraction

1. Collect 100 mg plant samples (use leaves from the same position), finely chop them with sharp razor blade, flash-freeze in liquid nitrogen and store at −80 °C prior to extraction.
2. For extraction, take the samples stored at −80 °C and place them in an ice-cold mortar with 5 mg white quartz sand. Crush samples with an ice-cold pestle for 1 min, then add 600 μL sulfate buffer and crush until homogenous.
3. Transfer samples to 2.0 mL SafeSeal microcentrifuge tubes and centrifuge at 18,400 × *g* for 10 min at 4 °C.
4. Collect the supernatant into new 2.0-mL tubes and then transfer 500 μL of supernatant into the G25 column equilibrated with sulfate buffer. Allow the sample to be completely absorbed into the G25 matrix.
5. To separate the proteins from the metabolites add 1 mL of sulfate buffer to the G25 columns. Allow the buffer to be completely absorbed into the G25 Sephadex. The 1 mL released from the column contains the proteins. They can be collected and used for other analyses. To collect the metabolites, transfer the column into a new 15-mL tube and add 1.5 mL of sulfate

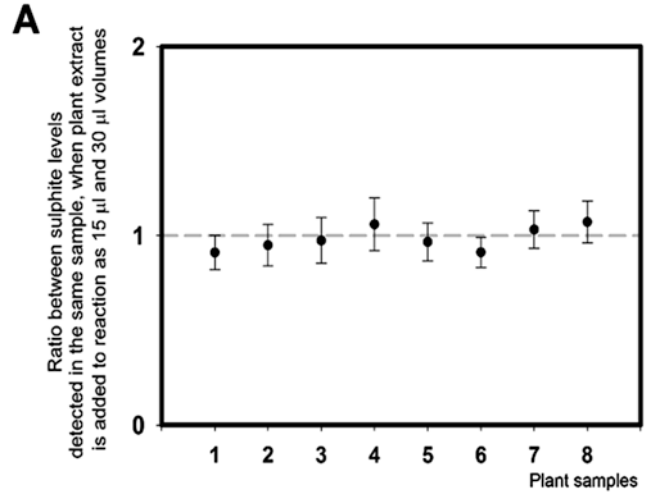

Sulfite levels in plants detected by fuchsin method

Plant sample	1	2	3	4	5	6	7	8
µg sulphite g-1 Fw	446.2	362.5	315.1	567.3	546.1	624.0	618.9	711.3

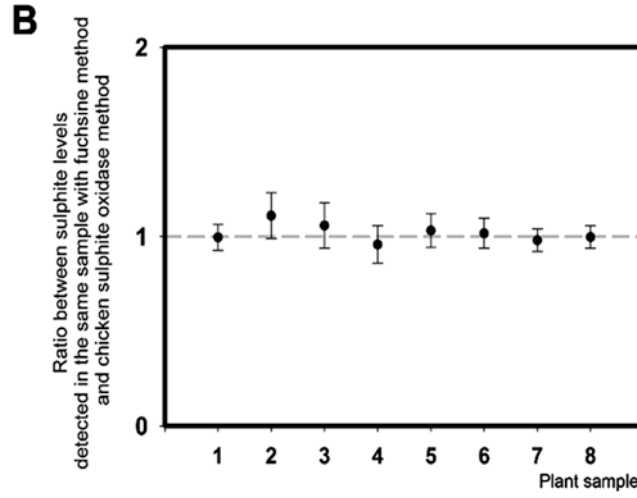

Sulfite levels in plants detected by chicken sulfite oxidase method

Plant sample	1	2	3	4	5	6	7	8
µg sulphite g-1 Fw	447.9	326.3	297.6	591.9	529.0	613.0	631.0	712.9

Fig. 2 Comparison of sulfite levels detected by fuchsin detection method in two different sample volumes (**a**) and between sulfite levels detected by fuchsin method and chicken sulfite oxidase method (**b**) in *Arabidopsis* plant samples (1–5) and tomato plant samples (6–8)

buffer to the column. According to the G25 column specification, the released 1.5-mL solution contains most of the metabolites.

6. Use the solution immediately.

Sulfite Detection

1. Load 100 μL of plant extract/standard/blank to the wells of a flat 96-well microplate, containing 40 μL of Milli-Q water.
2. Using a multichannel pipette simultaneously add 70.7 μL of freshly prepared 1&2&3 reagent and mix it with the sample/standard/blank.
3. Incubate samples for 10 min at room temperature (26 °C) and read the samples/standard/blank spectrophotometrically at 340 nm (use path length correction). The corrected results for 340 nm will be A1 point.
4. Using a multichannel pipette simultaneously add 3.2 μL of sulfite oxidase from the Bottle 4 (prewarmed to room temperature for 10 min and carefully mixed prior to adding to the wells) to each well.
5. Read the samples/standard/blank every 5 min for 30 min (or use the kinetic option on your spectrophotometer) at 340 nm. After 30 min the reaction should be completed.
6. Read the samples/standard/blank at 340 (use pathlength correction) at 30 min. The corrected results for 340 nm will be the A2 point.
7. Calculate the results either based on the standard curve or using the extinction coefficient. The results are comparable with sulfite levels detected in the same plant samples by the fuchsin method (Fig. 2b).
8. Below is described calculation of sulfite using the extinction coefficient.

Determine the absorbance differences ($A1-A2$) for blank, standards, and samples.

Subtract the absorbance difference of the blank from the absorbance difference of the sample:

$$\Delta A = (A1-A2)_{\text{sample}} - (A1-A2)_{\text{blank}}.$$

Make standard curve, then $C = \Delta A/a \times F$, where C is the concentration, "a" is from the standard curve equation $y = ax + b$, and F is the dilution factor.

The sulfite content can also be calculated using ε (extinction coefficient) of NADH at 340 nm according to the general equation for calculating the concentration:

$$C = \frac{V \times MW}{\varepsilon \times d \times v \times 1000} \times \text{“}\, A\left[g / l\right], \text{ where:}$$

V = final volume (mL),
v = sample volume,
MW = molecular weight of the substance to be assayed (g/mol).
d = light path (cm).

ε = extinction coefficient of NADH at 340 nm = 6.3 (L × $mmol^{-1}$ cm^{-1}).

It follows for sulfite (as SO_2).

$$C = \frac{0.306 \times 64.06}{6.3 \times d \times 0.2 \times 1000} \times \text{“} A[g/l] \quad \text{(g } SO_2 \text{ } L^{-1} \text{ sample solution)}$$

If the samples are diluted during the preparation, the results must be multiplied by the dilution factor F. Note that extraction through the column results in a threefold dilution.

3.4 Enzymatic Detection of Thiosulfate in Plant Tissues

3.4.1 Thiosulfate Extraction

1. Collect 100 mg of plant samples (use leaves from the same position on the plants), finely chop them with sharp razor blade, flash-freeze in liquid nitrogen and store at −80 °C prior to extraction.
2. For extraction take the samples stored at −80 °C and crush them in an ice-cold mortar and pestle with 5 mg white quartz sand. Add 600 µL 0.1 M Tris–HCl, pH 9.0 and crush until homogenous.
3. Transfer samples to 2.0 mL SafeSeal microcentrifuge tubes and centrifuge at 18,400 × *g* for 10 min at 4 °C.
4. Prepare G25 columns to separate proteins from metabolites. To do so, remove the cap and bottom from the column, allow the storage liquid to pass through the column, and saturate Sephadex G-25 with 0.1 mM Tris–HCl, pH 9.0 by passing 3 mL Tris–HCl pH 9.0 buffer through the column three times. Avoid column drying.
5. Collect supernatant and add 500 µL to the G25 column equilibrated with 0.1 mM Tris–HCl, pH 9.0. Allow sample to be completely absorbed into G25 matrix.
6. To separate the proteins from the metabolites add 1 mL 0.1 mM Tris–HCl, pH 9.0, to G25 columns. Allow all the buffer to be completely absorbed into G25 Sephadex. The 1 mL which is released from the column contains the proteins. They can be collected and used for other analyses.
7. To collect metabolites (including thiosulfate), transfer the column into a new 15-mL tube, add 1.5 mL 0.1 mM Tris–HCl, pH 9.0 to the G25 column. According to the G25 column specification, the released 1.5-mL solution contains most of the metabolites.
8. Use the solution immediately.

3.4.2 Thiosulfate Detection

1. To detect thiosulfate 95 µL of 10 mM dithiothreitol solution first should be added to the wells of a flat 96-well microplate.
2. Next, 100 µL of sample or standard should be added to the wells containing dithiothreitol solution.

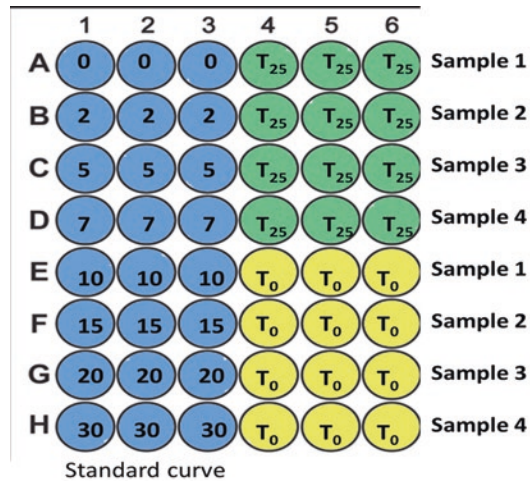

Fig. 3 96-well plate schematic to measure four samples and an 8-point standard curve. Use three repetitions for the standard curve. For each sample use 6 repetitions, since half will be used as time 0

3. To start the reaction, add 5 μL of enzyme solution according to the scheme in the Fig. 3. Add 5 μL water to the time 0 (T_0) wells.
4. Incubate samples for 25 min at room temperature (26 °C).
5. Color-develop the reaction by adding 20 μL solution D and 20 μL solution F to each well.
6. **Incubate for 1 h at room temperature; the final color of the reaction is light blue!** (Usually the reaction changes color very rapidly (orange, yellow, pink, green, and then developing stable blue color).
7. Read the absorbance of the blue color at 670 nm.

3.4.3 Thiosulfate Calculation

1. Calculate the slope and the R^2 of the standard curve after blanking all the numbers with their T_0 points (Fig. 4a).
2. Blank the OD data obtained for the samples by subtracting the OD of their corresponding T_0 points.
3. Calculate the thiosulfate content in samples based on the standard curve and dilution factor (Fig. 4b).

3.5 Detection of Sulfolipids in Plants

3.5.1 Lipid Extraction

1. Prepare 15 mL glass tube with Teflon-lined screw cap; add 2 mL of isopropanol with 0.01% BHT and heat at 80 °C (*see* **Note 8**).
2. Take 200 mg fresh plant tissue, transfer into the glass tube (preheated to 80 °C) and incubate for 15 min at 80 °C.
3. Centrifuge at 3500 × *g* for 5 min at room temperature and transfer isopropanol supernatant to a clean 4 mL glass tube and keep separately.

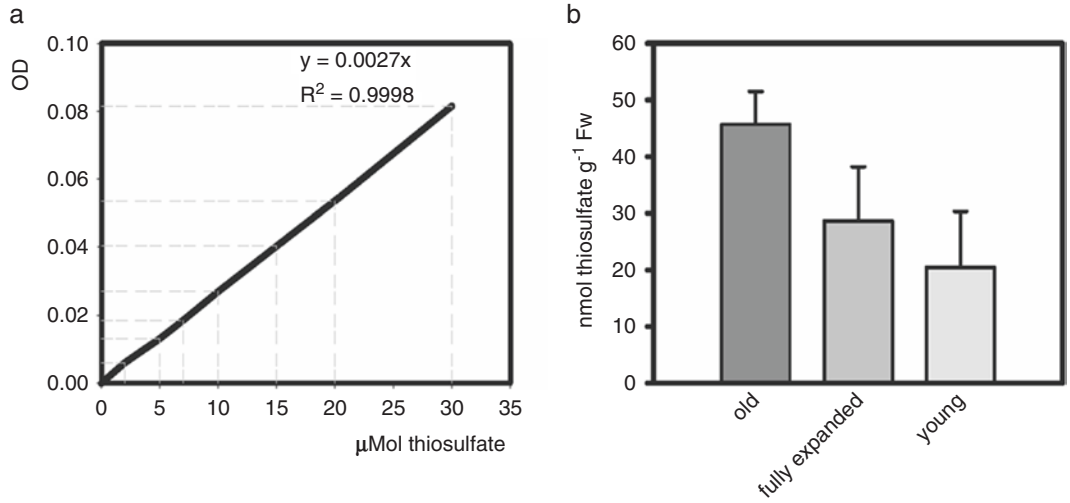

Fig. 4 Thiosulfate standard curve generated as described in Subheadings 3.3 and 3.4. Thiosulfate levels in old, fully expanded and young leaves of 6-week-old wild-type tomato plant

4. Continue extraction of residue by adding 2:1:0.8 mL methanol–chloroform–water solution. Keep at room temperature for 1 h with permanent stirring. If necessary continue at 4 °C until residue is colorless.
5. Centrifuge at 3500 × *g* for 5 min at room temperature. Transfer supernatant to a clean 15 mL glass tube and add 1:1 mL chloroform–water and mix well. This should create two phases.
6. Centrifuge at 3500 × *g* for 5 min at room temperature. Carefully collect the lower, lipid-containing fraction with a glass Pasteur pipette and transfer it to a 4 mL glass tube with isopropanol (from stage #4).
7. Dry the total lipid extracts under a stream of nitrogen and redissolve in 100 µL chloroform.
8. Keep samples at −20 °C.

3.5.2 Washing the TLC Plates

1. Add the washing solution to the TLC chamber and put the filter paper in to saturate it with vapor (*see* **Note 9**).
2. Place TLC plate (Silico 60 10 cm × 10 cm, 0.25 mm thickness, Silica Gel 60, Macherey-Nagel, Duren, Germany) into the washing solution and wait until all the solution is absorbed into the plate. Dry the TLC plate (*see* **Note 10**) in air ~5–10 min.

3.5.3 Separation of Lipids by 1D TLC

1. Load 10–20 µL of the samples onto the TLC plate (*see* **Note 11**).
2. Place TLC plate in polar lipids separation solution (*see* **Note 12**).
3. When the solvent front has reached 1 cm from the top of the plate, carefully remove the plate from the tank and dry completely in the fume hood for approximately 10 min.

3.5.4 Separation of Fatty Acids by 2D TLC

1. Load 20 μL of the samples onto the TLC plate as drops of 0.5 cm diameter.
2. Place the TLC plate in a TLC chamber containing **System A** and wait until all the solution is absorbed into the plate. Run for approximately 20 min till the front reaches 1 cm from the top.
3. Dry the TLC plate in air ~5–10 min.
4. Rotate the plate and place it in a TLC chamber containing **System B.**
5. Run for approximately 20 min until the front reaches 1.5 cm from the top.
6. Dry the TLC plate in air ~5–10 min.

3.5.5 Visualization

1. To visualize the lipids spray with 10% v/v sulfuric acid (concentrated) in methanol.
2. Heat at 120 °C for 10 min. The galactolipids bands are purple, while bands of sulfolipids are light pink. If the bands are heated longer, they become brown, but more visible (Fig. 5).

3.5.6 Alternative for GC: Transmethylation (Common Method for Total Fatty Acids and Spots from 1D and 2D TLC)

1. Spray with ANS UV solution.
2. Dry and mark the spots corresponding to SQDG under UV light (use suitable personal safety protection—do not expose your skin or eyes to UV light).
3. Prepare glass tubes and scrape lipid spots into the glass tubes.
4. Add 2 mL of 2% sulfuric acid in methanol solution (1 mL of sulfuric acid +49 mL methanol). Add 10 μL of heptadecanoic acid as an internal standard (0.5 mg/mL). This can be kept at −20 °C.
5. Add magnetic stirrers and put the tubes in a sand dry bath (80 °C) for 90 min mixing continuously.
6. Remove samples and cool on the benchtop until room temperature
7. Add 1 mL water and 1 mL hexane and vortex briefly.
8. Centrifuge at 3500 × *g* for 5 min. Take the upper fraction (hexane) and transfer it to a new tube.
9. Dry under nitrogen and then resuspend in 20 μL of hexane. Use for GS analysis.

Fatty acid methyl esters (FAME) were identified and quantified on a Trace GC Ultra (Thermo, Italy) equipped with a flame ionization detector and a programmed temperature vaporizing (PTV) injector.

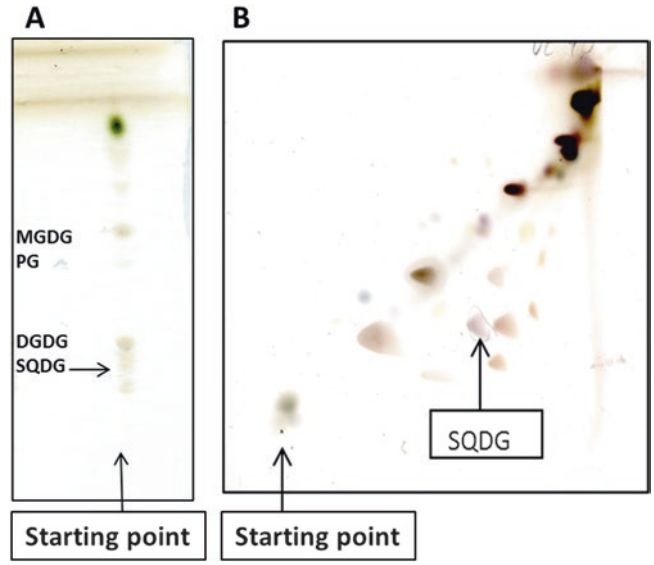

Fig. 5 Separation of fatty acids in TLC plates. 1D (**a**) and 2D (**b**) separation of fatty acids

4 Notes

1. If necessary, convert the detected amount of S to fresh weight by multiplying by the DW/FW ratio.
2. It is recommended to dry organic tissue at 65 °C and soils at 105 °C.
3. For S determination all standards and samples must be mixed with 5–10 mg vanadium pentoxide to ensure full conversion of any inorganic S to sulfur dioxide.
4. Close the tin capsule with tweezers (fold and squeeze the capsule as tightly as possible without breaking it) to minimize any air entering the sample.
5. There are four sample types: "Blank" (tin capsule only), "Bypass" (tin capsule containing standard used to condition the instrument and allow the operator to check the chromatogram), "Standard" (2–3 mg of known standard), and Sample (2–3 mg of sample).
6. For a detailed description of the EA the reader is referred to the Organic Elemental Analysis Flash 2000 Elemental Analyzer, Operating Manual available from Thermo Scientific (www.thermofisher.com). Many methods are available in the OEA Cookbook available from Thermo Finnigan Italia S.p.A
7. For a more detailed protocol of sulfate determination by ion chromatography refer to http://www.dionex.com.

8. It is extremely important that the plants be extracted immediately after sampling and that the isopropanol be preheated. Plants have very active phospholipase D, which is activated upon wounding; failure to place the sampled tissue quickly into hot isopropanol will result in generation of phosphatidic acid.
9. Work in a fume hood and always close the lid.
10. When the solvent front has reached 1 cm from the top of the plate, carefully remove the plate from the tank and dry completely in the fume hood for approximately 10 min under air or with a hairdryer.
11. Mark the starting point for the samples 1 cm from the bottom from left side and load the sample. Keep the spot smaller than 1 cm in diameter (for 1D and 2D TLC). Each plate can hold up to 4–5 samples for 1D TLC plate.
12. The liquid in the camera should be ~0.5 mm, which is around 50 mL.

Acknowledgment

With thanks to Mrs. Liron Summerfield for help and advice in using the EA.

References

1. Saito K (2000) Regulation of sulfate transport and synthesis of sulfur-containing amino acids. Curr Opin Plant Biol 3:188–195
2. Leustek T (2002) Sulfate metabolism. Arabidopsis Book 1:e0017
3. Shimojima M (2011) Biosynthesis and functions of the plant sulfolipid. Prog Lipid Res 50:234–239
4. Leustek T, Martin MN, Bick JA, Davies JP (2000) Pathways and regulation of sulfphur metabolism revealed through molecular and genetic studies. Annu Rev Plant Physiol Plant Mol Biol 51:141–165
5. Davidian J-C, Kopriva S (2010) Regulation of sulfate uptake and assimilation - the same or not the same? Mol Plant 3:314–325
6. Sanda S, Leustek T, Theisen MJ, Garavito RM, Benning C (2001) Recombinant Arabidopsis SQD1 converts UDP-glucose and sulfite to the sulfolipid head group precursor UDP-sulfoquinovose in vitro. J Biol Chem 276:3941–3946
7. Brychkova G, Xia Z, Yang G, Yesbergenova Z, Zhang Z, Davydov O, Fluhr R, Sagi M (2007) Sulfite oxidase protects plants against sulfur dioxide toxicity. Plant J 50:696–709
8. Murray F (1997) Urban air pollution and health effects. In: Brune D, Chapman DV, Gwynne MD, Pacyna JM (eds) The global environment: science, technology and management. Scandinavian Science Publisher, Weinheim, Germany
9. Vauclare P, Kopriva S, Fell D, Suter M, Sticher L, von Ballmoos O, Krähenbuhl U, Op den Camp R, Brunold C (2002) Flux control of sulfate assimilation in *Arabidopsis thaliana*: adenosine 5′-phosphosulfate reductase is more susceptible to negative control by thiols than ATP sulfurylase. Plant J 31:729–740
10. Amy NK (1988) Effect of dietary protein and methionine on sulfite oxidase activity in rats. J Nutr 118:941–944
11. Hänsch R, Mendel RR (2005) Sulfite oxidation in plant peroxisomes. Photosynth Res 86: 337–343
12. Heber U, Huve K (1998) Action of SO_2 on plants and metabolic detoxification of SO_2. Int Rev Cytol 177:255–286

13. Khan MS, Haas FH, Allboje Samami A, Moghaddas Gholami A, Bauer A, Fellenberg K, Reichelt M, Hansch R, RR M, Meyer AJ (2010) Sulfite reductase defines a newly discovered bottleneck for assimilatory sulfate reduction and is essential for growth and development in *Arabidopsis thaliana*. Plant Cell 22: 1216–1231
14. Eilers T, Schwarz G, Brinkmann H, Witt C, Richter T, Nieder J, Koch B, Hille R, Hänsch R, Mendel RR (2001) Identification and biochemical characterization of *Arabidopsis thaliana* sulfite oxidase: a new player in plant sulfur metabolism. J Biol Chem 276:46989–46994
15. Papenbrock J, Schmidt A (2000) Characterization of two sulfurtransferase isozymes from *Arabidopsis thaliana*. Eur J Biochem 267:5571–5579
16. Tsakraklides G, Martin M, Chalam R, Tarczynski MC, Schmidt A, Leustek T (2002) Sulfate reduction is increased in transgenic *Arabidopsis thaliana* expressing 5′-adenylylsulfate reductase from *Pseudomonas aeruginosa*. Plant J 32:879–889
17. Brychkova G, Yarmolinsky D, Fluhr R, Sagi M (2012) The determination of sulfite levels and its oxidation in plant leaves. Plant Sci 190: 123–130

Chapter 16

Determining Glutathione Levels in Plants

Smita Sahoo, Jay Prakash Awasthi, Ramanjulu Sunkar, and Sanjib Kumar Panda

Abstract

Upon exposure to abiotic stresses, plants tend to accumulate excessive amounts of reactive oxygen species (ROS) that inturn react with cellular lipids, proteins, and DNA. Therefore, decreasing ROS accumulation is indispensible to survive under stress, which is accomplished by inducing enzymatic and nonenzymatic antioxidant defense pathways. Glutathione, particularly reduced glutathione (GSH), represents a principal anitioxidant that could decrease ROS through scavenging them directly or indirectly through ascorbate–glutathione cycle or GSH peroxidases. Glutathione content can be determined using HPLC or spectrophotometric assays. In this chapter, we provided detailed assays to determine total, reduced, and oxidized gluathione using spectrophotometric method.

Key words Abiotic stress, GSH, GSSG, Oxidative stress, Reactive oxygen species

1 Introduction

Reactive oxygen species (hydrogen peroxide [H_2O_2], super oxide radicals [O_2^-], hydroxyl radicals, and singlet oxygen) are partially oxygnetaed molecules that are generated as by-products of aerobic cellular metabolism. In addition to other metabolic processes, being photosynthetic orgnisms, plants are more prone to produce ROS. The generation of ROS is further augmented by environmental stresses such as drought, temperature (high and low), salinity, heavy metals and other pollutants and UV-B [1, 2]. Although ROS serve many beneficial roles under stress by participating in signaling and acclimation responses, they are also extremely harmful and damage the lipid component of the membranes [3, 4]. To restrict the damaging effects of ROS, plants deploy enzymatic and nonenzymatic systems under stress. The enzymatic systems include superoxide dismutases, peroxidases (both glutathione and ascorbate-dependent peroxidases), catalases, and peroxiredoxin, while the nonenzymatic component

Ramanjulu Sunkar (ed.), *Plant Stress Tolerance: Methods and Protocols*, Methods in Molecular Biology, vol. 1631,
DOI 10.1007/978-1-4939-7136-7_16,

largely includes glutathione (GSH), ascorbate but also some of the sugars and sugar derivatives.

Glutathione is a thiol-containing low molecular-weight tripeptide (γ-glutamyl-cysteinyl-glycine) with a gamma peptide linkage between the carboxyl group of the glutamate side chain and the amine group of cysteine that distinguishes it from peptide bonds in proteins [5]. GSH is known to accumulate in all subcellular compartments of plant cells. Though GSH plays many roles in diverse aspects of plant processes including cell differentiation, cell death, enzymatic regulation, senescence and growth and development, its role as an antioxidant in cellular protection under stress is the most significant one [6]. Glutathione is an essential component of the sulfur metabolism and homesostasis by participating in signaling of sulphur status. It also regulates enzymatic activity, serves as a signaling molecule regulating gene expression, and participates in redox reactions controlling redox status. Further, it is a principal component of the ascorbate–glutathione cycle that scavenges hydrogen peroxide. In ascorbate–glutathione cycle GSH acts as a reducing agent that converts oxidized ascorbate into reduced form through dehydroascorbate reductase (DHAR) [6, 7]. GSH can also serve as an ROS scavenger because superoxide or hydroxyl radicals can oxidize GSH, which in turn reduces oxidation of other cellular components [5]. Oxidized glutathione forms disulfide with another molecule (GSSG). The GSSG can be reduced by glutathione reductases in various cellular compartments to regenerate GSH.

Spectrophotometric method is routinely used to determine glutathione levels in cells [5]. The spectrophotometric assay involves oxidation of GSH by the sulfhydryl reagent 5,5′-dithiobis(2-nitrobenzoic acid) (DTNB) to form the yellow derivative 5′-thio-2-nitrobenzoic acid (TNB), measurable at 412 nm. The oxidized glutathione or glutathione disulfide (GSSG) is measured by first reducing it to GSH with glutathione reductase (GR) in the presence of NADPH and then allowing GSH to react with DTNB again to produce more TNB.

2 Materials

All reagents should be prepared using deionized water and analytical grade reagents.

1. Eppendorf tubes.
2. Spectrophotometer (UV lamp).
3. Centrifuge.
4. Plant tissue.
5. 6% metaphosphoric acid containing 1 mM EDTA. Weigh 6 g of metaphosphoric acid and 0.029224 g of EDTA and transfer

to a glass beaker with distilled water and make up the volume to 100 mL.

6. 0.5 M potassium phosphate buffer (pH 7.5): Weigh 8.709 g of K_2HPO_4 and 6.8045 g KH_2PO_4 and dissolve in a glass beaker containing 80 mL of distilled water. Mix well and make up the volume to 100 mL. Adjust the pH of the reagent to 7.5 (*see* **Note 1**).
7. 10 mM BSA: Dissolve 6.6 g of BSA dissolved in 10 mL distilled water and store at −20 °C for further use.
8. 10 mM DTNB: Dissolve 99 mg in 25 mL ethanol and store at −20 °C for further use (*see* **Note 2**).
9. 0.5 mM NADH: Dissolve 8.292 mg in 25 mL distilled water and store at −20 °C for further use.
10. 2.5 mM NADPH: Dissolve 18.61 mg in 10 mL potassium phosphate buffer and store at −20 °C for further use (*see* **Note 3**).
11. 2-vinylpyridine. Dilute 2-vinylpyiridine (1:10) with potassium phosphate buffer and leave on ice until use (*see* **Note 4**).
12. Glutathione reductase.

3 Methods

The method provided below is slightly modified from Anderson's method [8].

3.1 Total Glutathione

1. Homogenize 0.2 g of tissue in 2 mL of 6% metaphosphoric acid containing 1 mM EDTA using chilled mortar and pestle.
2. Centrifuge the samples at 11,500 × *g* for 15 min at 4 °C and collect the supernatant.
3. Take 0.4 mL supernatant and add it to 1 mL of 0.5 M potassium phosphate buffer pH 7.5.
4. Then add 100 μL DTNB (10 mM), 200 μL (10 mM BSA), 100 μL NADH (0.5 mM) and incubate at 37 °C for 15 min.
5. Let cool and then measure the change in absorbance at 412 nm.

3.2 Oxidized Glutathione (GSSG)

1. For GSSG assay, the GSH is removed by addition of 2-vinylpyridine to the supernatant for 1 h at 25 °C.
2. Mix the sample extract (100 μL) with 600 μL reaction buffer (100 mM potassium phosphate buffer containing 5 mM EDTA, pH 7.5), 100 μL of diluted yeast GR (20 U/mL), and 100 μL of 10 mM DTNB.
3. The reaction is initiated by adding 100 μL of 2.5 mM NADPH; after mixing thoroughly, the rate of absorption change at 412 nm is monitored in a dual beam spectrophotometer.

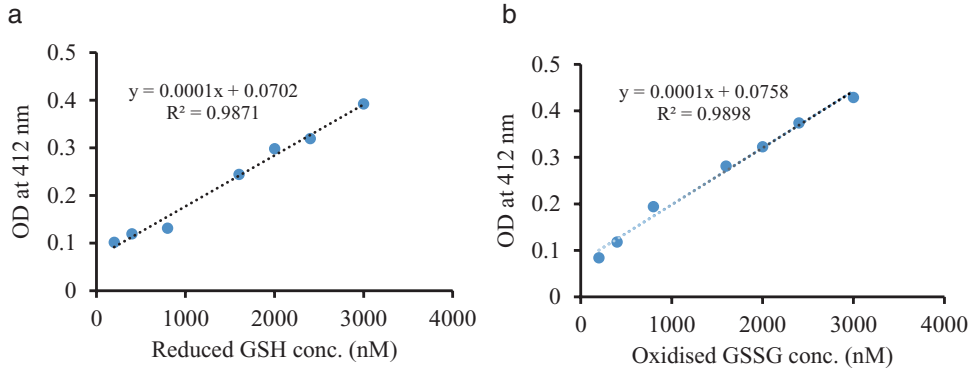

Fig. 1 Glutathione standard curve. Various amounts of reduced glutathione (GSH) and oxidized glutathione (GSSG) was used for standard. Absorbance was measured at OD 412 nm, reduced glutathione (**a**) and oxidized glutathione (**b**) standard curve

3.3 Reduced Glutathione (GSH)

1. GSH content is obtained after subtracting GSSG from the total glutathione.

Preparation of Solutions for Standard Curve: Standard curve (Fig. 1) for estimation of the reduced (GSH) and oxidized (GSSG) form of glutathione, 1 mM stock solution in diluted metaphosphoric acid (6%) is prepared.

4 Notes

1. Use a series of NaOH solutions (e.g., 1 and 0.1 N) to avoid sudden rise in pH.
2. DTNB is light sensitive. Exposure to light leads to nonspecific color intensification.
3. NADPH is also light sensitive and hence need to be prepared in a brown small vial or a vial covered with aluminium foil.
4. 2-vinylpyridine is a light-sensitive reagent and therefore need to be prepared in a brown small vial or a vial wrapped with aluminum foil.

References

1. Lnzé D, Van Montagu M (1995) Oxidative stress in plants. Curr Opin Biotech 6:153–158
2. Bartels D, Sunkar R (2005) Drought and salt tolerance in plants. Crit Rev Plant Sci 24:23–58
3. Nakano Y, Asada K (1987) Purification of ascorbate peroxidase in spinach chloroplasts; its inactivation in ascorbate-depleted medium and reactivation by monodehydroascorbate radical. Plant Cell Physiol 28:131–140

4. Mittler R, Vanderauwera S, Gollery M, Breusegem FV (2004) Abiotic stress series. Reactive oxygen gene network of plants. Trends Plant Sci 9:490–498
5. Noctor G, Queval G, Mhamdi A, Chaouch S, Foyer CH (2011) Glutathione. In: Arabidopsis book. American Society of Plant Biologists, Rockville, MD, p e0142. doi:10.1199/tab.0142
6. Ogawa K (2005) Glutathione-associated regulation of plant growth and stress responses. Antioxid Redox Signal 7:973–981
7. Noctor G et al (2012) Glutathione in plants: an integrated overview. Plant Cell Environ 35: 454–484
8. Anderson ME (1985) Determination of glutathione and glutathione disulfide in biological samples. Methods Enzymol 113:548–555

Chapter 17

Porous Graphitic Carbon Liquid Chromatography–Mass Spectrometry Analysis of Drought Stress-Responsive Raffinose Family Oligosaccharides in Plant Tissues

Tiago F. Jorge, Maria H. Florêncio, and Carla António

Abstract

Drought is a major limiting factor in agriculture and responsible for dramatic crop yield losses worldwide. The adjustment of the metabolic status via accumulation of drought stress-responsive osmolytes is one of the many strategies that some plants have developed to cope with water deficit conditions. Osmolytes are highly polar compounds, analysis of whcih is difficult with typical reversed-phase chromatography. Porous graphitic carbon (PGC) has shown to be a suitable alternative to reversed-phase stationary phases for the analysis of highly polar compounds typically found in the plant metabolome. In this chapter, we describe the development and validation of a PGC-based liquid chromatography tandem mass spectrometry ($LC\text{-}MS^n$) method suitable for the target analysis of water-soluble carbohydrates, such as raffinose family oligosaccharides (RFOs). We present detailed information regarding PGC column equilibration, $LC\text{-}MS^n$ system operation, data analysis, and important notes to be considered during the steps of method development and validation.

Key words Drought stress, Osmolytes, $LC\text{-}MS^n$, Mass spectrometry, Porous graphitic carbon, Raffinose family oligosaccharides

1 Introduction

Drought stress conditions are a major limitation for agriculture, and their impact leads to significant reductions in crop yield every year. This situation is anticipated to pose a real threat to food security in the next few years, as the most arable land worldwide is located in regions prone for example to either regular seasonal drought or floods. Because plants cannot escape from unfavorable situations, their survival relies on the initiation of adaptive responses. Central metabolism, i.e., carbohydrate, nitrogen, and energy metabolism, is essential for survival. Therefore, flexibility to reconfigure these primary metabolic pathways to maintain cellular homeostasis is essential for plants to help them alleviate the imposed stress. It is therefore very important to understand how

Ramanjulu Sunkar (ed.), *Plant Stress Tolerance: Methods and Protocols*, Methods in Molecular Biology, vol. 1631,
DOI 10.1007/978-1-4939-7136-7_17,

plants perceive constantly changing environmental signals and cope with such adverse conditions [1, 2].

Plants have developed different strategies at both morphological and physiological levels to cope with adverse environmental conditions, including leaf area reduction and the accumulation of osmolytes, respectively. Osmolytes, also known as compatible solutes, are small molecular weight organic compounds that do not inhibit cellular metabolism even at high concentrations (thus compatible), and include soluble sugars (e.g., glucose, sucrose, raffinose family oligosaccharides (RFOs)), polyols (e.g., mannitol, sorbitol), amino acids (e.g., proline), quaternary ammonium compounds (e.g., glycine betaine), and polyamines (e.g., putrescine, spermidine, and spermine) [3]. Among them, increasingly attention has been paid to RFOs which are known to have different stress-related physiological roles, such as osmoprotection during seed desiccation, carbon source to facilitate recovery on rehydration, antioxidant activity to counteract the accumulation of reactive oxygen species (ROS) and stabilization of the phospholipid membrane [4, 5]. Based on this, developments of target LC-MS methods for the analysis of RFOs will allow to better understand their physiological roles.

RFOs are nonstructural, water-soluble carbohydrates widely distributed in the plant kingdom, characterized by the formation of α-1,6 glycosidic linkages between a molecule of sucrose and galactosyl residues [6]. These residues are donated by a molecule of galactinol, and the sequential addition of one, two, and three galactosyl residues generates the most studied RFOs, namely raffinose, stachyose, and verbascose, respectively (Fig. 1). Common to all known osmolytes, RFOs are highly polar compounds, and consequently, show minimal retention on typical reversed phase stationary phases. High-performance anion exchange liquid chromatography (HPAEC) has been widely employed for the analysis of carbohydrates, including RFOs [7–10]. However, the mandatory use of mobile phases with high concentration of salts, such as sodium hydroxide and sodium acetate, strongly compromises its coupling with more sensitive mass spectrometry (MS) techniques.

Porous graphitic carbon (PGC) stationary phases are commercially available from Thermo Electron Corporation under the trade name Hypercarb [11, 12]. Due to its unique surface composed by a crystalline network of flat sheets of hexagonally arranged carbon atoms, PGC is highly reproducible and stable throughout the entire pH range 0–14, thus not limiting the use of pH-dependent mobile phases. The retention mechanism of analytes on the PGC surface is quite different from those observed on typical silica-based bonded stationary phases. Briefly, two essential processes account for the overall retention: (1) dispersive interactions of the analyte between mobile phase and graphite surface, by which retention increases as the hydrophobicity of the molecule increases

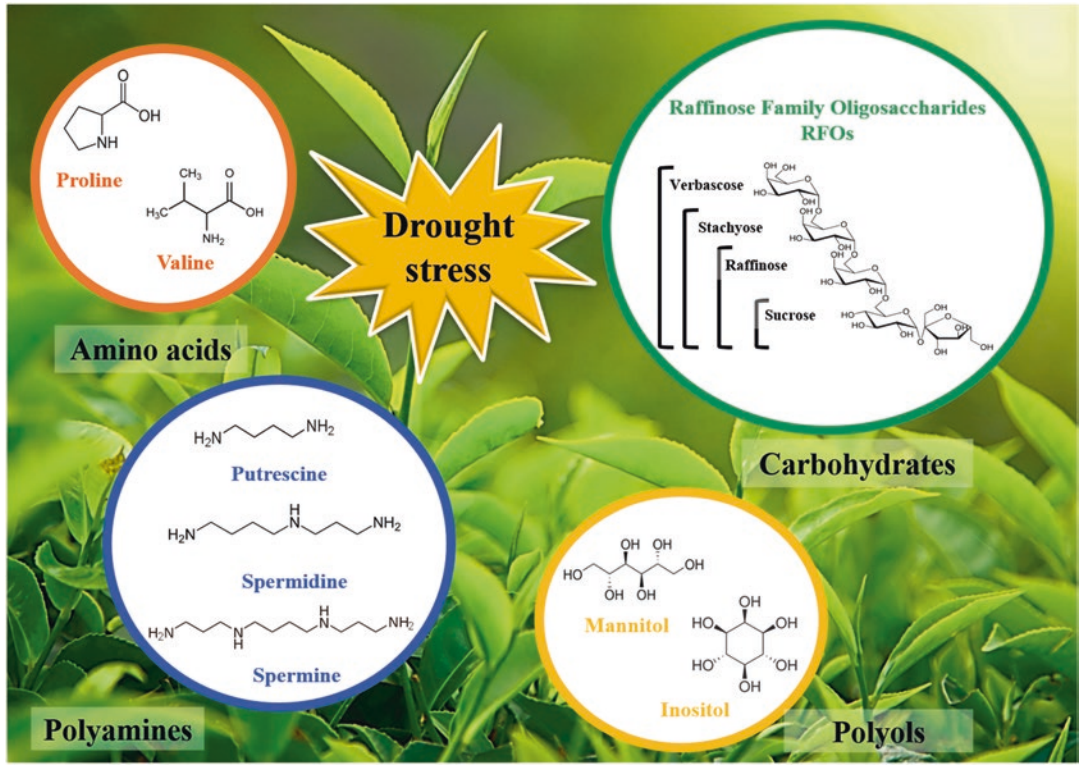

Fig. 1 Schematic diagram illustrating representative stress-responsive osmolyte classes

and (2) charge induced interactions of a polar analyte with the polarizable surface of graphite. In other words, the analyte retention strength depends on the molecular area in contact with the graphite surface and on the type and position of the functional groups at the point of interaction with the graphite surface. Thus, planar molecules are more retained on the PGC surface than highly structured, three-dimensional and rigid molecules, since more points of interaction are possible with the PGC surface [11, 12].

Considering these physicochemical properties, PGC has shown to be an excellent choice for the separation of closely related water-soluble carbohydrates from different biological matrices. Relevant applications include the analysis of a range of oligosaccharides from Triticum aestivum stems [13], phosphorylated carbohydrates from Arabidopsis thaliana leaves [14], RFOs from Lupinus albus stems [15] and leaves of the resurrection plant Haberlea rhodopensis [16], and nucleotide carbohydrates in A. thaliana tissues [17].

In this chapter we describe a detailed protocol for the development and validation of a PGC-LC-MS method for the target analysis of RFOs based on previous work published by Antonio and coworkers [15]. It must be highlighted that this protocol is broadly applicable to different plant tissues and can be transferred to other ion trap-based LC-MS systems with minor modifications.

2 Materials

2.1 Plant Material Sampling

1. Leaves, roots, or other tissue from any plant species.
2. Screw-cap polypropylene Falcon tubes (15 or 50 mL depending on the amount of material) for storage of frozen plant tissues.
3. 2.0-mL safe-lock polypropylene Eppendorf tubes for sample weighing and extraction.
4. Schott GL14 glass tubes for metabolite extraction.
5. Liquid nitrogen for sample quenching, grinding, and weighing of plant samples (*see* **Note 1**).
6. Protective gloves for handling frozen objects.
7. Metal spatula or small spoon.
8. Ceramic pestle and mortar or basic grinder with ball mill.

2.2 Equipment, Instrumentation, and Software

1. Freezer at −80 °C for long-term storage of the frozen plant tissues.
2. Pipettes and tips suitable for handling organic solvents.
3. Balance for accurate weighing of standard chemical powders and plant tissues.
4. 2.0-mL polypropylene Eppendorf tubes for standard solutions.
5. Vortex.
6. Thermoshaker with a 2.0-mL thermoblock.
7. Ultrasonic bath.
8. Centrifuge suitable for 15-mL tubes and centrifuge suitable for 2.0-mL polypropylene Eppendorf tubes.
9. Centrifugal concentrator.
10. 1.5-mL autosampler vials and caps with a PTFE/silicon septum.
11. Analytical column HyperCarb®, 2.1 mm diameter, 100 mm length, spherical particles of 3 μM (ThermoScientific).
12. Hypersep Hypercarb® (Thermo Scientific) solid phase extraction (SPE) cartridges containing 200 mg of porous graphitic carbon (PGC).
13. Syringe pump for direct infusion measurements.
14. Gas-tight Hamilton glass syringe 0.1–1.0 mL.
15. Surveyor high performance liquid chromatography system or equivalent, equipped with an automatic sample injector and a sample cooler.
16. Quadrupole ion trap mass spectrometer (QIT) Surveyor LCQ ThermoFinnigan equipped with an electrospray ionization (ESI) or equivalent.
17. MS data acquisition software: Xcalibur 2.2 (Thermo Scientific) or equivalent.

2.3 Solutions (See Note 2)

1. Individual standard stock solutions: Prepare 1 mM stock solutions in HPLC grade water, vortex until homogenization is completed, and store at −20 °C.
2. HPLC mobile phases: 0.1% formic acid (v/v) in HPLC grade water (eluent A), and 0.1% formic acid (v/v) in acetonitrile (eluent B). Prepare mobile phases freshly and sonicate (ultrasonic bath) them at least 15 min before use.
3. Needle, syringe, and purge lines cleaning solution: 100% methanol.
4. Individual standard working solutions: Prepare the individual standard working solutions in HPLC grade water by dilution of the standard stock solutions (1 mM), vortex and store at −20 °C before and after use.
5. Electrospray (ESI) solution: 50:50 (v/v) methanol–0.1% formic acid (v/v) in HPLC grade water.
6. Quality control (QC) mixture: Prepare a 50 μM standard mixture in HPLC grade water by dilution of each standard stock solution (1 mM), vortex and store at −20 °C before and after use.
7. Calibration curve of individual standard solutions: Prepare a 200 μM individual standard working solution in HPLC grade water by dilution of the individual standard stock solution (1 mM). From the 200 μM individual standard working solution prepare a dilution series of at least seven concentration points ranging from 1.25 to 100 μM (*see* **Note 3**).

3 Methods

3.1 Plant Growth and Sampling Conditions

Plants must grow under specific and controlled conditions to reduce biological variation between samples. Moreover, they must be representative of the total plant population under study, and at least six biological replicates should be used to normalize biological variation. It is expected that a large amount of samples is obtained in metabolomics studies, and thus it is recommended to prepare in advance an adequate sample identification file as well as prelabel all sample tubes. The use of liquid nitrogen in all sample preparation steps until extraction is especially important to avoid changes in metabolite levels. Hence, plant harvest followed by quenching (i.e., rapidly freezing the plant tissue in liquid nitrogen) should be performed, if possible, in the field or in the greenhouse. Additionally, to increase efficiency of the metabolite extraction, it is important to finely homogenize plant fresh frozen tissues—easily performed with a precooled pestle and mortar filled with liquid nitrogen or a ball mill. It must be highlighted that the most important issue during these steps is to guarantee that the plant material does not thaw [2, 18, 19]. Finally, all samples should be stored in a labeled box or bag at −80 °C.

3.2 Harvest and Tissue Sampling

1. Prelabel all sample screw-cap polypropylene Falcon tubes (15 or 50 mL depending on the amount of material) with freezer-compatible labels or pen markers.
2. Harvest a representative amount of the plant tissue of interest into a screw-cap polypropylene Falcon tube, and rapidly freeze it in liquid nitrogen (quenching).
3. Use a precooled pestle and mortar filled with liquid nitrogen, or a precooled ball mill, to finely homogenize the frozen plant tissue. While doing this, make sure that the plant material does not thaw by sequentially adding liquid nitrogen.
4. Once a fine homogenized powder is obtained, transfer it back to the precooled labeled screw-cap polypropylene Falcon tube with the help of a precooled metal spatula or small spoon.
5. Use precooled 2.0-mL safe-lock polypropylene Eppendorf tubes to weight aliquots of 100 mg of fresh weight (FW) powdered frozen tissue (*see* **Note 4**).
6. Prepare at least six biological replicates and make sure that they follow the same sample procedure to reduce biological variation.

3.3 Metabolite Extraction

Water-soluble carbohydrates, including RFOs, are extracted following a well-established protocol that uses 100 mg FW of plant tissue (with minor modifications) [18].

1. Add 1400 μL 100% methanol to the frozen plant tissue, and vortex (enzymatic activity stops here). Keep tubes on ice.
2. Place the 2.0 mL safe-lock polypropylene Eppendorf tubes in a thermoshaker during 15 min at 70 °C and 950 rpm. Attention! After 30 s, STOP thermoshaker and open the tubes to release pressure. Repeat 2× times.
3. Centrifuge for 10 min at 11,000 × *g* (room temperature).
4. Transfer all supernatant to a Schott (GL14) glass tube, leaving just the pellet. Attention! Keep the same volume per tube, approximately 1200 μL.
5. Add 750 μL of chloroform (*see* **Note 5**).
6. Add 1500 μL of water and vortex very carefully each glass tube during 30 s.
7. Centrifuge for 15 min at 2200 × *g* (room temperature).
8. Take a 150 μL aliquot from the upper phase (polar phase) into a new 2.0-mL safe-lock polypropylene Eppendorf tube.
9. Prepare a second aliquot (backup sample).

10. Evaporate to dryness using a centrifugal concentrator for at least 3 h without heating.
11. Fill tubes with inert gas (Argon) to prevent the extract from oxidation and degradation reactions through components of atmospheric air.

3.4 Preparation of the PGC-LC-MS System

3.4.1 HPLC Parameters and Considerations

1. Prepare HPLC mobile phase solvents as described in **item 2** of Subheading 2.3; switch on the HPLC pump and degas both solvents for at least 5 min, or until there are no air bubbles within the lines.
2. Wash needle and flush HPLC syringe at least twice. Check if there are no air bubbles within the lines.
3. Plug the PGC column carefully into the HPLC system. Place the outlet from the column directly to a waste bottle and check for leaks.
4. Precondition the PGC column (*see* **Note 6**) by slowly increasing the percentage of the aqueous eluent until the initial gradient conditions are reached. For a good PGC column equilibration, we recommend to keep the initial gradient conditions for at least 1 h (i.e., running to waste at a flow rate of 200 µL/min).
5. Program the HPLC method according to the linear gradient described in Table 1.
6. Set the flow rate to 200 µL/min, sample injection volume to 5 µL and the autosampler temperature to 4 °C.

Table 1
PGC-LC-MS gradient method for the target analysis of RFOs

Time/min	A (%)	B (%)	Gradient stage
0	96	4	Initial conditions
5	92	8	Elution
7	75	25	Elution
15	75	25	Elution
18	50	50	Washing
21	50	50	Washing
23	96	4	Equilibration
33	96	4	Equilibration

Mobile phase A: 0.1% FA (v/v) in HPLC grade water; Mobile phase B: 0.1% FA (v/v) in acetonitrile

7. After preconditioning the PGC column, connect the HPLC system to the ESI-QIT-MS and check if there are no leaks in the system. It is recommended to regularly register the pressure values (*see* **Note 7**).
8. Following long periods of column storage, regenerate the PGC column according to the manufacturer protocol. Start by inverting the column and pumbling it into the HPLC system with the outlet tubing running to waste. Flush a mixture of tetrahydrofuran–water (1:1, v/v) containing 0.1% trifluoroacetic acid (v/v) through the column at a flow rate of 100 μL/min during 30 min. Then, pump through the column a mixture of tetrahydrofuran–water (1:1, v/v) containing 0.1% sodium hydroxide (v/v) at a flow rate of 100 μL/min during 30 min. Afterward, repeat the flush with a mixture of tetrahydrofuran–water (1:1) containing 0.1% trifluoroacetic acid (v/v), and rinse the column with methanol–water (95:5, v/v) at a flow rate of 100 μL/min during 30 min. Finally, reinvert the column, plumb it back into the HPLC system, and reequilibrate the column to the initial mobile phase conditions.

3.4.2 ESI-QIT-MS Parameters and Considerations

To obtain a good performance of the MS system in terms of mass accuracy and resolution, it is highly recommended to set it up in advance as follows (*see* **Note 8**):

1. Prepare an ESI solution as described in **item 5** of Subheading 2.3; make use of the syringe pump to directly infuse the solution in the MS system at a flow rate of 5 μL/min.
2. Set the capillary voltage and ion source values to 35 V and 5 kV, respectively; the capillary temperature to 250 °C and the sheath and auxiliary gases to 40 and 20 (arbitrary units), respectively. Verify the MS signal and the presence of interfering background ions. If the MS signal is low or a high presence of interfering background ions is detected, clean the MS system by directly infusing ESI solution.

3.5 PGC-LC-MS Method Development for RFOs Analysis

The PGC-LC-MS method here described is divided into two parts. The first part describes ESI-QIT-MS direct infusion measurements of individual standard solutions while the second part guides you through the PGC-LC-MS method setup (development and validation).

3.5.1 ESI-QIT-MS Direct Infusion Measurements

1. Prepare a standard working solution for each target compound at a final concentration of 25 μM in ESI solution as described in **item 5** of Subheading 2.3. Vortex each solution before use.
2. Use the syringe pump to directly infuse the sucrose and raffinose standard working solutions in the MS system at a flow rate of 5 μL/min.

3. Search for the *m/z* peak of interest in both positive and negative ion modes and select the one that produces higher ion intensity and stability (*see* **Note 9**).
4. Make use of the instrument tune tool to maximize the MS signal.
5. Save the tune methods.
6. When acquiring full MS and MS^n data, set the mass range to *m/z* 100–1000 and the normalized collision induced dissociation (CID) energy values for each compound as listed in Table 2. If needed, these values can be adjusted for other MS instruments.
7. Prepare a MS method file for each compound with information regarding the respective tunes, the full MS and the MS^n data.
8. Prepare also a MS method file for a mixture with two scan events, the first one with the tune of sucrose and the second with the raffinose tune. This MS method is a full scan method to analyze the QC mixture sample (Fig. 2).
9. Clean the MS instrument between and at the end of measurements by infusing ESI solution into the MS system.

3.5.2 PGC-LC-MS Method Development and Validation

1. Connect the HPLC system to the ESI-QIT-MS equipment. Check if there are any leaks.
2. Prepare at least 500 mL of each HPLC mobile phase as previously described in **item 2** of Subheading 2.3.
3. Prepare in sample vials a blank solution (HPLC water) and a QC mixture as described in **item 6** of Subheading 2.3.
4. Run the blank solution and the QC mixture in triplicate. For the QC mixture, evaluate the chromatographic data (retention time, peak shape, peak area and resolution), the full MS data (ion current and peak intensity) and the system repeatability (retention time repeatability).

Table 2
Normalized collision induced dissociation (CID) energy values for each target compound

Standard compound	Normalised CID energy values		
	MS/MS	MS^3	MS^4
Sucrose	20	N.a.	N.a.
Raffinose	18	20	N.a.
Stachyose	20	25	N.a.
Verbascose	19	23	24

N.a. not applicable

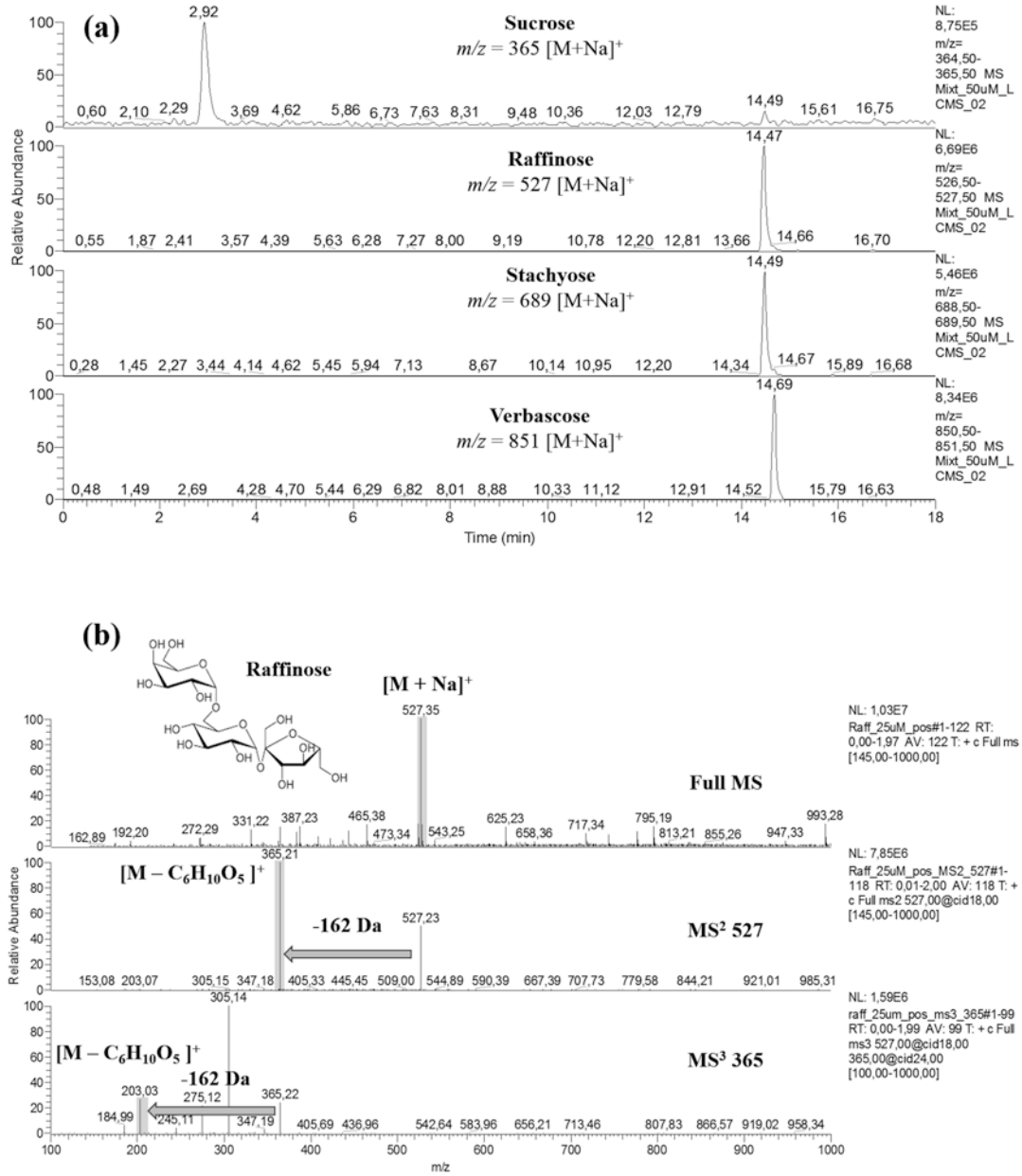

Fig. 2 (**a**) Extracted ion chromatograms obtained on a PGC-LC-MS separation (positive ESI ion mode) of a QC mixture (50 μM) containing the target compounds sucrose *m/z* 365, raffinose *m/z* 527, stachyose *m/z* 689, and verbascose *m/z* 851 detected as sodiated molecules $[M+Na]^+$; (**b**) CID MS^n ($1 \leq n \leq 3$) spectra of raffinose (precursor ion $[M+Na]^+$ *m/z* 527)

5. For retention time comparison purposes, prepare one individual standard working solution for example, raffinose at 50 μM as described in **item 4** of Subheading 2.3 and run it in triplicate.

6. Once the retention times are obtained, complete the MS method file of the mixture as described in **step 8** of Subheading 3.5.1 by including two time segments: the first segment from 0 to 6 min includes two scan events (full MS and MS/MS data) for sucrose data acquisition. The second segment from 6 to 33 min includes eight scan events (full MS and MS^n data) for raffinose, stachyose, and verbascose data acquisition (*see* **Note 10**).
7. Afterward, proceed with the PGC-LC-MS method validation strategy. Start by preparing the calibration curve of individual standard solutions for each target compound as described in **item 7** of Subheading 2.3. The calibration curves are important for later quantification of the target compounds in plant extracts (Fig. 3). Herein, we analyzed calibration curves that used five points for sucrose and six points for RFOs in a concentration range from 1.25 to 100 μM.
8. For repeatability evaluation (intraday precision) each concentration must be analyzed in triplicate using the MS method for each compound. The sequence order should start from the lowest concentration point to the highest concentration point. A blank solution should also be analyzed between each target compound.

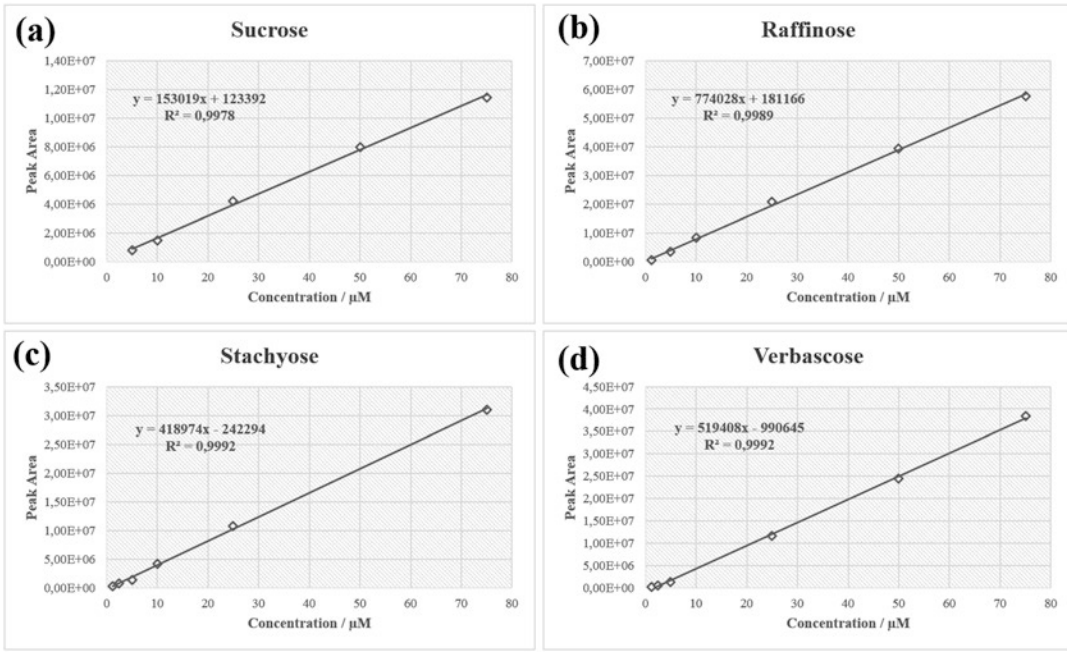

Fig. 3 Individual calibration curves for the target compounds: (**a**) sucrose, (**b**) raffinose, (**c**) stachyose, and (**d**) verbascose

9. Linearity range, limit of detection (LOD), and limit of quantification (LOQ) values were determined as described in Subheading 4.
10. Run in triplicate a point of the calibration curve in different days ($n = 6$) to obtain interday precision.
11. Prior to PGC-LC-MS analysis of plant extracts, it is recommended to perform a SPE cleanup step to reduce matrix effects. Our Hypersep Hypercarb® SPE protocol is as follows: (1) conditioning of the packing material with 2.0 mL 80:20 (v/v) acetonitrile–0.1% formic acid in HPLC water (v/v) followed by 2.0 mL of water; (2) loading of 1.0 mL of sample; (3) washing of the cartridge with 2.0 mL of water; and (4) elution of compounds with 2.0 mL of 25:75 (v/v) acetonitrile–water. Collect fractions of 1.0 mL in 2.0-mL polypropylene Eppendorf tubes and evaporate the eluates to dryness using a centrifugal concentrator. Eluates are reconstituted in 250 μL of mobile phase prior to PGC-LC-MS analysis (*see* **Note 11**). This elution protocol will allow the retention and elution of highly polar metabolites from plant extracts, including neutral carbohydrates (sucrose and RFOs).

3.6 Data Analysis

Herein we present our procedure to process LC-MS raw data using some of the tools available in the software Xcalibur 2.2 (ThermoScientific).

1. Prepare Xcalibur layout files for each target compound and for the QC mixture using the obtained *m/z* values in the direct infusion measurements.
2. Open the LC-MS raw file for both individual target compounds and QC mixture.
3. To apply smoothing to the chromatogram, select the Gaussian type with 9 smoothing points in a maximum of 15 possible points (*see* **Note 12**).
4. Select peak detection using the Genesis algorithm and include the area and signal to noise labels (Fig. 4).
5. Save Xcalibur layout files for target compounds and QC mixture.
6. Open the QC mixture LC-MS raw files and check peak reproducibility, peak area and mass accuracy between analysis in different days or weeks.
7. Open the LC-MS raw file of the calibration curve of individual standard solutions and register the peak area values to construct the plot of peak area vs concentration, i.e., calibration curve, as well as the signal-to-noise (S/N) values for LOD and LOQ evaluation.

Fig. 4 Software Xcalibur 2.2 (ThermoScientific) window displaying the settings to obtain peak area and signal-to-noise (S/N) values

8. Once this is done, evaluate the linearity of each calibration curve by visual inspection and then, using the Mandel's Fitting test (*see* **Note 13**).
9. To evaluate intraday and interday precision for each compound, calculate the relative standard deviation (RSD, %) of retention times and peak areas.

4 Notes

1. When handling and working with liquid nitrogen, all standard safety laboratory procedures must be followed.
2. Prepare all solutions in a fume hood with standard laboratory safety procedures as most of the organic solvents are toxic, flammable, volatile, and/or corrosive.
3. Our eight calibration points are: 1.25, 2.5, 5, 10, 25, 50, 75, and 100 μM. We recommend using a minimum of five points for the calibration curve.
4. Avoid to weight small sample amounts (less than 20 mg FW) because it will produce a high weighing error.
5. Chloroform is a very toxic solvent. This step must be done in the fume hood.
6. PGC column use and care instructions should be read in advance. When using the PGC column for the first time,

equilibrate it with a minimum of 20 column volumes of test mobile phase (column certificate of analysis).

7. If the HPLC system does not record the pressure values, we recommend preparing in advance a file to register the pressure values of the column to evaluate the behaviour throughout its life cycle.
8. It should be highlighted that LC-MS data is highly dependent on the type of mass spectrometer, ionization source, and chromatographic system used. Therefore, the procedure and settings here described for a QIT LCQ with ESI source might need minor modifications when applied to other LC-MS systems.
9. We used positive ion mode because it produced sodiated ions of higher intensity and stability. The negative ion mode usually originated deprotonated ions of lower intensity.
10. The MS method file of the mixture is prepared in advance for biological sample analysis.
11. If metabolite overloading is observed, then reconstitute SPE fractions in 500 μL of mobile phase prior to PGC-LC-MS analysis.
12. Xcalibur 2.2 (ThermoScientific) has two types of peak smoothing, Boxcar and Gaussian. The difference between them is the type of smoothing algorithm applied to the chromatogram. We have used Gaussian as it fits our data better.
13. This test is based on a mathematical model and is used as a complementary test to evaluate the linearity of a calibration curve.

Acknowledgments

This work was supported by the FCT Investigator Programme (IF/00376/2012/CP0165/CT0003) from Fundação para a Ciência e a Tecnologia and the ITQB NOVA research unit GREEN-it "Bioresources for sustainability" (UID/Multi/04551/2013). TFJ acknowledges FCT for the PhD grant (PD/BD/113475/2015) from the ITQB PhD programme "Plants for Life" (PD/00035/2013).

References

1. Obata T, Fernie AR (2012) The use of metabolomics to dissect plant responses to abiotic stresses. Cell Mol Life Sci 69:3225–3243
2. Jorge TF, Rodrigues JA, Caldana C et al (2015) Mass spectrometry-based plant metabolomics: metabolite responses to abiotic stress. Mass Spectrom Rev. doi:10.1002/mas.21449
3. Slama I, Abdelly C, Bouchereau A et al (2015) Diversity, distribution and roles of osmoprotective compounds accumulated in halophytes under abiotic stress. Ann Bot 115: 433–447
4. ElSayed AI, Rafudeen MS, Golldack D (2014) Physiological aspects of raffinose family oligo-

saccharides in plants: protection against abiotic stress. Plant Biol 16:1–8

5. Egert A, Eicher B, Keller F et al (2015) Evidence for water deficit-induced mass increases of raffinose family oligosaccharides (RFOs) in the leaves of three *Craterostigma* resurrection plant species. Front Physiol 6:1–6
6. Antonio C, Larson T, Gilday A et al (2008) Hydrophilic interaction chromatography/electrospray mass spectrometry analysis of carbohydrate-related metabolites from Arabidopsis thaliana leaf tissue. Rapid Commun Mass Spectrom 22:1399–1407
7. Sekiguchi Y, Mitsuhashi N, Inoue Y et al (2004) Analysis of sugar phosphates in plants by ion chromatography on a titanium dioxide column with pulsed amperometric detection. J Chromatogr A 1039:71–76
8. Lunn JE, Feil R, Hendriks JH et al (2006) Sugar-induced increases in trehalose 6-phosphate are correlated with redox activation of ADPglucose pyrophosphorylase and higher rates of starch synthesis in *Arabidopsis thaliana*. Biochem J 397:139–148
9. Delatte TL, Selman MHJ, Schluepmann H et al (2009) Determination of trehalose-6-phosphate in Arabidopsis seedlings by successive extractions followed by anion exchange chromatography–mass spectrometry. Anal Biochem 389:12–17
10. Gangola MP, Jaiswal S, Khedikar YP et al (2014) A reliable and rapid method for soluble sugars and RFO analysis in chickpea using HPAEC–PAD and its comparison with HPLC–RI. Food Chem 154:127–133
11. Pereira L (2008) Porous graphitic carbon as a stationary phase in HPLC: theory and applications. J Liquid Chromatogr Related Technol 31:1687–1731
12. Marriott AS, Antonio C, Thomas-Oates J (2015) Application of carbonaceous materials in separation science. In: White RJ (ed) Porous carbon materials from sustainable precursors. RSC Publishing, London, pp 103–126
13. Robinson S, Bergström E, Seymour M et al (2007) Screening of underivatized oligosaccharides extracted from the stems of Triticum aestivum using porous graphitized carbon liquid chromatography-mass spectrometry. Anal Chem 79:2437–2445
14. Antonio C, Larson T, Gilday A et al (2007) Quantification of sugars and sugar phosphates from Arabidopsis thaliana tissues using porous graphitic carbon liquid chromatography-electrospray ionization mass spectrometry. J Chromatogr A 1172:170–178
15. Antonio C, Pinheiro C, Chaves MM et al (2008) Analysis of carbohydrates in Lupinus albus stems on imposition of water deficit, using porous graphitic carbon liquid chromatography-electrospray ionization mass spectrometry. J Chromatogr A 1187:111–118
16. Gechev T, Benina M, Obata T et al (2013) Molecular mechanisms of desiccation tolerance in the resurrection glacial relic Haberlea rhodopensis. Cell Mol Life Sci 70:689–709
17. Behmüller R, Forstenlehner IC, Tenhaken R et al (2014) Quantitative HPLC-MS analysis of nucleotide sugars in plant cells following off-line SPE sample preparation. Anal Bioanal Chem 406:3229–3237
18. Lisec J, Schauer N, Kopka J et al (2006) Gas chromatography mass spectrometry-based metabolite profiling in plants. Nat Protoc 1:387–396
19. Kim HK, Verpoorte R (2010) Sample preparation for plant metabolomics. Phytochem Anal 21:4–13

Chapter 18

Profiling Abscisic Acid-Induced Changes in Fatty Acid Composition in Mosses

Suhas Shinde, Shivakumar Devaiah, and Aruna Kilaru

Abstract

In plants, change in lipid composition is a common response to various abiotic stresses. Lipid constituents of bryophytes are of particular interest as they differ from that of flowering plants. Unlike higher plants, mosses have high content of very long-chain polyunsaturated fatty acids. Such lipids are considered to be important for survival of nonvascular plants. Here, using abscisic acid (ABA)-induced changes in lipid composition in *Physcomitrella patens* as an example, a protocol for total lipid extraction and quantification by gas chromatography (GC) coupled with flame ionization detector (FID) is described.

Key words Lipid extraction, Gas chromatography, Flame ionization detector, Protonemata, Abscisic acid

1 Introduction

Bryophytes, unlike higher plants are known for their unique lipid composition and ability to withstand various abiotic stresses [1–3]. Lipid composition of bryophytes varies from that of higher plants by the occurrence of ether-linked glycerolipids containing a betaine moiety, high levels of esterified sterols, and triacylglycerols (TAGs) with acetylenic fatty acids [3–5]. Mosses also exhibit differential pattern of fatty acid composition compared to their vascular counterparts, mainly the presence of higher levels of long-chain polyunsaturated fatty acids (PUFAs) such as linoleic acid (18:2), α-linolenic acid (18:3), arachidonic acid (20:4), and eicosapentaenoic acid (20:5) [2, 3].

In general, response of plants under stress includes remodeling of the membrane lipid composition to modify membrane fluidity in order to maintain functions of critical integral proteins [6]. Membrane fluidity is typically affected by change in the levels of PUFAs [6]. Reactive oxygen species, which are typically induced by abiotic stress damage cellular membranes via lipid peroxidation and deesterification of membrane lipids, result in altered membrane lipid constitution [6–9]. Specifically, release of α-linolenic

Ramanjulu Sunkar (ed.), *Plant Stress Tolerance: Methods and Protocols*, Methods in Molecular Biology, vol. 1631,
DOI 10.1007/978-1-4939-7136-7_18,

acid (18:3) from membrane lipids and changes in PUFA levels is important to maintain membrane fluidity under stress [5]. Drought stress has shown to cause changes in phosphoglyceride composition of membranes in moss *Atrichum androgynum* [9]. Application of exogenous ABA, however, reduced the extent of membrane lipid damage indicating its role in membrane protection [10]. Under dehydration stress, moss protonemata accumulate significant levels of ABA, which regulate gene expression to induce stress tolerance [11]. Under freezing and drying stress, treatment with ABA also resulted in alteration of membrane phase properties to protect moss cells [12]. Increased stress tolerance in mosses in the presence of ABA is likely brought by changes in membrane lipid composition. Such changes, specifically in fatty acid profile, as induced by ABA or during stress can be routinely quantified by careful total lipid extraction and analyses. Protocols for routine lipid extraction from plant tissues and quantification are widely available [8]. High quality lipid extraction and sample preparation is key for accurate and reliable lipid profiling and quantification. Here, we provide a detail protocol for total lipid extraction and fatty acid analyses using GC-FID with emphasis on sample preparation for moss tissues cultured in the presence of exogenous ABA (10^{-5} M).

2 Materials

Prepare all solutions using ultrapure water and analytical grade reagents, and store at room temperature (unless indicated otherwise). Avoid use of plastic with organic solvents and use only detergent-free, clean glass tubes with Teflon screwcaps for lipid extraction, preparation, and storage (*see* **Note 1**). Diligently follow all waste disposal regulations, particularly when disposing of organic/hazardous waste materials.

2.1 Reagents and Materials

1. (±) Abscisic acid.
2. Agar.
3. Dimethyl sulfoxide (DMSO).
4. Hexanes.
5. Hydrochloric acid.
6. Isopropanol.
7. Methanol.
8. Potassium hydroxide and sodium sulfate (anhydrous).
9. Cellophane discs (9 mm AA Packaging Co., UK).
10. Ultrapure compressed air.
11. Hydrogen and helium gases.

12. Glass pasture pipettes.
13. Petri dishes.
14. Teflon-lined screw-cap glass tubes (16 × 125 mm) and 4-mL glass vials.
15. Micro-pore tape (Micropore™, GmbH, Germany).
16. Stainless steel beads (3.2 mm diameter).

2.2 Equipment

1. Mini bead beater (we used BioSpec Products, Inc. USA).
2. Nitrogen gas dryer (OA-SYS™, Organomation Asso. Inc. USA).
3. Varian 3800 GC system (or equivalent) equipped with FID (Varian, Inc. CA, USA).
4. Water bath (Isotemp 2320, Fisher Scientific).

2.3 Moss Media Stock Preparation

Composition of moss media given below is simplified from previous descriptions [13]

1. *Moss culture media (1 L)*: Dissolve 250 mg of $MgSO_4.7H_2O$ (0.1 mM), 250 mg of KH_2PO_4 (1.84 mM), 1.01 g of KNO_3 (1 M), 12.5 mg of $FeSO_47H_2O$ (4.5 mM), and 920 mg of $C_4H_{12}N_2O_6$ (5 mM) and 1 mL of microelement stock solution (see below recipe for micro stock solution), adjust pH to 6.5 with 4 M KOH and bring the final volume to 1000 mL with H_2O. Add 8 g of agar (0.8%), if solid media is required. Sterilize by autoclaving.
2. *Micro stock solution C (1000×)*: Dissolve 55 mg of $CuSO_4.5H_2O$ (0.22 mM), 614 mg of H_3BO_3, (10 mM), 55 mg of $CoCl_2.6H_2O$ (0.23 mM), 25 mg of $Na_2MoO_4.2H_2O$ (0.1 mM), 55 mg of $ZnSO_4.7H_2O$ (0.19 mM), 389 mg of $MnCl_2.4H_2O$ (2 mM), 28 mg of KI (0.17 mM) and make up the final volume to 1000 mL with H_2O.
3. *$CaCl_2$ (1 M)*: dissolve 110.98 g of $CaCl_2$ in water and make up the final volume to 1000 mL with H_2O, autoclave and store at 4 °C.
4. *ABA stock solution (10 mM)*: dissolve 2.64 mg of ABA in 1 mL DMSO and maintain the stock at −20 °C (*see* **Note 2**).

2.4 Moss Protonema Culture

1. Autoclave moss media with or without adding agar (Subheading 2.4), cellophane discs (lined with filter papers in a glass petri dish wrapped in foil), forceps, and mortar and pestle.
2. In a sterile workbench, add 1 mL of 1 M $CaCl_2$ stock solution (final concentration to 1 mM) to the autoclaved liquid and agar media, prior to its use. Mix well and pour the agar media (~25 mL) into sterile petri dishes.

3. Wet the cellophane discs by adding liquid media to soften them and minimize shrinkage, place them flat on the top of solidified media, and let them hydrate for 5–10 min.
4. Use mortar and pestle to homogenize 1-week-old protonemata in 2 mL of sterile liquid moss media. Homogenize until uniformity is achieved.
5. Add another 8 mL liquid moss media to the cell suspension, to achieve a total 10 mL cell suspension from one dish of protonemata tissue.
6. Pipette 1 mL green cell suspension on to a cellophane-covered plate and seal the plate with micropore tape.
7. Incubate cultures at 25 °C, under 16 h light and 8 h dark conditions (light intensity: 40 μmol photons m^{-2} s^{-1}).

2.5 ABA Treatment and Sample Preparation

1. Prepare moss media plates supplemented with ABA (final concentration 10^{-5} M) or DMSO (final concentration 0.1%).
2. Transfer cellophane discs with 2-week-old moss protonemata on to solid moss media supplemented with ABA (10^{-5} M) or DMSO (0.1%) as solvent control.
3. Incubate plates at 25 °C under 16 h light and 8 h dark conditions (light intensity: 40 μmol photons m^{-2} s^{-1}) for a week.
4. Harvest samples after 7 days. Dry protonemata tissues using blotting paper and use ~200 mg of tissues for lipid extraction.

3 Method

Lipid extraction and methyl esterification procedure described below can also be used for higher plant tissues.

3.1 Lipid Extraction from Moss

Preheated isopropanol is used for lipid extraction; it is generally preferred in pulverization of the tissues to prevent activity of lipid catabolic enzymes such as phospholipase D [8]. The selection of hexane–isopropanol as solvent for lipid extraction was based on volatility, low toxicity, and ability to form a two-phase system with water (to remove nonlipids) [14]. This solvent system has advantages over toxic chloroform-based lipid extractions [14, 15].

1. Weigh ~200 mg of moss protonemata tissues in screw-capped glass tube (*see* **Notes 3** and **4**).
2. Add 100 μg of heptadecanoic acid (C17:0, 10 mg/mL in hexane), which will serve as an internal standard (IS).
3. Homogenize the tissue samples by vigorously vortexing either in presence of liquid nitrogen or 2 mL hot isopropanol (70 °C), and ~10 steel beads (3 mm). Use bead beater to pulverize the sample (*see* **Notes 5**–7).

4. If the tissues were ground in liquid nitrogen then add 2 mL preheated isopropanol (70 °C) to the homogenized powder before it is thawed. Vortex and immediately place samples for 5 min in water bath preset at 70 °C to inactivate lipases.
5. Add 3 mL of hexane and 0.5 mL of water to achieve a monophase of water–isopropanol–hexane with 1:4:6 ratio, respectively. Vortex the mix vigorously and let the samples stand for 5 min.
6. Transfer solvent extracts carefully into new set of screw-capped glass tubes without taking any tissue samples. Reextract the remaining tissue with 3 mL of hexane and 0.5 mL of water for 3–5 times. Removal of chlorophyll from the tissues can act as an indicator for complete extraction of the lipids.
7. Add 2.5 mL of aqueous Na_2SO_4 (0.5 M) to pooled solvent extracts and vortex vigorously. Additional Na_2SO_4 can be added to induce phase separation. Samples may be allowed to stand at room temperature for 30 min or left overnight at 4 °C, for lipids to be extracted into the organic phase and a clear phase separation.
8. Bring samples to room temperature, if left overnight at 4 °C and vortex. Centrifuge for 5 min at 4415 × *g* to attain clear phase separation. Using Pasteur pipet, carefully discard the aqueous phase and retain the organic phase (upper, when hexane is used as a solvent). Dry the organic phase under gentle stream of nitrogen gas. When the volume reduces to ~1 mL, transfer the lipid extract to a preweighed glass vials (4-mL Teflon-lined screw-cap glass tubes).
9. Weigh the glass vial after complete drying and determine the amount of the dry lipid residue by subtracting the weight of the empty vial. Resuspend lipids in 200 μL hexane and store the samples in −20 °C until further use.
10. Total lipid extract, if necessary, can be separated on thin layer chromatography (TLC, one/two dimensional) to determine the distribution of various lipid classes. Separated lipids can be recovered from TLC and their fatty acid composition can be determined using GC-FID, as described below (*see* **Note 8**).

3.2 Preparation of Fatty Acid Methyl Esters (FAME)

In plants, fatty acids are mainly present in two forms, ester- (glycerides, sterols, and waxes) and amide-linked (sphingolipids) fatty acids; unesterified free fatty acids remain as a minor constituent. For analysis of the fatty acid composition of total lipids or individual lipid classes using GC or GC-MS based approach, derivatization is necessary. Transesterification of fatty acids, generating fatty acid methyl esters (FAME), is a common approach. Transesterification of total fatty acids is achieved via base catalysis using hydroxide of sodium (NaOH) or potassium (KOH) in methanol forming sodium or potassium methoxide, respectively [16–18] (*see* **Note 9**).

1. To about 10 mg of lipid extract (*see* **step 9** in Subheading 3.1), add 0.2 mL of 2 M methanolic KOH (*see* **Note 10**) and 2 mL of hexane, and vortex for 1–2 min. Allow the reaction to proceed for at least 2 min at room temperature. Avoid any water contamination (*see* **Note 11**).
2. Vortex with 400 μL of 2 M HCl (~pH 3–4) to neutralize the alkaline solution to stop the reaction.
3. Centrifuge for 5 min at 4415 × *g*.
4. Carefully transfer upper hexane/organic phase to a new Teflon-lined screw-cap glass tubes.
5. Extract the mixture for three times with 2 mL of hexane.
6. Combine the organic phases and dry using nitrogen gas and dry bath then resuspend in 200 μL hexane to achieve a final concentration of ~1 mg/μL lipid. Or use desired volume of hexane for GC-FID analysis.

3.3 Determination of Fatty Acid Composition Using GC-FID

1. Inject lipid samples (1 μL/sample, manual/auto injection) to a GC with DB-23 column (30 m × 0.25 mm × 0.25 μm or equivalent) (*see* **Note 12**). First wash the injector with hexane before loading standard (37-FAME mix) and samples.
2. Use helium as carrier gas at a total flow rate of 1.5 mL^{-1}, set inlet temperature to 250 °C, pressure to 27 psi and split ratio to 0.1:1.
3. Set FID detector temperature to 300 °C with hydrogen flow rate of 30 mL min^{-1}, air flow rate of 400 mL min^{-1} and helium flow rate of 25 mL min^{-1}.
4. Set initial oven temperature to 150 °C for 3 min and then ramp to 250 °C at rate of 6 °C min^{-1}. Total run time is 18 min.
5. Wash the injector with hexane before and after each injection.

4 Data Analyses

Identification of fatty acid peaks is done by using reference standard (37-FAME mix, Supleco, Sigma) and quantification using an IS of heptadecanoate.

1. The GC column suggested in this protocol separates the FAMEs based on their size and degree of saturation. The saturated and shorter chain fatty acids have shorter retention time. Separation of fatty acid isomers can also be achieved.
2. Fatty acids separated can be identified by comparing their retention time with that of the reference peaks (37-FAME mix, Supleco, Sigma) on the chromatogram.

3. The amount of individual fatty acid (mg g^{-1} fresh weight (FW)) in the moss protonemata tissue with and without ABA treatment can be determined using the peak area for that particular fatty acid, the amount of protonemata tissue (mg) and concentration of IS (mg L^{-1}), as indicated in the formula below:

$$\text{Fatty acid}\left(\frac{mg}{gFW}\right) = \frac{\left(\text{IS}\left(mg\right)\times\left(\text{Peak area of individual FAME} \,/\, \text{Peak area of IS}\right)\right)}{\text{Tissue Weight}\left(\text{g}\right)}$$

4. The total fatty acid content of the moss protonemata can be determined as the sum of all individual fatty acids. Also, the relative abundance of individual fatty acid in the sample can be obtained by dividing the amount of individual fatty acid by the total fatty acid content.
5. Effect of ABA on fatty acid composition can be determined by comparing the lipid profile between control and ABA-treated protonemata.

5 Notes

1. Clean glassware with residue-free detergent such as Alconox, 3–5 times soaking and rinsing with deionized water and one final soaking and rinsing with ultrapure water followed by drying at 60 °C.
2. ABA can be dissolved in the pure ethanol instead of DMSO. Maintain solvent control in the experiment, as needed.
3. Tissue amount used for extraction may differ as needed, depending on the amount of lipids to be extracted.
4. This method can be used for lipid extraction and GC-FID analysis from moss gametophores and other plant/animal tissues.
5. Rapid extraction of lipids immediately after removal of tissue from media plates is highly recommended to avoid autolysis of lipid molecules [18].
6. Snap freezing of the protonemata tissues in liquid nitrogen and ground to fine powder form might circumvent autolysis and it may also facilitate higher levels of lipid extraction.
7. Preheated isopropanol is generally preferred for pulverization of tissues to prevent activity of lipid catabolic enzymes such as phospholipase D, which results in formation of phosphatidic acid.
8. Neutral and polar lipids can be first separated by one and two-dimensional TLC respectively. Lipids recovered from specific spot on TLC are then transesterified to generate FAME before GC-FID analysis.

9. Base-catalyzed transesterification facilitates rapid transesterification of *O*-acyl lipids in anhydrous methanol in the presence of a basic catalyst; however, acid-catalyzed transesterification is also a commonly used method for synthesizing FAMEs [17].
10. Care should be taken while dissolving potassium hydroxide (KOH) in methanol as it causes a strong exothermic reaction.
11. Take special care to avoid any water contamination during FAME preparation (Subheading 3.2) as it may cause hydrolysis of lipids.
12. Run one or two solvent (blank) injections prior to the actual samples/standards.

Acknowledgments

National Science Foundation Grant (NSF-IOS#1456917) supports AK's research on moss.

References

1. Charron AJ, Quatrano RS (2009) Between a rock and a dry place: the water-stressed moss. Mol Plant 2:478–486
2. Beike AK, Jaeger C, Zink F, Decker EL, Reski R (2014) High contents of very long-chain polyunsaturated fatty acids in different moss species. Plant Cell Rep 33:245–254
3. Mikami K, Hartmann E (2004) Lipid metabolism in mosses. In: Wood AJ, Oliver MJ, Cove DJ (eds) New frontiers in bryology: physiology, molecular biology and functional genomics. Springer, New York
4. Dembitsky VM (1993) Lipids of bryophytes. Prog Lipid Res 32:281–356
5. Dembitsky VM (1996) Betaine ether-linked glycerolipids: chemistry and biology. Prog Lipid Res 35:1–51
6. Upchurch RG (2008) Fatty acid unsaturation, mobilization, and regulation in the response of plants to stress. Biotechnol Lett 30:967–977
7. Ayala A, Muñoz MF, Argüelles S (2014) Lipid peroxidation: production, metabolism, and signaling mechanisms of malondialdehyde and 4-hydroxy-2-nonenal. Oxidative Med Cell Longev. doi:10.1155/2014/360438
8. Welti R, Li W, Li M, Sang Y, Biesiada H, Zhou HE, Rajashekar CB, Williams TD, Wanf X (2002) Profiling membrane lipids in plant stress responses. Role of phospholipase D alpha in freezing-induced lipid changes in Arabidopsis. J Biol Chem 277:31994–32002
9. Guschina IA, Harwood JL, Smith M, Beckett RP (2002) Abscisic acid modifies the changes in lipids brought about by water stress in the moss *Atrichum androgynum*. New Phytol 156:255–264
10. Beckett RP (2001) ABA-induced tolerance to desiccation-induced ion leakage in the moss *Atrichum androgynum*. Plant Growth Regul 35:131–135
11. Shinde S, Nurul IM, Ng CK (2012) Dehydration stress-induced oscillations in LEA protein transcripts involves abscisic acid in the moss, *Physcomitrella patens*. New Phytol 195:321–328
12. Oldenhof H, Wolkers WF, Bowman JL, Tablin F, Crowe JH (2006) Freezing and desiccation tolerance in the moss *Physcomitrella patens*: an in situ Fourier transform infrared spectroscopic study. Biochim Biophys Acta 1760:1226–1234
13. Ashton NW, Cove DJ (1977) The isolation and preliminary characterization of auxotrophic and analogue resistant mutants of the moss *Physcomitrella patens*. Mol Gen Genet 154:87–95
14. Hara A, Radin NS (1978) Lipid extraction of tissues with a low toxicity solvent. Anal Biochem 90:420–426

15. Bligh EG, Dyer WJ (1959) A rapid method of total lipid extraction and purification. Can J Biochem Physiol 7:911–917
16. Ichihara K, Waku K, Yamaguchi C, Saito K, Shibahara A, Miyatani S, Yamamoto K (2002) A convenient method for determination of the C20–22 PUFA composition of glycerolipids in blood and breast milk. Lipids 37:523–526
17. Christie WW (1993) Preparation of derivatives of fatty acids for chromatographic analyses. In: Christie WW (ed) Advances in lipid methodology. Oily Press, Dundee. (also available online at http://lipidlibrary.aocs.org/)
18. Christie WW, Xianlin H (2010) Lipid analysis: isolation, separation, identification and lipidomic analysis, 4th edn. The Oily Press, Bridgewater

Chapter 19

Detection of Free Polyamines in Plants Subjected to Abiotic Stresses by High-Performance Liquid Chromatography (HPLC)

Xiaoqing Gong and Ji-Hong Liu

Abstract

High-performance liquid chromatography (HPLC) is a sensitive, rapid, and accurate technique to detect and characterize various metabolites from plants. The metabolites are extracted with different solvents and eluted with appropriate mobile phases in a designed HPLC program. Polyamines are known to accumulate under abiotic stress conditions in various plant species and thought to provide protection against oxidative stress by scavenging reactive oxygen species. Here, we describe a common method to detect the free polyamines in plant tissues both qualitatively and quantitatively.

Key words Benzoyl chloride, Gradient elution, HPLC, Perchloric acid, Polyamines

1 Introduction

Polyamines (PAs) are ubiquitously distributed in all living organisms, including bacteria, animals, and plants. It has been documented that the PAs are involved in a variety of biological processes [1–3]. In plants number of studies also focused on the elucidation of physiological role of PAs and more specifically in response to abiotic stresses. Given their accumulation under abiotic stresses, their levels need to be determined using a sensitive and accurate detection method. Since PAs are neither chromophores nor fluorophores, they cannot be detected by spectrophotometric or fluorescent methods. Therefore, almost all techniques developed so far to detect the PAs require the appropriate conversions of PAs via chemical or immune methods, for example, enzymatic analysis, thin-layer chromatography, high-performance liquid chromatography (HPLC), and HPLC coupled with different mass spectrometry [4–10].

HPLC coupled with derivatization steps is the most common and widespread method to determine PAs. The active and polar amino groups of PAs are transformed into chromophores or

Ramanjulu Sunkar (ed.), *Plant Stress Tolerance: Methods and Protocols*, Methods in Molecular Biology, vol. 1631,
DOI 10.1007/978-1-4939-7136-7_19,

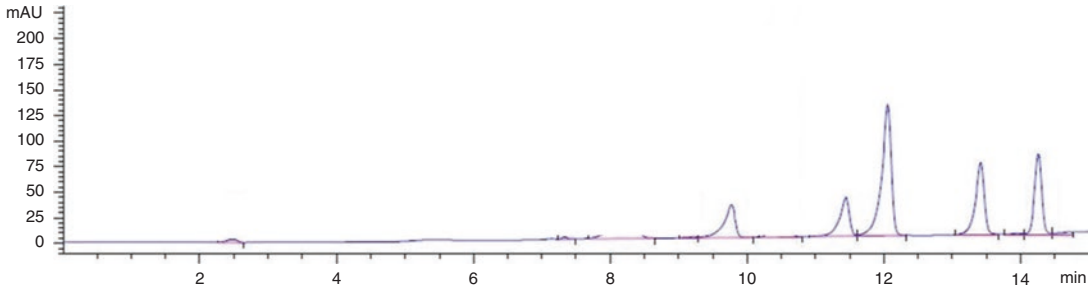

Fig. 1 A representative chromatogram showing the HPLC peaks of polyamines, including putrescine (Put), spermidine (Spd), and spermine (Spm). IS shows the internal standard. Numbers on the peaks show the time (minutes) for the corresponding polyamines to be recognized

fluorophores with various derivatization agents that can be detected by ultraviolet and/or fluorescence detectors [11, 12]. Typical derivatization agents include dansyl chloride, benzoyl chloride, dabsyl chloride, o-phthalaldehyde, 9-fluorenylmethyl chloroformate (FMOC), or 6-aminoquinolyl-N-hydroxysuccinimidyl carbamate (AQC) [9, 13–16]. After derivatization, the obtained products can be easily separated on the reversed phase columns with suitable mobile phases according to their polarity. The strongest polar products were eluted and detected first in the HPLC analytical system [17, 18].

In this protocol, we describe an optimal method to separate PAs extracted from different plants based on Schotten–Baumann reaction, and analyze them by reverse-phase HPLC system equipped with a diode array detector (DAD). The plant tissues are homogenized in perchloric acid buffer to extract crude PAs, which were benzoylated in alkaline solution. Benzoyl-PAs are then extracted into ethyl ether and vacuum-dried. After redissolving in methanol, the samples are applied to the Agilent 1260 Infinite system for the next analysis. According to this protocol, we successfully separated and determined three main types of PAs, diamine putrescine, triamine spermidine, and tetramine spermine, in various plants, such as Arabidopsis, apple, citrus, and tobacco (Fig. 1).

2 Materials

Prepare all solutions with ultrapure water (prepared by purifying deionized water to attain a sensitivity of 18 MΩ cm at room temperature [RT]) and HPLC grade reagents as far as possible. If not, at least chemicals of analytical grade might be used. All prepared solutions should be placed in autoclaved glassware or/and sterile tubes at an appropriate temperature. Strictly follow the appropriate disposal regulations when disposing of waste materials.

2.1 Standard Solutions for Polyamine Extraction and Analysis

1. Standard putrescine (Put): 1 mM Put (*see* **Note 1**). Dissolve 0.8815 g Put (MW = 88.15) with 10 mL water to prepare 1 M stock solution. Dilute the stock solution to 1 mM before use. Store at −80 °C.
2. Standard spermidine (Spd): 1 mM Spd. Dissolve 1.452 g Spd (MW = 145.2) with 1 mL water to prepare 1 M stock solution. Dilute the stock solution to 1 mM before use. Store at −80 °C.
3. Standard spermine (Spm): 1 mM Spm. Dissolve 2.0234 g Spm (MW = 202.34) with 10 mL water to prepare 1 M stock solution. Dilute the stock solution to 1 mM before use. Store at −80 °C.
4. Internal standard (IS): 1 mM 1,6-hexanediamine. Dissolve 1.162 g 1,6-hexanediamine (MW = 116.2) with 10 mL water to prepare 1 M stock solution. Dilute the stock solution to 1 mM before use. Store at −80 °C (*see* **Note 13**).

2.2 Preparation of the Reagents

1. Extraction buffer: 5% perchloric acid (PCA). Add about 80 mL of water to a glass beaker, and pipette 5 mL of PCA into the same beaker and mix thoroughly. Weigh 0.05 g DL-dithiothreitol (DTT) and dissolve it in the PCA solution. Then transfer the solution to a 100 mL volumetric flask, and add water to make up final volume (100 mL), and mix well. Store at 4 °C (*see* **Note 2**).
2. 2 M NaOH: Weigh 8 g of NaOH and dissolve it with about 80 mL double distilled water in a glass flask. Transfer the solution to a 100 mL volumetric flask, dilute with water to final volume, and mix well. Store at RT (*see* **Note 3**).
3. Saturated NaCl solution: Weigh 35.9 g of NaCl and dissolve it with 100 mL water (the solubility of NaCl is 35.9 g at room temperature). Store at RT (*see* **Note 4**).
4. Benzoyl chloride: HPLC grade for derivatization.
5. Ethyl ether (≥99%).
6. Methanol: HPLC grade.
7. Solvent A: 100% HPLC grade methanol. Degas before use, with an ultrasonicator for about 15 min (*see* **Note 5**).
8. Solvent B: 100% HPLC grade water. Degas ddH_2O to prepare solvent B (*see* **Note 5**).

2.3 The HPLC System

The HPLC system is an Agilent 1260 Infinite equipped with a C_{18} reversed phase column (4.6 mm × 150 mm, particle size 5 μm) and a diode array detector (DAD). The Agilent ChemStation B.04.03 version is used to record and analyze the HPLC chromatography data.

3 Methods

3.1 Extraction of PAs from Plant Samples

1. Collect and immediately freeze the plant samples in liquid nitrogen and store the frozen tissues at −80 °C (*see* **Note 6**).
2. Grind the frozen sample in a precooled mortar into fine powder using liquid nitrogen.
3. Weigh about 0.1 g of the ground tissue powder into a 2 mL Eppendorf tube (*see* **Note 7**).
4. Place the prepared extraction buffer (5% PCA solution) on ice before use. Add 1 mL of the buffer to the tube in **step 3**), tighten the tube and vortex for 30–60 s at RT.
5. Incubate the tube with the mixture on ice for 30 min.
6. Centrifuge the tube at 13,000 × *g* at 4 °C for 15 min.
7. Transfer the supernatant to another 2 mL Eppendorf tube and store it on ice in the dark (*see* **Note 8**).
8. For the deposition layer, homogenize it again with 1 mL more 5% PCA and repeat the **steps 4–6**.
9. Transfer the supernatant to the same tube in **step 7**, and vortex it well. The crude extract is ready for derivatization in the next step, otherwise store it at −20 °C (*see* **Note 8**).

3.2 Derivatization of the Extracted PAs

1. Pipette 1 mL of the crude extract into a precooled 10 mL tube, add 50 μL of IS and 1 mL of 2 M NaOH into the tube step by step, and mix them well.
2. Add 10 μL of benzoyl chloride into the tube and vortex for 20 s (*see* **Note 9**).
3. Incubate the tube containing the mixture in water bath at 37 °C for 20 min (*see* **Note 10**).
4. Add 2 mL of saturated NaCl into the tube, and then 2 mL of ethyl ether to leach benzoyl-polyamines into the organic phase. Tighten the lid securely and vortex slightly for several seconds (*see* **Note 11**).
5. Centrifuge the tube at 8000 × *g* at RT for 5 min.
6. Transfer 1 mL of the ethyl ether phase into a 1.5-mL Eppendorf tube, vacuum-dry in a concentrator (SCANVAC, Denmark).
7. Add 200 μL of HPLC-grade methanol to redissolve the dried samples using a disposable syringe. And filter into a 2-mL Agilent screw top vials for the next HPLC analysis, or store the benzoylated samples at −20 °C (*see* **Note 12**).

3.3 Derivatization of PA Standards

Set three to four different serial concentrations of the PA standards, for example, 1 nM, 10 nM, and 100 nM. And then pipette different volumes of the stock solutions of each standard into a precooled 10-mL tube, prepare the standard PAs samples following the steps in Subheading 3.2 (*see* **Note 13**).

Table 1
The elution procedure for PA separation by HPLC

Time (min)	Solvent A (%)	Solvent B (%)
0	45	55
15	95	5
17	100	0
18	45	55
25	45	55

3.4 The HPLC Program

The HPLC analysis is performed with a programmable Agilent 1260 Infinite liquid chromatograph, running at a gradient mode. For each sample, 20 μL of the working solution is loaded into the system for analysis. The solvent system consists of methanol (A) and water (B), changing from 45%: 55% (v/v, A: B) to 95%: 5% in 15 min to elute the benzoyl-PAs, and the total running time for each sample is approximately 25 min (including column regeneration) (Table 1). The flow rate is 0.7 mL/min and the temperature of the column is 25 °C. The DAD detector is used to detect the PAs derivatives being set at 230 nm (*see* **Note 14**). Finally, the HPLC data is analyzed using the Agilent ChemStation B.04.03 version, according to the instruction manual.

4 Notes

1. The standard solution of PAs can also be prepared with the concentration of 1 mg/mL, since it is more convenient for weighing and calculation.
2. As PCA is a strong acid, similar to concentrated sulfuric acid, it will release enormous heat during dilution. Thus the proper method to prepare 5% PCA is to add the PCA into water and stir slowly. Do not reverse the step, which can lead to an explosion. In addition, it is better to prepare fresh 5% PCA solution just before use.
3. NaOH is typical of strong alkali, similar to the preparation of 5% PCA, add the NaOH powder into the water bit by bit and stir slowly. In addition, NaOH solution is easy to generate Na_2CO_3 with the CO_2 in the air, cover the bottle as soon as the solution is prepared.
4. The saturated NaCl solution should be well mixed using the magnetic stirrers. Heating will accelerate the dissolution and increase the solubility of NaCl, thus make sure extra crystal can be seen when the solution cool down at RT.

5. Degassing is necessary before the solvents are applied to the HPLC system, only if the quaternary pump can degas the mobile phase automatically. Confirm it when running the HPLC system for the first time.
6. This protocol is most suitable for leaves, while for other tissues the method possibly needs slight modification.
7. The concentration of PAs may change according to different plant species, tissues, treatments, etc. Generally, it is suggested to carry out a preliminary experiment to determine the suitable sample magnitude.
8. When transferring the supernatant, pipette the same volume from each tube, for example, 800 μL each. The crude extracts of PAs are stable for HPLC analysis for more than 6 months when stored at −20 °C.
9. The amount of benzoyl chloride should be enough to derive all amino groups in the crude extracts. Otherwise the quantization of PAs would be inaccurate. Here, 10 μL of benzoyl chloride is enough for at least 0.2 g tobacco and Arabidopsis leaves, 0.1 g citrus and apple leaves. The amount needs to be calibrated for different plant species and tissues.
10. The incubation time for benzoylation at 37 °C can be changed from 20 to 30 min, depending on the plant species. For example, we found that 20 min is fine for Arabidopsis and tobacco, while 25 min is optimal for citrus and apple.
11. Ethyl ether is volatile, so make sure that the lid is securely tightened. Slightly whirl the tube on the vortex or by hand so as to thoroughly leach the benzoyl-polyamines into the ethyl ether phase.
12. When redissolving the dried samples, the amount of methanol can be flexible, depending on the amount of dried samples. In addition, note the difference among the disposable filters, a filter, 0.22 μm for organic solvent, is needed here. The benzoyl-PAs are stable at −20 °C for several months in the plastic Eppendorf tubes.
13. Standard PAs are prepared and analyzed to verify the retention time of each PA. The concentration of PAs in the sample is determined by normalizing with the IS.
14. The HPLC program needs to be reset on different systems so as to achieve the optimum results. PAs derivatives can be detected at both 230 nm and 254 nm, the former is much more sensitive to benzolyated substance, while detection at 254 nm needs more samples. In addition, if the detection is carried out at 254 nm, complete the HPLC analysis in a short period, as the absorbance of benzoyl-Spd at 254 nm increases within 2 weeks of storage.

Acknowledgment

This work was supported by China Postdoctoral Science Foundation (K3080215805) and Natural Science Foundation of China (31320103908).

References

1. Agostinelli E (2012) Role of polyamines, their analogs and transglutaminases in biological and clinical perspectives. Amino Acids 42: 397–409
2. Moschou PN, Wu J, Cona A, Tavladoraki P, Angelini R, Roubelakis-Angelakis KA (2012) The polyamines and their catabolic products are significant players in the turnover of nitrogenous molecules in plants. J Exp Bot 63: 5003–5015
3. Galitsopoulou A, Michaelidou AM, Menexes G, Alichanidis E (2015) Polyamine profiles in ovine and caprine colostrum and milk. Food Chem 173:80–85
4. Isobe K, Yamada H, Soejima Y, Otsuji S (1987) A rapid enzymatic assay for total blood polyamines. Clin Biochem 20:157–161
5. Seiler N (1971) Identification and quantitation of amines by thin-layer chromatography. J Chromatogr 63:97–112
6. Flores HE, Galston AW (1982) Analysis of polyamine in higher plants by high performance liquid chromatography. Plant Physiol 69:701–706
7. Liu R, Bi K, Jia Y, Wang Q, Yin R, Li Q (2012) Determination of polyamines in human plasma by high-performance liquid chromatography coupled with Q-TOF mass spectrometry. J Mass Spectrom 47:1341–1346
8. Magnes C, Fauland A, Gander E, Narath S, Ratzer M, Eisenberg T, Madeo F, Pieber T, Sinner F (2014) Polyamines in biological samples: rapid and robust quantification by solid-phase extraction online-coupled to liquid chromatography-tandem mass spectrometry. J Chromatogr A 1331:44–51
9. Ibarra AA, Wrobel K, Escobosa AR, Elguera JC, Garay-Sevilla ME, Wrobel K (2015) Determination of putrescine, cadaverine, spermidine and spermine in different chemical matrices by high performance liquid chromatography–electrospray ionization–ion trap tandem mass spectrometry (HPLC–ESI–ITMS/MS). J Chromatogr B 1002:176–184
10. Bashiry M, Mohammadi A, Hosseini H, Kamankesh M, Aeenehvand S, Mohammadi Z (2016) Application and optimization of microwave-assisted extraction and dispersive liquid-liquid microextraction followed by high performance liquid chromatography for sensitive determination of polyamines in turkey breast meat samples. Food Chem 190: 1168–1173
11. Lin JK, Lai CC (1982) Chromophoric determination of putrescine, spermidine and spermine with dabsyl chloride by high performance liquid chromatography and thin-layer chromatography. J Chromatogr 227:369–377
12. Slocum RD, Flores HE, Galston AW, Weinstein LH (1989) Improved method for HPLC analysis of polyamines, agmatine and aromatic monoamines in plant tissues. Plant Physiol 89: 512–517
13. Erim FB (2013) Recent analytical approaches to the analysis of biogenic amines in food samples. Trends Anal Chem 52:239–247
14. Subramanyam S, Sardesai N, Minocha SC, Zheng C, Shukle RH, Williams CE (2015) Hessian fly larval feeding triggers enhanced polyamine levels in susceptible but not resistant wheat. BMC Plant Biol 15:3
15. Gong XQ, Zhang JY, Hu JB, Wang W, Wu H, Zhang QH, Liu JH (2015) FcWRKR70, a WRKY protein of *Fortunella crassifolia*, functions in drought tolerance and modulates putrescine synthesis by regulating arginine decarboxylase gene. Plant Cell Environ 38: 2248–2262
16. Dai Z, Wu Z, Wang J, Wang X, Jia S, Bazer FW, Wu G (2014) Analysis of polyamines in biological samples by HPLC involving pre-column derivatization with o-phthalaldehyde and N-acetyl-L-cysteine. Amino Acids 46: 1557–1564
17. Horváth C, Melander W (1977) Liquid chromatography with hydrocarbonaceous bonded phases; theory and practice of reversed phase chromatography. J Chromatogr Sci 15: 393–404
18. Vailaya A, Horváth C (1998) Retention in reversed-phase chromatography: partition or adsorption? J Chromatogr A 829:1–27

Chapter 20

Determination of Polyamines by Dansylation, Benzoylation, and Capillary Electrophoresis

Gounipalli Veeranagamallaiah and Chinta Sudhakar

Abstract

Polyamines are polycationic nitrogenous compounds that accumulate in plants exposed to abiotic stresses. In higher animals, they influence gene expression, brain development, and nerve growth and regeneration. Because of their known roles in plant stress responses, quantitative determination of polyamines is very important. Polyamines in their native form cannot be detected by optical and/or electrochemical methods as they do not show any structural features, and hence derivatization of polyamines is essential to make them to produce either chromophores or fluorescence. Here we describe various methods of derivatization using different labeling agents and suitable separation and detecting methods for a vast source of polyamines existing in living cells.

Key words Benzoylation, Capillary electrophoresis, Dansylation, Derivatization, Polyamines

1 Introduction

Polyamines (PAs) are small aliphatic low-molecular weight polycationic nitrogenous compounds that are ubiquitious and found to be essential for growth and development in prokaryotes and eukaryotes [1]. The most common polyamines found in all living cells are putrescine (Put), spermidine (Spd), and spermine (Spm). PAs occur as free molecular bases (free form), or are often conjugated with small molecules (phenolic acids) or bound to macromolecules such as nucleic acids and proteins [2]. PAs have been implicated in a variety of cell functions involving growth and differentiation [3], during stress conditions and infection by pathogenic fungi and viruses [2]. Additionally, on the basis of their ability to form soluble conjugates with various phenol derivatives, Bouchereau et al. [4] demonstrated that PAs are involved in scavenging of reactive oxygen species. Further, the function of PAs in oxidative stress could be mediated by H_2O_2 produced during their oxidative degradation and that in turn could play a signaling role in plants [5]. Furthermore, one of the manifestations of the PAs

Ramanjulu Sunkar (ed.), *Plant Stress Tolerance: Methods and Protocols*, Methods in Molecular Biology, vol. 1631,
DOI 10.1007/978-1-4939-7136-7_20,

antioxidant effect is their ability to regulate the expression of genes encoding antioxidant enzymes. The capacity of PAs to induce expression of antioxidant genes such as peroxidase in tobacco plants was demonstrated for Spd [6] and SOD in the roots of the halophyte *Mesembryanthemum crystallinum* for cadaverine [7]. More recently, Sudhakar et al. [8] have described the role of PAs in modulating antioxidant defenses in foxtail millet cultivars differ in salt tolerance. Based on the type of the biological sample to be studied and based on the type and purpose of the study, several methods for quantitative determination of polyamines have been developed. These methods majorly include chromatographic such as gas chromatography (GS), liquid chromatography (LC), thin layer chromatography (TLC), and high performance liquid chromatography (HPLC) coupled with UV or fluorescence or chemiluminescence or mass spectrometric (MS) detectors; capillary electrophoretic and enzymatic (Note: the immobilized enzymatic chemiluminescence detection system is useful for the determination of PAs with the advantage of high specificity, but the enzyme polyamine oxidase (PAO) is expensive and can easily be denatured). However, direct measurement of PAs in biological samples is difficult because they are small aliphatic molecules that do not exhibit any structural features that would allow their sensitive detection without derivatization [9]. Moreover, they show neither UV absorption nor fluorescence properties. Hence, derivatization of polyamine samples is essential prior to the quantitative detection, as derivatization increases the sensitivity of the sample, and increases the analysis time and the risk of intermediate errors. Derivatization of polyamines is majorly achieved by employing either benzoylation method or dansylation methods. While in benzoylation method, benzyl chloride [10, 11] and dabsyl chloride [12] are used for derivatization which form chromophores, where as in dansylation method, dansyl chloride [9], fluorescamine [13], and O-pthalaldehyde (OPA) [14, 15] are used for derivatization which forms fluorophores. For determination of polyamines through capillary electrophoresis, derivatization of polyamines is also performed by using labeling reagents like fluoroscein isothiocyanate [16], *p*-toluenesulfonyl chloride [17], 1-pyrenebutanic acid succinimidyl ester [18], 6-aminoquinolyl-N-hydroxysuccinimidyl carbamate [19], 4-floro-7-nitro-2,1,3 benzoxadiazole [20], and 1-(3-succinimidyl-hexanate)-1′-methyl-3-3-3′3′-tetramethyllindocarbocyanine-5-5′-disulfonate [21]. In addition, Driouich et al. [22, 23] and Inoue et al. [24] demonstrated the use of salicylaldehyde-5-sulfonate (SAS) as labeling reagent for polyamines in capillary electrophoresis. Hence, in the following section, we describe both the methods with modifications in detail.

2 Materials

Prepare all solutions using ultrapure water (prepared by purifying deionized water to attain a sensitivity of 18 MΩ cm at 25 °C) and analytical grade reagents. Diligently follow all waste disposal regulations when disposing of waste materials.

2.1 Components for Polyamine Preparation

1. *Perchloric acid solution*: To prepare 5% and 10% perchloric acid solutions take 7.143 mL and 14.3 mL of 70% perchloric acid respectively and make up to 100 mL with ultrapure water.

2.2 Derivatization Components

1. *Preparation of dansyl chloride*: Dissolve 500 mg of dansyl chloride in 100 mL of acetone freshly at the time of use (*see* **Note 1**).
2. *Saturated sodium carbonate solution*: Dissolve excessive amount of sodium carbonate in 100 mL of ultrapure water.
3. *0.5 mM potassium hydroxide in methanol solution*: Dissolve 2.8 mg of potassium hydroxide in 20 mL of methanol and finally make it up to 100 mL with methanol.
4. *2 N NaOH*: Dissolve 8 g of sodium hydroxide in 50 mL of ultrapure water and finally make it up to 100 mL with ultrapure water.
5. *2% benzoyl chloride*: Dissolve 1 g of 4-(dimethylamino)benzoyl chloride (HPLC grade) in 20 mL of methanol (HPLC grade) and finally make it up to 50 mL with same methanol (*see* **Note 2**).
6. *Saturated sodium chloride*: Dissolve 35.7 g of sodium chloride in ultrapure water and finally make up to 100 mL.
7. *Cyclohexane-ethylacetate solvent*: Mix cyclohexane and ethyl acetate (TLC grade) in 2:3 ratio and store in an airtight bottle (*see* **Note 3**).
8. *Triethanolamine and 2-propanol solvent*: Mix triethanolamine and 2-propanol (HPLC grade) in 1:4 ratio and store in an airtight bottle.

2.3 HPLC Components

1. *10 mM sodium dihydrogen phosphate*: Dissolve 3.5814 g of sodium dihydrogen phosphate in 100 mL of ultrapure water and adjust the pH to 7.8 with HCL, finally make up to 1000 mL.
2. *10 mM sodium acetate buffer pH 5*: Dissolve 820.3 mg of sodium acetate in 100 mL of ultrapure water and adjust the pH to 5 with glacial acetic acid (HPLC grade) and finally make up to 1000 mL.

2.4 Components for Capillary Electrophoresis

1. *100 mM sodium dodecylbenzene sulfonate (DBS)*: Dissolve 3.4848 g of sodium dodecylbenzene sulfonate in 20 mL of ultrapure water and finally make up to 100 mL.

2. *1 mM phosphate buffer*: Dissolve 1.56 g of sodium dihydrogen phosphate dihydrate (monobasic) in 50 mL of water and make upto 100 mL with ultrapure water. Dissolve 3.5814 g of disodium hydrogen phosphate dodecahydrate (Dibasic) in 50 mL of water and finally make up to 100 mL with ultrapure water. Mix 90.8 mL of dibasic solution and 9.2 mL of monobasic solution to give 100 mM phosphate buffer with pH 7.8. Dilute 100 mM phosphate solution to 1 mM with ultrapure water.
3. *Synthesis of Salicylaldehyde-5-sulfonate (SAS)*: Prior to the SAS synthesis, prepare *n*-phenyl-salideneimine-5-sulfonic acid as previously described by Inoue et al. [24]. Mix 35 g of *n*-phenylsalicylaldimine in 95 mL of concentrated sulfuric acid and keep on heating for 2.5 h at 100 °C by vigorous stirring. Add this mixture into an equal volume of ice-water stepwise by continuous stirring. Recrystallize the resultant yellow precipitation in diluted sulfuric acid. Take the solid by filtration, wash with small quantity of ice-water and then with ethanol and acetone. Dry the product (*n*-phenyl-salideneimine-5-sulfonic acid) at ambient temperature (*see* **Note 4**).

   Take 25 g of *n-p*henyl-salideneimine-5-sulfonic acid and dissolve in aqueous solution of sodium carbonate (13.8 g in 125 mL of water). Boil the contents vigorously in an open flask for 2.5 h with periodic replenishment of the evaporated water. Cool 100 mL of the content to room temperature and to this slowly add acetic acid until pH of the solution reach to five. Allow the solution to cool 0 °C and filter off the resultant precipitation (salicylaldehyde-5-sulfonate). Wash the precipitation with ethanol and air-dry at room temperature (*see* **Note 5**).

   Alternatively, salicylaldehyde-5-sulfonate is readily is available as sodium salt with GFC chemicals, USA. The authors have not tested this readymade chemical, instead synthesized manually.
4. *50 mM salicylaldehyde-5-sulfonate solution*: Dissolve 1.0658 g of Salicylaldehyde-5-sulfonate in 50 mL of 10 μmol phosphate buffer (pH 7.8) and finally make up to 100 mL (*see* **Note 6**).
5. *100 mM HEPES buffer:* Mix 2.383 g of HEPES (4-(2-hydroxyethyl)piperazine-1-(ethanesulfonic acid) in 50 mL of ultrapure water and finally make up to 100 mL.

3 Methods

3.1 Preparation of Polyamines from Plant Samples (See Refs. 25, 26)

1. Take 0.1–0.5 g plant sample and grind in mortar with pestle using liquid nitrogen to fine powder. After transferring the resulting powder into a plastic tube add five volumes of 5% ice-cold perchloric acid (PCA), vortex the sample and leave it for 1 h on ice.

2. Centrifuge the suspension for 30 min at a speed of 15,000 × *g* at 4 °C. Take the supernatant and filter using a 0.2-μm filter syringe. Use this filtrate containing 5% perchloric acid (v/v) plant sample for derivatization.

3.2 Derivatization of Polyamines by Dansylation

Dansylation of polyamines was originally described by Seiler and Wiechann [27] and was adopted with modifications.

1. Take 200 μL of perchloric acid polyamines extracts into a fresh tube and to this add 400 μL of dansylchloride freshly prepared in acetone (5 mg/mL of acetone) and 200 μL of saturated sodium carbonate (*see* **Note 7**).
2. Vortex the mixtures briefly and incubate for at least 18 h in dark at room temperature.
3. To remove the excess dansylchloride from the samples, add 100 μL proline (100 mg/mL) and incubate for at least 30 min at room temperature (*see* **Note 8**).
4. Extract the dansylated polyamines into toluene or cyclohexane or benzene (3 × 1 mL) and pool the contents (*see* **Note 9**).
5. Process the standards in the same way as for samples and 20 nmol should be dansylated for each concentration alone or in combination.
6. Dry the organic phase at 40 °C under stream of air or nitrogen gas.
7. After this derivatization, clean the samples by adding 0.6 mL of 0.5 mM KOH in methanol [28] and left the mixtures to stand for 1 h at 40 °C.
8. To the mixtures add 1.5 mL of aqueous mixture containing 200 mg of KH_2PO_4 and 200 mg of Na_2HPO_4.
9. Extract the polyamines three times with organic solvent as described in **step 4**.
10. Dry the organic phase as described in **step 6** and finally dissolve the dry residues in 200 μL of methanol. Use polyamines in methanolic phase for analysis.

3.3 Derivatization of Polyamines by Benzoylation

Benzoylation of polyamines was originally described by Redmond and Tseng, [29] and further modified by Flores and Galston [25] and Slocum et al. [30].

1. Take 500 μL of perchloric acid extract of polyamines and to this add 1 mL of 2 N NaOH and 10 μL of 2% benzoyl chloride in methanol.
2. Vortex the contents for 30 s and incubate for 30 min at room temperature. To this add 2 mL of saturated NaCl (stop the reaction) and 2 mL of diethyl ether and mix vigorously.

3. Centrifuge the contents for 10 min at 3000 × *g* at 4 °C and phase separate the benzoyl-polyamines (collect the upper organic layer).
4. Evaporate the organic solvent phase under warm air and finally dissolve the dried polyamines in 50–100 μL of methanol (acetonitrile can also be used).
5. Filter this solution through a 0.45-μm Millipore filter to remove any particles. Use these polyamine derivatives for further analysis or store at −20 °C (stable up to 3 weeks).

3.4 Determination of Polyamines

After derivatization, polyamines can be determined by the following methods.

3.4.1 Separation and Determination of Polyamines by Thin Layer Chromatography (See Ref. 31)

1. Prepare 0.2 mm thick silica plates measuring 20 × 20 cm and air-dry the plates over night in dark.
2. Activate the air-dried TLC plates for 1 h at 110 °C (*see* **Note 10**).
3. Apply the samples in small spots to the thin layer plate by using sample applicator (Hamilton syringe). Apply the samples in 6-mm spots with a distance of 18 mm from one edge (*see* **Notes 11** and **12**).
4. Keep the solvent cyclohexane and ethyl acetate in 2:3 ratio in the chromatography tank (CAMAG, Switzerland) for saturation.
5. The plates are now exposed to ascending chromatography in the solvent saturated glass tank. Immerse the plates in the solvent mixture for 1.5–2 h or until the solvent front reaches just 2.5–5 cm below the end mark.
6. Remove the plates from the tank and allow to air-dry in the dark (*see* **Notes 13** and **14**).
7. After chromatographic separation of polyamines, visualize the chromatographic plates under 360 nm of UV source and then scrape off the zones containing dansyl derivatives with the scalpel blade and collect into a centrifuge tube.
8. To the individual sample tubes add 2 mL of ethyl acetate. After stirring for 2 min, centrifuge at 12,000 × *g* for 5 min and transfer into a new tube.
9. Measure the concentration of individual polyamine with fluorescent spectrophotometer at an excitation of 350 nm and a measuring emission of 495 nm.
10. The concentration of polyamines is determined with standards and normalized per milligram of sample protein.

3.4.2 Determination of Polyamines by HPLC

1. After derivatization, inject 20 μL of sample onto the HPLC. If the polyamine concentration is too high, it is better to dilute with the same solution used to dissolve dry residues of polyamines as in **step 10** of dansylation or as in **step 4** of benzoylation.

2. Follow the HPLC running conditions as mentioned.
   (a) Temperature: ambient.
   (b) Elution gradient: on injection: 45–80% B over 14 min.
   At 14 min: 80–90% B over 1 min.
   At 15 min. Hold at 90% B for 7 min.
   At 22 min. 90–45% over 1 min (stop data).
   At 29 min. Inject next sample.
3. Detect the fluorescence at 340 nm (excitation) and at 515 nm (emission).
4. Calculate the peaks using LCI-100 integrator and express the polyamines titers in nmol per mg fresh weight or number of cells initially used for polyamine extraction.

3.5 Determination of Polyamines by Capillary Electrophoresis

Capillary electrophoresis was initially employed by Driouich et al. [22–23] for separation and determination of n-alkylamines, histamine, lysine, and diaminopimelic acid by derivatizing them with salicylaldehyde-5-sulfonate (SAS) as labeling agent. Later Inoue et al. [28] used this technique for separation and determination of polyamines in *Arabidopsis thaliana*. SAS reacts with aliphatic primary amines to form stable Schiff's base and gives negative charge to the derivatives that results in selective manipulation of the separation [24]. Since these derivatives are water soluble it is possible to separate them in an aqueous phosphate buffer solution.

3.5.1 Preparation of Polyamines for Capillary Electrophoresis (See Ref. 24)

1. Polyamine samples in perchloric acid extract should be concentrated before subjecting them for capillary electrophoresis due to their insufficient sensitivity of UV detection. For this purpose employ the Ion-pairing solid-phase extraction (SPE).
2. Take A C18 cartridge column and wash it sequentially with 1 mL of acetone, methanol, water, and 10 mM acetate buffer (pH 5).
3. Take 3 mL of perchloric acid polyamine extract and to this add sufficient amount of potassium hydrogen carbonate powder, mix and cool it to 0 °C. See the solution with precipitation of potassium perchlorate (*see* **Note 15**).
4. Remove the precipitation by filtering or centrifugation.
5. To the solution add 600 µL of 100 mM acetate buffer and 60 µL of 100 mM sodium dodecylbenzene sulfonate (DBS), mix the contents and pass through the C18 cartridge to retain ion pairs of polyamine and DBS.
6. Wash the column with 1 mL of distilled water and then elute the ion pairs by adding 270 µL of ethanol. Use this effluent for derivatization with SAS.

3.5.2 Derivatization with Salicylaldehyde-5-Sulfonate and Separation by CE

The method of Driouich et al. [22–23] as adopted for plant tissues by Inoue et al. [24] iss used for derivatization of polyamines with SAS with modifications as follows.

1. Prepare polyamine standard solutions by dissolving an appropriate amount of polyamines in distilled water individually and adjust their concentration to 10 mM (*see* **Note 16**).
2. Take 350 µL of 0.1 µmol of each polyamine solutions individually in separate tubes and add 10 µL of 1 mM phosphate buffer (pH 7.8), 50 µL of 50 mM SAS, and 600 µL of ethanol.
3. Mix the contents thoroughly and incubate at 20 °C for 40 min.
4. Similarly take 270 µL of polyamine sample eluted from the SPE column and to this add 30 µL of HEPES buffer containing 50 mM SAS.
5. Mix the contents thoroughly and incubate at 20 °C for 40 min.
6. After incubation, filter the reaction mixtures using 0.45-µm membrane filter and use filtrates for electrophoretic separation.
7. Use the electrophoretic apparatus which has a capillary total length of 64.5 cm with an effective length of 56 cm. Inject 270 µL of polyamine standards and plant sample at 5 kPa for 5 s. Run the electrophoresis by applying a voltage of 30 kV and maintaining the temperature at 20 °C.
8. Detect the separated polyamines over 10 min by measuring the absorbance at 240 nm and express the electrophoregram as milliabsorbance units (mAU).
9. Calculate the concentration of the individual polyamines by using their correlation coefficients (R [2]) (CAD = 0.999; PUT = 0.996; SPD = 0.999; SPM = 0.952; and TSPM = 0.959; for more details read [24]).

4 Notes

1. Dansylchloride is highly corrosive to metals and causes serious corrosion to skin and eyes. Hence, dansyl chloride should be handled with extreme care. Since dansyl chloride is corrosive to metals use plastic spatulas while weighing. It is suggested to use Dermatril™ nitrile gloves while working with dansyl chloride. Dansyl chloride is fluorogenic and hence it is recommended to store the stock solution at 2–8 °C in bottles wrapped with aluminum foil.
2. Benzoyl chloride is highly corrosive to metals and cause serious corrosion to skin and eyes. Hence, benzoyl chloride should be handled with extreme care. Since benzoyl chloride is corrosive to metals and moreover it is highly moisture sensitive, do not try to weigh with metal spatulas; instead, it is suggested to use

one unit (1 gm) at once. It is suggested to use Dermatril™ nitrile gloves while working with benzoyl chloride. After preparation store the stock solution at 4 °C in bottles wrapped with aluminum foil.

3. Cyclohexane is acute toxic, shows respiratory sensitization, carcinogenic, shows reproductive toxicity, and hence care should be taken while using it. Since cyclohexane is hazardous to aquatic environment, diligently follow waste disposal regulations when disposing of the same.
4. *n*-phenylsalicyladimine is corrosive to metals and causes skin corrosion, serious eye damage, and acute toxicity. Hence, exercise extreme care while working with *n*-phenylsalicyladimine.
5. After every step during the synthesis of salicylaldehyde-5-sulfonate identify the product and confirm with NMR spectroscopy.
6. Prepare salicylaldehyde-5-sulfonate for samples in 100 mM HEPES buffer to prevent precipitation of buffer components in the reaction mixture containing more than 60% ethanol.
7. Dansylchloride reagent should be added in excess of quantity in order to obtain the reaction with all amino groups of polyamines.
8. Dissolve 100 mg of proline in 1 mL of ultrapure water and use this to remove excess dansylchloride.
9. Each time add 1 mL of toluene or cyclohexane or benzene, mix thoroughly, and let the contents stand for a while. Extract the upper organic layer containing polyamines. Dansylated polyamines in organic phase are stable up to 1 month.
10. Commercially available plates do not require activation for 1 h at 110 °C.
11. Polyamines at this stage are in the form of dansyl derivatives, which are light sensitive, and hence application of polyamines on TLC plates and separation should be carried out in the dark.
12. Volume of sample applied onto TLC is very critical and should be taken care of for reproducible results, and hence it is suggested to use fully automated devices such as Linomat V.
13. Since dansyl derivatives are light-sensitive and can be irreversibly destroyed on active surface by light, it is essential to keep the dry plate in the dark until they are ready for quantitative determination.
14. It is better to spray the chromatographic plates with 20 mL of triethanol amine and 2-propanol (prepared in 1:4 ratio) to stabilize the dansyl derivatives and increase the fluorescence. The intensity of fluorescence of chromatographic plates is quite stable for 3–4 days if stored in the dark.

15. Adding potassium hydrogen carbonate is necessary as it removes perchloric acid and adjusts the pH to 5.
16. SPD should be dissolved in ethanol; store standard solutions of PUT and CAD in refrigerator (4 °C) and SPM, SPD, and TSPM in freezer (−20 °C).

References

1. Tiburcio AF, Kaur-Sawhney R, Galston AW (1990) Polyamine metabolism. In: Miflin BJ, Lea PJ (eds) The biochemistry of plants, Intermediary nitrogen metabolism, vol 16. Academic Press, New York, pp 283–325
2. Baron K, Stasolla C (2008) The role of polyamines during *in vivo* and *in vitro* development. In Vitro Cell Dev Plant 44:384–395
3. Groppa MD, Benavides MP (2008) Polyamines and abiotic stress: recent advances. Amino Acids 34:35–45
4. Bouchereau A, Aziz A, Larher F, Martin-Tanguy J (1999) Polyamines and environmental changes: recent developments. Plant Sci 140:103–125
5. Kuznetsov VIV, Shevyakova NI (1999) Proline under stress: biological role, metabolism, and regulation. Russ J Plant Physiol 46:274–289
6. Hiraga H, Ito H, Yamakawa H, Ohtsubo N, Seo S, Mitsuhara I, Matsui H, Honma M, Ohashi Y (2000) An HR-induced tobacco peroxidase gene is responsive to spermine, but not to salicylate, methyl jasmonate, and ethephone. Mol Plant-Microbe Interact 13:210–216
7. Aronova EE, Shevyakova NI, Sretsenko LA, Kuznetsov VIV (2005) Cadaverine-induced induction of superoxide dismutase gene expression in *Mesembryanthemum crystallinum* L. Dokl Biol Sci 403:257–259
8. Sudhakar C, Veeranagamallaiah G, Naareshkumar A, Sudhakarbabu O, Shivakumar M, Pandurangaiah M, Kiranmai K, Lokesh U (2015) Polyamine metabolism influences antioxidant mechanism in foxtail millet (*Setaria italica* L.) cultivars with different salinity tolerance. Plant Cell Rep 34:141–156
9. Ducros V, Ruffieux D, Belva-Besnet H, de Fraipont F, Berger F, Favier A (2009) Determination of dansylated polyamines in red blood cells by liquid chromatography-tandem mass spectrometry. Anal Biochem 390:46–51
10. Schenkel E, Berlaimont V, Dubois J et al (1995) Improved high performance liquid chromatographic method for the determination of polyamines as their benzoylated derivatives: application to P388 cancer cells. J Chromatogr B 668:189–197
11. Sethi R, Raghuveer CS, Bashir S, Castro ME (2011) An improved high performance liquid chromatographic method for identification and quantization of polyamines as benzoylated derivatives. Am J Analyt Chem 2:456–469
12. Koski P, Helander IM, Sarvas M, Vaara M (1987) Analysis of polyamines as their dabsyl derivatives by reversed-phase high-performance liquid chromatography. Anal Biochem 164: 261–266
13. Hunter KJ, Fairlamb AH (1998) The determination of polyamines and amino acids by a fluorescamine -HPLC method. Methods Mol Biol 79:125–130
14. Campı'ns-Falco´ P, Molins-Legua C, Sevillano-Cabeza A et al (2001) O-Phthalaldelhyde-N-acetylcysteine polyamine derivatives: formation and stability in solution and in C18 supports. J Chromatogr B 759:285–297
15. Marton LJ, Lee PL (1975) More sensitive automated detection of polyamines in physiological fluids and tissue extracts with ophthalaldehyde. Clin Chem 21:1721–1724
16. Mattusch J, Huhn G, Wennrich R (1995) Sensitive laser induced fluorescence detection of polyamine-fluoresceinisothiocyanate-derivatives after capillary zone electrophoretic separation. Fresenius J Anal Chem 351:732–738
17. Legaz ME, Vicente C, Pedrosa MM (1998) Separation of tosylated polyamines by high-performance capillary zone electrophoresis. J Chromatogr A 823:511–521
18. Paproski RE, Roy KI, Lucy CA (2002) Selective fluorometric detection of polyamines using micellar electrokinetic chromatography with laser-induced fluorescence detection. J Chromatogr A 946:265–273
19. Liu G, Chen J, Ma Y (2004) Simultaneous determination of catecholamines and polyamines in PC-12 cell extracts by micellar electrokinetic capillary chromatography with ultraviolet absorbance detection. J Chromatogr B 805:281–288
20. Zhang LY, Tang XC, Sun MX (2005) Simultaneous determination of histamine and polyamines by capillary zone electrophoresis with 4-fluor-7-nitro-2,1,3-benzoxadiazole derivatiza-

tion and fluorescence detection. J Chromatogr B 820:211–219

21. NN F, Zhang HS, Ma M, Wang H (2007) Quantification of polyamines in human erythrocytes using a new near-infrared cyanine 1-(1-succinimidyl-hexanoate)- 1′-methyl-3,3,3′,3′-tetramethyl- indocarbocyanine-5,5′-disulfonate potassium with CE-LIF detection. Electrophoresis 28:822–829
22. Driouich R, Takayanagi T, Oshima M, Motomizu S (2001) Separation and determination of *n*-alkylamines and histamine by capillary zone electrophoresis using salicylaldehyde-5-sulfonate as a derivatizing reagent. J Chromatogr A 934:95–103
23. Driouich R, Takayanagi T, Oshima M, Motomizu S (2003) Investigation of salicylaldehyde-5-sulfonate as a precolumn derivatizing agent for the determination of n-alkane diamines, lysine, diaminopimelic acid, and isoniazid by capillary zone electrophoresis. J Pharm Biomed Anal 30:1523–1530
24. Inoue G, Kaneta T, Takayanagi T, Kakehi J, Motosec H, Takahashic T (2013) Determination of polyamines in *Arabidopsis thaliana* by capillary electrophoresis using salicylaldehyde-5-sulfonate as a derivatizing reagent. Anal Methods 5:2854–2859
25. Flores HE, Galston AW (1982) Analysis of polyamines in higher plants by high performance. Plant Physiol 69:701–706
26. Naka Y, Watanabe K, Sagor GHM, Niitsu M, Pillai MA, Kusano T, Takahashi Y (2010) Quantitative analysis of plant polyamines including thermospermine during growth and salinity stress. Plant Physiol Biochem 48:527–533
27. Selier N, Wiechmann M (1967) Mikrobestimmung von Spermine und Spermidine als dimethylamino-naphthalin-5-sulfonsaure-derivate. Hoppe Seylers Z Physiol Chem 348:1285–1290
28. Seiler N, Knodgen B (1979) Determination of the naturally occurring monoacetyl derivatives of di- and polyamines. J Chromatogr 164:155–168
29. Redmond JW, Tseng A (1979) High-pressure liquid chromatographic determination of putrescine, cadaverine, spermidine and spermine. J Chromatogr 170:479–481
30. Slocum RD, Flores HE, Galston AW, Winstein LH (1989) Improved method for HPLC analysis of polyamines, agmatine and aromatic monoamines in plant tissue. Plant Physiol 89:512–517
31. Madhubala R (1998) Thin layer chromatographic method for assaying polyamines. Methods Mol Biol 79:131–136

Chapter 21

Rapid Quantification of Abscisic Acid by GC-MS/MS for Studies of Abiotic Stress Response

Paul E. Verslues

Abstract

Drought and low water potential induce large increases in Abscisic Acid (ABA) content of plant tissue. This increased ABA content is essential to regulate downstream stress resistance responses; however, the mechanisms regulating ABA accumulation are incompletely known. Thus, the ability to accurately quantify ABA at high throughput and low cost is important for plant stress research. We have combined and modified several previously published protocols to establish a rapid ABA analysis protocol using gas chromatography–tandem mass spectrometry (GC-MS/MS). Derivatization of ABA is performed with (trimethylsilyl)-diazomethane rather than the harder to prepare diazomethane. Sensitivity of the analysis is sufficient that small samples of low water potential treated *Arabidopsis thaliana* seedlings can be routinely analyzed in reverse genetic studies of putative stress regulators as well as studies of natural variation in ABA accumulation.

Key words Drought, Water stress, Abscisic acid, GC-MS, Polyethylene glycol, Agar plates, *Arabidopsis thaliana*, *Brachypodium distachylon*

1 Introduction

Drought, along with related abiotic stresses such as salinity, is a major factor limiting plant productivity and is of increasing concern because of the predicted effects of climate change. Drought and osmotic stress cause rapid and substantial accumulation of the plant stress hormone Abscisic Acid (ABA). ABA is in turn a central controller of downstream drought responses [1, 2]. Recent studies have elucidated a core ABA signaling pathway consisting of the PYR/PYL/RCAR family of ABA receptors (PYLs), protein phosphatase 2Cs (PP2Cs), SnRK2 kinases, and SnRK2 phosphorylation targets such as ion channels and ABF transcription factors [3, 4]. In this pathway, increased ABA concentration promotes interaction of PYLs with PP2Cs, leading to inhibition of PP2C activity. This in turn allows the SnRK2 kinases to activate by autophosphorylation and in turn phosphorylate

Ramanjulu Sunkar (ed.), *Plant Stress Tolerance: Methods and Protocols*, Methods in Molecular Biology, vol. 1631,
DOI 10.1007/978-1-4939-7136-7_21,

their downstream targets. Different PYL-PP2Cs interactions have different ABA affinities [5], suggesting that they may respond differently depending on the level of ABA. Thus, precise regulation of the amount of ABA accumulated in the plant tissue is important for controlling the signaling output of the PYL-PP2C-SnRK2 signaling pathway and thereby affecting the activation of downstream stress responses.

In contrast to the rapid advances in signaling downstream of ABA, progress in understanding how ABA levels are controlled has been more limited. Endogenous ABA levels reflect the net effects of ABA synthesis and catabolism as well as conjugation and deconjugation of ABA-glucose ester, and perhaps other ABA-sugar conjugates (reviewed in [1]). Both the rapid turnover of ABA [6] and conjugation–deconjugation to signaling inactive sugar esters [7–9] make ABA a dynamic signal that can respond rapidly to environmental changes. When plants are exposed to a defined, reproducible low water potential stress it can be seen that the level of ABA accumulation is matched to the stress severity (example data reviewed in [1]). How the different pathways of ABA synthesis, catabolism, conjugation, deconjugation, and transport are coordinated and how the set-point level of ABA accumulated is changed in response to different stress and different environmental conditions are not known. There are some clues. For example, PP2C mutants have altered ABA accumulation [10, 11], likely as a result of ABA signaling exerting feedback regulation over ABA accumulation. Also, ongoing work in our laboratory has observed that *Arabidopsis thaliana* natural accessions exhibit a wide variation in ABA accumulation (Verslues Laboratory, unpublished). Given how many downstream responses are controlled by ABA, the molecular mechanisms that control of ABA levels is one of the major unanswered questions of abiotic stress. Thus, methods to accurately quantitate ABA, preferably with low cost and high throughput, continue to be important for plant stress biology.

While research on ABA is challenging, it also presents an opportunity to uncover new aspects of stress sensing and signaling. If ABA can be quantified with sufficient accuracy and throughput, then the level of ABA can be used as an "output" to tell when the unknown stress sensing and signaling events regulating ABA accumulation have been perturbed. ABA-responsive promoter-reporter constructs have been used with some success to report changes in endogenous ABA levels as well as find mutants deficient in ABA accumulation or ABA response [12, 13]. However, such approaches do introduce a level of uncertainty as to whether or not the promoter activity is influenced by factors other than ABA. Recent efforts to produce ABA biosensors [14, 15] are also extremely promising but need further refinement and necessitate the generation of transgenic plants, sometimes in specific genetic backgrounds to prevent silencing of the sensor construct. Like ABA-responsive

reporter constructs, ABA biosensors are not applicable in situations where ABA needs to be analyzed in a large set of genotypes or in nonmodel plants. Direct measurement of ABA in tissue extracts, and the accuracy and throughput of such measurement, is still a limiting factor for many studies.

Traditional methods of quantifying ABA can be divided into immunoassays and mass spectrometry based methods. Immunological methods include either ELISA or radioimmunoassay using ABA-specific antisera [2, 16–18]. The advantage of these techniques is that they require little in the way of specialized equipment (especially for ELISA methods). However, such assays tend to be expensive, relatively low throughput, and have a narrow working range. The latter point necessitates prior knowledge of the approximate level of ABA in the samples to be assayed or the assay of multiple dilutions of each sample, thus further limiting the numbers of samples that can be analyzed. Recently, liquid chromatography (LC)-mass spectrometry (MS) has become more common and accessible. Several methods for LC-MS/MS quantification of plant hormones, including ABA, have been published (*see* for example [19–22]). LC-MS/MS techniques can be very accurate, especially when stable isotope labeled ABA is used as an internal standard for quantification, and do not require derivatization of ABA. Disadvantages are the expensive instrumentation required and susceptibility of liquid chromotography to interferences from the sample matrix. For example, our laboratory commonly uses PEG-infused agar plates for stress experiments [23, 24]. In this case the samples contain residual high molecular weight PEG which can foul the nano-LC columns used for LC-MS/MS analysis. Samples either have to be laboriously rinsed to remove the PEG, PEG removed during sample extraction, or another method must be used.

Another long standing method of ABA quantification is GC-MS and GC-MS/MS. When combined with use of isotope labeled internal standard, the method is accurate and the use of tandem MS rather than single stage MS drives down the detection limit and allows ABA to be accurately quantified even in complex sample matrix. Gas chromatography is less sensitive to chromatography interferences than liquid chromatography. The same residual PEG that is problematic for LC poses no issue for GC as it does not volatilize when injected into the GC. A drawback of GC-MS/MS is the need to methylate ABA to make it sufficiently volatile to separate by GC. Traditionally this has been done using diazomethane, a toxic and explosive chemical that must be specially prepared before use [25]. Some studies have used (trimethylsilyl)-diazomethane (TMSD) as an alternative derivatization reagent [26, 27] but this has not yet been widely adopted.

Our laboratory has developed a rapid GC-MS/MS ABA quantification protocol which combines an abbreviated sample preparation,

TMSD derivatization and slight modification of previously reported GC-MS/MS analysis conditions [25, 28]. We have used this method for samples of *Arabidiopsis thaliana* and *Brachypodium distachylon* and find that the sensitivity and sample through put is suitable for reverse genetic and natural variation studies aimed to find novel regulators of low water potential-induced ABA accumulation. The method should be readily adaptable to other plant species; although, in some cases modifications of sample extraction and cleanup procedures may be needed. The reproducibility of ABA measurements depends not only on the analytical aspect but also the stress treatment protocols. We use PEG agar plates which allow a constant, reproducible stress to be applied and we typically measure ABA after plants have had a chance to acclimate to the stress. Readers are referred to previous discussion of stress treatment methods and descriptions of the PEG-agar plate system [23, 24].

2 Materials

1. Library tubes/racks.
2. Grinding beads (2 mm).
3. Freeze dryer.
4. Bead-beater. We use a Rentsh Mixer Mill MM301. Other bead beaters or grinding samples with microfuge pestles are alternatives.
5. (±)-abscisic acid (Sigma A1049) or (+)-abscisic acid (Sigma A4906 or 90,769) to generate the standard curve. ABA stock solution: 26.4 mg of S(+)ABA (264.3 g/mol) is dissolved in 1 mL Methanol (100 mM stock) and sequentially diluted to make 1 μM working stock.
6. Deuterated ABA for use as internal standard: ABA[$^2H_6$] (+)-*cis,trans*-abscisic acid (D6-ABA) [29].
7. Vacumm manifold.
8. C_{18} solid phase extraction cartridges: Supelclean™ LC-18 SPE Tube, bed wt. 100 mg, volume 1 mL (Sigma-Aldrich, No. 504270), or equivalent product available from other manufacturers.
9. Water bath-type sonicator.
10. Autosampler vials with low volume inserts suitable for 12–15 μL sample volume.
11. Speed-Vac or similar type vacuum concentrator with rotor for microcentrifuge tubes.
12. (Trimethylsilyl)-diazomethane, 2 M solution in hexane.
13. Reagent grade methanol, diethylether and ethyl acetate, glacial acetic acid.

14. GC-MS/MS capable of chemical ionization using methanol. In our laboratory a Varian model 431GC with VF-14MS (Varian/Agilent) column coupled to a Varian model 220 MS is used. Other types of instrument or GC-column can be used but analysis parameters may need to be adjusted.

3 Methods

The method described here was developed for Arabidopsis seedlings and has also been successfully used for leaf tissue of drought treated *Brachypodium distachylon*. Use for other species or stress treatments may require adjustments in how much tissue is used, how much internal standard is added and the extraction procedure. For example, we were unable to measure ABA in leaf samples of drought treated switchgrass using this procedure because of low recovery of ABA (presumably caused by high wax content and cell wall material in the sample). We have not quantitatively compared this procedure to procedures involving derivatization with diazomethane; however, it is likely that the derivatization efficiency is somewhat lower with TMSD. We have found this not to be a major concern for analyzing stress treated samples where ABA levels are high; however, it could be more of concern when analyzing other acidic hormones that may be present at lower concentration.

1. Prepare either library tubes in 96-well plate format or microcentrifuge tubes by adding 4–6 grinding beads.
2. Collect and weigh plant tissue samples and place in the tubes with grinding beads. Typically samples consist of 30–100 mg of tissue for Arabidopsis thaliana seedlings exposed to low water potential or up to 300 mg for unstressed seedlings (*see* **Note 1**). Samples should be frozen immediately using liquid nitrogen or dry ice.
3. Lyophilize samples until dry (typically 24–48 h).
4. Grind samples to a fine powder using grinding beads and sample homogenizer. After grinding, samples can be kept at room temperature or in refrigerator for short term storage (up to a few weeks) or at −20 °C for longer term storage.
5. Label two sets of microcentrifuge tubes for each sample being processed.
6. Calculate the amount of diluted D6-ABA solution needed (20 μL, approximately 20 pmol, for each sample and standard curve point) and prepare appropriate amount of working D6-ABA solution (*see* also **Note 2**).
7. Prepare standard curve tubes by adding the amounts of ABA standard and 20 μL of d6-ABA as indicated in Table 1. These can be directly put in the vacuum concentrator (**step 10**) without further processing.

Table 1
Standard curve set up

	pmol ABA	1 μM ABA stock (μL)	10–50 μM D6-ABA working solution (μL)
Blank	0	0	0
Standard 1	2	2	20
Standard 2	5	5	20
Standard 3	10	10	20
Standard 4	20	20	20
Standard 5	30	30	20
Standard 6	40	40	20
Standard 7	60	60	20

ABA and D6-ABA stock and working solutions are prepared as described in **Note 2**

8. Add 1 mL of 80% MeOH and 20 μL of ~50 μM d6 ABA to each plant tissue sample. Vortex thoroughly.
9. Spin down the samples for 5 min at ≥1000 × *g* using microplate centrifuge or standard microcentrifuge (*see* **Note 3**).
10. Prepare C_{18} SPE columns using vacuum manifold: wash with 600 μL of methanol and then equilibrate with 600 μL of 80% methanol (*see* **Note 4**).
11. Place labeled microfuge tube for collection under each SPE column and apply the corresponding sample to the SPE column by pipetting or gently pouring (to avoid disturbing the pellet). Elute into microfuge tube. Add additional 300 μL of 80% MeOH to the sample tubes, apply to SPE column and elute into the same tube as (*see* **Note 5**).
12. Dry the sample eluates as well as standard curve tubes overnight in vacuum concentrator (or until dry; typically 5–8 h needed, *see* **Note 6**). A small pellet of material will typically remain in each tube. (This is the usual stopping point for day 1 of the sample preparation, remaining steps are performed the following day.)
13. Resuspend samples in 200 μL of diethylether–methanol (9:1) and sonicate for ~10 min to resuspend pellet as much as possible (*see* **Note 7**).
14. Pulse each tube in microfuge (approximately 30 s at maximum speed) to pellet any insoluble material. Transfer supernatant to new microfuge tube.

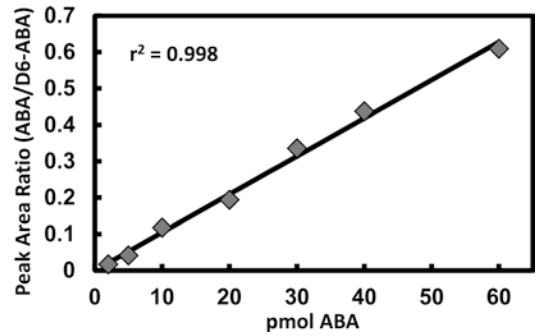

Fig. 1 Standard curve for ABA quantitation. Standard curve prepared as described in Table 1 and **Note 2** and is based on the ratio of ABA (daughter ion 229) and D6-ABA (daughter ions 233 + 234) peak areas

15. Let tubes stand open under fume hood to evaporate completely. This typically takes 2–3 h (avoid exposing the samples to bright light).
16. Add 20 μL of HPLC-grade methanol to each tube followed by 20 μL of 2 M TMSD. Close the tube caps, wrap tubes and tub rack in aluminum foil (to protect from light) and let stand ≥4 h (or overnight) in fume hood (*see* **Note 8**).
17. Add 20 μL of 0.5 M acetic acid in hexane (*see* **Note 9**). Evaporate to dryness by leaving tubes open in fume hood (1or 2 h).
18. Resuspend each sample and standard in 15 μL of ethyl acetate and transfer to autosampler vial with low volume insert (*see* **Note 10**). Cap each autosampler vial immediately to prevent evaporation. Check that the sample is in the bottom of the vial insert and tap down if needed.
19. Analyze each sample and standard by GC-MS/MS (*see* **Note 11**). Methanol chemical ionization is used to generate precursor ions (261 mass-to-charge ratio [*m/z*] for ABA and 267 *m/z* for D6-ABA). Daughter ions of 229 *m/z* (ABA) and 233 + 234 *m/z* (D6-ABA) are used for quantification. Analysis parameters are based on previous protocols [25, 28] and are given in detail in **Note 12**. Spectra generated in our analyses are essentially the same as those previously published [28].
20. Acquire peak areas and calculate the ratio of ion 229 (ABA) peak area to ion 233 + 234 (D6-ABA) peak area. Use this ratio to construct standard curve and calculate ABA amount in each sample. A typical standard curve is shown in Fig. 1.

4 Notes

1. For unstressed Arabidopsis seedlings where ABA contents are very low (around 1 ng/g fresh weight), it may necessary to combine two samples processed this way to get good signal-to-noise ratio for the ABA peak. Alternatively, a larger sample amount can processed using a larger volume SPE tube with appropriate scale up of extraction and elution volumes.
2. D6-ABA stock solution: dissolve 1 mg in 270 μL methanol and dilute tenfold to generate 1 mM stock solution. This is then diluted 50- to 100-fold to generate working solution added to each sample and standard. As quantification of ABA is determined by the ratio of the ABA peak area to D6-ABA peak area, the amount of D6-ABA used is not as critical as ensuring that all standards and samples have the same amount of D6-ABA added; thus, a volume of D6-ABA working solution sufficient for all samples and standards must be diluted at one time.
3. We have found that it is possible to remove a 50- or 100-μL aliquot of sample for proline analysis without affecting the ABA quantification. In this case the aliquots removed for proline analysis should then be dried down in a vacuum concentrator, resuspended in water and assayed for proline as previously described [30].
4. Do not let the resin dry out before applying the samples. For this and **step 11** the accuracy of dispensing the methanol solutions used is not as critical; thus, a repeater syringe-dispenser can be used to speed up the sample processing.
5. The eluate should be colorless or light yellow at this point for Arabidopsis seedlings with most of the green pigment and particulate matter retained on the SPE resin. Adding the additional 300 μL to wash the sample pellet is optional but does increase recovery of ABA.
6. Capacity of the vacuum concentrator is typically the limiting factor for how many samples can be processed at one time. We are able to use two standard Speed-Vacs (40-tube rotors) at once so that 72 samples and 8 standards can be dried simultaneously.
7. Sonication to resuspend the pellet is not be absolutely required but may increase recovery of ABA.
8. Use caution as TMSD is a very toxic chemical. TMSD must only be handled under a properly functioning fume hood and protective gloves and lab coat worn to prevent skin contact or

inhalation. Samples and methanol used must be free of water which will interfere with the derivatization reaction.

9. To make 0.5 M acetic acid in hexane add 30 μL of glacial acetic acid to 1 mL hexane. Adding this to the sample destroys any remaining TMSD.
10. Pipette up and down 2–3 times to increase recovery of sample. It is not needed to quantitatively recover all the ethyl acetate as the final quantitation is based on the ABA to D6-ABA ratio; but, enough volume must transferred to the bottom of each vial to allow the autosampler needle to pick it up.
11. Samples can be stored at room temperature on the autosampler for 1–2 days before analysis or stored at −4 C for several days. As there are still substantial impurities in the sample, we typically replace the GC inlet liner every 150 samples and remove a front section of the GC column and clean the MS ion trap every 500–800 samples.
12. These parameters are for a Varian 431 GC with VF14MS column coupled to a Varian 240 MS and are based on methods described by [28] but with the GC temperature program changed to allow more rapid runs while still having good separation of ABA from potentially interfering peaks. GC-Conditions: Splitless injection (1 μL), splitter opening 1:20 after 0.8 min, injector and transfer line temperature 250 °C; GC temperature program: 0.8 min at 70 °C, linear ramp to 270 °C at 15 °C/min, hold at 270 °C for 0.5 min, linear ramp to 310 °C at a rate of 80 °C/min, hold for 5 min. Total time for the GC temperature program is 20.1 min. MS Settings are generally as described previously [25, 28] with the MS set for CI Auto Ionization mode using methanol as the reagent gas. Scan time is 0.38 s, multiplier offset +300 V, emission current 30 μA. Ion preparation is set to MS/MS mode with two parent ions selected for fragmentation: ABA parent ion 261 m/z with excitation storage level of 115.0 and excitation amplitude of 0.45; D6-ABA parent ion 267 m/z with excitation storage level of 117.5 and excitation amplitude of 0.45. For both parent ions the resonant waveform type is used with a mass isolation window of 3.0 mass units. ABA elutes at 14.0–14.3 min (depending on age and condition of the GC column) D6-ABA elutes at 13.9–14.2 min. The mass spectrometer is turned to scan mode from 13.8 to 14.8 min and idled for the rest of the run. For ABA, the daughter ion of 229 m/z is used as the quantitative ion to determine the ABA peak area. For D6-ABA, the sum of daughter ions 233 and 234 is used to determine the peak area.

Acknowledgments

Work in the Verslues laboratory is supported by Academia Sinica and the Taiwan Ministry of Science and Technology. I thank Trent Z. Chang for laboratory assistance and help with GC-MS maintenance.

References

1. Verslues PE (2016) ABA and cytokinins: challenge and opportunity for plant stress research. Plant Mol Biol 91:629–640
2. Jones AM (2016) A new look at stress: abscisic acid patterns and dynamics at high-resolution. New Phytol 210:38–44
3. Raghavendra AS, Gunugunta VK, Christmann A, Grill E (2010) ABA perception and signalling. Trends Plant Sci 15:395–401
4. Cutler SR, Rodriguez PL, Finkelstein RR, Abrams SR (2010) Abscisic acid: emergence of a core signaling network. Annu Rev Plant Biol 61:651–679
5. Szostkiewicz I, Richter K, Kepka M, Demmel S, Ma Y, Korte A, Assaad FF, Christmann A, Grill E (2010) Closely related receptor complexes differ in their ABA selectivity and sensitivity. Plant J 61:25–35
6. Ren H, Gao Z, Chen L, Wei K, Liu J, Fan Y, Davies WJ, Jia W, Zhang J (2007) Dynamic analysis of ABA accumulation in relation to the rate of ABA catabolism in maize tissues under water deficit. J Exp Bot 58:211–219
7. Lee KH, Piao HL, Kim HY, Choi SM, Jiang F, Hartung W, Hwang I, Kwak JM, Lee IJ, Hwang I (2006) Activation of glucosidase via stress-induced polymerization rapidly increases active pools of abscisic acid. Cell 126: 1109–1120
8. Xu ZY, Lee KH, Dong T, Jeong JC, Jin JB, Kanno Y, Kim DH, Kim SY, Seo M, Bressan RA, Yun DJ, Hwang I (2012) A vacuolar beta-glucosidase homolog that possesses glucose-conjugated abscisic acid hydrolyzing activity plays an important role in osmotic stress responses in Arabidopsis. Plant Cell 24:2184–2199
9. Priest DM, Ambrose SJ, Vaistij FE, Elias L, Higgins GS, Ross AR, Abrams SR, Bowles DJ (2006) Use of the glucosyltransferase UGT71B6 to disturb abscisic acid homeostasis in *Arabidopsis thaliana*. Plant J 46:492–502
10. Bhaskara GB, Nguyen TT, Verslues PE (2012) Unique drought resistance functions of the highly ABA-induced clade A protein phosphatase 2Cs. Plant Physiol 160:379–395
11. Rubio S, Rodrigues A, Saez A, Dizon MB, Galle A, Kim TH, Santiago J, Flexas J, Schroeder JI, Rodriguez PL (2009) Triple loss of function of protein phosphatases type 2C leads to partial constitutive response to endogenous abscisic acid. Plant Physiol 150:1345–1355
12. Christmann A, Hoffmann T, Teplova I, Grill E, Müller A (2005) Generation of active pools of abscisic acid revealed by in vivo Imaging of water-stressed Arabidopsis. Plant Physiol 137: 209–219
13. Ishitani M, Xiong L, Stevenson B, Zhu JK (1997) Genetic analysis of osmotic and cold stress signal transduction in Arabidopsis: interactions and convergence of abscisic acid-dependent and abscisic acid-independent pathways. Plant Cell 9:1935–1949
14. Waadt R, Hitomi K, Nishimura N, Hitomi C, Adams SR, Getzoff ED, Schroeder JI (2014) FRET-based reporters for the direct visualization of abscisic acid concentration changes and distribution in Arabidopsis. elife 3:e01739
15. Jones AM, Danielson JA, Manojkumar SN, Lanquar V, Grossmann G, Frommer WB (2014) Abscisic acid dynamics in roots detected with genetically encoded FRET sensors. elife 3:e01741
16. Weiler EW (1979) Radioimmunoassay for the determination of free and conjugated abscisic acid. Planta 144:255–263
17. Weiler EW (1982) An enzyme-immunoassay for cis-(+)-abscisic acid. Physiol Plant 54: 510–514
18. Quarrie SA, Whitford PN, Appleford NEJ, Wang TL, Cook SK, Henson IE, Loveyes BR (1988) A monoclonal-antibody to (S)-abscisic acid – Its characterization and use in a radioimmunoassay for measuring abscisic acid in crude extracts of cereal and lupin leaves. Planta 173:330–339
19. Balcke GU, Handrick V, Bergau N, Fichtner M, Henning A, Stellmach H, Tissier A, Hause B, Frolov A (2012) An UPLC-MS/MS method for highly sensitive high-throughput analysis of phytohormones in plant tissues. Plant Methods 8:47

20. Forcat S, Bennett MH, Mansfield JW, Grant MR (2008) A rapid and robust method for simultaneously measuring changes in the phytohormones ABA, JA and SA in plants following biotic and abiotic stress. Plant Methods 4:16
21. Ross AR, Ambrose SJ, Cutler AJ, Feurtado JA, Kermode AR, Nelson K, Zhou R, Abrams SR (2004) Determination of endogenous and supplied deuterated abscisic acid in plaint tissues by high-performance liquid chromatography-electro-spray ionization tandem mass spectrometry with multiple reaction monitoring. Anal Biochem 329:324–333
22. Chiwocha SDS, Abrams SR, Ambrose SJ, Cutler AJ, Loewen M, Ross AR, Kermode AR (2003) A method for profiling classes of plant hormones and their metabolites using liquid chromatography-electrospray ionization tandem mass spectrometry: an analysis of hormone regulation of thermodormancy of lettuce (*Lactuca sativa* L.) seeds. Plant J 35:405–417
23. Verslues PE, Agarwal M, Katiyar-Agarwal S, Zhu J, Zhu JK (2006) Methods and concepts in quantifying resistance to drought, salt and freezing, abiotic stresses that affect plant water status. Plant J 45:523–539
24. van der Weele CM, Spollen WG, Sharp RE, Baskin TI (2000) Growth of *Arabidopsis thaliana* seedlings under water deficit studied by control of water potential in nutrient-agar media. J Exp Bot 51:1555–1562
25. Muller A, Duchting P, Weiler EW (2006) Hormone profiling in Arabidopsis. In: Salinas J, Sanchez-Serrano JJ (eds) Methods in molecular biology, vol vol 323. Humana, Totowa, NJ, pp 449–457
26. Schmelz EA, Engelberth J, Tumlinson JH, Block A, Alborn HT (2004) The use of vapor phase extraction in metabolic profiling of phytohormones and other metabolites. Plant J 39:790–808
27. Schmelz EA, Engelberth J, Alborn HT, O'Donnell P, Sammons M, Toshima H, Tumlinson JH (2003) Simultaneous analysis of phytohormones, phytotoxins, and volatile organic compounds in plants. Proc Natl Acad Sci U S A 100:10552–10557
28. Muller A, Duchting P, Weiler EW (2002) A multiplex GC-MS/MS technique for the sensitive and quantitative single-run analysis of acidic phytohormones and related compounds, and its application to *Arabidopsis thaliana*. Planta 216:44–56
29. Abrams SR, Nelson K, Ambrose SJ (2003) Deuterated abscisic acid analogs for mass spectrometry and metabolism studies. J Labelled Comp Radiopharm 46:273–283
30. Verslues PE (2010) Quantification of water stress-induced osmotic adjustment and proline accumulation for *Arabidopsis thaliana* molecular genetic studies. In: Sunkar R (ed) Plant stress tolerance. methods and protocols. Humana, New York, pp 301–316

Chapter 22

Silencing of Stress-Regulated miRNAs in Plants by Short Tandem Target Mimic (STTM) Approach

Sachin Teotia and Guiliang Tang

Abstract

In plants, microRNAs (miRNAs) regulate more than hundred target genes comprising largely transcription factors that control growth and development as well as stress responses. However, the exact functions of miRNA families could not be deciphered because each miRNA family has multiple loci in the genome, thus are functionally redundant. Therefore, an ideal approach to study the function of a miRNA family is to silence the expression of all members simultaneously, which is a daunting task. However, this can be partly overcome by Target Mimic (TM) approach that can knockdown an entire miRNA family. STTM is a modification of TM approach and complements it. STTMs have been successfully used in monocots and dicots to block miRNA functions. miR159 has been shown to be differentially regulated by various abiotic stresses including ABA in various plant species. Here, we describe in detail the protocol for designing STTM construct to block miR159 functions in Arabidopsis, with the potential to apply this technique on a number of other stress-regulated miRNAs in plants.

Key words Arabidopsis, miRNA, miR159, Short tandem target mimic (STTM), Stress-responsive miRNAs, Target mimic (TM)

1 Introduction

Small RNAs including microRNAs (miRNAs) play an important role in regulating endogenous target gene expression. Twenty to twenty-two nucleotide (nt) miRNAs achieve this function by binding to the near perfect complementary sites of the target genes. This binding leads to target mRNA degradation and/or translational repression. This regulation of the target mRNA by miRNAs is crucial in plant functioning and development. The main approaches to study functions of miRNAs include either overexpression or silencing their expression, which will result in down-regulation and upregulation of their target genes, respectively. While means of overexpression include expressing miRNAs under the control of *CaMV* 35S promoter, the knock-downs are created through target mimics [1], molecular sponges [2] and short

Ramanjulu Sunkar (ed.), *Plant Stress Tolerance: Methods and Protocols*, Methods in Molecular Biology, vol. 1631,
DOI 10.1007/978-1-4939-7136-7_22,

tandem target mimics (STTMs) [3]. Each approach has a variable efficiency in downregulating a particular miRNA [4].

STTM is a recently created technique to effectively downregulate a number of miRNAs expressed in various plant species. STTM is an artificial short (~96 nt) DNA segment that expresses noncoding RNA that can be introduced into plants either through stable transformation or virus-based transient expression systems [5]. STTM consists of two complementary binding sites which bind to the target miRNAs. The binding sites are separated by empirically tested 48–88 nt spacer (*see* **Note 1**). The binding sites have trinucleotide mismatches at a position complementary to 11th–13th nt of the target miRNA (*see* **Note 2**). These mismatched bases will not bind to the target miRNA and consequently form a bulge which will enable the artificial binding sites to escape the cleavage by the target miRNA [3] (Fig. 1). This resistance to cleavage will help STTM degrade/sequester target miRNAs. The spacer forms a weak stem-loop which helps in separating two miRNA binding sites from RNA-induced silencing complex (RISC) collision [4].

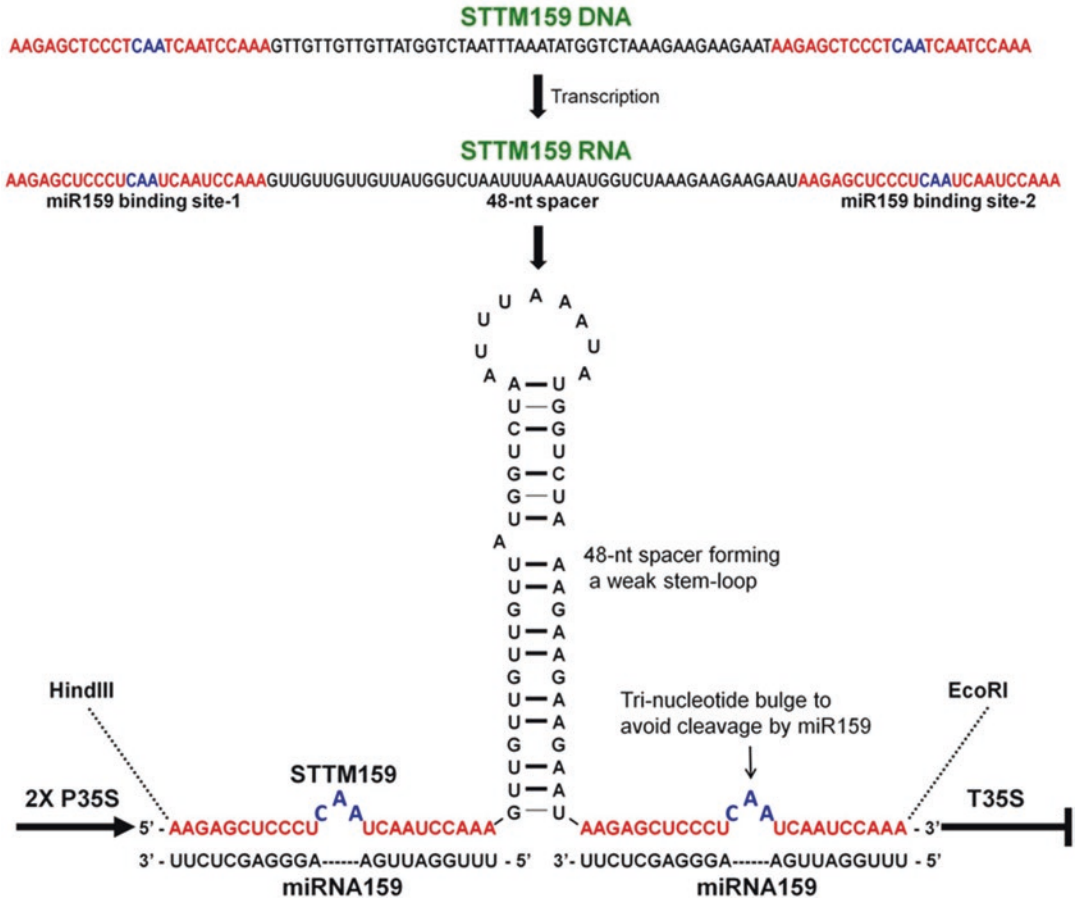

Fig. 1 STTM159 construct with miRNA159 binding sites (in *red*) on flanking sides separated by a 48-nt spacer forming a weak stem loop. The tri-nucleotide bulge is shown in *blue*. The complementary miRNA159 is shown in *black*. *2x P35S, double, enhanced 35S promoter; T35S, terminator*

A number of miRNAs are implicated for their roles in plant abiotic stress responses [6]. One such miRNA is miR159. Initial studies showed that miR159 levels in Arabidopsis increase under drought treatment or by exogenous ABA application during seed germination, indicating toward its possible role in drought tolerance [7, 8]. Further studies showed miR159 to be regulated by a number of stresses in many plant species. miR159 is upregulated: by drought and ABA in *Phaseolus vulgaris* [9]; by drought in *Vigna unguiculata* [10], wheat [11], rice [6], and maize [12]; by salt in wheat [11], banana [13], Phaseolus [9], Arabidopsis [6], and potato [14]; by heat in wheat [15]; by hypoxia in Arabidopsis [6]; by cold in wheat [11]; by UV-B radiation in wheat [16] and Arabidopsis [6]. miR159 has been found to be downregulated: by drought in potato [17] and rice [18]; by heavy metals in many plant species [19]; by hypoxia in maize [6]; by UV-B radiation in *Populus tremula* [6]. The precise roles of these miRNAs in stress responses can be determined by knocking down their expression through approaches such as STTM. STTM has been effective to downregulate many miRNAs in a number of plant species [4]. It has been previously mentioned that STTM was weakly effective to downregulate miR159 in Arabidopsis [2]. We show that STTM has been effective in knocking down the expression of miR159 in Arabidopsis with a concomitant increase in the target genes expression. Here, we describe the protocol to create STTM construct to knockdown miR159. This protocol can be applied to silence other stress-regulated miRNAs in Arabidopsis and other plant species.

2 Materials

2.1 Plant Growth Conditions

Arabidopsis is grown in a growth room/growth chamber with 16-h day photoperiod at 22–24 °C.

2.2 Arabidopsis Transformation

1. LB broth.
2. Silwet-L77.
3. Sucrose.
4. 50-ml falcon tubes.
5. Rifampicin, gentamycin, chloramphenicol, kanamycin.

2.3 Construction of Recombinant pOT2 and pFGC5941 Vectors

1. Vectors: pOT2-poly-cis, pFGC5941-PacI (Fig. 2).
2. *Taq* DNA polymerase (2.5 U/μl).
3. PCR cleanup kit.
4. G-25 sephadex columns.
5. Agarose.
6. Gel electrophoresis units.
7. T4 DNA ligase (400 U/μl)

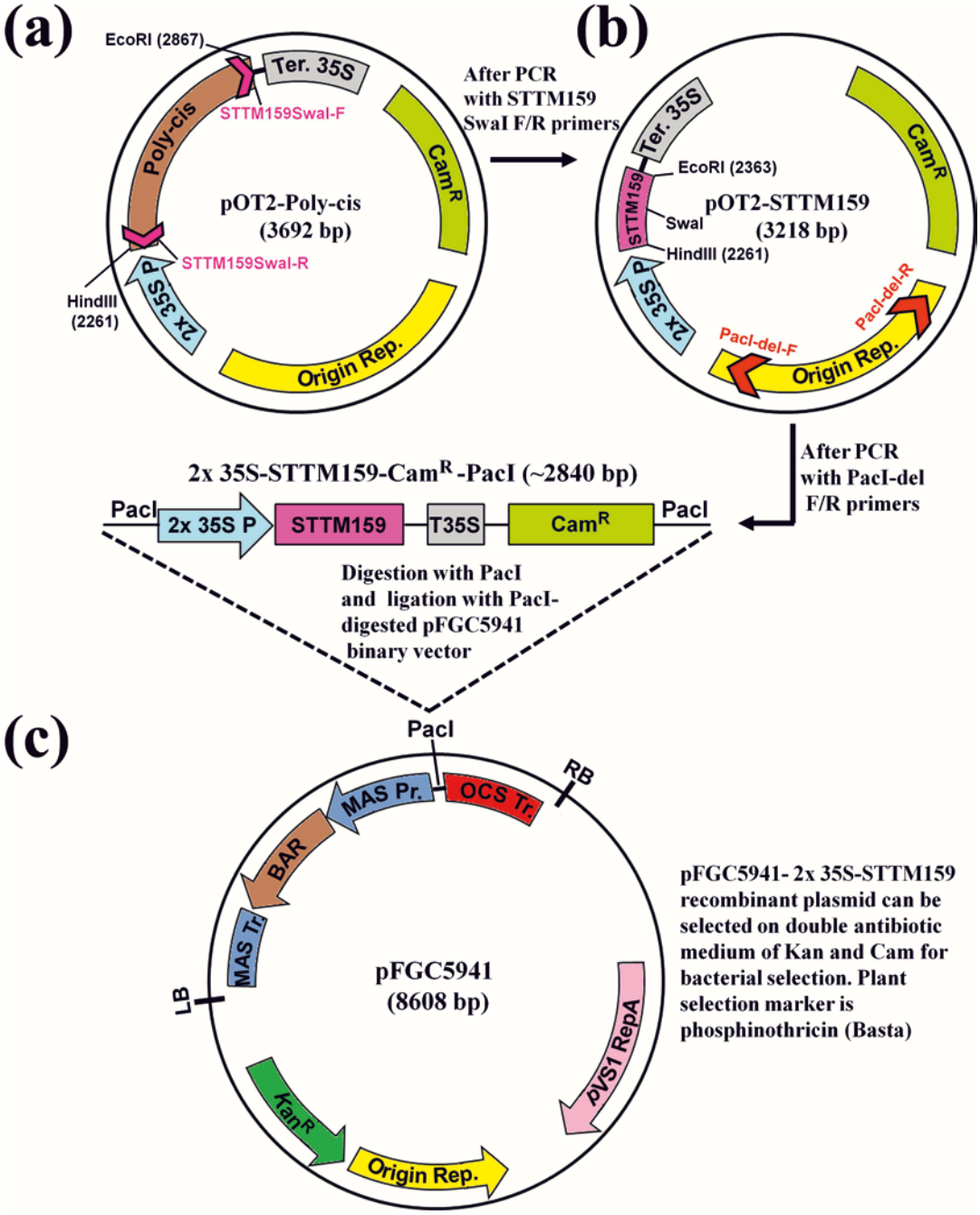

Fig. 2 Vectors used to silence miRNA159. (**a**) pOT2-poly-cis vector with STTM159SwaI-F/R primers binding sites and 2× 35S promoter and terminator; (**b**) pOT2 vector with a Poly-Cis site replaced with STTM159 construct (in *pink*) and origin-PacI-del primers to delete replication origin region and create PacI site; (**c**) pFGC5941 vector with PacI restriction site. The plant selection marker gene is *bar. Cam, chloramphenicol; Kan, kanamycin; Rep, replication; Pr./P, promoter; Tr./Ter., terminator*

8. Incubators and shakers for growing *E. coli* and Agrobacterium.
9. Laminar hood.
10. Luria–Bertani (LB) broth.
11. 30 mg/ml chloramphenicol.
12. 50 mg/ml kanamycin.
13. 35 mg/ml rifampicin.
14. Transformation competent *Escherichia coli* (DH5α).
15. Transformation competent *Agrobacterium tumefaciens*, GV3101 (MP90).
16. Plasmid miniprep kit.
17. Restriction enzymes: PacI, SwaI.
18. 10× reaction buffers for restriction digestion.
19. Primers synthesized in Integrated DNA Technology (IDT): STTM construction primers, the origin deletion primers (Table 1).

2.4 RNA Isolation, cDNA Synthesis, and Quantitative Real-Time (qRT) PCR Analysis

1. TRIzol Reagent.
2. 40 U/μl RNase inhibitor.
3. DNase−/RNase-free water.
4. Random hexamers or oligo dT as RT primers.
5. cDNA Reverse Transcription (RT) Kit.
6. Real-time PCR kit, SYBR® Select Master Mix, (Applied Biosystems).
7. Sequence-specific primers for Real-time PCR of target genes [Integrated DNA Technologies (IDT), Coralville, IA].
8. Nanodrop 2000 (Thermoscientific).
9. Real-time PCR cycler (StepOnePlus™ System, Applied Biosystems).
10. PCR Primers for Arabidopsis EF1α gene as an endogenous control:

    Forward: 5′-CACCACTGGAGGTTTTGAGGC-3′.

    Reverse: 5′-GGTGGCATCCATCTTGTTACAAC-3′.
11. miR159 Stem-loop real-time qRT-PCR primers:

    miR159-stemloop-RT-primer.

    5′-CTCAACTGGTGTCGTGGAGTCGGCAATTCAGT TGAGaagagctc-3′.

    Universal reverse primer.

    5′-GTGCAGGGTCCGAGGT-3′

    miR159-F.

    5′-ACACTCCAGCTGGGtttggattgaaggga-3′
12. DNeasy Plant Mini Kit—Qiagen.

Table 1
Primers used for production of STTM159–48 using pOT2-Poly-Cis template

STTM159-F (5′ to 3′)	gccATTTAAATatggtctaaagaagaagaatAAGAGCTCCCTCAATCAATCCA AAgaattcggtacgctgaaatcaccag
STTM159-R (5′ to 3′)	gccATTTAAATtagaccataacaacaacaacTTTGGATTGATTGAGGGAGCTC TTaagcttgggctgtcctctccaaatg
PacI-del-F (5′ to 3′)	TCCCTTAATTAAGTTTGCAAGCAGCAGATTACGCG
PacI-del-R (5′ to 3′)	TCCCTTAATTAAGAAAGGCGGACAGGTATCCGGTAAG

3 Methods

3.1 Designing STTM Construct

Arabidopsis has three members in miR159 family: a, b, and c whose sequences are as below:

miR159a 5′ UUUGGAUUGAAGGGAGCUCUA 3′.
miR159b 5′ UUUGGAUUGAAGGGAGCUCUU 3′.
miR159c 5′ UUUGGAUUGAAGGGAGCUCCU 3′.

The first 19 nt of these three members including the key seed region are the same. Only the last 2 nt (20 and 21) differ, which are not critical for efficacy of STTMs. For our purposes, we selected to design STTM against miR159b, which has at least one base common in the last two bases with both miR159a and c. The sequence for miR159 binding site in STTM should be complementary to it, which is: 5′-AAGAGCUCCCUUCAAUCCAAA-3′. We selected the same sequence for both binding sites in the STTM construct. Alternatively, one binding site can target miR159b and the other binding site can target miR159a or c, without any difference in STTM efficacy, as the dissimilar nucleotides are outside the seed region. For designing of STTM against miRNA165/166 also, this approach was taken where one binding site corresponds to miRNA165 and the other one to miRNA166, when both the miRNAs differ by 1 nt (#17) [3].

To make STTM binding sites resistant to the cleavage by the mature miR159, a trinucleotide bulge must be designed in the cleavage region of the binding sites, corresponding between the 10th and 11th positions of the mature miR159 [3]. In Arabidopsis *IPS1* this trinucleotide bulge is CUA which corresponds to 10th and 11th positions of miR399. When using CUA as the trinucleotide bulge no severe phenotype was observed (Tang lab, unpublished data and [2]). Therefore, in place of CUA we used CAA which was used to create TM construct, *MIM159* [20]. The STTM159 with CAA trinucleotide bulge produced severe

phenotype as reported [20]. This could be possible due to the effect on STTM binding site complementarity to miR159 or with the stability of overall STTM structure. After adding "CAA" as the trinucleotide bulge, the binding sequence becomes 5′-AAGAGCTCCCTcaaTCAATCCAAA-3′. Finally, the two binding sites, separated by 48-nt spacer, will form a STTM fragment which appears like this:

5′-AAGAGCTCCCTcaaTCAATCCAAAgttgttgttgttatggt ctaatttaaatatggtctaaagaagaagaatAAGAGCTCCCTcaaTCA ATCCAAA-3′ (Fig. 1).

3.2 Cloning STTM Fragment in pOT2-Poly-Cis Vector

pOT2-Poly-Cis vector has been described previously [21]. STTM fragment is first cloned into pOT2-Poly-Cis vector and then subcloned into pFGC5941 binary vector.

1. Design STTM specific primers (STTM159-F/R) with SwaI site at the 5′ site as shown in Table 1. The middle lower case letters form the spacer and the lower case letters toward the 3′ side of the primer form the bases complementary to bind with the pOT2-vector for inverse PCR (Fig. 2a).
2. Take the DNA template of pOT2-Poly-cis plasmid and amplify it by PCR using STTM159-F/R primers (Table 1) using LongAmp® *Taq* DNA Polymerase (NEB). Use the cycling conditions as: 94 °C, 2 min; [94 °C, 30 s; 58 °C, 30s; 68 °C, 4 min (30 cycles)]; 68 °C, 10 min.
3. Verify the PCR product (~3200 bp) on 1% agarose gel.
4. Purify the PCR product by desalting by passing through G25 sephadex column or PCR purification column (Promega).
5. Digest 10–20 µl of the purified PCR product with SwaI in a 50 µl reaction in NEB buffer 3 at 25 °C for 4 h.
6. After digestion, heat-inactivate the SwaI enzyme by incubating at 70 °C for 10 min and then again pass through the G25 sephadex column.
7. Self-ligate 10–20 µl of the SwaI-digested and purified products in 25–30 µl reaction using 1 µl T4 DNA ligase and 10× ligase buffer. Keep the above reaction overnight at 16 °C.
8. Transform the above reaction into chemically competent *Escherichia coli* (DH5α) cells by heat shock at 42 °C.
9. Select positive colonies by selecting on LB-agar plate supplemented with 30 µg/ml of chloramphenicol (Cam).
10. Test positive clones by colony PCR in 25 µl reaction using primers PacI-del-F/R (Table 1), using same conditions as above. After this PCR the "Replication origin" of the pOT2 vector is deleted and a PCR product is formed of 2846 bp which has PacI sites on both ends.

11. Digest 5 μl of the PCR product with SwaI and run on 1% agarose gel. Positive clones will have a SwaI site in the spacer region and will form two products: one of ~1 kb and the other of about ~2 kb. The original pOT2-Poly-Cis vector has no SwaI site and will form only one product of about ~3 kb.
12. Send the positive clone for sequencing using the sequencing primers: STTM-common-real-F (5′-catttggagaggacagcccaag-3′) and STTM-common-real-R (5′-ctggtgatttcagcgtaccgaa-3′).

3.3 Subcloning STTM Fragment from pOT2-Poly-Cis Vector into Binary Vector pFGC5941-PacI

After PCR with PacI-del-F/R primers in **step 10** of the previous section, the "origin of replication" is removed. What remains is the structure of STTM159 together with CaMV d35S (2× enhanced) promoter, the 35S terminator and Cam^R selection marker, which is subcloned into a binary vector pFGC5941 for Agrobacterium-mediated transformation. Vector pFGC5941 has a unique PacI site (Fig. 2c).

1. Mix the remaining 20 μl PCR product from **step 10** of the previous section with 500 ng of pFGC5941 and digest them with 1 μl PacI in NEB buffer 1 in 50 μl reaction volume and incubate for 4 h at 37 °C (*see* **Note 3**). After digestion, heat-inactivate the reaction mix at 65 °C for 20 min.
2. Purify the digested products using PCR purification column.
3. Take 26 μl of the above purified mix of PacI-digested pFGC5941 vector and PacI-digested origin-deleted PCR product and set up a 30-μl reaction volume by adding 1 μl T4 DNA ligase and 3 μl of ligation buffer. Incubate the reaction mix and ligate at 16 °C overnight.
4. Transform the ligation reaction into DH5α*E. coli* cells and plate on a LB agar plate with both kanamycin (50 mg/ml) and Cam^R (30 mg/ml) for screening the colonies containing the recombinant pFGC5941-STTM construct. Kan^R comes from the pFGC5941 backbone and Cam^R comes from origin-deleted PCR product of pOT2 backbone. The possibility of false positive colonies is removed by the double selection (*see* **Note 4**).
5. Verify the correct clones by isolating plasmid DNA from a few positive colonies by Promega miniprep kit and digesting with PacI enzyme. After digestion, correct construct will give two DNA bands on agarose gel (one of about ~8.6 kb and the other is about ~2.8 kb). The positive construct is further verified by DNA sequencing using the primers STTM-common-real-F/R (step 12 of the previous section).

3.4 Transforming Recombinant pFGC5941-STTM159 Vector into A. tumefaciens by Freeze–Thaw Method

The recombinant pFGC5941-STTM159 vector is transformed into *Agrobacterium* strain GV3101 (MP90) by freeze–thaw method [22].

1. Thaw a vial of transformation-competent Agrobacterium cells thawed in ice and add 1 μg plasmid DNA dissolved in sterile water to it.
2. Perform transformation by freeze–thaw method and plate the transformed Agrobacterium cells on LB plates supplemented with 50 mg/ml rifampicin, 50 mg/ml kanamycin, 50 mg/ml gentamycin, and 30 mg/ml chloramphenicol.
3. Incubate the plates at 28 °C for 2–3 days until the colonies become bigger.
4. For screening the transformants, perform colony PCR using previously described primers, STTM-common-real-F/R.
5. Prepare a glycerol stock of the correct Agrobacterium transformant and store at −80 °C for further use.

3.5 Transformation of Arabidopsis with the Agrobacterium harboring pFGC5941-STTM159 Vector

Transform Arabidopsis with the above construct using modified floral dip method [23] and select the transformed seeds by spraying with herbicide Basta.

3.6 Validation of miR159 Silencing by Real-Time PCR Analysis

Transgenic Arabidopsis expressing STTM159 shows very severe phenotype like reduced stature, with rounder, upward curled leaves (Fig. 3). The flowers are smaller with short sepals and petals and siliques are shorter with fewer seeds (data not shown). Validate the given transgenic lines for knockdown of miR159 and upregulation of target gene expression, *MYB33* and *MYB65* [24].

1. Isolate DNA from plants exhibiting severe phenotypes using DNeasy Plant Mini Kit, and confirm the transgene integration by STTM-common-real-F/R primers, as mentioned above.
2. Isolate RNA from the confirmed plants showing integration of STTM159 and wild type (WT) using Trizol reagent using manufacturer's instructions (*see* **Note 5**).
3. Quantify the RNA samples by measuring the absorbance of the sample at 260 nm using a Nanodrop 2000 (Thermo Scientific). Check quality of RNA by running in 1% Agarose gel.
4. Take 1 μg of RNA from three independent transgenic lines and make cDNA using High-Capacity cDNA Reverse Transcription Kit (Applied Biosystems) using random hexamers (for target genes) and miR159-stemloop-RT-primer (for miR159 stem-loop PCR). In both reactions, first incubate RNA at 70 °C for 5 min. And then immediately put in ice. The conditions are as follows: For stem-loop PCR—30 °C for 10 min, 42 °C for

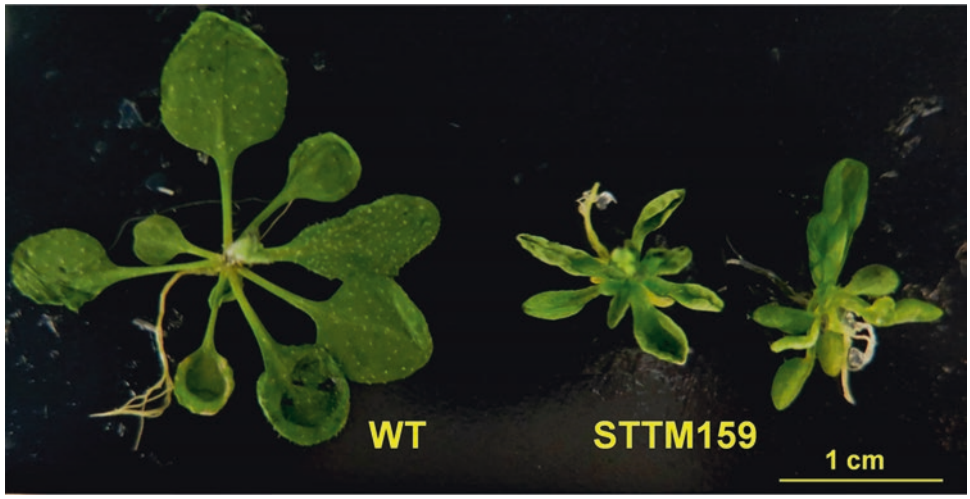

Fig. 3 Transgenic Arabidopsis expressing STTM159 show very severe phenotype like stunted growth, with upward curled leaves, which are less rounded

50 min, 85 °C for 5 min; for mRNA RT-PCR—25 °C for 30 min, 42 °C for 30 min, 85 °C for 5 min.

5. Design real-time PCR primers by selecting a unique region from the target genes. The primers should not form a product more than 200 bp. Check the primers by using BLAST search engine in NCBI database to see if they are not binding elsewhere.
6. Take 1 μl of the cDNA, 6 μl of 2× SYBR Green PCR Master mix (Applied Biosystems), and 0.5 μl each of 10 μM primers to set up 12 μl of reaction. Set up each reaction in triplicate on a StepOnePlus™ System (Applied Biosystems) with the following conditions: heat activation of reverse DNA polymerase at 95 °C for 10 min followed by 40 cycles of 95 °C for 15 s, 60 °C for 1 min.
7. Analyze the data thus obtained by the $2^{-\Delta\Delta CT}$ method [25] (Fig. 4). Take EF1α as an endogenous control and WT as a sample control.

4 Notes

1. The spacer in STTM can be 48–88 bp, but minimum spacer should be at least 48 bp for STTM efficacy.
2. The trinucleotide bulge in the STTM sequence is important to escape cleavage by the target miRNA. The trinucleotides should not be complementary to the 11th–13th nt of the

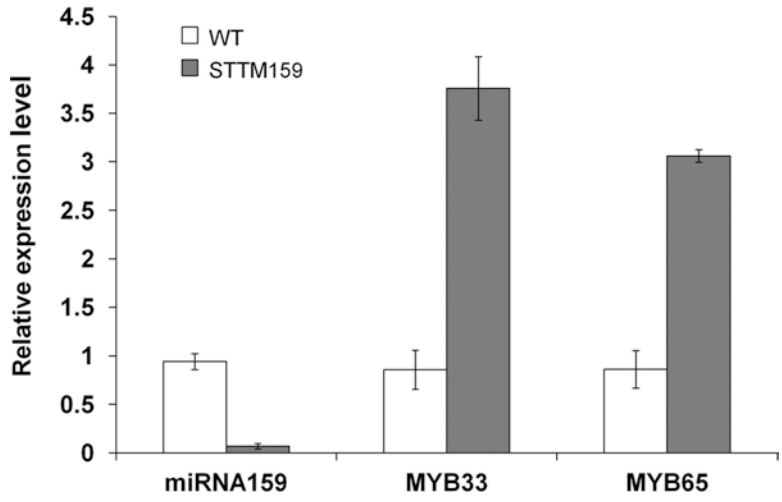

Fig. 4 Real-time PCR analysis of transgenic plants expressing STTM159. miRNA159 expression is suppressed in Arabidopsis plants expressing STTM159 construct. The target genes of miRNA159, *MYB33* and *MYB65*, are upregulated in plants expressing STTM159 construct

target miRNAs. These trinucleotides can be other than (CAA) depending upon the mismatches to the complementary bases of the target miRNA.

3. Before ligating the mixture of PacI-digested pFGC5941-STTM159 and origin-del-pOT2 PCR, specific dephosphorylation of pFGC5941 vector, but not the pOT2-STTM, may be required to increase the colonies bearing recombinant clones on the double antibiotics selection plates. In that case PacI digestion of the two vectors will be done separately.
4. The selection of pFGC5941-STTM159 on double antibiotics (Kan + Cam) plates ensures all correct colonies.
5. TRIzol contains phenol and GITC is hazardous to humans. Always wear laboratory coat, gloves, and eye protection while handling this solution.

Acknowledgements

This study was partially supported by funds from Henan Agricultural University (HAU) and NSFC (31571679), China. G.T. is supported by the National Science Foundation (NSF; grants IOS-1048216 and IOS-1340001). S.T. is supported by a postdoctoral scholarship from HAU.

References

1. Franco-Zorrilla JM, Valli A, Todesco M, Mateos I, Puga MI, Rubio-Somoza I, Leyva A, Weigel D, Garcia JA, Paz-Ares J (2007) Target mimicry provides a new mechanism for regulation of microRNA activity. Nat Genet 39:1033–1037
2. Reichel M, Li Y, Li J, Millar AA (2015) Inhibiting plant microRNA activity: molecular SPONGEs, target MIMICs and STTMs all display variable efficacies against target microRNAs. Plant Biotechnol J 13:915–926
3. Yan J, Gu Y, Jia X, Kang W, Pan S, Tang X, Chen X, Tang G (2012) Effective small RNA destruction by the expression of a short tandem target mimic in Arabidopsis. Plant Cell 24:415–427
4. Teotia S, Singh D, Tang X, Tang G (2016) Essential RNA-based technologies and their applications in plant functional genomics. Trends Biotechnol 34:106–123
5. Sha A, Zhao J, Yin K, Tang Y, Wang Y, Wei X, Hong Y, Liu Y (2014) Virus-based microRNA silencing in plants. Plant Physiol 164:36–47
6. Khraiwesh B, Zhu JK, Zhu J (2012) Role of miRNAs and siRNAs in biotic and abiotic stress responses of plants. Biochim Biophys Acta 1819:137–148
7. Reyes JL, Chua NH (2007) ABA induction of miR159 controls transcript levels of two MYB factors during Arabidopsis seed germination. Plant J 49:592–606
8. Sunkar R, Zhu JK (2004) Novel and stress-regulated microRNAs and other small RNAs from Arabidopsis. Plant Cell 16:2001–2019
9. Arenas-Huertero C, Pérez B, Rabanal F, Blanco-Melo D, De la Rosa C, Estrada-Navarrete G, Sanchez F, Covarrubias AA, Reyes JL (2009) Conserved and novel miRNAs in the legume *Phaseolus vulgaris* in response to stress. Plant Mol Biol 70:385–401
10. Barrera-Figueroa BE, Gao L, Diop NN, Wu Z, Ehlers JD, Roberts PA, Close TJ, Zhu JK, Liu R (2011) Identification and comparative analysis of drought-associated microRNAs in two cowpea genotypes. BMC Plant Biol 11:127
11. Gupta OP, Meena NL, Sharma I, Sharma P (2014) Differential regulation of microRNAs in response to osmotic, salt and cold stresses in wheat. Mol Biol Rep 41:4623–4629
12. Wang Y-G, An M, Zhou S-F, She Y-H, Li W-C, F-L F (2014) Expression profile of maize microRNAs corresponding to their target genes under drought stress. Biochem Genet 52:474–493
13. Lee WS, Gudimella R, Wong GR, Tammi MT, Khalid N, Harikrishna JA (2015) Transcripts and microRNAs responding to salt stress in *Musa acuminata* Colla (AAA Group) cv. Berangan Roots. PLoS One 10:e0127526
14. Kitazumi A, Kawahara Y, Onda TS, De Koeyer D, de los Reyes BG (2015) Implications of miR166 and miR159 induction to the basal response mechanisms of an andigena potato (*Solanum tuberosum subsp. andigena*) to salinity stress, predicted from network models in Arabidopsis. Genome 58:13–24
15. Xin M, Wang Y, Yao Y, Xie C, Peng H, Ni Z, Sun Q (2010) Diverse set of microRNAs are responsive to powdery mildew infection and heat stress in wheat (*Triticum aestivum* L.) BMC Plant Biol 10:123
16. Wang B, Sun YF, Song N, Wang XJ, Feng H, Huang LL, Kang ZS (2013) Identification of UV-B-induced microRNAs in wheat. Genet Mol Res 12:4213–4221
17. Yang J, Zhang N, Mi X, Wu L, Ma R, Zhu X, Yao L, Jin X, Si H, Wang D (2014) Identification of miR159s and their target genes and expression analysis under drought stress in potato. Comput Biol Chem 53:204–213
18. Barrera-Figueroa BE, Gao L, Wu Z, Zhou X, Zhu J, Jin H, Liu R, Zhu JK (2012) High throughput sequencing reveals novel and abiotic stress-regulated microRNAs in the inflorescences of rice. BMC Plant Biol 12:132
19. Yang ZM, Chen J (2013) A potential role of microRNAs in plant response to metal toxicity. Metallomics 5:1184–1190
20. Todesco M, Rubio-Somoza I, Paz-Ares J, Weigel D (2010) A collection of target mimics for comprehensive analysis of microRNA function in *Arabidopsis thaliana*. PLoS Genet 6:e1001031
21. Tang G, Yan J, Gu Y, Qiao M, Fan R, Mao Y, Tang X (2012) Construction of short tandem target mimic (STTM) to block the functions of plant and animal microRNAs. Methods 58:118–125
22. Weigel D, Glazebrook J (2006) Transformation of Agrobacterium using the freeze-thaw method. Cold Spring Harbor Protoc 7:pdb.prot4666
23. Narusaka M, Shiraishi T, Iwabuchi M, Narusaka Y (2010) The floral inoculating protocol: a simplified *Arabidopsis thaliana* transformation method modified from floral dipping. Plant Biotechnol 27:349–351
24. Allen RS, Li J, Stahle MI, Dubroue A, Gubler F, Millar AA (2007) Genetic analysis reveals functional redundancy and the major target genes of the Arabidopsis miR159 family. Proc Natl Acad Sci U S A 104:16371–16376
25. Livak KJ, Schmittgen TD (2001) Analysis of relative gene expression data using real-time quantitative PCR and the $2-\Delta\Delta CT$ method. Methods 25:402–408

Chapter 23

Rhizosphere Sampling Protocols for Microbiome (16S/18S/ITS rRNA) Library Preparation and Enrichment for the Isolation of Drought Tolerance-Promoting Microbes

Venkatachalam Lakshmanan, Prasun Ray, and Kelly D. Craven

Abstract

Natural plant microbiomes are abundant and have a remarkably robust composition, both as epiphytes on the plant surface and as endophytes within plant tissues. Microbes in the former "habitat" face limited nutrients and harsh environmental conditions, while those in the latter likely lead a more sheltered existence. The most populous and diverse of these microbiomes are associated with the zone around the plant roots, commonly referred to as the *rhizosphere*. A majority of recent studies characterize these plant-associated microbiomes by community profiling of bacteria and fungi, using amplicon-based marker genes and next-generation sequencing (NGS). Here, we collate a group of protocols that incorporate current best practices and optimized methodologies for sampling, handling of samples, and rRNA library preparation for variable regions of V5-V6 and V9 of the bacterial 16S ribosomal RNA (rRNA) gene, and the ITS2 region joining the 5.8S and 28S regions of the fungal rRNA gene. Samples collected for such culture-independent analyses can also be used for the actual isolation of microbes of interest, perhaps even those identified by the libraries described above. One group of microbes that holds promise for mediating plant stress incurred by drought are bacteria that are capable of reducing or eliminating the plant's perception of the stress through degradation of the gaseous plant hormone ethylene, which is abundantly produced in response to drought stimuli. This is accomplished by some types of soil bacteria that can produce the enzyme 1-aminocyclopropane-1-carboxylate (ACC) deaminase, which is the immediate precursor to ethylene. Here we provide a high-throughput protocol for screening of ACC deaminase-producing bacteria for the applied purpose of mitigating the impact of plant drought stress.

Key words ACC deaminase, Dual index PCR, Phytobiome, Plant growth-promoting microbes

1 Introduction

The microbial component of plant-associated communities is incredibly diverse, consisting of bacteria, fungi, protozoa, and other microfauna and mesofauna [1–3]. The impact of these individual community members on the neighboring plants can vary from highly detrimental, or pathogenic, to highly beneficial, or mutualistic. Yet in most natural ecosystems, the community must also be considered as a collective, or "phytobiome," that when

Ramanjulu Sunkar (ed.), *Plant Stress Tolerance: Methods and Protocols*, Methods in Molecular Biology, vol. 1631,
DOI 10.1007/978-1-4939-7136-7_23,

healthy is capable of synergistic functioning to impart division of labor, productivity, and stability or resilience to the community as a whole [4, 5]. Traditionally, phytobiomes have been characterized by using cultivation-based methods and a battery of different medias and growth conditions. To further screen bacteria potentially involved in plant growth promotion, culture- and coculture-based methods were routinely used [6]. These techniques generally include simple plate assays or growing the microbes in broth and supplementing the plant growth medium with culture filtrate to identify strains with properties beneficial to the plant of interest. Unfortunately, cultivation-based methods generally rely on a rather limited number of media compositions, and the nutritional and environmental requirements of rhizospheric microbes are extraordinarily diverse and largely unknown. Hence, there is no general method or media composition that can be used to isolate all or even most species of root-associated microbes. Accordingly, a variety of alternative methods have been developed.

As discussed above, culture-dependent studies provide an incomplete account of overall diversity within and between microbial species and lack the sensitivity to detect shifts in community composition [7]. As a consequence, culture-independent techniques have been rapidly developed over the last 10 years, and these tools have dramatically changed our view of microbial diversity in any particular environment, suggesting that as few as 1% of rhizospheric microbes are cultivable [8]. Perhaps most importantly, the advancements underlying next-generation sequencing (NGS) technologies have enabled miniaturization, enhanced sensitivity *and* dramatically reduced costs. A second major development was the identification of genomic regions with short, highly conserved sequences flanking more variable gene sequence. Due to its ubiquity across all domains of life [9], the small subunit rRNA gene [16S rRNA gene in Bacteria and Archaea or 18S rRNA gene (and associated internal transcribed spacer, or ITS) in Eukarya] fits this bill, and amplicon sequencing based upon these regions gives researchers access to the tools to study the composition, organization, and spatiotemporal patterns of the fungal and bacterial microbial community development and function. Already, pioneering work has established robust experimental methods and analytical frameworks for studying the microbiome [10–13]. The microbiome analysis currently combines careful sample collection and processing, NGS and rigorous bioinformatics analysis to provide unprecedented detail of the composition of microbiota, not only at the whole plant level but even those populations inhabiting different plant organs or tissues.

We are at a nexus in agriculture, where a burgeoning world population is emerging at a time of significant climate change, the likes of which are unseen since the dawn of civilization. We must

act quickly to engage in extensive research to develop strategies to cope with abiotic stresses, including the development of heat and drought-tolerant plant varieties, shifting crop calendars, and recalibration and optimization of resource management practices. Microorganisms have always played a critical role in alleviating abiotic stress in plants, imparting properties to their host that reduces the perception of the stress (avoidance) or enhances tolerance to the stress [14–16]. Despite this extensive coevolutionary history, we currently utilize (at least knowingly) only a fraction of the microbes that could enhance plant growth and stress resistance. We propose that evaluation of the impact of microbial inoculations to alleviate stresses in plants could be integrated with plant breeding programs. Thus, a measure of plant responsiveness to symbiosis could be scored as a phenotype during the breeding process, instead of evaluation later, almost as an afterthought. Here we have reviewed recent work on the role of microorganisms in ameliorating drought stress in crops and subsequently outline (a) culture-dependent microbiological techniques and (b) culture-independent molecular techniques for microbiome analyses and screening of drought-tolerant microbes (Fig. 1).

In Protocol 1 we describe a pipeline for microbiome analysis from the living soil of an experimental site, and subsequent sampling and handling, as well as preparation of 16S libraries for DNA sequencing [18] using the Illumina MiSeq sequencing platform. Secondly, in Protocol 2 we describe a method for the isolation of microbes (culture-dependent) and downstream methods for screening for drought tolerance-promoting microbes.

Protocol 1. Sampling, and 16S/18S rDNA library preparation for microbiome analyses.

2 Materials

2.1 Sampling

Phosphate buffer saline (6.33 g of $NaH_2PO_4H_2O$, 16.5 g of $Na_2HPO_4H_2O$, and 200 μL Silwet L-77 in 1 L of water).

Nylon membrane.

DMSO.

Formaldehyde.

Ethanol, 200 proof.

50-mL conical tubes.

2.2 DNA Isolation

MoBio PowerSoil DNA kit.

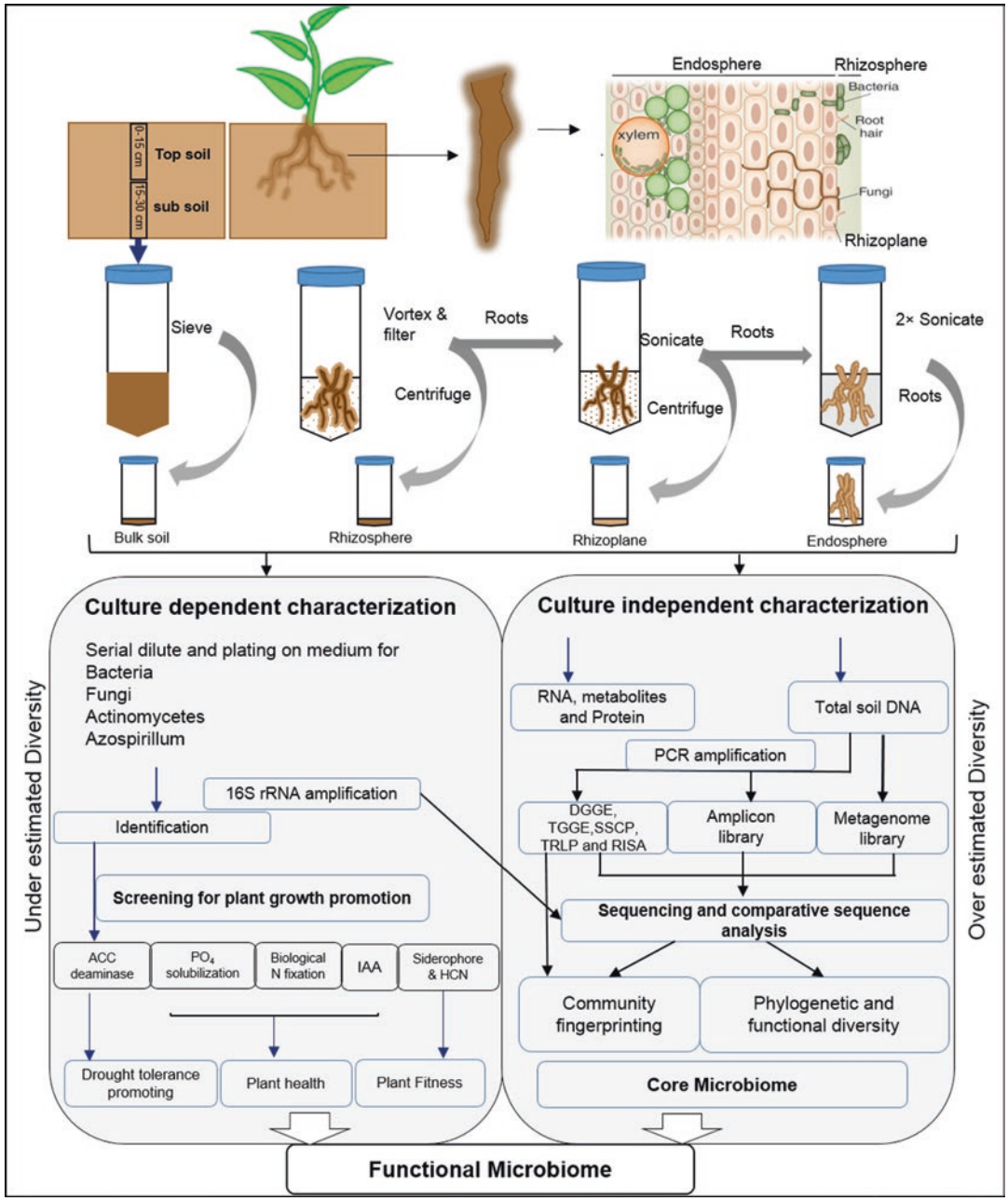

Fig. 1 Scheme for the isolation and analysis of plant-associated microbial diversity as well as bulk soil (adopted from Bakker et al. [17], Bulgarelli et al. [11], Edwards et al. [10]). The plant functional microbiome primarily includes bacteria and fungi of the rhizosphere, rhizoplane, and endosphere (*top right*) that are recruited from the bulk soil and colonize the root surface (rhizoplane) and potentially the inside of the plant (endosphere). These microbes can be characterized by culture-dependent (*lower left*) and independent (*lower right*) protocols

2.3 16S Amplification and Library Preparation Primers

Target region	Primers	Sequence (5′–3′)	References
16S_V4-V5	515F-Y 926R	GTGYCAGCMGCCGCGGTAA CCGYCAATTYMTTTRAGTTT	[19]
18S_V9	1391F EukBr_R	GTACACACCGCCCGTC TGATCCTTCTGCAGGTTC ACCTAC	[20]
ITS2	ITS86F ITS4 R	*GTGAATCATCGAATCTTTGAA* *TCCTCCGCTTATTGATATGC*	[21]

KAPA HiFi HotStart ReadyMix kit.

AmPure XP Beads.

Nextera index kit.

Nuclease-free water.

3 Methods

3.1 Experimental Site

Generally, there are no specific sites on earth where microbiome cannot be found since bulk soil as well as all plant parts are associated with numerous species of microorganisms, beneficial as well as pathogenic. However, some guidelines are here provided that may facilitate the identification and isolation of plant-associated beneficial microbes: (a) the center of biological diversity for any plant-associated microbiome is likely to be found near the center of biological diversity for the plant species harboring that microbiome; (b) the best place to search for a biological control agent is likely in the same ecological niche as the target pathogen; (c) when a target plant is introduced into a new or nonnative soil, it may enrich certain native beneficial microbes in the soil to "engineer" its own rhizosphere to assist the host plant in its recovery and adaptation to the new habitat; (d) taxonomy of the bacteria and/or fungi can serve as a useful indicator of potentially beneficial microbes, i.e., some bacterial and fungal families or divisions tend to contain beneficial species or genotypes (e.g., Rhizobiaceae or Glomeromycota).

3.2 Sampling

The number of replicate samples to be collected is directly related to the level of soil heterogeneity. A general guideline we could suggest would be three to five replicates for bulk soil per treatment. Within each replicate field, soil and plants are sampled at the same time in four fixed quadrats (50 × 50 cm, varies accordingly the nature of plants) (*see* **Note 1a**). Within 48 h after sampling, the

different compartments, i.e., bulk soil, rhizosphere, rhizoplane, and endosphere, are prepared as follows:

3.2.1 Bulk Soil

1. Bulk soil samples are collected from unplanted quadrats. Five soil cores (4.5 cm Ø, 0–15 cm for top soil and 15–30 cm for subsoil) are taken from each quadrat.
2. Four cores from each of the four corners and a single core from center of the quadrat and are sampled simultaneously and pooled. One portion is used for soil analysis.
3. The other portion is passed through 2-mm sieve and defined as "bulk soil."

3.2.2 Rhizosphere Soil

1. Five to ten plants with roots from each quadrat are removed from the soil. The excess soil is manually shaken from the roots, leaving approximately 1 mm of soil still attached to the roots.
2. The roots are placed in a clean and sterile 50-mL conical tube containing 25 mL of sterile phosphate buffered saline (PBS) solution and vortex for 15 s.
3. The resulting turbid solution is filtered through a 100-μm nylon mesh and the filtrate is centrifuged to form tight pellets, defined as "rhizosphere soil."

3.2.3 Rhizoplane

1. The roots designated for rhizoplane collection are cleaned and placed in sterile 50 mL conical tube containing 15 mL PBS.
2. The roots in the conical tube are sonicated for 30 s at 50–60 Hz. The sonication procedure strips the rhizoplane microbes from the root surface as well as portions of the rhizodermis as evidenced by the gradient of organellar reads from the rhizoplane to the endosphere.
3. The roots are removed and discarded and the liquid PBS fraction.
4. Transfer to 2-mL tubes and concentrate the rhizoplane compartment by multiple centrifugation.

3.2.4 Endosphere

1. The roots designated for the endosphere collection are rinsed in sterile distilled water and remove the debris aseptically.
2. Roots are subsequently placed in new sterile PBS buffer for sonication to remove soil or microbial aggregates remaining on the root surface as described Subheading 3.2.3.
3. Discard the PBS buffer and the clean sonicated roots constitute the endosphere compartment (*see* **Note 1b**).

3.3 Handling of Samples and DNA Extraction from Rhizo-Compartments

3.3.1 Storage and Handling

The handling of samples after collection is a critical aspect of the study design when using culture-dependent as well as DNA-based methods to compare the composition and diversity of microbial communities from environmental samples. It is not always possible or ideal to directly isolate DNA from all of the samples. Recently, several studies have been conducted to optimize the handling of samples and storage conditions [22–24] and we summarize their findings in this cartoon (Fig. 2).

1. Freeze. For long-term storage, all the samples of bulk soil, rhizo-components are mixed with or without DMSO, freeze them and stored at −80 °C. Then, when it is time to do DNA extractions, thaw them out and extract DNA.
2. Buffer. Mix with some PBS buffer or DNA stabilization/extraction solution and then let sit, possibly at 4 °C or room temperature, for an extended period of time. Then extract DNA.
3. Process.Direct processing is needed for isolation of culture dependent microbes. Alternatively, extract DNA from fresh samples and then store the DNA for later use.
4. Dry. Collect samples and dry them and then store them dried. This is done usually in cases where the main goals do not involve DNA analysis or culture dependent microbiomes.
5. Fix. Collect samples and then mix them with fixatives like formalin and alcohol. This is done with all sorts of samples where the main goal is to do something other than DNA analysis.

3.3.2 DNA Extraction

1. Thaw the stored samples. The endosphere fraction is pre-homogenized before the DNA extraction by bead beating for 1 min.
2. The DNA of each sample is then extracted using the MoBio PowerSoil DNA isolation kit according to the manufacturer's protocol eluted in 50 μL of elution buffer (*see* **Note 1c**).
3. Quality and quantity of DNA are checked.

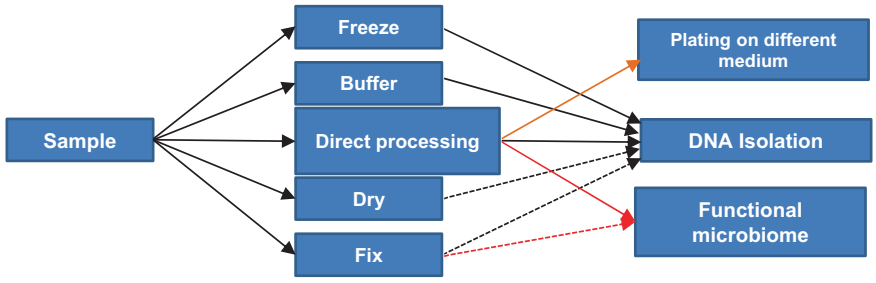

Fig. 2 A flowchart for the handling of samples collected for microbiome analyses

3.4 16S rRNA Gene Amplification and Sequencing Library Preparation

Here we present a protocol that incorporates best practices [11, 12, 18]. This protocol uses a two-step PCR process, where the marker gene of interest is amplified with a pair of adapter-tailed primers in a primary PCR reaction, and sample-specific dual indices and flow cell adapters are added in a subsequent indexing (Fig. 3). The protocol includes the primer pair sequences with sequencing adapters for V4 and V5 region that creates an amplicon size of ~412 bp. Next, after adding Illumina sequencing adapters and dual index barcodes to the mplicon target, up to 96 libraries can be pooled together for sequencing (Fig. 3). The same protocol can be used for sequencing other regions with appropriate region-specific primers.

3.4.1 PCR Amplification of 16S rDNA Gene

Thaw the KAPA HiFi HotStart ReadyMix kit, target gene specific primers and genomic DNA on ice. This step uses PCR to amplify the template out of a DNA sample using region of interest-specific

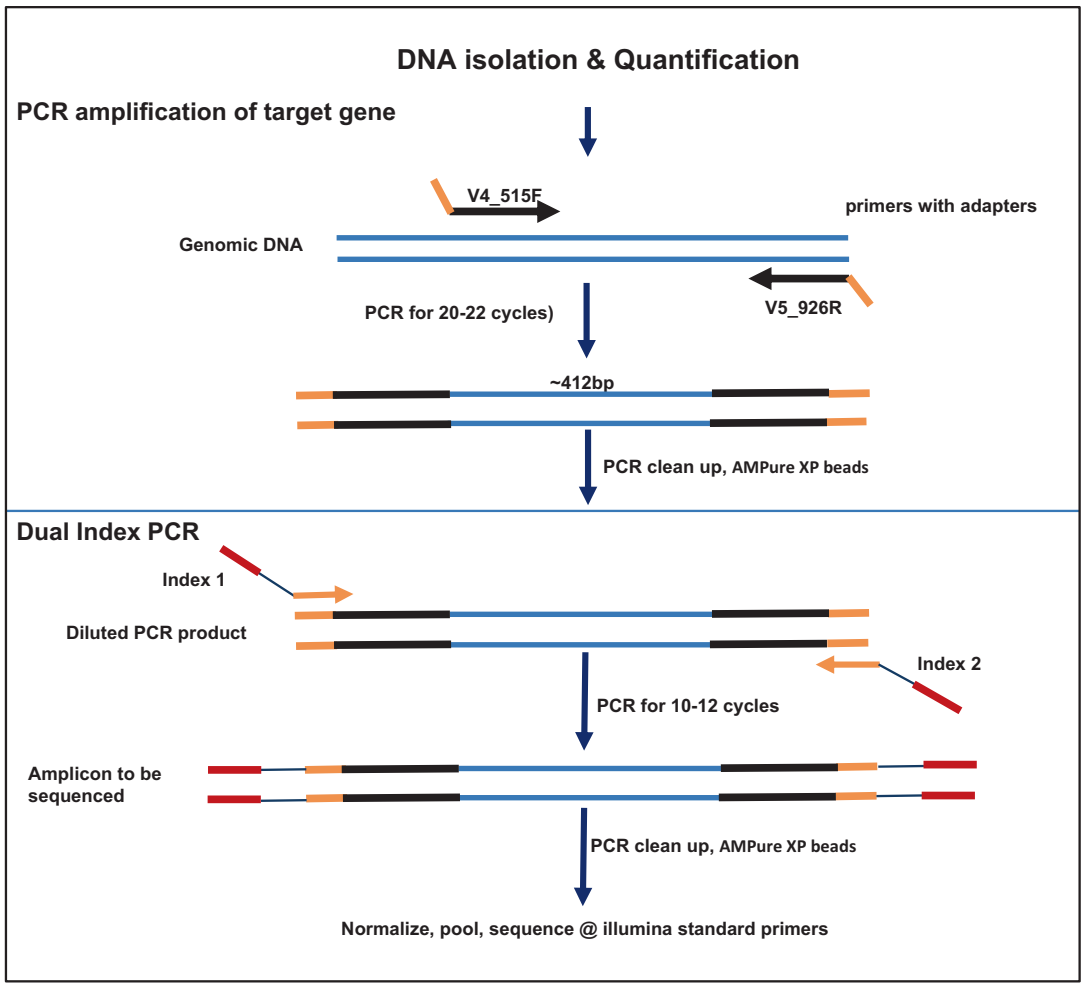

Fig. 3 Outline of the protocol for 16S rRNA gene microbiome profiling, which uses an amplification with primers targeting the V4 and V5 variable region of the 16S rRNA gene. Illumina flow cell adaptors and dual indices are added in a secondary amplification

primers and overhanging adapters attached. Set up the following PCR reaction (For samples with low template abundance, to reduce adapter dimer contamination final concentration of 0.5× KAPA HiFi HotStart Ready Mix is desirable)

Genomic DNA (5 ng/μL)	2.5 μL
Target specific forward primer with adapters (1 μM)	5.0 μL
Target specific reverse primer with adapters (1 μM)	5.0 μL
KAPA HiFi HotStart Ready Mix (2×)	12.5 μL

1. Run the following PCR protocol on the Bio-Rad (or equivalent PCR machine). Typically, this should be run for 20–25 cycles and stopped at the end of the final extension phase (*see* **Notes 1d** and **e**). PCR conditions are,

   95 °C—5 min.

   20 or 25 cycles of:

   98 °C—30 s.

   65 °C—15 s.

   72 °C—15 s.

   72 °C—5 min.

   Hold at 4 °C.
2. The quality and quantity of PCR amplification is verified on a Bioanalyzer (*see* **Note 1f**).
3. Primers and primer dimer species can be removed by AMPure beads according to the manufacturer's protocol.
4. If you are not immediately proceeding to Dual Index PCR, store the purified PCR product at −20 °C for up to a week.

3.4.2 Dual Index PCR

1. Determine how many samples are to be pooled together for sequencing and select Index 1 (i7) and index 2 (i5) dual indexing scheme, ensuring no index overlap between samples to be pooled for sequencing.
2. Follow the Illumina's guidelines and attach selected dual indices and Illumina sequencing adapters using the Nextera XT index kit. Briefly, set up the following PCR reaction.

Purified 16S rRNA amplicon	5.0 μL
Nextera XT Index primer 1 (i7)	5.0 μL
Nextera XT Index primer 1 (i5)	5.0 μL
KAPA HiFi HotStart Ready Mix (2×)	25.0 μL
Nuclease free water	10.0 μL

Run the following PCR protocol:

95 °C—3 min.

8 cycles of:

98 °C—30 s.

65 °C—30 s.

72 °C—30 s.

72 °C—5 min.

Hold at 4 °C.

3. After the PCR program is complete, centrifuge the plate to collect the sample.
4. Use the AMPure beads and clean up the library before quantification.
5. If you are not immediately proceeding to library quantification, normalization and pooling, store the purified product at −20 °C for up to a week.
6. Library quality is verified using a Bioanalyzer and quantified using a fluorometric method.
7. Dilute the concentrated final library using 10 mM Tris–HCl pH 8.5 to 4 nM.
8. Aliquot 5 μL from each library and mix aliquots for pooling libraries.

Protocol 2. Microbiological screening of drought tolerance-promoting microbes.

The plant hormone ethylene is an important modulator of normal plant growth and development as well as a key feature in the response of plants to a wide range of stresses. Plants respond to environmental stress by producing stress ethylene [25]. Out of various roles in drought stress played by plant growth-promoting bacteria (PGPB), one mechanism involves lowering plant ethylene levels through the action of the enzyme 1-aminocyclopropane-1-carboxylate (ACC) deaminase. This enzyme catalyses the cleavage of ACC, the immediate precursor of ethylene in plants, to ammonia and α-ketobutyrate [26]. This results in an overall decrease in plant ethylene levels, and an upregulation of plant genes involved in growth and protein production. Reportedly, as a direct consequence of adding ACC-degrading bacteria, plants develop longer roots and are thus more resistant to stress related to water limitation. The following protocol describes a method for screening microbes isolated from environmental samples following the steps as illustrated in Fig. 1. In particular, a method for the high-throughput screening for ACC deaminase activity adapted from Ali et al. [27] and Li et al. [28], which may be used for the identification of bacteria capable of imparting drought tolerance to a host plant.

4 High-Throughput ACC Deaminase Assay for Isolation of Drought-Tolerant Bacteria

4.1 Materials

DF salts minimal medium amended with 3 mM ACC.

DF salts minimal medium per liter [29]: KH_2PO_4 (4.0 g); Na_2HPO_4 (6.0 g); $MgSO_4 \cdot 7H_2O$ (0.2 g); $FeSO_4 \cdot 7H_2O$ (1 mg); H_3BO_3 (10 μg); $MnSO_4$ (10 μg); $ZnSO_4$ (70 μg): $CuSO_4$ (50 μg); MoO_3 (10 μg); Glucose, 1.0%.

Polyethylene glycol 6000.

Ninhydrin reagent 2% solution.

4.2 Methods

1. Screen the bacterial collection as illustrated in Fig. 1 in DF salts minimal medium containing 3.0 mM ACC as the sole source of nitrogen (*see* **Note 2a**).
2. Pick up single colonies of bacteria growing on this minimal media.
3. Inoculate 5 mL of rich media in a culture tube and incubate overnight at 28 °C till they rich stationary phase (*see* **Note 2b**). Add PEG 6000 to the suspension solution to induce drought stress. For control, do not add PEG (*see* **Note 2c**).
4. Take 2 mL of bacterial culture in a microcentrifudge tube and harvest by centrifugation at 5000 × *g* for 5 min.
5. Wash the bacterial pellet twice with 1 mL of DF salts minimal medium.
6. Suspend the bacterial pellet in 2 mL of DF medium supplemented with 3 mM final concentration of ACC in a culture tube. Incubate at 28 °C on a shaker for 24–36 h (*see* **Note 2b**).
7. Incubate a 2 mL sample of DF-ACC medium without inoculation to use as blank in subsequent steps.
8. Centrifuge the bacterial culture at 8000 × *g* for 5 min to obtain cell free supernatant. Dilute the supernatant tenfold with DF salts minimal medium.
9. Dispense 120 μL of ninhydrin reagent into wells of a standard 96-well PCR plate. To each well add 60 μL of diluted supernatant and mix by pipetting.
10. For quantification of enzymatic activity, prepare DF-ACC working solutions ranging from 0.005 to 0.50 mmol/L, and mix 60 μL of each concentration with 120 μL of ninhydrin reagent and dispense into wells of 96-well PCR plate.
11. Heat the PCR plates in a boiling water bath for 30 min or till color development.
12. Development of red color indicates degradation of ACC, i.e., ACC deaminase positive bacterial culture. Purple color indicates

nondegradation of ACC, i.e., ACC deaminase negative bacterial culture.

13. Transfer 100 μL of reaction solution, blank solution, and standard solution into a standard microplate reader and record the absorbance at 570 nm with the spectrophotometer to quantify microbial enzyme activity in drought stressed condition with respect to control.

5 Notes

1. Sampling, and 16S/18S rDNA library preparation for microbiome analyses.
   (a) Plants should be carefully removed from the soil, stored in ice chests or coolers and transported immediately to the lab and stored at 4 °C and immediately (within 48 h) processed for the determination of microbial biomass and potential enzymatic activities.
   (b) CARD-FISH on whole nonsonicated roots and thrice sonicated roots was used to analyze the efficacy of this procedure for removing microbes from the rhizoplane (for CARD-FISH protocol *see* Edwards et al. [10]).
   (c) The rhizoplane samples typically had low DNA yield and were subsequently concentrated in a SpeedVac down to 10 μL.
   (d) KAPA HiFi HotStart ReadyMix has a higher salt concentration than conventional PCR ready-mixes, which affects DNA melting and primer annealing. To ensure that targets are completely denatured, use a temperature of 98 °C for denaturation and optimal annealing temperature for a specific primer set is likely to be higher than when used in a conventional PCR ready-mix. An annealing temperature gradient PCR is recommended to determine the optimal annealing temperature with the KAPA HiFi HotStart ReadyMix. In our hand anneal at 65 °C is worked for different environmental samples.
   (e) To ensure the highest fidelity, use high-quality DNA and the lowest possible number of cycles.
   (f) Samples that amplify poorly can be amplified with increased cycle numbers. It is recommended that a water blank be run to allow assessment of potential contamination in reagents. Ensure that all sample mixing and all sample transfer steps are done carefully to avoid any cross-contamination.

2. Microbiological screening of drought tolerance-promoting microbes.
   (a) ACC is thermolabile. Prepare stock solution separately, sterilize by filtration, and add to autoclaved media just before pouring.
   (b) Estimate the incubation time empirically by recording O.D using standard spectophotomer. Harvest at O.D 1.00 (A_{600}).
   (c) The osmotic potential of 10% PEG 6000 is about −1.48 [29].
   (d) The inoculated plates should be incubated at no higher than 35 °C, as ACC deaminase is inhibited above this temperature.

Acknowledgments

This work was supported by the US Department of Energy, the BioEnergy Science Center (BESC), through the Office of Biological and Environmental Research in the DOE Office of Science and The Samuel Roberts Noble Foundation. We declare no conflict of interests inherent to this submission.

References

1. Turner TR, James EK, Poole PS (2013) The plant microbiome. Genome Biol 14:209–219
2. Berendsen RL, Pieterse CM, Bakker PA (2012) The rhizosphere microbiome and plant health. Trends Plant Sci 17:478–486
3. Vorholt JA (2012) Microbial life in the phyllosphere. Nat Rev Microbiol 10:828–840
4. Beattie GA, Lindow SE (1995) The secret life of foliar bacterial pathogens on leaves. Annu Rev Phytopathol 33:145–172
5. Rosenblueth M, Martínez-Romero E (2006) Bacterial endophytes and their interactions with hosts. Mol Plant Microbe Interact 19:827–837
6. Beneduzi A, Peres D, Vargas LK, Bodanese-Zanettini MH, Passaglia LMP (2008) Evaluation of genetic diversity and plant growth promoting activities of nitrogen-fixing bacilli isolated from rice fields in South Brazil. Appl Soil Ecol 39:311–320
7. Bakker PA, Berendsen RL, Doornbos RF, Wintermans PC, Pieterse CM (2013) The rhizosphere revisited: root microbiomics. Front Plant Sci 4:165
8. Hugenholtz P, Goebel BM, Pace NR (1998) Impact of culture-independent studies on the emerging phylogenetic view of bacterial diversity. J Bacteriol 180:4765–4774
9. Olsen GJ, Lane DJ, Giovannoni SJ, Pace NR, Stahl DA (1986) Microbial ecology and evolution: a ribosomal RNA approach. Annu Rev Microbiol 40:337–365
10. Edwards J, Johnson C, Santos-Medellín C, Lurie E, Podishetty NK et al (2015) Structure, variation, and assembly of the root-associated microbiomes of rice. Proc Natl Acad Sci 112:E911–E920
11. Bulgarelli D, Rott M, Schlaeppi K, van Themaat EVL, Ahmadinejad N et al (2012) Revealing structure and assembly cues for Arabidopsis root-inhabiting bacterial microbiota. Nature 488:91–95
12. Gohl DM, Vangay P, Garbe J, MacLean A, Hauge A et al (2016) Systematic improvement of amplicon marker gene methods for increased accuracy in microbiome studies. Nat Biotechnol 34:942–949

13. Mendes R, Kruijt M, de Bruijn I, Dekkers E, van der Voort M et al (2011) Deciphering the rhizosphere microbiome for disease-suppressive bacteria. Science 332:1097–1100
14. Ngumbi E, Kloepper J (2016) Bacterial-mediated drought tolerance: current and future prospects. Appl Soil Ecol 105:109–125
15. Rolli E, Marasco R, Vigani G, Ettoumi B, Mapelli F et al (2015) Improved plant resistance to drought is promoted by the root-associated microbiome as a water stress-dependent trait. Environ Microbiol 17:316–331
16. Marasco R, Rolli E, Ettoumi B, Vigani G, Mapelli F et al (2012) A drought resistance-promoting microbiome is selected by root system under desert farming. PLoS One 7:e48479
17. Bakker P, Berendsen R, Doornbos R, Wintermans P, Pieterse C (2012) The rhizosphere revisited: root microbiomics. Front Plant Sci 4:165
18. (2013) Illumina 16S metagenomic sequencing library preparation (Illumina Technical Note 15044223 Rev. A). Illumina. http://support.illumina.com/content/dam/illumina-support/documents/documentation/chemistry_documentation/16s/16s-metagenomic-library-prep-guide-15044223-b.pdf
19. Parada AE, Needham DM, Fuhrman JA (2015) Every base matters: assessing small subunit rRNA primers for marine microbiomes with mock communities, time series and global field samples. Environ Microbiol 18:1403–1414
20. Amaral-Zettler LA, McCliment EA, Ducklow HW, Huse SM (2009) A method for studying protistan diversity using massively parallel sequencing of V9 hypervariable regions of small-subunit ribosomal RNA genes. PLoS One 4:e6372
21. Vancov T, Keen B (2009) Amplification of soil fungal community DNA using the ITS86F and ITS4 primers. FEMS Microbiol Lett 296:91–96
22. Kerckhof F-M, Courtens EN, Geirnaert A, Hoefman S, Ho A et al (2014) Optimized cryopreservation of mixed microbial communities for conserved functionality and diversity. PLoS One 9:e99517
23. Prakash O, Jangid K (2015) Preservation of uncultivated microbial cells for single cell genomics and cultivation in future. Single Cell Biol. doi:10.4172/2168-9431.S1-003 2015
24. Lauber CL, Zhou N, Gordon JI, Knight R, Fierer N (2010) Effect of storage conditions on the assessment of bacterial community structure in soil and human-associated samples. FEMS Microbiol Lett 307:80–86
25. Glick BR (2014) Bacteria with ACC deaminase can promote plant growth and help to feed the world. Microbiol Res 169:30–39
26. Glick BR, Cheng Z, Czarny J, Duan J (2007) Promotion of plant growth by ACC deaminase-producing soil bacteria. Eur J Plant Pathol 119:329–339
27. Ali SZ, Sandhya V, Rao LV (2014) Isolation and characterization of drought-tolerant ACC deaminase and exopolysaccharide-producing fluorescent *Pseudomonas* sp. Ann Microbiol 64:493–502
28. Li Z, Chang S, Lin L, Li Y, An Q (2011) A colorimetric assay of 1-aminocyclopropane-1-carboxylate (ACC) based on ninhydrin reaction for rapid screening of bacteria containing ACC deaminase. Lett Appl Microbiol 53:178–185
29. Michel BE, Kaufmann MR (1973) The osmotic potential of polyethylene glycol 6000. Plant Physiol 51:914–916

INDEX

Ramanjulu Sunkar (ed.), *Plant Stress Tolerance: Methods and Protocols*, Methods in Molecular Biology, vol. 1631,
DOI 10.1007/978-1-4939-7136-7, © Springer Science+Business Media LLC 2017

I

K

L

M

N

O

P

Q

R

S

T

V

W